

*Tectonic-sedimentary evolution of the  
Cenozoic Hatay Graben, South Central  
Turkey.*



Sarah J. Boulton

M.Sci (Hons) (Lon)

Thesis submitted for the degree of Doctor of Philosophy

University of Edinburgh

2006



“Geology is the study of pressure and time. That's all it takes, really.

*Pressure and time.”*

Red – The Shawshank Redemption

From the screenplay of the book by Stephen King.

## Abstract

The Mediterranean region is important for understanding the processes of diachronous continental collision. The Hatay Graben, Turkey, is located near the Bitlis suture zone, the Misis-Andırın Lineament, the Dead Sea Fault Zone, the East Anatolian Fault Zone and the Cyprus Arc. Fieldwork focused on the Palaeogene to Quaternary geology of the Hatay Graben and lead to a new two-stage tectonic model of a foreland basin that was dissected into a transtensional graben, a result of the westward tectonic escape of Anatolia.

Arabian platform carbonates of Late Cretaceous-Eocene age are the oldest sediments studied. The Oligocene was characterised by a regional hiatus. In the Early Miocene (Balyatağı Formation), braided-rivers and alluvial fans drained uplifted areas to the S. Syn-tectonic sedimentary features indicate that normal faulting was active by Mid-Miocene time; a time when shallow-marine carbonate deposition (peritidal, lagoonal, reefal and slope environments) predominated (Sofular Formation). Water-depth increased during Mid-Late Miocene due to increased subsidence, resulting in the deposition of hemipelagic carbonates (Nurzeytin Formation). The Middle to Upper Miocene units record the lower and middle units of a typical underfilled foreland basin sequence. After the Messinian Salinity crisis, the area was initially marine but regressed to marginal-marine and eventually to non-marine from Late Pliocene time onwards.

The orientation of the graben was probably influenced by pre-existing zones of crustal weakness related to the Early Mesozoic rifting of Neotethys. Normal faults are common in all formations and areas, but strike-slip faults are mainly observed within the Plio-Quaternary fill of the graben. Three main trends of fault strike are observed within the Hatay Graben (NW-SE, N-S, NE-SW); these appear to have been active synchronously, suggesting an overall transtensional setting.

During the Miocene the basin developed in the distal (southerly) part of a foreland basin of the Tauride allochthon, represented by the Misis-Andırın Mountains to the N. Crustal loading initially triggered the development of a flexural bulge to the south and normal faulting within the foreland basin. During the Plio-Quaternary; however, a pronounced topographic, fault-controlled, graben developed. The formation of this Hatay Graben *sensu stricto* is inferred to have been influenced by the westward tectonic escape of Anatolia along the East Anatolia Fault Zone and left-lateral offset along the northward extension of the Dead Sea Transform Fault. The Hatay Graben is located at the interface between a zone of continental collision in the east and a pre-collisional area to the west, a setting that played a key role in its Plio-Quaternary development

## Acknowledgements

Where do I start? There have been so many people who have helped and supported me over the last few years, who have helped me along the way. I thank you all.

Most of all I'd like to thank Alastair Robertson, without whom this project would not have happened. His advice, knowledge and humour have been invaluable, no one could ask for a better supervisor. I'd also like to thank Hugh Sinclair and Ulvi Can Ünlügenç, my other supervisors for their input. Especially Ulvi Can at Çukurova University who provided maps, papers, cars, field assistants and of course *çay*!

I would like to thank all the technical staff who have assisted me in various ways, Geoff Angel, Ann Menim with the XRD work, Nikki Cayzer with the SEM and Mike Hall for many thin sections. Additionally, I'd like to thank the staff at SUERC (East Kilbride), especially Rob Ellam, for helping with the strontium isotope work, and Ümit Safak at Çukurova University for undertaking microfossil analyses for me. I'd like to thank my Turkish field assistants, Pinar and Mustafa and also Tolga, for Turkish lessons and fending off the inevitable invitations of hospitality.

I'd also like to thank Iain Stewart (Plymouth), James Jackson (Cambridge) and Mark Allen (Durham) for enlightening discussions and nuggets of information that have been invaluable to this project.

I guess the people who have shaped my time most; however, are my friends. To Sam, Jason and Emma, my flatmates; thanks for putting up with my highs and lows, especially Sam who has not only been a great friend but also my field assistant. These last three years would have been harder without you. Thanks to Tim I and Alex, for fun holidays here and abroad, hill walking and of course cheeky Tuesdays! To Jon H for always appreciated computer advice; thanks to Pete and Tim K, for completing the Eastern Med research group with Sam and myself and for games of backgammon in exotic places. Finally, to Nick, Kev, Clare B, Clare W, Zana, Rich, Robin, Chris B, Helen, Ira and all the other Ph.D students to numerous to mention, thanks for the memories – I hope there will be many more. Thanks too to my friends from home, you have been there for me through everything for as long as I can remember. Sume, Emma and Jenny, I hope that will never change.

Also a mention should go Berlington Berties! Thanks to Doogie, Jude, Chris H, Richie, Tim D and Thomas for many a late night and early morning!

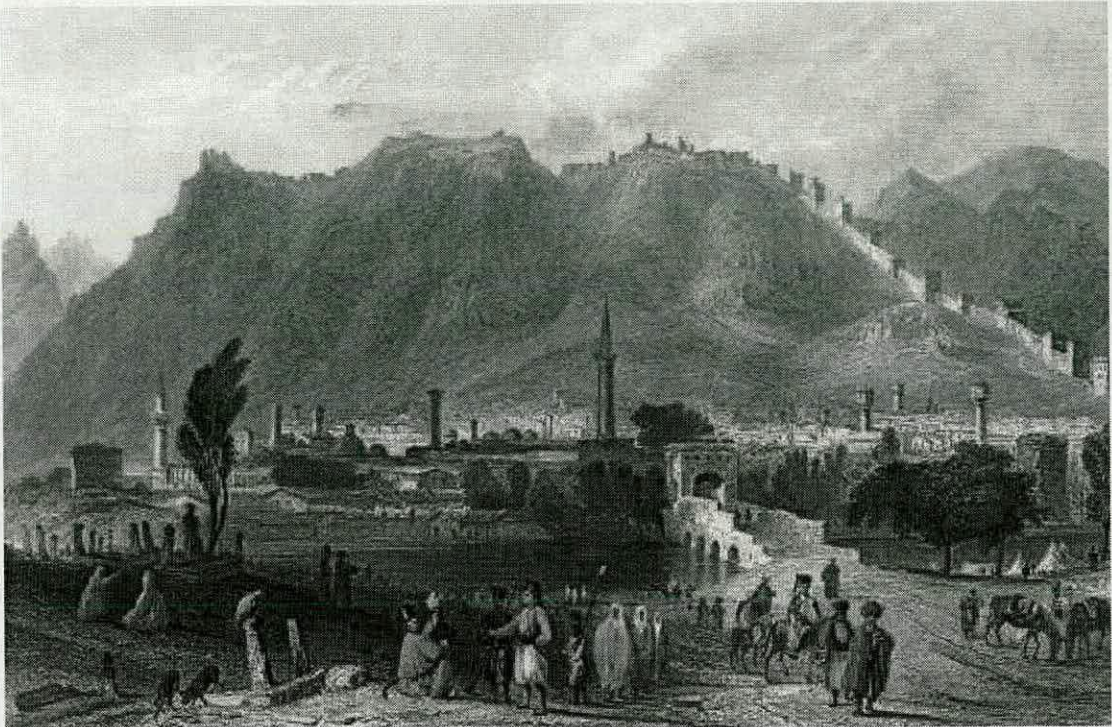
But I guess as with any good speech, the final word is reserved for my family. You have always had unswerving belief that I could do anything and you have supported me all the way, never questioning whether at the end of it all I would be able to get a "proper job"! Thank you Mum, Thank you Dad, Thank you Charles. I hope that your new life in Canada brings you everything that you want.

<b>1</b>	<b>INTRODUCTION AND RATIONALE</b>	<b>1</b>
1.1	INTRODUCTION	1
1.2	OVERVIEW OF THE GEOLOGY OF THE HATAY GRABEN	8
1.3	PROJECT AIMS	10
1.4	PROJECT METHODS	11
1.5	THESIS ORGANISATION	13
1.6	USE OF TURKISH WORDS IN THE THESIS	14
<b>2</b>	<b>REVISED STRATIGRAPHY OF THE CENOZOIC ROCKS OF HATAY</b>	<b>15</b>
2.1	INTRODUCTION	15
2.2	CENOZOIC UNITS OF THE HATAY GRABEN	18
2.3	CENOZOIC UNITS OF THE KIRIKHAN AREA	27
2.4	INITIAL INTERPRETATIONS	32
2.5	CONCLUSIONS	33
<b>3</b>	<b>SR<sup>87</sup>/SR<sup>86</sup> ISOTOPE ANALYSIS</b>	<b>35</b>
3.1	INTRODUCTION	35
3.2	METHODOLOGY	37
3.3	RESULTS	42
3.4	DISCUSSION	43
3.5	CONCLUSIONS	46
<b>4</b>	<b>SEDIMENTOLOGICAL EVOLUTION</b>	<b>47</b>
4.1	INTRODUCTION	47
4.2	THE SEDIMENTOLOGY OF THE HATAY GRABEN	49
4.3	SEDIMENTS FROM THE AREAS AROUND SERINYOL, BELEN AND KIRIKHAN	123
4.4	SERINYOL	141
4.5	PROVENANCE	147

<b>5</b>	<b>BASIN ANALYSIS</b>	<b>175</b>
5.1	INTRODUCTION	175
5.2	LATE CRETACEOUS AND EOCENE UNITS	176
5.3	EARLY MIOCENE – AQUITANIAN TO BURDIGALIAN AGE	182
5.4	MIDDLE MIOCENE – UPPERMOST BURDIGALIAN/BASE-LANGIAN TO TOP-LANGIAN AGE	195
5.5	UPPER MIOCENE	204
5.6	LATEST MIOCENE TO PLIOCENE	214
5.7	QUATERNARY	221
5.8	SUMMARY PALAEOENVIRONMENTAL MODELS	223
<b>6</b>	<b>SUBSIDENCE CURVES</b>	<b>231</b>
6.1	INTRODUCTION AND METHODOLOGY	231
6.2	RESULTS	236
6.3	DISCUSSION	239
6.4	CONCLUSIONS	241
<b>7</b>	<b>STRUCTURAL GEOLOGY OF THE HATAY GRABEN</b>	<b>243</b>
7.1	INTRODUCTION	243
7.2	EXTENSIONAL TECTONICS	246
7.3	OBLIQUE-SLIP FAULTS	259
7.4	STRIKE-SLIP FAULTS	261
7.5	COMPRESSIONAL TECTONICS	264
7.6	TIMING OF FAULTING	268
7.7	FAULT ORIENTATION DATA	278
7.8	B FACTOR	289
7.9	STRESS ANALYSIS	290
7.10	PAST AND PRESENT SEISMICITY	296

7.11 DISCUSSION	303
7.12 CONCLUSIONS	307
<b>8 TECTONIC GEOMORPHOLOGY OF THE HATAY GRABEN</b>	<b>309</b>
8.1 INTRODUCTION	309
8.2 DRAINAGE PATTERNS	315
8.3 KARASU RIFT	325
8.4 STREAM PROFILES	327
8.5 DISCUSSION	337
8.6 CONCLUSIONS	340
<b>9 REGIONAL COMPARISONS AND DISCUSSION OF THE GEOLOGICAL EVOLUTION OF THE HATAY GRABEN</b>	<b>341</b>
9.1 GEOLOGICAL HISTORY OF THE HATAY GRABEN AND THE KIRIKHAN AREA	341
9.2 REGIONAL COMPARISONS	350
9.3 TECTONIC MODELS FOR THE FORMATION OF THE HATAY GRABEN	372
9.4 WIDER IMPLICATIONS	384
9.5 FUTURE WORK	385
<b>10 CONCLUSIONS</b>	
<b>REFERENCES</b>	
<b>APPENDIX 1</b>	<b>CDVII</b>
<b>APPENDIX 2</b>	<b>CDXII</b>
<b>APPENDIX 3</b>	<b>CDXVII</b>
<b>APPENDIX 4</b>	<b>CDLXXXVII</b>
<b>APPENDIX 5</b>	<b>CDXCI</b>
<b>APPENDIX 6</b>	<b>CDXCII</b>
<b>APPENDIX 7</b>	<b>CDXCVI</b>
<b>APPENDIX 8</b>	<b>CDXCVII</b>

## Chapter 1



Antioch on the approach from Suadeah [Samandağ]

The plates at the beginning of each chapter are taken from the book: CARNE/BARTLETT: SYRIA, THE HOLY LAND, ASIA MINOR, ETC ILLUSTRATED. Published by Fisher Sons & Co. London. Paris and America. c.1836

<http://www.antiquemapsandprints.com/BOOKS/SYRIA-ASIA-MINOR-1836.htm>



# 1 Introduction and Rationale

## 1.1 Introduction

The relative motions of the African, Arabian and Eurasian plates shape the tectonics of the Eastern Mediterranean. The northward motion of Africa and Arabia towards Eurasia has caused convergence and collision in this region since the Late Cretaceous (Robertson 1998). Convergence between Africa and Eurasia began ~90 Ma ago (Şengör & Yılmaz 1981) resulting in the progressive closure of the Mesozoic Neotethys Ocean and the amalgamation of surrounding continental fragments. This also resulted in the development of an arcuate fold belt (Figure 1.1) that extends from Egypt through Sinai into Syria and Lebanon, known as the Syrian Arc (i.e. Krenkel 1924; Reches et al. 1981; Eyal 1996; Walley 1996). The development of these structures is generally considered to have taken place in two phases (Syrian Arc I and II) with Syrian Arc I deformation occurring ~90-85 Ma (Walley 1998) and Syrian Arc II deformation occurring ~37-24 Ma (Walley 1998).

Subduction took place along the Bitlis-Zagros Suture Zone from the Early Cretaceous to the Mid-Late Miocene (Yılmaz 1993; Robertson *et al.* 2004) when continental-continental collision occurred. Continuing N-S directed compression due to the motion of the Arabian plate, lead to the uplift and crustal thickening of Anatolia (Şengör & Kidd 1979; Jaffey & Robertson 2005) during Late Miocene/Early Pliocene time.

Following the cessation of collision across the suture zone in SE Turkey and Iran, compressional tectonics across Anatolia was replaced by tectonic escape by the Early Pliocene (Bozkurt 2001), causing the westward extrusion of the Anatolian block along the North Anatolian Fault zone (NAFZ) and the East Anatolian Fault zone (EAFZ) (McKenzie 1978a; Şengör *et al.* 1985). The NAFZ is older than the EAFZ, and is generally considered to have become active in the earliest Pliocene (~5 Ma) (Barka & Kadinsky-Cade 1988). The age of the EAFZ is thought to either be Late Miocene-Early Pliocene (i.e. Şengör *et al.* 1985; Arpat & Şaroğlu 1972) or Late Pliocene (Yürür & Chorowicz 1998; Westaway & Arger 1998).

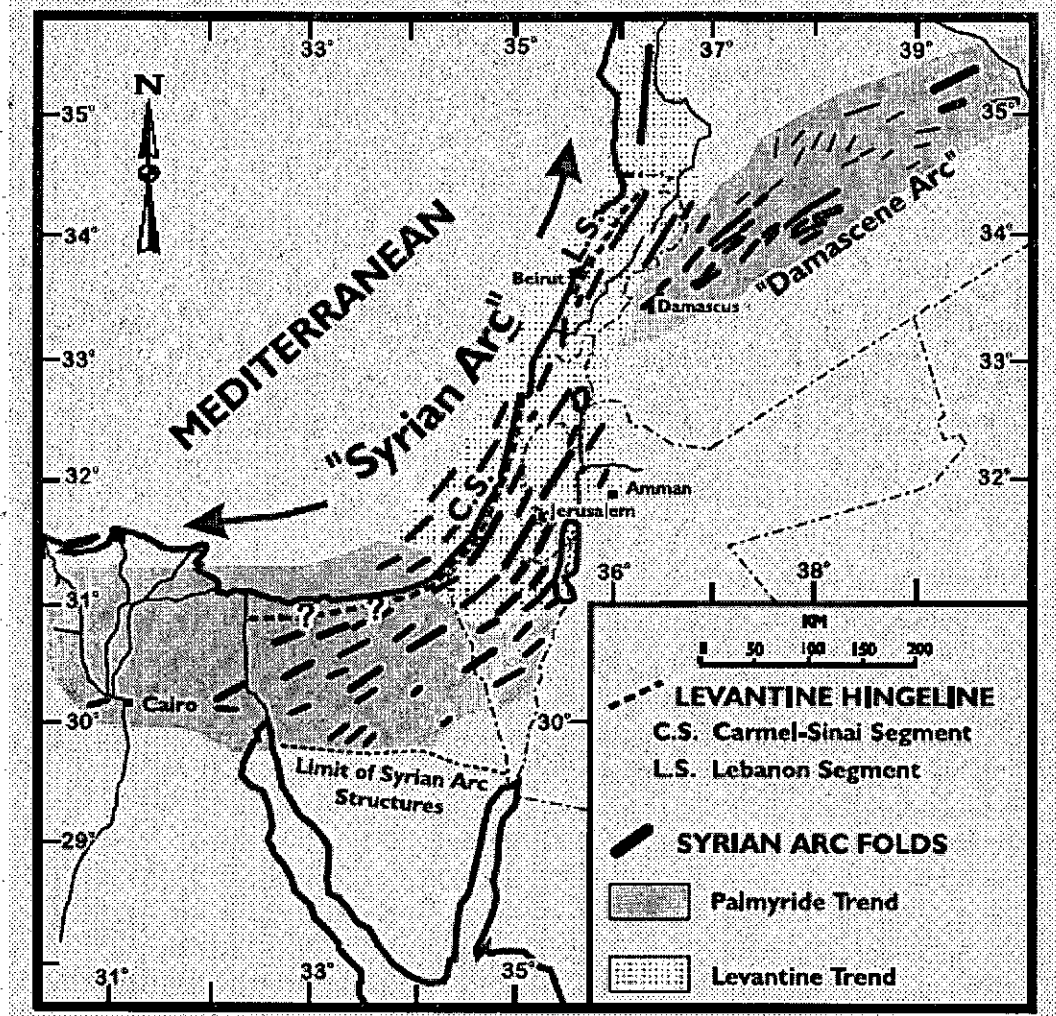


Figure 1.1. Map of Syrian Arc structures and Levantine and Palmyride trends in the Eastern Mediterranean region, from Walley 1998.

The relative motion between the African and Arabian plates is accommodated by left-lateral motion (Mart & Rabinowitz 1986) along the Dead Sea Fault zone (DSFZ) (Figure 1.2). The DSFZ links the area of sea-floor spreading in the Red Sea to the northern boundary of the Arabian plate and the zone of continental collision. The DSFZ may possibly have influenced the tectonics of the Cyprus Arc since the Neogene (Perinçek & Çemen 1990; Robertson 1998; Bozkurt 2001). The DSFZ was initiated in the south sometime in the Miocene (variously dated as <20 Ma, Lyberis 1998; 18 Ma, Garfunkel & Ben Avraham 1996; as Late Miocene, Steckler *et al.*: 1988) due to the opening of the Gulf of Suez.

The Cyprus Arc is generally considered to be the active plate boundary to the south of Cyprus, which accommodates the convergence between Africa and Anatolia (Ben Avraham

1978; Kempler & Garfunkel 1994). To the west and south of Cyprus the position of the arc is well defined; however, to the east this is not the case and there is no arc-trench system present. There are several views on the position of the plate boundary after this point: that there is no boundary in the area (Ben Avraham 1978); there are two boundary segments to the north and south Cyprus (Lort 1971; Le Pichon & Angelier 1979); there is a zone of active convergence from Cyprus to the Iskenderun Basin towards the Kahramanmaraş triple junction where the EAFZ and DSFZ may meet (McKenzie 1978a; Dewey & Şengör 1979); the arc is partitioned into a series of strike-slip systems forming a wide zone and not a discrete plate boundary (Kempler & Garfunkel 1994; Robertson 1998; Vidal *et al.* 2000) and finally southernmost boundary of the plate boundary runs from Cyprus onshore in northern Syria (Hardenberg 2004).

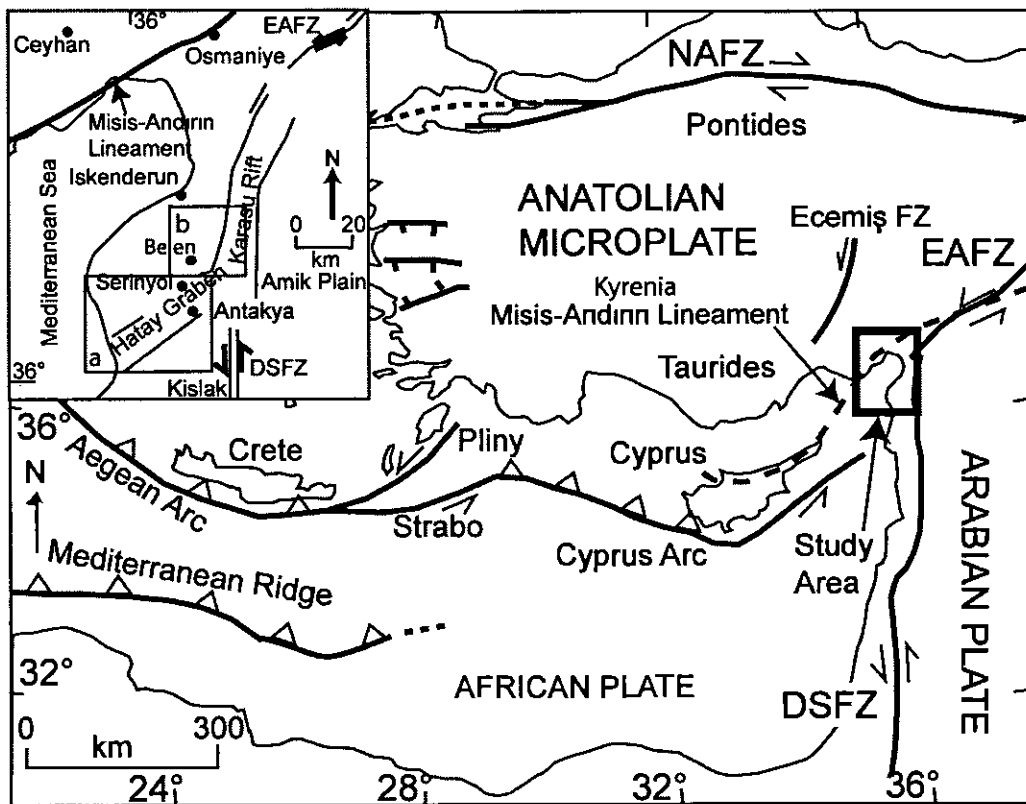


Figure 1.2. A simplified tectonic map of Turkey and the surrounding area showing the major Neotectonic structures. Box indicates location of inset map showing close up of study areas; box a. is the main study area around the Hatay Graben and box b. shows the secondary area around Belen.

Another regionally important strike-slip lineament, the Ecemiş Fault Zone, situated to the NE of the study area (Fig. 1.2) is considered to show a left-lateral offset of ~60km mainly

since Mid-Miocene time (Yetiş 1978; Koçayığıt & Beyhan 1998; Jaffey & Robertson 2002). Much early displacement of Anatolia was accommodated along this lineament, prior to the Plio-Quaternary activation of the EAFZ.

The region of Hatay is located in the Eastern Mediterranean on the border between Turkey and Syria (Fig 1.2). It is an area of active neotectonics where three major structural lineaments intersect: the southern end of the EAFZ, the northern end of the DSFZ and the Cyprus Arc (Robertson 1998) (Figure 1.2). The main study area for the research project is a graben that trends NE-SW from the city of Antakya to the Mediterranean Sea; an area that was previously considered as an extension of a graben, known as the Hatay Graben (Perinçek & Çemen 1990), the Amanos Fault Zone (Lyberis *et al.* 1992), or the Karasu Rift (Lovelock 1984; Westaway 1994; Rojay *et al.* 2001; Över *et al.* 2002), which appears to link the EAFZ with the DSFZ through the Amik Plain. In this study this structure will be termed the Karasu Rift and the main study area from Antakya towards the sea will be termed the Hatay Graben. As well as field work around the Hatay Graben, the eastern margin of the Karasu Rift (between Kırıkhan and Belen; Fig 1.2) was also investigated in order to study the differences and similarities between the areas, and to gain a broader perspective on the palaeogeography of the region as a whole. A few days were also spent along the coast of the Iskenderun Bay to the north, in order to find out if there are any major differences between the sedimentary and structural characteristics of the two areas.

The Hatay Graben is orientated NE-SW and is bounded to the NW by the Kızıl Dağ, a range of mountains that extends northwards for about 80km and rise sharply from the Mediterranean Sea and the Gulf of Iskenderun to ~1800m in elevation. To the SE the basin is bounded by the Ziyaret Dağ, which rise to ~1300m. The Hatay Graben, situated between these mountain ranges, falls from 160m at the Amik Plain (NE of Antakya; Fig 1.2), inland, to the coast. The Hatay Graben is a topographic low formed due to transextension accommodated by normal faults. The Karasu Rift runs northwards from the Amik Plain, with the Kızıl Dağ/Amanos Dağ to the west and Syria to the east.

The Karasu Rift and the Hatay Graben developed following the emplacement of the Late Cretaceous Hatay ophiolite, which was thrust southwards due to the closure of the of the Southern Neotethys ocean in the latest Cretaceous (Robertson 1998). Post-collisional changes in the stress regime related to foreland basin formation and the development of the

DSFZ resulted in extensional and strike-slip faulting that formed in the various structures present today.

There is a large body of research on the geological evolution of the Misis-Andırın lineament (e.g., Kelling *et al.* 1987; Kozlu 1987; Gökçen *et al.* 1988; Robertson *et al.* 2004) and the structure and sedimentology of the associated foreland basin fill (e.g., Aktaş & Robertson 1984; Gökçen *et al.* 1988; Derman 1996; Robertson *et al.* 2004; Kelling *et al.* 2005).

Several models have been proposed for the formation of the Misis-Andırın lineament:

- That continental collision had ceased in the latest Cretaceous, following this low-angle detachment faulting in the Eocene – Oligocene lead to basin and melange formation. A second phase of extension then took place in the Early Miocene. In the Mid-Late Miocene the basin was infilled and subsequently underwent transpression and strike-slip faulting (Karig & Kozlu 1990).
- Similar to the above model but after the cessation of subduction, transtensional basins formed due to sinistral strike-slip faulting until the Early Miocene. A period of sedimentation took place in the Middle Miocene infilling basins, after that strike-slip faulting resumed in the Late Miocene-Late Pliocene. (Ünlügenç 1993; Kozlu 1997).
- In this model the rocks of the Misis-Andırın lineament are seen as an accretionary prism formed during northward subduction from the latest Cretaceous to Late Miocene (Yılmaz 1993; Yılmaz & Gürer 1995). Continental collision was complete by the Middle Miocene and there was a regional switch to left-lateral strike-slip during the Plio-Quaternary.
- The last model is similar to the above only that subduction occurred in two phases beginning in the Latest Cretaceous with emplacement of ophiolites leaving a remnant of oceanic crust. Little subduction took place from this time until the Middle Eocene when subduction recommenced, resulting in diachronous continental collision. Strike-slip faulting then took place from the Plio-Quaternary (Aktas & Robertson 1984; Yılmaz 1993; Derman 1996; Robertson 1998, 2000; Robertson *et al.* 2004).

Although there has been much speculation on the Neotectonic plate configuration of the field area and surroundings, there is a lack of information in the literature about the possibility that the Hatay Graben was part of the foreland basin to this suture zone.

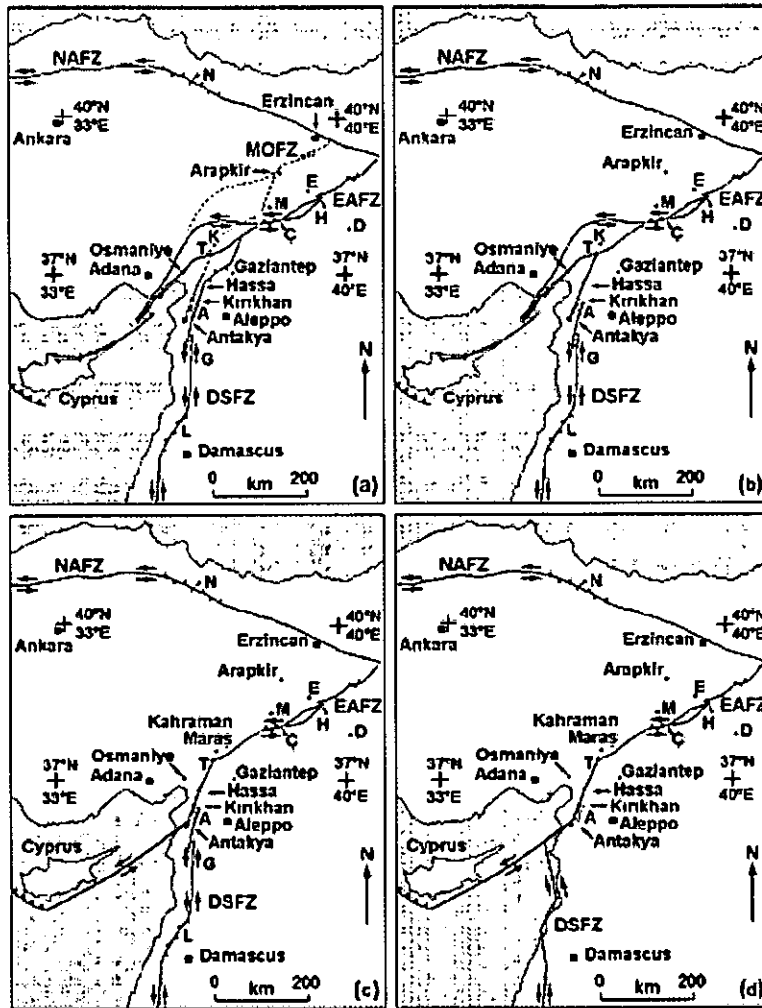


Figure 1.3. Summaries of the different regional kinematic interpretations proposed for the Neotectonic configuration of Eastern Mediterranean; a. Westaway (1994), b. Karig & Kozlu (1990), c. Over *et al.* (2004); Yurur & Chorowicz (1998), d. Girdler (1990), from Yurtmen *et al.* (2002). See text for explanation.

The above models were mostly based on work on the EAFZ or DSFZ. Little work has actually been carried out on the Neogene to recent geology of the Karasu Rift or the Hatay Graben. There is little work especially on the sedimentology and there are no facies models; additionally, published structural information is sparse. Much work has been undertaken on the underlying ophiolite (e.g. Coğulu 1974; Delaloye *et al.* 1980; Tinkler *et al.* 1981; Parlak *et al.* 1998) and some on the Quaternary setting of the area (Erol & Pirazzoli 1992; Pirazzoli *et al.* 1991; Rojay *et al.* 2001). It is, therefore, apparent that there is much scope for new insights to be gained on the geological evolution of this important area by conducting field research in the Hatay Graben.

## 1.2 Overview of the Geology of the Hatay Graben.

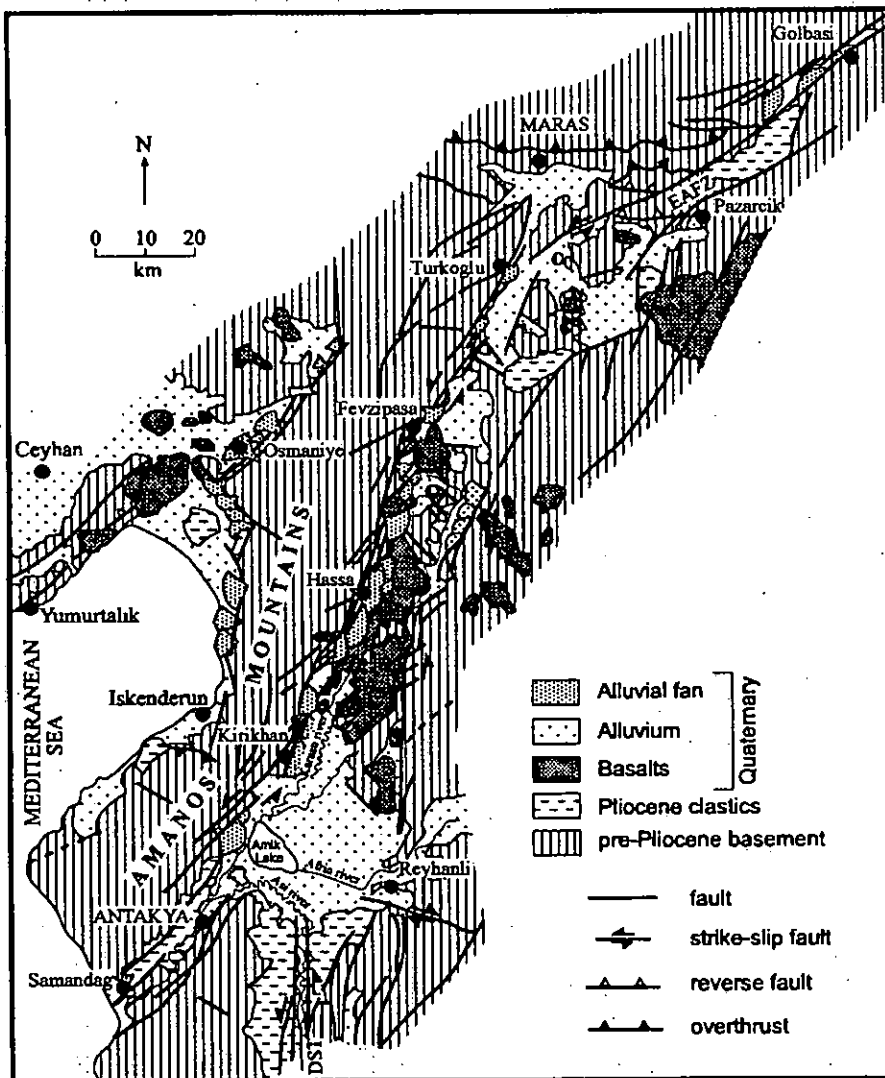


Figure 1.4. Simplified regional geological map of the faults and Plio-Quaternary rocks of the Karasu Rift and its vicinity, from Rojay *et al.* 2001.

The Upper Cretaceous Hatay Ophiolite (Appendix 8) forms the basement to the study area; this ophiolite was emplaced southwards during the Campanian to Maastrichtian (Tinkler *et al.* 1981) due to the closure of the Neothethys to the north (Robertson 1998). Upper Cretaceous limestones were deposited unconformably onto the ophiolite. Tinkler *et al.* (1981) and Pişkin *et al.* (1986) report that an extensive conglomerate is present at the base of the sedimentary cover sequence; this is suggested to be Maastrichtian in age and had originated due to erosion along a fault scarp; however, little evidence is presented in support of this

statement. Parlak *et al.* (1998) do not mention this conglomeratic material and describe the formation as being composed of shallow-marine calcarenites, marls and clayey limestones.

Upper Cretaceous shallow-marine carbonates pass transitionally upwards into Late Palaeocene – Middle Eocene calcarenites and limestones rich in microfossils. These carbonates form part of the Arabian carbonate platform (Gvirtzman *et al.* 1989). Uplift took place during the Middle to Late Eocene triggered by continued closure of the Tethys Ocean (Robertson 1998), resulting in a period of non-deposition that continued until the Early Miocene. Tinkler *et al.* (1981) and Pişkin *et al.* (1986) record the presence of an extensive conglomeratic horizon composed of limestone and ophiolitic debris at the base of the Miocene sedimentary sequence.

Parlak *et al.* (1998) describes the overlying Middle – Late Miocene sediments in the Karasu Rift as being discordant to the conglomerates. Tinkler *et al.* (1981) and Pişkin *et al.* (1986) when discussing the Hatay Graben do not mention this feature; they describe the Middle Miocene limestones as being composed of reef-derived material, transitional to the Late Miocene sediments composed of marl with intercalculated sandstone and mudstone beds. There is no information in the literature on the nature of the Pliocene sediments.

During the Quaternary active volcanism occurred in parts of the Karasu Rift; the lavas are basaltic in nature. However, they are confined to a limited section of the rift and none are found within the Hatay Graben. A number of different basaltic flows have been dated spanning a range of ages from 2.2 – 0.5 Ma (K-Ar; Parlak *et al.* 1998; Rojay *et al.* 2001). It is possible that the volcanism was intermittent in nature thus resulting in the spread of ages. Geochemical analysis carried out by Parlak *et al.* (1998) suggests that the magma originated from an enriched mantle source; this is consistent with other basalts found in rift zones i.e. East African Rift, the Ethiopian Rift, Rio Grande Rift (Wilson 1989).

The Quaternary sediments of the area were sub-aerially deposited and are mainly composed of fluvial and lacustrine sediments; recent alluvium, alluvial fans, talus and lake deposits that dissect the older stratigraphy. Tufa and caliche can additionally be observed (Rojay *et al.* 2001) especially near the town of Harbiye. Rojay *et al.* (2001) undertook a brief analysis of sediments from borehole data, which showed that the sediment thickness was variable within the Amik Plain and Karasu Rift, with sediment thickness being greatest on the western



margin of the Karasu Rift and in the centre of the Amik Plain; this was attributed to the presence of buried faults that presumably were active during deposition.

Erol (1969) and Pirazolli *et al.* (1991) observed uplifted Quaternary shorelines in several localities along the Mediterranean coast in the Hatay area. Pirazolli *et al.* (1991) determined that two rapid phases of uplift took place at around  $2500 \pm 100$  yrs B.P from marine terraces at 2.5 – 3m absl and at  $1345 \pm 70$  yrs B.P from terraces at 0.7-0.8m absl using carbon-14 dating. It was proposed that the youngest uplift event is related to the historical earthquake of July 551.

Evidence for normal faulting is abundant from the Maastrichtian onwards (Över *et al.* 2002; Rojay *et al.* 2001; Tinkler *et al.* 1981). Rojay *et al.* (2001) observed mainly sinistral oblique-slip faults and normal faults with lesser numbers of dextral and sinistral strike-slip faults. In that study 114 fault plane measurements were taken giving a mean orientation of  $045^{\circ}$ - $225^{\circ}$ . Över *et al.* (2002) conducted a more extensive, but still limited, fault kinematic study in order to determine the orientation of the principle stress axis from the Pliocene to the present day. It was suggested that the present stress regime is dominantly normal with a minor strike-slip component trending NE-SW; this replaced an earlier Late Cenozoic sinistral strike-slip regime. This change is attributed to a decrease in the maximum stress direction over time due to the roll-back of the subducting slab along the Cyprus Arc.

### **1.3 Project Aims**

The aims of this research project were:

- To develop an integrated tectonic-sedimentary history of the graben in order to constrain the evolution of the graben and its relationship to the development of the wider region.
- To develop facies models and palaeo-environmental interpretations for the graben from the Latest Cretaceous to the present-day.
- To develop a model of the structural evolution of the graben and to use various lines of evidence to constrain the timing of fault motion.
- To test existing models of the graben formation (Fig. 1.3) and, if necessary, to construct a new model incorporating new data.

## **1.4 Project Methods**

The data for this project were collected over 3 field seasons lasting a total of 15 weeks. Large amounts of data were gathered and over three hundred samples were collected. Fieldwork included sample collection, fossil collection, measurement of structural and sedimentological data, field descriptions, sketches and measuring sedimentary logs. Provenance studies on conglomerates were undertaken in the field where ~100 clasts were recorded at each locality. Field mapping was undertaken in certain areas in order to extend the coverage of geological maps of the area made by Turkish M.Sc students (Dokumacı 1997; Kop 1996; Mistik 2002; Temizkhan 2003) and also to investigate more fully areas of intense faulting.

Field descriptions and sedimentary logs were used in the interpretation of lithological units and to develop facies and palaeoenvironmental models. This was aided by the use of thin sections. Over 60 samples were made into thin sections and used for petrographic and provenance studies including point-counting. Fine-grained samples were additionally used in X-ray diffraction (XRD) to help determine their provenance.

Prior to this study, there was an existing stratigraphic scheme and some micropalaeontology (Şafak, 2000a, b) had been undertaken in the study area; however, this was not comprehensive. The incomplete nature of the stratigraphy made it desirable that a reassessment and revision of the stratigraphy was carried out. This included the acquisition of new age data for the sedimentary succession, which was achieved through strontium isotopic dating carried out in SUERC, at East Kilbride with the help of Dr. Rob Ellam, and new micropalaeontological dating was undertaken by Prof. Dr. Ümit Şafak of Çukurova University (Adana, Turkey).

The revised stratigraphic scheme erected during this work aids the interpretation of the history of the graben, both sedimentological and structural. Additionally, it has enabled comparisons between the Hatay Graben and areas to the north (around Belen and Kırıkhan) as well as other sedimentary basins especially in the Eastern Mediterranean region. This new stratigraphic framework combined with environmental interpretations of the sediments observed in the field area allowed the construction of subsidence curves with the assistance of Dr Jon Turner (University of Edinburgh).

However, a sequence stratigraphic approach was not used. Sequence stratigraphy can be a powerful tool for understanding sedimentary successions and even though potential sequence boundaries can be recognised in the Hatay Graben, it was not felt appropriate to use this method for a number of reasons. Although, sequence stratigraphy was initially developed for passive continental margins and foreland basins, the applicability to extensional grabens of these models remains unproven (Jordan 1995; Miall 1995). In practice, there is insufficient evidence for the underlying controls on the formation of sequence boundaries, whether they represent tectonic, climatic, eustatic variation or a combination of these factors especially in tectonically complex areas. Additionally, although the sedimentary succession in the Hatay Graben is well-exposed, the 3D architecture and age control on the boundaries is still not well enough known to make an accurate sequence stratigraphic model and offshore correlations are not possible in the absence of linking seismic data.

A digital elevation model (DEM) and topographic maps were utilised in the investigation of the geomorphology of the basin and the construction of longitudinal stream profiles provided insights into the present-day fault activity of the graben.

A large structural data set of was collected and used to determine the structural evolution of the area. This combined with observations of the sediments allows the timing and development of faults to be reconstructed and integrated into the overall picture of graben development. Additionally, palaeostress orientations were calculated from these data using the computer programme Daisy 2.4 (Salvini 2001) allowing comparisons with a previous study.

The overall aim of the project was to determine the role of this basin in the Neotectonic development of the Eastern Mediterranean and to test existing models on the plate configuration of this area. Models of basin history will be presented here, discussed and compared to the overall tectonic history of the region.

## **1.5 Thesis organisation**

This introductory chapter is followed in chapter 2 with a review of the existing literature on the stratigraphy of the area, followed by the new stratigraphic framework used in this study. The rationale, methods and results of the strontium isotope dating carried out on foraminifera constitute chapter 3. Chapter 4 gives detailed field descriptions, presents logs of the formations and the results of the provenance studies on the fine, medium and coarse-grained sediments studied. In chapter 5, this is then integrated with other information, such as age data, thin-section descriptions and benthic:planktic foraminifer ratios, to determine facies associations and develop a sedimentary model for the study area. The data from the previous chapters are used to calculate subsidence curves for the Hatay Graben in chapter 6. Chapter 7 deals with the structural data and evidence for the timing of graben formation. Chapter 8 examines some of the geomorphological aspects of the graben and discusses the data from the plotting of longitudinal stream profiles and the significance of these data. The Hatay Graben is then compared with other Tertiary basins of the Eastern Mediterranean and placed into the regional plate tectonic evolution in chapter 9; the major conclusions are then listed.

## 1.6 Use of Turkish words in the thesis

Due to the nature of the project this thesis contains many Turkish words that the reader may not be familiar with. The following are some notes to make the reading of these words easier. Essentially, the Turkish alphabet is the same as the Latin alphabet but with the addition of some letters. These are:

ç	like 'ch' in church
ğ	lengths the preceding vowel but is silent
ı	(without a dot) is like the i in cousin
ö	as the German ö
ş	like the 'sh' in shoe
ü	as the German ü

Most of the other letters are pronounced in the same way as English with the exception of c that is pronounced j; u is as in 'put' not 'cup' and a is a long sound like in the father.

In the thesis many of the places and features in the field area are referred to by the Turkish name. The following is a brief glossary of geographic features used.

<i>tepe</i>	hill	<i>çay</i>	stream
<i>dağ</i>	mountain	<i>dere</i>	valley
<i>nehir</i>	river	<i>kalesi</i>	castle
<i>köy</i>	village		

Turkish place names can often be translated easily into English. Here are a few from the field area.

<i>Büyükkaraçay</i>	Big black stream	<i>Nurzeytin</i>	Light Olive
<i>Kızıldağ</i>	Red Mountain	<i>Gökdere</i>	Sky valley
<i>Asi Nehir</i>	Rebel river	<i>Hacıdağ</i>	Pilgrim Mountain
<i>Samandağ</i>	Straw Mountain		

## Chapter 2



Part of the walls of Antioch over a ravine.

## 2 Revised Stratigraphy of the Cenozoic rocks of Hatay.

### 2.1 Introduction

In this chapter, I will formally redefine the stratigraphy for the Cenozoic rocks of the Hatay Graben and Kırıkhan area to provide a framework for sedimentological and structural studies (i.e. Boulton *et al.* in press) and to facilitate comparisons between the two areas. This has been achieved by combining the existing stratigraphy with field observations, new (Appendix 1) and published micropalaeontology and new strontium dating results (the strontium results are discussed more fully in the following chapter). However, further simplification of the stratigraphy was not seen as necessary as the units are sufficiently different between the Hatay and Kırıkhan areas to warrant different formation names. The formations are lithostratigraphic mappable units and, therefore, the boundaries of some of the units are diachronous.

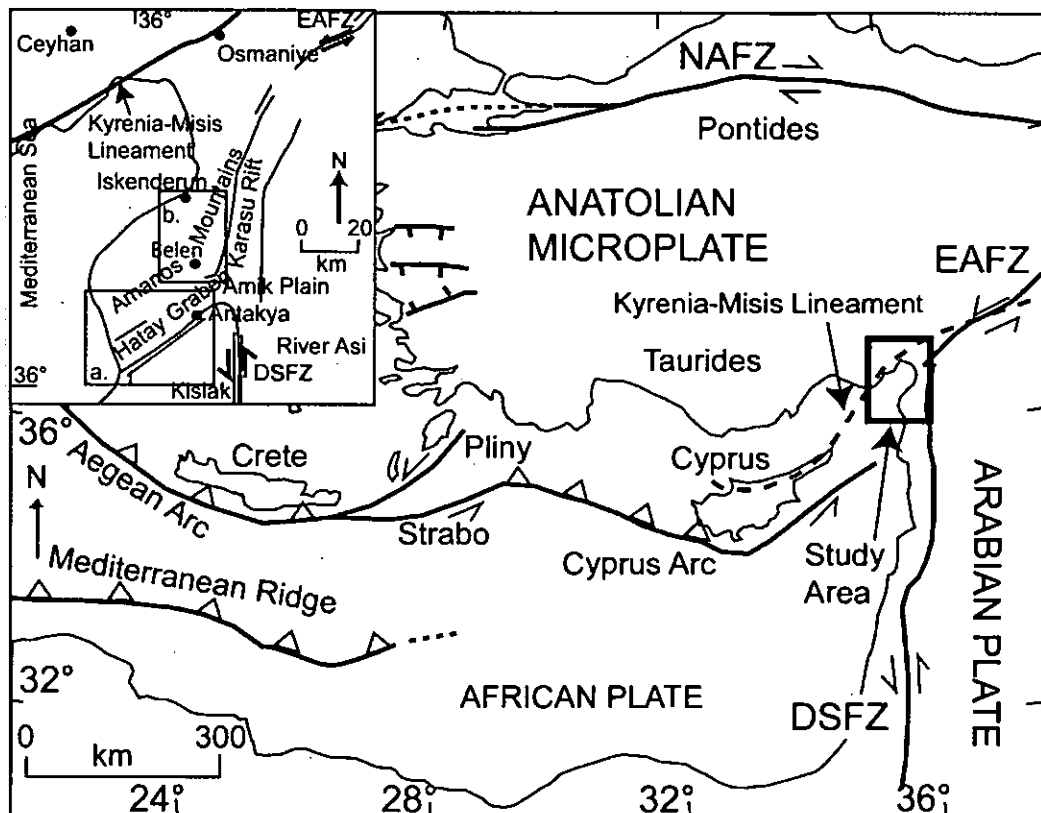


Figure 2.1. A) Map showing the regional plate tectonics of the Eastern Mediterranean, box indicates location of B; B) Enlargement of the Hatay region of southern Turkey, showing features referred to in the text.

### 2.1.1 Previous stratigraphic nomenclature

The geology of the area has attracted much interest due to the location of the basins in an area of active neotectonics; to the north there is the East Anatolian Fault Zone (EAFZ); to the west the Cyprus Arc and directly to the east of the Hatay Graben is the Dead Sea Fault Zone (DSFZ) that is considered to border the Karasu Rift (Fig. 2.1) (Freund *et al.* 1968; Rojay *et al.* 2001).

The sediments of the Hatay Graben and around the towns of Kırıkhan and Belen, in the Karasu Rift, share some lithological similarities and span the same period of geological time (Upper Cretaceous to Quaternary). Dubertret (1939, 1953) carried out early studies of the area, but a stratigraphic time scale was not confirmed until Atan (1969). His work divided the Miocene sediments into two formations, the Yazir and Enek Formations, with the Enek Formation consisting of two members. Palaeocene to Eocene limestones were also divided into two formations by Atan (1969) but these were given different names for the areas around Antakya and Kırıkhan (Fig. 2.2).

In the Hatay Graben these formations are named the Eşmişek and Almacık Formations; whereas, in the Karasu Rift sediments of the same age and similar lithology were termed the Cona Formation and Almacık Limestone. Dubertret and Atan studied the area as a whole, but subsequently the sedimentology and stratigraphy of the two areas were considered separately. Atan's (1969) terminology continued to be used in the Hatay Basin (Selçuk 1981; Pişkin *et al.* 1986), until Şafak (1993a,b) used micropalaeontology to divide the Miocene succession into five new formations: the Balyatağı, Sofular, Tephehan, Nurzeytin and Vakıflı Formations. This terminology was subsequently used by Mıstık (2002) and Temizkhan (2003). In the northern area a greater variety of nomenclature and divisions were introduced (Fig. 2.2) creating some confusion in the literature.



Figure 2.2. Various stratigraphic nomenclature used in the areas of Antakya and Kirikhan.

T E R T I A R Y		Antakya (Southern) Area				Kirikhan (Northern) Area					This Study		
		Atan 1969	Selçuk 1981	Pişkin 1986	Şafak 1993	Atan 1969	Derman 1979	Kozlu 1982	Yılmaz 1982	Günay 1984	Kop 1996	South	North
		Neogene	Pliocene	Samandağ	Samandağ	Samandağ	Samandağ						Karasu Basalt
Neogene	Miocene	Yazir Sofular Mb Enek Balyatağı Mb	Yazir Enek	Yazir Enek	Vakıfî Nurzeytin Tepehan Sofular Balyatağı	Yazir Sofular Mb Enek Balyatağı Mb	Kuzgun Seyhan Karaisali Gildiri	Kızıdere Horu Mb Kalecik		Altınözü Teknepinar	Gökdere Kepez Kıcı	Vakıfî Mb Nurzeytin Sofular Balyatağı	Gökdere Kepez Kıcı
	Palaeocene / Eocene	Almacık Eşmişek	Kıslak Okçular	Kıslak Uluyol - Oçular	Kıslak Okçular	Almacık Lmst Cona	Gercüş + Midyat Belveren + Antak	Cona	Kocagedik Cona	Hacıdağı Cona	Hacıdağı Cona	Kıslak Okçular	Hacıdağı Cona

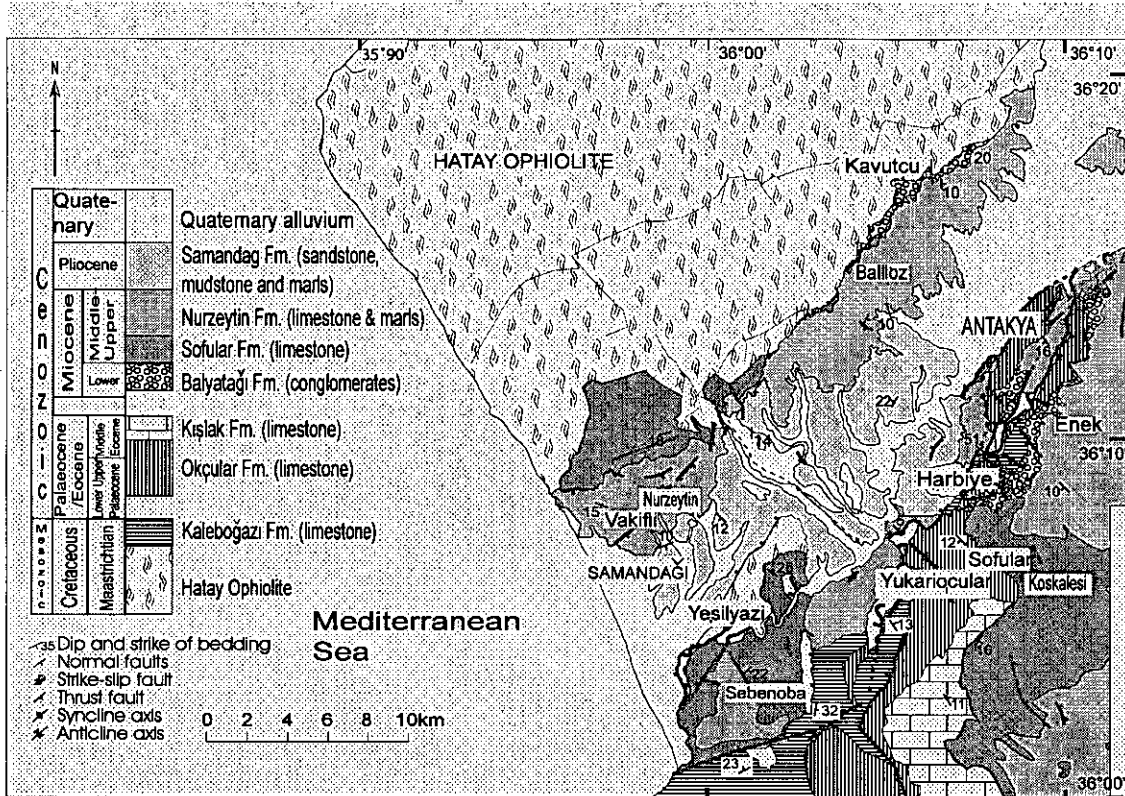


Figure 2.3. Geological map of the area around Antakya (Hatay Graben), place names are referred to in the text.

## 2.2 Cenozoic Units of the Hatay Graben

### 2.2.1 Okçular Formation: fine-grained wackestones

*Synonymy.* Uluyol-Oçular Formation; Pişkin *et al.* 1986.

*Name and type location.* The formation is named after Yukarıoçular village, 12km south of Antakya (Fig. 2.3).

*Lithology and variation.* The Okçular Formation is composed of creamy white limestones, biomicrite-biosparite (after Folk, 1959) or wackestones (after Dunham, 1961) and fine-grained calcarenite. Beds are generally <50cm thick with sharp bases and tops; ripples are developed on the surface of some beds. The limestones are rich in microfossils, especially large benthic foraminifera such as *Nummulites* sp., *Discocyclina* sp. and also macrofossils, although much fossil material has been replaced by secondary calcite. Weathered surfaces of this unit are usually karstified. There is little variation within this formation, although the

abundance of detrital material increases upwards and is also laterally variable (Decrouez and Selçuk 1981).

*Lower and upper boundaries.* The base of the Okçular Formation can be observed to the east of Antakya (Fig. 2.3). In some places the limestone directly overlies the Hatay Ophiolite along an erosional surface; in other locations there is a complete sedimentary sequence and the base of the Okçular Formation is taken as the first limestone bed above a sequence of red and brown mudstones that forms the top of the underlying formation (Upper Cretaceous Kaleboğazı Formation). The contact between the Okçular and Kaleboğazı Formations is conformable. The upper boundary of the Okçular Formation is unconformable with younger Neogene units.

*Thickness and regional extent.* The formation is regionally extensive, very similar to the Hacıdağı Formation (see 2.3.2). The thickness of the unit is estimated as 200-320m (Selçuk, 1981).

*Dating evidence.* The Okçular Formation corresponds to the lower part of the *Acarinina bulbrooki* (Bolli) biozone of Safak (1993a), assigned to the Lutetian stage of the Eocene. The lower boundary is additionally defined by the first occurrence of *Turborotalia centralis* (Cushman and Bermudez) (Safak 1993a). The ranges of *Morozovella aragonensis* and *Truncorotaloides topilensis* are entirely contained within the Okçular Formation (Safak 1993a) (Fig. 2.4).

## **2.2.2 Kışlak Formation: marl and marly limestone.**

*Synonymy.* Defined by Atan 1969; retained in the same sense by later workers.

*Name and type location.* The formation is named after the Kışlak village, 20km south of Antakya. The type section is on the Antakya-Yayladağı road near the village.

*Lithology.* The lower part of the formation is composed of marl and marly limestones, whereas the upper part of the formation is made up of marl and calcarenites. The limestones are cream to white in colour, fine to medium grained and fossiliferous (microfossils and macrofossils).

*Lower and upper boundaries.* The lower boundary of the Kışlak Formation is transitional to the underlying Okçular Formation. The upper boundary is an unconformity with the Nurzeytin Formation.

*Thickness and regional extent.* The Kışlak Formation is only exposed in the far south of the study area; further north this formation does not overlie the Okçular Formation and thus appears not to be laterally extensive. The thickness of the unit is 200-250m (Selçuk, 1981).

*Dating Evidence.* The Kışlak Formation forms the upper part of the *Acarinina bullbrooki* bio-zone and contains *Morozvella spinulosa* and *Morozvella lehneri* (Safak 1993a) (Fig. 2.4).

		Formation	Planktonic Foraminifera zones	Ostracod zones	
<b>Pliocene</b>		Samandağ			
<b>Miocene</b>	<b>Messinian</b>	Vakıfı Mb			
	<b>Tortonian</b>	Nurzeytin		<i>Cypriideis</i>	
	<b>Serravallian</b>		N10	<i>Orbulina universa</i>	
	<b>Langhian</b>	Sofular	N9	<i>Orbulina suturalis</i>	<i>Carinocythereis</i>
			N8	<i>Præorbulina glomerosa curva</i>	
<b>Burdigalian</b>	Balyatağı	N7	<i>Globigerinoides trilobus</i>	<i>Neomonoceratina helvetica</i> <i>Aurila soummamensis</i>	
<b>Eocene</b>	<b>Lutetian</b>	Kışlak Okçular	P10	<i>Acarinina bullbrooki</i>	

Figure 2.4. Biostratigraphic zones for the Hatay Graben, after Safak 1993a, b.

### 2.2.3 Balyatağı Formation: Conglomerates, coarse litharenites and mudstones.

*Synonymy.* Enek Formation (in part); Pişkin *et al.* 1986; Selçuk 1981 and Atan 1969.

*Name and type locality.* The formation is named after Balyatağı Tepe, 1km west of Enek village. The type section is exposed on the NW side of the hill (Fig 2.3).

*Lithology and variation.* The formation consists of bodies of interbedded lenticular matrix- and clast-supported conglomerates, coarse litharenites and mudstones (various colours; cream, brown and red). The proportion of mudstone increases up section and the clast size of the conglomerates generally decreases, from a maximum size of >1m near the base of the formation to <50cm at the top. In the southeast, the mudstones form a minor component of the formation, only occurring as interbeds in the uppermost part of the succession. In the northwest; however, the upper part (~25m) of the formation is composed entirely of mudstones.

*Lower and upper boundaries.* The base of the Balyatağı Formation varies from the north to the south: in the north, it overlies the Hatay Ophiolite along an erosional surface. However, in the south the base of the formation is an angular unconformity with the Eocene Kışlak Formation. The upper boundary is a sharp contact between the Balyatağı Formation and the limestones of the Sofular Formation. This contact is locally variable and has been observed both as a conformity and as a slight angular unconformity.

*Thickness and regional extent.* The thickness of the formation is very variable; in the type section the formation is ~50m thick. To the northeast of the type locality the thickness increases to a maximum of ~175m, whereas to the southeast the formation thickens to ~65m, and then gradually disappears. In the northeast the formation thins to the south from >100m to zero near the village of Balliöz.

*Dating evidence.* The Balyatağı Formation is dated as Aquitanian to Burdigalian (Early Miocene) in age. Planktic foraminifera are found only within basal and uppermost marine horizons, the majority of the formation contains no fossil material. The base of the formation is marked by the first occurrence of *Globigerinoides trilobus*, which gives its name to the biozone, as defined by Safak (1993a). There is also the first occurrence of

*Globigerinoides ruber* and *Globorotalia obesa*. Ostracods have also been identified in the uppermost part of this formation, characterised by *Aurila soummamensis* (Safak 1993b), but also marked by the first occurrence of *Hemicyprideis helvetica* and *Falunia plicatula*. The appearance of *Cytherella vulgata* and *C. ramosa subalevis* is used to indicate the position of the Aquitanian to Burdigalian boundary (Safak 1993b). The top of the formation is marked by the last occurrence of *Cytheretta simplex* and *Cytheretta orthozensis* (Fig. 2.4).

#### **2.2.4 Sofular Formation: Bioclastic wackestones.**

*Synonymy.* Enek Formation (in part); Pişkin *et al.* 1986; Selçuk 1981 and Atan 1969. Sofular and Tepehan Formations; Şafak 1993; Mistik 2002; Temizkhan 2003

*Name and type locality.* The formation is named after Sofular village, 10km south of Antakya (Fig. 2.3). The type location is exposed in a gorge system that runs WNW-ESE to the south of the village, as far as Kozkalesi village 1.5 km away.

*Lithology and variation.* In the type section the lower part of the formation comprises bioclastic calcirudite, mainly wackestone rich in shallow-marine fauna (i.e. bivalves, corals and echinoids). These limestones are massively bedded and often muddy with evidence of intense bioturbation. Cream to red mudstone is interbedded with the limestone; these beds have sharp bases, often capped by a thin conglomerate layer. Up sequence, the mudstone beds disappear and the formation is composed entirely of bioclastic limestone. The formation shows little variability with most exposures consisting of calcirudite; however, in exposures along the River Asi, near Yeşilyazı village (Fig 2.3), the lower part of the succession consists of thinly bedded red and brown mudstone passing upwards into thin-bedded calcilutite. The upper part of the succession consists of bioclastic calcirudite and medium-grained calcarenite.

*Lower and upper boundaries.* In the type section the base of the formation is not observed. In other areas the Sofular Formation was exposed variably overlying the Kızıldağ Ophiolite, the Okçular Formation or the Balyatağı Formation. The contact is sharp with an abrupt change in lithology to bioclastic limestones. The upper boundary is gradational, normally over several metres, and is defined as the point where marl of the Nurzeytin Formation dominates.

*Thickness and regional extent.* In the type area the Sofular Formation exceeds 200m in thickness. Thick exposures of the formation crop out in coastal exposures and along the River Asi (Fig. 2.3). The formation thins inland (to the northeast) on both margins of the basin until eventually it disappears.

*Dating evidence.* The Sofular Formation is dated as uppermost Burdigalian/base-Langhian to top-Langhian in age. It encompasses the whole of the planktonic foraminifera biozones of *Praeorbulina glomerosa curva* and *Orbulina suturalis*, which is equivalent to the whole of the ostracod biozone *Neomonoceratina helvetica* and the base of the *Carinocythereis baslangic* biozone (Safak 1993a, b) (Fig. 2.4). The base is marked by the first occurrence of several ostracod species including *Cymocytheridea contracta* and *Cytherella petrosa*. The top of the formation is marked by the last occurrence of several ostracod species including *Cyamocytheridea reversa* and *Falunia retiformis* and the planktonic foraminifer species *Globorotalia obesa*.

## 2.2.5 Nurzeytin Formation: Marl

*Synonymy.* Yazir Formation; Pişkin *et al.* 1986; Selçuk 1981 and Atan 1969.

*Name and type locality.* The formation is named after Nurzeytin village, 5km north of Samandağı (Fig. 2.3). The type section is located in the valley to the east of the village.

*Lithology and variation.* The Nurzeytin Formation mainly consists of fossiliferous marls. Within the marl sequence laterally discontinuous beds of sand, limestone and conglomerate are present. Thick litharenite beds are more common in more northerly outcrops, often massively bedded, although laminations and ripples are observed, with thin chalk horizons and mud rip-up clasts. Thin sand horizons are found throughout the formation. Limestones are more common in southerly outcrops, where flutes and grooves are observed on the base of beds. One metre-thick matrix-supported conglomerate was observed, composed of marl clasts set in a marl matrix. The Vakıflı Member, composed of gypsum (selenitic and alabastrine gypsum), occasionally caps the top of this formation.

*Lower and upper boundaries.* The lower boundary is gradational with the underlying Sofular Formation. The upper boundary is poorly exposed but appears to be either

conformable with the Samandağı Formation or marked by a gypsum horizon (Vakıflı Member).

*Thickness and regional extent.* The formation is laterally extensive, exposed both within and outside the present-day topographic basin. The maximum thickness is ~300m; the upper gypsum horizon is exposed at four locations and varies in thickness from 5-25m.

*Dating evidence.* The Nurzeytin Formation is dated as Serravallian to Tortonian, based on the planktonic foraminifera zone of *Orbulina universa* and the ostracod zones of *Carinocythereis* and *Cyprideis* (Safak 1993a, b) (Fig. 2.4). Samples were taken from a number of intervals within the Nurzeytin Formation for strontium dating and these give a range of ages from a maximum of 13.24 M yr to a minimum of 7.17 M yr, corresponding to Serravallian to Tortonian time.

## 2.2.6 Vakıflı Member: Gypsum

*Synonymy.* Vakıflı Formation; Safak 1993. The Vakıflı Member has been down-graded from a formation as in previous nomenclature, as the evaporite facies are limited in extent and size, and do not constitute a mappable unit. However, the facies is considered significantly different from the rest of the Nurzeytin Formation to form a member.

*Name and type location.* The Vakıflı Member is named after the village of the same name to the north of Samandağı (Fig. 2.3). The type section is ~ 1.5 km to the ENE.

*Lithology and variation.* The type section is mainly composed of alabastrine (fine-grained) gypsum. This exposure includes large angular blocks (>2m) of laminated alabastrine gypsum set in a gypsiferous marl matrix. In places, the alabastrine gypsum is seen to have undergone diagenetic alternation to coarse selenitic gypsum. Other exposures consist of coarse-grained selenitic gypsum, including one location where the basal gypsum is made up of banded selenite (repeated layers of selenite crystals, 1-5cm in size) and the upper part is composed of thick (>1m), massive fragmented selenite crystals, 5cm or more in size.



*Lower and Upper Boundaries.* The lower boundary is conformable with the Nurzeytin Formation and the Upper boundary is conformable with the Samandağ Formation.

*Thickness and regional extent.* The Vakıflı Formation is only present in four locations in the field area; the thickest deposit (the type section) is 25 m thick with the other locations being in the order of 5-10m thick.

*Dating evidence.* This formation is dated as Messinian in age based on the ostracod species *Cyprideis ruggeri* and the presence of the planktonic foraminifera *Globoquadrina altispira altispira* at the very top of the formation (Safak 1993a, 1993b) (Fig. 2.4).

### **2.2.7 Samandağ Formation: Marl and sandstone.**

*Synonymy.* Defined by Atan 1969; retained in same sense by later workers.

*Name and type locality.* The Samandağ Formation is named after the town of Samandağ (Fig. 2.3).

*Lithology and variation.* The lithology of lower part of the formation is dominated by fossiliferous marl and is difficult to distinguish from the Nurzeytin Formation in the field. Thin litharenite horizons are common; these are often laterally discontinuous, as are rare conglomerate horizons. Intraformational slumps and channel incisions are also observed. The upper part of the sequence is composed of fossiliferous and non-fossiliferous orange-weathering litharenites, which become generally coarser upwards. Locally, these sandstones contain stringers of shallow-marine fauna (mostly bivalves), cross-bedding and parallel laminations. Rare conglomerate lenses are present. The contact between the lower and upper Pliocene is transitional.

*Lower and Upper boundaries.* The lower boundary often conformably overlies the Nurzeytin Formation. Also at one location the Samandağ Formation overlies an erosion surface cut into the Sofular Formation.

*Thickness and regional extent.* No complete section is exposed and regional faulting affects the formation. The estimated thickness of the Samandağ Formation is 100-400m. The formation is only exposed within the present topographic basin towards the coast.

*Dating evidence.* The base of the Pliocene is characterised by the first appearance of *Globigerinoides trilobus sacculifer*, *Globigerinoides obliquus obliquus* and *Globorotalia scitula* (Safak 1993a) (Fig 2.4). One sample provided a reliable Pliocene date using strontium analysis, giving a date of 5.35 Ma (See Chapter 3).

### 2.3 Cenozoic Units of the Kırıkhan Area.

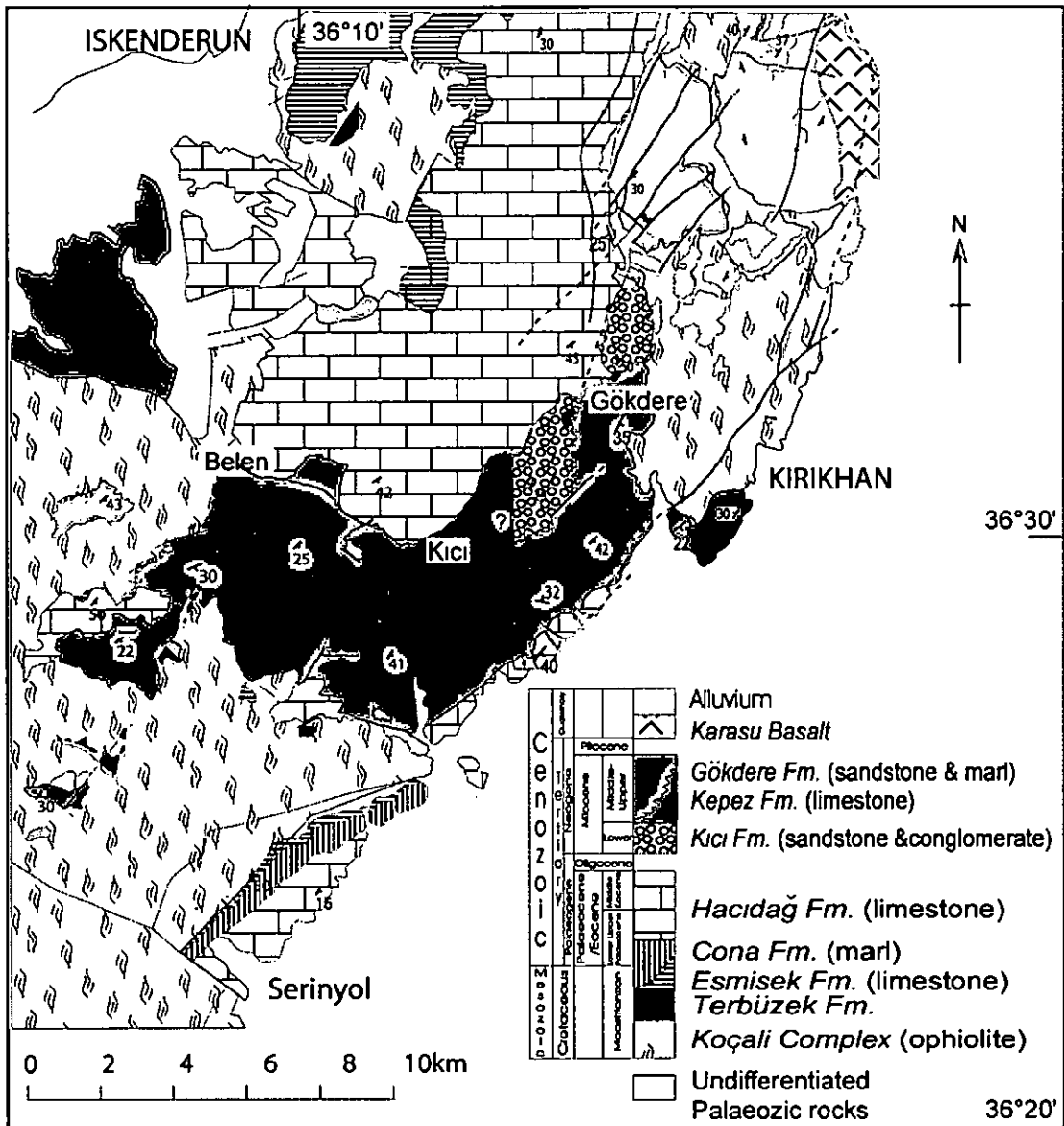


Figure 2.5. Geological map of the area around Kırıkhan, places on map are referred to in the text.

### 2.3.1 Cona Formation: Calcarenite

*Synonymy.* Süleymandede Formation; Bryant 1960.

*Name and type location.* The type section of this formation is the Süleymandede Tepe east of Osmaniye. The name Cona comes from the town of the same name, 7km to the northeast of Osmaniye (Fig. 2.1).

*Lithology and variation.* The Cona Formation comprises calcarenite, marly sandstone and clayey limestones and is rich in bioclastic material.

*Lower and upper boundaries.* The lower boundary is conformable with the underlying Eşişek Formation. The upper boundary is transitional to the Hacıdağı Formation.

*Thickness and lateral extent.* The thickness of the unit is estimated at 120-390m (Bryant 1960). It is laterally very extensive with exposures from the Belen area to Osmaniye (~100km).

*Dating evidence.* Planktonic foraminifera date this formation as Maastrichtian to Early Palaeocene; these include *Omphalocyclus* sp, *Siderolites* sp. and *Globotruncana stuartiformis* (Yılmaz *et al.* 1984)

### 2.3.2 Hacıdağı Formation: Calcarenite

*Synonymy.* Kocagedik Formation; Yılmaz 1982; Cona Formation (in part); Kozlu 1982. Almalgamated into the Cona Formation in the Osmaniye area by Yılmaz *et al.* 1984.

*Name and type location.* The type location of the Hacıdağı Formation is to the northwest of Kaypak (Serdar) town near the city of Osmaniye (Günay 1984).

*Lithology and variation.* The Hacıdağı Formation is composed of white calcarenites and limestone. Beds are generally <50cm thick and contain foraminiferal lags, bioturbation and fine laminations. Many beds also exhibit normal grading and chert nodules, mostly within

the upper parts of beds. Intraformational slumps have been recognised, but overall there is very little variation in lithology.

*Lower and upper boundaries.* The lower boundary is transitional with the underlying Cona Formation. The upper boundary is marked by an angular unconformity with the Kıcı Formation.

*Thickness and lateral extent.* The formation is laterally extensive and greater than 400m thick. It is difficult to estimate the thickness as the formation has been extensively folded in this area.

*Dating evidence.* The Hacıdağı Formation is rich in microfossils which dates the formation as Palaeocene to Eocene in age. Planktic foraminifera identified include *Discocyclina archiachi*, *Alveolina rutimeeri*, *Assilina* cf. *laminose* Gill and *Globorotalia velascoensis* (Atan 1969).

### **2.3.3 Kıcı Formation: Conglomerate and sandstone**

*Synonymy.* Gildiri Formation, Derman 1979; Enek Formation (Sofular Member); Selçuk 1981; Kalecik Formation (Horu limestone Member); Kozlu 1982.

*Name and type location.* The Kıcı Formation is named after Kıcı village on the Antakya-Belen road (Fig. 2.5). It is proposed that the Kurtisoğuksu section becomes the new type location.

*Lithology and variation.* The lower part of the formation is composed of thick matrix-supported conglomerates composed of large angular, to subrounded clasts of limestone, basalt and sandstone. The upper part of the sequence is composed of red-purple conglomerates and coarse litharenites, with occasional dark grey and black mud horizons. The sandstones are cross-bedded and parallel laminated; bioturbation is common. There is some variation in the formation as the basal conglomerates are only locally developed.

*Lower and upper boundaries.* The lower boundary of the Kıcı Formation is a sharp angular unconformity with the underlying Hacıdağı Formation. The upper boundary with the Kepez

Formation or Gökdere Formation is poorly exposed but may be an unconformity (Kop 1996).

*Thickness and lateral extent.* The Kıcı Formation is only observed around the Kırıkhan area and is ~100-150m thick.

*Dating evidence.* No microfossils have been identified in the formation to date.

#### **2.3.4 Kepez Formation: Biosparite/biomicrite.**

*Synonymy.* Karaisalı Limestone, Derman 1979; Enek Formation, Selçuk 1981; Kalecik Formation, Kozlu 1982, Teknepınar Formation, Günay 1984.

*Name and type locality.* This formation is named after Kepez Tepe (also the type locality) 6km west of Kırıkhan (Fig. 2.5).

*Lithology and variation.* The Kepez Formation is composed of white biosparite and biomicrite. The bioclastic material is completely fragmented. The formation is poorly exposed and is usually karstified. There is little lithological variation in the observed outcrops.

*Lower and upper boundaries.* The lower boundary with the Kıcı Formation is poorly exposed. The upper boundary is a lateral and vertical transition with the Gökdere Formation.

*Thickness and lateral extent.* The formation is restricted in extent, as it is only exposed on a two hill tops near Gökdere village and just to the southwest of Kırıkhan (Fig), where it is probably exposed due to faulting. The maximum thickness is estimated to be ~345m (Derman 1979) but is often thinner.

*Dating evidence.* None.

### 2.3.5 Gökdere Formation: Marl

*Synonymy.* Arbo Formation, Bryant 1960; Seyhan Formation, Derman 1979; Enek and Yazır Formations, Kozlu 1982; Altınözü Formation, Günay 1984.

*Name and type location.* The Gökdere Formation is named after Gökdere village, 5km west of Kırıkhan (Fig. 2.5). The type section is exposed along the Gökdere-Kırıkhan road to the SE of the village.

*Lithology and variation.* The Gökdere Formation is dominated by marl, although there is a significant amount of litharenite. The sandstones typically form several metre-thick units. Two main types of sand body have been observed: i) where sand beds are thin and interbedded with marl, contain plant material and abundant ostrea, also ripples and flutes, and ii) where sand beds are thicker and there are no marl interbeds, but ripples and load casts are present. Although the marl is laterally continuous the sands tend not to be. Near the top of the formation sandstone predominates.

*Lower and upper boundaries.* The lower boundary is unconformable on the Kıcı Formation or conformable with the Kepez Formation. The top of the formation is usually marked by an erosional surface with Quaternary alluvium.

*Thickness and lateral extent.* The formation is laterally extensive and very thick. The thickness of the formation is in the order of 700m.

*Dating evidence.* The presence of the ostracod species *Cyprideis seminulum* and *C. antolica*, indicate that this formation is Tortonian to Messinian in age (Kozlu 1982).

## 2.4 Initial Interpretations

The sedimentary rocks of the Hatay Graben and the Karasu Rift in the area around Belen and Kırıkhan record the change from regional shelf deposition to a more active tectonic regime, marked by a greater variety of sub-environments. The Okçular, Kışlak, Cona and Hacıdağı Formations record carbonate deposition in a shallow-marine shelf that covered the whole area during the latest Cretaceous to Eocene times. This period of deposition was followed in the Oligocene by a widespread hiatus linked to relative sea-level fall. The Oligocene was a period of significant eustatic sea-level fall; however, in this area compressional deformation was also significant as Eocene and older strata exhibit widespread folding that younger sediments do not, this deformation is likely to be related to Syrian Arc II deformation. Indicating that during the Oligocene experienced regional uplift probably as a result of regional continental collision to the north along the Bitlis suture zone (Robertson *et al.* 2004); in addition to eustatic sea-level fall resulting in a widespread unconformity surface. After this hiatus, sedimentation in the area resumed in the Burdigalian. The Balyatağı Formation of the Hatay Graben is generally a fining-upwards sequence of polymict conglomerates and sandstones that fine-up into sandstones and muds. These are interpreted to represent gravelly braided river deposits that became more channelised over time, perhaps reflecting loss of relief in the source area (Section 5.3.1). The Kıcı Formation is also continentally derived; however, the coarse lower conglomerates are possibly alluvial fan debris that fine up into sandy braided river deposits or upper delta plain sediments.

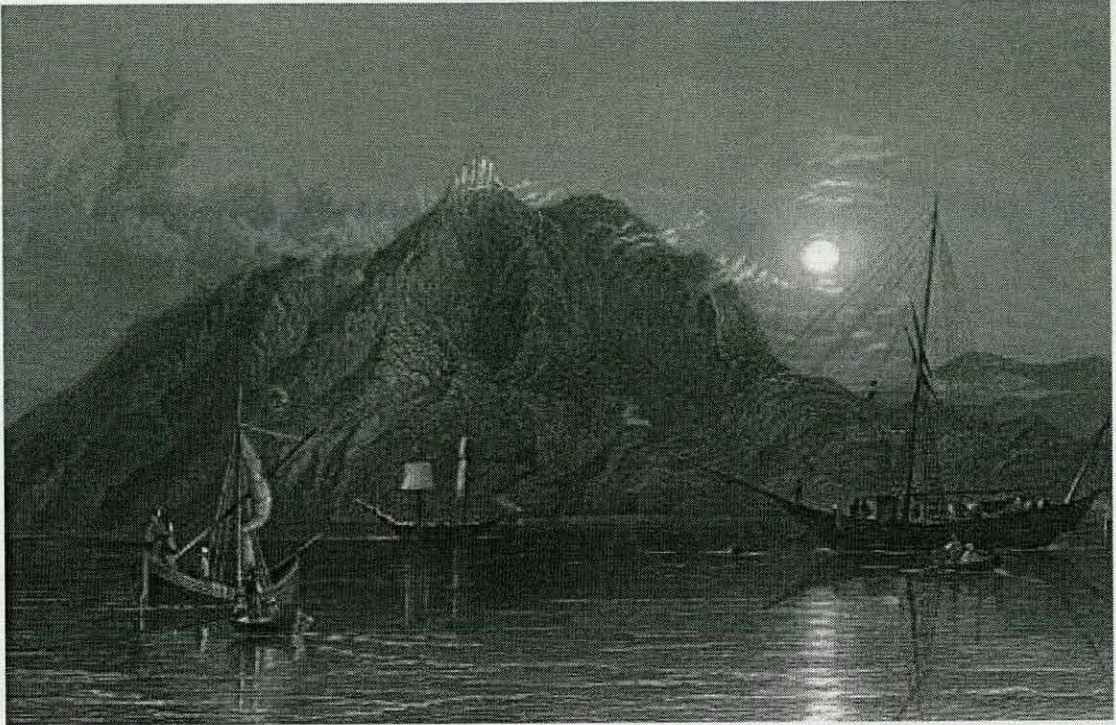
The Sofular and Kepez Formations represent a return to shallow-marine carbonate deposition during the Langhian. The greater thickness of the Sofular Formation suggests that greater accommodation space was available in the Hatay Graben by this time compared to areas to the northeast, possibly due to greater extension in the former. Subsequently, during the Serravallian to Tortonian, the Nurzeytin and Gökdere Formations record progressive deepening of the area due to continued relative sea-level rise. Sand beds in the upper part of the Gökdere Formation are possibly representative of pro-delta deposits suggesting that the area around Kırıkhan appears to have been shallower than the Hatay Graben at this time. This is supported by the presence of Messinian evaporites and Pliocene sediments only within the Hatay Basin, probably because by this time the Karasu Rift had become fully continental. The Hatay Basin continued to be marine until the latest Pliocene/Holocene when shallow-marine/coastline sedimentation was succeeded by continental conditions.



## **2.5 Conclusions**

- The sedimentary evolution of the Hatay Graben and the area of the Karasu Rift around Belen and Kırıkhan share many similarities and have a shared history.
- The stratigraphic nomenclature has been redefined and simplified in order to aid correlation across the field areas.
- The Palaeogene units: the Cona and Hacıdağ Formations of the north correlate to the Okçular and Kışlak Formations of the Hatay Graben.
- The Neogene units: The Early Miocene Balyatağı Formation of the Hatay Graben is equivalent to the Kıcı Formation of the north; the Sofular Formation equivalent to the Kepez Formation and the Nurzeytin Formation is equivalent to the Gökdere Formation.
- The Tepehan Formation (Safak 1993a, b) is not included in this scheme as it was deemed an unnecessary interval due to the similarity to the Nurzeytin Formation.
- The Vakıflı Formation of Safak (1993a, b) has been downgraded to a member of the Nurzeytin Formation due to the limited extent and thickness of the unit. This member is only present in the Hatay Graben.

## Chapter 3



Mount Cassius from the sea.

## 3 Sr<sup>87</sup>/Sr<sup>86</sup> isotope analysis

### 3.1 Introduction

The aim of this chapter is to detail the Sr<sup>87</sup>/Sr<sup>86</sup> isotopic analysis that was carried out as part of this research project. This was primarily undertaken in order to obtain numerical dates for the sedimentary units in the Hatay Graben, especially for the marl units of the Upper Miocene to Pliocene. There has previously been no Sr<sup>87</sup>/Sr<sup>86</sup> analysis carried out on sediments from this area, and pre-existing age determinations are based on micropalaeontological studies (Safak 1993a,b); thus, there is a lack of precision in the existing age data. In addition, identifying the age of samples in question also allows better facies correlations and a more complete picture of basin evolution to be developed. In this chapter the rationale, methodology and results are detailed for the Sr<sup>87</sup>/Sr<sup>86</sup> analysis that was undertaken in order to quantify sediment ages.

Sr<sup>87</sup>/Sr<sup>86</sup> isotope analysis works on the principle that the Sr<sup>87</sup>/Sr<sup>86</sup> isotope ratio in sea-water is relatively constant throughout the world's oceans at any one time due to the fact that the residence time of strontium in sea-water (~2.5-5Ma) is much greater than the mixing time of the ocean (Broeker & Peng 1982; McArthur 1994). The Sr<sup>87</sup>/Sr<sup>86</sup> ratio in sea-water varies mainly due to variations in the amount of high Sr<sup>87</sup>/Sr<sup>86</sup> terrigenous detrital flux into the ocean from continental weathering relative to the low Sr<sup>87</sup>/Sr<sup>86</sup> ocean crust input from hydrothermal exchange at mid-ocean ridges. The dissolution of carbonates on the sea-floor acts as a buffer by adding strontium with a ratio similar to that of sea-water (Brass 1976; Oslick *et al.* 1994; McArthur 1994).

Therefore, if the variations in Sr<sup>87</sup>/Sr<sup>86</sup> ratio in sea-water through time are known, Sr<sup>87</sup>/Sr<sup>86</sup> ratios can be determined for samples of unknown age and compared to published curves in order to find the age of the sample. Much work has been undertaken recently to confine the shape of the Sr<sup>87</sup>/Sr<sup>86</sup> ratio curve through time (i.e. Miller *et al.* 1991; Hodell & Woodruff 1994; Oslick *et al.* 1994; Gleason *et al.* 2002), this is important because the highest temporal resolution is obtained for parts of the sea-water curve that have the highest rate of change of Sr<sup>87</sup>/Sr<sup>86</sup> ratio as a function of time.

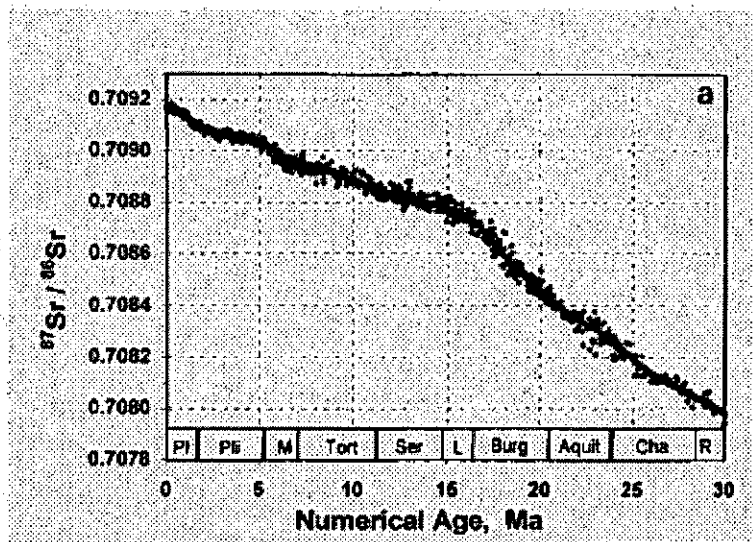


Figure 3.1. Strontium Isotope curve for the last 30 million years, from McArthur et al. 2001.

In general, the Sr<sup>87</sup>/Sr<sup>86</sup> ratio in seawater has been increasing since the Jurassic (Hodell & Woodruff 1994) and continues to show an increase throughout the Cenozoic, due to the increasing intensity of glacial activity and/or the increasing rate of tectonic uplift of the continents (Hodell 1994) supply more continental strontium to the oceans. During the Cenozoic, the steepest part of the curve is for the Early Miocene (Figure 3.1). Therefore, during this time the temporal resolution is in the order of  $\pm 0.5\text{My}$  (Hodell & Woodruff 1994). The slope continues to increase although at lower gradient until the Late Miocene. During the Late Miocene, the Mediterranean became isolated from the world's oceans; this resulted in anomalous (reduced) Sr<sup>87</sup>/Sr<sup>86</sup> ratios from the area during that time. Thus, dating using Sr is not possible for the Messinian in the Mediterranean area due to this isolation effect. Dating is also problematic for the Pliocene as the reference curve shows little change through this period, this consequently results in poor resolution for this time (Fig. 3.1).

Sr is obtained from biogenic carbonate; this is the main sink of Sr in the oceans (Brass 1976; Hodell 1994). Organisms forming carbonate shells or tests do not appear to prefer one isotope of Sr over another, so it can be assumed that the Sr<sup>87</sup>/Sr<sup>86</sup> ratio in the biogenic carbonate is the same as sea-water at the time of precipitation. Radiogenic Sr<sup>87</sup> from the decay of Rb<sup>87</sup> can be ignored as biogenic carbonate generally contains low concentrations of Rb relative to Sr, as long as no diagenetic alteration has occurred (Elderfield 1986).

## 3.2 Methodology

### 3.2.1 Sample selection and preparation

Benthic and planktic foraminifera were selected for strontium analysis. Bulk rock analysis was considered but there is a risk of including unknown and reworked components within the sample that would result in erroneous results. Additionally, there is an increased risk of including a diagenetic signature (Richter & DePaolo 1988). Other marine organisms that construct a calcite shell (such as corals, echinoids and oysters) can be used for Sr<sup>87</sup>/Sr<sup>86</sup> analysis; however, Flecker (1995) showed that these samples are generally more affected by diagenesis and have larger error bars than for measurements on foraminifera alone, so it was decided to use only microfossils for Sr<sup>87</sup>/Sr<sup>86</sup> ratio determination.

To extract the foraminiferal tests from the marls, first the whole rock was washed through a 62µm sieve until the water ran clear and all clay minerals were washed away. If the rock sample was too hard, it was left in distilled water overnight or until the sample had begun to disintegrate. The sample was then dried overnight, and then dry sieved through 600µm and 250µm sieves. The foraminifera were picked from the 250µm fraction. There is no evidence in the literature to suggest that benthic and planktic foraminifera incorporate strontium into the tests differently so both were picked. Specimens were carefully picked and those that appeared very abraded or had specks of orange material on the outside or dark inclusions (pyrite or clay minerals) were ignored.

Sample No	Location No/Name	Grid ref.	Fauna
SB44	70	65297/02478	Mixed foraminifera
SB50	Karacay Log	31268/05890	Mixed foraminifera
SB67	4	64775/02250	Mixed foraminifera
SB80	140	38087/11348	Mixed foraminifera
SB81	141	37995/11340	Mixed foraminifera
SB18A	Mizrakli Log	69443/03491	Planktic foraminifera
SB20A	Mizrakli Log	69443/03491	Mixed foraminifera
SB22A	Mizrakli Log	69443/03491	Mixed foraminifera
SB39A	178	34832/08647	Planktic foraminifera
SB42A	180	32902/08285	Mixed foraminifera
SB47A	188	35351/07667	Planktic foraminifera
SB56A	206	39264/15134	Mixed foraminifera

Table 3-1. List of samples and fauna used in the Sr<sup>87</sup>/Sr<sup>86</sup> analysis, location of samples is shown on Figure 3.2.

After the foraminifera were picked samples were cleaned in pure ethanol in a sonic bath for 2-8 minutes depending on the individual samples, while the samples were being cleaned they were regularly checked for signs of disintegration. When the samples appeared clean or on the point of disintegration they were removed from the sonic bath. Previous workers (Miller *et al.* 1991; Oslick *et al.* 1994) report cleaning their samples for only 2-3s; either their foraminifera are much cleaner or less lithified than those from this study. Flecker (1995) favoured cleaning foraminifera for up to 40 minutes, while Hodell and Woddruff (1994) do not mention cleaning their samples at all. Specimens of cleaned and dirty foraminifera were observed under the SEM to observe the effect of the cleaning process; this showed that the cleaning process removed the majority of superficial 'dirt' but was inconclusive as to its effect on internal material (Figure 3.3). As the samples may be partly lithified it is unlikely that all trace material was removed (for a full discussion see Flecker 1995). After cleaning the samples were re-inspected and any individual tests that seemed insufficiently cleaned were discarded.

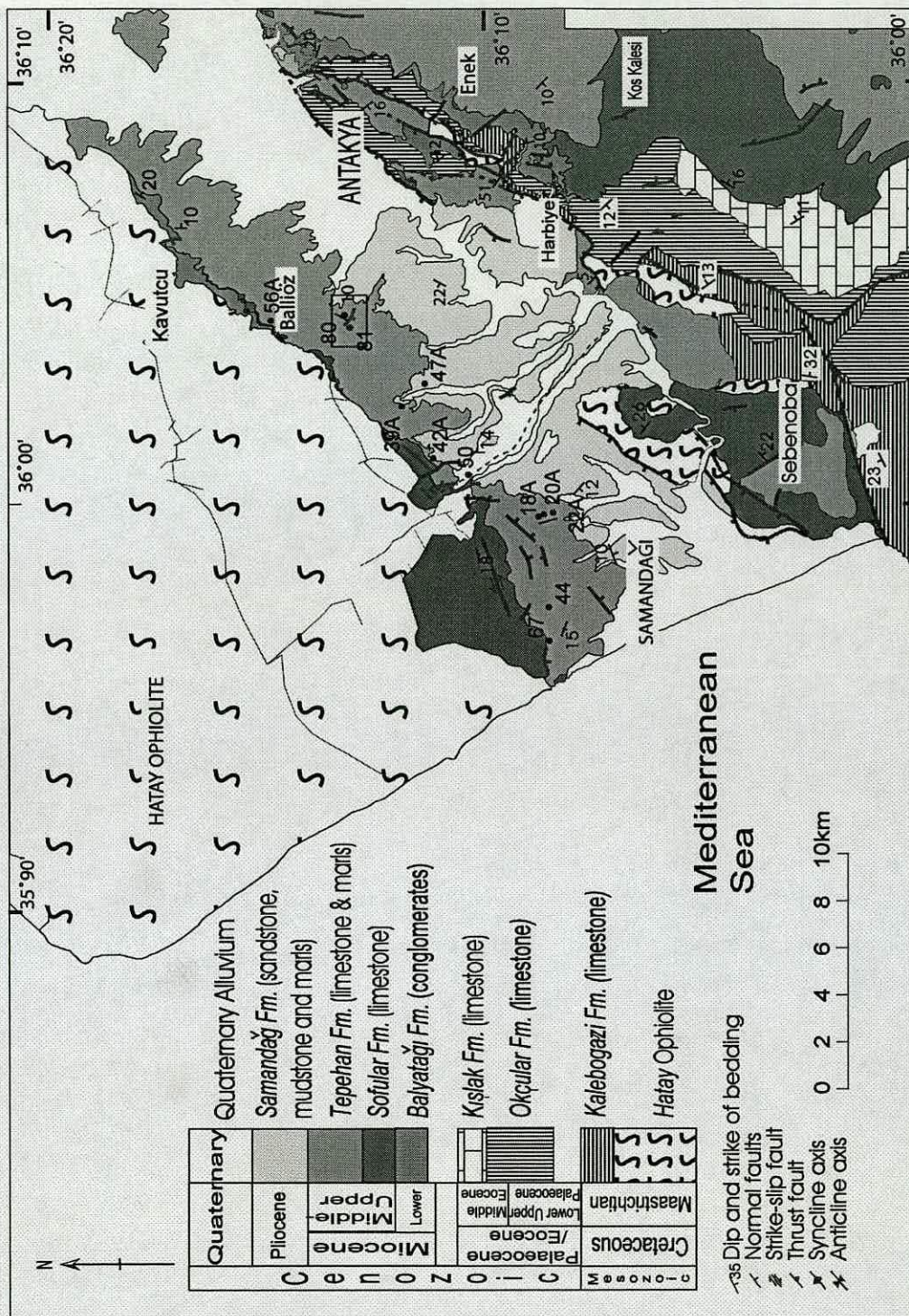


Figure 3.2. Geological map of the Hatay Graben showing the location of samples collected for strontium analysis. The box around samples 80 and 81 shows the location of Fig. 3.5.

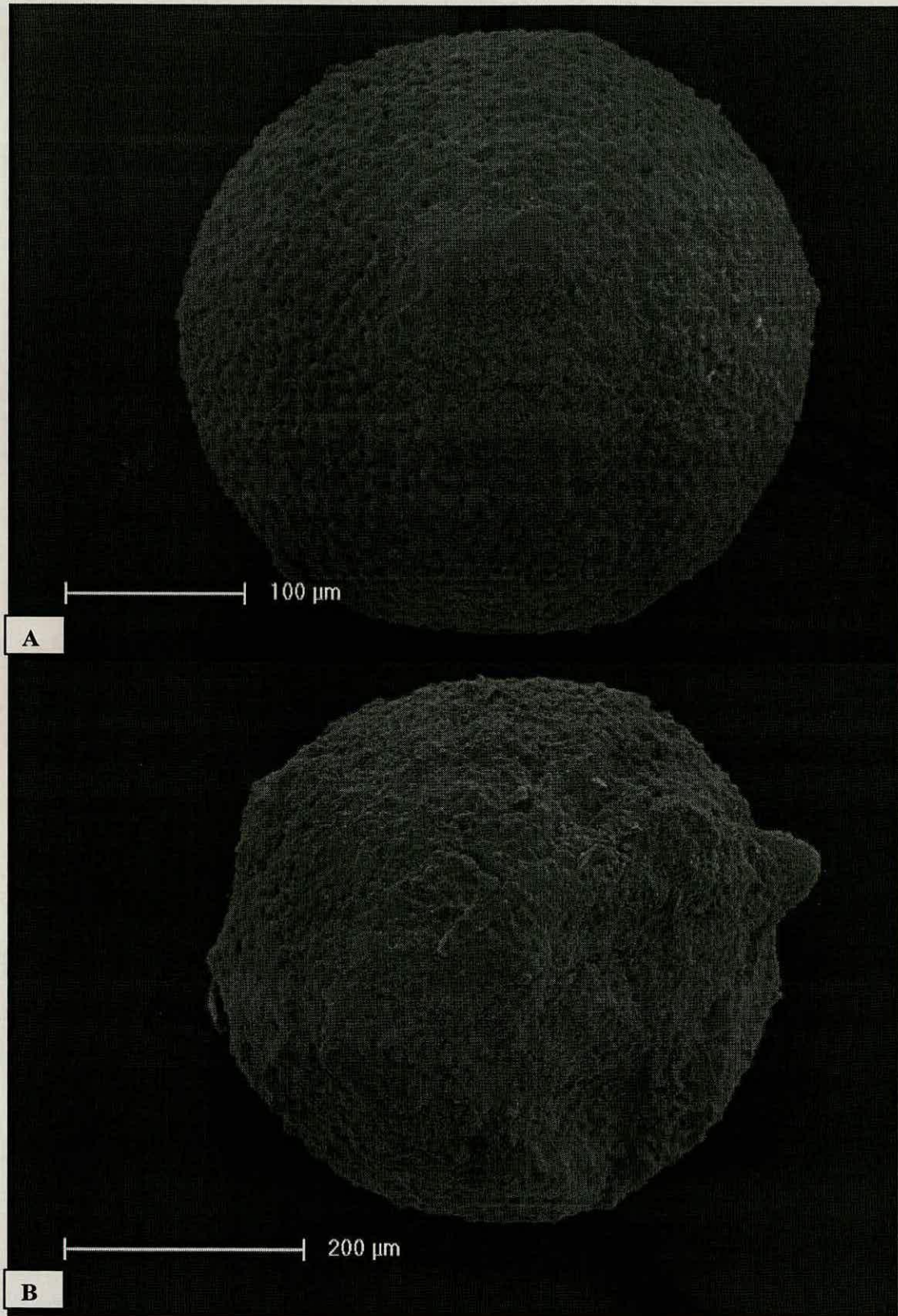


Figure 3.3. A) *Orbulina universa* after cleaning; B) *Orbulina universa* before cleaning. Note reduction in surface debris.



### 3.2.2 Chemistry

Weighed samples were placed in teflon beakers and 2ml of ammonium acetate were added. This was to leach and remove any remaining clay minerals and strontium adhering to the foraminifer tests. After standing for 1.5 hours the tests were cleaned twice in milli-q water (milli-q water is distilled and then further filtered through an ion-exchange cartridge to make it very pure), which was removed from the sample with the aid of centrifuging. The cleaned samples were then dissolved by adding 2ml of 2.5M HCl and left overnight to ensure full dissolution. The resulting solution was then centrifuged for 2 minutes and then the fluid was removed while being careful to leave any remaining particulate matter behind. Milli-q water was then added to the test-tube containing the remaining particulate material; this was centrifuged again and the liquid removed to ensure that as much of the dissolved sample as possible was collected. The samples were then dried. When dry, 1ml of 8M HNO<sub>3</sub> was added and left to stand until all of the residue was dissolved.

The sample was then ready to load into a cation exchange column. The column contained strontium specific resin, which was washed and conditioned for the sample using 0.01M and 8M HNO<sub>3</sub> respectively. The sample then was loaded into the column and washed down with 1ml of 8M HNO<sub>3</sub>. The sample was eluted with 5ml of 8M HNO<sub>3</sub>, followed by 10ml of 3M HNO<sub>3</sub>, thus removing the Ca and Ba contained within the sample. Then a clean teflon beaker was placed under the column and 5ml of 0.01M HNO<sub>3</sub> is washed through to collect the Sr. The acid was subsequently dried down and ready to run on the mass spectrometer.

The samples were loaded onto Ta filaments in the standard manner and loaded into a 20 sample turret head. The isotope ratios were measured on a VG Sector 54-30 mass spectrometer in dynamic multicollection mode with mass fractionation normalized to a Sr<sup>87</sup>/Sr<sup>86</sup> ratio of 0.1194.

### 3.3 Results

Sample	87Sr/86Sr	2SE	Age		Range	(inc
			(Ma)	Range	2SE)	Stage
SB18A	0.708919	21	9.05	8.82-9.28	7.42-10.04	Tortonian
SB20A	0.708925	18	8.68	8.41-8.93	7.17-9.79	Tortonian
SB22A	0.708878	23	10.84	10.53-10.74	9.87-11.33	Tortonian
SB39A	0.708812	23	13.24	13.08-13.39	12.09-14.57	Serravalian
SB44	0.70893	21	8.33	8.03-8.60	6.93-9.68	Tortonian
SB42A	0.708894	21	10.06	9.93-10.19	9.04-10.91	Tortonian
SB47A	0.709023	23	5.35	5.20-5.41	4.59-5.80	Mio/Plio
SB50A	0.70891	18	9.46	9.39-9.81	8.03-10.34	Tortonian
SB56A	0.708907	21	9.58	9.42-9.72	7.53-10.48	Tortonian
SB67	0.709009	23	5.61	5.56-5.66	5.01-6.06	Messinian
SB80	0.708861	21	11.22	11.11-11.33	10.39-12.13	Tortonian
SB81	0.708924	21	8.75	8.48-8.99	7.17-9.86	Tortonian

Table 3-2. Results of the Sr<sup>87</sup>/Sr<sup>86</sup> analysis

The sample number is followed by the strontium isotope ratio with a 2SE error and the corresponding age. Two age ranges are given, the first includes the uncertainty in the sea-water curve and the second includes the analytical uncertainty as well as the error in the sea-water curve. The second gives the real error in the measurements. The ages were calculated using the excel table of Howarth and McArthur (1997).

Samples SB80, 81 and 67 initially contained large Rb concentrations, although further treatment produced viable errors it is still possible that the results for these samples are less accurate than for the other samples. Especially as SB67 has resulted in an Messinian age, given the problems with this time period in the Eastern Mediterranean this would suggest that this is a dubious result.

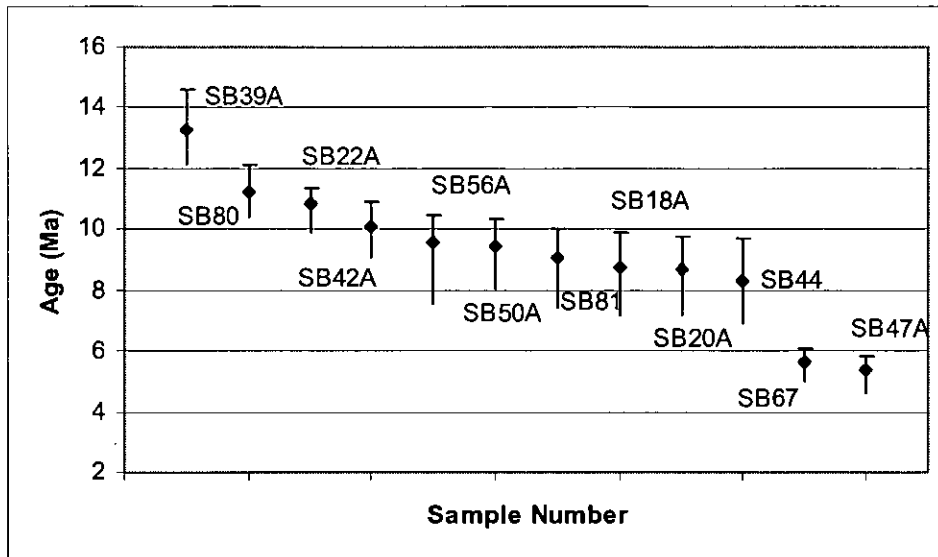


Figure 3.4. Graph showing the age and calculated error for each sample.

### 3.4 Discussion

Some samples were chosen in order to date sediments of unknown age. Samples SB39A and SB44 yield Late Miocene ages as expected (Fig 3.4), although SB39A at an average age of 13.24 Ma was older than believed in the field as field relationships indicated that the sample location is near the upper boundary of the formation. SB47A is Pliocene in age. Surprisingly sample SB67 is Messinian in age (average age - 5.35Ma). This sample is from a location near to the basin margins in what was considered to be Upper Miocene marls, although a high Rb content in the sample has probably resulted in an anomalous result as it is highly unlikely to be Messinian from that location and strontium dating does not work for the Messinian.

Samples SB18A, SB20A and SB22A were collected from an Upper Miocene section near the village of Mızraklı (Fig. 3.2), samples SB18A-20A shows a decrease in age, as expected, from 9.05 Ma to 8.68 Ma over ~16m, indicating a Tortonian age for these marls. However, sample SB22A ~10m higher in the sequence yields a much older age than expected, of 10.84 Ma. Even when the error on the age derived is taken into account this holds true. If this sample had come from the upper part of the section this anomalous result could be the result of basin isolation leading to reduced Sr<sup>87</sup>/Sr<sup>86</sup> values and thus erroneous age values. However, as the sample is near the base of the sequence this seems unlikely (although not impossible) and may be the result of reworked material or the effects of diagenesis, as the

horizon the sample was collected from is associated with small iron nodules. Another alternative is that the formation is faulted, which was not observed in the field.

Samples SB18A, SB50 and SB42A were taken from the Middle-Upper Miocene boundary (Sofular to Nurzeytin Formations) in order to investigate the nature of this contact. SB18A was taken from the base of the Mızraklı log (Fig. 4.45) in the southwest of the basin; as stated above this sample yielded an average age of 9.05Ma. Sample SB50 was taken from the boundary section exposed in the Karaçay valley; this sample yielded an average age of 9.46Ma (Fig 3.4). Sample SB42A was collected to the northwest of SB50 at location 180 (0232902/4008285). At this location, thick bioclastic limestone with interbedded marl and marly limestones are exposed in the hanging wall of a normal fault. This lithology is similar to the Middle to Upper Miocene boundary limestone, sample SB42A was taken from the first marl interval above this hard limestone. The footwall of the fault is composed of hard bioclastic limestone. This sample yielded an average age of 10.06 Ma. Sample SB56A was collected near the Middle to Upper Miocene boundary even further to north and this sample gave an average age of 9.58Ma.

Taking the average ages and assuming that these samples come from the same lithostratigraphic boundary this could indicate that the boundary in the northeast of the basin (i.e. inland today) is generally older than to the southwest (towards the present coast). Another factor to take into account is the planktic and benthic foraminiferal ratio, which is indicative of water depth. Samples SB50 and SB56A have a planktic:benthic ratio (P/P+B) of 0.59, whereas SB18A has a ratio of 1 and SB42A has a ratio of 0.08. This suggests that SB18A is a shallow-water sediment; whereas, SB42A is fully marine (~200m) and the other samples come from intermediate water depths (for more on sedimentary facies see chapter 5).

This suggests that the samples come from different locations on the shelf: SB42A is the deepest and SB18A is the shallowest; if we envisage a simple case where sediments onlap onto a slope, one would expect SB42A to be the youngest and SB18A the oldest sample. However, when the range of ages determined for the samples is taken into account, all the samples fall within a similar range, this then suggests that the boundary is the same age across the whole area, and samples were taken from various depths along a carbonate ramp with onlap being synchronous.

Samples SB80 and SB81 were collected from the footwall and hanging wall of an inferred fault (no exposure but topographic and lithological information implied a structural feature, Fig. 3.5). SB80 is dated to ~11.22Ma, whereas SB81 is dated ~8.75Ma. Considering that only ~200m separates the two sample locations and that bedding dips only at 10°, this result supports the presence of a fault, probably a normal fault dipping to the west (Fig. 3.5).

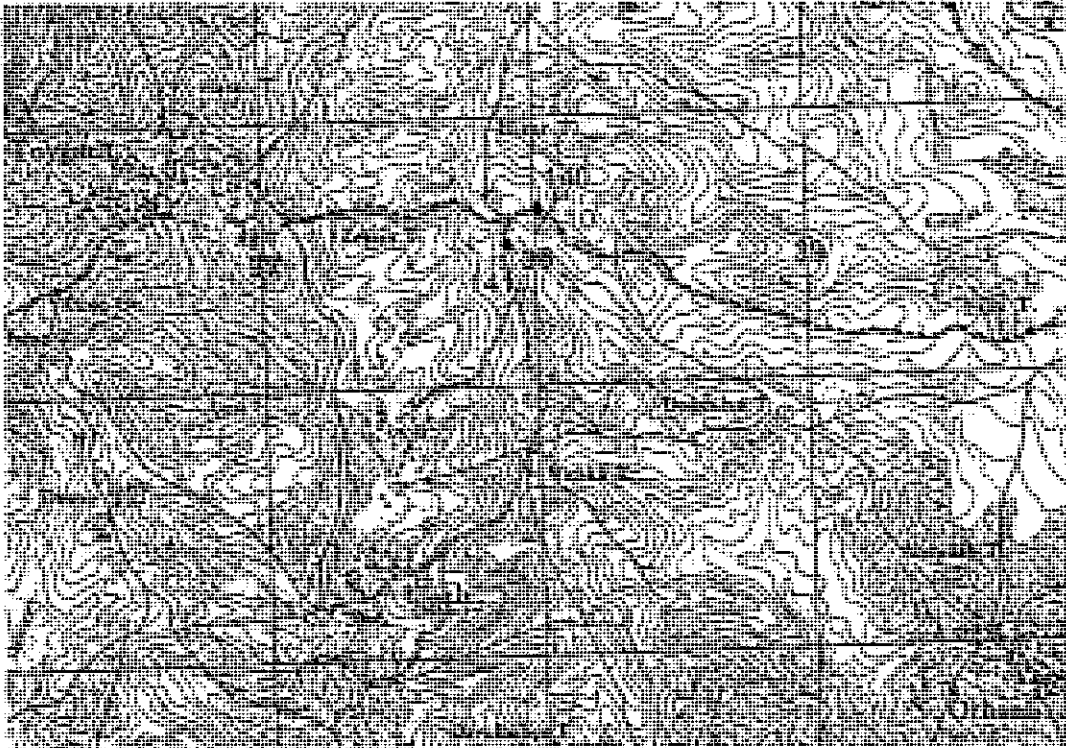


Figure 3.5. Topographic map showing the locations 140 and 141 where samples SB80 and SB81 were collected respectively. An age difference between the two locations suggests the presence of a fault running down the valley between the localities. Location of the map is indicated by a box on Fig. 3.1.

### **3.5 Conclusions**

- The Late Miocene samples yielded ages of between 13.25 Ma and 8.33 Ma, i.e. Serravallian to Tortonian in age.
- Sample SB67 resulted in a Messinian date that may be erroneous
- The Pliocene sample yielded ages of 5.35 Ma.
- The base of the Late Miocene Nurzeytin Formation is likely to be the same age across the whole of the field area.
- The top of the Late Miocene Nurzeytin Formation has probably been differentially eroded.
- Dating sediments has given evidence for the presence of a fault plane that is not exposed; this fault is probably normal.

## Chapter 4



Beit El Ma near Antioch. Supposed site of Daphne [modern Harbiye].

## 4 Sedimentological Evolution

### 4.1 Introduction

This chapter discusses the sedimentology of the Hatay Graben and the areas around the towns of Serinyol, Belen and Kırıkhan (Fig 4.1 and 4.70). This is based upon field data and laboratory studies of collected samples. The chapter firstly discusses the field characteristics of each lithostratigraphic unit in turn; these units are based upon the revised stratigraphy as outlined in Chapter 2. This is achieved by focussing on the type locality and other selected locations for each unit. Laboratory analyses of collected samples are then discussed in the second half of the chapter. The observations are then drawn together in the chapter 5 and interpreted in terms of lithofacies in order to develop a facies models and palaeoenvironmental maps of the study area.

Although this results in the raw sedimentological data and the interpretation of these data to be presented in separate chapters with some minor repetition of data in the next chapter, it was felt that this approach would be advantageous for a number of reasons. Setting the information out in this way will firstly aid the transformation from thesis chapters into papers for publication, as this represents important new knowledge of the field area. Additionally, chapter 4 presents the data with locations and specifics, which need not be repeated in chapter 5, making this chapter more process orientated and interesting. Finally, setting out the information in this way prevents the chapters from becoming too long.

Techniques used in the collection of sedimentological field data included measuring sedimentary logs, collecting samples, measuring palaeocurrent data and the general description of lithology and facies. Lithological descriptions form the first part of this chapter with photographs, field sketches, graphic logs and maps to illustrate observed features. Palaeocurrent data are also presented here with maps.

The second part of this chapter presents petrological and provenance studies from samples taken during the fieldwork. This includes X-ray diffraction (XRD) studies of fine-grained sediments (laboratory data in Appendix 2), point-counting of thin sections (individual thin section descriptions are to be found in Appendix 3 and information from them is incorporated into this chapter and Chapter 5, letter/number codes in bold indicate thin section with description in Appendix 3) and conglomerate clast counts.



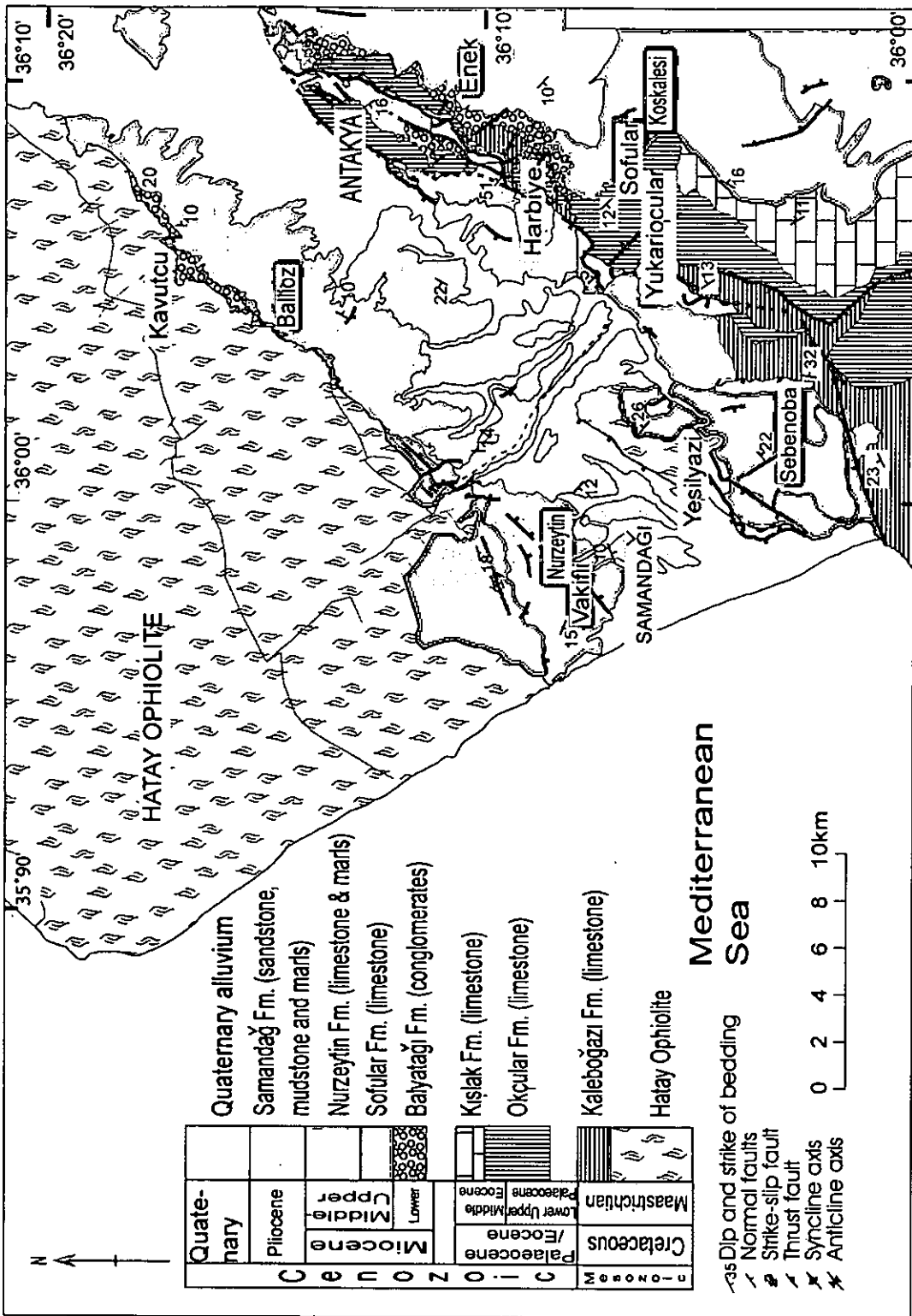


Figure 4.1. Map of the main study area based around the city of Antakya showing the main locations discussed in the text. Map based on field work carried out in this study and the maps of Temizkhan (2003), Mistik (2002) and Pişkin (1985).

## 4.2 The Sedimentology of the Hatay Graben

### 4.2.1 Cretaceous to Eocene – Kaleboğazı and Okçular Formations: limestones and marl.

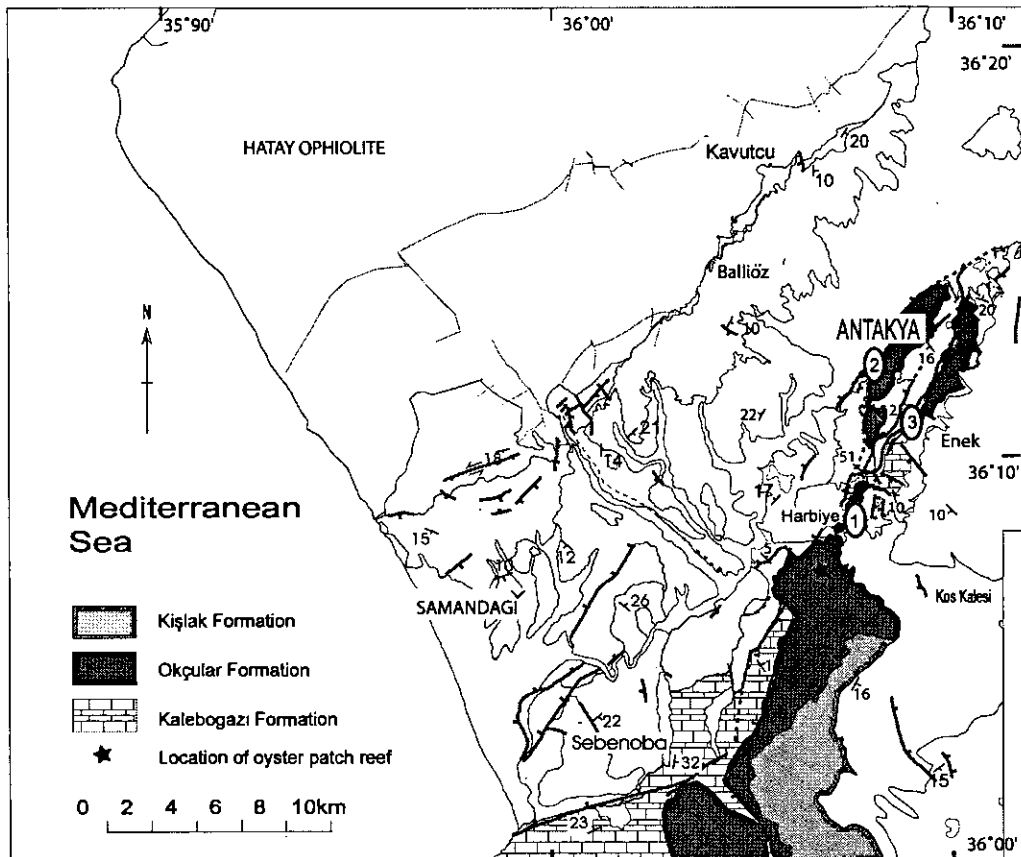


Figure 4.2. Map of the Hatay Graben showing the distribution of Upper Cretaceous and Eocene sediments. Numbers indicate locations described in the text.

Cretaceous and Eocene sediments only outcrop in the eastern part of the field area (Fig. 4.2); both formations are dominated by limestones. There is very limited exposure of the Upper Cretaceous limestones, and the Eocene limestones are mostly karstified.

## 4.2.1.1 Harbiye Gorge (1)

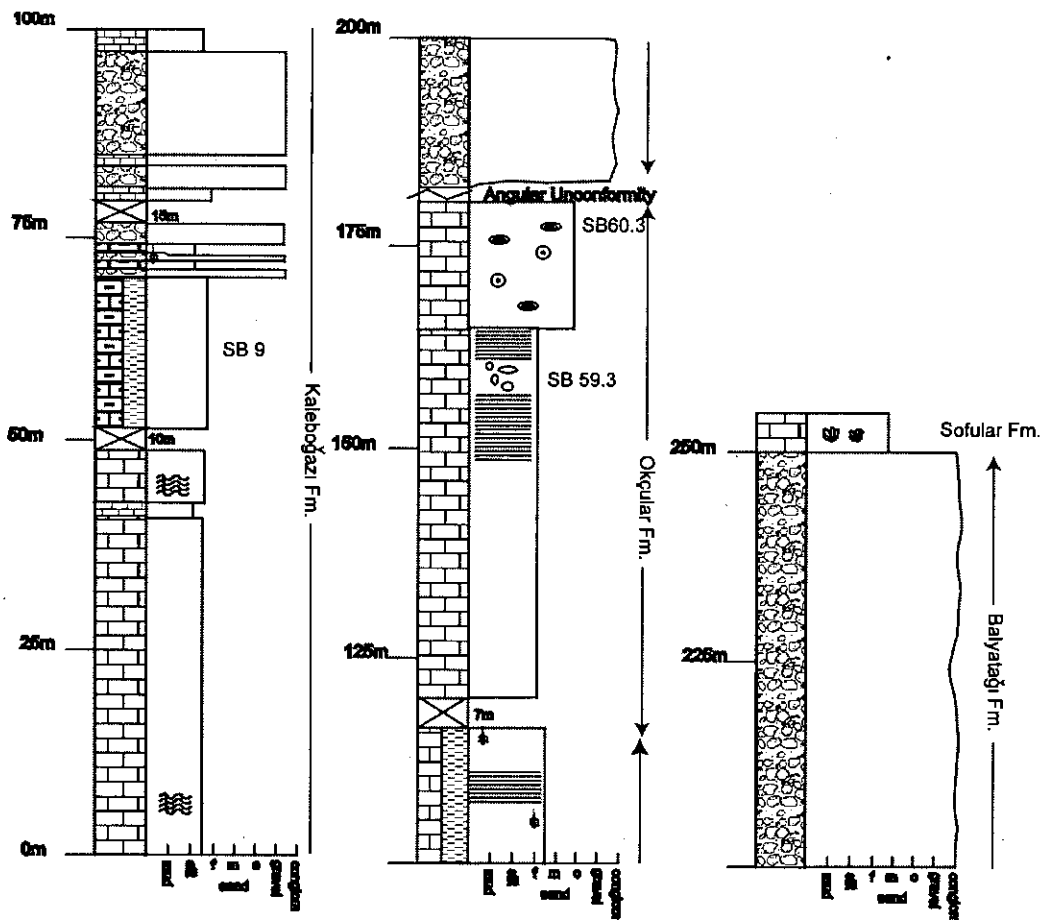


Figure 4.3. Log showing the sedimentary succession measured along the Harbiye Gorge. Figure 4.11 shows the location where the log was measured. Key for all the logs presented in this chapter is to be found in Appendix 7.

The Harbiye Gorge trends eastwards from the town of Harbiye, exposing a sequence of rocks of latest Cretaceous (Kaleboğazı Formation) to Late Miocene (Sofular Formation) in age (Fig 4.3). The base of the Kaleboğazı Formation is not exposed at this location; however, when it is exposed limestone is observed to overlie the ophiolite, which has an eroded and leached top. The basal sediments are composed of hard, white microbial limestone (Fig. 4.3); bedding thickness is less than 1m. Wavy algal lamination, fenestral porosity and desiccation breccia are common and vertical burrows are present in some horizons; chert nodules are found at some locations.

The upper section of this formation is composed of interbedded marl, conglomerate, sandstone and limestone (Fig 4.3). Conglomerate and coarse litharenite dominates this part. Generally, the conglomerate is matrix supported, with poorly sorted, sub-angular, to rounded, clasts of ophiolitic and carbonate composition. The colours of these carbonates range from creamy pink to red. The marl horizons are pink, red or reddish brown and often contain cream-coloured caliché nodules (SB9). The upper parts of these beds are often laminated (parallel and convoluted) and rootlets are common. Lime mudstone horizons are less abundant in the succession; they are generally cream coloured but the outer surface is stained red due to contact with the surrounding sediments. Some silicic material (ophiolite clasts) is present. Occasional limestone beds are completely chertified and microbial laminations are preserved within these beds.

There is a slight angular discordance between these beds and the overlying Okçular Formation (7°). However, this may be due to the presence of a small fault at the boundary of the logged section. The base of the Okçular Formation is composed of thinly bedded (5-20cm), very fine-grained cream lime mudstone (SB59.3), with occasional lenses and horizons of red mudstone. Wavy microbial laminations are common, as is fenestral porosity and chert nodules. This lithology often becomes karstified.

These interbedded lime mudstones and mudstone pass upwards in medium-grained white packstone/rudstone (SB60.3). No sedimentary structures were observed. However, bioclastic material is common especially large benthic foraminifera, including *Nummulites* sp; oncolites are also abundant.

Along the road to Bözlu, that runs along the top of the Okçular Formation, a biogenic build up of oysters was observed (Fig. 4.2).

#### 4.2.1.2 Antakya (2)

The base of the Eocene Okçular Formation can be observed at location 287 (0244702/4009163), east of the city of Antakya. A basal clastic sediment rests on an irregular surface of serpentinite (Fig. 4.4). This breccia is matrix supported and is formed of angular clasts of serpentinite in a fine-grained carbonate matrix. Clast abundance decreases laterally away from the boundary completely disappearing after ~1m. The fine-grained limestone (wackestone, SB98A & SB100A) is thinly bedded (5-30cm) and has sharp bedding surfaces. Beds are also laterally discontinuous and occasionally separated by thin



marl horizons, <5cm thick. Chert nodules are common; these are often parallel to the bedding planes. Straight crested ripple marks are developed on the top surface of some beds. Higher in the formation, bioclastic material increases in abundance and Nummulites sp. and Milliolid sp can be observed in hand specimen; planktic foraminifera, echinoid fragments, coralline algae (possibly reworked) and coral fragments are also present.

#### 4.2.1.3 *Enek Pass (3)*

A new road cutting exposes the ophiolite-cover boundary (Fig. 4.5) at location 161 (0246952/4006503). The top of the ophiolite at this location is very irregular and mounds of pillow lavas are observed. These pillow lavas are overlain by ~10-15m of mudstone and marl, which drape the underlying topography. The sediments are very fine-grained and are brown-red, cream and maroon in colour. No sedimentary structures were observed within these sediments.

The mudstone and marl are overlain by thinly bedded, Nummulitic packstone. This is very similar to that observed in the upper sections of the Okçular Formation.



Figure 4.4. Photograph showing the basal limestone breccia observed near Antakya. To the left is the underlying serpentinite, the contact is left of the compass-clinometer.

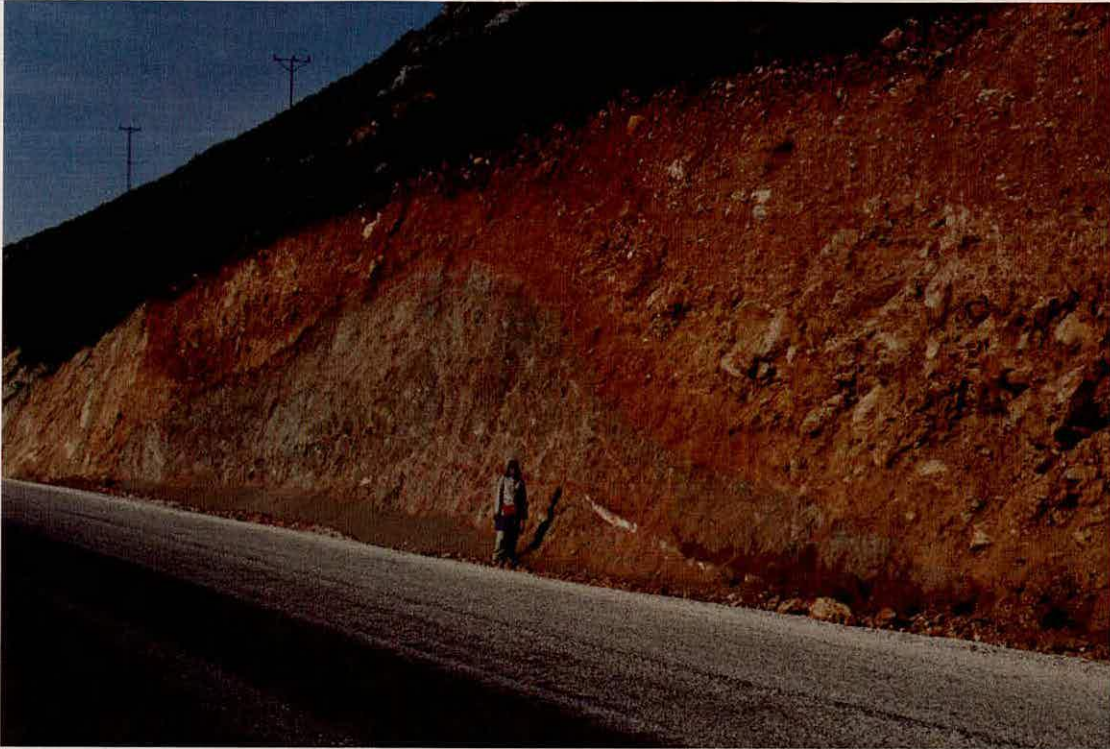


Figure 4.5. Photograph showing the contact between the pillow lavas and the sedimentary cover at location 161.

#### **4.2.2 Summary of the Cretaceous and Eocene.**

The basal Upper Cretaceous sediments rest upon the irregular surface of the Hatay Ophiolite. The Kaleboğazı Formation is composed of uniform microbial limestones with wavy laminations and fenestral porosity. The upper part of the Kaleboğazı Formation is composed of interbedded marl, mudstone, conglomerate and limestone. The Palaeocene to Eocene Okçular Formation is made up of a lower microbial limestone and an upper wackestone/packstone rich in large benthic foraminifera. Sedimentary structures include planar laminations. The base of the Eocene Okçular Formation is observed to overlie both the Hatay Ophiolite and the Kaleboğazı Formation.

### 4.2.3 Lower Miocene - Balyatağı Formation: conglomerate and mudstone.

The Balyatağı Formation outcrops extensively along the eastern flanks of the present topographic graben (Fig. 4.6). There are also isolated exposures of conglomerate along the western margin; however, the Balyatağı Formation was not observed to the south. The formation is composed mainly of conglomerates and mudstone.

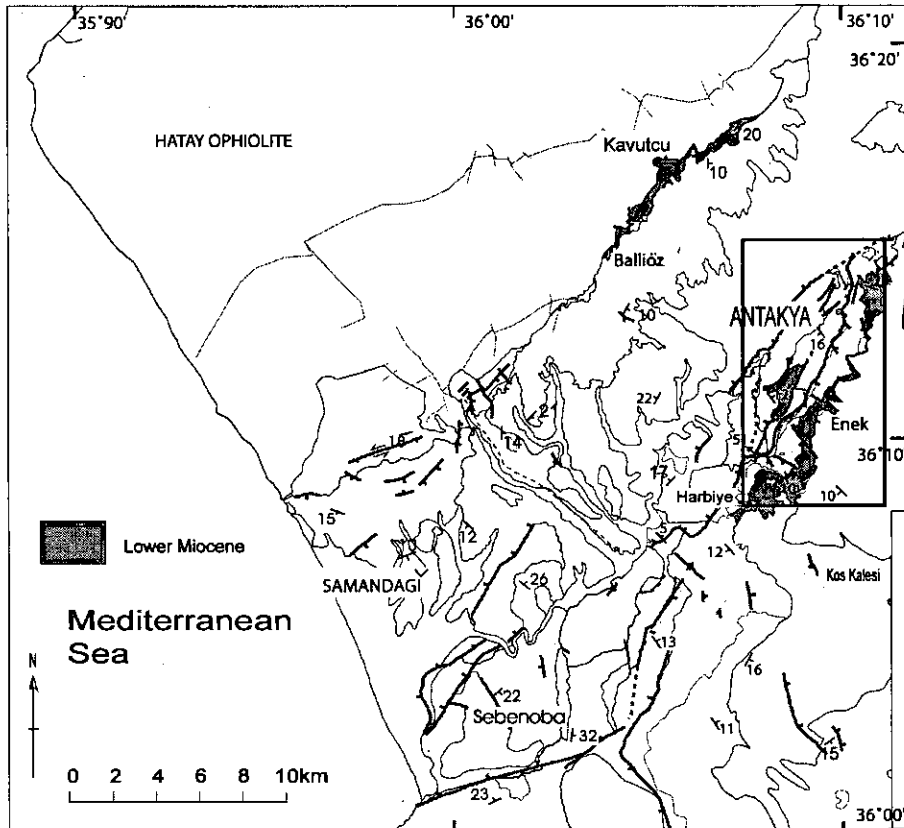


Figure 4.6. Map showing the outcrop extent of the Lower Miocene (shaded grey). The box indicates the position of Fig. 4.19. Numbers indicate position of locations discussed in the text.

#### 4.2.3.1 Enek/Balyatağı (type location) (1).

The type location for the Balyatağı Formation is on the main road from Antakya to Altınöz, near the village of Enek. The base of the formation rests on an angular unconformity with the underlying Eocene Okçular Formation and is composed of interbedded conglomerates and mudstones. The conglomerate is composed of ophiolite- and limestone-derived clasts (Fig 4.7); these are sub-angular to rounded, and generally poorly sorted. Clast size varies greatly between beds, with some conglomerates having clasts greater than 1m in size (these



are more common in the lower part of the formation) to beds with maximum clast size of up to 10cm. The conglomerates vary between being matrix- and clast-supported but are generally clast-supported. The composition of the matrix ranges from micrite to fine siliciclastic material. This has the same composition as the large clasts to pale-coloured weathered serpentinite material (SB30.3).

The fine-grained mudstone varies in colour and hardness; some beds are soft and dark reddish brown, whereas others are hard and pink to white in colour. “Floating” pebbles of dominantly serpentinite are common; these are generally < 0.5cm in size, sub-rounded, to sub-angular and are quite well sorted. These beds generally exhibit less pebbly material upwards.

A log was measured at this section from 0247339/4006037 to 0247796/4006188 (Fig 4.8 and 4.10). However, the Balyatağı Formation is laterally discontinuous making the logged section not wholly representative of the formation. The section shows a number of thick conglomerate beds, fining upwards from a clast size often in excess of 30cm, to a fine-grained mudstone. Pebble imbrication and cross-bedding can be observed within the conglomerate beds, whereas the mudstone beds contain occasional stringers of single pebbles and scattered nodular carbonate (caliche).

Near the top of the formation within the logged section, sedimentary structures become much more common: large-scale, low-angle cross-bedding, pebble imbrication and parallel lamination are all observed. Additionally, there is much less mudstone in the upper part of the succession. Above the conglomerates there is an abrupt transition to limestones of the Middle Miocene Sofular Formation.

Figure 4.9 shows the laterally discontinuous nature of the conglomerate beds in the middle to upper part of the formation; these form lenses that appear to be thicker at one end compared to the other. In between the conglomerate beds is pebbly sandstone mudstone. Below this, the conglomerates exhibit greater continuity with possibly a sheet-like geometry.



Figure 4.7. Close up photograph of the conglomerates in the field.



Figure 4.8. Photograph of the top of the type section near Enek, at the top of the hill limestones of the overlying formation are exposed. Note the continuous parallel bedding. Softer, less prominent, beds are palaeosols interbedded with coarse sandstone and conglomerates.

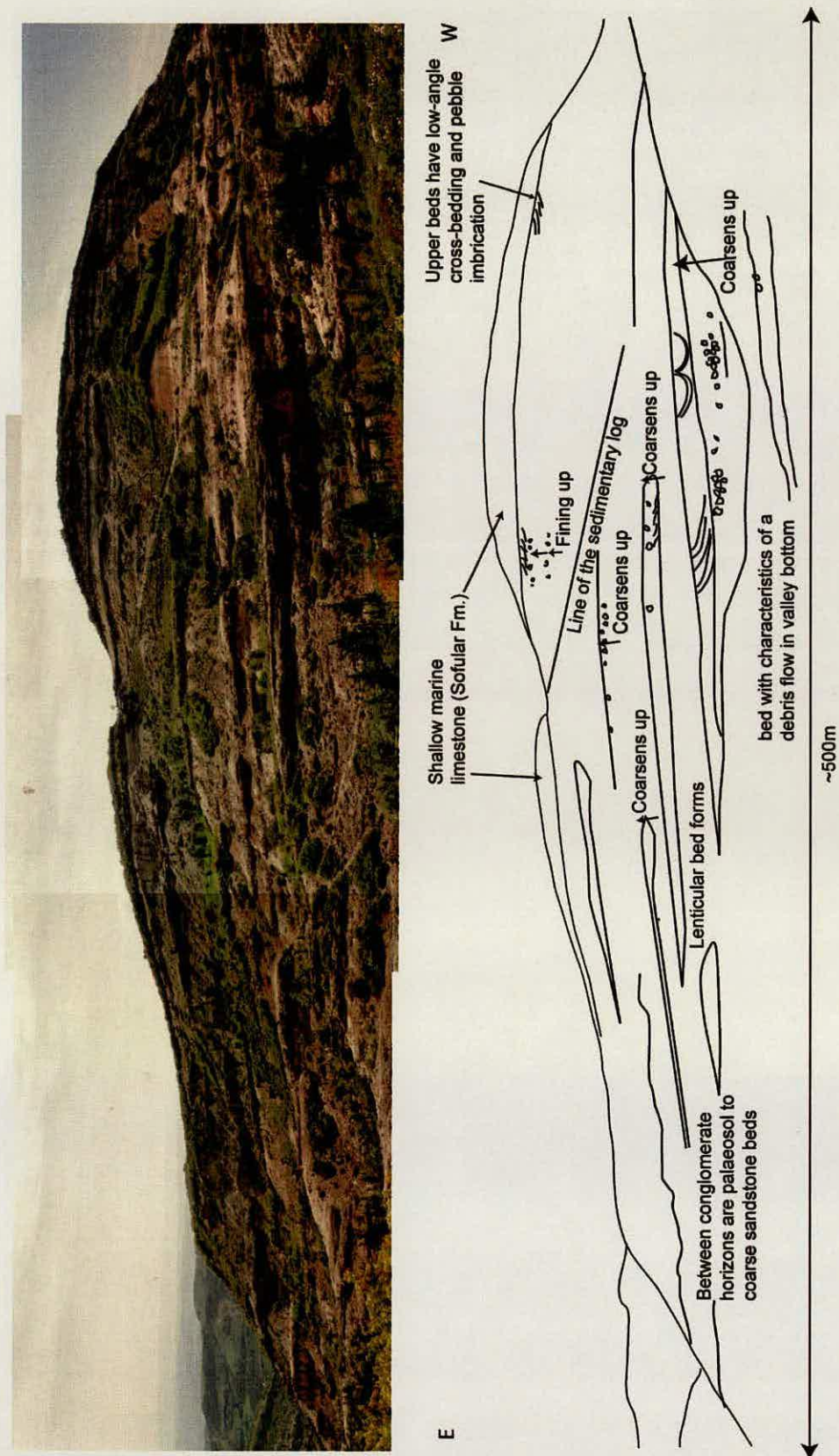


Figure 4.9. Panorama of Balyatağı Tepe, note that the beds have a lenticular morphology in the lower part of the photograph.

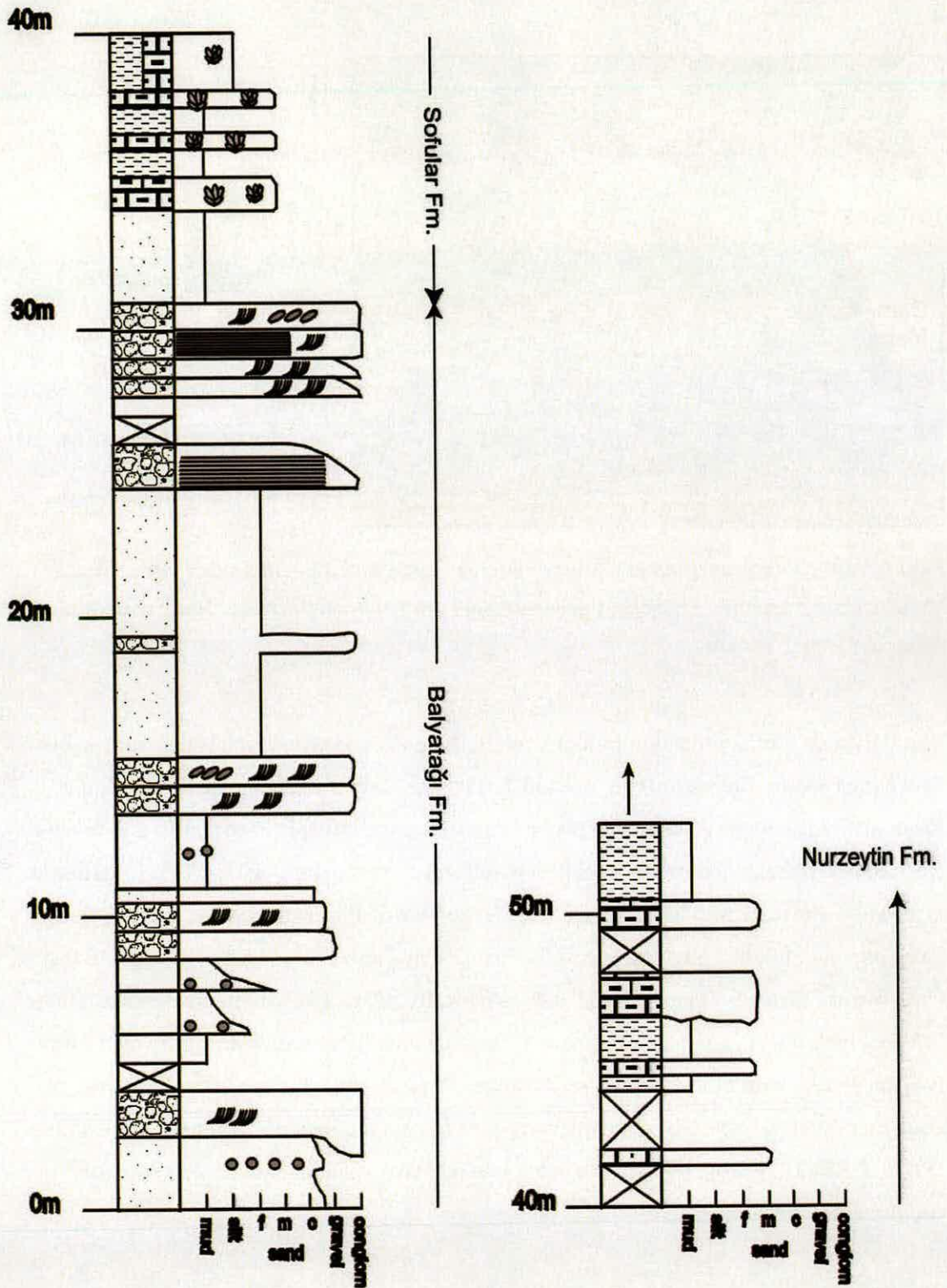


Figure 4.10. Log of the type section for the Balyatağı Formation, at Balyatağı Tepe.

## 4.2.3.2 Harbiye Gorge (2)

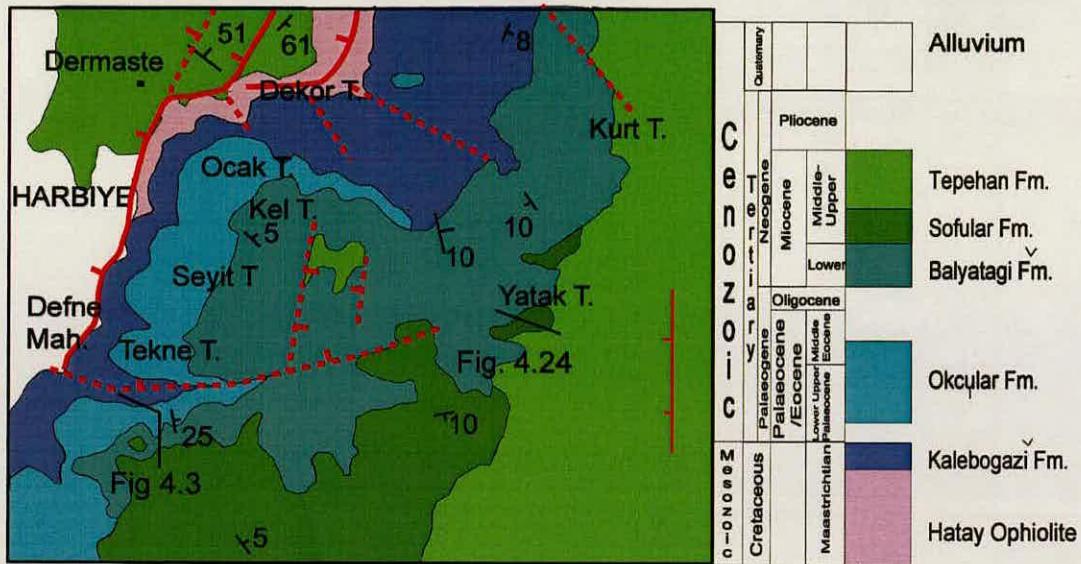


Figure 4.11. Geological map and key of Harbiye Gorge and the surrounding area. Black lines indicate measured sections, figure numbers are given on the map. North is up and width of the map is 4km.

The Balyatağı Formation outcrops along the Harbiye Gorge section, and is unconformable above the Okçular Formation (Fig 4.3 and 4.12). The base of the Balyatağı Formation at location 497 is composed of coarse pebbly sandstone containing marine debris, e.g. bivalves (including *Ostrea*), oncolites and pebbles with algal coatings (Figs. 4.13). This fossiliferous interval is ~6m thick and lies upon an irregular surface of Eocene limestone. Above this basal interval of thick conglomerate, beds then fine upwards into mudstone, similar to that observed at Balyatağı Tepe; bed thickness is typically >2m. The maximum clast size varies between beds but is generally <40cm; and clasts are angular to rounded. Clast composition is again mixed, with limestone and serpentinite clasts; also, the texture varies from matrix- to clast-supported. The matrix is mostly composed of cream-coloured, weathered serpentinite (SB59 & SB61). Pebble imbrication and low-angle cross-bedding are present in some conglomerate horizons.

The fine-grained mudstone facies is very hard and varies from pink to white in colour and often contains “floating” clasts <5 cm in size, the majority being < 0.5cm in size, and mostly derived from the ophiolite. In places, these mudstones are nodular and calichefied.



Figure 4.12. Photograph of the base of the Lower Miocene conglomerates unconformable upon Eocene limestones (paler rocks bottom left); note break of slope along the boundary.



Figure 4.13. Photograph of a clast with an algal coating in the basal conglomerates in the Harbiye gorge.

4.2.3.3 Gökçeğöz (3)

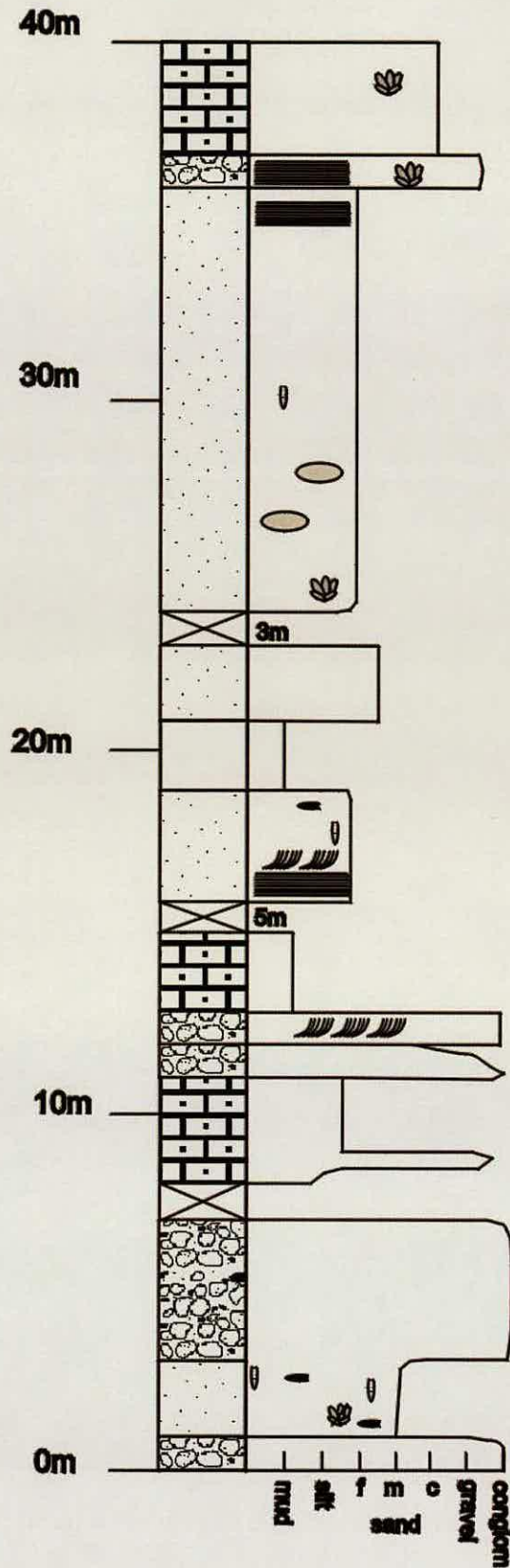


Figure 4.14. Log of the Gökçeğöz section.

The upper part of the Balyatağı Formation is well exposed along the road from Antakya to Gökçeğöz. Interbedded conglomerate and mudstone 100-150m thick (similar to that described previously in 4.2.3.1) is overlain by ~45m of interbedded conglomerate, sandstone and marl. The conglomerates and sandstones often occur together as fining upwards sequences. Cross-bedding, parallel lamination and burrowing are common within the sandstone. Also, small lenses of conglomerate and marl were observed in some sandstone beds. At the very top of this interval, bivalve material starts to appear. There is a minor amount of fine-grained sandy marl and mudstone present, which tends to form rather structureless beds, although some of the sediment is nodular.

4.2.3.4 *Kavutcu (4)*

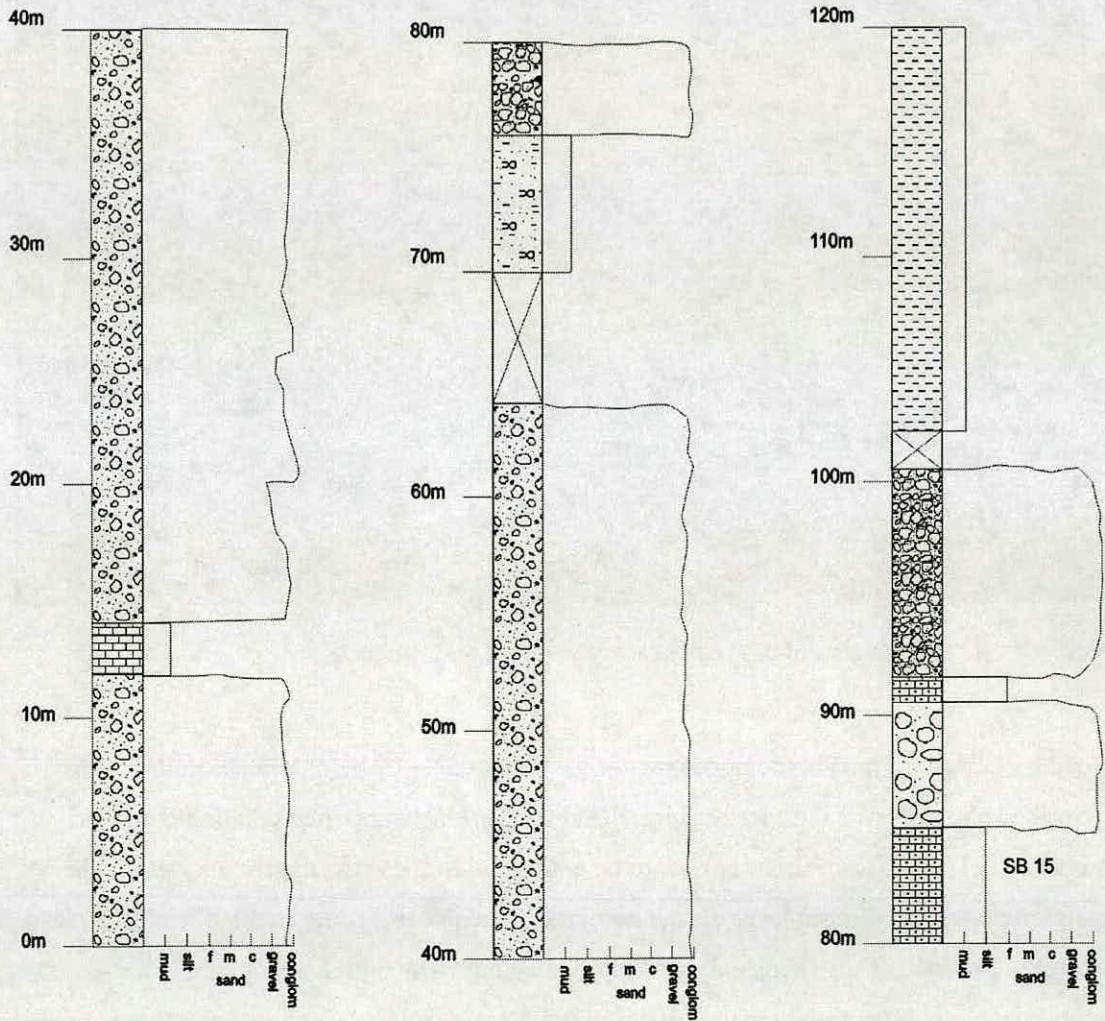


Figure 4.15. Log of the section at Kavutcu.

On the northwestern margin of the Hatay Graben, Lower Miocene sediments crop out at the village of Kavutcu (Fig 4.15 and 4.16); however, the base of the formation was not observed



at this location. The conglomerates are more massive than those observed on the southeastern margin. At Kavutcu, the succession is relatively uniform, the lowermost 80m being formed of massive conglomerates (~65m thick). Bedding planes are difficult to distinguish and there are no obvious structures. The conglomerate is matrix supported; the clasts are sub-angular to sub-rounded; maximum clast size is ~40cm, but the mean clast size is nearer to 5-10cm; also some beds appear to fine upwards. The conglomerate is polymict but is dominantly composed of serpentinite and chert. The matrix is white in colour and derived from weathered serpentinite (**SB15 & SB65A**).

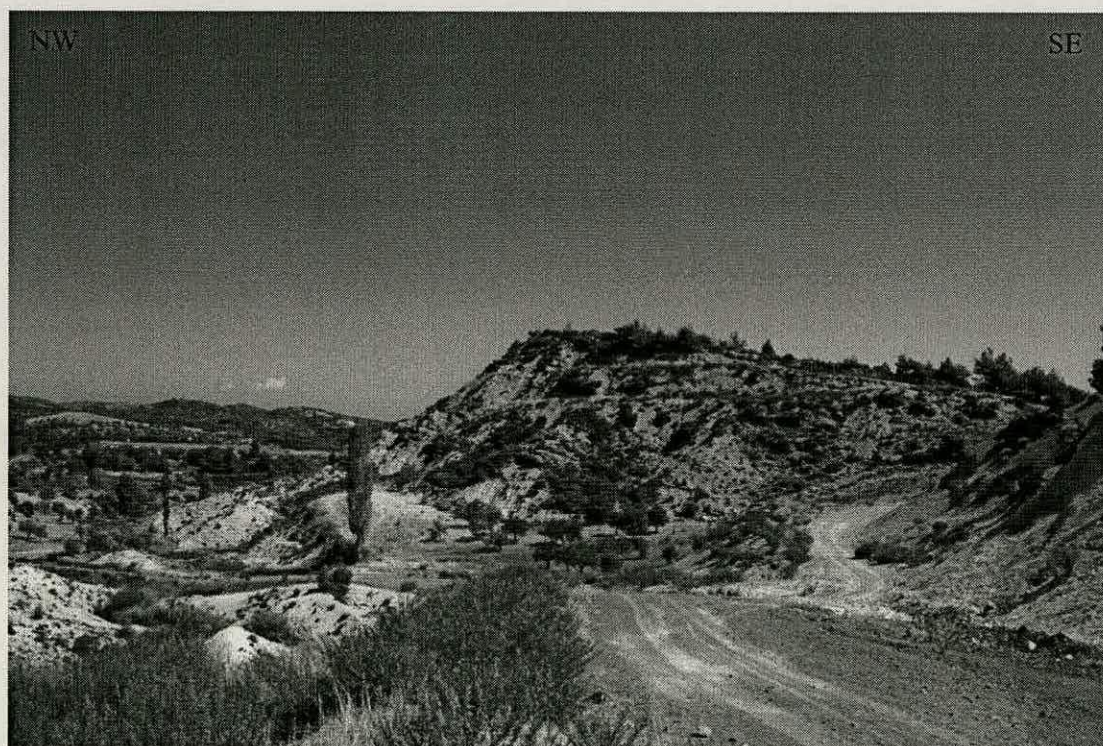


Figure 4.16. Photograph of the sedimentary sequence at Kavutcu.

Bedding is well defined in the upper part of the formation. Conglomerates similar to that described above persist but these are interbedded with clast-supported conglomerate and mudstone. The mudstone beds appear to be composed of the same matrix material as the conglomerates but without large clasts; however, there are still some small siliciclastic clasts within these beds. These beds exhibit a mottled colour: white, pink and green. Clast-supported conglomerates are made-up of polymict gravel (clasts <5cm in size): these are also mottled red and white. Upwards, there is a conformable boundary with marls of the Upper Miocene succession.

#### 4.2.3.5 *Dikmece (5)*

There is very good exposure of Lower Miocene sediments at the village of Dikmece. The base of the sedimentary sequence can be observed at 0243641/4019688 (Fig 4.17). White matrix-supported conglomerate overlies the sheeted dyke complex of the Kızıldağ Ophiolite. Clasts are primarily derived from the ophiolite (serpentinite) and are <10cm in size. Above this basal conglomerate, there is ~60m of finer grained sediments, mostly composed of mudstone and marl, with some levels containing small (~2mm) “floating” pebbles of serpentinite. The colour of these sediments varies from pure white to a red and white mottled appearance. In the middle part of this mudstone is a conglomerate bed in which clasts are mostly composed of Eocene Nummulitic limestone. This facies is matrix-supported and poorly sorted.

Notably, the sediment shows considerable lateral and vertical facies variation. The thickness of the mudstone unit varies and two conglomerates were observed with different clast compositions; one was dominantly carbonate derived, the other ophiolitic.

#### 4.2.3.6 *Palaeocurrent Analysis*

Eight of the locations studied possessed palaeocurrent indicators. These are generally imbricated elongate clasts, although occasionally cross-bedding provided current directions. Figure 4.17 shows that locations in the NE have palaeocurrent directions that are orientated to the N or NE; in contrast, locations to the SW exhibit a greater variety of palaeocurrent, orientations varying from south, west/northwest to east. No measurements were made on the NW basin margin as no palaeocurrent indicators were present in the sediments.

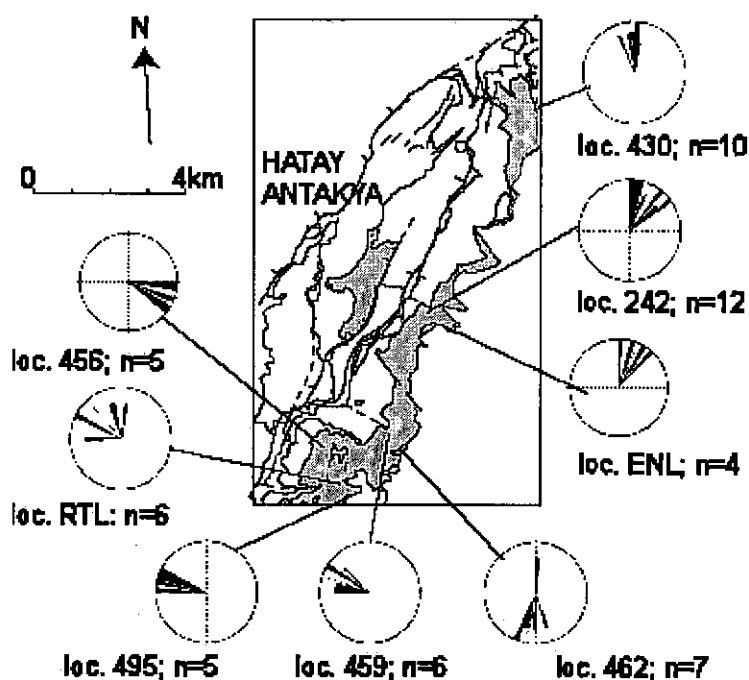


Figure 4.17. Palaeocurrents measured from the Balyatağı Formation, location numbers and the number of data points are given for eight localities. Palaeocurrent measurements were either taken from cross-bedding or pebble imbrication.

#### 4.2.4 Summary - Balyatağı Formation

This formation varies across the field area. On the southeastern margin of the graben the Balyatağı Formation is characterised by a variable thickness of matrix-supported conglomerate that fines upwards near the top of the formation into interbedded conglomerates and palaeosols.

On the northwestern margin the nature of the conglomerates differs; generally the thickness of the basal conglomerate is thinner, and proportionally, the amount of matrix in these sediments is higher. In this area, in contrast to the south, the uppermost part of the formation is dominated by palaeosol.

### 4.2.5 Middle Miocene – Sofular Formation: limestone with marl and conglomerate.

The Sofular Formation outcrops extensively along both the southeastern and northwestern margins of the Hatay Graben. The base of the formation is composed of marl and limestones; the percentage of limestone increases upwards until there is no marl or conglomerate remaining.

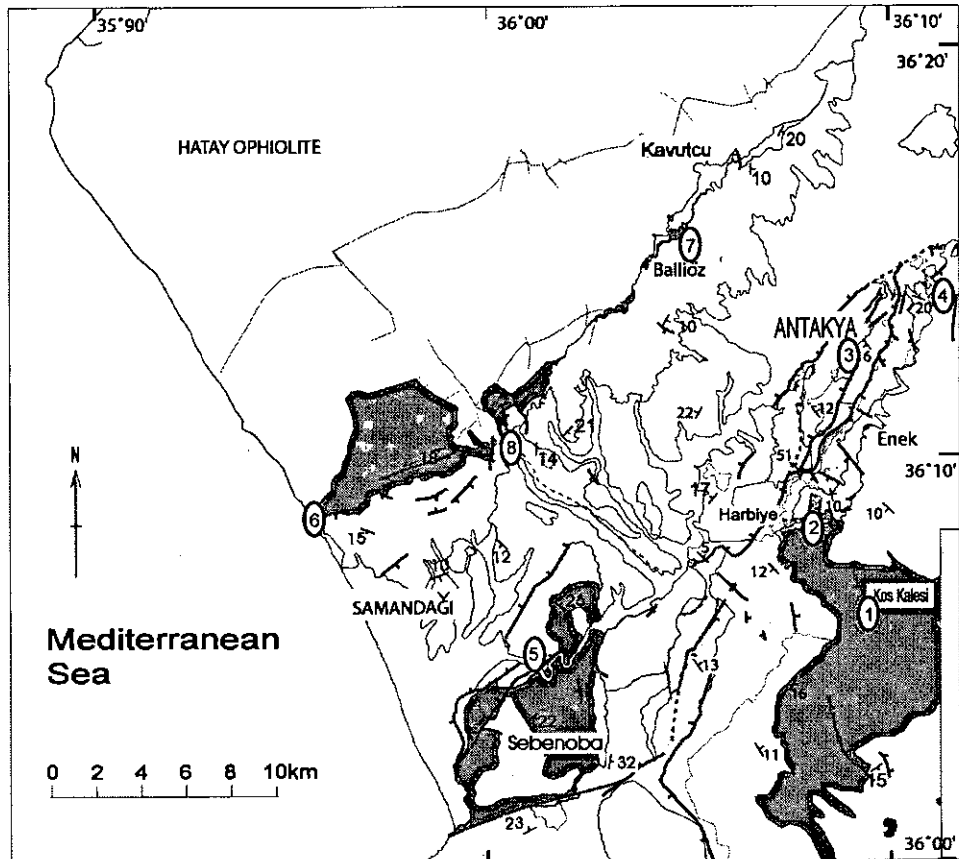


Figure 4.18 Map showing the extent of the outcrop of the Middle Miocene Sofular Formation (shaded grey). Numbers indicate localities discussed in the text.

4.2.5.1 *Kozkalesi (type location)(1).*

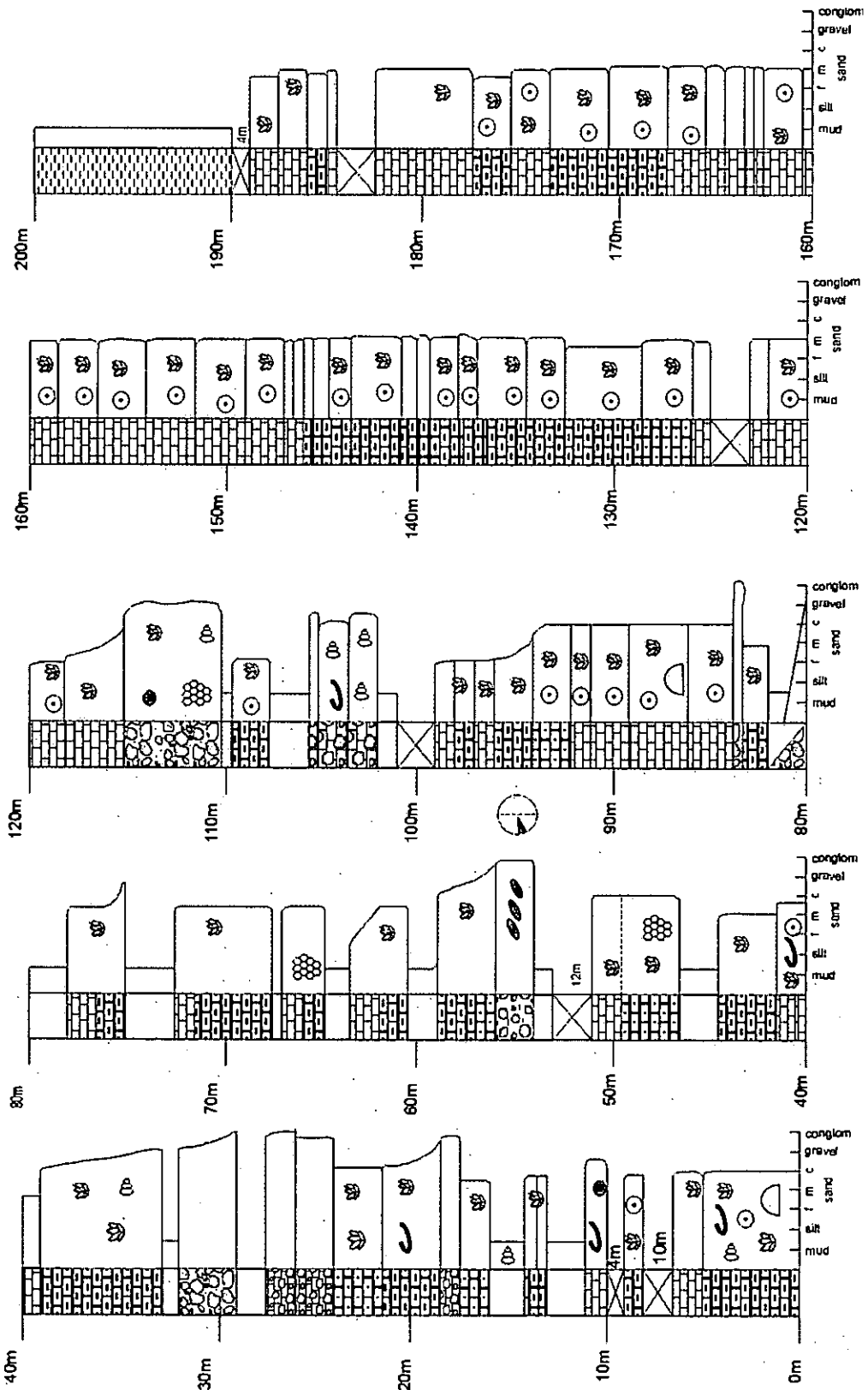


Figure 4.19. Log of the section measured near the village of Kozkalesi.

Near the village of Kozkalesi (0247400/3998450), the confluence of two gorges results in an excellent exposure of Middle to Upper Miocene sediments, >215m in thickness. A sedimentary log was measured from 0247022/3998693 in the west, up section to 0249220/3998275 (Fig. 4.19). The log can be broadly described in terms of four lithological assemblages (A, B, C, D). The basal sediments contain repeating cycles of the lithologies, forming fining upwards cycles generally c. 5-15m in thickness.

A.

This lithology is a conglomerate horizon that exhibits a sharp contact with the underlying bed. It is laterally discontinuous and of variable thickness (maximum observed thickness ~5m). The conglomerates are clast- and matrix-supported and are polymict; the lithoclasts are well rounded and occasionally bored. The clasts include limestones and serpentinite; and often the conglomerates contain fossil material, such as bivalves, gastropods and coral (Fig. 4.20).

B

The conglomerates fine upwards into coarse bioclastic marly limestones, generally wackestones and rudstones (**SB13.3**). Fossil material is partly fragmented and composed of a variety of bivalve and gastropod species (e.g. *Ostrea*, *pectens*) echinoids (*Chlypeaster* sp., *Echamolampas* sp., *Schizaster* sp., *Psammechinus* sp. (Piskin *et al.* 1982), oncolite and coral. Beds are 1-6m thick lacking sedimentary structures. This limestone is quite soft and grades into a harder bioclastic limestone (C).

C.

The harder limestone (wackestone – packstone **SB12.3**) contains the same faunal assemblage, but additionally rare *in situ* coral heads were observed, and there are often numerous oncolites (algal balls) in these beds. The top surface is sharp but irregular.

D.

This facies is fine-grained pink-grey carbonaceous mudstone. The beds are 50cm to 2m thick, generally lacking sedimentary structures. However, the beds sometimes exhibit a mottled appearance. This appearance is in part due to the presence of caliche, the development of which varies with some beds having no or only minor amounts caliche but other palaeosol horizons exhibit advanced calichification. Small gastropods, roots and other plant material are present in some beds.

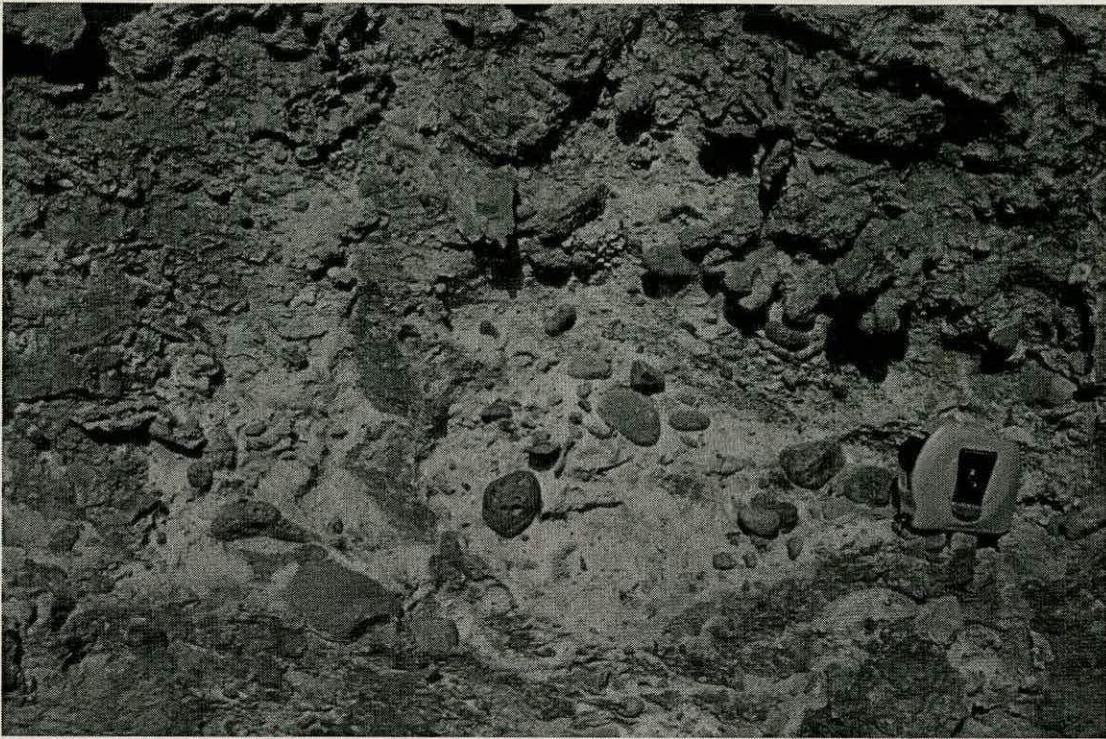


Figure 4.20. Photograph showing detail of the basal conglomerate observed in one bed. Note bored pebble (centre) and coral fragments (above tape measure).

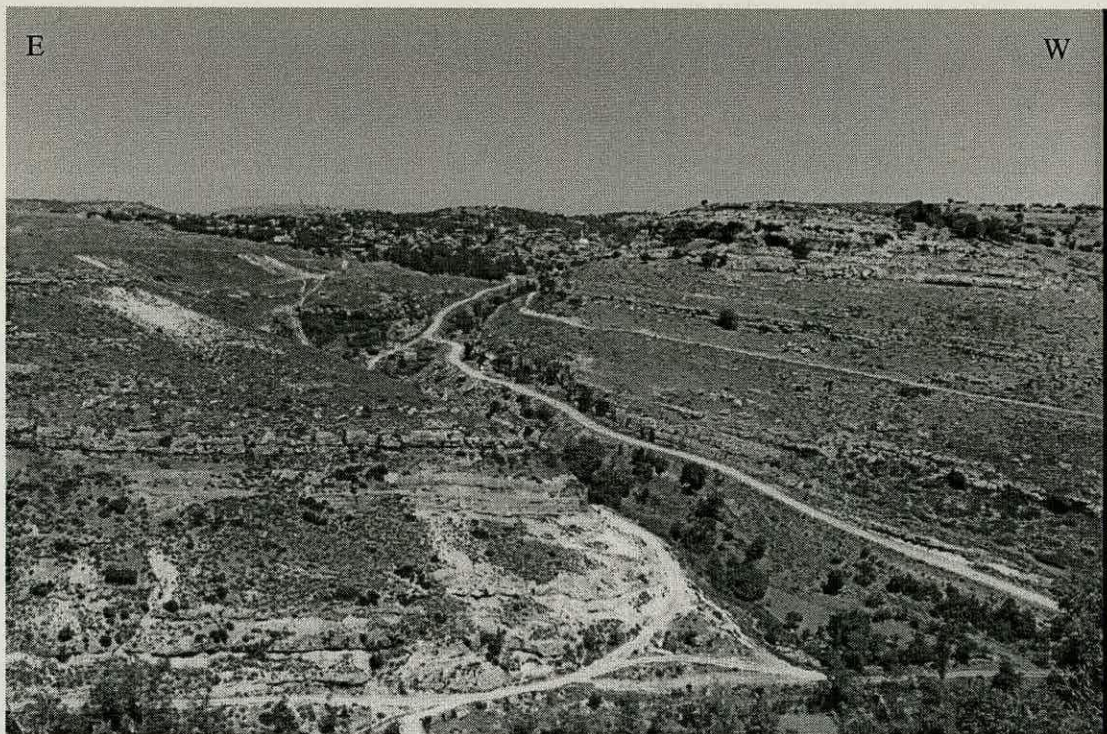


Figure 4.21. Photograph showing view towards Kozkalesi village showing the lower part of the Sofular Formation; note the rhythmic nature of the hard limestone beds.



Figure 4.22. Photograph showing the top of the Sofular Formation and the overlying Nurzeytin Formation, far hillside. Note that compared to the previous photograph there are fewer soft weathered beds and the formation is dominated by hard limestone.

Higher in the sequence the sediments become more uniform in composition; the mudstone and conglomerate horizons (lithologies A and D) then decrease in frequency until eventually none are present and the limestone is more homogeneous. The limestones are muddy, with a high bioclastic component, including whole and fragmented bivalves (e.g. *Ostrea*, *Glycymeris* sp.) gastropods (e.g. *Conus* sp.), echinoids and abundant oncolites (SB20.3). Beds are massive (1-5m thick), with transitional contacts.

At the top of the logged section there is 10-15m thick interval of marly limestone, interbedded with a poorly exposed lithology, possibly marl. Above this interbedded section there are no further exposed limestone beds. The last bed of thick limestone defines the top of the Sofular Formation (Fig 4.22).



4.2.5.2 Harbiye Gorge and surroundings (2).

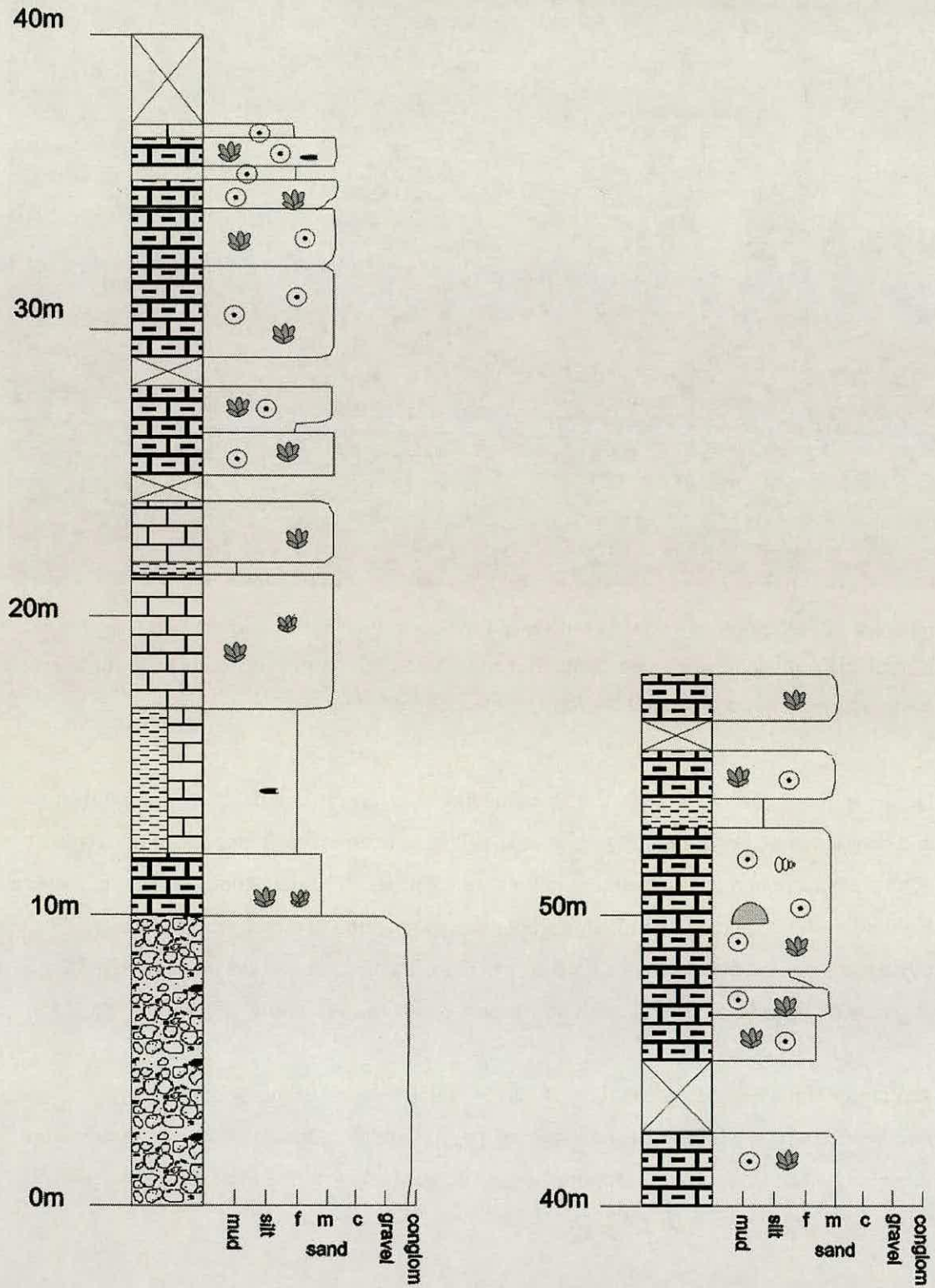


Figure 4.23. Log of the Sofular Formation exposed along the Harbiye Gorge, see Fig. 4.11 for the location of the log.

The Sofular Formation is exposed at the top of the sequence exposed within the Harbiye Gorge. The thickness of the formation is rather variable in this area with ~10m of this formation being exposed on the southern side of the gorge, but reaching ~60m in the north. The basal contact is poorly exposed. Basal sediments are interbedded marl and marly limestone (wackestone/packstone); beds are ~25-50cm thick. These sediments are fossiliferous with bivalves, echinoids, and gastropods present; large *Ostrea* are only present in the lowermost beds.

Upwards, the marl beds decrease in frequency and the limestone becomes harder and less marly. Bedding thickness increases to metre-scale. There is an increase in oncolitic material upwards; other fossil material is also present and there is much bioturbation (e.g. horizontal and vertical burrows).

#### 4.2.5.3 Antakya Sub-basin (3)

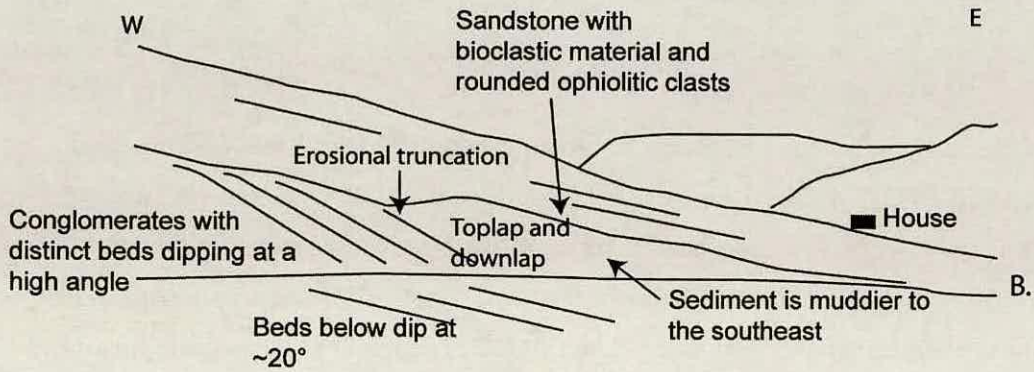
Nodular bioclastic limestone (packstone-rudstone) is exposed in the Antakya sub-basin at location 486 (0247333/4009509 Fig. 4.18), this contains plentiful fossil material, for example echinoids, oncolite, large benthic foraminifera, bivalve fragments (including *Ostrea*, *Cypraea* (Cowry), *Glycermyeris* sp., *Pectinids*), gastropods and scaphopods. This limestone is interbedded with grey calcarenite (SB43.3) and marl. The bioclastic limestone coarsens upwards; well-rounded pebbles <4cm in size start to appear along with large *Ostrea* that can reach 20cm length.

The nodular limestone beds have an average dip of ~20°, at 0246923/4009602, these beds are directly overlain by beds dipping ~35° that down-lap onto the underlying conglomerate and oyster bed. These steeper beds are composed of very coarse-grained orange sandstone to conglomerate (clasts <3cm in size, sub-angular to rounded). They are poorly sorted, occasionally beds appear to be normally graded (Fig. 4.24).

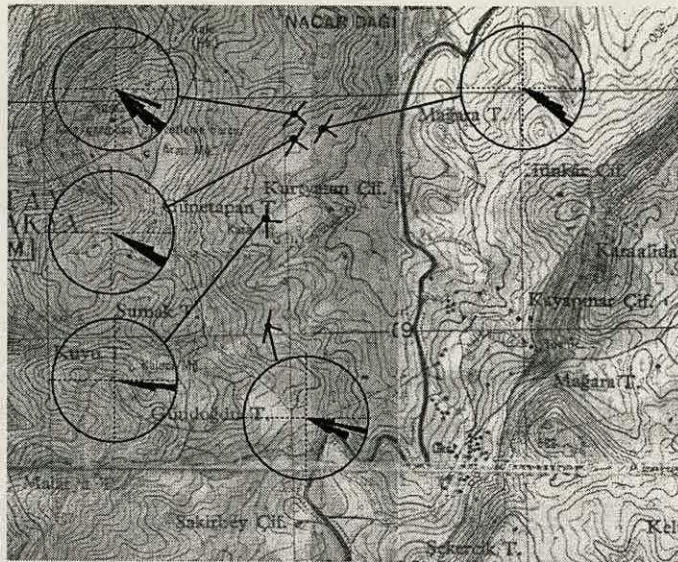
At the top of this unit the steeply dipping beds (foresets) curve to become subparallel with the overlying beds, which dip at ~20°. These overlying beds are composed of very coarse sandstone to pebbly sandstone (clasts <5cm, rounded). Clasts are composed of ophiolite and bioclastic limestone; bivalve and coral fragments are also present. The sediments fine upwards away from the boundary into pebbly mudstone.



A.



B.



C.

Figure 4.24. Map and photographs showing the geometry of the features observed at location 486. Top photograph of exposure; middle field sketch illustrating main features; bottom rose diagrams showing variation in dip direction of foresets around locality.

4.2.5.4 *Gökçegöz (4).*

At this location there is ~6m of Middle Miocene sedimentation. Above the Balyatağı Formation conglomerates, 2m of pale cream, medium-grained calcarenite is exposed. Within this bed are pebble horizons; pebbles are <3cm in size. Shell fragments, horizontal burrows and rip-up clasts are also present. The upper bedding surface is rippled.

Above this sandstone horizon there are several bioclastic limestone beds, rich in bivalve, gastropods, echinoids, coral, oncolite and surpulid worm tubes. Horizontal burrows are present near the base of one bed.

4.2.5.5 *Asi Nehir (5).*

Three locations on the Asi Nehir warrant a full description. On the north side of the Asi at 0223550/3996343 the Middle Miocene sequence overlies serpentinite. The base of the sequence is a thick red conglomerate. The clasts are 100% serpentinite derived, angular to sub-angular and clast supported, with apparently no bedding.

Above these coarse clastic sediments are several metres of very fine-grained mudstone and lime mudstone. The mudstones are pink and white-mottled with wavy laminations and occasional small lenses of sandy material. The limestones are also very fine-grained with irregular bedding surfaces. The beds are variable from a couple of centimetres to 1m in thickness.

Above the thinly bedded mudstones, very fine-grained limestone (**SB52 & SB53** mudstone Dunham) beds 50cm-2m thick, form a sequence >40m thick. The beds are irregular, often laterally discontinuous, and contain laminations and ripples. Bedding thickness varies from 5-50cm. Near the base of the limestone sequence there are three horizons of reddish brown mudstone that are very irregular in thickness and exhibit irregular laminations.

The basal sediments are again observed at location 183 (0234571/3996220). A thick basal conglomerate unit overlies the ophiolite (> 5m thick). Above, are fine-grained sediments ~8m thick, composed of pink-white nodular lime mudstones, brown mudstone with desiccation cracks and thin interbeds of nodular chalk and rippled cream mudstone. Upwards, this passes into fine-grained lime mudstone, as described above.

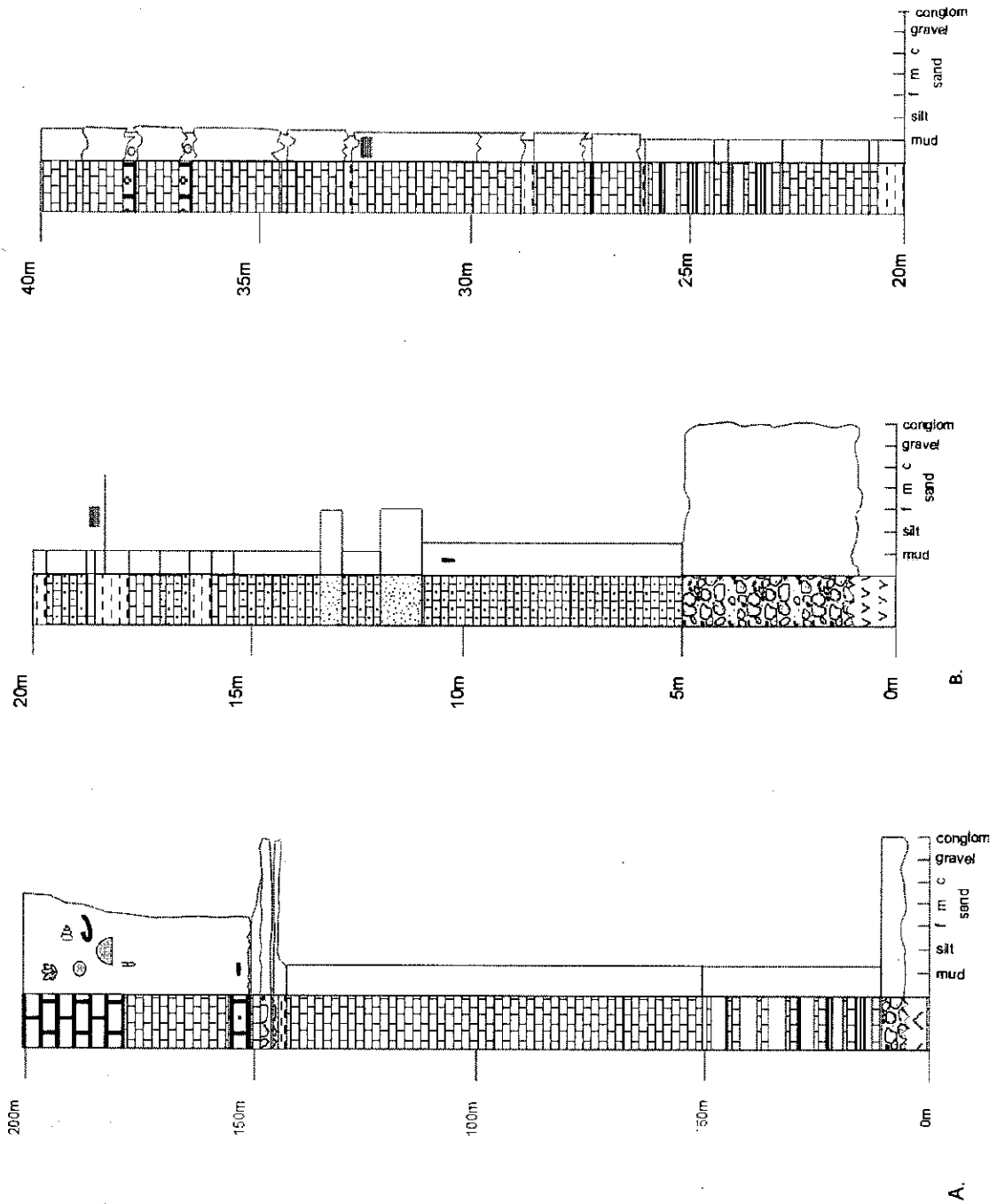


Figure 4.25. Logged section from the north side of the Asi Nehir (5). A. Is a composite log for the entire sequence. B. Shows the basal 40m in greater detail.



Figure 4.26. Photo of the fine-grained facies observed above the conglomerates along the north side of the Asi Nehir. 5m of section shown here. In the top right harder white limestone can be seen. Hammer circled for scale.



Figure 4.27. Photograph of two palaeosol horizons observed near the base of the limestones. Hammer circled for scale.



Figure 4.28. Photograph of the fine-grained sediments seen at the base of the sequence on the southern side of the Asi Nehir. GPS for scale.

The upper part of the sedimentary succession in this area is exposed further north (0235097/3998128). The base of this sequence is composed of the fine-grained lime mudstone, with algal laminations, occasional small gastropods and fenestral porosity. The upper contact of this lithology is bored and there is an angular discordance with the overlying beds (a few degrees). Above this disconformity the sediments exhibit an increasing clastic component. Fine- to coarse-grained calcarenites are interbedded with clast-supported conglomerate horizons of sub-angular to sub-rounded serpentinite clasts (up to 40cm in length) and occasional thin beds of mudstone and carbonate. The sandstones are rich in shelly material (e.g. gastropods, bivalves, echinoids, benthic foraminifera). Sedimentary structures are rare but horizontal laminations were observed. The lower part of this sequence is more variable; upwards, the lithologies become more uniform in nature.

Similar lithologies are exposed at Yesilyazı köyü (0233660/3996810), where there is a small exposure of calcarenite, conglomerate and mudstone that pass upwards into marly wackestone with a large bioclastic component, very similar to Kozkalesi and Çevlik.

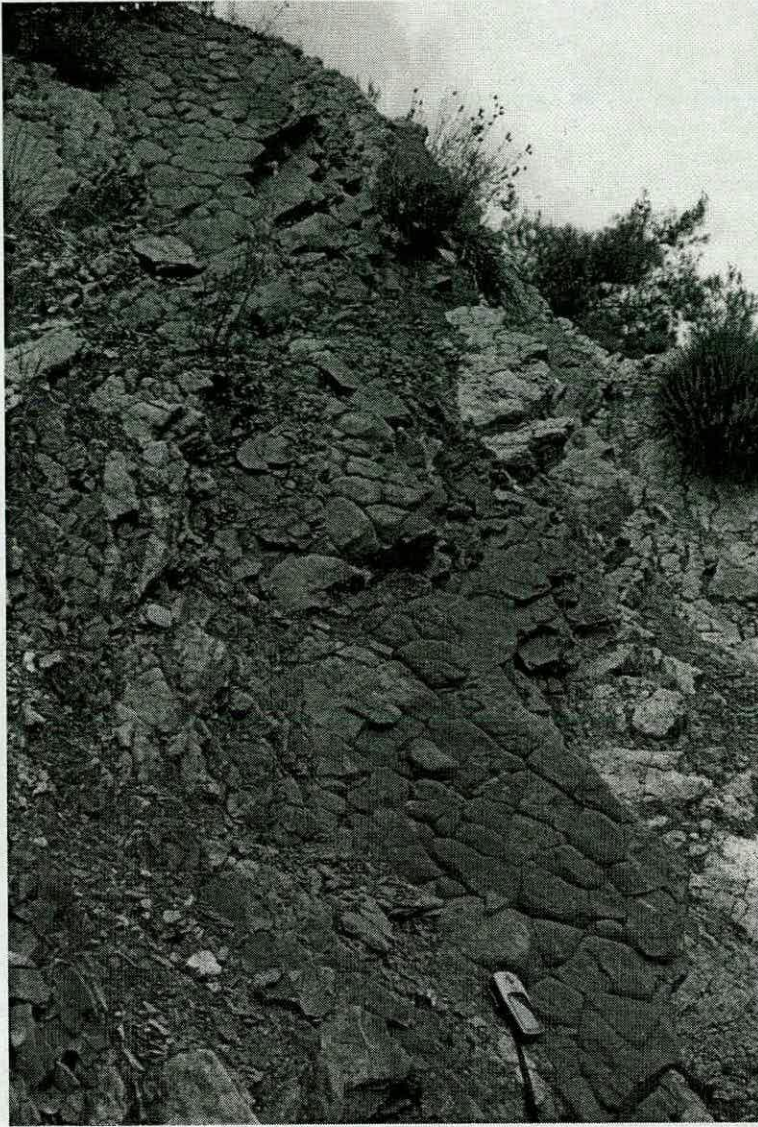


Figure 4.29. Photograph showing desiccation cracks on the top surface of a bed at the same location as Fig. 4.28.





Figure 4.30. Photograph of the unconformity surface showing boring on the contact.



Figure 4.31. Photograph of conglomeratic horizons in the sediments above the unconformity. Hammer for scale circled at the bottom.

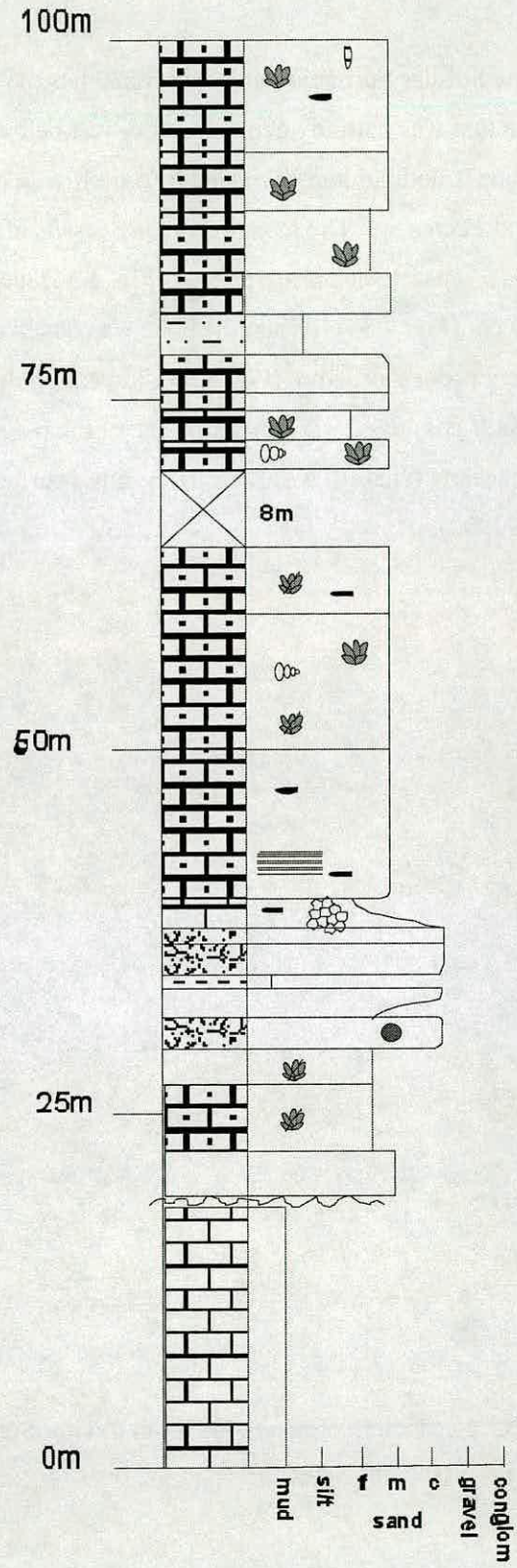


Figure 4.32. Log of the section described above and shown in the photographs.

## 4.2.5.6 Location 230

The bedding surface of the Sofular Formation at location 230 has the appearance of a hardground (i.e. a horizon that was partially cemented at or just below the sediment-water interface) in that the surface is nodular and encrusted by a multitude of whole bioclasts, mostly large echinoids and *Pecten* sp. The most interesting fossils at this location are a collection of bones; over 15 separate bones are present (Fig. 4.33) including large vertebrae that measures 30 cm x 19 cm (Fig. 4.34). When the bone was observed in thin-section it conclusively showed a very porous structure (Fig. 4.35), indicating these would have been very light bones. This factor combined with the large size of the bones indicates that they are probably that of a Cetacean (Whale). A similar hardground surface can be observed at location 14 (0231350/3992900).

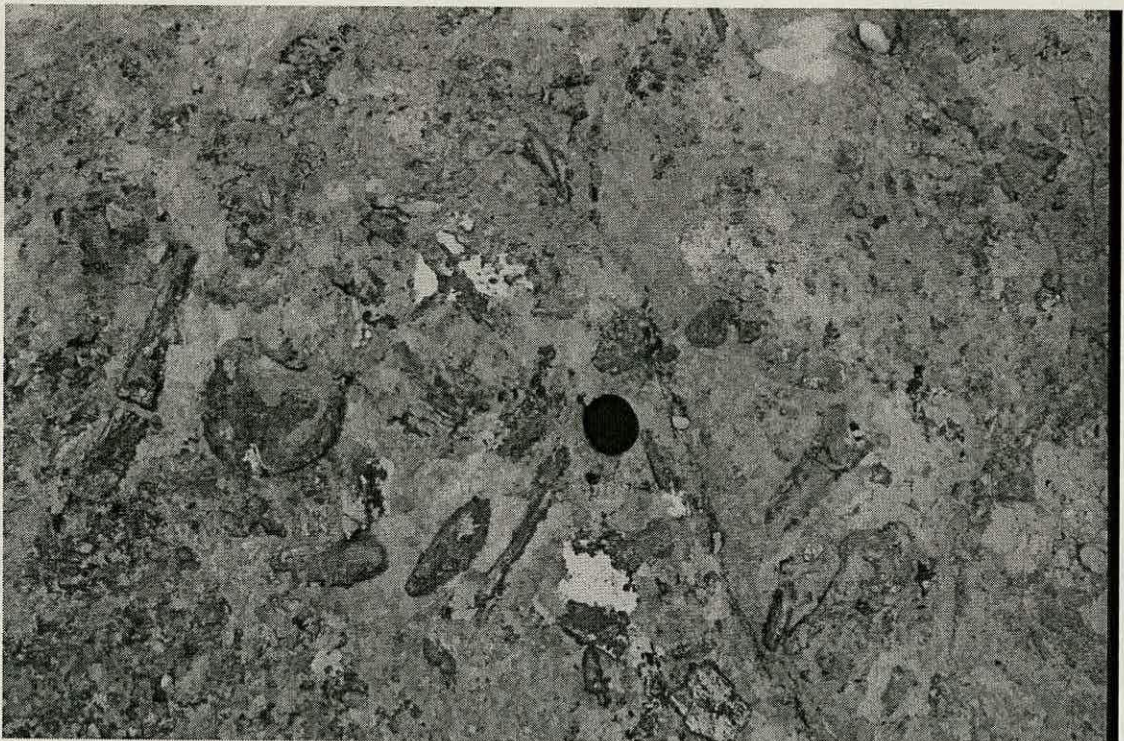


Figure 4.33. Photograph of a collection of bones found on the hard-ground surface at location 230, note that they are disarticulated.



Figure 4.34. Photograph of the large vertebrae that measures 30x19cm.

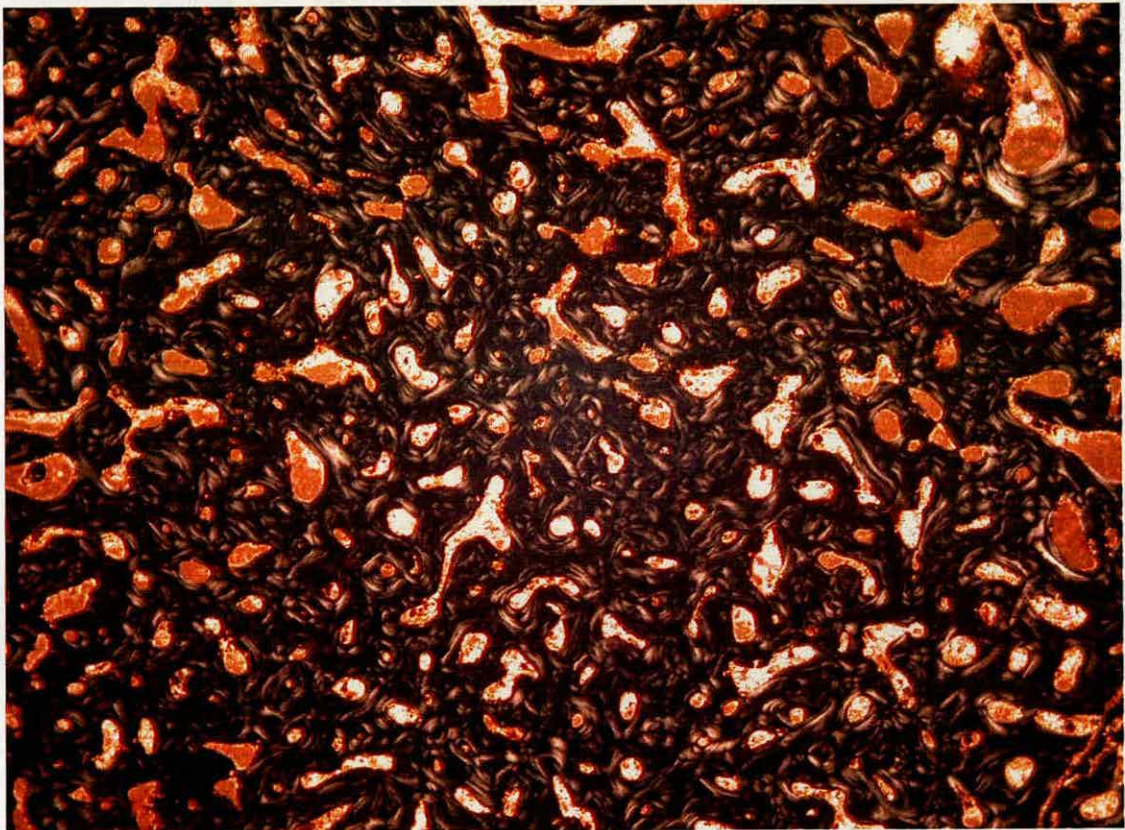


Figure 4.35. Photomicrograph of the bone under cross-polarised light, field of view is 5mm.

4.2.5.7 Çevlik (6).

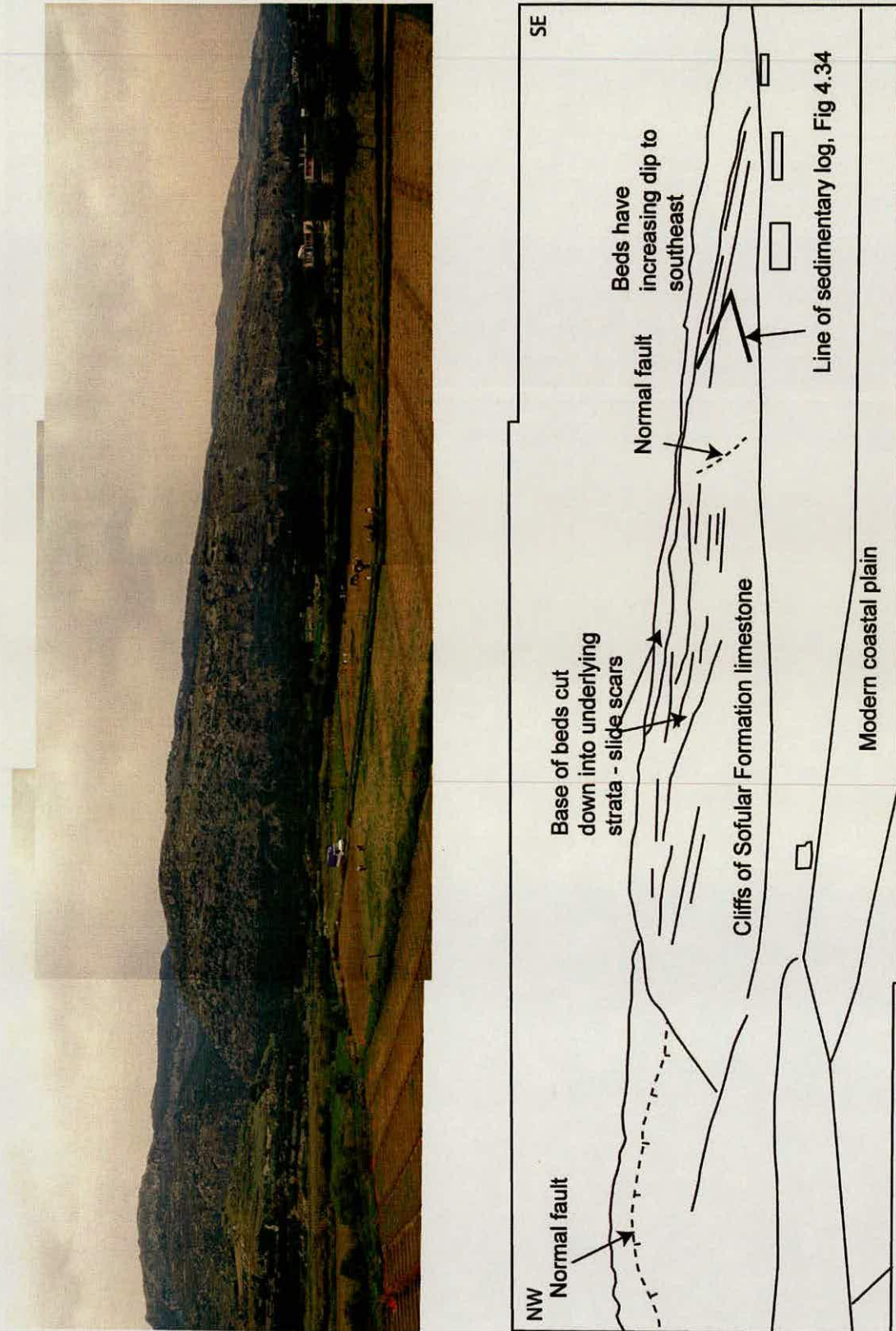


Figure 4.36. Photo montage showing exposure along cliff east of Çevlik. Logged section in Figure 4.37.

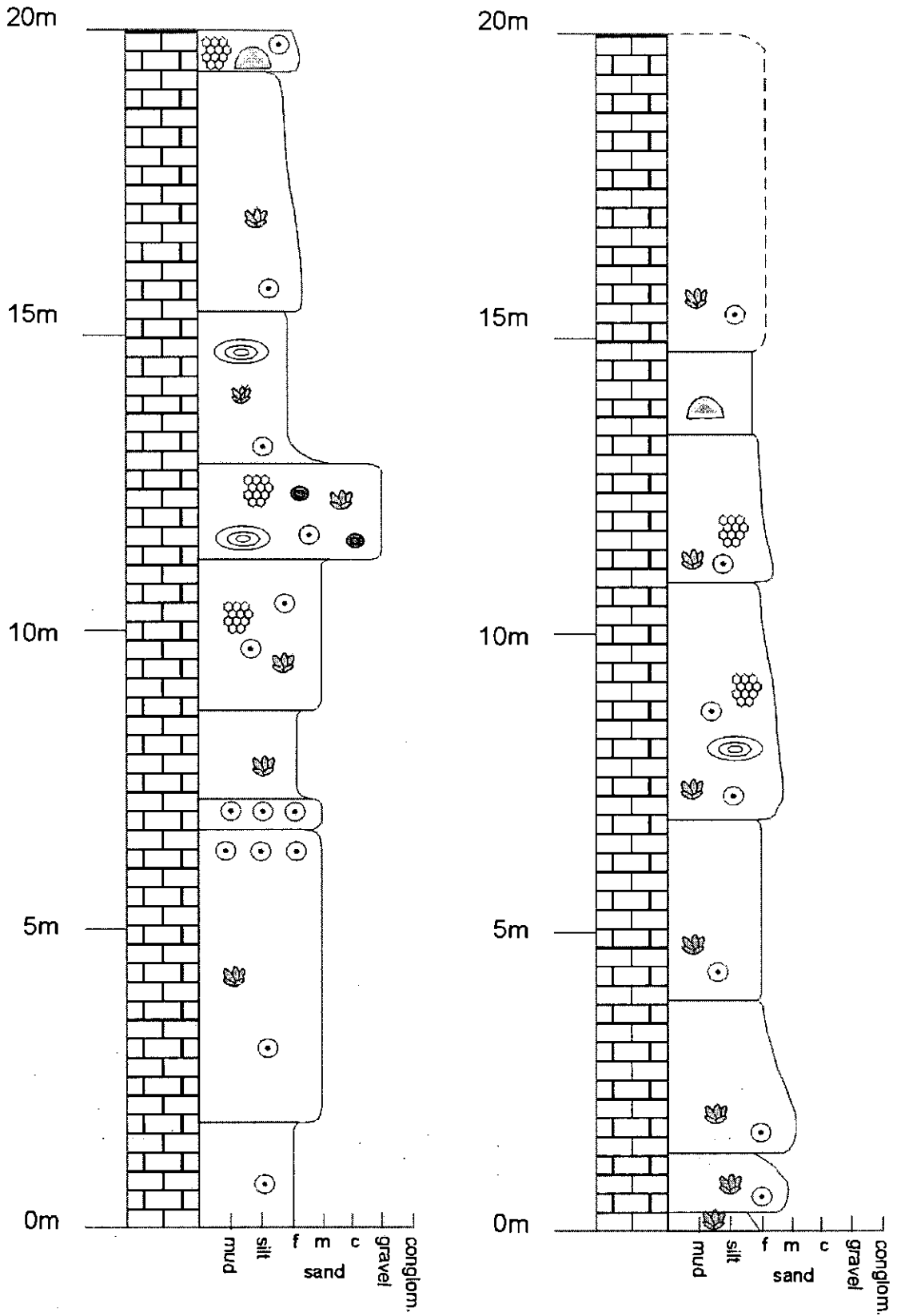


Figure 4.37. Log of cliff section, position of log shown in Figure 4.36.

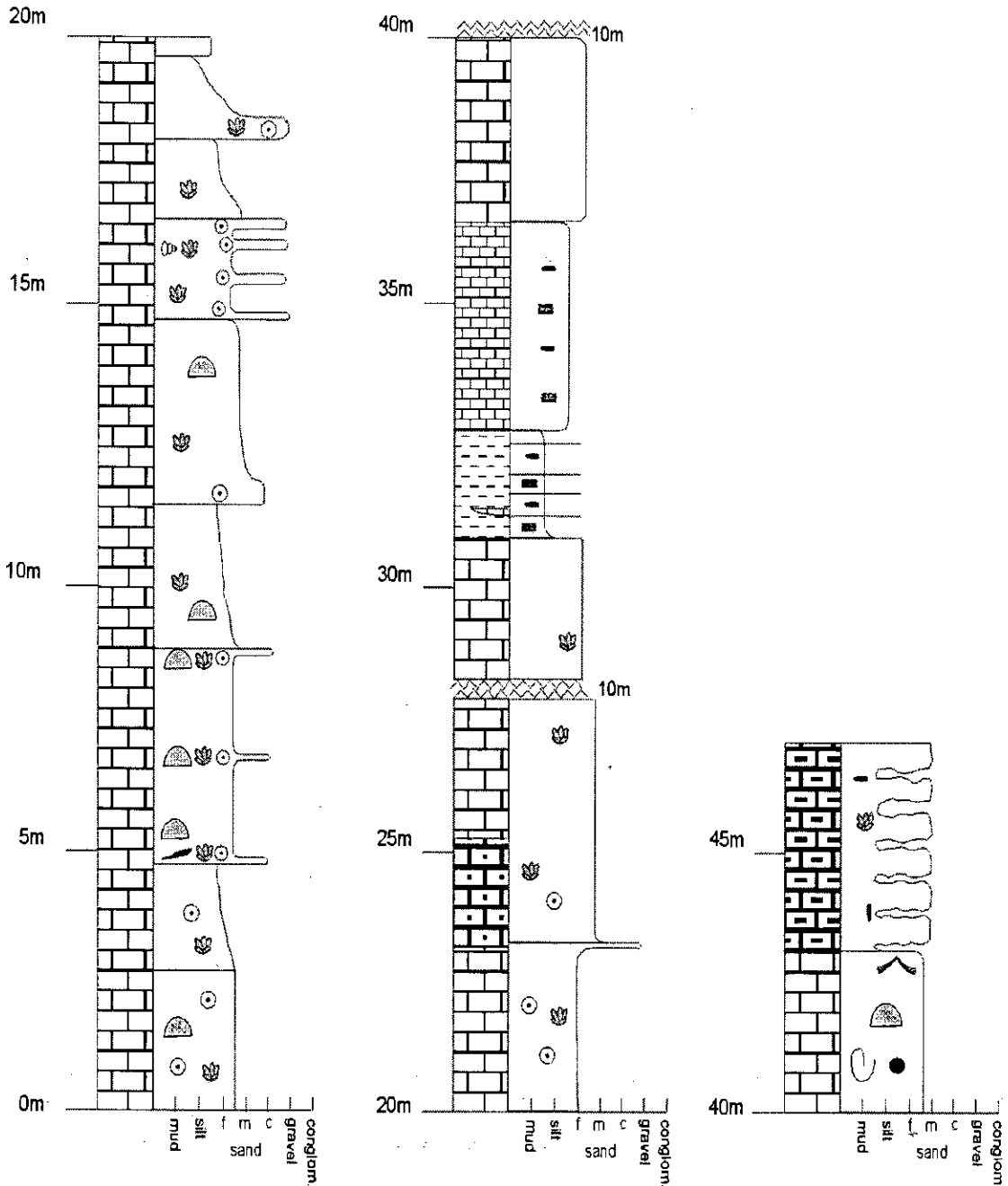


Figure 4.38. Composite section from two localities exposed west of the town of Çevlik along the coast.

Limestones are exposed around the coastal town of Çevlik. A cliff exposure at 0764250/4001300 shows large-scale erosional surfaces (Fig. 4.36).

The lithology is rather uniform, marly limestones (wackestone **SB49**), 1-5m thick, with a substantial bioclastic component of algal material (oncolites), benthic and planktic foraminifera, echinoids, bivalves (including oysters), crinoids, gastropods and coral. The

beds show evidence of intense bioturbation, including *Ophiomorpha* and *Planolites*. At the top of the cliff section the limestone is capped by a poorly exposed marl/mud sequence.

At Çevlik, the limestone sequence is faulted but good exposures of the base and top of the limestone sequence can be observed locally (Fig. 4.38). The base of the limestone is exposed on the coast at 0763100/4001375, where coarse bioclastic wackestone overlies serpentinite; however, the actual boundary is not exposed.

Upper beds of the Sofular Formation can be observed at 0763768/4001584. Bioclastic wackestone is interbedded with marl beds that are laminated and rippled. Rip-up clasts of marl are found in some of the harder unlaminated beds. Above, there is a regular repeating sequence of bedded marl and marly limestone; beds are ~50cm thick and bedding surfaces are very irregular. There are abundant chert nodules, apparently infilling vertical burrows. A dewatering pipe ~1.5m long was also observed (Fig. 4.39).



Figure 4.39. Photograph of the dewatering pipe (centre), position of pipe ~43m in logged section shown in Fig. 4.39.



## 4.2.5.8 Kesecik (7).

The thickness of the Sofular Formation decreases from ~150m at Çevlik to less than 20m near the village of Kesecik, at location 210 (0238982/4015161). The base of the formation is conformable on the underlying Lower Miocene succession and is composed of rubbly wackestone-packstone containing bivalves (fragmented and whole, e.g. *Pecten* sp. *Mya* sp.), gastropods (e.g. *Conus* sp., *Architectonica simplex*), echinoids (e.g. *Opissaster polygonalis*), coralline fragments, other shelly material and rounded ophiolitic pebbles. Stratigraphically above this packstone is coralline rudstone, 5-10m in thickness; this limestone is not conformable with the underlying succession and has an asymmetric dome-like morphology (Fig. 4.40). This is overlain by 2m of packstone-rudstone mainly composed of fragments of coralline algal and bivalves. Benthic and planktic foraminifera are also present.

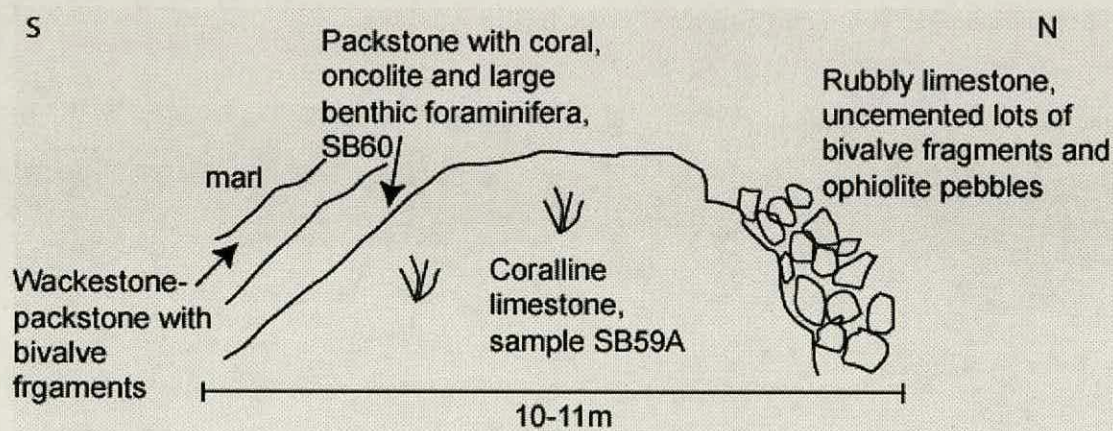


Figure 4.40. Field sketch of location 210 showing asymmetric shape of the coralline build-up and the different lithologies present.

At an exposure along strike to the southwest of location 210 (at 0238686/4015181) (Fig. 4.41), reddish-brown, pebbly sandstone and conglomerate beds overlie the Lower Miocene succession. Bed thickness is variable, some beds are lenticular and thickness is <1.5m. Clasts are sub-angular to sub-rounded, <20cm in size, and dominated by ophiolite, although micrite and conglomerate clasts are also present. The coarse to pebbly sandstone beds are cross-bedded. The top of this exposure is white rudstone, ~1.5m thick, dominantly composed of coral fragments.

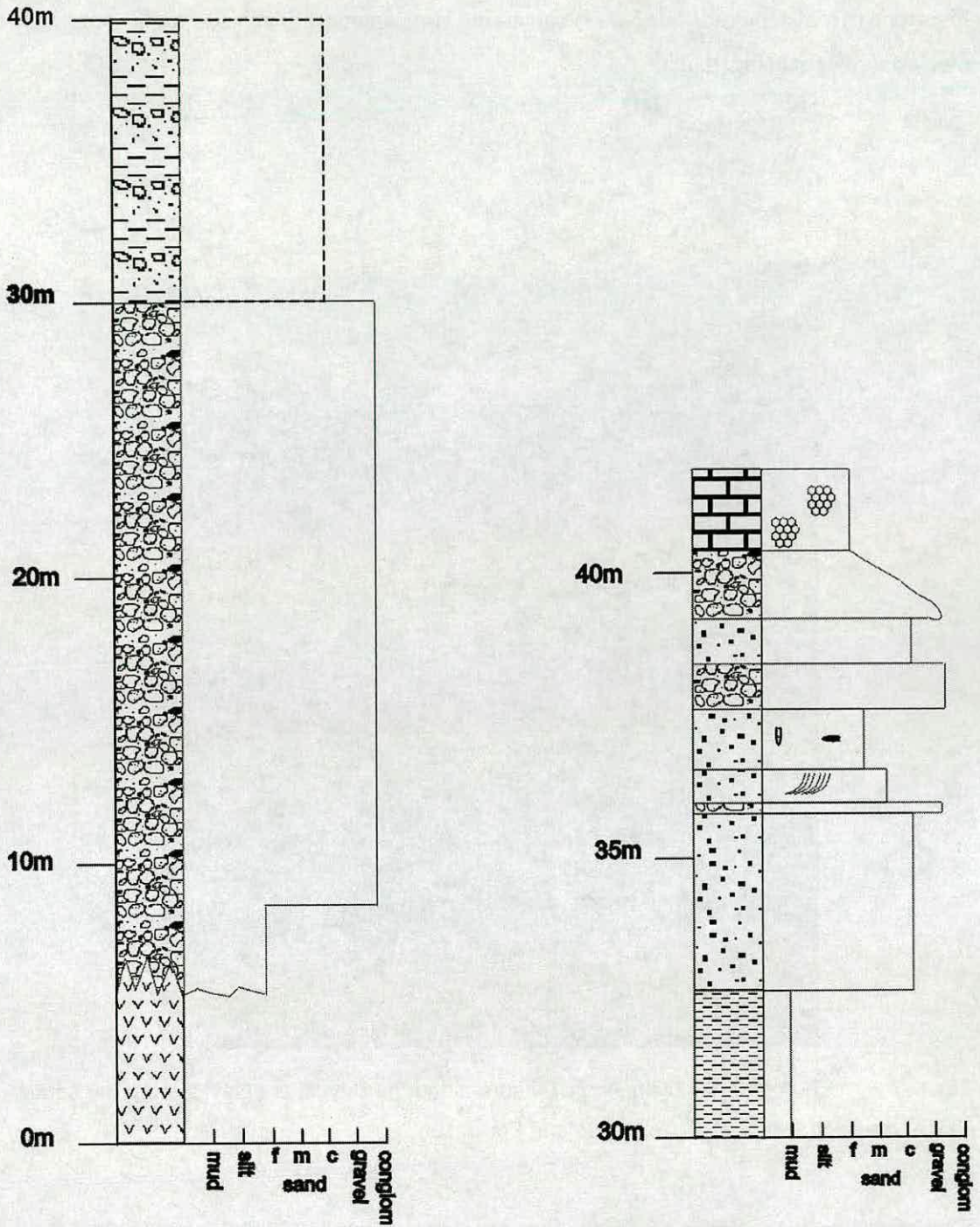


Figure 4.41. Log of the section described above at location 210.

4.2.5.9 *Other exposures along the northern basin margin*

The Middle to Upper Miocene succession is exposed along the Büyükkara Çay (0231300/4006059). The Middle Miocene here is composed of thick beds (>50cm) of marly

limestone (floatstone/rudstone **SB49**) containing large amounts of coarse fragmented bioclastic material (Fig. 4.42).

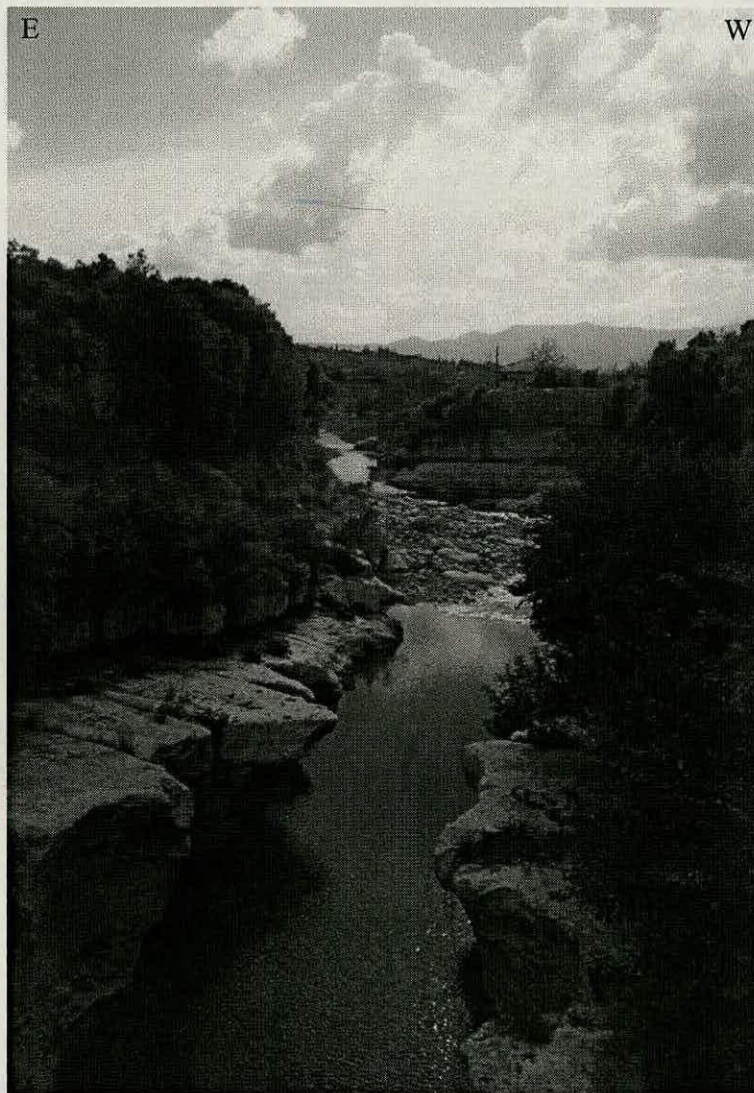


Figure 4.42. Photograph showing the exposure along the Buyukkara Cay, view to the south. Thick limestone beds belong to the Sofular Formation.

Two other localities warrant a brief description. At location 385 (0768889/4004132), distorted bedding planes were observed within an otherwise undeformed sequence of bioclastic limestone (Fig. 4.43). At location 482 (0769542/4004564), hummocky cross-bedding was observed within hard wackestone, which is interbedded with marl (Fig. 4.44).



Figure 4.43. Photograph of the disrupted bedding at location 385. Beds to the right have been pushed over those to left (southwest). Hammer for scale circled.



Figure 4.44. Photograph of the hummocky cross-bedding observed at location 482.

#### **4.2.6 Summary – Sofular Formation**

The Sofular Formation unconformably overlies the Balyatağı Formation in the north of the study area and overlies the Kılıdağ Ophiolite to the south along an erosional surface.

At Kozkalesi, the basal contact of the Sofular Formation consists of interbedded mudstone, bioclastic limestone and conglomerate that contain bioclastic material and rounded limestone clasts.

Along the Asi Nehir, the base of the succession is marked by a thick red conglomerate composed of ophiolite clasts, overlain by interbedded mudstone and limestone. Desiccation cracks and ripples were observed in these rocks.

At Kesecik, the basal sediments are coarse sandstones and conglomerates with cross-bedding. Elsewhere the basal sediments were generally coarse bioclastic limestone.

The middle part of the formation is dominated by either hard carbonate mudstone or coarse bioclastic wackestone-rudstone.

The upper part of the formation at Kesecik is marked by coralline limestone. In contrast, the upper part of the formation along the Asi Nehir is composed of interbedded bioclastic calcarenites and conglomerates, whereas at all other locations the top of the formation is marked by the uppermost bed of thick limestone before an interval of thinly interbedded marl and marly limestone.

### 4.2.7 Upper Miocene – Nurzeytin Formation: marl with calcarenites, limestones and conglomerates.

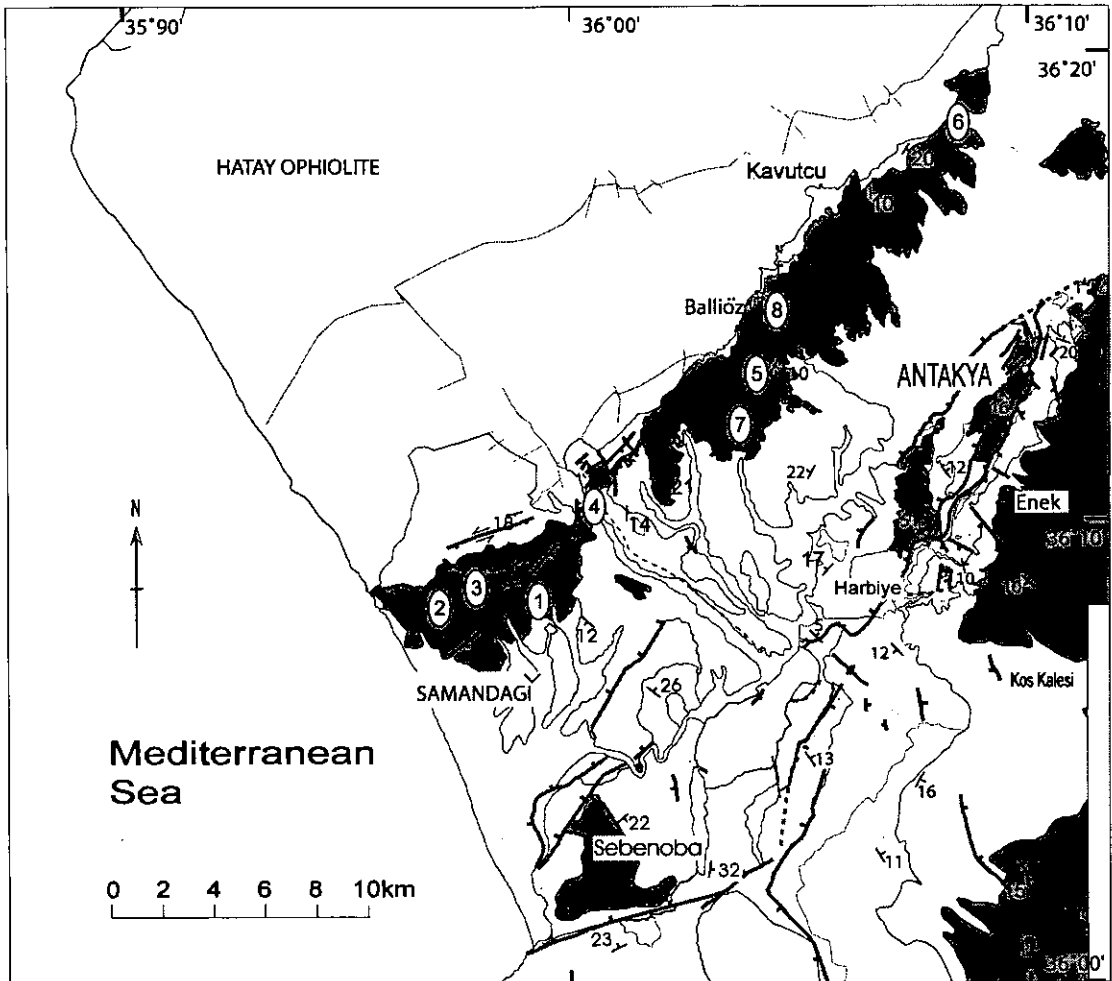


Figure 4.45. Outline map showing the outcrop extent of the Nurzeytin Formation (shaded in grey), numbers show the position of localities described in the text.

The Nurzeytin Formation is a thick, variable unit of marl with interbedded calcarenites, limestone and conglomerates. The formation has a wide outcrop extent and can be observed all over the field area. The upper levels of the formation is composed of the Vakifli Member, which is composed of gypsum and gypsiferous marl.

4.2.7.1 Nurzeytin (type location) (1).

conglomer

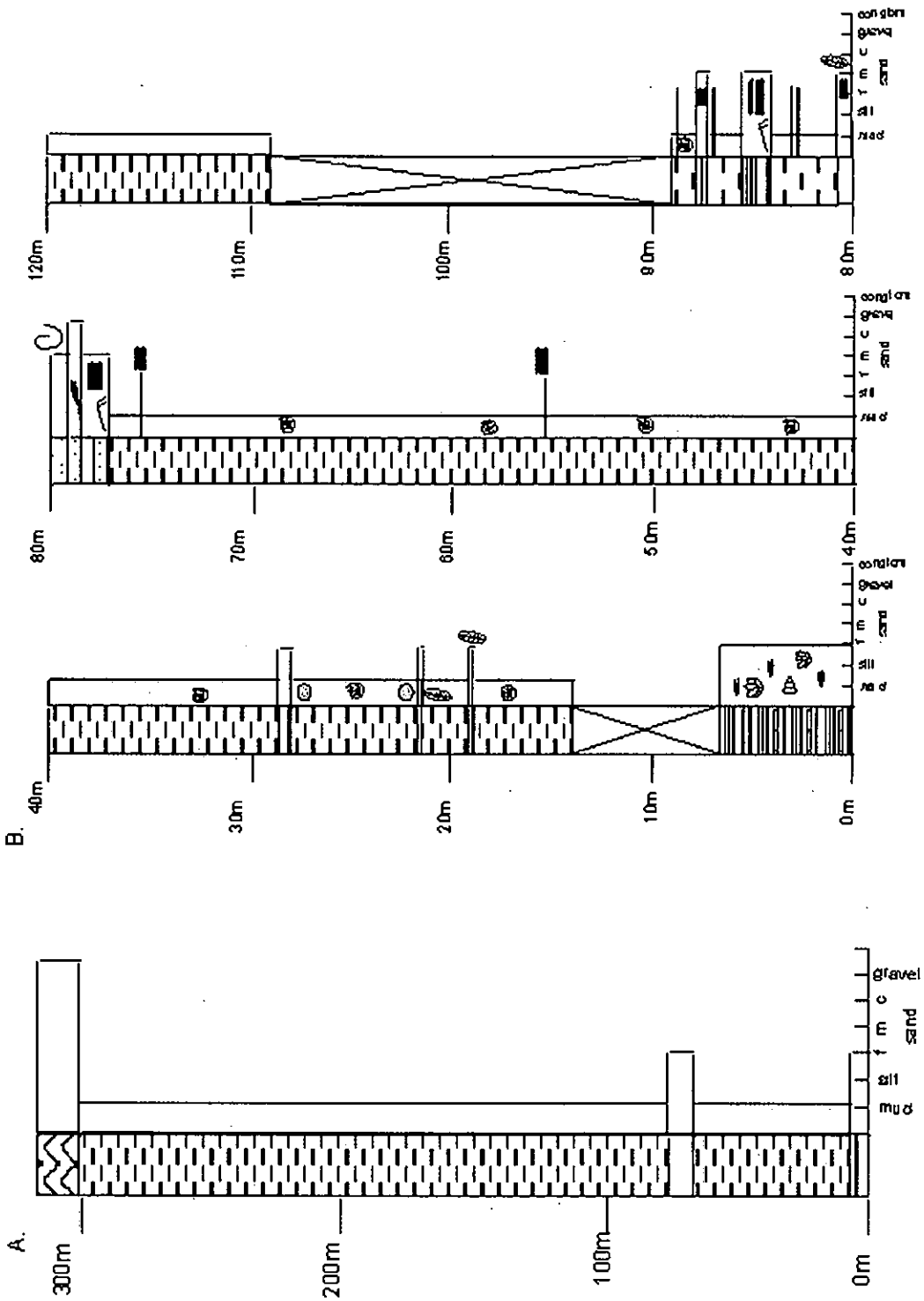


Figure 4.46. Log of the Nurzeytin Formation at the type location.

To the east of the village of Nurzeytin, there is a well-exposed succession as logged from 0769443/4003491 to 0230000/4002521. The base of the formation is not exposed in this location; the lowermost sediments observed are interbedded grey marl and grey lime mudstone. Beds are 30-130cm thick and fine upwards. The beds are bioturbated and horizontal burrows were observed; fragments of body fossils are also present and include bivalve and gastropod fragments as well as planktic foraminifera. These interbeds are replaced upwards after 10-15m by a dominantly marl lithology with only occasional interbeds. The marl is fine-grained and poorly exposed. Planktic foraminifera and plant material occurs within these beds.

Interbeds within the marl occur either singularly or in groups. Isolated interbeds, often calcarenites <1m thick, exhibit sharp bases and tops but lack sedimentary structures. Small iron-stained nodules were found in the underlying or overlying marl in some horizons. Interbeds occurring in packages tend also to be calcarenites, <50cm thick, with sharp bases, that then fine upwards and grade into a marl bed above (Fig. 4.46). Sedimentary structures such as parallel laminations, cross-laminations, ripple marks, flutes casts and rip-up clasts are present. Additionally a slumped horizon composed of marl, sandstone and chalk, 60cm thick was observed. The top of the logged sequence is capped by 10-15m of selenitic gypsum (see 4.2.9).

#### 4.2.7.2 *Thick limestone bed (2) and debris flow (3).*

On the northern margin of the graben at location 71 (0765081/4002244; 2 on Fig. 4.45), there is an exposure of limestone and marl, these are two thick (1.5m and >3m) calcarenite beds separated by a variable thickness of marl. These beds exhibit rare parallel laminations and rip-up clasts and also have erosive bases with flute casts. The palaeocurrent direction is to the southeast based on flutes and groove casts that are present on the base of the limestone beds. The limestone is unfossiliferous but planktic foraminifera are present within the marl.

In a field cutting at location 104 (3 on Fig 4.45), >4m of matrix-supported conglomerate (Fig. 4.47) is exposed. Clasts are sub-angular to sub-rounded, composed of marl, laminated marly limestone and nodular limestone; the matrix is of marl. Above the conglomerate horizon are several beds of thinly bedded calcarenite and marls. The calcarenite (packstone) is coarse-grained and bioclastic (bivalve fragments, benthic and planktic foraminifera,



gastropods); clasts of limestone are present but there is no ophiolitic material. This is, in turn, overlain by further conglomerate horizon.

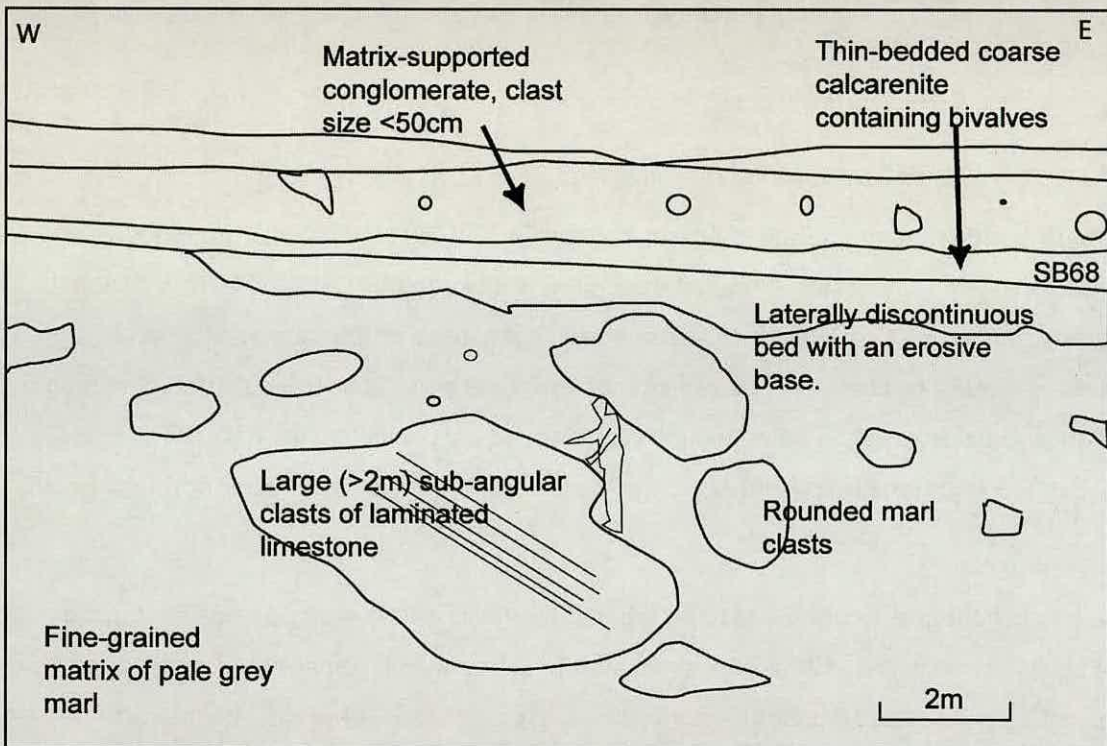


Figure 4.47. Photograph and field sketch of the large conglomerate horizon at location 104.

#### 4.2.7.3 *Büyükkara Çay (4).*

The Middle to Upper Miocene boundary is exposed along the Büyükkara Çay at 0231300/4006059 (Fig. 4.45). Upper Miocene sediments here are conformable on the underlying limestone (rudstone) and are composed of interbedded grey marl and grey limestone (mudstone). The beds grade upwards from the softer marl into harder limestone; the upper surface of the limestone is a sharp contact. Bed thicknesses are <1m. Fossils (bivalve and echinoid fragments) are found near the top of the limestone beds and the sediment is rich in planktic foraminifera. Trace fossils are common, on surfaces of beds and burrows into the bed, such as *Ophiomorpha*, *Thalassinoides* and *Planolites*. A cliff section marks the end of the exposure at 0231710/4005825, where a broad marl horizon appears to cut down into the underlying limestone bed.

#### 4.2.7.4 *Locations 140 and 141(5).*

Thick sandstone interbeds were observed in the Nurzeytin Formation at location 140 (0238087/4011348; Fig. 4.45). The location is composed of three thick litharenite beds (1.25-2.2m thick) separated by thinner (0.2-0.3m) marl and chalk beds. The litharenite is composed of angular to sub-rounded, poorly sorted grains and is clast supported; the grain size is 0.1-2mm (**SB79**). The litharenite beds have sharp erosional bases. Rip-up clasts of marl are found in layers within the thick beds but other sedimentary structures are absent. Occasional oyster shells are present. Similar beds are observed in other locations in the vicinity.

Thin beds (<20cm) of micaceous litharenite are interbedded with thin beds (<40cm) of marl and sandy marl at location 141 (Fig. 4.48). The sandstone beds exhibit sharp erosive bases and fine upwards from coarse sandstone to mud. The basal portions of beds are often structureless, but parallel laminations, cross-bedding and lamination are present in the upper part of the beds. Small carbonate nodules are present in some horizons. The sediments are rich in fossil material, bivalve fragments, planktic foraminifera and plant material. There is also much evidence of bioturbation.

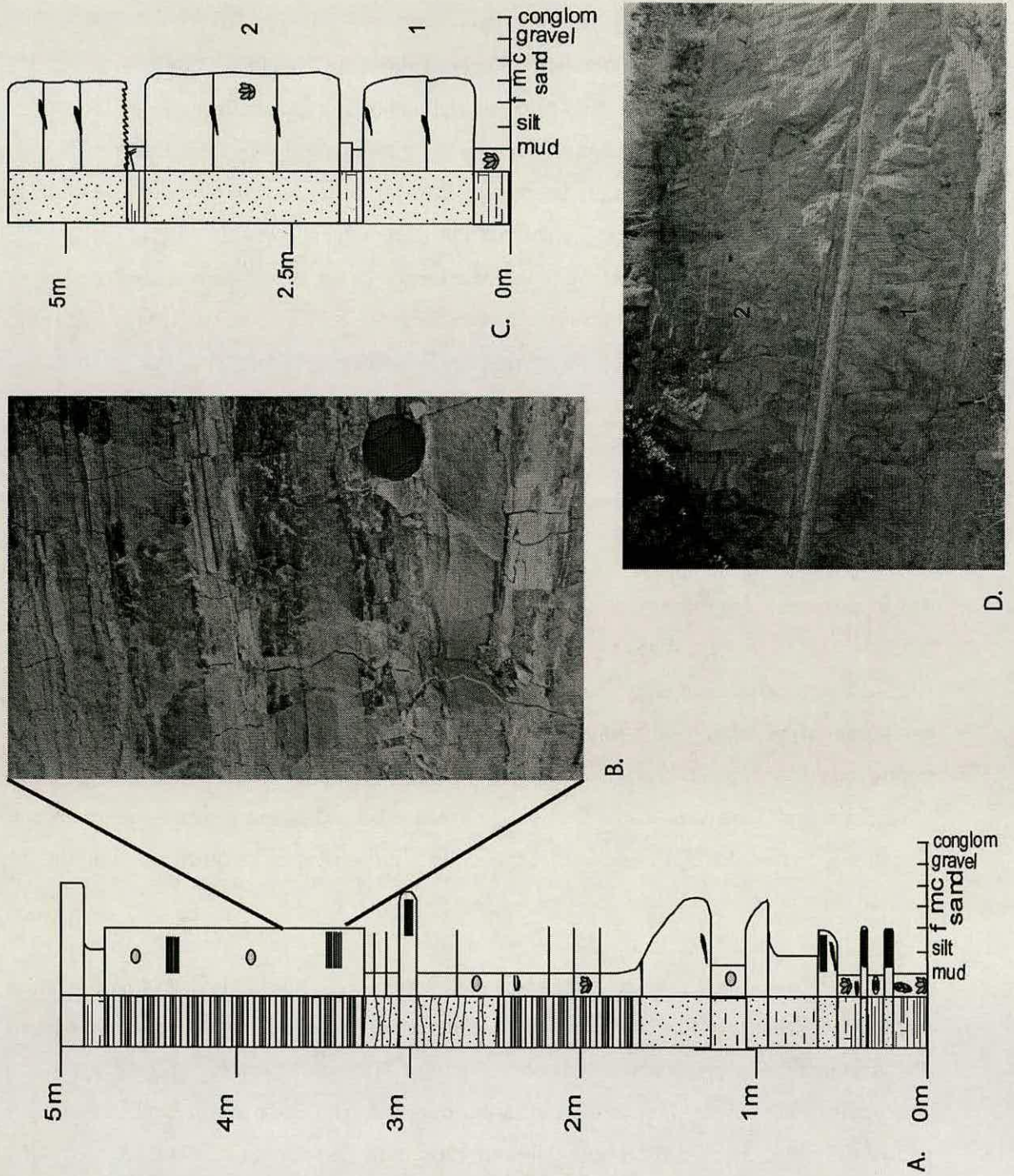


Figure 4.48. Logs of locations 140 (C) and 141 (A). Photograph of location 141 (B) showing thin bedded parallel laminated sandstone and photograph of location 140 (D) showing thick amalgamated sandstone beds (1 & 2) with thin marl beds in between.

4.2.7.5 Karaali (6).

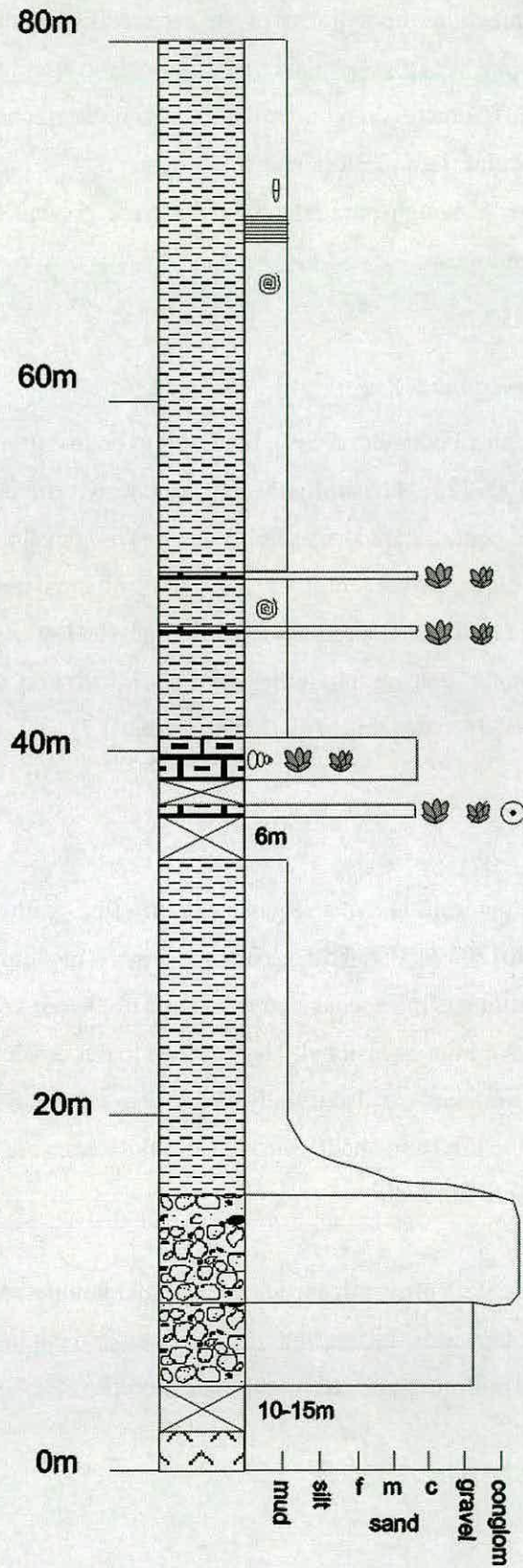


Figure 4.49. Log of the section at Karaali

Only 6m of bioclastic wackestones/rudstones are present along the Karaalı log (Fig. 4.49) for the Middle Miocene succession, the majority of the section is composed of Upper Miocene marls. These sediments are very fine-grained, grey and rich in fossil material (e.g. echinoid fragments, bivalves both fragmented and articulated). Some horizons are especially rich in fauna including large benthic foraminifera and small oysters. The marl is generally lacking in sedimentary structures although parallel laminations are present in some horizons and vertical burrows are common.

#### 4.2.7.6 *Northern sandstone (7).*

There is an exposure of thick bedded (1.5-2m), medium- to coarse-grained litharenite at location 189 (0237541/4007722). Generally this is very poorly cemented but cemented nodules are present. Bed contacts are sharp, and flute casts are developed on the base of some beds. Mud rip-up clasts are present in the basal parts of some beds. Shell fragments are also present and large oyster shells are scattered through the lower part of the section. Between the thick sandstone beds are thin horizons of marl, with very small bivalves and foraminifera. Sample SB50A dates this to Tortonian (Table 3.2).

#### 4.2.7.7 *Location 212 (8).*

Thick-bedded sandstone outcrops above a sequence of very fine-grained grey marls at location 212 (0239008/4012969) (Fig. 4.50). The sandstone is medium- to fine-grained and uncemented. The sandstone is micaceous and fragments of *Ostrea* shells are also present. The base of the beds is sharp but occasionally is observed to cut down into the underlying beds; the upper bedding surfaces are also usually sharp. Rip-up clasts of marl are observed near the top of some of the sandstone beds. Groove and flute casts are present, as are parallel laminations and cross-bedding

The interbedded marls are dark grey, micaceous and parallel laminated. Abundant plant material is also present. Upwards the marl interbeds die out and medium- to coarse-grained sandstone is interbedded with fine-grained muddy sandstone.

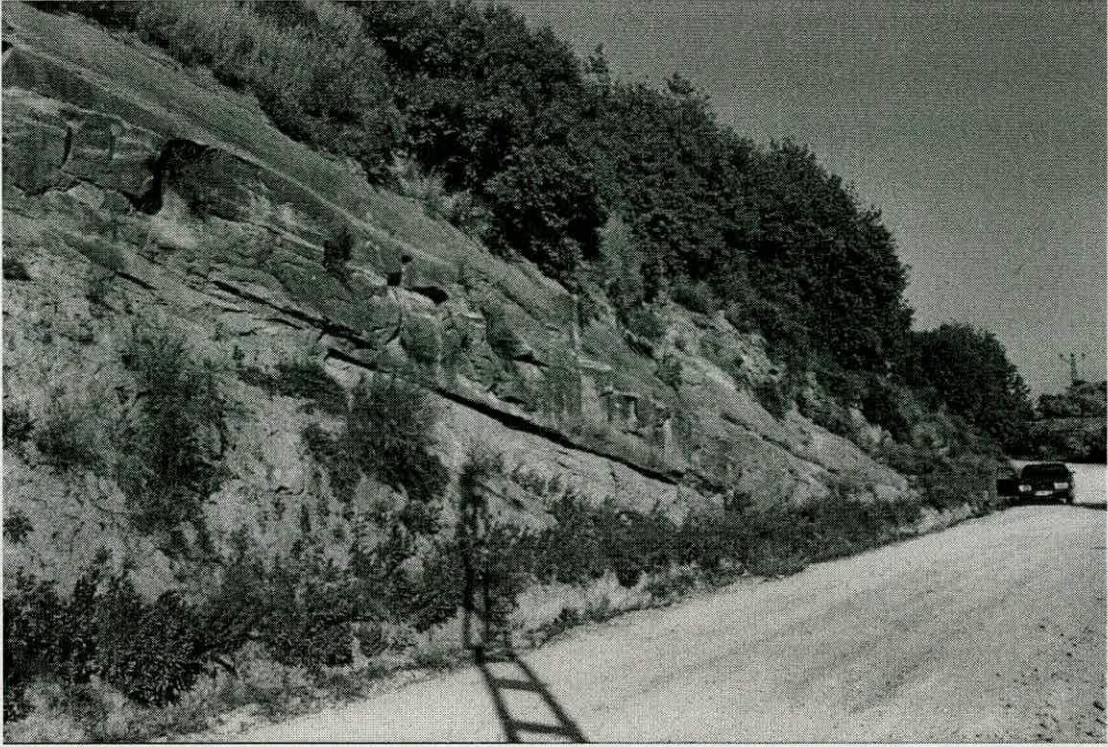


Figure 4.50. Photograph of section at location 212 near the village of Balliöz.

#### 4.2.7.8 *Palaeocurrent analysis*

Good palaeocurrent indicators are rare within this formation; however, at four locations measurements could be made, mostly from sole structures (Fig. 4.51; flute and groove casts). These show varied current orientations, with greater scatter as the numbers of measurements increase. The northerly exposures exhibit palaeocurrents flowing to the south and the west, whereas in the south the palaeocurrents indicate an easterly flow.

### 4.2.8 Summary of the Nurzeytin Formation

The Nurzeytin Formation is dominated by grey marl. The base of the formation is characterised by an interval of interbedded marl and limestone above the Middle Miocene Sofular Formation, with which the Nurzeytin Formation is conformable. Interbeds are common throughout the area. The composition of these beds varies; conglomerate, calcarenite and litharenite beds are all present. The top of the formation is marked either by the Vakifli Member composed of evaporates or alternatively, there is a conformable sequence from sandy marl into Pliocene sandstones.

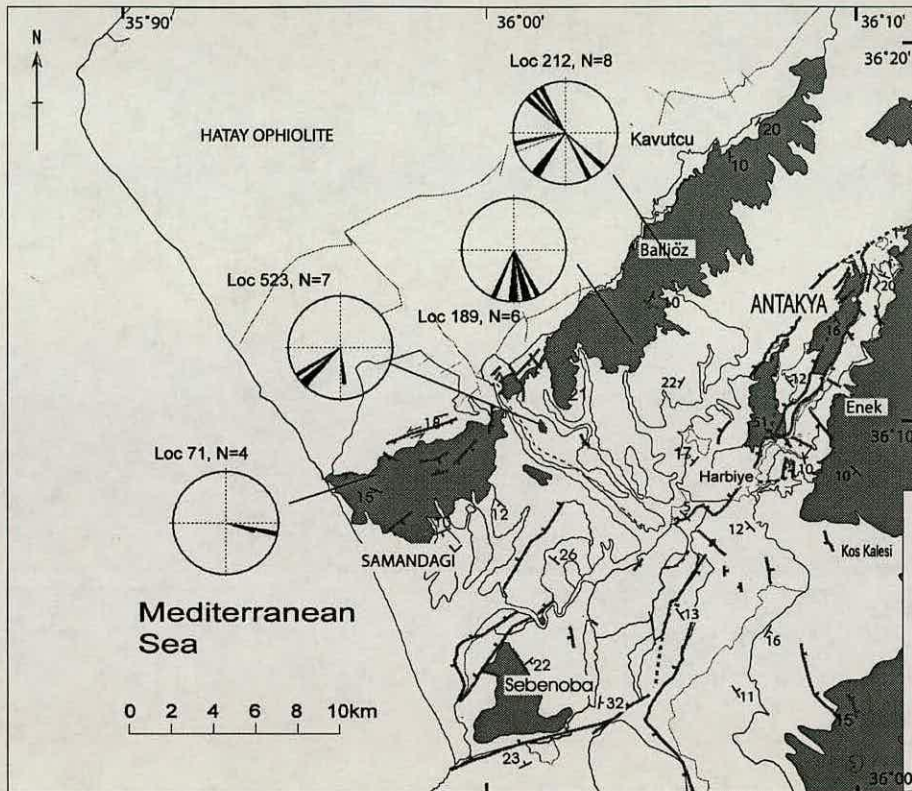


Figure 4.51. Palaeocurrent directions as recorded for the Nurzeytin Formation, location numbers and number of data given on map.

#### 4.2.9 Messinian – Vakıflı Member: evaporites.

The uppermost part of the Nurzeytin Formation is the Vakıflı Member, which is characterised by the presence of evaporite minerals. Four *in situ* evaporite localities are known in the Hatay Graben; three of these are near the axis of the modern basin and one on the southeastern flank of the basin (Fig. 4.52). The present altitude of gypsum ranges from 130m above sea-level (a.s.l) near the basin axis to 320m a.s.l (Fig. 4.52) on the southeast flank of the basin.

The thickest gypsum deposit (25m) is located near the village of Nurzeytin, the type location. The gypsum at this location is mainly composed of alabastrine (fine-grained) gypsum (location a; Fig. 4.53) that occasionally has dark laminae, which may be due to the presence of iron. This exposure includes large angular blocks (>2m) of laminated alabastrine gypsum set in a matrix of gypsiferous marl and sandy marl with caliche nodules; that are very soft and uncemented. The marl appears to drape the alabastrine blocks. In places, the

alabastrine gypsum is seen to have undergone diagenetic alteration to coarse selenitic gypsum.

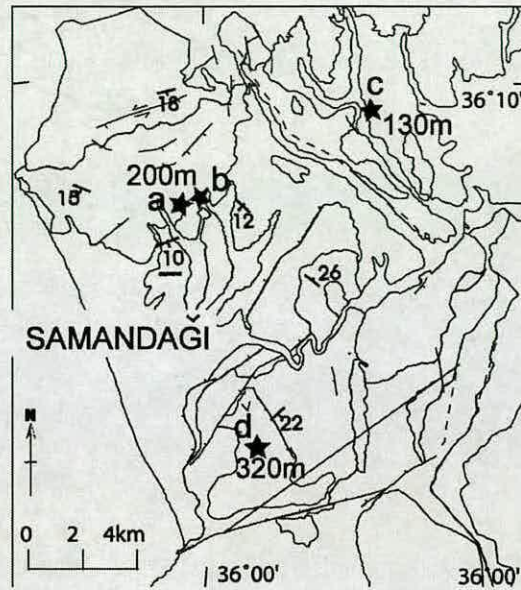


Figure 4.52. Map showing the location of Messinian evaporites.

The other sequences (5-10m thick) comprise coarse-grained selenitic gypsum (locations b, c, d; Fig. 4.49). Exposures b and c consist of massive selenitic gypsum. However, it is not clear whether this material represents primary gypsum or secondary gypsum. Location d, in contrast, consists of several exposures where a succession can be identified. The basal gypsum is made up of banded-stacked selenite, with repeated layers of selenite crystals, 1-5cm in size. The upper part of the sequence is composed of thick (>1m), massive fragmented selenite crystals, 5cm or more in size.

#### 4.2.10 Summary of the Vakıflı Member

This member is characterised by the presence of gypsum, either as alabastrine or selenite.



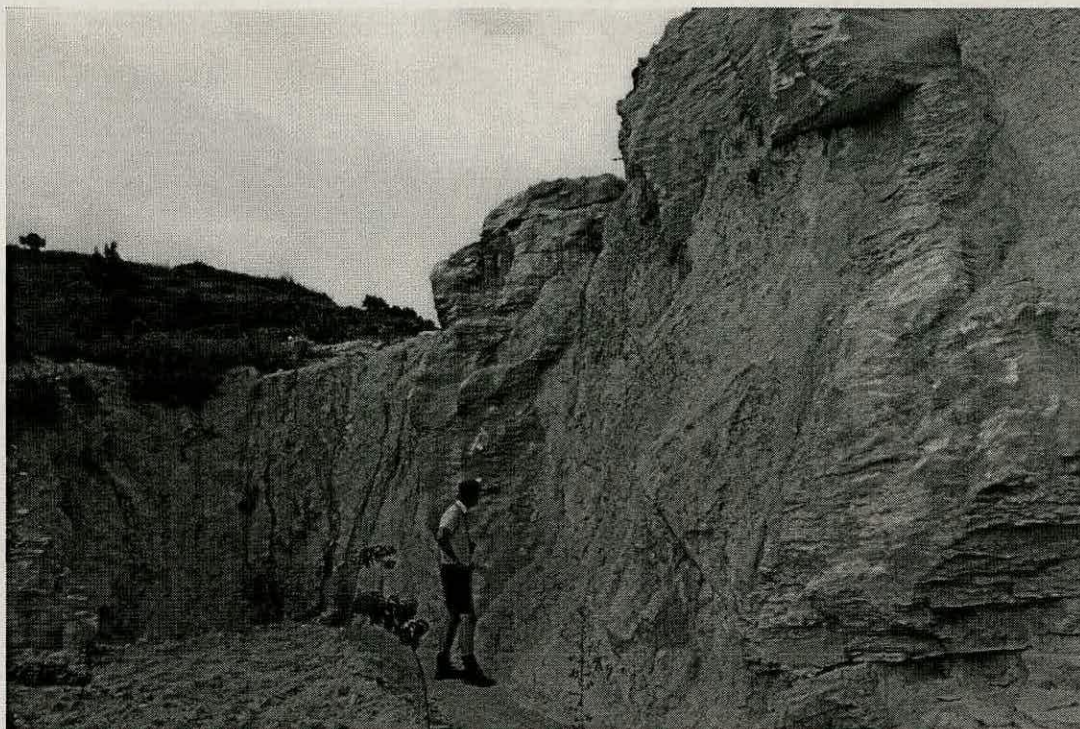


Figure 4.53. Photograph of alabastrine blocks in a gypsiferous marl matrix as observed at location a.



Figure 4.54. Photograph of laminated alabastrine gypsum.

### 4.2.11 Pliocene – Samandağ Formation: sandstone

The Samandağ Formation crops out only in the centre of the present topographic basin. This unit is composed of mainly lithic greywackes and litharenites.

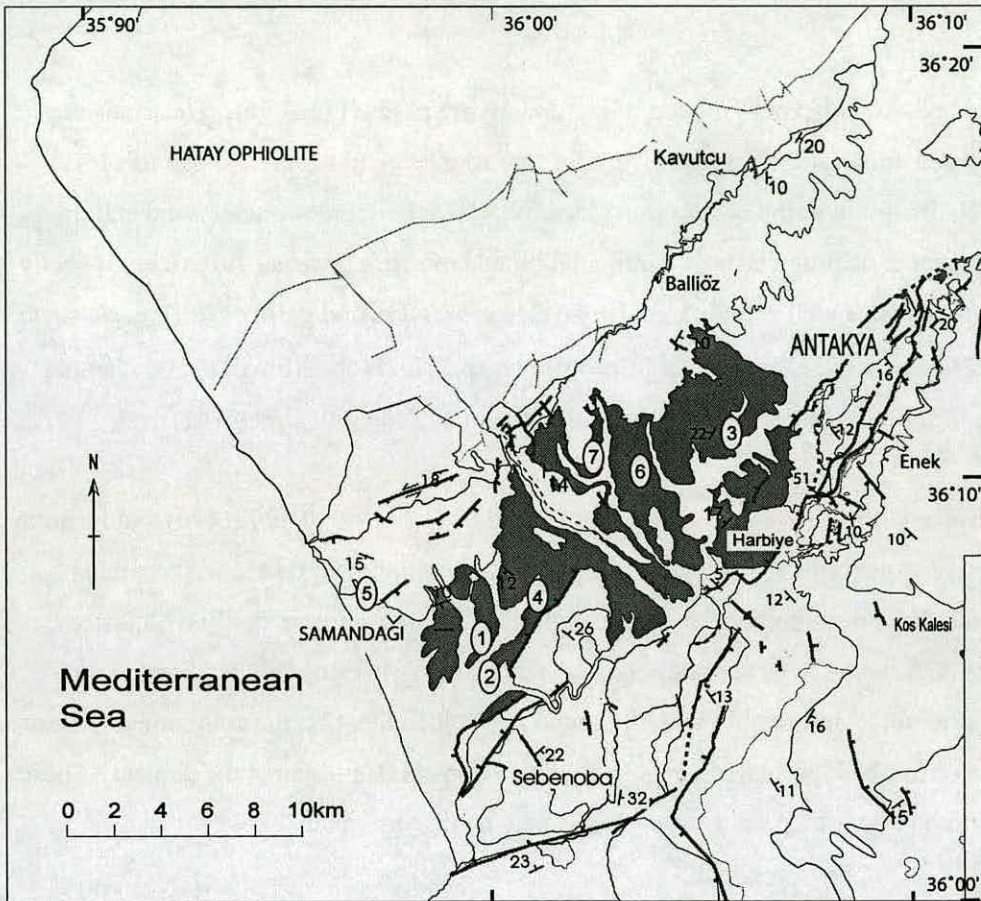


Figure 4.55. Outline map showing the extent of exposure of the Pliocene Samandağ Formation (shaded grey), numbers indicate position of locations discussed in the text.

#### 4.2.11.1 Samandağ terraces(1).

Incised river terraces near the town of Samandağ expose good sections of the Late Miocene and Pliocene basin fill. The river terrace with Kireci Tepe as the highest point, provides a good exposure of the Late Miocene and Pliocene from 0769682/3998307 to 0769999/3999200 going up sequence. Late Miocene sediments are composed of marl/mud and silt but thin (<20cm) sandstone beds are common; these sediments are unlithified. The sands are generally fine-grained and fine upwards into the marl/mud. Some of these sand horizons have parallel laminations and scoured bases. There are occasional thin shell lags of fragmented material with abundant scattered bivalves and gastropods.

The Miocene/ Pliocene boundary occurs in the lower sediments. There was no evidence in the field for this boundary and it was identified using microfossil dating (see appendix 1). Eight metres above the boundary there is an abrupt change to micaceous sands at 0769750/3998399.

These upper beds downlap onto the top of the underlying muds (Fig. 4.56). The sands are medium-grained, bioclastic calcarenites. Grains are rounded and sorted. Above this level there is much distortion in the bedding. At location 419, a horizon of orange sand and mud has been disturbed. Rip-up clasts of parallel laminated mud are present. A horizon of shelly conglomerate contains well-rounded sandstone clasts, bivalves and gastropods (e.g. *Neverita josephina*, *Ringicula* sp., *Demoulia* sp., *Calliostoma* sp., *Turris* sp.). Small (~5m) channel structures and slumped horizons are present at location 422 (0230015/3999141).

Thick (>4m) conglomerates were observed at location 421 (0230080/39991470) and location 423. These conglomerates are polymict, limestone and ophiolite clasts are well rounded, some of which have been bored into. The conglomerates are also very shelly with *Ostrea*, bivalves (e.g. *Glycymeris glycyeris*, *Cyclocardia* sp., *Crasostrea* possibly *C. angusta*) and gastropods present. Conformable with the sequence, at location 421, the conglomerate fines upwards into cross-bedded coarse sandstone with *Ostrea* shells present at the contact. These conglomerates are not observed everywhere so may be discontinuous.

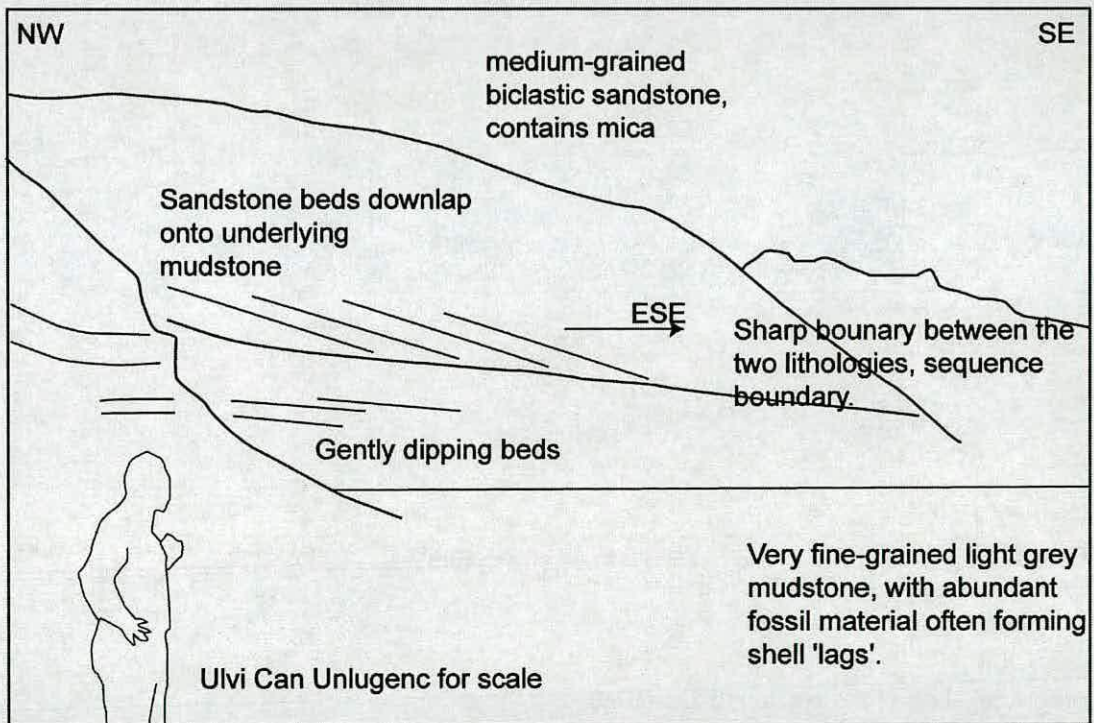
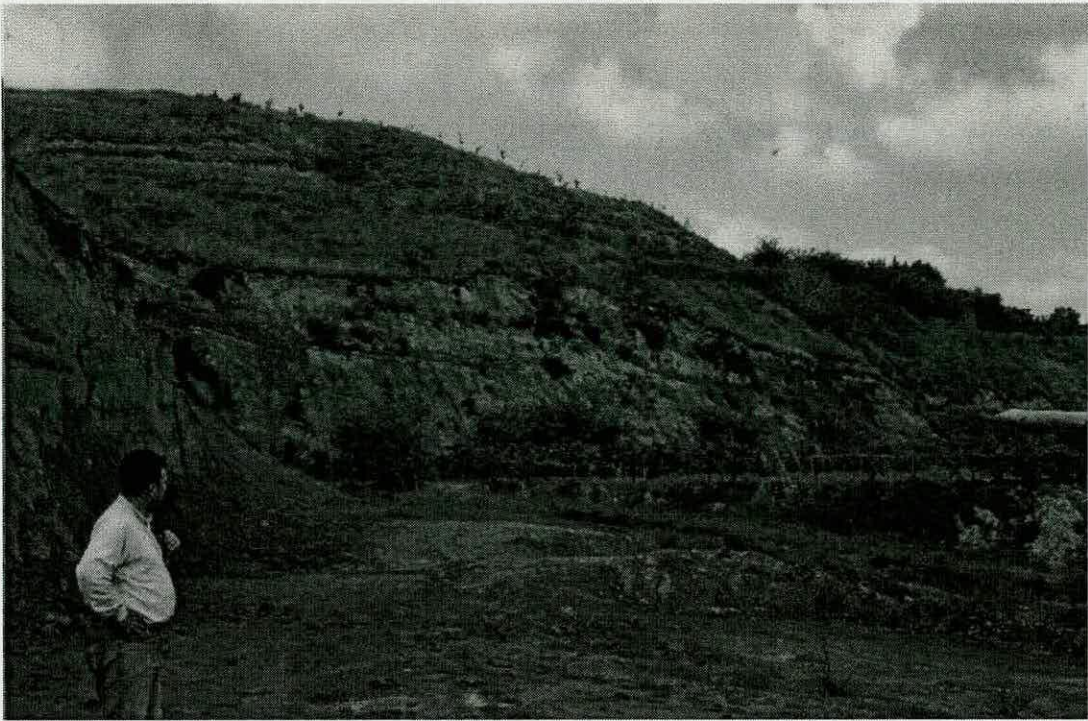


Figure 4.56. Photograph and field sketch of the downlap surface observed along the terrace at Kireci Tepe, micropalaeontology indicates the Upper Miocene to Pliocene boundary is 8m below this horizon.

4.2.11.2 Location 8 and associated locations(2).

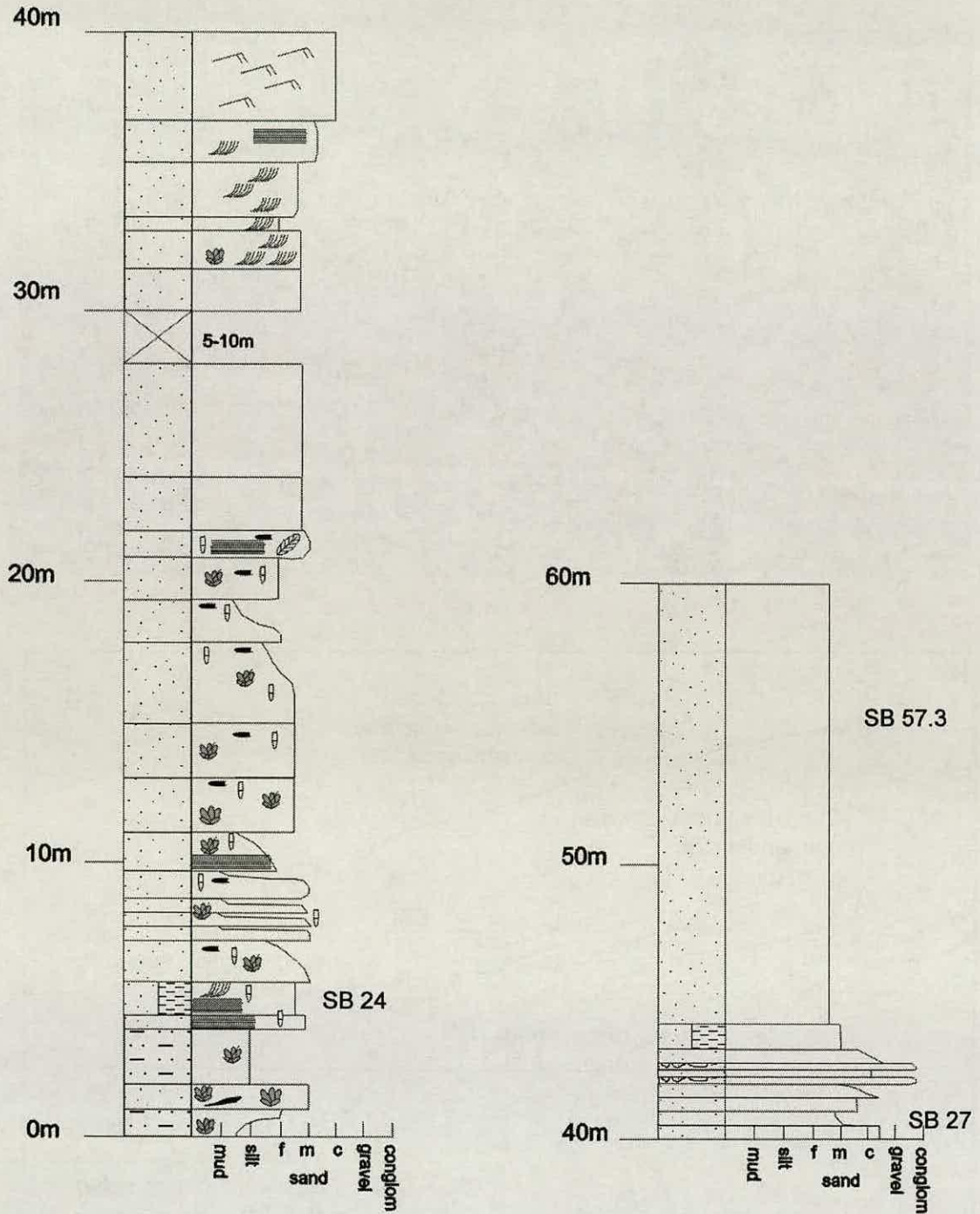


Figure 4.57. Log of the section at location 8.

A section of Late Miocene to Pliocene sediments were logged near the village of Sutasi, along the edge of a river terrace. The base of the section is Late Miocene in age and composed of orange-coloured, muddy sandstone (greywacke-lithic calcarenite **SB24** & **SB26**), with bedding thickness 0.25-3m thick. Grain size is medium to coarse with some

beds fining upward to very fine-grained. Sedimentary structures are common, e.g. parallel laminations, cross-lamination, horizontal and vertical burrows, rip-up clasts and lags of shell material and small rounded pebbles. Common shell fragments are mostly composed of bivalve and gastropod material and occasional articulated bivalves are observed. Reworked oncolites and rare plant material are also present.

The Miocene-Pliocene boundary was identified using microfossil dating (see appendix 1), but there is also change in the character of the sediments. The sandstone (lithic calcarenite) becomes coarser and cross-bedding is common. The thickness of the bedding decreases with many beds <10cm thick. These beds have rippled tops. Above this are slightly thicker parallel laminated beds interbedded with lenticular polymict conglomerates of up to 75cm in thickness with interbedded coarse sandstone and mudstone above. There is no fossil material in these beds.

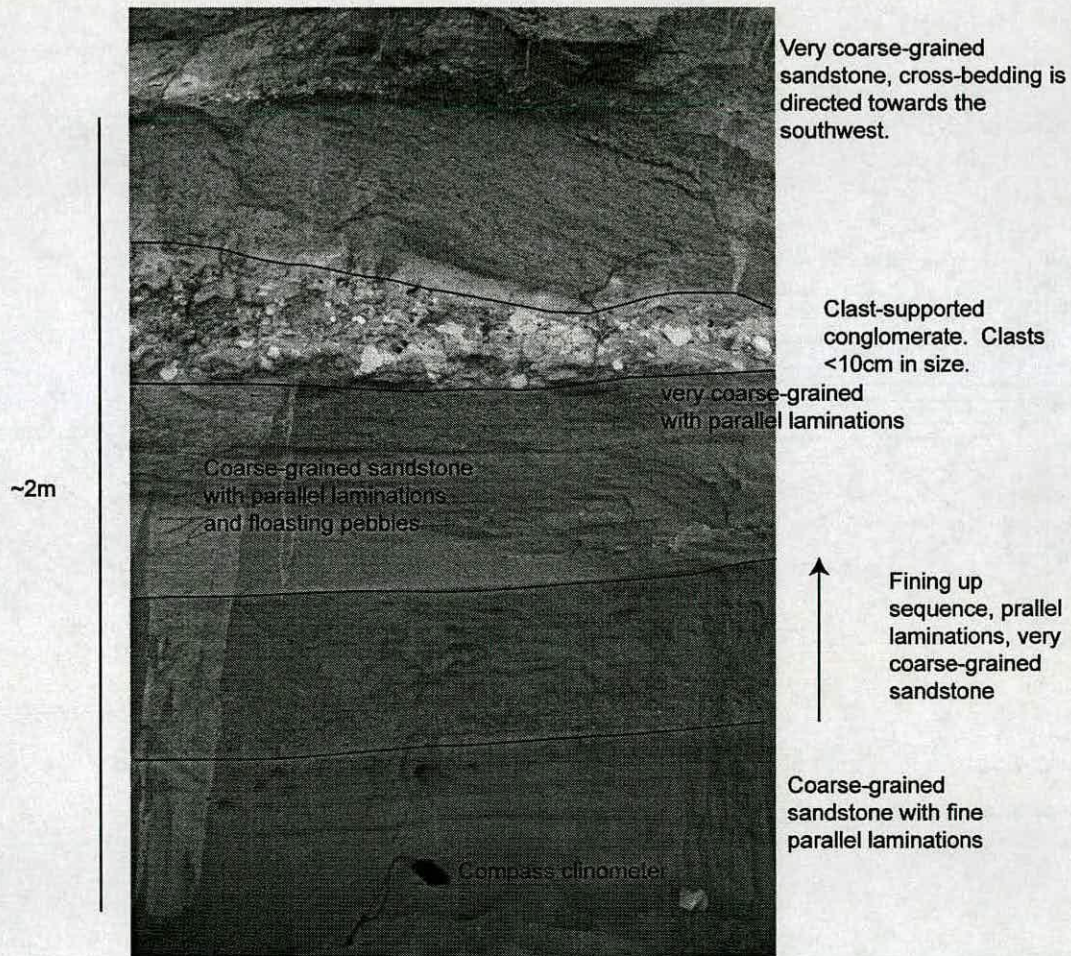


Figure 4.58. Photograph and field sketch of parallel laminated sandstone overlain by a conglomerate lens and cross-bedded sandstone at location 8. Position of the photograph 40-45m on Figure 4.57.

Above this interval of diverse structures, the uppermost part of the sequence is composed of thick sandstone, in which, bedding surfaces cannot be distinguished (**SB57.3**). The sandstone is medium- to coarse-grained and micaceous. There are numerous of horizontal and vertical burrows, such as *Skolithos*, but parallel laminations are preserved in some horizons. There is no fossil material present within these beds.

The sequence is also exposed along the top of the terrace, and generally consists of uncemented orange sandstone, lacking in sedimentary structures. Cemented nodules (similar to doggers) are present. At location 454, however; low-angle cross-bedding is present.

Quaternary stream incision into this terrace level has exposed, at location 451 (Fig. 4.59) (0231201/3998123), a sequence composed of lower massive sands cut into at the top by a series of channel features composed of pebbly sand.

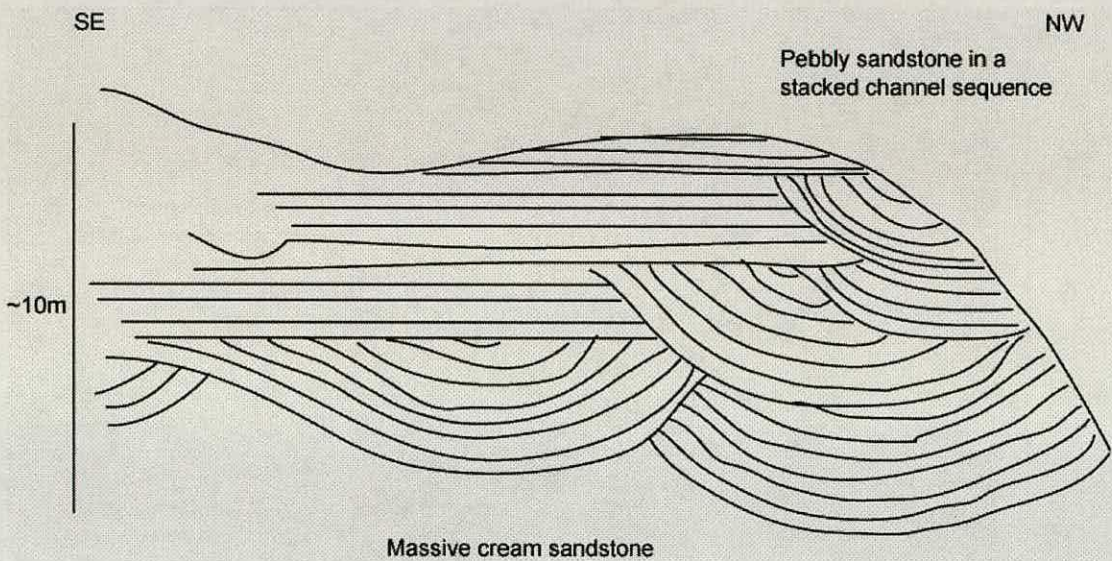


Figure 4.59. Field sketch of location 451 showing stacked channel features exposed in the side of a Quaternary terrace near Samandağ.

4.2.11.3 Main road cuttings (3).

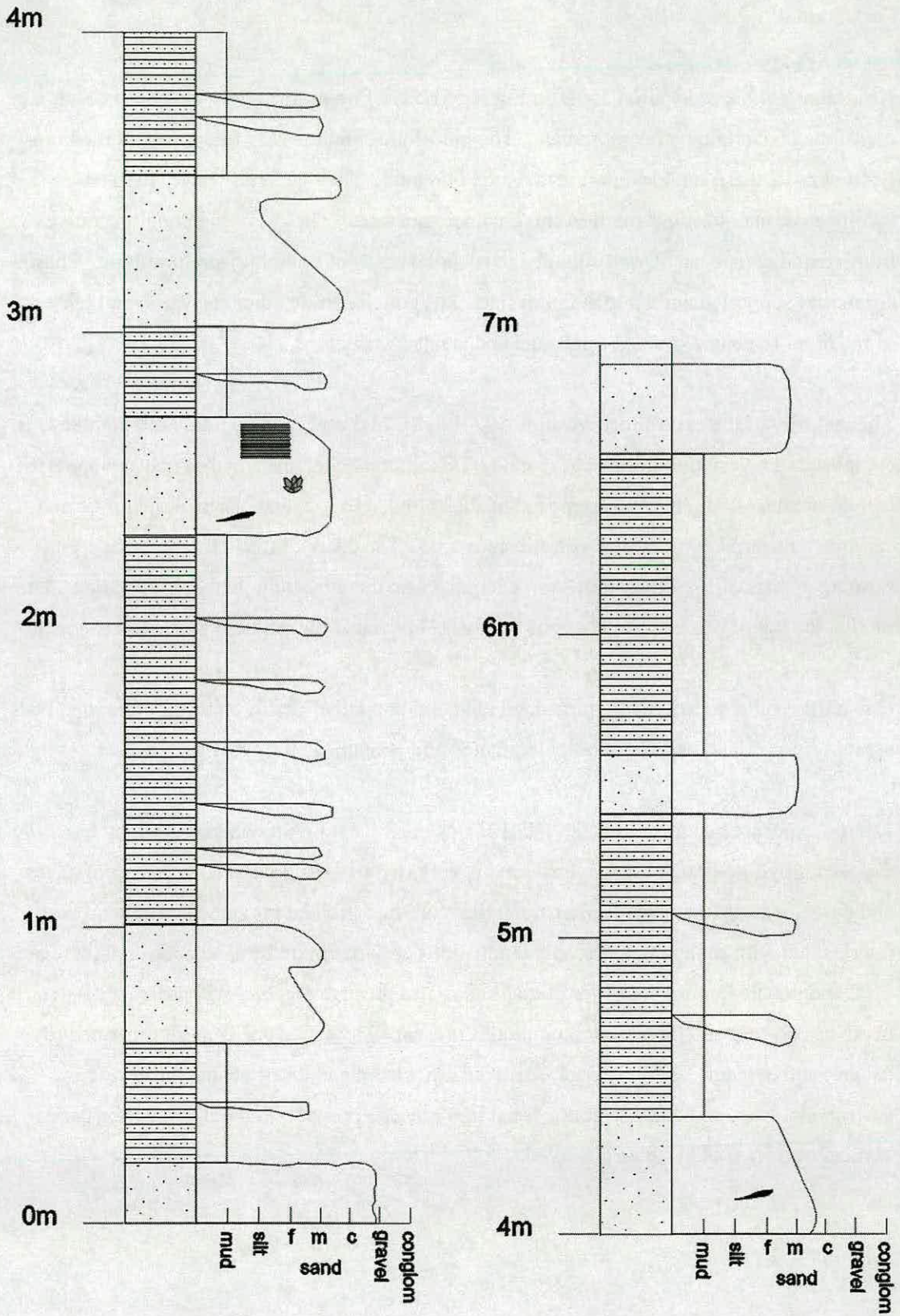


Figure 4.60. Log of road cutting at location 56.



Along the main Antakya to Samandağ road there are good exposures of the Samandağ Formation.

Near Güneysöğüt, at location 56 (3 on Fig. 4.55), very fine-grained grey micaceous mudstone is overlain by conglomerate. The mudstone contains very fine layers of medium-grained sand; these sand layers fine upwards into mud. They generally have sharp bases, locally erosional, forming small (<2m) channel structures. The overlying conglomerate is lithified and composed of well-rounded to rounded clasts of ophiolite and limestone. These are matrix supported and up to 30cm in size. The conglomerate contains occasional lenses of medium- to coarse-grained sandstone and is not fossiliferous.

The majority of the exposure at location 57 (10m SE of 3 on Fig. 4.55; 0239750/4006864) is composed of a very fine-grained grey mud. This interval contains a bed of matrix-supported conglomerate, ~40cm thick. Composed of sub-rounded to rounded clasts of ophiolitic and carbonate material, which fines upwards into sand. The bases of the beds are erosive forming a channel-like structure (~8m in length), and there is slight pebble imbrication. The sand at the top of this interval contains bivalve (*Pecten* and *Ostrea*) and gastropod fragments.

Down the road at location 58 interbedded mud and lenticular sand is exposed. The sand beds contain rip-up clasts and are parallel laminated and contain shell fragments.

A large exposure occurs at 0232590/4001241 (4) near Koyunoğlu, where quarrying has exposed grey fine-grained sand. This sand is very rich in fossil material, including bivalves and gastropods. Moving up section along the road, fine-grained grey micaceous sand is interbedded with sandy mud. Parallel laminations are present in the sandstone, and there are shell and pebble lags. A lot of fossil material is still present, together with articulated bivalves. At the top of the section no mud is present. The sandstone is more cemented (by calcite) and contains fossil material, scattered articulated and disarticulated bivalves, gastropods, scapopod and polyzoan. Shell lags are also present. Parallel laminations and vertical burrow could also be observed.

4.2.11.4 Location 7 (5)

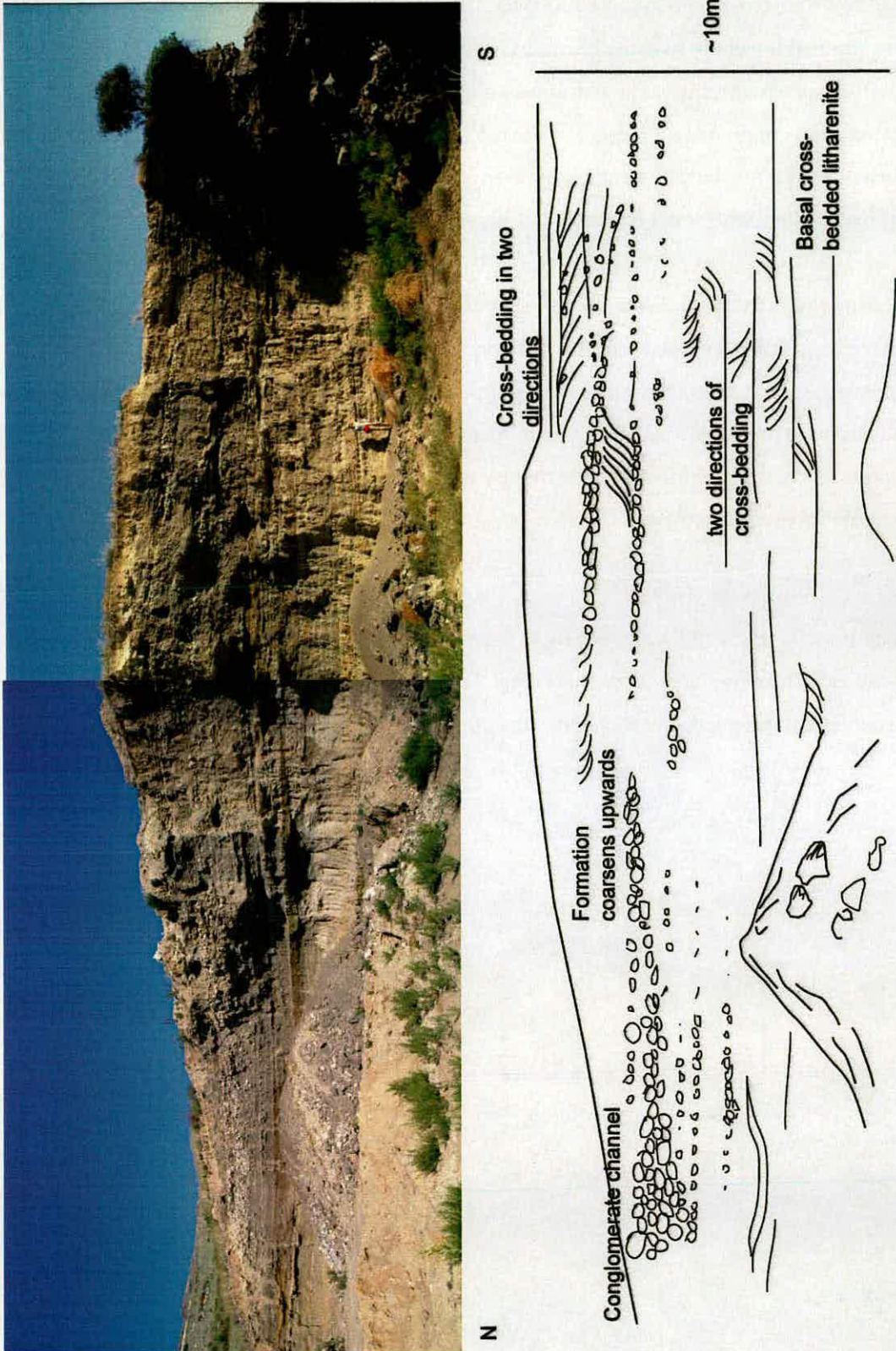


Figure 4.61. Photograph and field sketch of location 7, note increasing proportion of conglomerate higher in the exposure.

Approximately 10m of cross-bedded, poorly lithified, sandstone is exposed in a quarry, to the west of Samandağ, at 0765400/4000510. The sandstone (litharenite) is medium- to coarse-grained to pebbly in some places. Grains are sub-angular to rounded and beds generally coarsen upwards. The outcrop as a whole coarsens upwards with coarse pebbly sandstone and conglomerate present at the top of the outcrop. There is some evidence of bioturbation as a few burrow can be observed; although at first glance there appears to be no fossil material present, small fragments of bivalves (e.g. *Ostrea*, *Cardium*) were found.

The base of the sandstone can not be directly observed but nearby the upper surface of the Sofular Formation is exposed, eroded and bored. Thus suggesting that the Pliocene sediments rest on this erosion surface, this appears to dip down under the Pliocene sandstone to the east. On top of the quarry exposure there is ~5-6m of palaeosol; the base of this section is leached and cemented, followed by brown palaeosols with caliche. There are also some limestone clasts present.

#### 4.2.11.5 Coarse Sandstone (6)

At location 192 (0237890/4005964) there is an outcrop of very coarse-grained sandstone and conglomerate forming large cross-beds (Fig. 4.62). The sandstone is very poorly sorted with sub-rounded, to rounded, clasts of limestone, ophiolite and red chert.



Figure 4.62. Photograph of location 192 showing cross-bedding in pebbly sandstone.

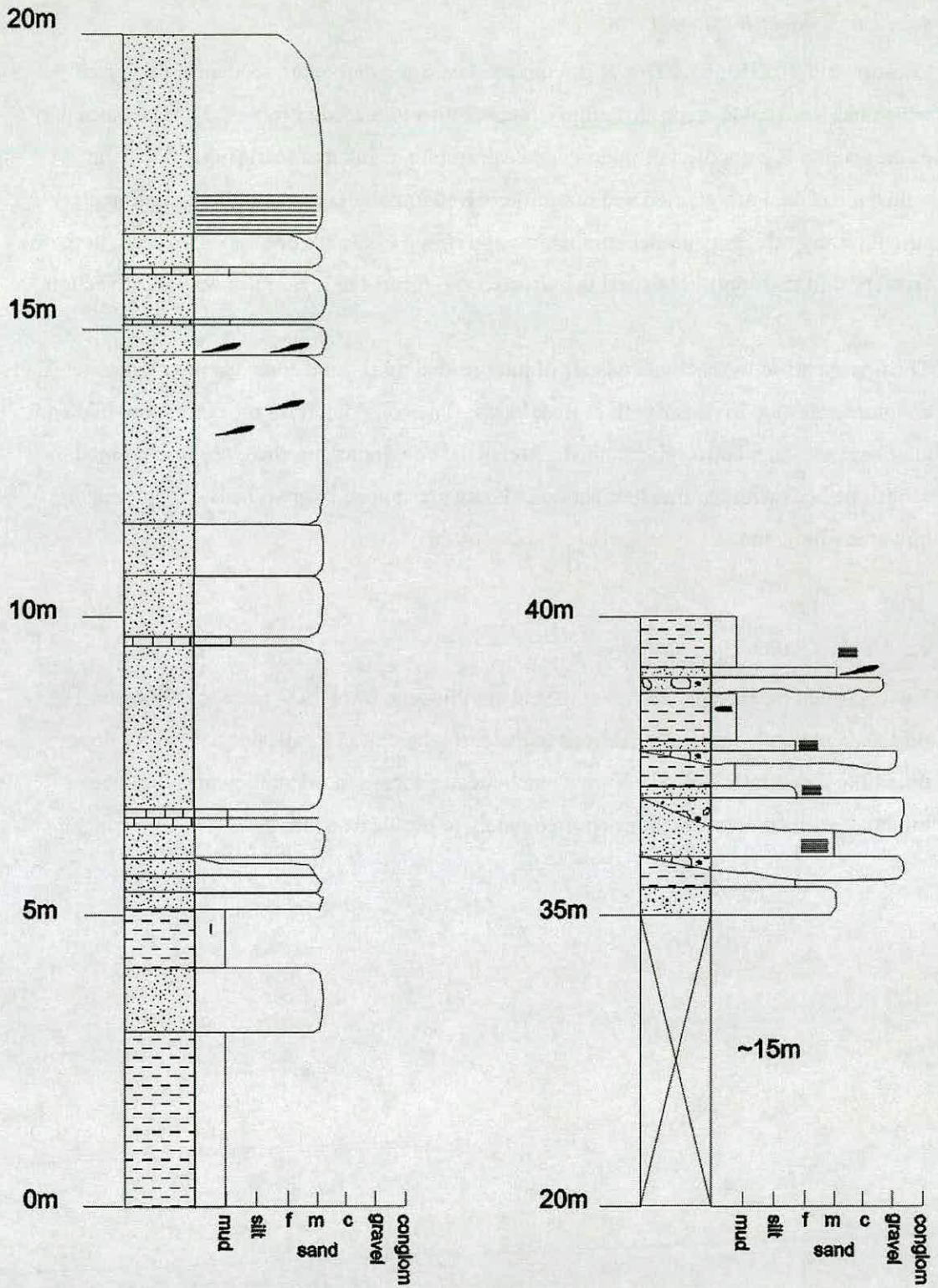


Figure 4.63. Log of location 188

#### 4.2.11.6 *River Section(7)*

Location 188 (0235357/4007667) is a mixed clastic and carbonate sequence, the top of which has been dated using strontium isotopic ratios to 5.35Ma (Table 2.3). The basal part of the section is composed of interbedded calcarenite, chalk and marl (Fig.4.63). The sandstone is medium-grained and unlithified. Bedding thickness is 0.3-3m. Sedimentary structures are rare, but parallel laminations and rip-up clasts are present. The chalk horizons are very thin (5-15cm). The marl is burrowed and forms the lowermost bed of the section.

The upper part of the section consists of interbedded marl, sandstone and conglomerate. The conglomerates are irregular with erosive bases. The conglomerates are clast supported and clasts are sub-angular to sub-rounded. Above the conglomerates there are fine-grained sandstone beds with parallel laminations. These are capped by marl beds, completing an upwards fining unit.

#### 4.2.11.7 *Palaeocurrent Analysis*

Palaeocurrent measurements were taken at six Pliocene locations. Locations 406 and 192 furnished unimodal current directions to the east whereas 523 indicates a westerly flow direction. Locations 7, 8, 519 have a much greater spread in orientation and could be bimodal, with current directions approximately to northeast-southwest.

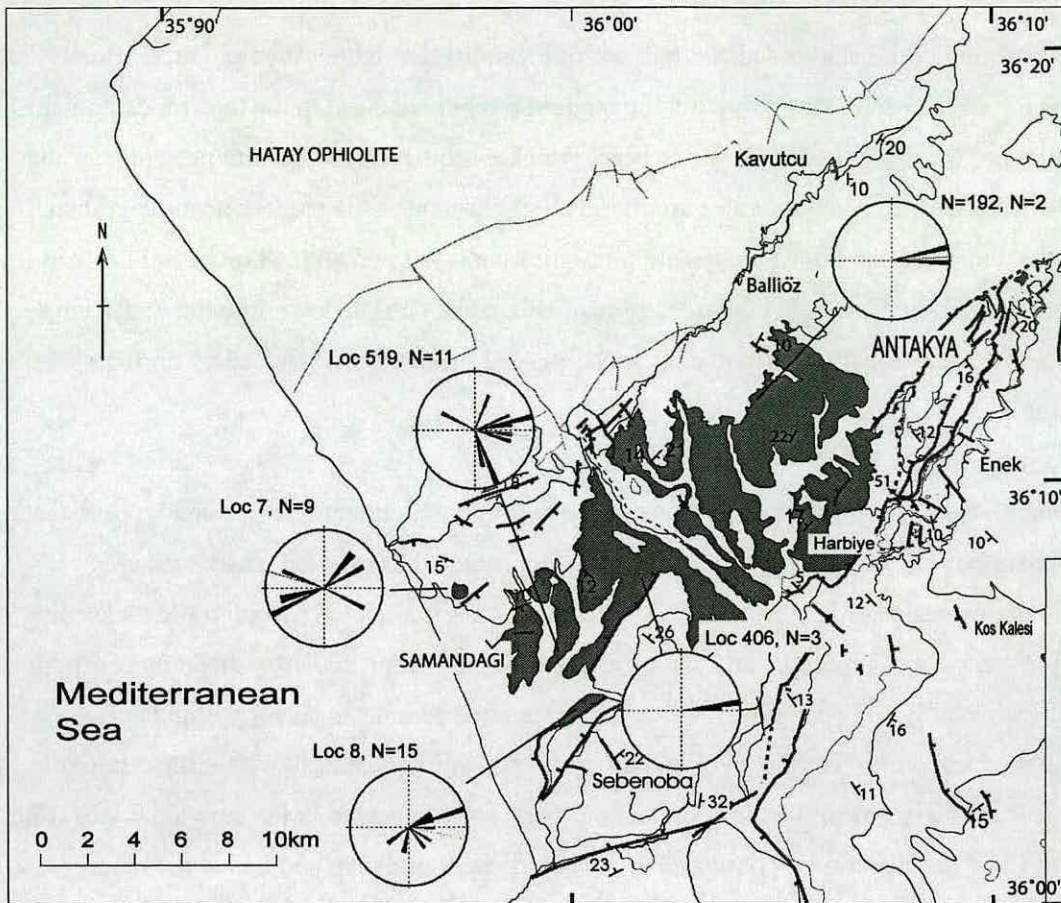


Figure 4.64. Map showing palaeocurrent orientations for the Pliocene Samandağ Formation. Location number and number of data shown on the map.

#### 4.2.12 Summary of Samandağ Formation

The Samandağ Formation only outcrops in the centre of the modern topographic basin. The formation is dominated by sandstone. The base of the formation is in general muddy and could be termed lithgreywacke. Sedimentary structures are generally lacking but fossil material is very common.

Upwards, the sandstone becomes less muddy (litharenite) and fossil material becomes less abundant. Sedimentary structures that are present include parallel laminations and low-angle cross-bedding. Occasional laterally discontinuous conglomerate horizons are present. The very top of the formation is characterised by massive orange sandstone.

### 4.2.13 Quaternary Alluvium

Quaternary alluvium is exposed at a number of locations throughout the field area, usually on the top of river terraces and within the modern river channels. On the tops of terraces the thickness of the unit is usually 2-3m, whereas thicker sequences of >8m are present near the Asi Nehir. Alluvial conglomerates are found along the axis of the graben; near the graben margins and along the flanks older sediments are usually capped with a brown soil horizon <50cm thick. The base of the Quaternary is often erosive cutting down into the underlying sediments. Occasionally this boundary was observed to have been affected by normal faulting.

In general, the Quaternary sediments are composed of conglomerates; these can be clast- or matrix-supported, are often poorly sorted with sub-rounded to rounded clasts with a maximum clast size of 0.5-1m. The clast composition is dominated by ophiolitic rocks with varying amounts of limestone and sandstone. Clast imbrication and cross-bedding is often observed. Pebbly and coarse-grained sandstone is often present as lenses within the conglomerates, cross-bedding, parallel and cross-lamination is present within these horizons. At one location large cross-beds (>1m in thickness) were observed in the conglomerates (Fig 4.65). Clast imbrication was observed in the conglomerates above and below the cross-bedded horizon. Clast size was up to 30cm.

The nature of the conglomerates are variable. At location 133 (0239222/4001019) an exposure of conglomerates with sandy lenses can be observed. The conglomerates are clast and matrix-supported, with clast-supported conglomerates generally present within channel features. The sorting of the sediment is also variable, generally the sorting is poor but within the channels sorting improves especially towards the edges. Cross-bedding is present and indicates palaeoflow towards the southeast.

A large block of limestone is surrounded and overlain by river gravels can be observed at location 90 (0235438/4098173, Fig. 4.66). The gravels and coarse sandstone exhibit trough cross-bedding and are dominated by well-rounded pebbles (<10cm in size).

At location 138 (40966/02298) there is a matrix-supported conglomerate outcropping above a horizon of matrix-supported pebbly sandstone. Clasts include coarse-grained sandstone containing mud clasts, coarse-grained sandstone without mud clasts, and mudstone some of

which is laminated. The pebbly sandstone below exhibits convoluted and contorted bedding and large angular clasts were observed along the boundary between the two facies.

Erosional channels are observed in various places in the field area. At location 8, a channel 100-150 m wide (although this might be an oblique section) cuts into the underlying Pliocene. The channel fill is composed of polymict (sandstone, limestone and ophiolitic rocks) conglomerate. Clasts are poorly sorted and up to 1m in size. Matrix and clast supported horizons are present but there is no clast imbrication or other sedimentary structures. A normal fault at location 172 (0233702/4002760) has formed the margin of a channel. Pliocene sediments dip at a high angle in the hanging wall and the conglomerates overlie these along an angular unconformity.



Figure 4.65. Photograph showing large cross-beds in the middle of Quaternary fluvial conglomerates exposed along river cutting of the Büyükaraçay at location 38.





Figure 4.66. Photograph showing a block of limestone in cross-bedded sandstone, from location 90.

#### 4.2.13.1 Other Quaternary Deposits

There is a large thickness of tufa exposed around the town of Harbiye. The thickness of the deposit exceeds 50m and appears to form the terrace on which the town is situated. Flugel (2004) defines tufa as a porous carbonate that forms in non-marine cold waters the formation of which is strongly controlled by aquatic plants. As opposed to travertine, a term now used for hot water springs ( $>20^{\circ}\text{C}$ ). Studies of modern tufa deposits have revealed specific facies types (Pedley 1990; Glover & Robertson 2003), some of which can be recognised in the tufa near Harbiye. Phytoherm framestone and Phytoherm boundstone facies are both present (Figs. 4.67 & 4.68). Phytoherm framestone is composed of *in situ* carbonate-encrusted plant material, particularly forming radially around plant stems that have now decayed leaving carbonate tubes. Phytoherm boundstone is formed by algal mats creating laminated stromatolite-like textures. Small fragmentary layers were also present; it was not clear if these clasts were plant fragments or algal balls but the facies is unconsolidated and laminated and can thus be termed microdetrital tufa.

Palaeosols are commonly associated with tufa, these sediments are no exception. The palaeosols are laterally discontinuous and maroon in colour.

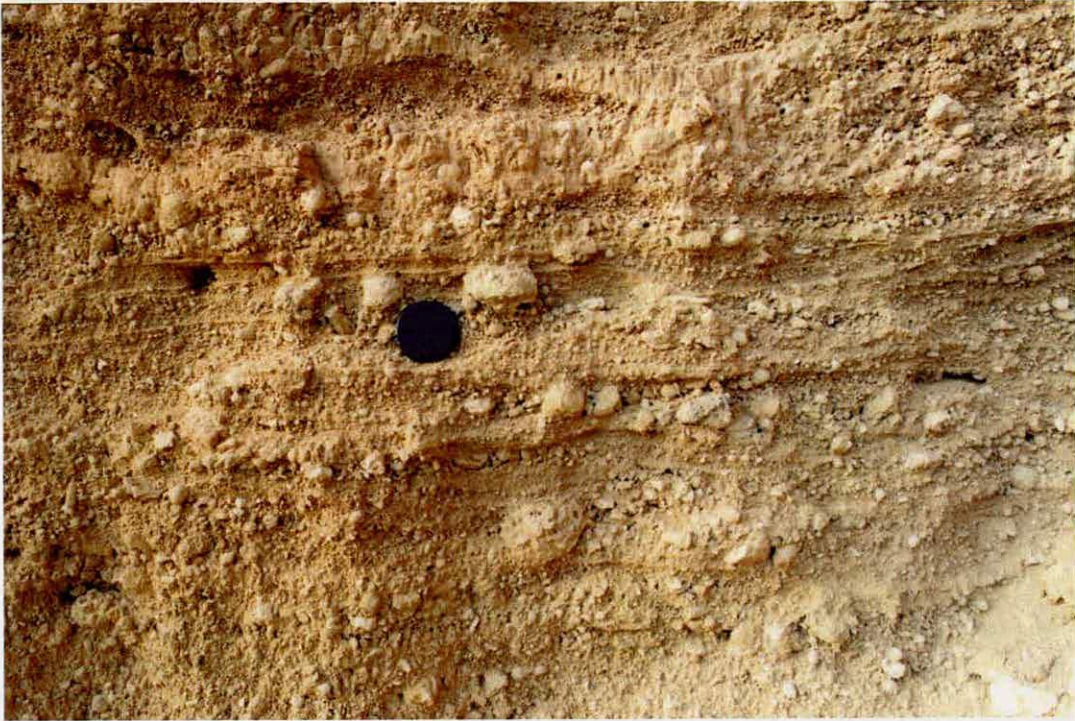


Figure 4.67. Photograph of tufa forming the Harbiye terrace note horizontal laminations. Possible microdetrital tufa facies



Figure 4.68. Photograph showing close-up texture of the tufa, note tube structures and wavy laminations forming Phytoherm boundstone and framestone facies.

Well sorted and rounded, quartz arenite is exposed near the top of a Quaternary river terrace at location 406 (0233118/40011490). The sandstone has tabular cross-beds indicating an easterly palaeocurrent direction. The exposure is poor and appears to be plastered onto the side of the terrace. The sandstone is variably cemented and has a honeycomb-weathering pattern.

Quaternary *terra rossa* soil is present in some areas of the field area. This soil commonly forms on limestone basement in areas with a Mediterranean climate (i.e. warm, dry summers and cool, wet winters) and can be seen in many areas on the flanks of the basin where limestone is exposed. Rare terra rossa is present within the axis of the basin preserved within cavities (palaeokarstic caves?) in the Sofular Formation exposed mainly in road cuttings. In one exposure, exposed along the Titus Tunelli at Çevlik, the terra rossa was observed to also contain fragments of bone and gastropods (Fig. 4.69).



Figure 4.69. Photograph of terra rossa containing bone material (white clasts) preserved in an erosional feature (palaeokarstic cave?) in Miocene limestone.

### **4.3 Sediments from the areas around Serinyol, Belen and Kırıkhan.**

A substantial amount of sediment is exposed around the towns of Belen, Kırıkhan, and Serinyol. These towns lie to the north of the Hatay Graben, on the western margin of the Amik Plain. Sedimentary studies (e.g. Bryant 1960, Derman 1979, Kozlu 1982, Günay 1984) have been carried out on areas around Belen and Kırıkhan and the sedimentary units, although of a similar age to those observed in the Hatay Graben have been given different formation names (see Chapter 2) due to the differing lithological characteristics. The area around Serinyol has not been studied previously and will be considered separately in section 4.4.

#### **4.3.1 Eocene - Hacıdağı Formation:limestone.**

The Hacıdağı Formation is exposed in the northern part of this area to the east of Belen and to the west of Kırıkhan. This unit is composed of limestone.

##### *4.3.1.1 Location 241 (0255391/4036316)*

A road cutting exposes a fresh outcrop of the Eocene Hacıdağı Formation at location 241. The limestones of the Hacıdağı Formation vary from fine-grained wackestone to rudstone, often fining upwards. Bedding is thin (10-20cm thick) with sharp bases and tops. The base of some beds is erosional, but they are not laterally continuous. Bedding is disrupted in places where some beds have slumped (Fig. 4.72). Parallel lamination is common, and there is abundant bioturbation, burrows can be seen to cut and disrupt the laminations in some beds (Fig. 4.71). There are numerous large benthic foraminifera e.g. *Nummulites*, *Discocyclina*) often concentrated in the bases of the beds in lags, when the microfossils are not present at the very top of the beds. Chert nodules are common; these are dark grey to black in colour and form elongated shapes parallel to the bedding planes. Occasionally there are horizons of coarse, angular- to well-rounded clasts, composed of clasts of limestone and serpentinite.

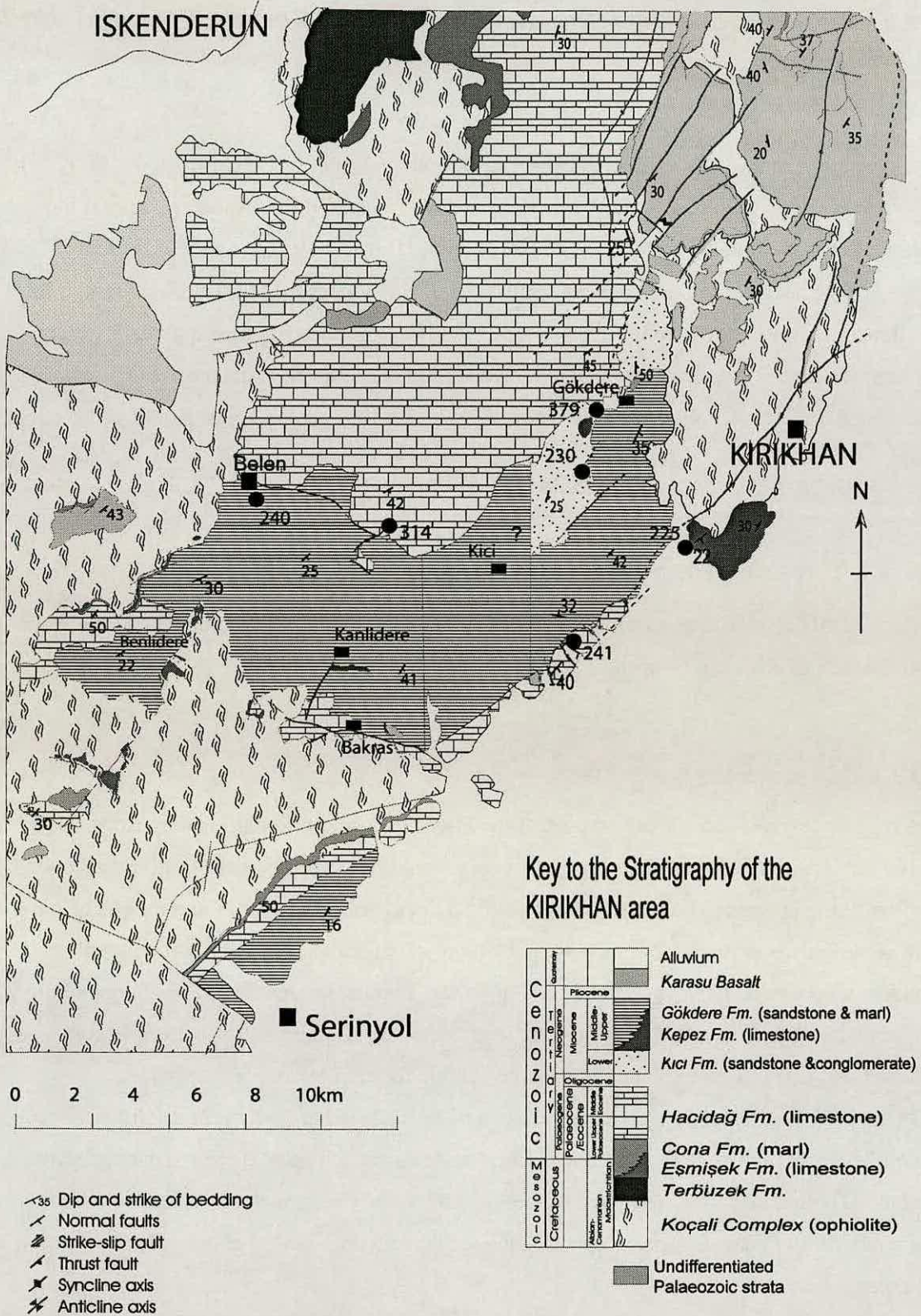


Figure 4.70. Geological map of the northern part of the field area, showing the location of the main locations discussed in the text.

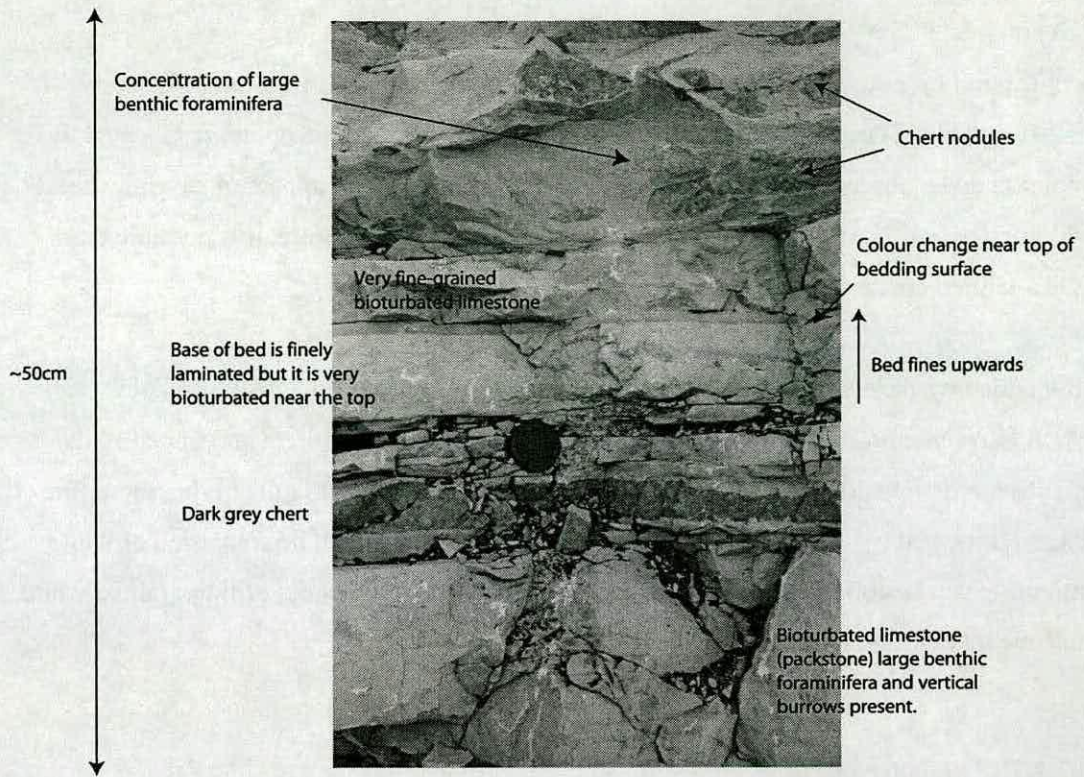


Figure 4.71 Annotated photograph of sedimentary structures in calcarenite observed at location 241.



Figure 4.72. Photograph of incipient slumping in basal bed, northwards directed.

#### 4.3.1.2 *Quarry Exposures*

There is good exposure of the limestones in a series of quarries. At location 257 (0252919/4032418) the basal contact between the limestones and the ophiolite (sheeted dyke complex) can be observed. The contact is very sharp and does not appear to have any basal conglomerate or other lithological changes associated with it; therefore, it is possible that this is a faulted contact.

Thin-bedded wackestone and packstone are exposed, at locations 252 and 253. These beds are rich in *Nummulites* (2-3mm in size); other large benthic foraminifera and trace fossils were observed on bedding planes. Nodular grey chert is also present. Overlying these thin-beds is a thick bed (~10m) that has an erosive base. This appears to be composed of white nummulitic wackestone/floatstone within which are sub-rounded clasts of fine-grained white limestone that does not contain any benthic foraminifera.

#### 4.3.1.3 *Abandoned Village of Kanlıdere*

Eocene limestones are exposed in the bottom of the valley near the abandoned village of Kanlıdere, at 0251163/4036881. These are thin-bedded, wackestone with chert nodules. The top of the formation at this locality is a 7-10m thick conglomerate bed; this is clast supported, clasts are sub-angular to sub-rounded, with a maximum clast size of 30cm. Although generally poorly sorted there does appear to be some size layering within the conglomerate. Clasts are composed of limestone and chert.

#### 4.3.1.4 *Belen Road*

Thin-bedded limestone contains an impressive slumped horizon (Fig. 4.73) at location 314 (0252481/4041026) just off the Belen road. Chert nodules are common especially in the upper parts of the bedding planes. The Eocene – Miocene boundary is located further up the main road towards Belen. The top of the Eocene limestone is very eroded and bedding is sub-vertical. Basal Miocene sediments contain well rounded clasts of Eocene limestone.

### 4.3.2 **Summary of the Hacıdağı Formation**

This formation is composed of limestone rich in large benthic foraminifera. Grey coloured chert nodules are common throughout the formation. Beds are thin with sharp bedding surfaces. Sedimentary structures are present and include parallel laminations and slumps.



Figure 4.73. Photograph showing the slump structure at 314, note that beds above and below are undeformed. Nose of slump fold is orientated to the north. Compass-clinometer circled for scale.

### **4.3.3 Lower Miocene - Kıcı Formation: Sandstone and conglomerates.**

The Kıcı Formation is composed of a mixture of conglomerate, sandstone, mudstone and limestone. Good exposures are found to the west of Kırıkhan.

#### *4.3.3.1 Location 230 (0257106/4041687)*

The base of the Kıcı Formation rests unconformably on the Eocene Hacıdağı Formation. In this location the basal sediments of this formation is 50-60m of thick-bedded conglomerate (Fig. 4.74). Clasts are up to 1m in size and generally angular to sub-rounded. The clasts are matrix supported and dominantly of carbonate composition although there is some basalt and red sandstone present.

Above this basal conglomerate there is a sequence of coarse purplish-red sandstone (SB77A). Beds are in the order of 30-300cm thick with sharp bedding planes. Grain-size is



generally very coarse but also conglomerate and mudstone horizons are present and many sandstone beds show normal grading.

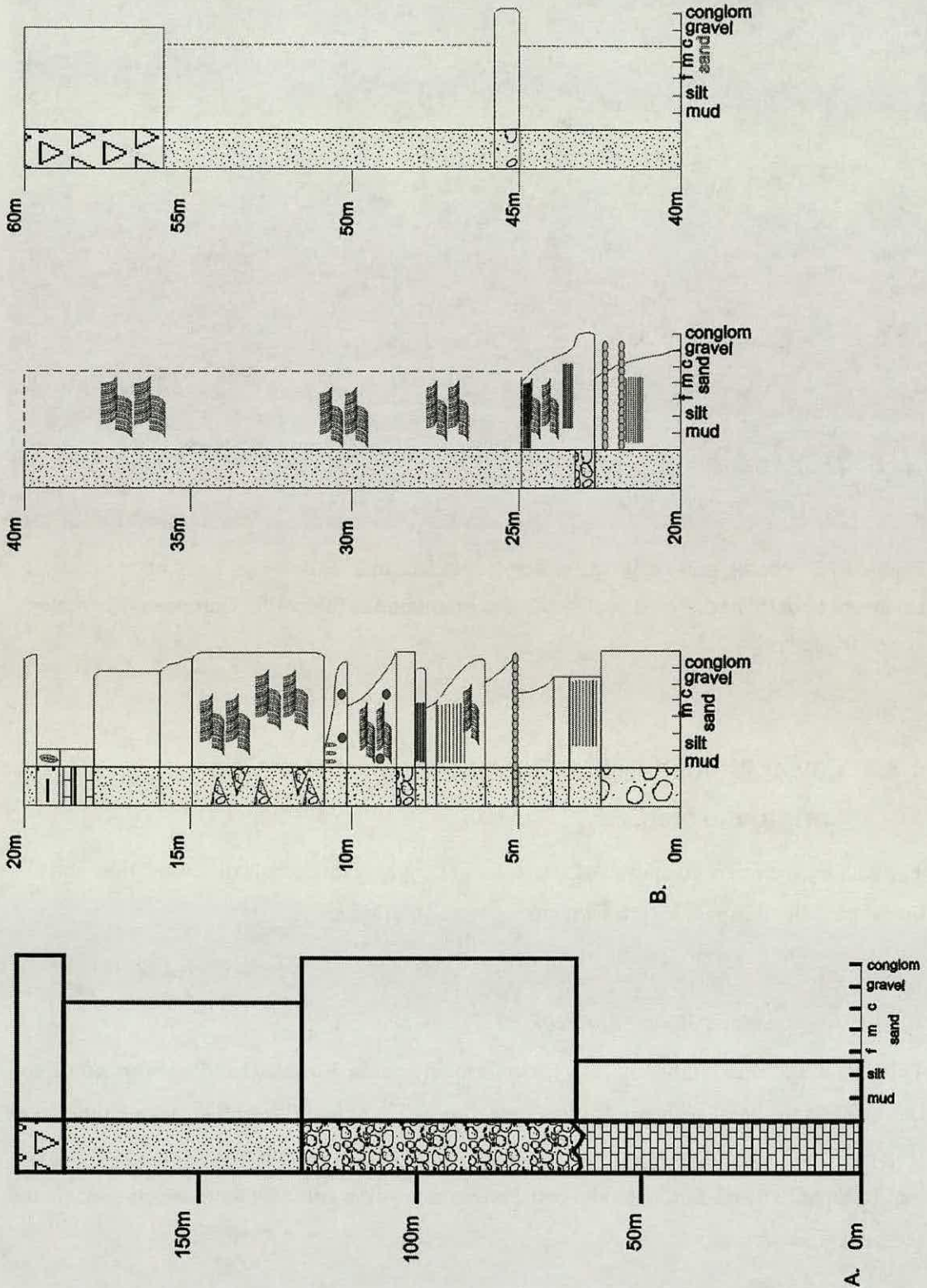


Figure 4.74. A. Summary log of the measured section at location 230 showing broad lithological changes. B. Detailed log of the top 60m of Kici Formation.

The sandstone (litharenite) beds often containing “floating” rounded pebbles and pebble horizons a single pebble thick; these generally have an ophiolitic derivation. Sedimentary structures are common, such as parallel lamination, cross-bedding and bioturbation (Fig. 4.75).

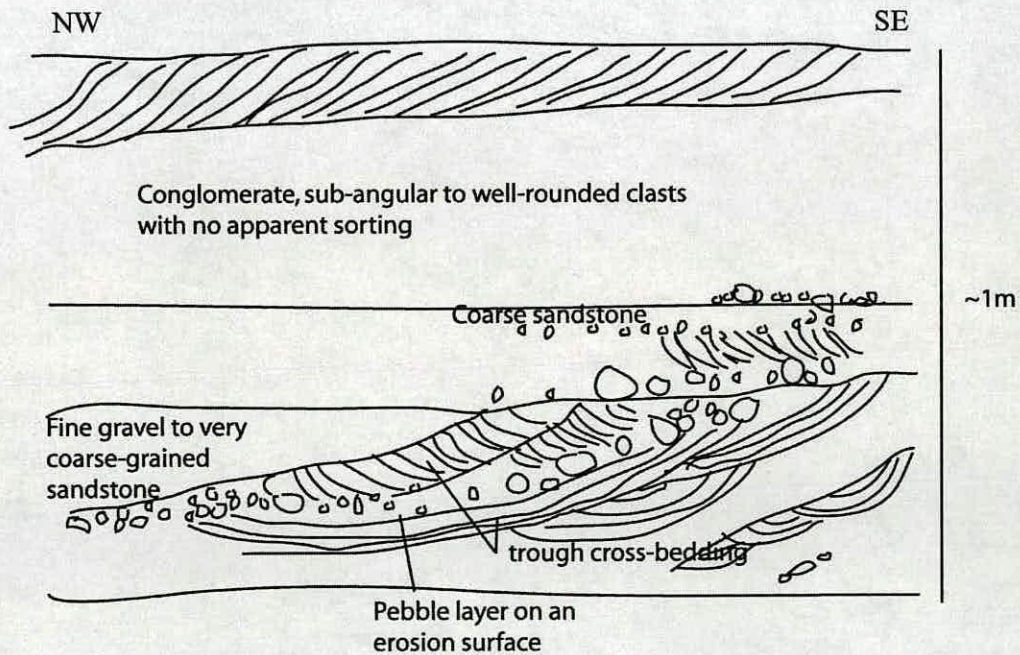


Figure 4.75 Photograph and field-sketch of cross-bedding observed at location 230.

Conglomerate beds are clast supported, with well-rounded clasts of a generally ophiolitic composition, but limestone clasts are also present. The conglomerates are either found at the base of sandstone beds or they form laterally variable lenses. There is also an interval with 1.75 m of mudstone exposed. The bottom 1m is composed of very thin interbeds of white and pale lilac coloured chalk and black mudstone, which is overlain by dark grey mudstone containing roots and plant material. The mudstone has in places a scaly texture. The base of the overlying sandstone bed is conglomeratic.

The uppermost beds of the formation are thick sandstones that have some “floating” pebbles and occasional conglomerate horizons. The exposure is terminated by an erosional surface above this there is cemented talus (thickness undetermined).

4.3.3.2 Location 379 (0257656/4043600)

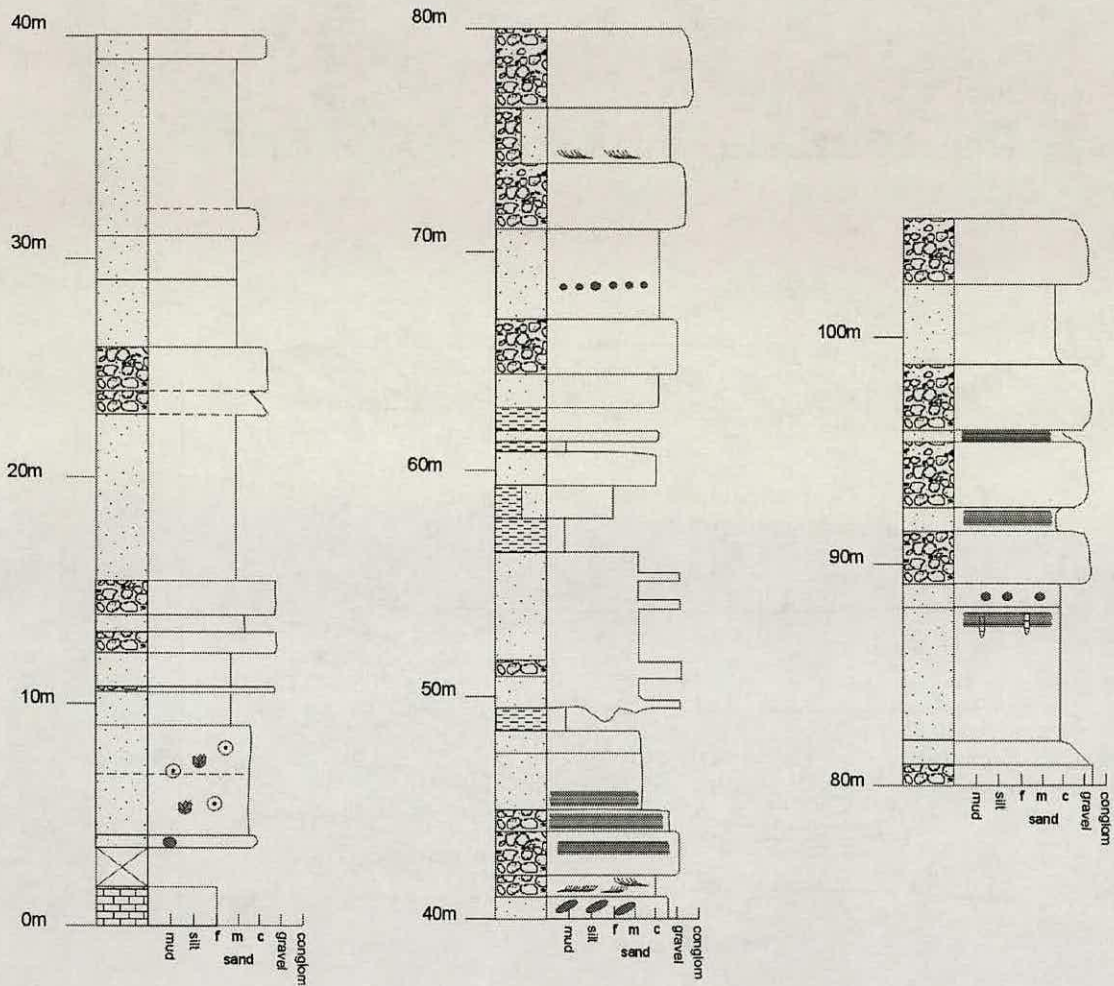


Figure 4.76. Log of the section at 379/380.

At this location the Kıcı Formation is again observed to overlie the Hacıdağı Formation above an erosional unconformity; however, at this location there is no large thickness of conglomerate developed, only 1.5m of mixed breccia and red palaeosol (Fig. 4.76). Above this basal horizon there is ~5m of coarse-grained boundstone, composed mostly of large fragments of algal material, other bioclastic and some siliciclastic material (SB154A & 155A).

Upwards, the sequence is dominated by coarse litharenite and conglomerate. Conglomerates are matrix-supported and composed of rounded clasts of dominantly ophiolite material, but limestone clasts are present and these sometimes show evidence of boring. Clasts are well-rounded and their size varies between beds. Rounded “floating” pebbles are very common within the sandstone beds. Higher in the section, sedimentary structures become more common and parallel lamination, cross-bedding, pebble imbrication, sediment loading and bioturbation are present. Additionally, there are occasional mudstone beds of very fine-grained, mostly black in colour with a shaley fabric. The top of the sequence is poorly exposed but it appears that there is an upward transition to the Kepez Formation.

#### 4.3.3.3 *Abandoned Village of Kanlidere*

Above the Eocene strata at Kanlidere, ~40m of Lower Miocene sediments outcrop; in this location the nature of the sediments is markedly different to those observed further to the north (Fig. 4.77). Fine-medium grained, poorly sorted, brown sandstone is exposed. This sandstone exhibits onion-skin weathering. There are no sedimentary structures or fossils.

Interbedded with the massive sandstone there are three conglomerate horizons. These conglomerates are clast-supported, poorly sorted with well-rounded to sub-rounded clasts up to 40cm in size (Fig. 4.78). The matrix is composed of fine-grained, brown sandstone, the clasts have a mixed composition of limestone and ophiolite derivation. Many of the limestone clasts exhibit *lithophaga*-like borings. The top of the formation is conformable with the overlying limestone (Kepez Formation).

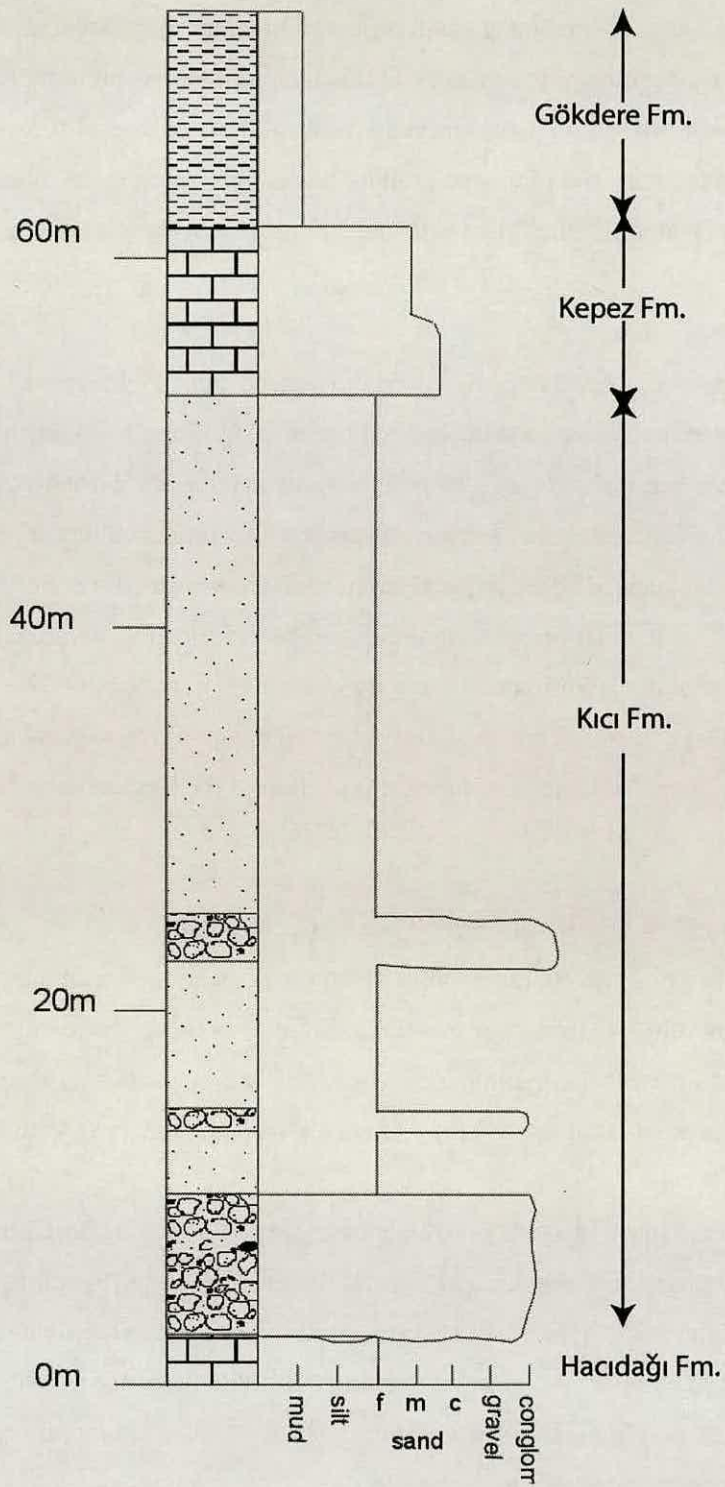


Figure 4.77. Log of the section at Kanlıdere.



Figure 4.78. Photograph of one of the conglomerate horizons observed, note the pebble that have been bored into.

#### **4.3.4 Summary of the Kıcı Formation**

The Kıcı Formation is generally composed of coarse-grained sandstones and conglomerates. Rip-up clasts, cross-bedding and parallel lamination are all common. Within this sequence there are rare mudstone and carbonate beds. At one location a thickness of conglomerate was observed at the base of the formation, but is not present elsewhere.

### **4.3.5 Middle Miocene - Kepez Formation:limestone.**

The Kepez Formation is very poorly exposed and is only found a very few locations.

#### *4.3.5.1 Location 380 (0257650/4043585)*

This location is up the road from the K1c1 Formation section described above. Here there is a small exposure of rubbly limestone (packstone **SB158A**). This is composed of shallow-marine debris, such as fragments of oncolite, coral, bivalves, gastropods and echinoids.

#### *4.3.5.2 Abandoned Village.*

At Kanlidere 10-15m of Kepez limestone is exposed. The basal beds are marly wackestone and pass upwards into hard packstone. There is abundant bioclastic debris, bivalve fragments, bryozoan, echinoids, small gastropods, coral and oncolites. The upper surface of the outcrop is planar, but the lower surface appears to slope downhill towards the present river valley; there is also variation in the dip of beds.

#### *4.3.5.3 Location 225 (0260097/4039793)*

The Kepez Formation forms small rounded hills with very poor exposure in this area. However, there is a small outcrop, at location 225, of fine-grained crystalline limestone (wackestone **SB68A**) containing coralline algae, foraminifera and echinoid fragments. This bed is variable in thickness (2-3m) and has an uneven basal surface. This overlies a very poorly exposed soft marly limestone.

### **4.3.6 Summary of the Kepez Formation**

This formation is composed of bioclastic limestone.

### 4.3.7 Upper Miocene - Gökdere Formation: mudstone with sandstone interbeds.

The Gökdere Formation is laterally very extensive and is extensively present in the southern part of this area. It is composed of marl and sandstone.

#### 4.3.7.1 Gökdere

The type section of the Gökdere Formation outcrops near the village of Gökdere (Fig. 4.79). The base of the formation is not exposed; the measured log starts at 0258444/4043872. The majority of the formation is composed of massive, fine-grained, grey marl. The marl is fossiliferous with foraminifera and gastropods. Near the base of the formation are very thin (5cm) Interbeds of fine-grained micaceous sandstone (litharenite). Some of these thin beds exhibit parallel laminations and contain plant fragments.

Upwards the proportion of sand increases; sandstone beds become thicker (<50cm) and more numerous (Fig. 4.80). The sandstone beds are usually found in packets with significant a thickness of marl between. The sandstone is often laterally discontinuous with sharp upper and lower bedding surfaces. There are a plethora of sedimentary structures present in these sandstones, including small channel structures, parallel lamination (**SB27.3**), cross-bedding, ripples, rip-up clasts, load casts, flutes and current-aligned plant material.

The amount of sand continues to increase upwards until bedding thickness exceeds 1m; these beds continue to be interbedded with marl. The sandstone weathers orange in this interval and sedimentary structures are uncommon; although mud-rip clasts and bioturbation was observed. There are; however, many elongate carbonate cemented concretions. Occasional oyster beds are present, individual *Ostrea* can exceed 20cm in length. *Turitella* gastropods and plant material are also common within these thick beds. Near the very top of the exposed sequence there are rare chalk beds interbedded with the sandstone and marl.



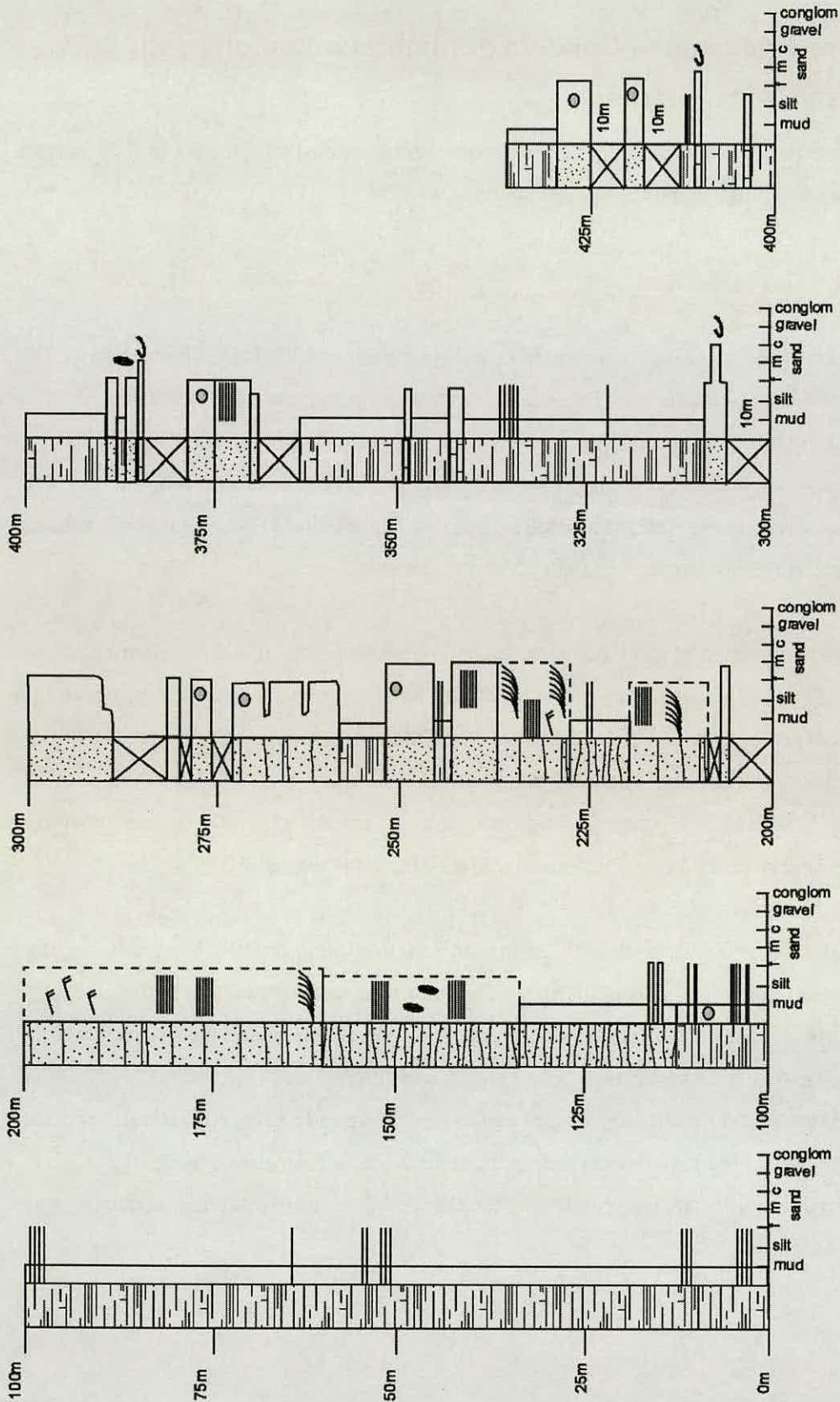


Figure 4.79. Log of the Gökdere Formation at the type section.



Figure 4.80. Photograph of part of the logged section showing the interbedded sandstone and marl.

#### 4.3.7.2 *Belen*

The Gökdere Formation is well exposed around the town of Belen where it is composed of interbedded sandstone and marl/mudstone. The mudstone is very fine-grained, cream and micaceous and dominates the formation.

The sandstone (litharenite/calcarenite) is fine- to coarse-grained; beds are normally graded and micaceous. Bed thickness is <40cm, but most beds are <10cm thick; laterally, these beds are locally discontinuous. The sandstone beds tend to form packets within the marl. Sedimentary structures are common; parallel laminations, ripples (Fig. 4.81), cross-laminations were all observed. Fossils are not generally present but *Ostrea* fragments were identified and plant material is quite common.



Figure 4.81. Photograph of current ripples on top surface of sandstone bed, palaeoflow is down the page towards the northeast.

4.3.7.3 *Location 240 (0254512/4036394)*

A considerable thickness of interbedded micaceous sandstone and mudstone is exposed at location 240. The sandstone is well bedded, <50cm thick. The upper bedding surfaces commonly exhibit straight-crested ripples; rip-up clasts and parallel laminations are present in some of the beds. Fallen blocks reveal that the bases of the beds have sole marks (formed by erosion and bioturbation). Fossil material is rare but *Ostrea* fragments are present and a well-preserved leaf was found.

#### 4.3.7.4 *Bakras Valley*

Marl with sand-bodies is also exposed along a valley from 0252679/4036337 to 0251825/4037008. Marl again dominates the sequence; the sediments are generally fine-grained and grey in colour commonly with mica. Rare horizons; by contrast, are non-micaceous and black in colour.

The sand-bodies are composed of thin-beds (<40cm) of litharenite that are dark grey, medium-coarse grained and micaceous. The bases of these beds are planar and exhibit trace fossils. Parallel laminations, ripples, ripple lamination and load casts (Fig. 4.82) are all present. Plant material is also common in these sandstones.



Figure 4.82. Photograph of base of a sandstone bed with well developed load casts.

#### 4.3.7.5 *Palaeocurrent Analysis*

Palaeocurrent measurements from this formation were measured generally on ripples, sole marks and, in one case, from a log measured at Gökdere, from flow oriented plant debris. Although there is some spread in palaeocurrent orientation, in general they indicate a southerly to westerly flow (Fig. 4.83).

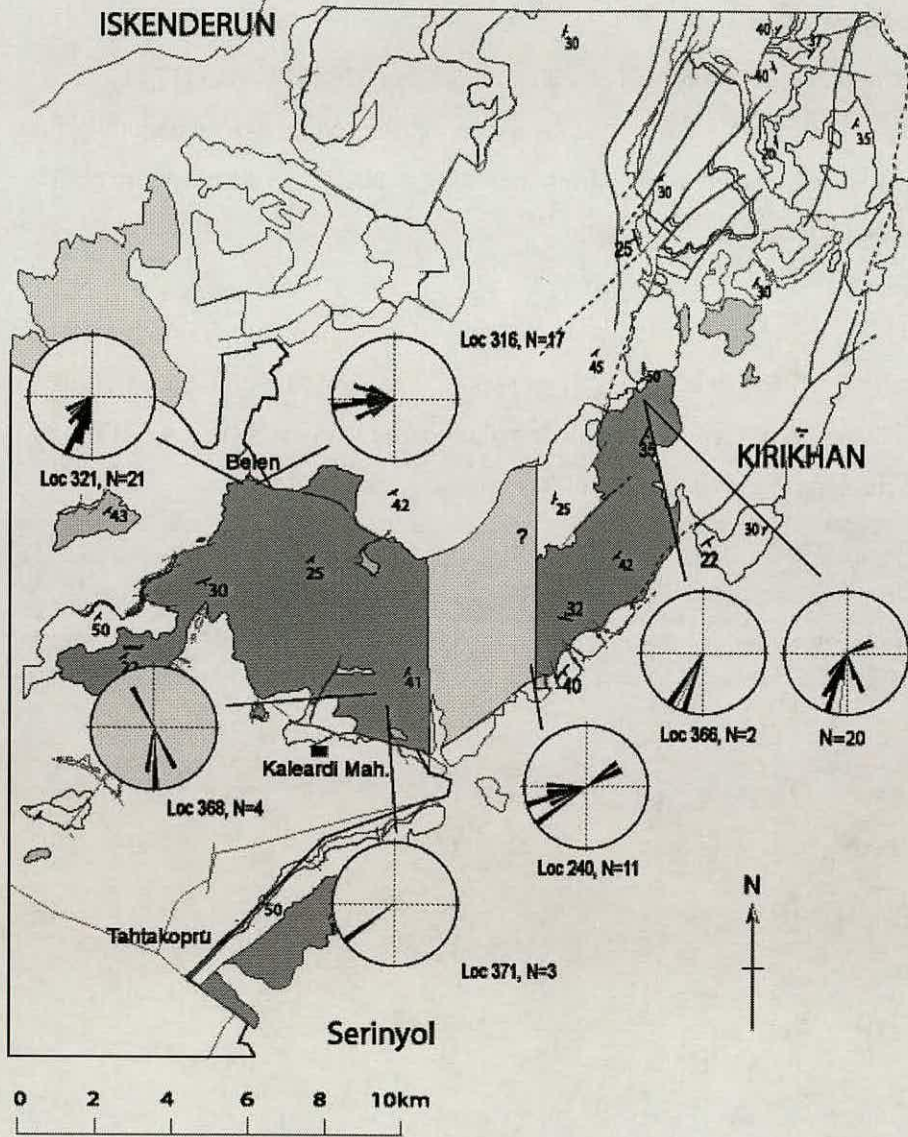


Figure 4.83. Map showing the location of measured palaeocurrents and rose diagrams.

#### 4.3.8 Summary of the Gökdere Formation

The majority of the Gökdere Formation is composed of micaceous marl; within this background sedimentation there are numerous packages of sandstone beds. These sandbodies are commonly composed of 10-20m of interbedded sandstone and marl, where sandstone is the dominant lithology present. The sandstone generally forms thin beds <20cm thick with sharp bases and tops. Sedimentary structures are common and include cross-bedding, ripples, parallel lamination, sole marks (flutes and grooves) and load casts. Fossil material is not very common but *Ostrea* and *Turitella* are present in some horizons in large numbers. Plant material is also common.

### 4.4 Serinyol

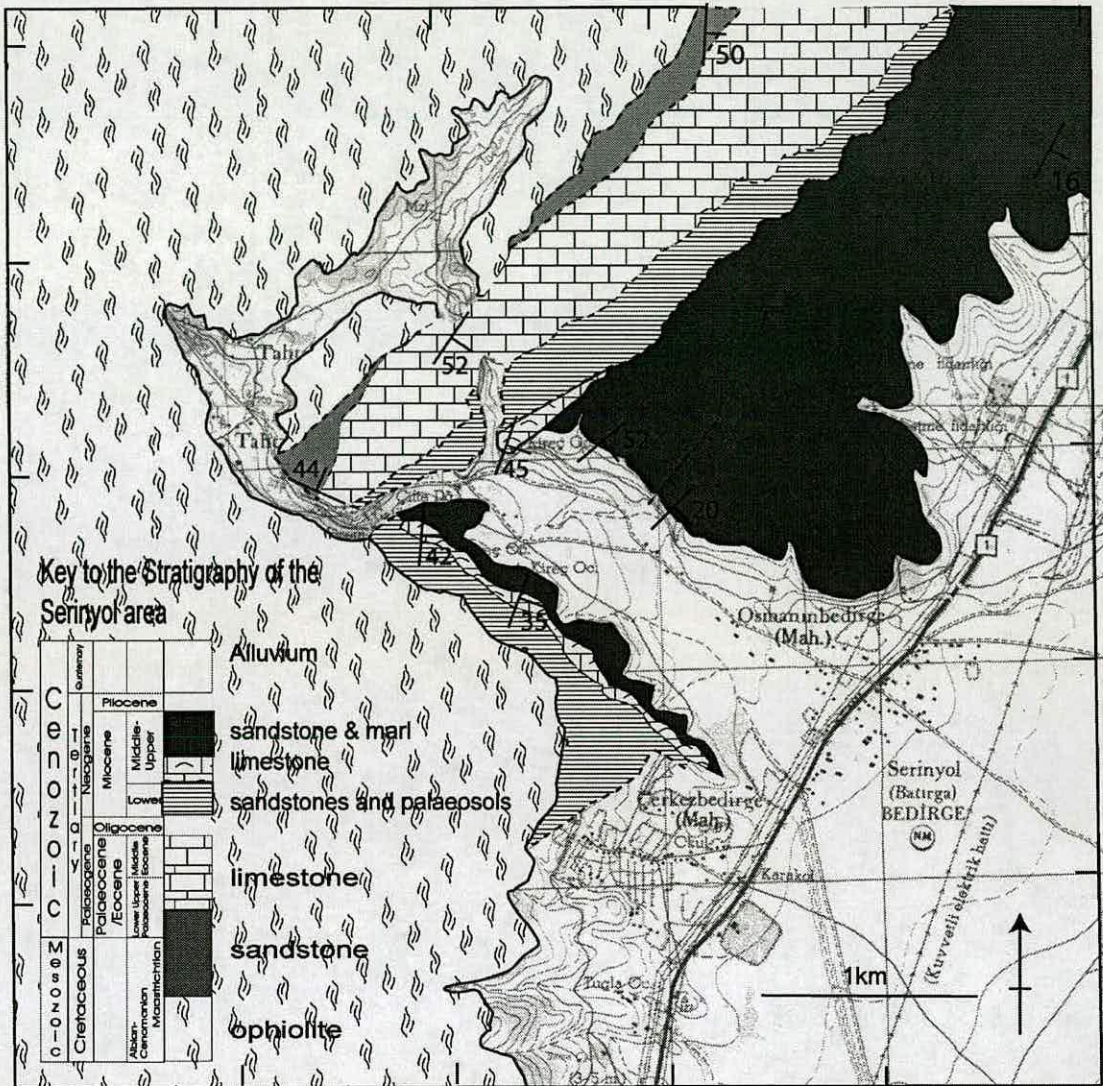


Figure 4.84. Geological map of the area around Serinyol. Key as Figure 4.8.1.

Around the town of Serinyol, to the north of Antakya, there is a small area of Cenozoic sediment preserved on the edge of the Amik Plain. This area lies just outside the northern end of the Hatay Graben, within a re-entrant of the ophiolite. A complete sequence of sediments from the Upper Cretaceous to Upper Miocene is exposed in this small area (Fig. 4.84 and 4.85).

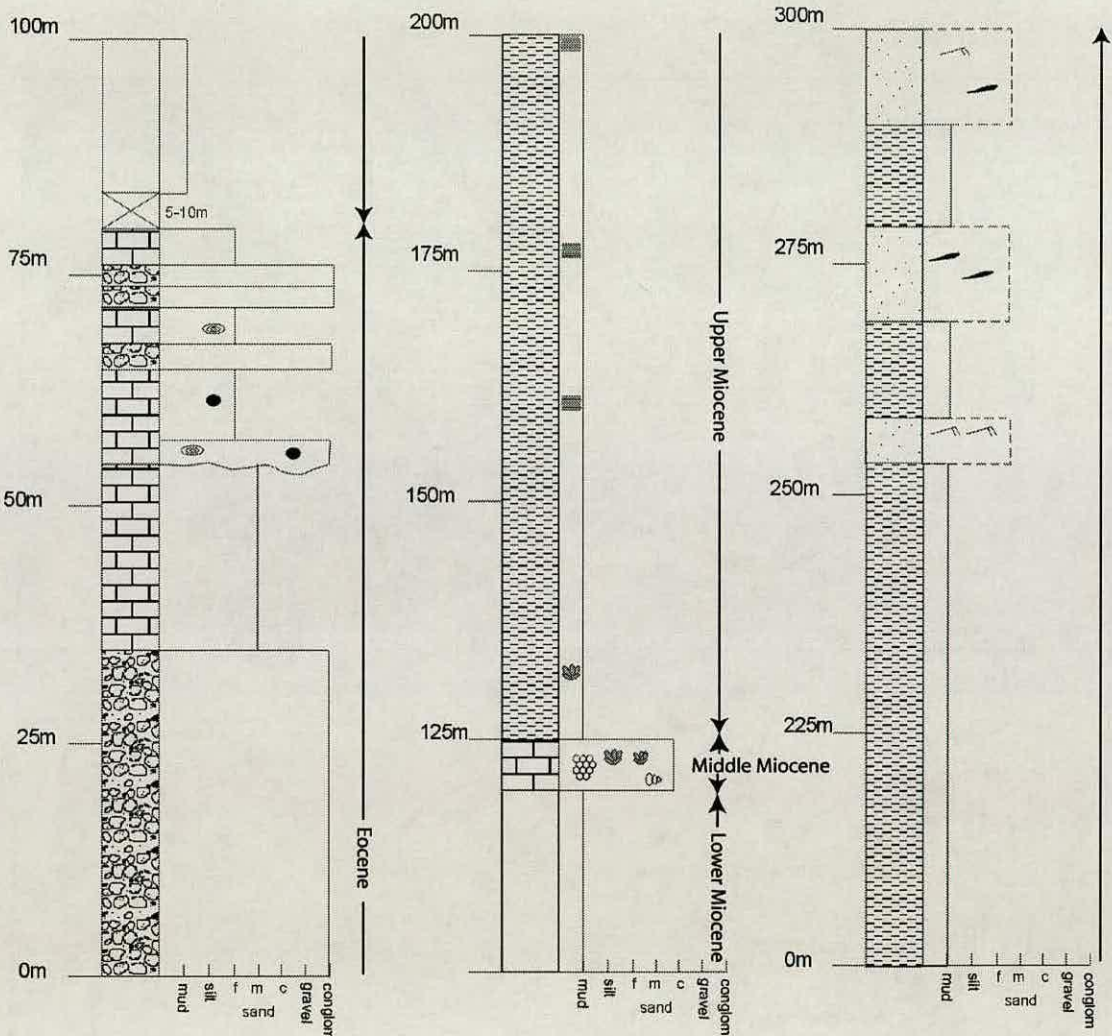


Figure 4.85. Log of the Serinyol succession.

#### 4.4.1.1 Upper Cretaceous

Pink coarse-grained sandstone (litharenite **SB92A**) outcrops along the road at location 273. This sediment is thinly bedded (<10cm), alternating between hard well-lithified beds and soft, poorly-lithified beds of the same composition. Bedding planes are sharp with trace fossils and straight-crested ripple marks on the upper surfaces. Bed-thickness and mean grain size increases up the section.

#### 4.4.1.2 Eocene

Eocene sediments also directly overlie the eroded upper surface of the ophiolite. The best exposure of the Eocene sediments occurs along a stream-cutting at location 259 (0248123/4029755). Basal sediments consist of hard white limestone (wackestone-packstone) containing large benthic foraminifera. Chert nodules are common. Within this basal limestone there is a large, laterally discontinuous conglomerate horizon (Fig. 4.86), the

base of which is irregular and cuts down to the top of the ophiolite to the north. This conglomerate is composed entirely of sub-angular to sub-rounded, limestone and chert clasts, of up to 90cm in size; the mean clast size is nearer to 10-20cm and the conglomerate is poorly sorted and clast supported.

Above this conglomerate, there is a return to limestone (fine-grained sparite). Bedding is thin and irregular; the upper surfaces of the beds are occasionally rippled. Chert nodules are very common and *Nummulites* are sometimes observed in dense accumulations (lags). Within this sequence there are several clast supported conglomerate horizons; the clasts are angular to sub-rounded, <50cm in size and composed of limestone and chert. There is also a thick (2.5m) rudstone bed that has a very irregular base that cuts down into the underlying beds. *Nummulites* and *Discocyclusina* exhibit a rough parallel alignment. Additionally, there is a small change in bedding orientation above and below this bed. The top of this unit is not well exposed.

It is interesting to note that 4.5km northeast of this area, there are some small outcrops of red mudstone overlain by white limestone. These sediments unconformably overlie the ophiolitic complex and occur high up in the mountains a significant distance from the present day depocentre. The limestone is fossiliferous with bivalves and plant material present. Higher in the sequence *Nummulites* are present indicating a Palaeocene to Eocene age, although the basal sediments may be older.

#### 4.4.1.3 Early Miocene

The base of the Miocene in this area is taken to lie directly above the last bed of Eocene limestone. The Early Miocene sediments are composed of 30-40m of red and brown mudstone (i.e. palaeosol) with abundant caliche. Individual beds cannot be distinguished. There is no conglomerate present in this area.

#### 4.4.1.4 Middle Miocene

The Middle Miocene exposure is very irregular and is mostly composed of a variable thickness (2 to 6m) of recemented rubbly material at location 466 (0248346/4029129). Blocks are ~10cm in size, angular and clast supported. The limestone is very rich in bioclastic material, such as *Pecten*, *Ostrea*, poritid corals and gastropods (Fig. 4.87). Underlying this material there is an irregular basal bed of limestone rich in fragmented bivalves.



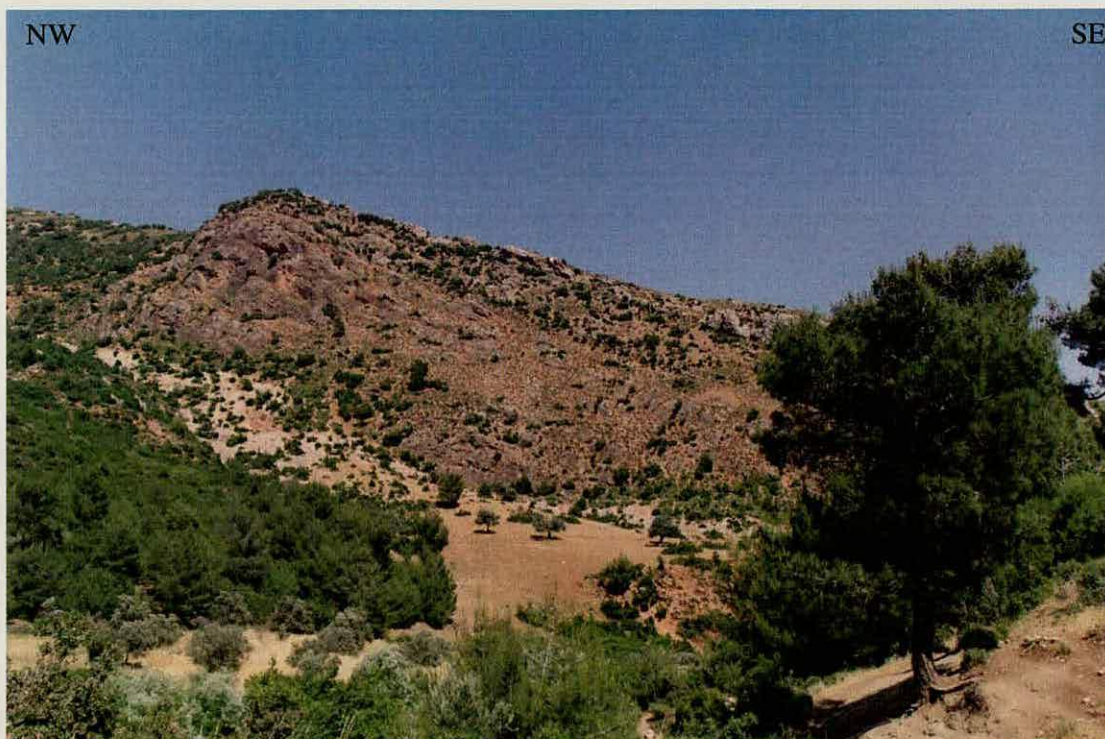


Figure 4.86. Photograph of Eocene section, showing large conglomerate that has cut down through the Upper Cretaceous strata to the ophiolite.



Figure 4.87. Photograph of Middle Miocene corals in rubble limestone.

This material can be observed at other locations in the immediate vicinity of location 466, and at locations 468 and 469, although the thickness of the conglomerate and underlying limestone varies from location to location.

#### 4.4.1.5 *Late Miocene*

The Late Miocene sediments are overlain by grey marl. This contains tiny pelagic bivalves and foraminifera and also larger bivalves and polyzoans. Upwards, the colour changes to brownish. There are occasional horizons with parallel laminations but there are no lithological variations.

The upper part of the formation, includes four sand-bodies. These are 10-20m thick and formed from thin, irregular beds of medium-grained calcarenite (**SB61.3**). They are separated by a similar thickness of marl. Ripples, cross-lamination, tepee structures and rip-up clasts are present. Some fossil material is present, mostly as fragmented bivalves.

### **4.4.2 Summary of the sediments around Serinyol**

The sediments around Serinyol exhibit similarities to those observed in other areas. The Upper Cretaceous sediments are; however, different as they are sandstones not carbonates. Eocene sediments on the other hand are *Nummulitic* limestones, similar to those observed around Belen and they contain a conglomeratic horizon also observed near Kanlidere, thus illustrating a similar history to the northern area. The Lower Miocene sequence of palaeosols and the Middle Miocene reef talus does; however, most resemble the Early to Middle Miocene sequence of the northwestern margin of the Hatay Graben. The Late Miocene sequence of marl is similar to that observed in both of the main areas, but the presence of discrete sand-bodies is more like that observed in the areas around Belen and Bakras kalesi. This indicates that the Serinyol area has had a sedimentary history that incorporates aspects of both areas and as such is important in linking the sedimentary evolution of these areas together.

## 4.5 Provenance

### 4.5.1 Introduction

The second part of this chapter on the sedimentology of the field area concerns the petrographic analysis of selected sediment samples from the Hatay Graben and from around the towns of Belen, Kırıkhan and Serinyol. Sediment petrography and petrology were undertaken in order to determine their provenance. Clays were analysed using X-ray diffraction (XRD; Appendix 2); sandstones were studied using thin sections (Appendix 3) and point counting (Appendix 4); and the proportion of different clast types in conglomerates was counted in the field.

### 4.5.2 Clay Mineralogy

#### 4.5.2.1 Methodology

Forty-four samples of fine-grained sediments were analysed using XRD. These samples consisted of muds, marls and soils where the grain size was too small to determine the mineralogical composition through optical methods. XRD uses the crystal lattice of minerals to diffract x-rays as described by Bragg's Law ( $\lambda = 2d \sin \theta$ ). When an x-ray is incident upon a sample, the x-ray will be either transmitted or scattered. Generally, scattered x-rays will destructively interfere; however, when Bragg's Law is satisfied the x-rays will constructively interfere producing a strong response or peak. When x-rays are transmitted through a powder sample, the powder acts like a crystal lattice, resulting in a series of peaks at different  $2\theta$  wavelengths allowing the identification of the minerals present within the sample.

The 44 samples were chosen from the main two field areas, around Antakya and the Kırıkhan/Belen area, and span the period from the Late Palaeogene/Eocene to the Pliocene (Figure 4.5.1.).

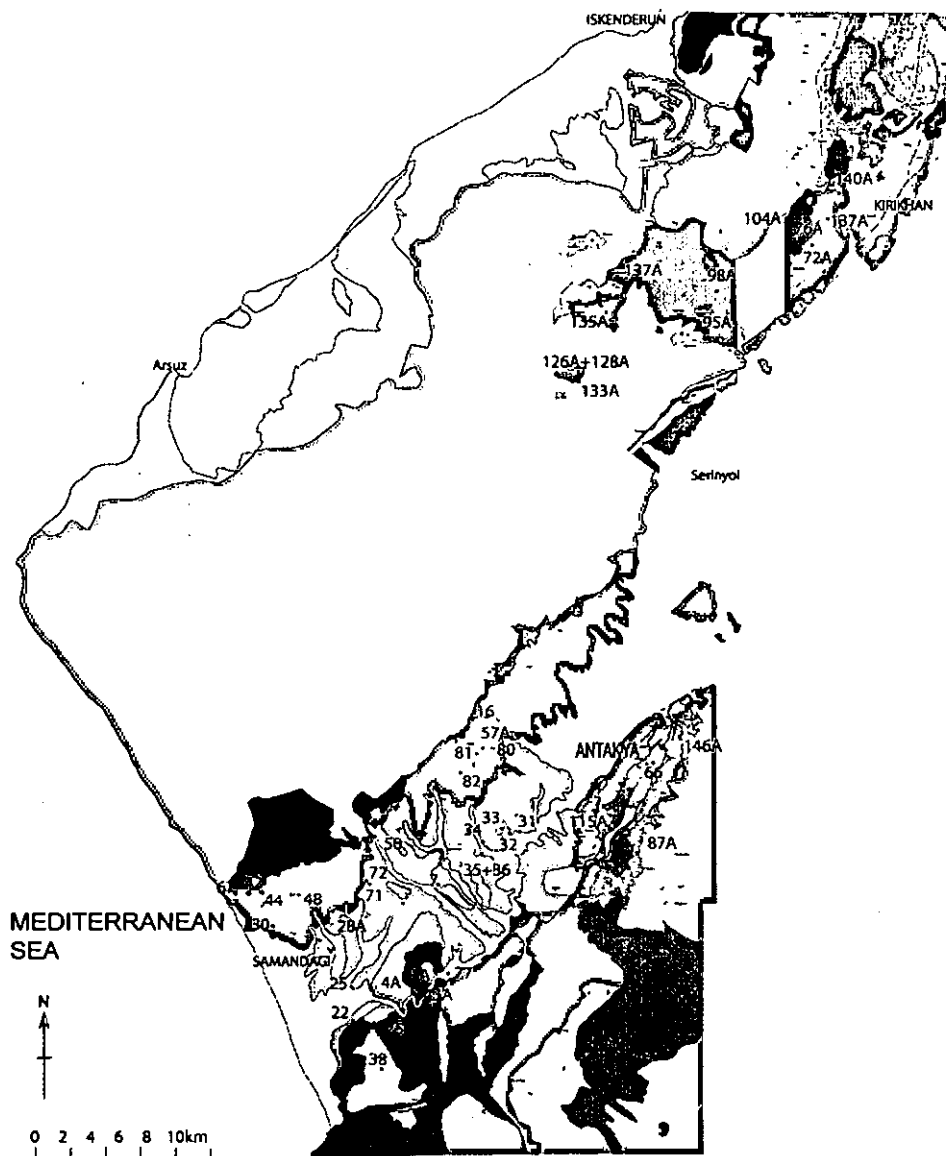


Figure 4.5.1. Map showing the location of samples used in XRD analysis.

Each sample was tested in several ways.

- The first procedure was to run the sample as a simple powder produced by crushing the sample; this was to determine the bulk composition.
- Secondly, the powder was added to distilled water and left for 3 hours to settle, the water and remaining suspended sediment were then decanted and left overnight. The following morning a small amount of the remaining water/sediment solution was placed

on a glass disc to be run in the XRD instrument. This process concentrates the very fine material within the samples, such as mica.

- The fines were then treated with ethylene glycol. This technique was used to further identify the type of clay minerals in the sample as the addition of ethylene glycol causes the crystal lattice of smectite to expand and as a result the peak wavelength shifts to lower wavelengths.
- Finally, some samples were heated to 500°C; heating to this temperature has the effect of translating the peak wavelengths of smectite allowing confident clay mineral identification and higher precision in determining relative peak heights.

This method is essentially a qualitative one that determines the mineralogical composition only. However using peak height, a semi-quantitative value for the individual minerals can be derived. It is not 100% accurate and depends on the composition of the sample. The simpler the composition is, the more accurately concentrations can be calculated. This is done by measuring the height of the major peak for each mineral, multiplying this number by a standard factor for that particular mineral and then working out the percentage of each mineral within the sample.

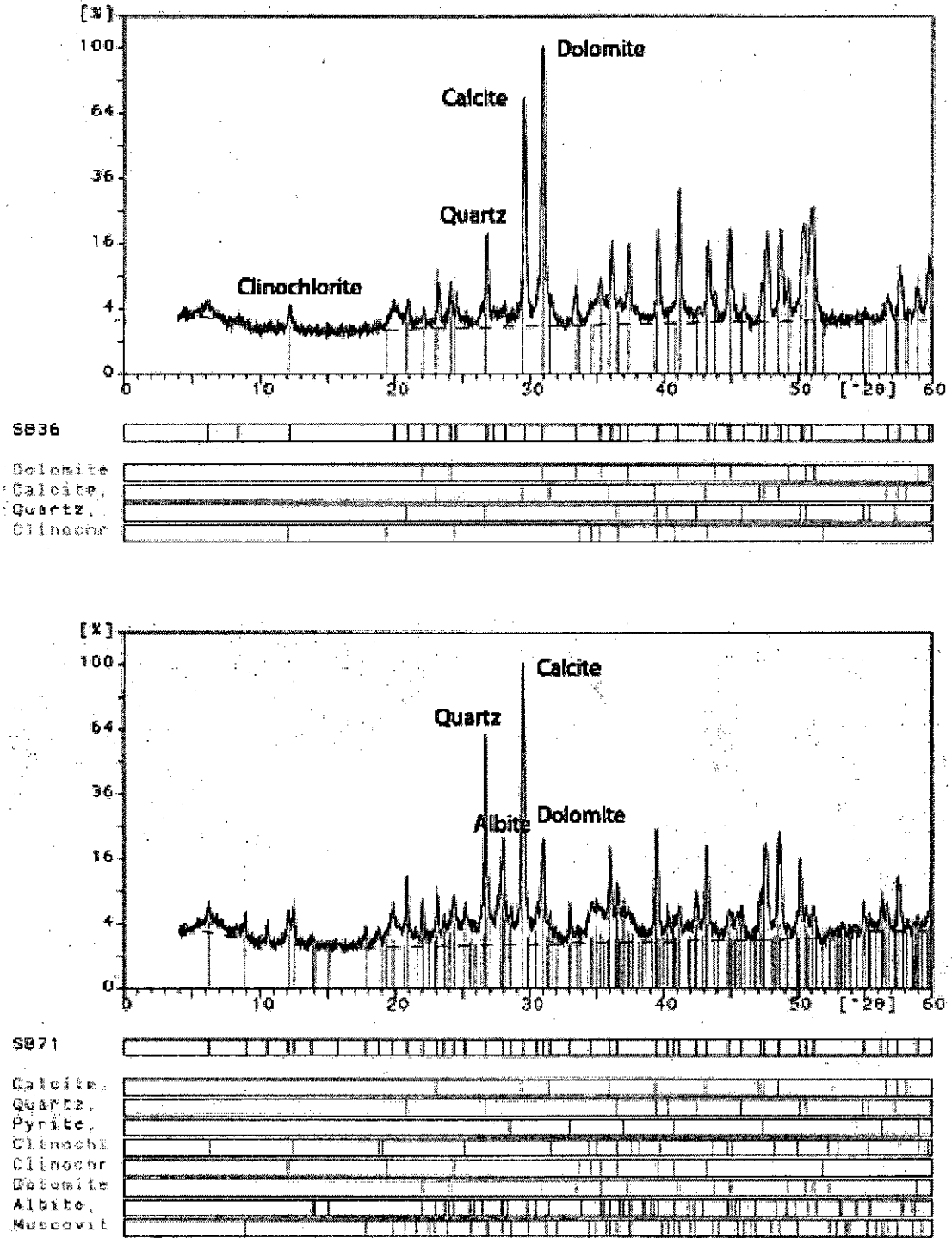


Figure 4.5.2. Sample XRD traces showing the form the raw data takes.

#### 4.5.2.2 *Results*

The results are discussed, firstly in terms of the general trends seen in the mineralogy of the sediments; then in the context of the area from which the individual samples were taken.

Data can be found in Appendix 2.

The following are general trends observed in the results.

- i. The majority of the samples are mostly composed of calcite (30-95%) and quartz. Only 5 samples analysed contain no calcite and only two samples contain <10% calcite. Five of these seven samples are palaeosols. Quartz is present in the majority of samples (0-64%); the highest concentrations are found in samples from the Gökdere Formation and in palaeosols. Dolomite and aragonite are also present; dolomite is present at high concentrations (up to 72%) in some of the palaeosols, whereas the amount of aragonite is variable.
- ii. A variety of clay minerals are present in the samples. Smectite is the most common, with some samples containing >60%. Illite is present in a number of samples at low concentrations (<10%); however in three samples illite is present in higher concentrations. Smectite and illite are mostly found in the Samadağı and Nurzeytin Formations and are very rare in the Gökdere Formation. Palygorskite and kaolinite are present in a few samples at low concentrations (<10%). Kaolinite is more abundant in the Gökdere Formation and palygorskite is generally found in palaeosols.
- iii. Albite and clinochrysotile (serpentine) are present in the majority of samples; chlorite is occasionally present in trace amounts. Although albite and chrysotile are found throughout the sequence, there is a higher concentration of these minerals in the older samples, especially in the palaeosols.
- iv. Pyrite, haematite, ankerite, muscovite and trenolite are other minerals that are found in significant amounts in some samples.

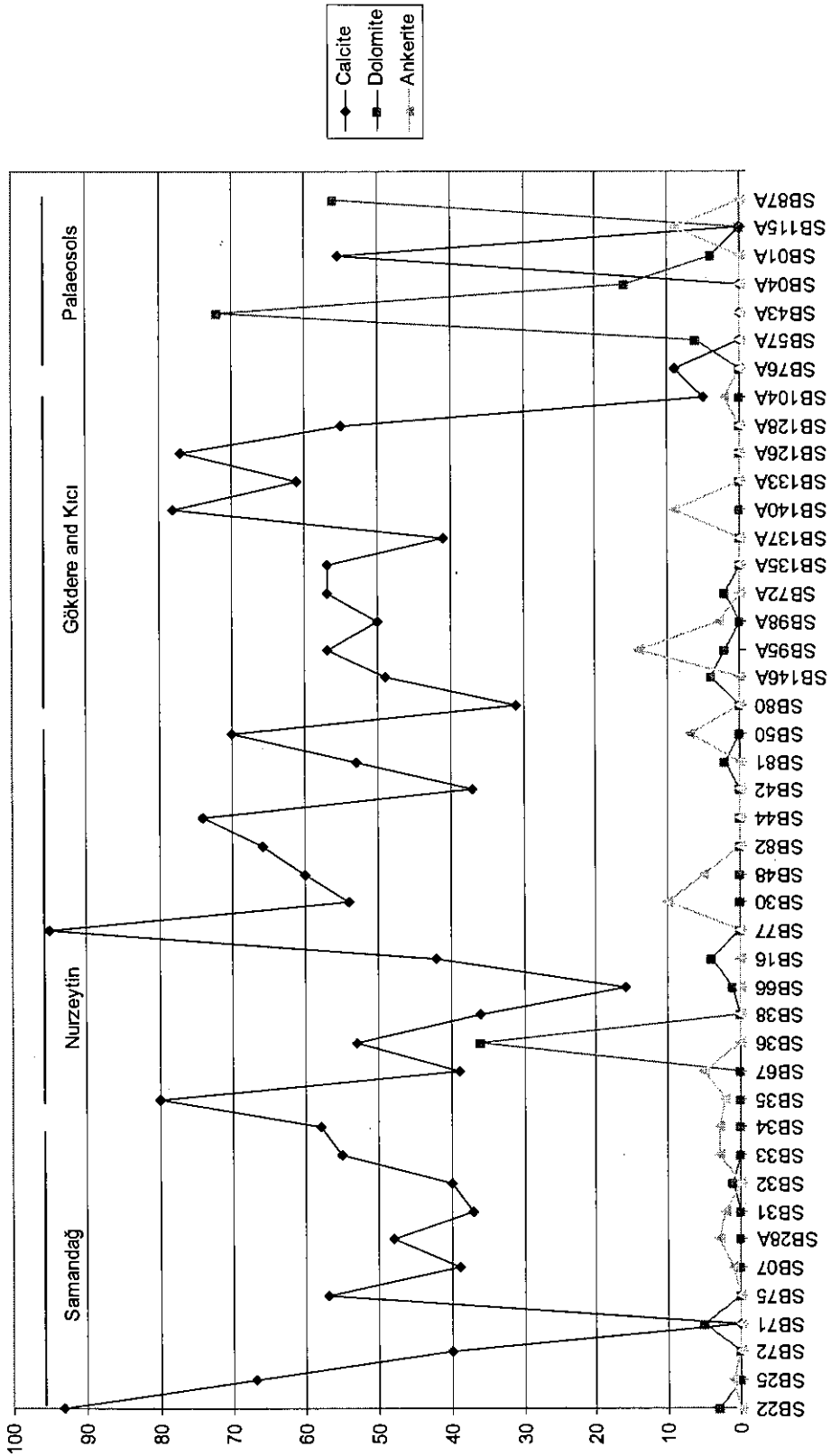


Figure 4.5.3. Graph showing percentage of calcite, dolomite and ankerite in samples analysed.



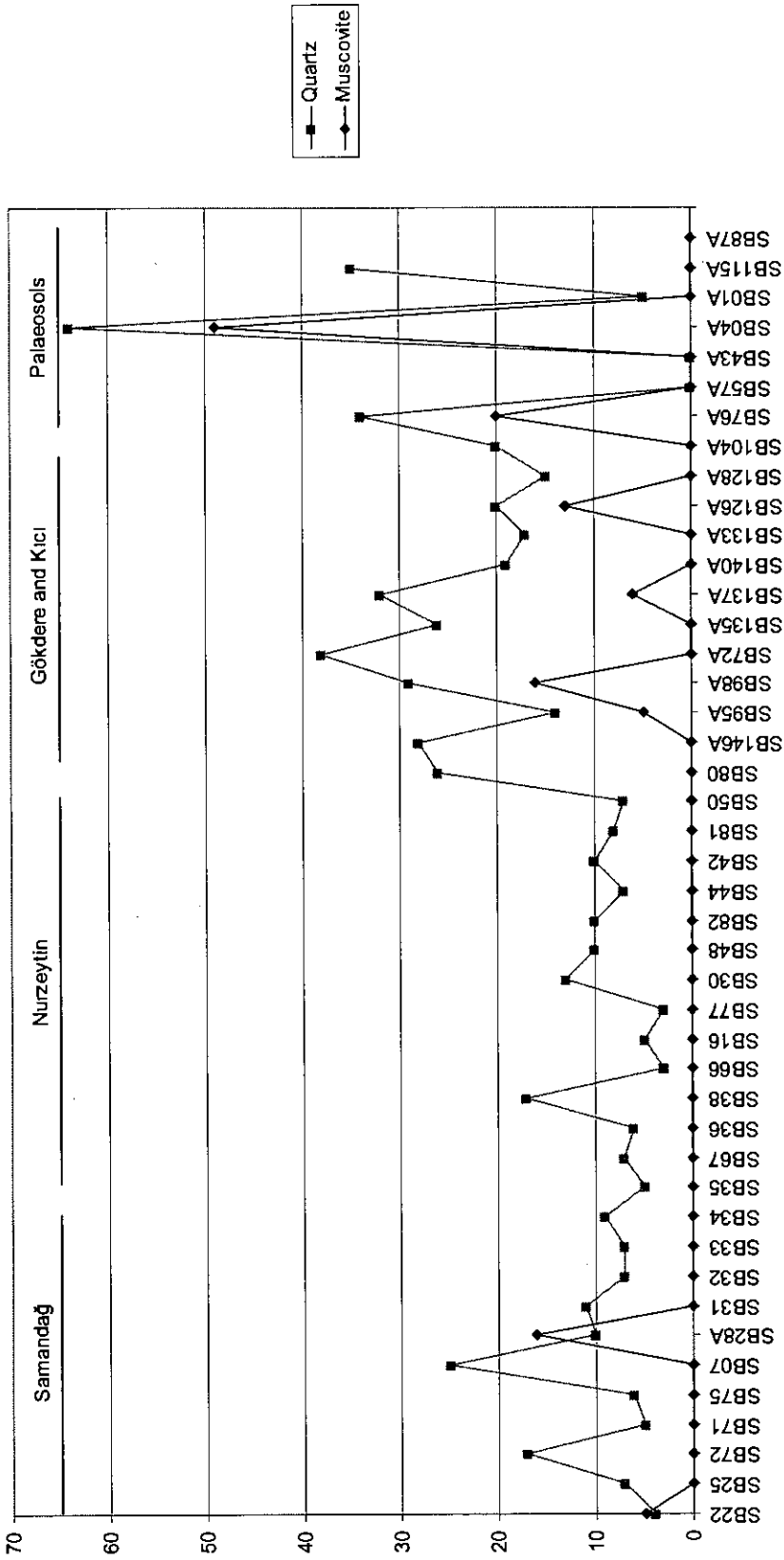


Figure 4.5.4. Graph showing the percentage of quartz and muscovite mica in the samples analysed.

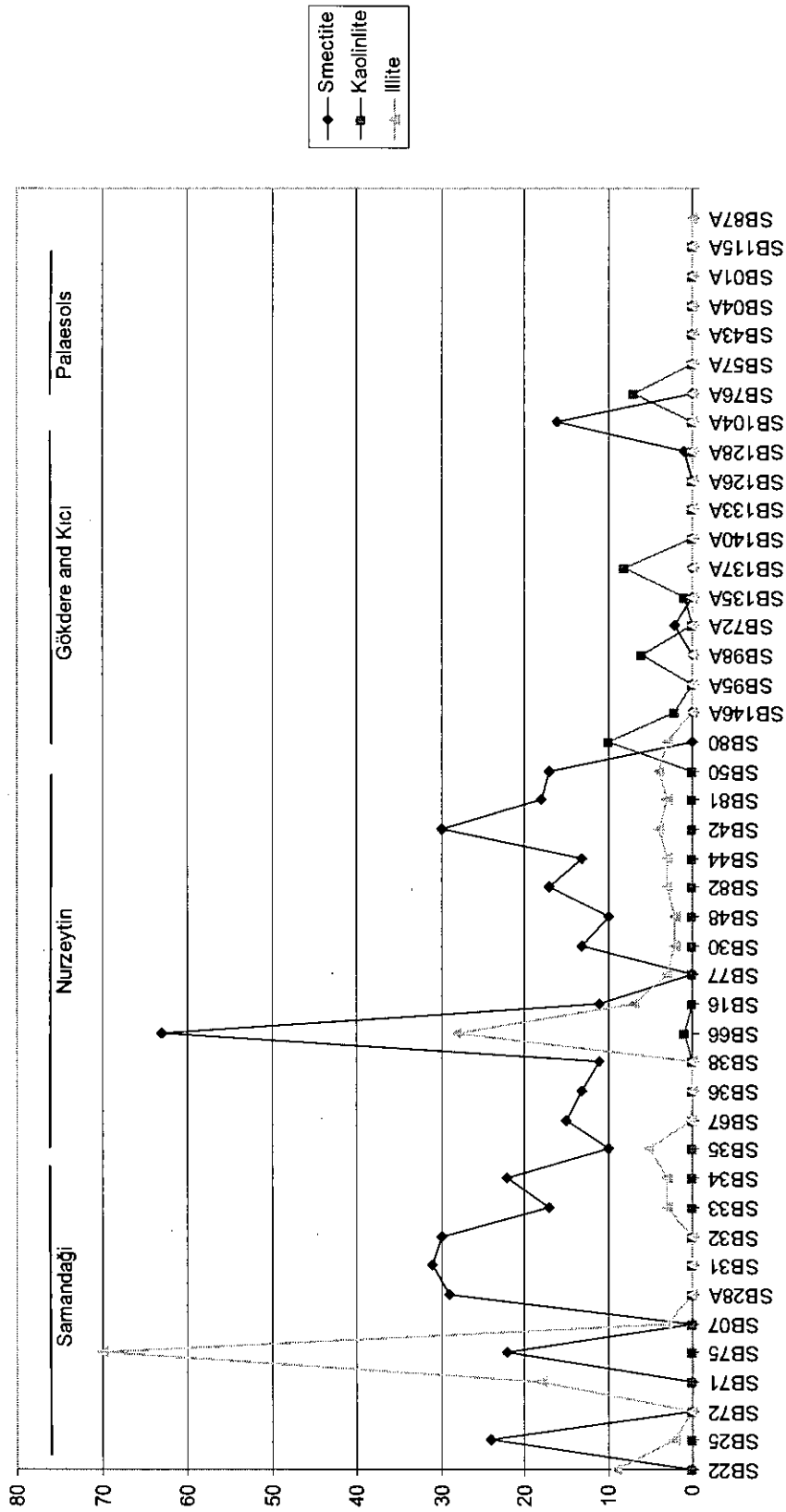


Figure 4.5.5. Graph showing the percentage of smectite, kaolinite and illite in the samples analysed.

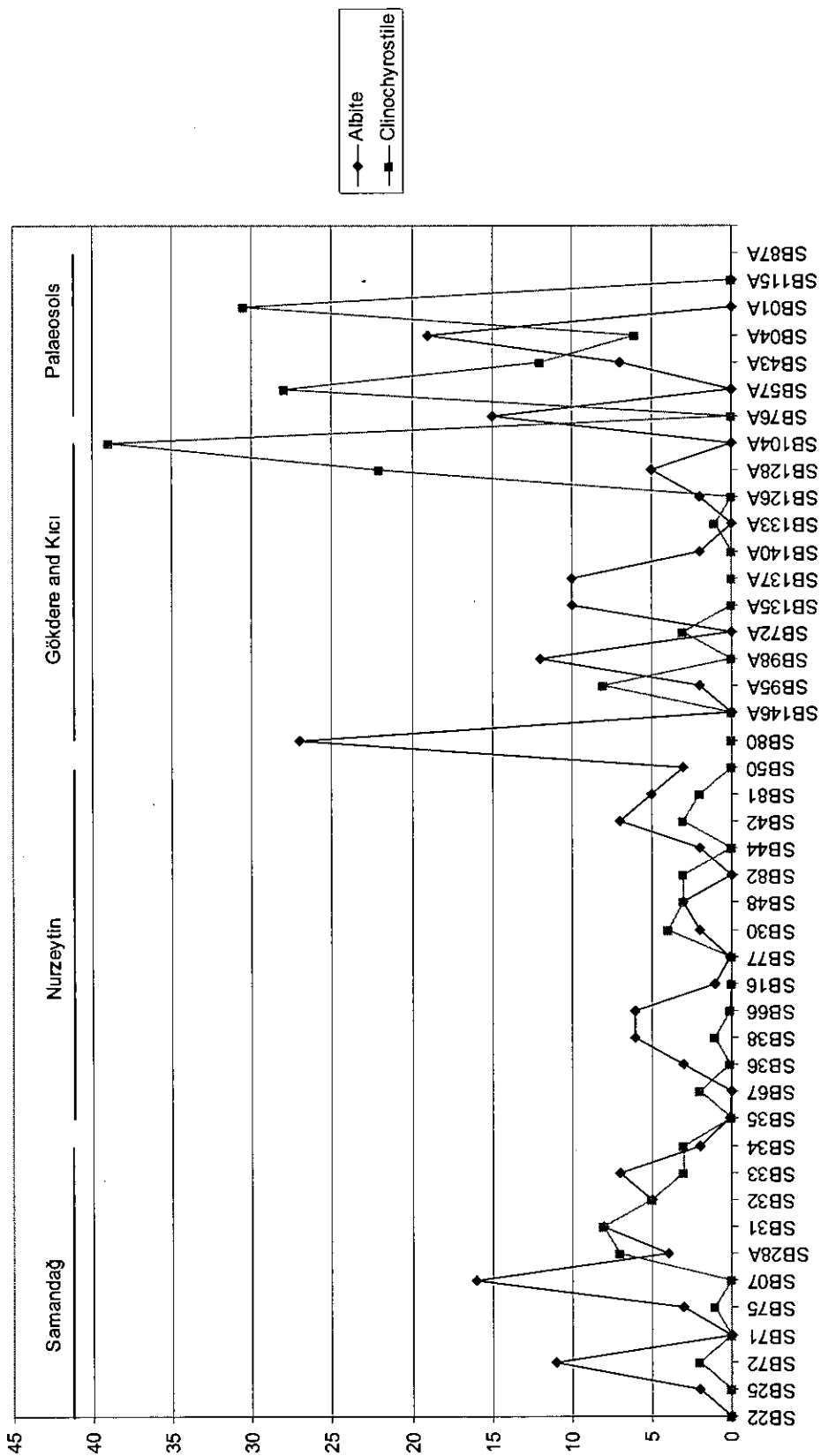


Figure 4.5.6. Graph showing the percentage of albite and clinocrysotile in the samples analysed.

#### 4.5.2.3 *Palaeosols*

Sample SB87A was taken from a soil horizon below Eocene Nummulitic limestones. It is, therefore, interpreted to be Palaeocene or older in age. This sample has a simple composition of dolomite, calcite and palygorskite (by decreasing abundance). Sample SB115A was collected from the base of the Lower Miocene sequence and is composed of calcite, clinocrysotile, ankerite and quartz. Several samples were taken from the base of the Middle Miocene succession, these are variable but generally contain clinocrysotile and albite; haematite is the cause of red colour in two of the samples. In general, the mineralogy of these samples is very different to mud and marl samples from other part of the succession.

#### 4.5.2.4 *Kırıkhan Area*

Two samples were analysed from the Kıcı Formation (Lower Miocene), both have compositions rich quartz and clinocrysotile. Sample SB76A contains abundant smectite (16%) and muscovite (20%) but low calcite (5%). Sample SB104A, by comparison, has no smectite or muscovite but has a high (56%) calcite content.

Ten samples were analysed from the Gökdere Formation. All have significant amounts of quartz (14-38%) and high calcite (31-78%) contents. Albite and muscovite also are quite abundant.

#### 4.5.2.5 *Antakya Area*

Samples from the Upper Miocene Nurzeytin Formation have high quartz, calcite and smectite concentrations; most have illite, clinocrysotile and albite in small to trace amounts. Dolomite and ankerite are present in a few samples.

Samples from the Samadağı Formation are compositionally similar to the Upper Miocene Nurzeytin Formation, in that the samples are rich in calcite, quartz and smectite with trace amounts of other minerals.

#### 4.5.2.6 Discussion

The most common mineral to be found in the fine-grained sediments is calcite, leading to the majority of very fine-grained samples being termed marls. Therefore, we can conclude that the background sedimentation in the graben was calcareous in nature. In general, the non-calcareous mudstones were sampled from palaeosol horizons and thus can be termed silcretes; however, three palaeosol samples did contain calcite, probably in the form of caliche as this was observed in some horizons. In addition to a calcite component from deposition from suspension, some of the calcite present may be from calcareous shelled organisms, such as foraminifera. Aragonite was present in some samples and this probably had a biogenic source. The presence of dolomite and ankerite suggests that in some samples diagenesis has occurred. Ankerite often forms as veins in shales due to low temperature metasomatism or the oxidation of sulphides.

Minerals formed from weathering of the ophiolite, mainly clinocrysotile, albite and tremolite are present in the majority of the samples showing that the surrounding ophiolites have been a sediment source since at least the Lower Miocene. The palaeosol horizons generally have the highest proportions of ophiolitic material and are some of the oldest rocks tested. This may be because during periods of low sea-level the ophiolite underwent greater erosion, thus indicating the importance of relative sea-level change over time, or due to the relative enrichment of minerals due to the low accumulation rate of palaeosol compared to the rate of ophiolite erosion.

The other mineral present in the majority of the samples is quartz. The highest concentrations occur in samples from palaeosol horizons and from the Kılcı and Gökdere Formations. Quartz is not expected to be present in high volumes if erosion of the underlying ophiolite is the main sediment source. This suggests that material is being sourced from elsewhere, possibly from lithologic quartzites exposed to the north in the Amanos Mountains near Kırıkhan (e.g. Sadan, Sosink, Seydişehir Formations), or further away from the Taurus Mountains. Alternatively, the quartz may be sourced from chert; chert is relatively common in some intervals of the succession.

Muscovite is present in some samples and is likely to have an extrabasinal source, from metamorphic rocks. It is quite common in palaeosol horizons and in the Kılcı and Gökdere Formations, although it is rare in the main Hatay Graben. This is the same pattern as seen

for quartz and suggests that the Hatay Graben was more distal from these detrital sediment sources than the northern area.

The last main components of the fine-grained sediment are the clay minerals. Smectite is very common in the Nurzeytin and Samandağ Formations and illite is present in low concentrations. Smectite forms in sedimentary rocks by diagenetic processes; deep burial diagenesis causes conversion of smectite to illite/ smectite and illite (Deer et al. 1992). Also, smectite, mixed with illite, is widely found in soils derived from the weathering products of basic rocks. Illite forms from the breakdown of muscovite, kaolinite and feldspar but principally from the diagenetic alteration of smectite. As it is unlikely that these sediments have undergone deep burial diagenesis, it is more likely that the illite present is detrital in nature. The weathering of feldspars can form kaolinite; it is present in the Kıcı and Gökdere Formations and probably is related to the high proportion of ophiolitic material found in them.

Pyrite and haematite are present in a few samples. Pyrite has been observed to infill fossils and in is likely to have formed during diagenesis. Haematite has given a red colour to some of the sediments, and probably formed during diagenesis in oxidising conditions.

### **4.5.3 Medium-grained sediments.**

In order to investigate the nature of the medium-grained sediments found in the field area, thin-sections were cut from limestones and sandstones. Petrographic descriptions were made of the samples and representative sandstones were point-counted in order to give quantitative results for compositions. Full thin-section descriptions can be found in Appendix 3, and individual samples are cross-referenced in Chapter 4.1. In this section the result of the sandstone point-counting will be presented and discussed.

### **4.5.4 Point-counting of sandstones**

#### *4.5.4.1 Point-counting methodology*

Samples of sandstone were collected from various stratigraphic heights and localities within the field area. Thirteen samples of coarse-grained sandstone (mean grainsize > 1mm) and ten of medium-grained sandstone (mean grainsize ~0.5mm) were examined in thin-section and point-counted; point-counting is a quantitative measurement of the proportion of different grain types that compose the sandstone or other lithology.

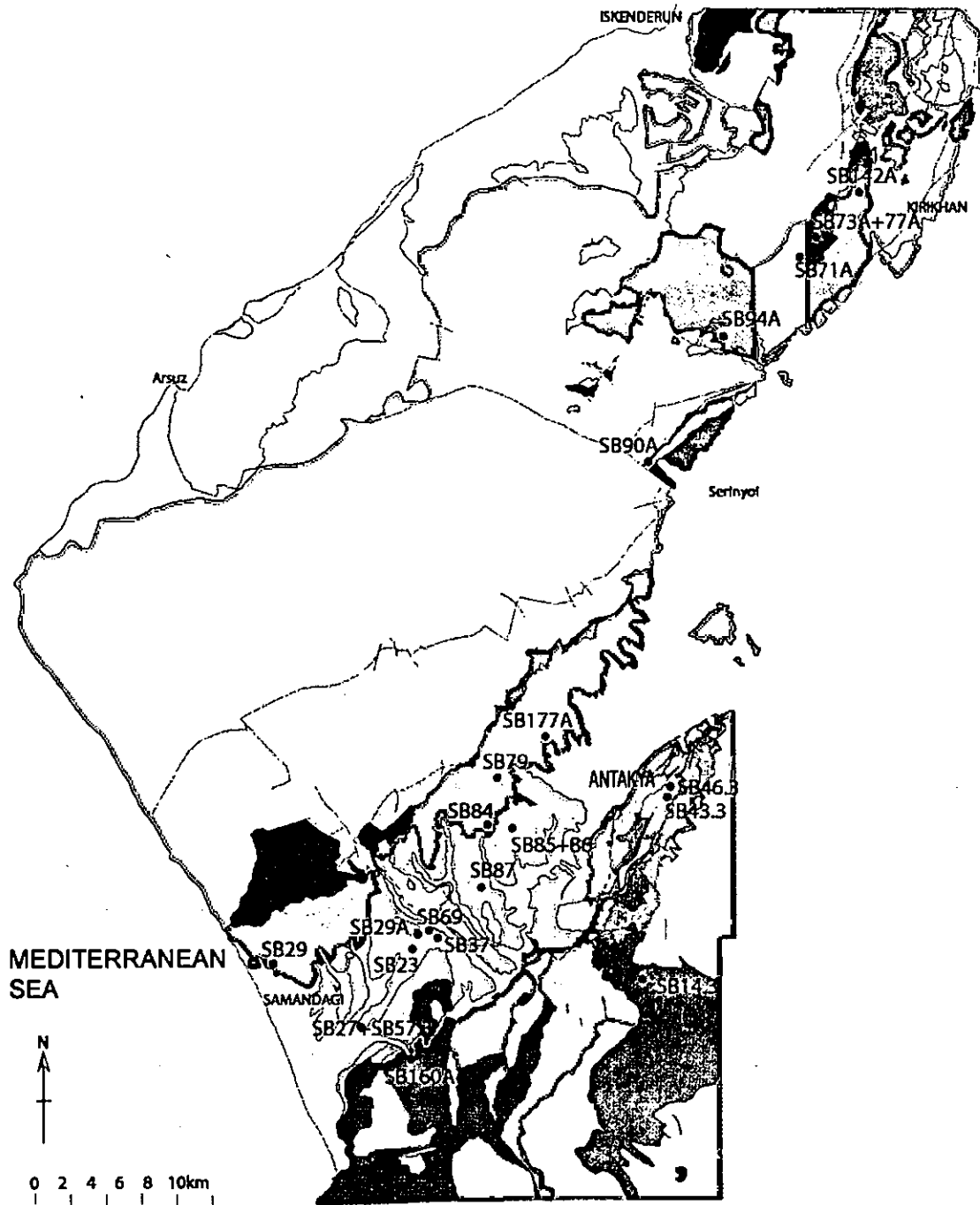


Figure 4.5.7. Map showing the location of samples used in point-counting.

Two hundred points were counted for each thin-section in order to have a statistically meaningful sample group. In the technique used, rock fragments were recorded as either having been derived from the underlying ophiolitic basement or having a carbonate or siliciclastic origin; no further differentiation was made. In addition to lithic fragments, individual quartz (monocrystalline and polycrystalline) and feldspar (plagioclase mainly but also alkali) crystals were recorded, as were any other individual grains that appeared under the cross hairs such as micas or bioclastic material. The matrix was counted either as primary matrix (micrite) or as cement (sparite).

The results are summarised in Appendix 4 and were also plotted as ternary diagrams; the classic monocrystalline quartz-feldspar-lithic fragments (Q(m)FL) diagram and also a polycrystalline quartz-sedimentary-lithic fragments-ophiolite lithic fragments (Q(p)LsLv) diagram. (Dickinson 1983).



## 4.5.4.2 Point-counting results

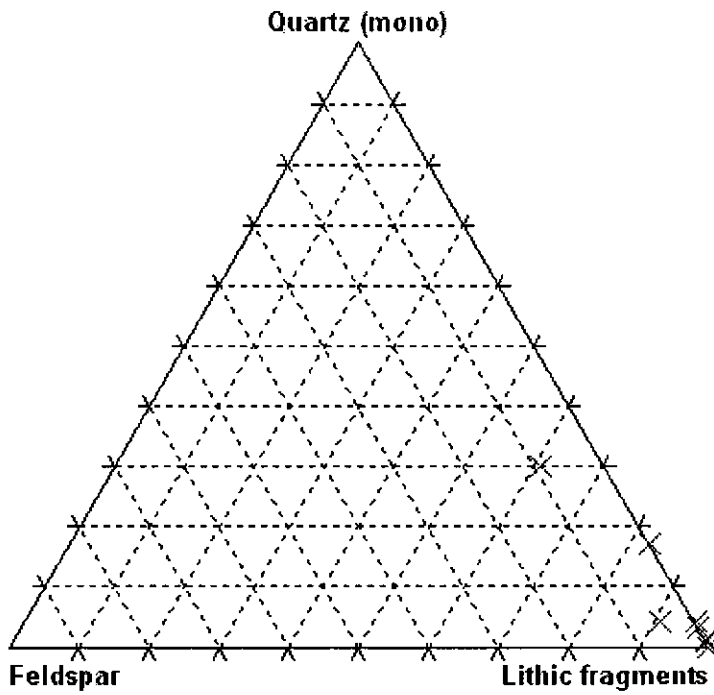


Figure 4.5.8. Q(m)FL diagram for coarse-grained (&gt;1mm) sandstones

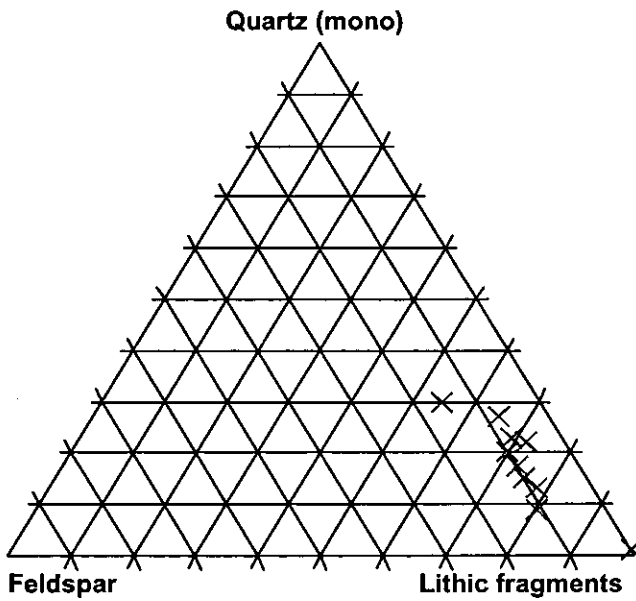


Figure 4.5.9. Q(m)FL diagram for medium-grained (~0.5mm) sandstones.

Figure 4.5.8 shows a cluster of results in the lithic fragment corner. This is not surprising as the majority of sandstones are classified as litharenites (>50% lithic fragments). Samples SB160A and SB29 lie slightly off the trend due to a higher quartz composition. Using the provenance diagram of Dickinson (1983), all the samples plot within the lithic recycled area of the recycled origin.

Medium-grained samples (Fig 4.5.9) exhibit a range of compositions from 100% lithic fragments to ~60% quartz; 10% lithics and 10% feldspar. This variation does not seem to be related to the age of the sediments as samples of Late Miocene and Pliocene age plot in amongst each other.

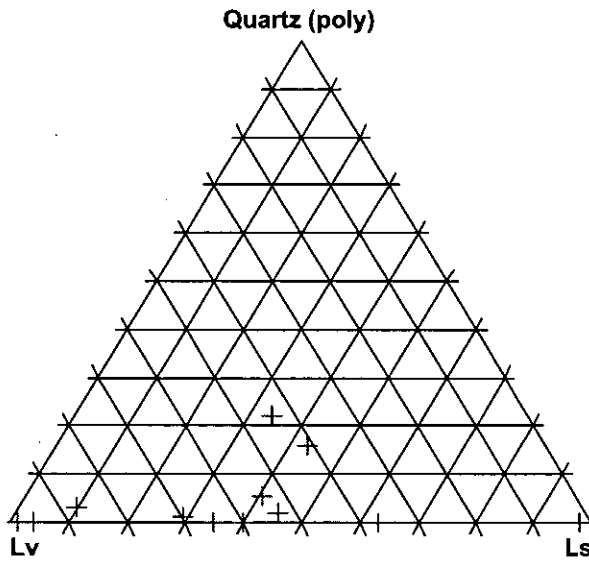


Figure 4.5.10. Q(p)LsLv diagram for coarse-grained (>1mm) sandstones, N.B. Lv includes serpentinite material

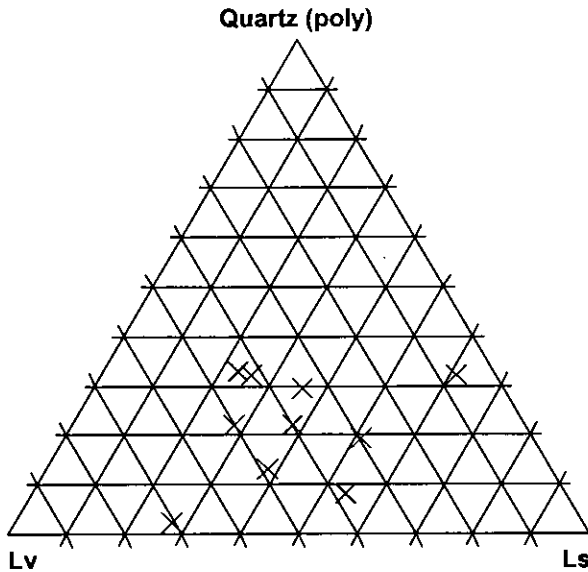


Figure 4.5.11. Q(p)LsLv diagram for medium-grained (~0.5mm) sandstones.

When the lithic fragments and polycrystalline quartz are considered there is much greater variety exhibited in the composition of the sandstones for both grain sizes. The coarse sandstones (Figure 4.5.10) generally have low concentrations of polycrystalline quartz; only samples SB69 and SB73.3 contain significant amounts of polycrystalline quartz. The samples do have a range of compositions between the two end members of sedimentary and volcanic fragments. In contrast, the finer grained samples (Figure 4.5.11) have a higher proportion of quartz than the coarse sandstones, but these too show variation in the proportions of different types of lithic fragments.

#### 4.5.4.3 Discussion

These results show that the composition of all the point-counted sandstones is dominated by clasts derived from pre-existing rocks and therefore can be called litharenites. Coarse-grained rocks show very little compositional variation, with only SB160A and SB29 (both Pliocene in age) not falling in the same area as all the other samples. Finer-grained samples are also all litharenites but there is a slightly wider spread of compositions. There is no age trend, as samples from different ages plot in amongst each other.

When polycrystalline quartz and lithic fragments are considered, the coarse-grained samples contain very little polycrystalline quartz (apart from SB57.3 and SB69, both Pliocene in age). The majority of the samples contain more ophiolitic material than sedimentary, apart

from sample SB90A, which is Late Cretaceous in age. This indicates that since the Early Miocene the most important clastic source into the basin has been the ophiolite, but prior to this very little material was shed from it. Fine-grained samples also are dominated by ophiolitic clasts but there is a much greater component of polycrystalline quartz. This is perhaps due to current action causing separation of mineral fractions.

Samples of rocks were collected from the Palaeozoic sediments exposed in the Karasu Rift in order to investigate potential sources for the siliciclastic sediments of the Hatay. Two main lithologies were identified and sampled; a pink quartz arenite and a greywacke. The greywacke also contained a large percentage of quartz, plus plagioclase and clay minerals and rare muscovite. It is thus possible that some of the quartz observed in the sediments in the Hatay Graben was sourced from these Palaeozoic sediments; however, muscovite is not common suggesting that the source of this mineral is from further afield.

## 4.5.5 Diagenesis

### 4.5.5.1 Sandstone diagenesis

Late Miocene and Pliocene sandstones in the field area have undergone varying degrees of carbonate cementation. In some outcrops this is evenly distributed while in others carbonate concretions can be observed.

Lower Miocene limestones of the K1c1 Formation (northern area) contain a small percentage of sparite cement (<10%).

Upper Miocene sandstones (Nurzeytin Formation) and occasional calcarenites in the Sofular Formation (Middle Miocene) are cemented with drusy sparite; this can be clear or cloudy and has effectively reduced the porosity of the sandstones to zero in most of the samples. Isopachous fringes have developed around clasts in some samples (e.g. SB160A, Middle Miocene, Figure 4.5.12)

Sandstones of the Gökdere Formation also have calcite cements with poikilotopic textures in some samples. A few samples contain clasts that have optically continuous overgrowths and micritic envelopes.

Sandstone is the dominant lithology of the Pliocene (Samandağ Formation). Again mostly the cement is clear drusy sparite that has infilled the majority of the original porosity, although some samples do retain some primary porosity. In some sandstones the clasts have micrite envelopes (e.g. SB69; Figure 4.5.13), and there are occasional poikilotopic textures and optically continual overgrowths of calcite clasts. Sample SB4.3 shows a variety of textures; the carbonate clasts often have micritic envelopes and there are apparently two stages of drusy sparite growth, firstly the formation of small crystals on edges of clasts (good nucleation sites) and then the later infilling of the remaining pore space by large sparite crystals.

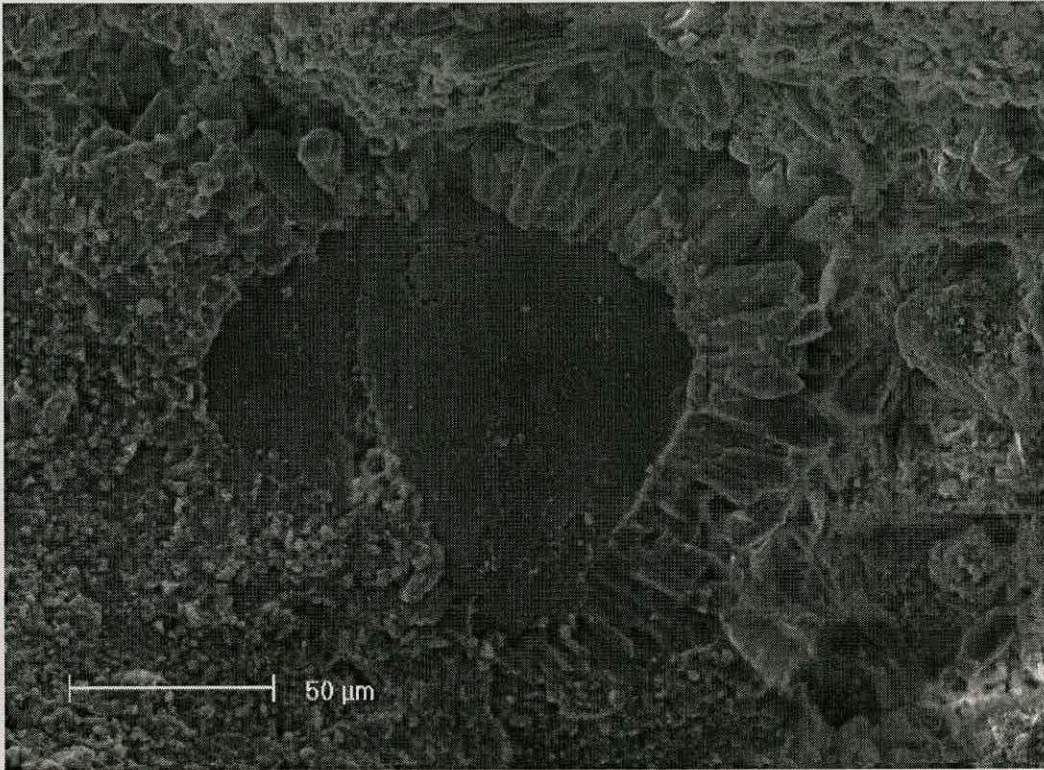


Figure 4.5.12. SEM picture showing a calcite clasts from sample SB160A with a partial fibrous isopachous fringe. This represents the first stage of cement; subsequent cementation took the form of fine drusy sparite.

Micrite envelopes may be the result of grain degradation through the activity of endolithic bacteria. If this is the case it indicates that the grains were deposited within the photic zone but subsequent transportation to deeper water may have taken place (Tucker 1991).

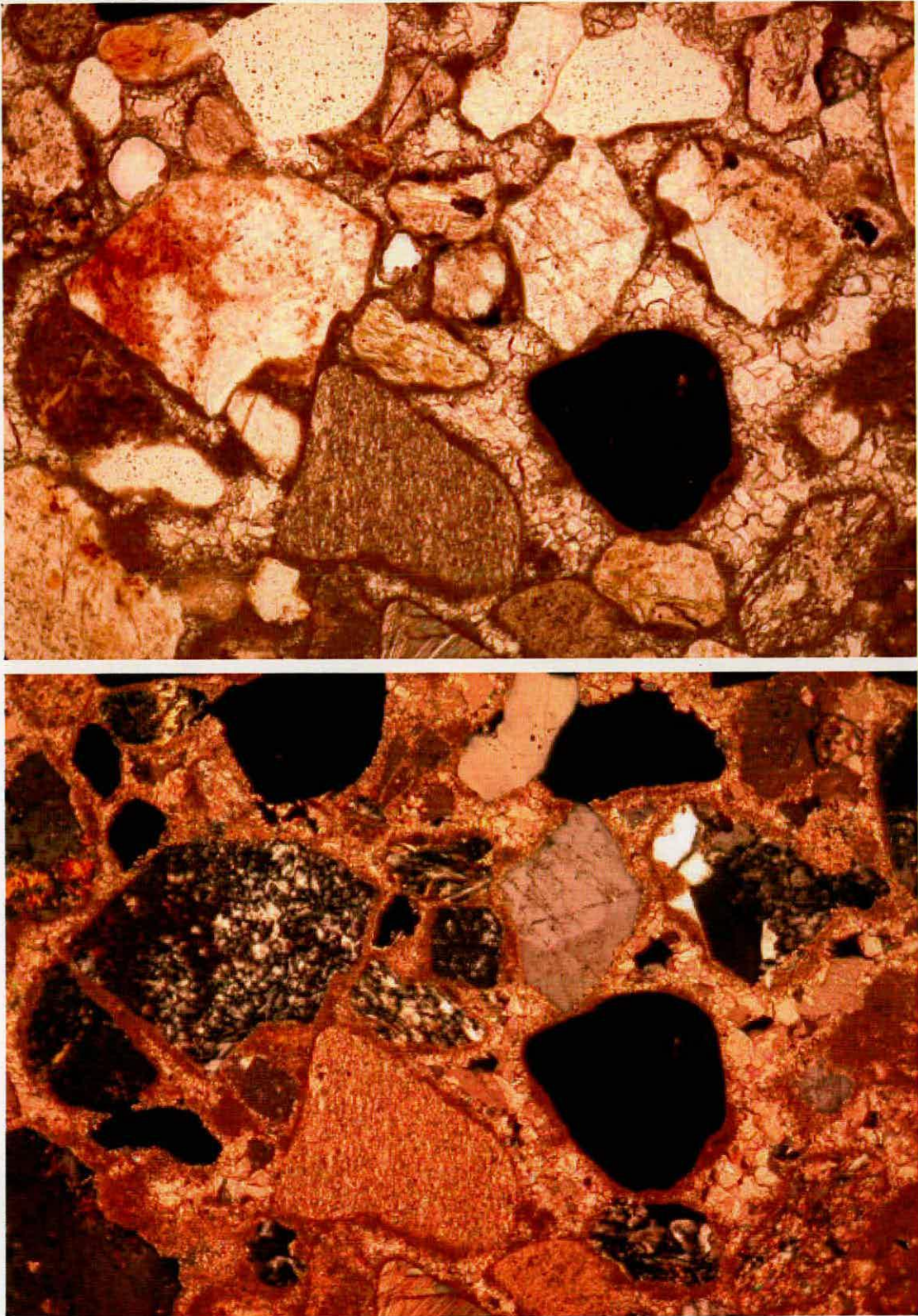


Figure 4.5.13. Photomicrographs of SB69, top plane polarised light, bottom crossed polars. Note the dense micrite envelope encasing the grains. Later sparite cementation filled in the porosity. Note how the crystal size of the sparite crystals increases into the centre of the void.

#### 4.5.5.2 *Limestone diagenesis*

Eocene limestones from the north and the south both have calcite cements that form optically continuous overgrowths, commonly on top of echinoid fragments, and have poikilotopic texture. There is no primary porosity generally preserved.

The Middle Miocene Sofular Formation is composed of bioclastic wackestones, packstones and grainstones. The percentage of primary porosity present is variable with none in some samples and porosity of >10% in others (i.e. SB41, Figure 4.5.14). Secondary porosity caused by the dissolution of aragonitic bivalve shells does occur in some samples but this is rare and generally they have been replaced by calcite. For example, SB21.3 from Kozkalesi contains some primary porosity preserved in bioclasts only partially filled with sparite and there is also some secondary porosity due to the dissolution of bioclasts. Syntaxial overgrowths are often present on fragments of echinoid and crinoid.

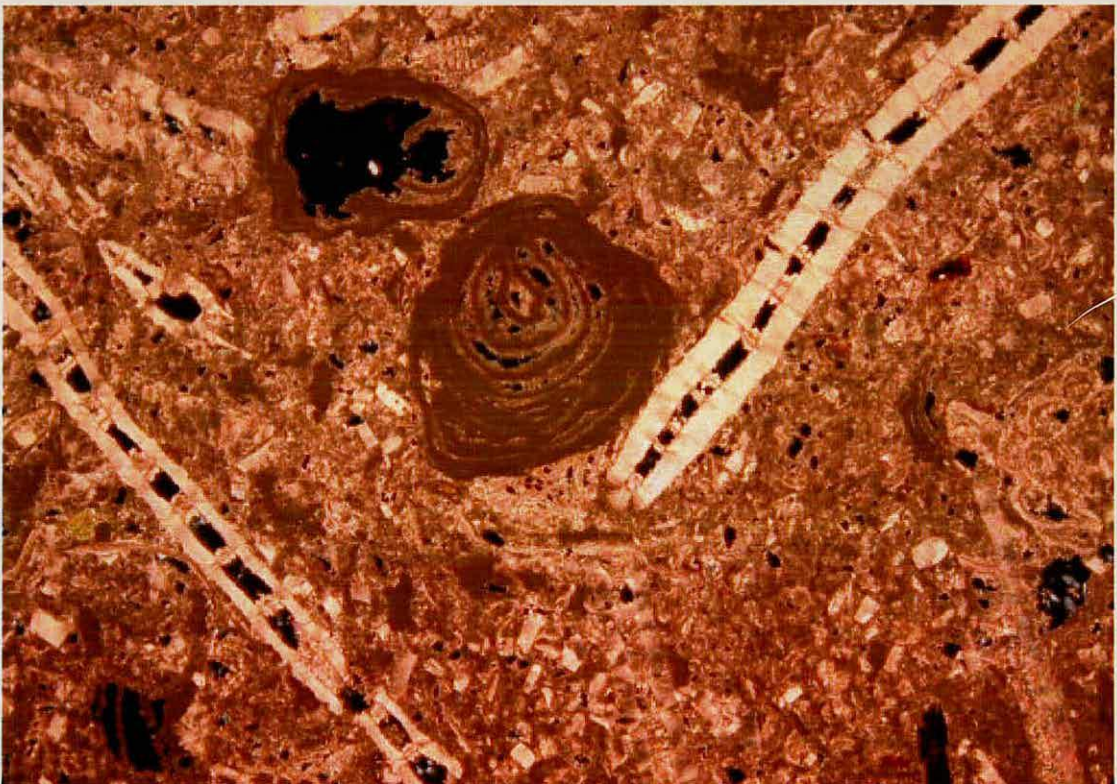


Figure 4.5.14. Photomicrograph of SB41 in crossed polarised light showing primary porosity (black) preserved in bioclasts (benthic foraminifera and oncolites) and within the matrix.

In general these limestones contain high proportions of micrite and the amount of cement is small. However, good textures can be observed in some samples. For example, in SB47 there are isopachous fringes of fibrous calcite crystals around some clasts and in SB70, drusy calcite crystals are coarser in the centre of filled voids.



Limestone of the Kepez Formation from the northern study area and rare Upper Miocene limestone in general have the same diagenetic characteristics as those of the Sofular Formation.

The presence of isopachous fringes indicates that these sediments were below the water table during diagenesis. The dominance of calcite cement and general lack of dissolution indicates that the pore water was saturated with calcium carbonate. These factors indicate diagenesis took place in the marine realm.

### 4.5.6 Conglomerate Petrology

In order to understand the origins of the conglomerates *in situ* clast counting was performed in the field (Appendix 5). Where possible a grid was constructed on the outcrop and around 100 clasts were identified and counted; this was done at 26 locations (Figure 4.5.15). The conglomerates contain a range of clasts that are mainly sedimentary in origin (limestones, chert, sandstone, mud, conglomerate and chalk) or serpentinite. Rarely, clasts of basalt or schist are present. Figure 4.5.16 shows that there are three main compositional groups: serpentinite dominated, sedimentary dominated and mixed sedimentary and serpentinite.

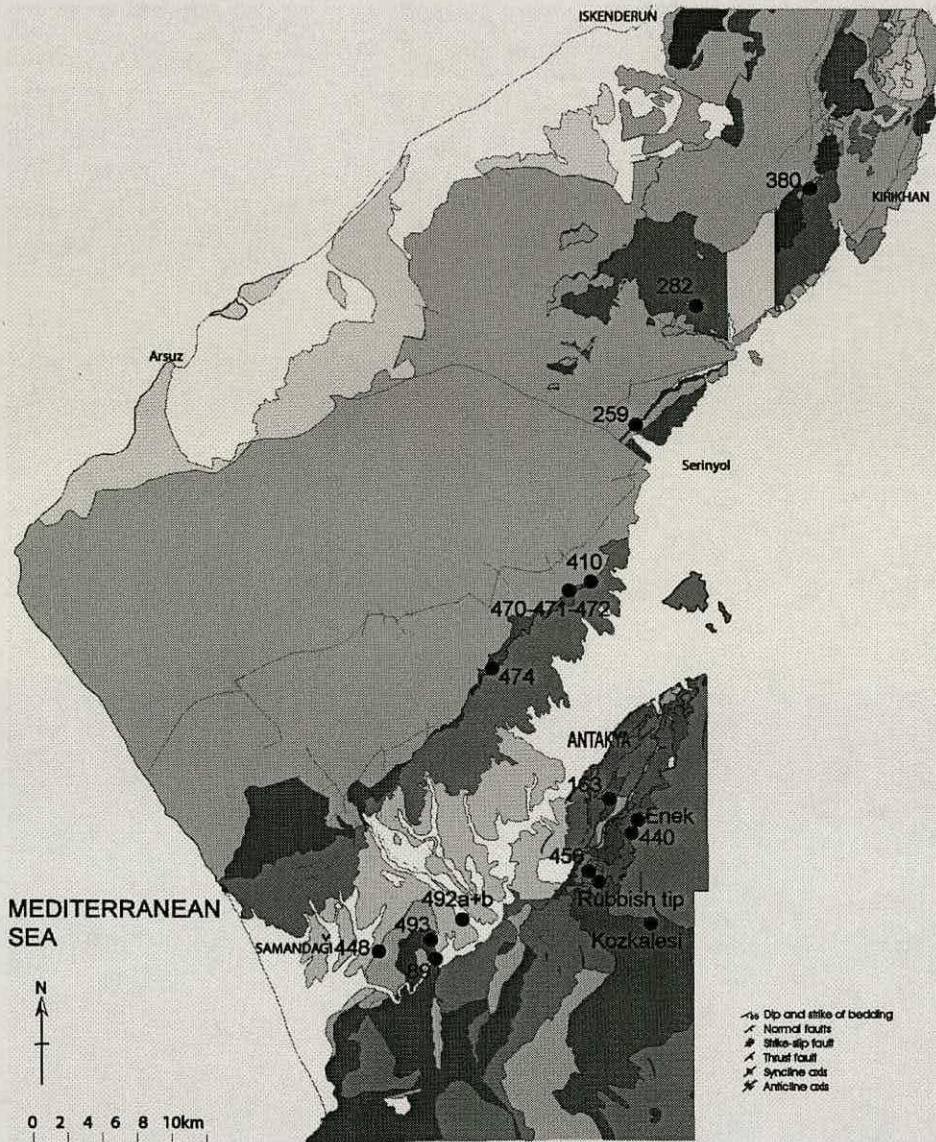


Figure 4.5.15. Map showing the locations of outcrops where conglomerates were clast counted.

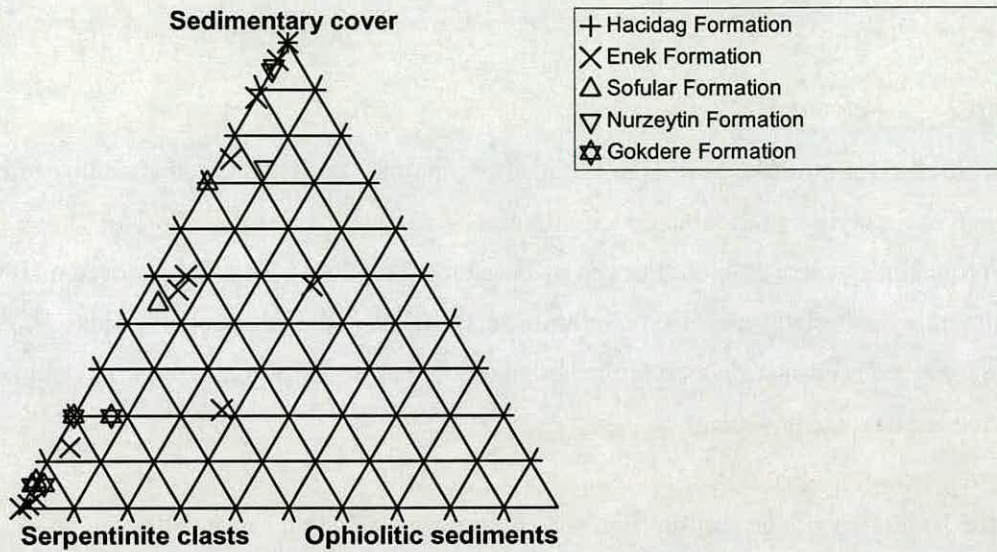


Figure 4.5.16. Ternary diagram showing the composition of conglomerates, for a description of the different classes refer to text below.

The serpentinite clasts that were derived from the ophiolites are usually too weathered to determine the original composition, although from grain-size it is likely that basalts and dolerite dominate, while gabbro is also present in smaller amounts. Occasionally, fresh samples of all these lithologies were observed.

Sedimentary clasts are much more varied and divided into two classes. Red chert, similar to that observed in Baer Bassit, and jasper are present in basal conglomerates of the Balyatağı Formation and are possibly from the sedimentary cover of the ophiolite or from older sediments underlying the ophiolite and thus termed ophiolitic sediments. Nummulitic, algal and pink pelagic limestone clasts were derived from the Late Cretaceous to Eocene cover. Smaller numbers of clasts of bioclastic limestone, marl, conglomerate and sandstone were reworked from the Neogene sediments found in young conglomerates. Rare exotic clasts of schist, pink calcarenite and fresh basalt are sourced from upstream in the Karasu Graben or from further afield.

The texture of the conglomerates varies between formations but there is no consistent trend. Conglomerates are clast and matrix supported, poorly to well sorted and clasts are generally well-rounded to sub-angular.

#### 4.5.6.1 *Belen and Kırıkhan Areas*

The oldest conglomerates (from the Hacıdağ Formation) counted are in the vicinity of the village of Serinyol and the abandoned village of Kanlıdere (SE of Belen). The conglomerates observed in the Eocene succession at both locations are composed of 100% sedimentary material; limestone (calclutite and bioclastic) and black chert. This conglomerate is clast-supported with sub-angular to sub-rounded clasts, up to 50cm in size; the mean clast size is ~10cm.

At the Kanlıdere village section (Fig. 4.5.15, location 282), two Lower Miocene conglomerate horizons (<10m apart in the section) are present above the Eocene interval. The composition of these conglomerates is dominated by sedimentary clasts (varied limestones often with borings and chert) but there are also serpentinite clasts. These conglomerates are matrix supported, poorly sorted, with sub-rounded to well-rounded clasts and form discrete horizons.

Near Gökdere, the Early Miocene sediments differ from those near Kanlıdere. In this area there is an abundance of coarse clastics and the composition of the conglomerate horizons is dominantly serpentinite. There are also a few limestone clasts present. These conglomerates are generally poorly sorted and matrix-supported conglomerates with sub-rounded to well rounded clasts.

#### 4.5.6.2 *Antakya Area*

The Early Miocene was a period of conglomeratic deposition in the area around Antakya and eight locations were clast counted. The composition of this unit is variable; serpentinite and sedimentary clasts change proportion. Composition varies laterally and vertically, and no lateral trend is obvious, but it seems that the formation fines upwards and that there are more clasts of pelagic limestone, red chert and Jasper in the bottom half of the formation. Texturally, these sediments are very poorly sorted and clast- and matrix-supported horizons were identified; clast shape also varies from sub-angular to rounded.

Lower Miocene conglomerates are also present on the northwest margin. At the village of Karaali (location 410) and at location 472 conglomerates at the base of the sedimentary succession were observed. Both have a mixed sedimentary/serpentinite composition, but the sedimentary clasts (limestone and grey chert) are the most significant.

Fewer conglomerates are present higher in the sequence. Basal Middle Miocene conglomerates were measured at locations 474 and 448. Location 474 on the NW margin is dominated by serpentinite clasts but has a few sedimentary clasts (limestone and sandstone), whereas at location 448 serpentinite dominates with occasional limestone clasts. Two conglomeratic horizons within the Middle Miocene succession were also counted. At Kozkalesi, two thirds of the clasts are limestones, the rest serpentinite. Along the Asi river, there is a greater variety of clast compositions but sedimentary and serpentinite clasts are present in equal proportions.

Conglomerate horizons from the Late Miocene succession show variability between different levels, e.g. at location 492, although the clast composition is a mixture of sedimentary and serpentinite-derived material, the sedimentary clasts are more important and show a greater variety of clast types than in older conglomerates (i.e. muds, basalt, sandstone).

#### 4.5.6.3 *Discussion*

Eocene conglomerates are composed entirely of limestone clasts, i.e. Nummulitic limestone or pinkish fine-grained limestone; no serpentinite material is present indicating that at this time ophiolitic material was not undergoing erosion as the ophiolite was still covered by limestone and unroofing had not yet taken place. By contrast, the erosion of Upper Cretaceous and Palaeocene/Eocene limestones was taking place. However, by Early Miocene time, variable amounts of serpentinitised material were appearing in the conglomerates. In the lower part of the Enek Formation there are also significant amounts of jasper and radiolarian cherts, possibly from the Baer Bassit ophiolite or older sediments from below. This indicates that erosion, and by inference uplift, of ophiolite had taken place by the Early Miocene (possible during the Oligocene hiatus, Robertson 1998); this ophiolitic material dominated the supply of clastic material throughout the Early Miocene. Basal Middle Miocene conglomerates are also composed mostly of ophiolitic material indicating that this was the most important source during this time too. However, higher in the Sofular

Formation, sedimentary clasts are just as significant as serpentinite. This suggests that by this time erosion of the sedimentary succession had increased (due to erosion of these rocks) or that erosion of the ophiolite declined possibly due to submergence. This trend continued into the Late Miocene as serpentinite material continued to compose a smaller fraction of the clast compositions. No clast counts were made of Pliocene conglomerates, as horizons were generally small. However, it can generally be said that clast composition is polymict and that serpentinite clasts may form the most significant clast type. Quaternary to modern conglomerates are dominated by serpentinite clasts but contain various sedimentary clasts.

#### 4.5.7 Conclusions

- Fine-grained basin sediments are dominated by calcium carbonate.
- There are high concentrations of ophiolite derived minerals in samples from palaeosols; these range in age from Palaeocene to Middle Miocene, and probably represent relative sea-level lows.
- Mica has an extrabasinal source.
- Sandstones of Middle Miocene age and younger are rich in ophiolite-derived material.
- Conglomerates of Eocene age contain no ophiolite-derived material but do contain Eocene, Palaeocene and Upper Cretaceous sediments.
- Early Miocene and younger conglomerates contain ophiolitic material.
- Thus prior to the Lower Miocene some erosion of the ophiolites took place but this was confined to periods of relative low sea-level, whereas it seems that the sedimentary cover underwent greater erosion. From the Early Miocene to present day there has been continual (although variable) erosion of the ophiolite and cover sediments.

## Chapter 5



The pass at Beilan [Belen].

## 5 Basin Analysis

### 5.1 Introduction

In this chapter, the sedimentological field observations and petrography (Chapter 4 and Appendix 3) will be combined in order to define the facies and facies associations for the southwest study area near Antakya and the northeast study area around the towns of Serinyol, Belen and Kırıkhan (Fig 4.1 and 4.70). This will be achieved by organising facies by age with different locations discussed separately and then integrated and summarised. Additionally, this information allows the reconstruction of sedimentary environments over time and from that the construction of conceptual models for the sedimentary evolution of the region. These interpretations will be compared and contrasted to other basins in the Eastern Mediterranean in Chapter 7.

South western Units	Age	Section in Chapter 4	North eastern Units	Age	Section in Chapter 4
Samandağ Formation	Pliocene	4.2.11	Gökdere Formation	L.Miocene	4.3.7
Nurzeytin Formation Vakıflı Member	L.Miocene Messinian	4.2.7 4.2.9	Kepez Formation	M.Miocene	4.3.5
Sofular Formation	M.Miocene	4.2.5	Kıc1 Formation	E.Miocene	4.3.3
Balyatağı Formation	E.Miocene	4.2.3	Hacıdağ Formation	Eocene	4.3.1
Okçular Formation	Eocene	4.2.1			
Kaleboğazı Formation	L.Cretaceous	4.2.1			

Table 5.1. Summary of the units of the south western (Antakya area) and north eastern (Kırıkhan area) study areas and the age of these units.



## 5.2 Late Cretaceous and Eocene Units

### 5.2.1 Southwestern area

The Upper Cretaceous and Eocene sediments of this area share many similarities and were deposited before continental collision took place to the north and before extension resulted in the formation of the Hatay Graben. Thus, these sediments are passive margin sediments of the Arabian Platform and therefore, I will interpret these sediments together as a precursor to foreland basin development and the formation of the Hatay Graben.

### 5.2.2 Kaleboğazı Formation – Late Cretaceous

The Late Cretaceous sediments of the Kaleboğazı Formation are thin bedded, white limestones exhibiting microbial lamination, fenestral porosity, desiccation breccia and chert nodules (section 4.2.1). Some of these features are indicative of sub-aerial exposure during deposition, and suggest that sedimentation took place in an *intertidal zone*. This is an area that lies between the normal low and high-tide levels and is alternatively flooded and exposed. Low-energy intertidal zones typically include microbial flats. Modern carbonates can be classified in terms of the amount of exposure during the tidal cycle, the ‘exposure index’ (Ginsburg *et al.* 1977) based on common sedimentary structures. The presence of irregular lamination (Section 4.2.1.1) indicates that where this is present these sediments have an exposure index of 40-90% corresponding to the *lower intertidal zone* (Figure 5.1).

The upper part of the Kaleboğazı Formation is composed of interbedded marl, limestone, sandstone and conglomerate (section 4.2.1.1). The exact composition is spatially very variable. Palaeosol horizons are common and caliche is present in some beds indicating that the sediments were deposited in a continental setting (100% exposure) that was probably semi-arid. The siliciclastic layers are generally structureless and quite thin; these are possibly alluvial in nature.

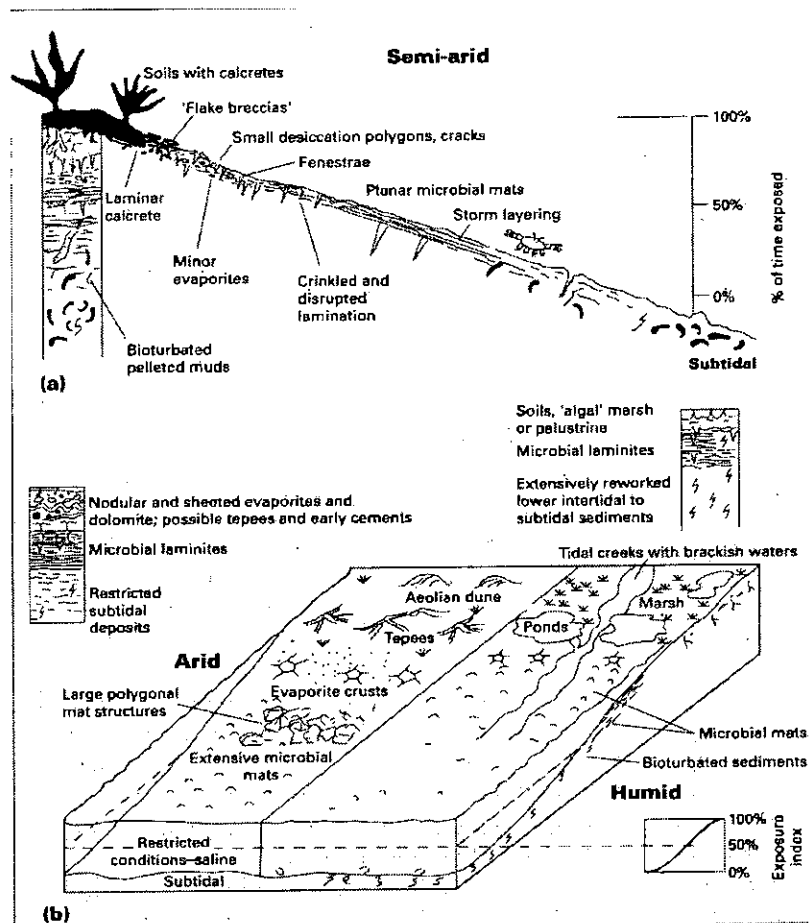


Figure 5.1. (a) Variations in sedimentary structures across a carbonate tidal flat, related to exposure index (Ginsburg *et al.* 1977); irregular and microbial lamination and fenestrae are observed in the Kaleboğazı Formation. (b) Contrasting environments and resulting sediments across an arid versus a humid tidal flat zone, microbial mats are found in both arid and humid conditions. The structures observed indicate a semi-arid to arid environment during the Late Cretaceous. From Wright and Burchette (1996).

#### 5.2.2.1 Okçular Formation - Lutetian

The basal part of the Eocene Okçular Formation is composed of thin-bedded, fine-grained lime mudstone with occasional lenses and horizons of red mudstone; beds are generally irregular and laterally discontinuous. Microbial laminations and fenestral porosity are present (section 4.2.1.2). These factors suggest that the environment of deposition of this formation is very similar to that of the Kaleboğazı Formation, i.e. within the *intertidal zone* (Figure 5.1). The mudstone horizons may represent immature soils, due to their mottled colour and lack of fossil material, suggesting that the exposure index was higher during the Lutetian than the lower part of the Kaleboğazı Formation, reaching 100% at times (Ginsburg *et al.* 1977).

The upper part of the Okçular Formation is composed of bioclastic packstone/rudstone. The main bioclastic components are large benthic foraminifera including *Nummulites*, *Discocyclusina* and *Milliolidids*, but planktic foraminifera are also present in some samples. Reworked oncolitic material is also occasionally present. This indicates that these limestones were deposited on the shelf-edge to slope (Figure 5.2) (Sartorio & Venturini 1988). *Nummulites* tend to prefer waters depths of 20-100m (Saller *et al.* 1993) and the presence of an accumulation of reworked oysters at one location (section 4.2.1.1) suggests that water depth was relatively shallow and restricted in places, perhaps indicating a shelf-edge position at the shallower end of the depth range of *Nummulites* or that the water depth was not constant in the area possible due to an irregular sea-floor topography.

The Eocene and Upper Cretaceous limestones both contain chert nodules that are often parallel to bedding planes. Nodular chert is often present in shelf limestones such as the Lower Carboniferous of the U.K. (Tucker 1991) and has a diagenetic origin. It is not clear where the silica for the chert originated but it is possible that sponge spicules, radiolarians or diatoms were the source. The shelf edge setting may make it more likely that diatoms are the source of the silica due to high productivity from upwelling.

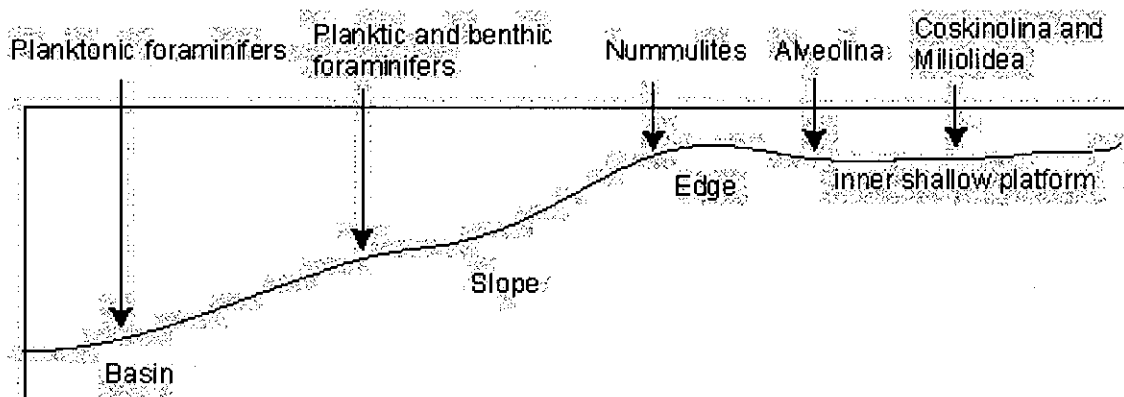


Figure 5.2. Carbonate-slope facies showing typical foraminiferal faunal assemblages for the Early-Middle Eocene, adapted and redrawn from Sartorio and Venturini (1988)

Thin-sections reveal that bioclastic material is the most common clast type (appendix 3), including some clasts derived from a lithified limestone. No ophiolitic material was found in the limestone apart from one sample taken directly above the ophiolite/Eocene boundary. Some erosion of Upper Cretaceous limestones may have taken place, but the ophiolite underwent only very local erosion during this time. Generally, there was no siliciclastic input during the Lutetian indicating that there was little erosion of older units taking place.

### 5.2.3 North eastern area.

### 5.2.4 Hacıdağ Formation – Palaeocene to Eocene.

A large thickness of Eocene limestones is exposed in the northeast. The majority of the formation is composed of thinly bedded wackestone and rudstone. Bedding planes are usually sharp, occasionally with erosive bases, and are laterally discontinuous. Parallel lamination is common at location 241 (section 4.3.1.1). These sediments include abundant large benthic foraminifera (mostly *Nummulites*), present mostly at the base of beds resulting in normal grading; the top of some beds is capped by a very-fine grained chalk. The characteristic sharp planar beds, fining upwards and the presence of parallel laminations suggest that these limestones were deposited from *turbidity currents* consisting of the  $T_A$ - $T_B$  -  $T_E$  divisions of the classical Bouma sequence (Bouma 1962). The  $T_C$ - $T_D$  divisions of the Bouma sequence generally appear to be absent although occasionally they were present, suggesting that partial flow separation took place resulting in incomplete sequences.

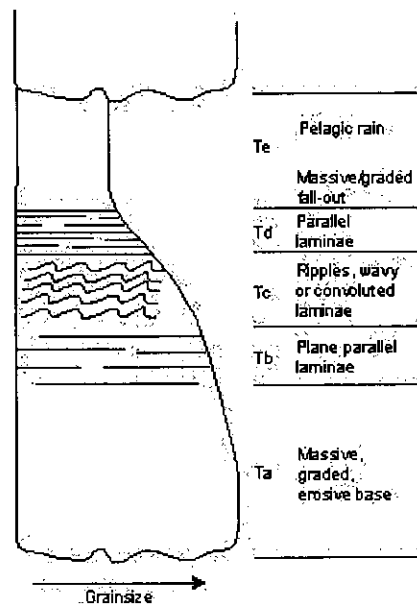


Figure 5.3. An idealised  $T_{a-e}$  Bouma sequence, adapted from Bouma (1962) and Howell and Normark (1982).

It was noted that some horizons were distorted and broken; these were interpreted as incipient slumps as the bedding was broken but significant offset in the bedding planes had not occurred (see 4.8.1.1, Fig 4.72). Other horizons show more obvious evidence of slumping including a spectacular sheath fold. There is sparse evidence for the direction of

slumping; however, the data seem to indicate that the slope may have dipped to the north (section 4.3.1.4) as facies trends show an increase in water depth in this direction.

The thin-bedded limestone facies are commonly capped by a thick bed (<10m) of conglomerate, composed of matrix-supported, sub-rounded clasts (up to ~7cm in size) of Nummulitic limestone. The base of this thick bed is irregular and erosional, distorting the underlying bedding in some areas. The clast size and shape suggest the conglomerate was laid down by a powerful flow and the texture of the sediment suggests that it was probably a *debris flow* (Nilsen 1982).

Clast-supported conglomerates with sub-angular to sub-rounded clasts composed of Eocene and Upper Cretaceous limestone and chert, and poor sorting were also observed at Serinyol and Kanlıdere (sections 4.4.1.2 and 4.3.1.3 respectively). The clast-supported nature suggests deposition was not by a debris-flow process but rather was perhaps deposited from a hyperconcentrated sediment flow.

Several conglomerate horizons are present at Serinyol (section 4.4.1.2). The main conglomerate bed is >10m thick, laterally discontinuous and of varying thickness (maximum thickness ~20m) and cuts out the basal part of the underlying bedded Eocene limestone and sits directly on top of the underlying ophiolite. It is probable that this conglomerate is channelised; however, it was not possible to determine the orientation. Above this conglomerate horizon, the thin-bedded limestone facies dominates, with occasional conglomerate horizons. Near the top of the sequence there is a slight angular discordance within the formation, directly below this there is a thick bed of Nummulitic rudstone with an erosive base; this may represent a tectonic event. Only one conglomerate horizon was observed at Kanlıdere. The lenticular nature of these clast-supported conglomerates suggests that these could be channel-fill deposits.

This evidence suggests that during the Eocene in this northern area, carbonates were being deposited on a slope, possibly orientated towards the north. The slope was unstable generating debris flows and turbidity currents and was cut into by channels that were infilled by coarse-grained sediments.

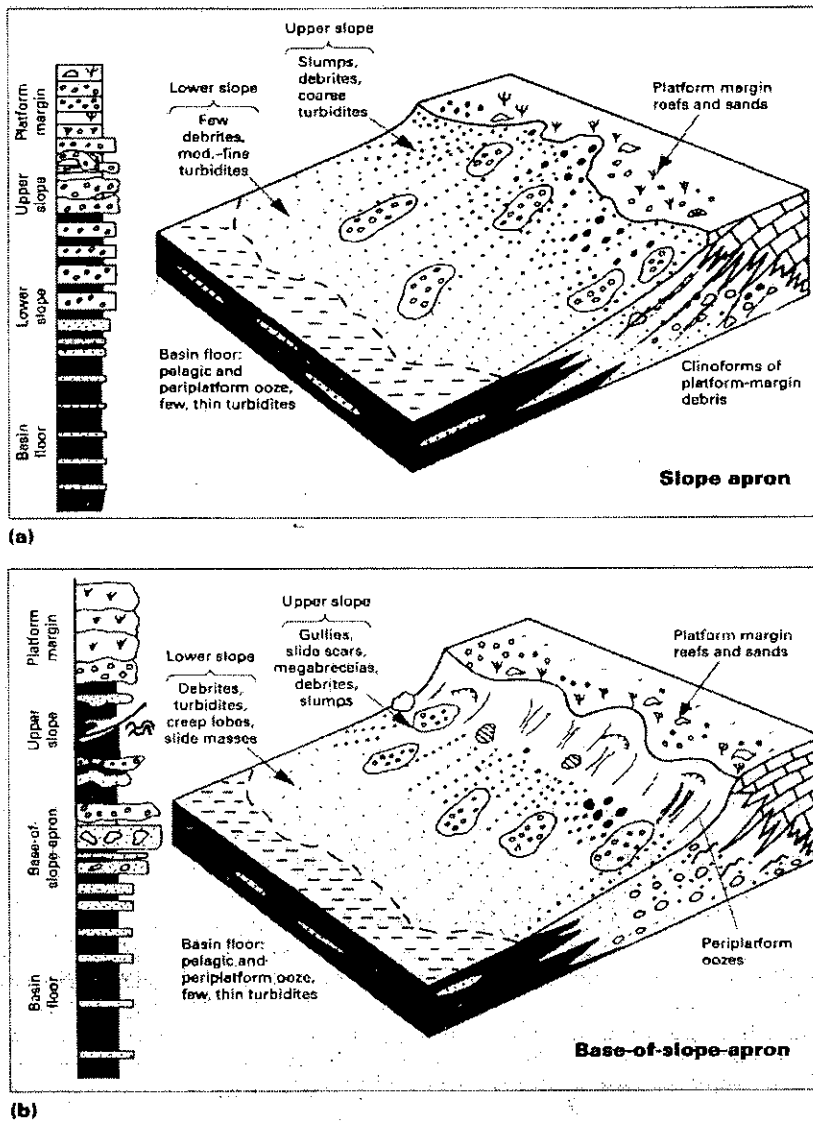


Figure 5.4. Apron facies models, from Wright and Burchette (1996). Many of the features shown in these models can be observed in the Hacidağ Formation, such as turbidites, slumps and conglomerates. The Hacidağ Formation does not conform exactly to either of these specific cases but the similarities suggest a slope environment for the unit, probably in the upper slope area with the turbidite dominated areas, near Kırıkhan, being the more distal. Scale of block diagrams is in the order of 70km across.

### **5.3 Early Miocene - Aquitanian to Burdigalian Age.**

#### **5.3.1 Balyatağı Formation – south western area.**

The Balyatağı Formation is observed along the eastern flank of the Hatay Graben unconformably overlying the Okçular Formation. The formation is characterised by a lower section of laterally continuous sheet-like conglomerates and an upper section of lenticular conglomerates with pebbly to massive sandstone, with an increasing proportion of mudstone/palaeosol occurring at the very top (Section 4.2.3). This is especially well observed at the type location near the village of Enek. The lower section can be observed over a wide area, whereas the upper section is less extensive. Although there are extensive Lower Miocene outcrops on the graben margin in the north, to the south of Harbiye Gorge there are no known outcrops of the Balyatağı Formation.

These sediments exhibit many of the features of fluvial environments. There is no coeval fossil material observed within the formation and the sediments are texturally and compositionally immature. Fluvial conglomerate bodies are commonly lenticular with cross-bedding poorly developed and sandstones can exhibit lenticular and laterally continuous bed morphologies (Tucker 1991). Additionally, palaeosols are common in some fluvial sequences.

The lower conglomerates are characterised by large angular to sub-angular clast sizes, poorly sorted and matrix supported, forming sheets of massive conglomerate with poorly defined bedding planes and rare grading (see section 4.2.3. for a full description). Using standard nomenclature for fluvial sediments (Miall 1978, 1996) these conglomerates can be termed facies Gmm, Gcm, Gmg (Table 5.1); this facies association is typical of sediment gravity flows (facies association SG; Miall 1985, 1996), which form sheet conglomerates. Sheet-like conglomerates are commonly inferred to be the products of infrequent catastrophic flows (Collinson 1996).

Facies Code	Facies	Sedimentary Structures	Interpretation
Gmm	Matrix-supported massive gravel	Weak grading	Plastic debris flow (high-strength, viscous)
Gmg	Matrix-supported gravel	Inverse to normal grading	Pseudoplastic debris flow (low strength, viscous)
Gci	Clast-supported gravel	Inverse grading	Clast-rich debris flow (high strength) or as Gmg
Gcm	Clast-supported massive gravel	-	Pseudoplastic debris flow (inertial bedload, turbulent)
Gh	Clast-supported, crudely bedded gravel	Horizontal bedding, imbrication	Longitudinal bedforms, lag deposits, sieve deposits
Gt	Gravel, stratified	Trough cross-beds	Minor channel fills
Gp	Gravel, stratified	Planar cross-beds	Transverse bedforms
St	Sand, fine to v. coarse, may be pebbly	Solitary or grouped trough cross-beds	Sinuuous-crested and linguoid (3-D) dunes
Sp	Sand, fine to v. coarse, may be pebbly	Solitary or grouped planar cross-beds	Transverse and linguoid bedforms (2-D) dunes
Sr	Sand, v. fine to coarse	Ripple cross-lamination	Ripples (lower flow regime)
Sh	Sand, v. fine to coarse, may be pebbly	Horizontal lamination parting or streaming lineation	Plane-bed flow (critical flow)
Sl	Sand, v. fine to coarse, may be pebbly	Low-angle (<15°) cross-beds	Scour-fills, humpback or washed-out dunes, antidunes
Ss	Sand, fine to v. coarse, may be pebbly	Broad shallow scours	Scour fill
Sm	Sand, fine to coarse	Massive, or faint lamination	Sediment-gravity flow deposits
Fl	Sand, silt, mud	Fine lamination, v small ripples	Overbank, abandoned channel or waning flood deposits
Fsm	Silt, mud	Massive	Backswamp or abandoned channel
Fm	Mud, silt	Massive, desiccation cracks	Overbank, abandoned channel or drape deposits.
Fr	Mud, silt	Massive, roots, bioturbation	Root bed, incipient soil
C	Coal, carbonaceous mud	Plant, mud films	Vegetated swamp
P	Palaeosol carbonate	Pedogenic features	Soil with chemical precipitation

Table 5.2. Facies classifications for fluvial sediments (from Miall 1996).



Element	Symbol	Principle facies assemblage	Geometry and relationships
Channels	CH	Any	Finger, lens or sheet; concave-up erosional base; scale and shape highly variable; internal concave-up 3 <sup>rd</sup> -order erosion surfaces common
Gravel bars and bedforms	GB	Gm, Gp, Gt	Lens, blanket; usually tabular bodies; commonly interbedded with SB
Sandy bedformss	SB	St, Sp, Sh, Sl, Sr, Se, Ss	Lens, sheet, blanket, wedge, occurs as channel fills, crevasse splays, minor bars
Downstream-accretion macroform	DA	St, Sp, Sh, Sl, Sr, Se, Ss	Lens resting on flat or channelled base, with convex-up 3 <sup>rd</sup> order internal erosion surfaces and upper 4 <sup>th</sup> -order bounding surfaces
Lateral-accretion macroform	LA	St, Sp, Sh, Sl, Se, Ss, less commonly, Gm, Gt, Gp	Wedge, sheet, lobe; characterised by internal lateral-accretion 3 <sup>rd</sup> Order surfaces
Scour hollows	HO	Gh, Gt, St, Sl	Scoop-shaped hollow ith asymmetric fill
Sediment gravity flows	SG	Gmm, Gmg, Gci, Gcm	Lobe, sheet, typically interbedded with GB
Laminated sheet sand	LS	Sh, Sl, minor Sp, Sr	Sheet blanket
Overbank fines	FF	Fm, Fl	Thin to thick blankets; commonly interbedded with SB; may fill abandoned channels

Table 5.3. Architectural elements in fluvial systems (from Miall 1996).

Higher in the section clast-supported conglomerates and sandstones become increasingly more common. Pebble imbrication and poorly developed cross-bedding are found within the lenticular coarse-grained conglomerate beds (Facies Gcm, Gh, Gp, Sm). This texture suggests deposition from stream flows (Collinson 1996). This association of facies may indicate deposition in channels (CH) or from gravel bars and bedforms (GB). Indeed, gravel bars and bedforms (GB) are commonly associated with sediment gravity flow deposits (SG). Additionally, the shape of many of the gravel deposits is suggestive of channels (Fig. 4.9).

Bedding planes become more defined towards the top of the formation; grain-size also decreases. Cross-bedding, parallel lamination and pebble-imbrication are all present (Gh, Gp, Sl, Ss, St). This facies association is suggestive of deposition on lateral accreting macroforms (LA) or downstream accreting macroforms (DA; Miall 1996) characterised by internal lateral accretion 3<sup>rd</sup>-order surfaces.

Interbedded with the conglomerates and sandstone near the top of the succession are a number of palaeosol horizons (P). Although some braided river systems lack significant amounts of palaeosols, other ancient systems like the Escanilla Formation (Spanish Pyrenees) include >40% palaeosol (Bentham *et al.* 1993), interpreted as overbank deposits mainly deposited from unconfined flows during times of overbank flooding. High proportions of immature palaeosol have been interpreted to indicate high rates of subsidence and sediment accumulation (Kraus & Middleton 1987).

The Balyatağı Formation, therefore, is interpreted as a gravel-dominated river with characteristics of a *braided* system. Braided-rivers can show a range of different features depending on a number of factors including the grain size of the sediment being transported, the depth of the river, the slope and the sinuosity. Braided-river deposits often have sheet-like or wedge-shaped geometry due to the lateral migration of channels within the area undergoing alluvium. Coarse-grained clast-supported sediments are indicative of proximal braided-streams. Miall (1977) developed a series of depositional models for braided-streams, that has since been revised and refined (see Miall 1996 for a full discussion).

The basal sediments of the Balyatağı Formation are dominated by SG architecture elements, with SB, GB and CH elements becoming more common upwards. The SG element is characteristic of gravel braided rivers with sediment gravity flows (Miall 1996), sinuosity is low, braiding is high suggesting that the lower part of the formation was deposited from this environment. GB and SB elements increase upwards, although also found in gravel braided rivers with sediment gravity flows; Gb with subordinate SB are characteristic of shallow gravel braided *Scott-type* (Figure 5.5.) rivers (Miall 1977, 1996) that consist of horizontally bedded gravels filling stacked, shallow channels, suggesting an evolution in river type over time.

In contrast, when the sediment load is mixed sand and conglomerate, a variety of bed forms can develop as seen in the uppermost part of the succession. The presence of GB and SB elements with LA or DA elements and the presence of palaeosols suggests deposition from a deep gravel braided *Donjek-type* river (Miall 1977, 1996)(Figure 5.5.). Due to the greater topography generated by these mixed sediment rivers compared to a gravel dominated one, floodplain deposits are more likely to be preserved. Sinuosity in this type of river is low to intermediate and the braiding parameter is intermediate to high.

Therefore, there is a progression in river type over time from a braided-river dominated by sediment gravity flows, possibly on an alluvial fan (although there is no evidence for a fan-shaped morphology) to a shallow and then deep gravel-bed braided river. This progression over time could be due to the decrease in the size of the sediment bedload and a corresponding increase in stream power, a more uniform discharge, a change in basin topography or greater incision of the river network.

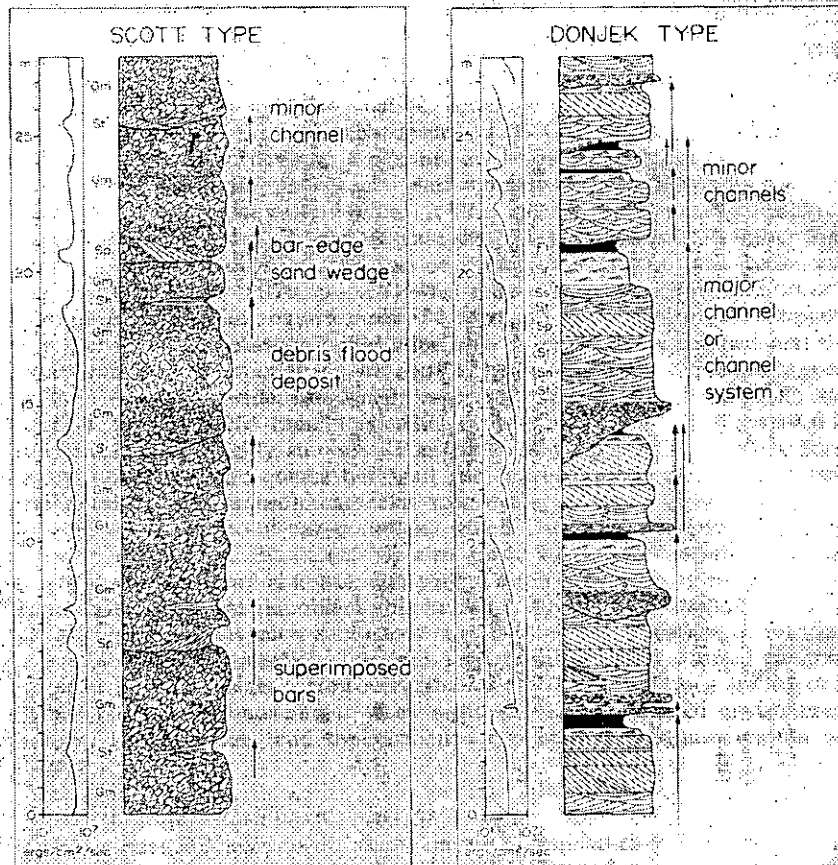


Figure 5.5. Logs showing grain size and sedimentary structures for the Scott- and Donjek-type braided rivers, from Miall 1977.

The lower part of the Balyatağı Formation, exposed on the north-western margin of the graben, is similar to that observed in the east dominated by Gmm and Gmg lithofacies (SG facies association); however, the upper part of the formation is composed of a much greater proportion of palaeosol (sections 4.2.3.4 & 4.2.3.5). This suggests that the basal part of the formation was deposited from gravel-braided rivers with sediment gravity flows (Miall 1996). The palaeosols are likely to represent distal floodplain deposits (FF facies association), the thickness of palaeosols indicates prolonged soil formation possibly due to more stable channels and bars in the river or the diversion of the river away from this area.

Floodplain deposits are common in many river types but do suggest a lower energy more stable system. It is interesting to note that Lower Miocene sediments directly overlie serpentinite in this area and not older sediments as in the east. This suggests that in this area uplift and erosion had taken place after the Eocene but the effect of this was perhaps less to the south.

The Balyatağı Formation has a varied clast composition consisting of both sedimentary and ophiolite-derived clasts, indicating that some Eocene and older sedimentary cover rocks and an ophiolite were being eroded. The northerly directed palaeocurrents (see 4.2.3.6.) suggest the sediments came from the south.

### 5.3.2 Kıcı Formation – Kırıkhan area.

Although there is no dating evidence for this formation, the stratigraphic position suggests an Early Miocene age. The sedimentary characteristics of the Kıcı Formation can be broadly differentiated into four facies.

In the east, near the village of Gökdere, the formation is well exposed at two locations (see section 4.3.3). At location 230, the basal part of the succession is composed of a polymict, matrix- and clast-supported conglomerate, 50-60m thick. The presence of both matrix- and clast-supported sediments suggest that both debris-flow and grain-flow processes contributed to deposition. Clasts are generally angular, up to 1m in size, composed of mainly Hacıdağ limestone but also minor red sandstone, serpentinite and basalt. The large size of the clasts indicates that the flows were probably high-energy and may have transported the sediment some considerable distance. There is no fossil material present, consistent with a non-marine origin.

These lithofacies can also be classified using standard nomenclature (Miall 1977, 1985, 1996), as Gmm and Gcm, indicating a SG facies association and interpreted as very coarse *alluvial fan* sediments. Bull (1972) and Nilsen (1982) outlined a number of characteristics for the recognition of alluvial fan deposits including deposition near the source area, deposition by high-energy flows, poorly sorted and poorly rounded sediments consisting of a mixture of partly sorted stream-flow and debris flow deposits. These features can all be observed in this basal facies.

In contrast, at location 379 (section 4.8.3.2), the basal sediments consist of 1.5m of breccia (angular clasts) and palaeosol, formed through exposure and weathering of the underlying unit (Hacıdağ limestone). This is overlain by 5m of microbial boundstone also containing coralline algae, bivalve fragments, benthic and planktic foraminifera. These features indicate a very shallow-marine origin for this material with some reworking and abrasion causing fragmentation of the bioclasts. The encrusting nature of the algae and some of the foraminifera cause biological binding of the carbonate and suggests a high-energy shallow-marine setting (Wright & Burchette 1996).

The upper part of the succession, at both locations, is composed of conglomerate and coarse litharenites with occasional mudstone horizons. However, location 230 in general is a fining-upwards sequence (Figure 5.6), whereas location 379/380 is a coarsening up sequence (Figure 5.7).

Conglomerates are clast-supported with well-rounded clasts at location 230. The composition is dominantly serpentinite but limestone clasts are also present. Conglomerate horizons generally occur at the base of sandstone beds or as laterally discontinuous lenses (Fig.5.6). St is the most common lithofacies identified but Gm, Gt, Sh, Sp, Fr and P lithofacies are also present.

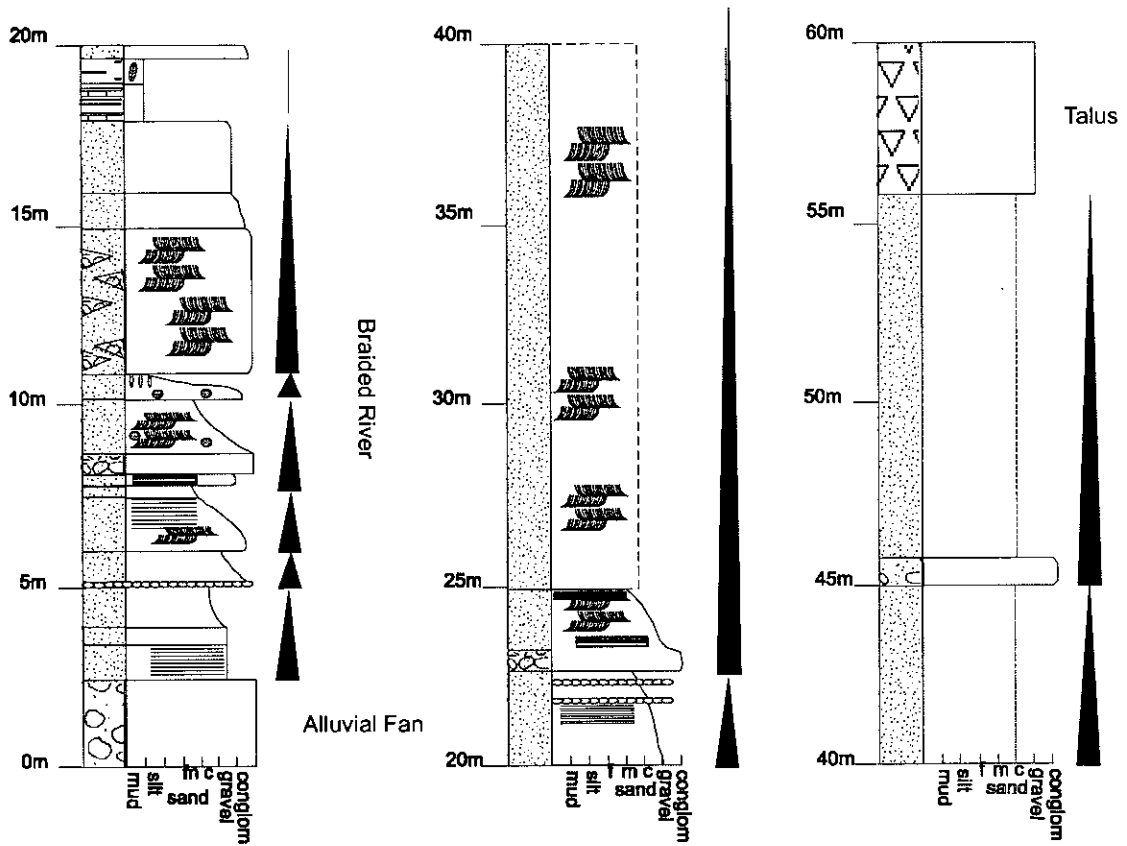


Figure 5.6. Sedimentary log measured at location 230 (Fig. 4.70) with sedimentary environments and fining-upwards cycles shown. Fining-upwards sequences may represent bar processes or where a basal conglomerate is present, may be a channel fill deposit. For key see Appendix 7.

In contrast, there is a higher proportion of conglomerate present in the section at location 379. The conglomerate is mostly matrix-supported, but clasts are well-rounded and composed of serpentinite and limestone. The limestone clasts locally show evidence of boring, indicating that some pebbles were formed and reworked in a sub-aerial setting before being incorporated into the these conglonerates.

The coarse litharenite is light purple to red in colour due to the high content of altered serpentinite; thin-sections reveal that basalt and polycrystalline quartz are also common. The sandstones do not contain much bioclastic material; only rare, probably reworked, planktic foraminifera and coralline algae, echinoid and *Ostrea* fragments. Sedimentary structures, such as trough cross-bedding (some of which have a herringbone pattern), parallel lamination, pebble imbrication and bioturbation are present in the sequence. Additionally, 'floating' pebbles are very common within this sandstone.

There are also occasional mudstone beds: black, red and cream mudstones are present often with a scaly or shaly texture. One bed contains abundant plant material and rootlets. Therefore, the lithofacies present at this location are Gmm, Gt, Gh, St, Sp, Fr and possibly C.

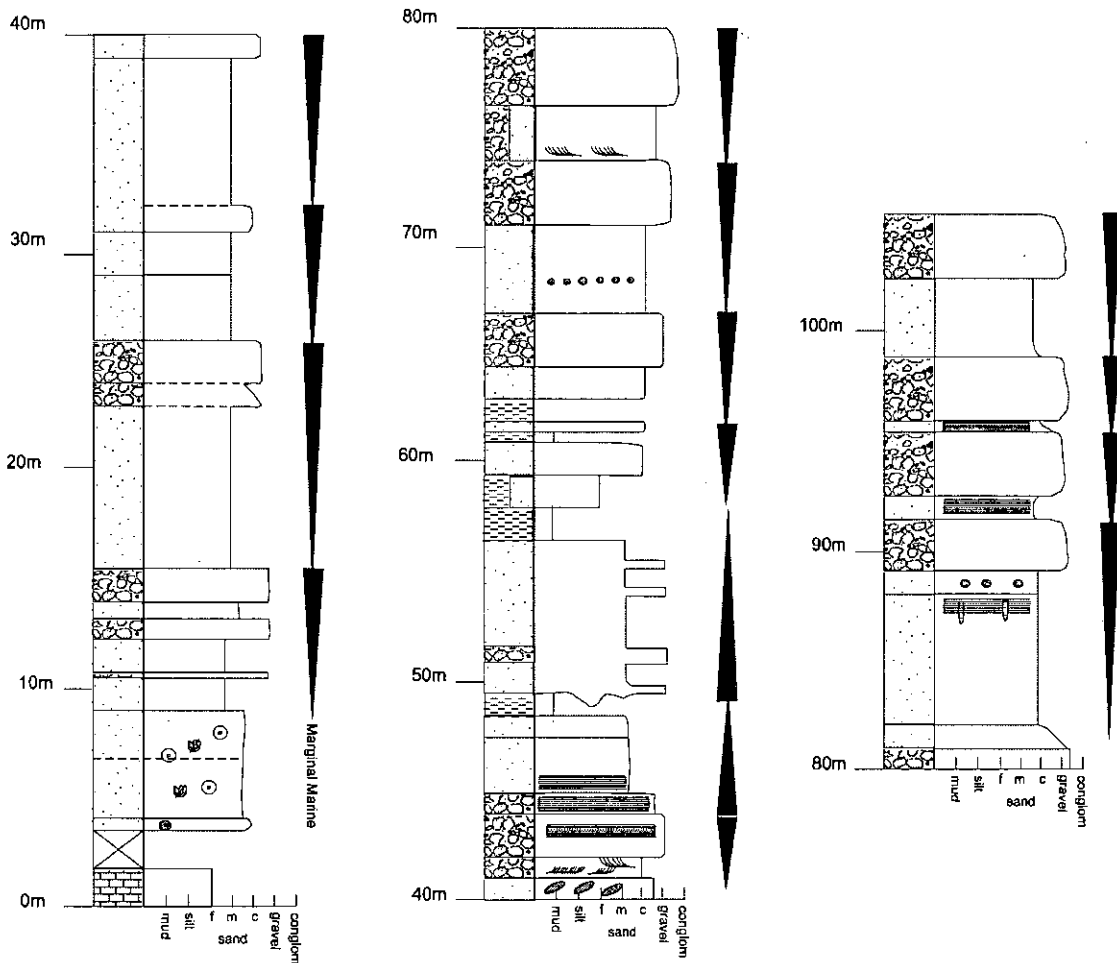


Figure 5.7. Sedimentary log showing sequences in this inferred alluvial fan deposit (location 379, see Fig. 4.76). Coarsening-upward cycles possibly formed by the progradation of individual fan lobes.

The presence of marine fossils in these sandstones, low species diversity, the presence of large oysters combined with the presence of plant material and rootlets in the mudstone facies suggests a marginal-marine environment of deposition.

The cross-bedded sandstones with basal lags of conglomerate seen at location 230 are suggestive of lateral and downstream accretion macroforms (LA and DA) and possibly

sandy bedforms (SB), similar to the deep gravel braided Donjek-type (Miall 1996) river discussed in section 5.3.1 but with a greater proportion of sand that suggests possible deposition from a gravel-sand meandering river (Miall 1996). The fine-grained sediments consisting of soft dark grey to black mudstone indicate a high organic matter content suggesting water-logged conditions. The presence of rootlets and plant material suggests non-marine conditions and colonisation by plants. This suggests that these mudstones were deposited in a flood plain, abandoned channel, or in a marsh environment.

Location 379 shows more evidence of marine influence (i.e. basal boundstone and herringbone cross-bedding) suggesting that this location was more proximal to the coast than location 230. This would suggest that these locations represent a lateral transition of alluvial fan-braided/meandering river-deltaic environments. As such this association could be termed a *fan-delta* as defined by Holmes (1965) as a coastal prism of sediments delivered into an alluvial fan and deposited either in the sea or a lake and distinguished from alluvial fans by evidence of the interaction of marine and alluvial processes.

The K1c1 Formation is different near the abandoned village of Kanlıdere (section 4.3.3.3). Here ~50m of brown, fine- to medium-grained, poorly sorted sandstone with onion-skin weathering is present between the Eocene Hacıdağ and Middle Miocene Kepez Formations. This sandstone contains bioclastic material including coralline algae, gastropod and bivalve fragments, and both benthic and planktic foraminifera, indicating a marine origin for this facies. Three conglomerate beds are interbedded with the sandstone; these are clast-supported, with well-rounded clasts of various composition; they are also poorly sorted, and these features suggest a grain-flow origin. Some of the limestone clasts have borings, indicating reworking in a shallow-marine environment.



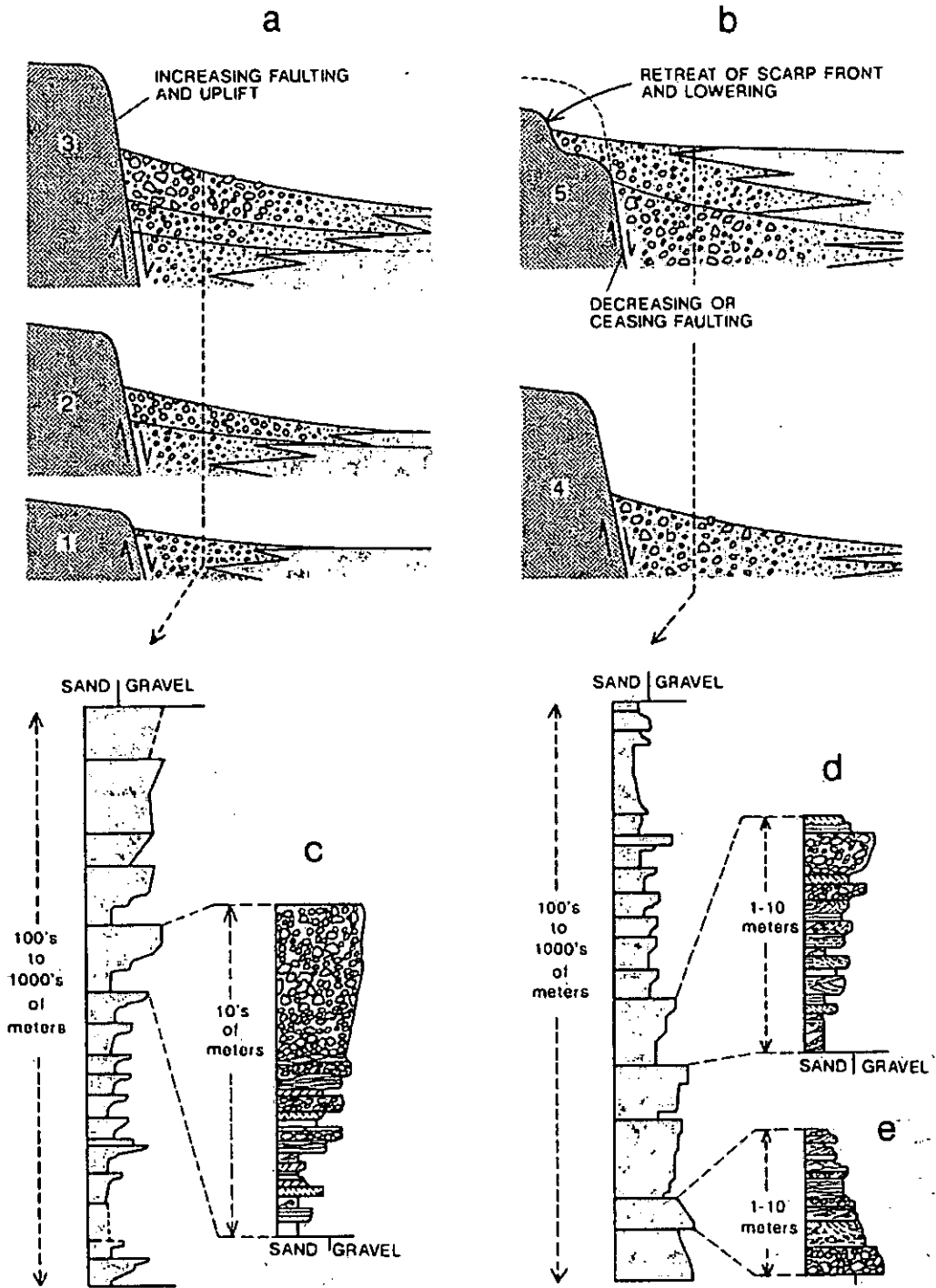


Figure 5.8. Idealised vertical sequences in alluvial fan deposits and their possible cause. a) Large-scale coarsening-upward sequence due to continuous faulting and fan progradation. b) Large-scale fining-upward sequence caused by retreat of scarp front and lowering of relief in source area or lateral shifting and abandonment of fan (not shown). c and d, Small-scale coarsening-upward cycles due to the prograding of individual fan lobes. e) Small-scale fining-upward cycle with channelised base generated by bar processes or filling of braided channel. From Einsele (1992).

The presence of fossil material in thin-sections indicates that these sediments were deposited in a marine environment and the fragmentary nature of the fossils shows that they have been reworked. The massive nature of the sandstone suggests that it was deposited from a grain-flow, , this suggests deposition in a shelf setting and may represent the *pro-delta* of the coarse grained sediments observed to the north.

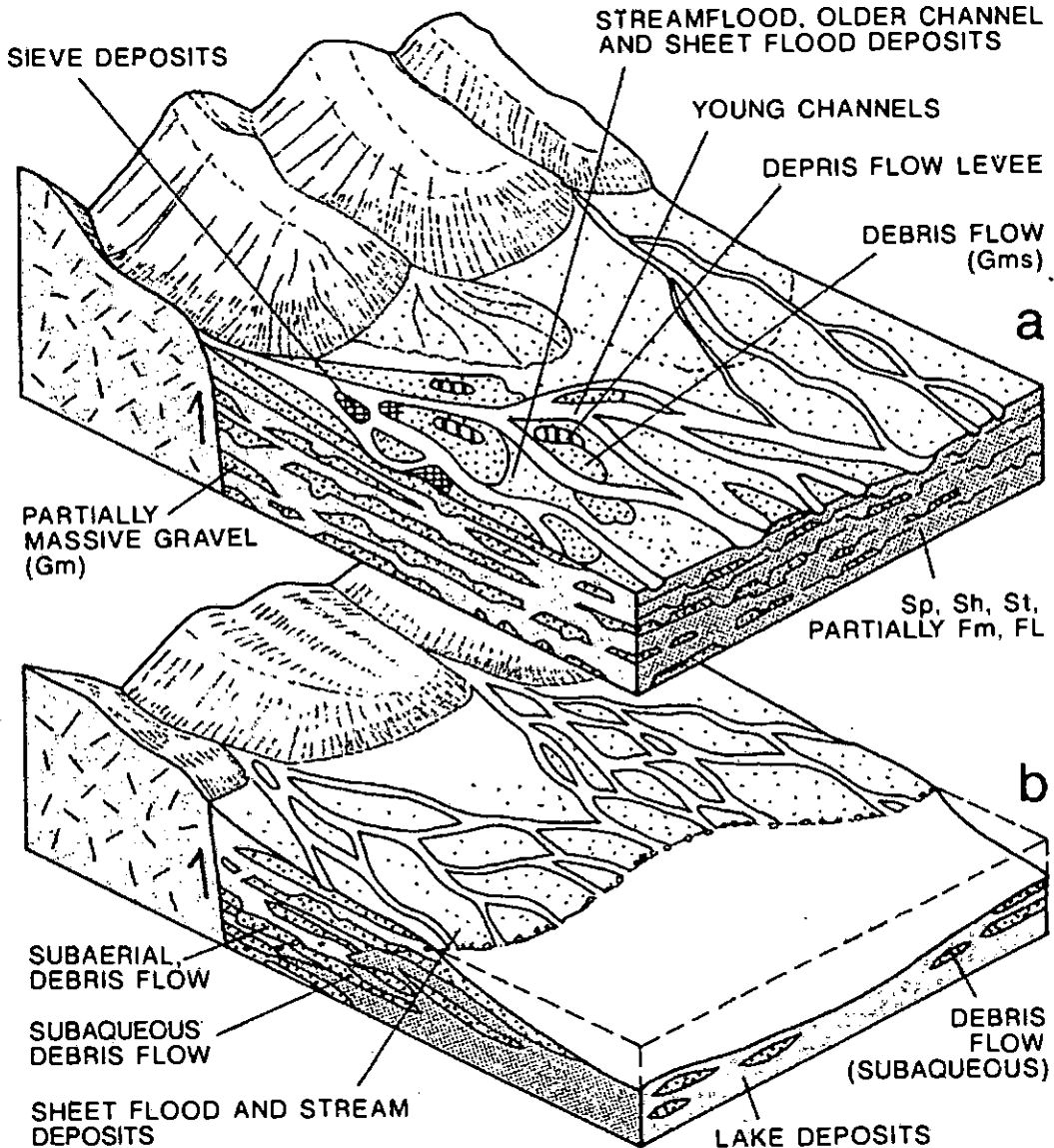


Figure 5.9. Simplified facies models of a) alluvial fan (proximal to mid-fan region) and b) fan-delta. From Einsele (1992).

The nature of the sediments of Early Miocene age are again different near the town of Serinyol (Fig. 4.84) where there are ~30m of red and brown palaeosols with some caliche, indicating this area was emergent and undergoing soil formation during this time.

The composition of the sandstone of the K1C1 Formation is dominated by serpentine, basalt and radiolarian chert clasts and there is very little matrix or cement present. This indicates that the sediment source was probably the ophiolite and related rocks. In contrast, the conglomerate horizons at Kanlidere were dominantly derived from the sedimentary cover (mainly limestone and chert). Fine-grained sediments contain abundant quartz and muscovite; these are probably extrabasinal: the fine-grained nature of these sediments could indicate that the source was some distance away.

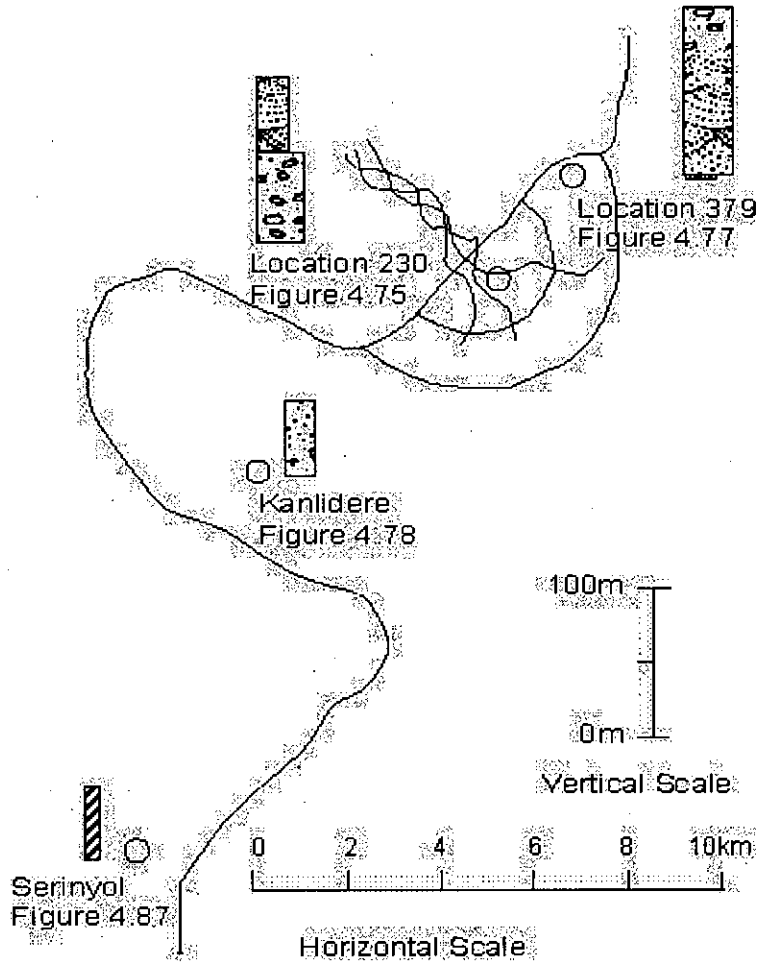


Figure 5.10. Sketch map showing locations discussed in the text and the envisaged local environment of deposition for the K1C1 Formation.

## 5.4 Middle Miocene - uppermost Burdigalian/base-Langhian to top-Langhian Age.

### 5.4.1 Sofular Formation, Hatay Graben.

The type section of the Sofular formation is located near the village of Kozkalesi (Section 4.2.5.1). The sediments of the basal section are composed of repeating lithologies dominated by marine carbonates, which are interpreted as cyclic transgressive-regressive events. The base of each cycle is marked by a conglomeratic lag (Facies A), probably formed during a rapid sea-level rise. Subsequently, carbonate formation began in shallow-marine conditions. The lower limestone beds (Facies B – wackestones and rudstones) above the conglomerate horizon contain abundant reworked shallow-marine fauna and lack sedimentary structures; these may be sub-tidal sediments. This facies is overlain by Facies C, composed of wackestone and packstone containing a similar faunal assemblage and rarely near the base of the sequence bio-accumulations of oysters and coral heads that appear to be *in situ*, thus suggesting an intertidal environment and implying that a relative sea-level fall had taken place. This trend in falling sea-level continued and the environment became sub-aerial, as indicated by the presence of palaeosols (Facies D). Palaeosol formation was halted by a rapid transgression resulting in the formation of another cycle of carbonate deposition.

The cyclicity and low relative-sea level suggests that deposition was taking place in the interior of a *carbonate platform*. In particular these carbonates are probably *peritidal cyclothems*, shallowing upwards cycles that form thick successions in a variety of settings (Ginsburg 1975; Pratt *et al.* 1992). The formation of such cyclothems may be due to autocyclic controls such as the progradation of the shoreline (e.g. the Massiccio Formation of the Apennines, Fig; Coliacicchi *et al.* 1975) combined with tectonic subsidence creating accommodation space, or due to allocyclic factors such as tectonic control or eustatic sea-level change (Wright & Burchette 1996).

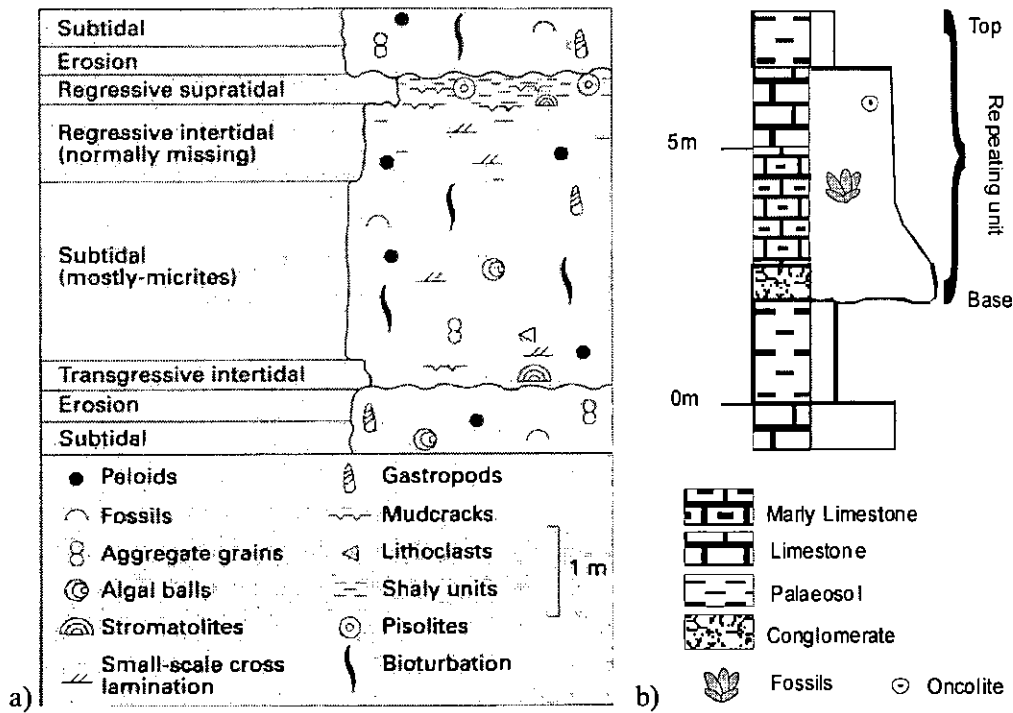


Figure 5.11. a) Peritidal cyclothem from the Massiccio Formation (Lower Jurassic) of the central Apennines, from Wright & Burchette (1996) based on the work of Coliacci *et al.* (1975). b) Cyclothem from the Sofular Formation; note that the thickness of the palaeosol unit is greater in the Sofular Formation.

The bio-accumulations, palaeosol and conglomerate horizons decrease in abundance upwards until eventually none are present, suggesting a more stable shallow-marine relative sea-level. The upper part of the succession is composed of oncolitic wackestone/rudstone. The oncolite and other shallow-marine fossil material are reworked, benthic:planktic foraminifera ratios suggest a water depth of up to 200m, implying that this material was reworked offshore down a *carbonate slope* adjacent to a platform (Figure 5.4).

The limestones exposed near Çevlik (Section 4.2.5.6, Fig. 4.37) closely resemble the upper part of the succession at Kozkalesi, suggesting a common depositional process. Bioclastic wackestone (exposed along a relict sea-cliff) dips basinward and the beds exhibit erosive bases that cut down towards the centre of the basin; these features are interpreted as slide scars (Fig.4.34). Similar features, but on a larger scale, have been described from the Jurassic Sumeini Group of Oman (the intraformational truncation surfaces of Watts 1990; Watts & Garrison 1986), which is interpreted as a carbonate slope with these features characteristic of the upper slope. This limestone facies consists of shallow-marine material, bivalves, gastropods, echinoids, microbial material that was being reworked offshore.

Therefore, these limestones are interpreted as being deposited on a *carbonate slope* adjacent to the platform as for Kozkalesi. This interpretation is supported by the recognition of slide scars and slumped horizons, typical of slope environments especially in the upper slope area (Figure 5.4). Hummocky cross-bedding was also identified (Section 4.2.5.8); this is indicative of storm processes and common in this facies (Wright & Burchette 1996).

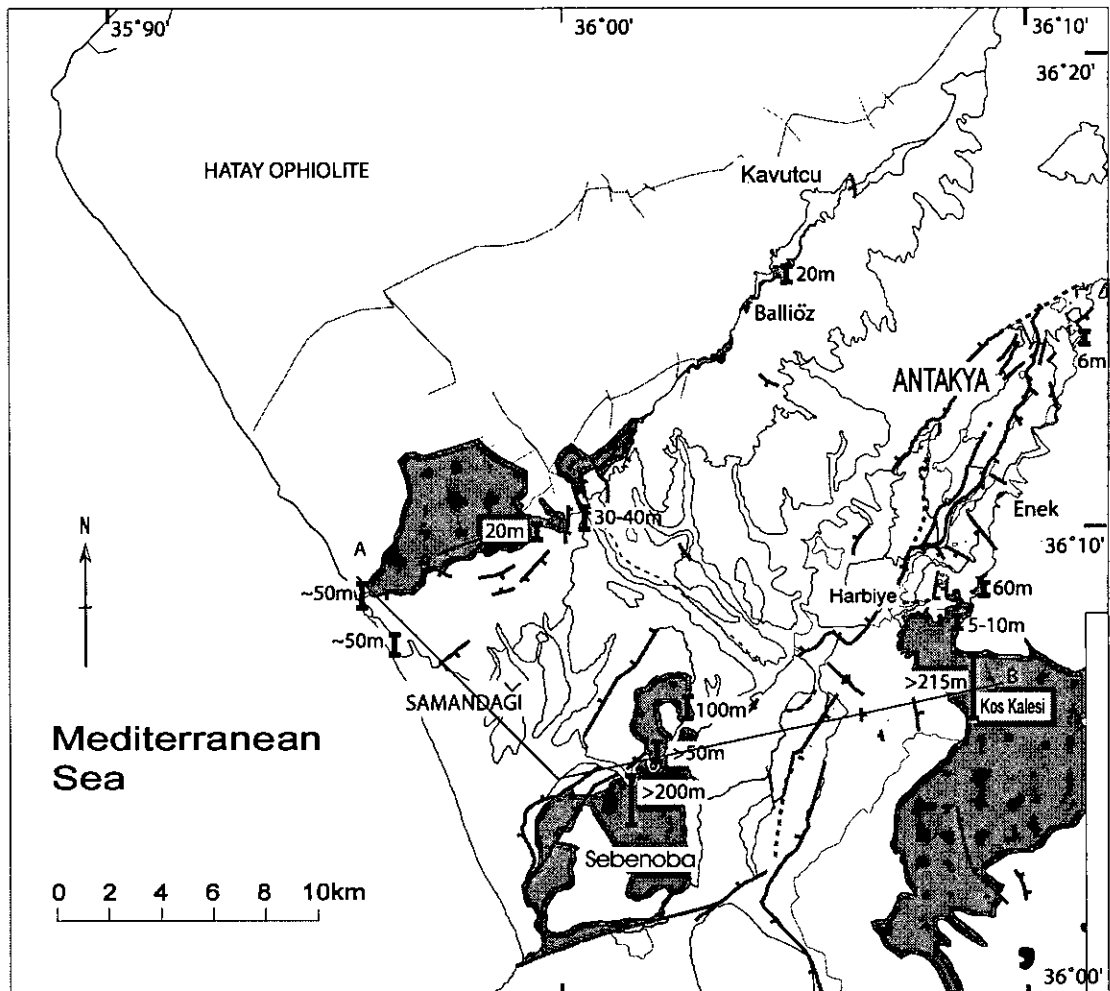


Figure 5.12. Map showing location of Middle Miocene sediments, thickness of the main sedimentary successions recorded and the line of the 2D line sketch of Figure 5.14.

This change to a deeper water slope setting records a rise in relative sea-level that caused the shallow carbonate platform to drown or move landwards; they also record a change in basin morphology. Thus, these carbonates represent a deeper water facies than the cyclothem. Above this level interbedded marl and limestone of the Nurzeytin Formation are observed, indicating a further increase in water depth.

The other main outcrop of the Sofular Formation occurs along the Asi Nehir, and has quite a different character from the limestones around Kozkalesi and Çevlik. These limestones overlie a variable thickness of conglomerate and interbedded limestone, mudstone and marl. The conglomerate is red and composed of angular serpentinite clasts that are massive-bedded. The fine-grained sediments overlying the conglomerate have very thin and irregular beds; a mottled colour is common and also wavy laminations and desiccation cracks are present (see section 4.2.5.5).

The lack of structure and the immature, angular clasts suggest that the clasts have not been transported very far and may have formed within an *alluvial fan*. The overlying thin-bedded sediments show evidence of a shallow-water environment and periodic sub-aerial exposure forming desiccation cracks and immature palaeosols. The close association of the two facies could indicate formation in a fan-delta environment. This was defined by Holmes (1965) as an alluvial fan prograding into a standing body of water. Nemec and Steel (1988) revised the terminology to a coastal prism of sediments delivered by an alluvial-fan system to the interface between the fan and a standing body of water. As there is evidence for the presence of an alluvial fan in this location overlain by sub-aerial sediments possibly of the prograding delta plain this interpretation seems reasonable.

The limestone beds that overlie the lower mixed clastic and carbonate sequence are thin-bedded micrite with <1% siliciclastic material, with irregular and lenticular beds and no fossil material. Near the base there are two irregular red mudstone beds, possibly palaeosol. Combined with the presence of ripple marks and irregular laminations (possibly microbial) it points to a shallow marine, possibly *lagoonal* or peritidal setting for this facies. This facies is in the order of 100m thick and appears to be split into three sediment packages by the presence two horizons visible in outcrop. It is not clear what these horizons represent (Figure 5.13) but they may be due to sea-level change, a pause in deposition or due to a tectonic event.

There is an upward transition along the Asi Nehir (that is not well exposed) to coarse bioclastic calcirudites (section 4.2.5.5) similar to that described previously at Kozkalesi (see 4.2.5.1). This transition suggests that this basal lagoonal-type facies is laterally equivalent to that observed in the basal sequence at Kozkalesi (peritidal carbonates). These very shallow-marine sediments are not present further to the west, near Çevlik; this may be due to deeper

water conditions in that area at the time of deposition or that they are not present today due either to erosion or lack of exposure.

SE

NW



Figure 5.13. View across the Asi Nehir; to the right the lower fine-grained limestone facies consisting of three cycles is exposed; these are interpreted as having been formed in a shallow-marine environment possibly a lagoonal setting. Above are bioclastic rudites deposited on the upper slope of a carbonate ramp; note the change in colour between the two facies.

By contrast, in another exposure along the Asi Nehir, the top of the shallow-marine facies is exposed (see 4.2.5.5). Here, the sediments have experienced some deformation and now have a dip of  $90^\circ$  to  $45^\circ$ . There is a gradual decrease in dip along the exposure and this is interpreted as syn-sedimentary deformation resulting from normal faulting (see section 6.5 for a full discussion of this feature). The basal sequence is made-up of fine-grained microbial limestone (as before); whereas the top surface is irregular and has been bored into (possibly by *Trypanites* or *Lithophaga*), indicating that this horizon is a hardground and thus represents a period of very low or non-deposition.

The sediments overlying this bored horizon contain a significant bioclastic component and also some siliciclastic material. Clast-supported conglomerate horizons composed predominantly of serpentinite are present near the base of this unit, but the sediment becomes



more uniform upwards, composed of fossiliferous calcarenite. Sedimentary structures are rare; however, occasionally parallel lamination is observed. The diversity of biological material, mostly fragmentary and reworked, indicates a marine setting for this facies. The conglomerates could be channel fills and thus possibly the equivalent of the slope facies described at Kozkalesi.

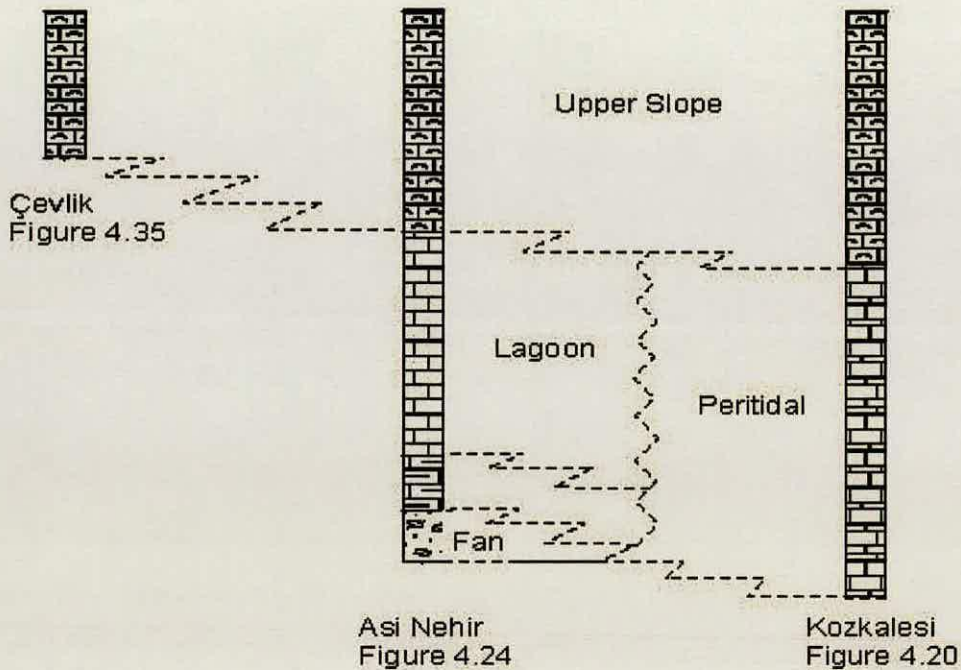


Figure 5.14. A 2D line sketch showing three sections and how the differing environments may be related to each other across the study area. Position of the line is shown on Figure 5.13.

Moving north-eastwards along the graben away from the coast the thickness of the Sofular Formation decreases until the unit is less than 10m thick at many localities. The limestone is rich in reworked shallow-marine fossil material; many bivalves are articulated suggesting that significant transport of the bioclastic material has not taken place.

A localised carbonate build-up was identified at Kesecik (Section 4.2.5.7). This patch-reef has developed on bioclastic rubble overlying a thick succession of Lower Miocene palaeosol and is associated laterally with shallow-marine siliciclastic facies (low-angle cross-bedding; Fig. 4.41). These associated sandstones can be compared with the 'Marginal Terrigenous Complex' (Esteban 1996), an association of coral reef and siliciclastic facies that is common

in a number of areas, e.g. Sicily (Catalano & Esteban 1978) and Tuscany (Bossio *et al.* 1978).

The reef core of the patch-reef is massive and composed of *poritids*. *Porites* is known for its ability to withstand high levels of fine-grained clastic sedimentation (Hubbard & Pocock 1972) but upwards corals disappear and oncolites predominant indicating a change in environmental conditions away from the optimal growth for corals. Coral reefs with low species diversity have been observed in other locations around the Eastern Mediterranean, such as the Serravalian Koronia Member of Cyprus (Follows 1996), where four coral species were identified.

Although this was the only patch-reef observed in the field, coralline rubble and coral fragments (probably from the fore-reef) were observed in other locations, suggesting that localised build-ups were once more common but have subsequently been eroded.

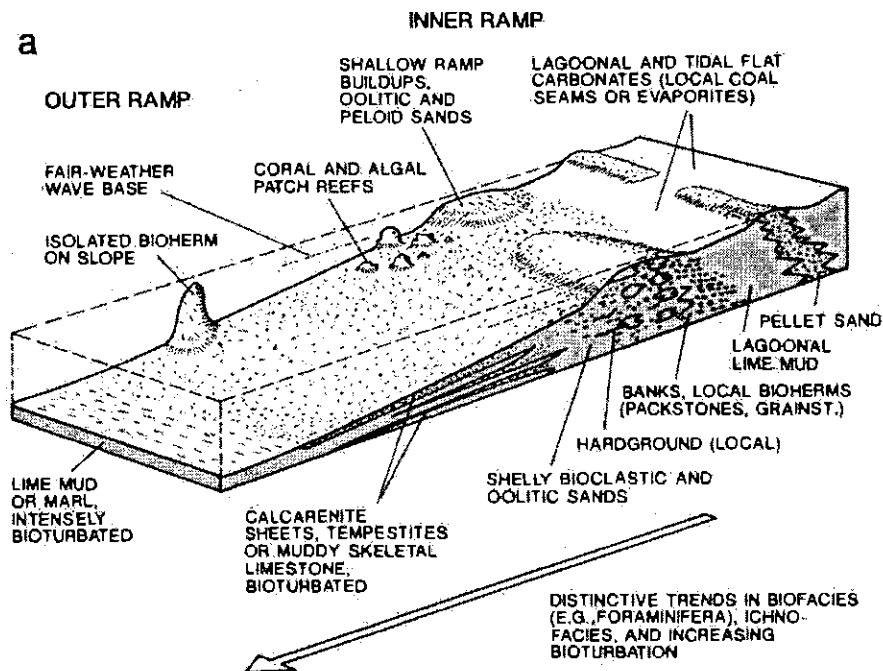


Figure 5.15. Idealised carbonate ramp with an inner ramp barrier complex separating a lagoonal-tidal zone from the open marine ramp facies (from Einsele 1992) based on the Arabian/Persian Gulf. It is envisaged that the Sofular Formation, although on a much smaller scale, represents a similar environment of shallow-marine carbonate formation with a diverse range of sub-environments. The deeper water marls associated with this model probably may represent the lower part of the Nurzeytin Formation although strontium dating would argue against this interpretation.

Coral reefs are common in the Mediterranean during the Langhian (Esteban 1996). This appears to be related to 2<sup>nd</sup> order eustatic sea-level highstands (Haq *et al.* 1987). Other major phases of coral reefs formation occur during the Aquitanian and Late Tortonian/Messinian and also correlate with 2<sup>nd</sup> order highstands. Langhian carbonate platforms with numerous coral reefs are found in the Red Sea (Coniglio *et al.* 1996; Purser *et al.* 1996), Catalonia, Spain (Permanyer & Esteban, 1973; Alvarez *et al.* 1977) and Israel (Buchbinder 1996), generally composed of *Porites*, *Tarbellastrae* and *Stylophora*. True barrier reef systems are uncommon with the majority of reefs being small fringing reefs with a variety of morphologies (Esteban 1996).

Miocene patch reefs are found on Cyprus, where they are termed the Terra Member (Aquitanian/Burdigalian) and the Koronia Member (Tortonian/Messinian) (Follows *et al.* 1996). Terra Member reefs are often circular ~10m in diameter but can reach 500m in width (Follows *et al.* 1996) and are faunally diverse. In contrast, the Koronia Member reefs form irregular mounds with low faunal diversity and appear to be more similar to the reef material observed in the Hatay field area. Tectonics were very important in controlling the formation of the patch reefs in Cyprus, the Terra Member in stable uplifted areas and the Koronia Member on uplifted fault controlled lineaments, perhaps suggesting that tectonic controls were also important in the formation of reefs in the Hatay area.

Late Miocene patch reefs have also been described from the Antalya region of southwest Turkey (Hayward *et al.* 1996). Here patch reefs are located within a prograding fan delta sequence part of a foreland basin succession. This confirms that such reefs can form in areas of significant terrigenous input and be associated with siliciclastic facies as seen by the association of the patch reef observed with coastal sediments in Hatay.

Another interesting feature of the northern outcrops, described in section 4.2.5.3, is the presence of steeply dipping foresets that overlie bioclastic rudstone. This rudstone contains articulated bivalves and, locally, oyster patch-reefs, suggesting that this is a *marginal marine facies*. The overlying foresets have a sigmoidal morphology and the sandstones are very coarse-grained (Fig. 4.24). The well-defined foresets have original dips of ~15-30° suggesting that this is a small *Gilbert-type delta*. Neinec (1990) states that slope gradients in gravelly deltas are commonly 30-35°, and is similar to the model by Wescott & Ethridge (1990), although in this case it appears that the foresets prograde over a transitional beach zone as well as being overlain by a beach transition zone. Topsets beds are not present, as

they were possibly eroded, but it is likely that some of the poorly exposed fine-grained sediments represent a prodelta. This delta developed on the footwall of one of the basin-bounding faults, with palaeocurrent directions (Fig. 4.24) away from the graben, thus indicating that topography controlled by fault motion must have been present at that time.

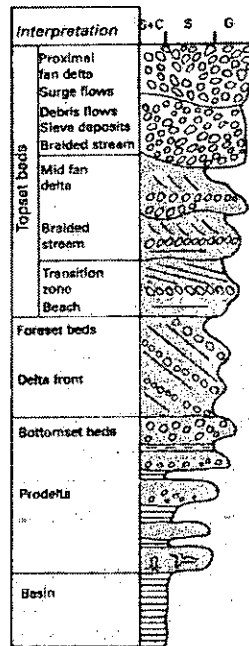


Figure 5.16. Idealised composite vertical section for a Gilbert-type delta, from Wescott & Ethridge (1990).

#### 5.4.2 Kepez Formation, Kirikhan area.

The Kepez Formation is very poorly exposed; therefore, there is little information on which to base an environmental reconstruction. Generally, the Kepez Formation is composed of bioclastic packstone containing fragments of bivalves, oncolites, coral, gastropods and echinoids. This indicates that the formation is shallow-marine in nature and possibly accumulated slightly offshore as the fragmentation of the bioclastic material indicates that it was reworked. The depositional setting was perhaps similar to the Sofular Formation.

Near the town of Serinyol, Middle Miocene limestone is slightly better exposed. At this location rubbly bioclastic rudstone contains large heads of poritid corals, bivalves and gastropods. The large coral fragments and the rubbly nature of the limestone indicate that this may be *reef talus*, confirming the presence of shallow-marine reefs. As this facies is observed in a number of different locations (see Fig. 4.84) and as large fringing reefs are uncommon in the Mediterranean, it is most likely that this material was derived from small patch reefs.

## 5.5 Upper Miocene

### 5.5.1 Nurzeytin Formation, Hatay Graben - Serravallian to Tortonian Age.

The Nurzeytin Formation is mainly composed of marl with interbeds of varied composition. The marl and then the various interbeds will be discussed below.

#### 5.5.1.1 *Marl*

Throughout the graben the marl of the Nurzeytin Formation is remarkably uniform; it is light to medium grey in colour, generally fossiliferous with numerous foraminifera, mostly planktic but also some benthic foraminifera. The ratio of benthic to planktic foraminifera suggests a water depth of up to 700m (Meschede *et al.* 2002). Detrital plant material is also often present.

Due to the fine-grained nature and uniformity of this sediment it is interpreted as having been deposited from sediment suspended within the water column and is typical of a *basin-floor facies*.

#### 5.5.1.2 *Interbeds*

There are four main types of interbed observed within the Nurzeytin Formation. The first type is a matrix-supported conglomerate (see 4.2.7.2; Fig. 4.47), >4m thick, with sub-angular to sub-rounded clasts of marl and limestone and a marl matrix. Although there is only one bed it is exposed in several locations indicating some lateral continuity. The matrix-supported fabric indicates that the conglomerate probably formed by debris-flow processes from the graben margin.

The second type of interbed is limestone (calcarenite) of various thicknesses (10cm-2m). The limestone is not fossiliferous, but does exhibit sedimentary structures such as parallel laminations, mud intraclasts and flute casts. The flute casts indicate that the limestone was deposited from a turbulent flow, combined with the presence parallel laminations and cross-lamination, is suggestive of low-density turbidity current processes (see 4.2.7.2). No beds exhibit the complete Bouma sequence.

The third type of interbeds are thin, <50cm thick, calcarenite beds, that tend to occur in packages with interbedded marl. These beds have sharp bases and fine upwards; sedimentary structures are present including parallel laminations, cross-lamination, ripple marks, flute casts and marl intraclasts. These sedimentary structures are indicative of high-density turbidites. Sometimes these sandstone beds are associated with small-scale slumped horizons.

Finally, thick sandstone beds are common in the more northern part of the Hatay Graben (away from the present coast). Thick litharenite beds were observed at location 140 (section 4.2.7.4) and several other places, suggesting that these beds are laterally extensive. They consist of three massive beds separated by thin marl or chalk and have horizons of marl intraclasts; no other sedimentary structures are present. Oyster shells are occasionally present. There is a lack of sedimentary structures but the presence of rip-up clasts suggests these beds were deposited from either grain flows or are the T<sub>A</sub> interval from high-density turbidity currents. Also present in the same area are thick litharenites, these are very similar but occur in thick (m scale) packets in which the base of the beds preserve flute and groove casts; these beds were possibly deposited from turbidity currents. Palaeocurrents suggest that sediment transport was mainly taking place at a high angle to the present basin margins, although there may have been some flow parallel to the basin as well (see 4.2.7.8). Unfortunately, palaeocurrent indicators are rare and not much data could be acquired.

The marl facies and the presence of a range of lithologically different interbeds are consistent with material being reworked down slope to the basin-floor. It appears that a variety of processes were operating, possibly relating to the grain-size, composition and volume of the unstable sediment. The density of the material was likely to have been a major control on the behaviour of the sediment flow. Plantic:benthic foraminifera ratios yield an estimation of the water depth, suggesting a water depth of between 0-250m.

Class	Group	Facies				
		1	2	3	4	5
A GRAVELS + PEBBLY SANDS	A1 Disorganized grvt + p. sst					
	A2 Organized p. sst					
B SANDS	B1 Disorganized					
	B2 Organized					
C SAND-MUD UNITS	C1 Disorganized					
	C2 Organized					
D SILTS + SILT-MUD UNITS	D1 Disorganized					
	D2 Organized					
E MUDS	E1 Disorganized					
	E2 Organized					
	F1 Isolated displaced clasts					
F CHAOTIC MIXED-GRADE UNITS	F2 Contorted + disturbed beds					
	F3 Muddy gravel + pebbly mud					
	G1 Ooze					
G OOZES + HEMIPELAGITES CHALKS, CHERTS, MARLSTONES	G2 Hemipelagite					

Figure 5.17 The main classes and groups of sediment facies recognised in the deep sea. The facies classes are distinguished based on grainsize (A-E), internal organisation (F) and composition (G), from Pickering *et al.* 1986.

Location No	Mean Age	No Planktic	No Benthic	Total	P/P+B
1SB50A	9.46	58	40	98	0.591837
2SB18A	9.05	113	0	113	1
3SB42	10.06	13	141	154	0.084416
4SB39A	13.24	100	0	100	1
5SB80	11.22	135	13	148	0.912162
6SB81	8.75	141	7	148	0.952703
7SB56A	9.58	77	52	129	0.596899
8SB44	8.33	107	5	112	0.955357
9SB20	8.68	100	4	104	0.961538
10SB22	10.84	110	5	115	0.956522

Table 5.4. Numbers of benthic and planktic foraminifera present in marls from the Late Miocene; these were dated using stontium isotopic techniques (see chapter Chapter 2 for location of samples).

The facies observed can be classified using Pickering *et al.*'s (1986) classes for deep sea sediments. In this case the Nurzeytin Formation would consist of E1 and E2 facies with interbeds of A1-2, B1-1, B2-1, B2-4, and G. The turbidites may be unconfined flows or possibly part of a sub-marine fan.

The lower boundary of this formation is was deposited simultaneously over the Sofular Formation, which is >200m thick in the southwest; however, to the north only a thin layer was deposited (<20m). Foraminiferal ratios also suggest that in the north of the area sediments were deposited in deeper water compared to those sediments in the south indicating a general decrease in water depth towards the south/southwest. Therefore, it is possible that the base of the Nurzeytin Formation in the north is the deeper water facies due to the presence of inherited topography from the Middle Miocene or due to contemporaneous tectonism; however, as relative sea-level rose deposition in the graben became more uniform.



### 5.5.2 Gökdere Formation, Kırıkhan area – Tortonian Age.

The Gökdere Formation is a coarsening-upward sequence, which is laterally very extensive and, although the precise details vary, the pattern of sedimentation is quite constant. The basal sediment is massive, fine-grained marl; the colour varies laterally from light grey to brown. The marl contains microfossils (both benthic and planktic foraminifera) and gastropods, with plant material being relatively common. Thin sandstone beds are interbedded with the marl; these often exhibit parallel laminations, flute and groove casts.

The proportion of sandstone increases higher in the Gökdere Formation (section 4.3.7.1 and Fig. 4.79). Litharenite beds increase in thickness (up to 50cm) and are generally found in ‘packets’ or ‘sand-bodies’. Bedding surfaces are sharp. The main sedimentary structures present are parallel lamination and cross-bedding. Sand-bodies higher in the sequence also exhibit ripples, load casts and flute casts. Many beds are laterally discontinuous (Fig. 4.80). These sedimentary features, combined with the fact that the beds often fine upwards indicate that deposition was from high-density turbidity currents producing the characteristic Bouma sequence with  $T_A$ - $T_E$  intervals present; however, not all intervals are present in all beds.

In the type section, at Gökdere, the sequence continues to coarsen upwards. This is not observed at other localities where the upper parts of the sequence are marked by numerous sand-bodies. At Gökdere, however, fine-grained mud is virtually absent for ~50m, occurring only as very thin beds. The sandstone beds there are thick (>1m) with occasional intraclasts. Biodiversity is very low and only one species of *Turitella* and occasional *Ostrea* are present. The *Ostrea* tend to occur in beds, with individual specimens exceeding 20cm in length. The low diversity fossil assemblage suggests a brackish water environment.

Above these thick sandstone beds the amount of marl increases again. In addition, thin chalk beds are also present. Sedimentary structures are usually absent although some parallel lamination is present. The fauna are still limited to large *Ostrea* and *Turitelid* gastropods suggesting that the environment was still brackish. There is also a lot of plant material present suggesting a marginal setting.

This succession is interpreted to be a progradational deltaic succession the main characteristic of which is a shallowing and coarsening-upwards sequence from offshore muds to silt and sand facies (Reading & Collinson 1996). The basal sediments dominated by

marl deposition are interpreted as basin mudstones. Above this basal marl facies there are numerous sand-bodies, which are interpreted to be the result of turbidity currents, and mark the onset of coarse clastic supply to the basin. The thickness of the sandstones and the sand-bodies increases upwards, marking the transition from distal to proximal turbidites.

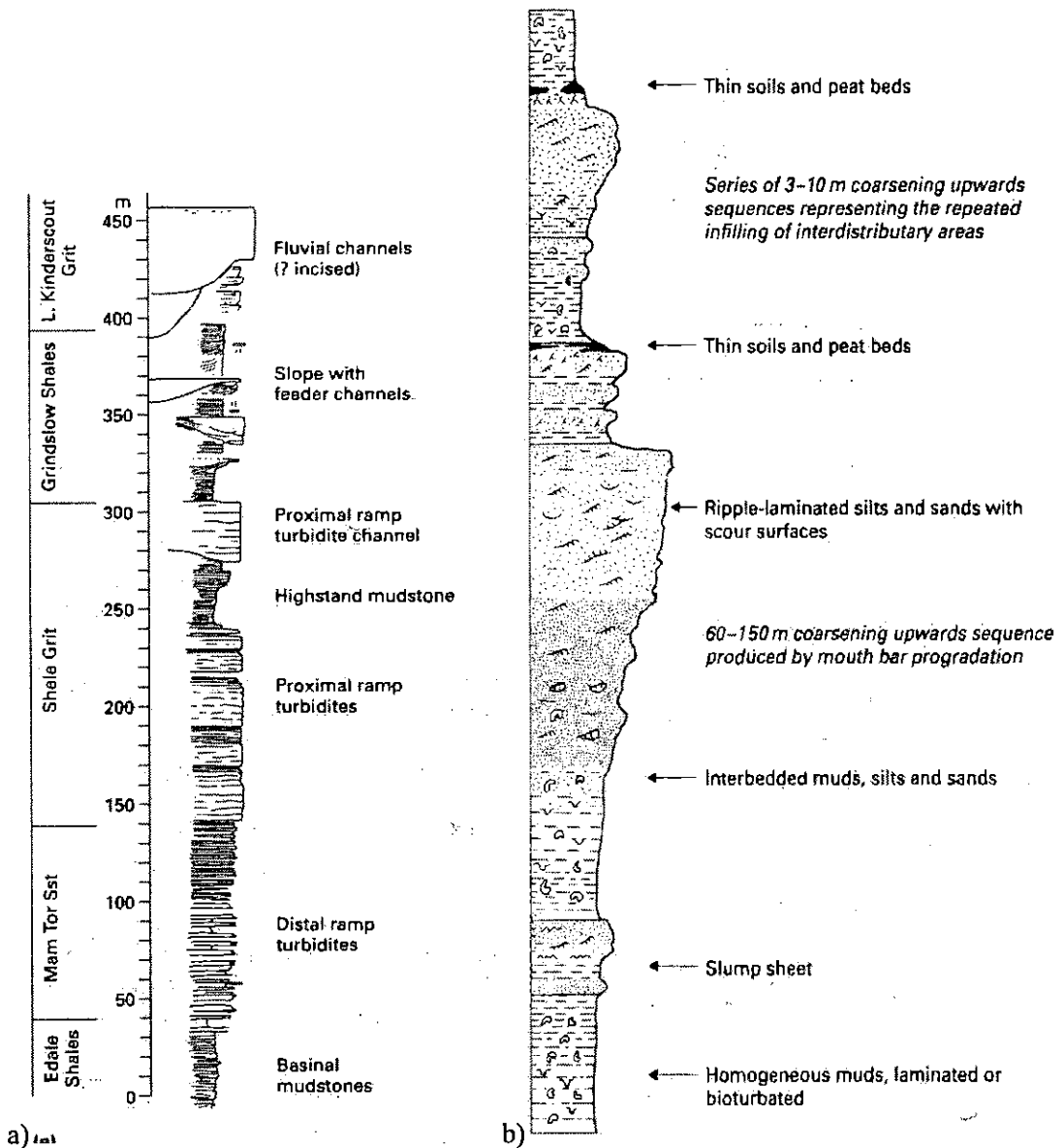


Figure 5.18. a) Vertical facies log of the Kinderscoutian of North Derbyshire where large volumes of sandy sediment apparently bypassed the slope through feeder channels; note how the lower units are similar to that observed in the Hatay but the upper part of the sequence is different (after Collinson *et al.* 1991, from Reading & Collinson 1996). b) Composite idealised sequence produced by mouth bar progradation in the Mississippi delta (after Coleman & Wright 1975, from Reading & Collinson 1996).

This transition from the basin floor to ramp may represent the *pro-delta* to *delta front* succession. The thick sandstones that overlie this mud-dominated sequence are of a different character; the lack of sedimentary structures suggests that they were bioturbated, while the low faunal diversity suggests stressed environmental conditions. The lack of sedimentary structures renders the interpretation of these sandstones problematic; they could represent a *mouth bar* environment or alternatively the intense bioturbation could indicate abandonment in a delta front setting (Reading & Collinson 1996). Locations other than the type section may be more distal to the sediment source thus accounting for the lack of this coarse sandstone facies. Palaeocurrent analysis indicates a general direction of sediment transport to the west/southwest (Section 4.3.7.5, Fig. 4.83); consistent with the more proximal character of the sediments in the most easterly locations.

Typically, overbank and shallow-bay deposits overlie sediments of a distributary mouth bar. The overbank deposits or crevasse splays typically form coarsening upward sequences. This is not observed. It is more likely that these mixed sediments represent a restricted sub-aerial setting such as an interdistributary bay or lagoon.

This succession has some similarities with fluvial-dominated deltas described from the Upper Carboniferous of the British Isles (i.e. Svela 1988; Martinson 1990; Collinson *et al.* 1991; Collinson *et al.* 1992) and the sequence can also be compared to an idealised sequence for mouth bar progradation from the Mississippi river delta (Coleman & Wright 1975). Additionally, similar sequences have been described from the Mediterranean region such as the Pliocene Çalkaya Formation of the Aksu Basin, Southern Turkey (Glover & Robertson 1998) and the Pleistocene of the Mesaoria Basin, Cyprus (McCallum & Robertson 1995b).

### 5.5.3 Vakıflı Member, Hatay Graben – Messinian.

Evaporites are present in four known locations in the Hatay Graben. The best exposed location (the type section, see section 4.2.9) is composed of blocks of laminated alabastrine gypsum set in a gypsiferous marl matrix. The alabaster has been diagenetically altered to selenite in places. The other locations are composed of selenite crystals. At one locality banding of small selenite crystals was observed that appears to be a primary structure and could be equivalent to the banded-stacked selenite of Robertson *et al.* (1995) from Cyprus, but generally there is no organisation to the crystals and it is unclear whether the selenite crystals are reworked primary or secondary diagenetic gypsum.

Gypsum is thought to have formed when the basin became semi-isolated from the Mediterranean Sea due to a fall in sea-level during the Messinian (Hsü 1972). Fine-grained alabastrine gypsum can be formed during the initial stages of desiccation by precipitation at the sediment-water and air-water interfaces (e.g. Schreiber *et al.* 1976). After precipitation, basin processes reworked these small crystals into depocentres. In contrast, selenitic gypsum forms in very shallow sub-aqueous environments. Thus, the alabastrine gypsum is interpreted as material that was precipitated and then reworked towards basin depocentres or deposited directly into the basin depocentre. This is in line with the present position of the deposits near the axis of the modern graben.

Alabastrine gypsum from Cyprus is interpreted to have been formed in a comparable way (Robertson *et al.* 1995). The banded-stacked selenite facies are interpreted as having formed in a shallow subaqueous setting, the banding recording repeated pulses of selenite growth (Robertson *et al.* 1995). In contrast, the selenitic gypsum at locality d (Section 4.2.9 and Fig 5.21) probably formed near the margin of the basin in a very shallow-water environment. The broken selenite crystals at the top of the succession perhaps represent gypsum debris flows that were possibly triggered by tectonic activity; again similar facies have been described from the Messinian of Cyprus (Robertson *et al.* 1995).

There is some evidence that significant erosion also took place during the Messinian. An erosional unconformity is observed at location 7, where the Sofular Formation is bored and eroded with Pliocene sediments directly overlying this erosion surface. Evidence is presented in Chapter Three which suggests that some of the Upper Miocene Nurzeytin

Formation has been eroded, especially in the northeast of the Hatay Graben. Suggesting that there could be a significant disconformity representing this period.

There are two main models for the depositional environment of evaporites; a closed basin creating a 'bull's eye' facies pattern and an open system creating a 'tear drop' facies pattern (Fig. 5.19). Evaporation occurs due to more water being lost by evaporation than is gained through precipitation and river influx, usually in arid to semi-arid climates. Unfortunately, exposure of the evaporites in the field area is limited; however, some generalisations can be made. Only gypsum is present, indicating that the concentration of brine remained low so that no halite formed. All the outcrops are found in the southwest of the study area and no evaporites were found any significant distance inland, and the deposits are <25m thick.

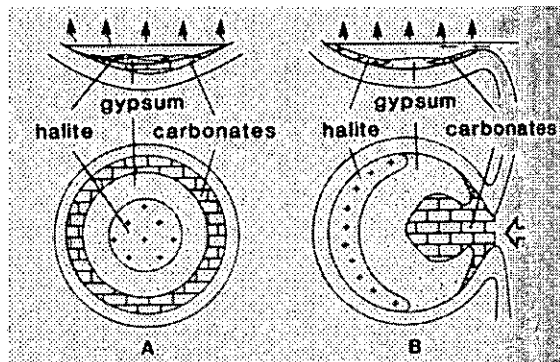


Figure 5.19. Broad patterns of evaporite facies. A) 'Bull's eye' pattern typical of closed basin. B) 'Tear drop' pattern, typical of restricted basin with near permanent connection to the open ocean, from Tucker 1991.

It is likely that at this time the Hatay Graben was isolated from the Mediterranean due to the falling sea-levels and became a small marginal basin. In the depocentres of this semi-isolated basin, some brine remained and lead to the deposition of carbonate and evaporite. The lack of halite suggests that the basin may have been at least semi-open; this situation has been suggested for other marginal basins of the Mediterranean, i.e., Polemi and Maroni Basins, Cyprus (Robertson et al. 1995); Veno del Gesso Basin, Appenines (Manzi *et al.* 2005). Similar evaporite facies to those observed in the Hatay Graben have also been reported from Mediterranean Basins, such as the Polis Graben, Cyprus. Gypsiferous turbidites, detrital selenite and slumped blocks have been described from this area (Payne & Robertson 1995); additionally, Messinian aged erosional surfaces, karst and fluvial

sediments are also present. It was determined that basin bounding and transverse faults controlled facies distributions, which may also be the case for the Hatay Graben.

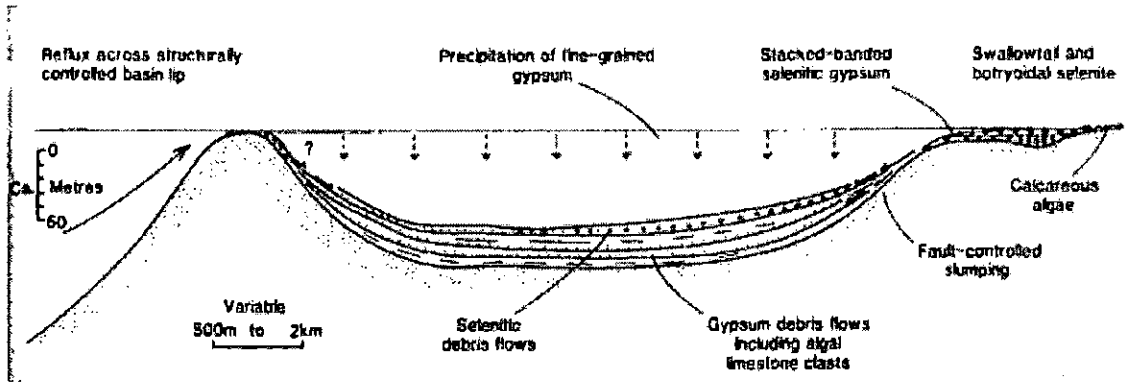


Figure 5.20. Simple facies model showing inferred processes of primary gypsum formation in Cyprus, in which the water depth is important (From Robertson *et al.* 1995). It is envisaged that the gypsum of the Hatay Graben formed in a similar manner.

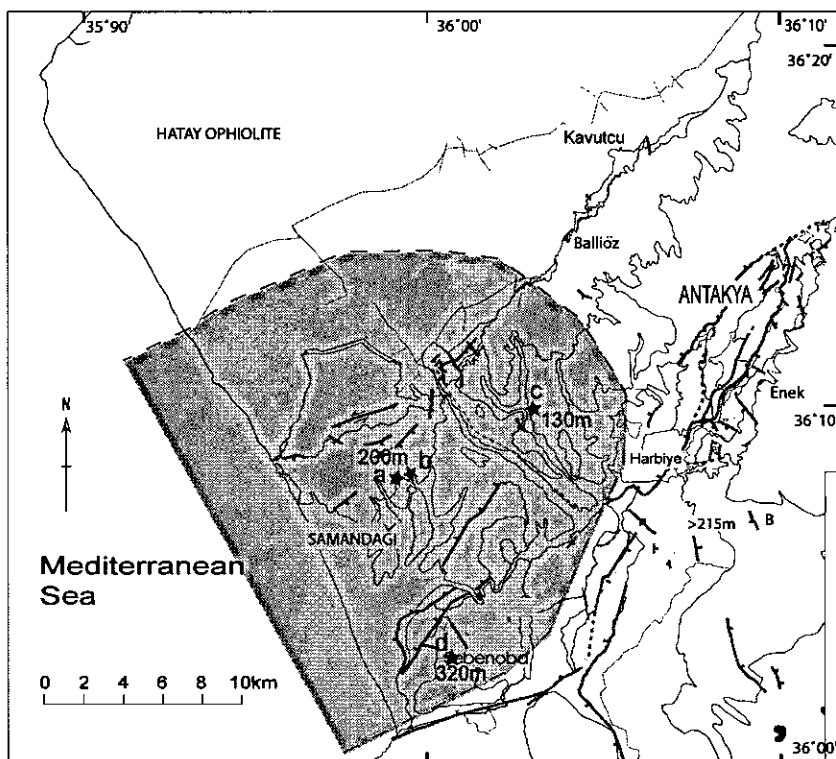


Figure 5.21. Map of the Hatay Graben showing location and elevation of Messinian evaporite deposits. Shaded area indicates possible extent of evaporite basin, assuming that locations c and d are marginal and therefore near the edge and that a and b were near the centre of a symmetrical basin.

## 5.6 Latest Miocene - Pliocene

### 5.6.1 Samandağ Formation, Hatay Graben.

The Samandağ Formation is composed of three main sedimentary facies: interbedded lithic greywacke and marl, litharenites with many sedimentary structures and massive orange litharenite. Each facies will be considered broadly in turn, although there is much spatial variation in this formation.

Where the Samandağ Formation is seen to overlie the Vakıflı Member (Nurzeytin Formation), the sediments are composed of very fine-grained grey marl. The similarity to the sediments of the Nurzeytin Formation suggest that after the sea-level rose at the end of the Messinian initial conditions in these basinal areas of the Hatay Graben were very similar to those prior to the end of the Mid-Miocene time.

Interbeds of different types are present within this basal marl and siltstone facies. Lenticular conglomerate beds are present, composed of matrix-supported and polymictic with sub-rounded to rounded clasts (up to 30cm in size). The matrix-supported texture of the conglomerate indicates debris flow processes, and the shape of the bed combined with the erosive base is channel-like, suggesting that this is a channel-fill deposit.

Fine-grained micaceous lithic greywacke beds are present in this facies. The bases of these beds are sharp and occasionally erosional; the beds often fine-upwards and are generally laterally discontinuous on an outcrop scale (section 4.2.11.3). Parallel laminations and 'rip-up' clasts are occasionally observed. These beds could again be channel-fill sediments. At one location stacked channels were observed at the top of the fine-grained facies (Fig. 4.59).

The progression from this dominantly marl facies to the sand dominated facies is generally poorly exposed (like the rest of the formation). However, there is good exposure along a river terrace near Samandağ. The lower part of this sequence includes the Late Miocene to Pliocene boundary. This boundary was identified through the use of microfossil dating; it is not marked by evaporite, an unconformity or a marked change in lithology.

The basal sediments of this of this exposure are composed of interbedded marl and thin sand beds, with rare parallel laminations and erosive bases (see 4.2.11.1). Shallow-marine bioclastic material, often found in layers, is abundant and there are many species of bivalves

and gastropods present in this sediment. The layered nature of the shelly material is suggestive of reworking by high-energy events, possibly storms. This combined with the lack of sedimentary structures implying that intense bioturbation has occurred could indicate that these sediments accumulated in an *offshore shelf environment*.

There is a sharp transition to bioclastic micaceous calcarenite, which down-laps onto a planar surface at the top of the muddier sediments. The sands are arranged in metre-scale low-angle foresets that prograde to the ESE. These foresets may represent a prograding delta. Above the foresets, there is evidence of slumping and soft-sediment deformation. There is still abundant shell material present.

The upper part of the section is poorly exposed uncemented sandstone, possibly of the *lower to upper shoreface*. Two thick, laterally discontinuous (but size indeterminate due to poor exposure), matrix-supported conglomerate horizons were observed, which are possibly coarse channel-fill conglomerates.

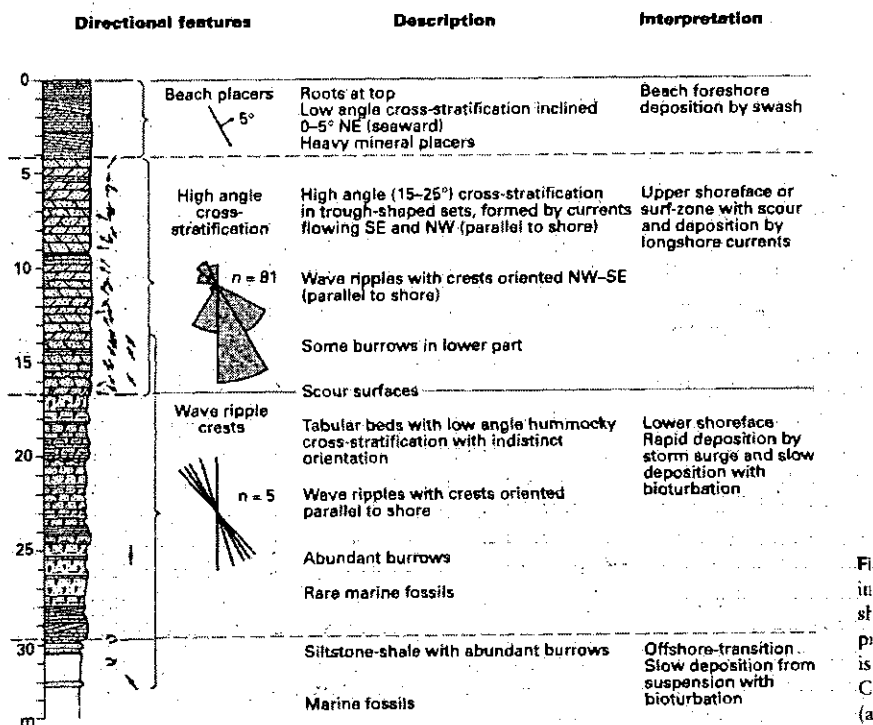


Figure 5.22. A prograding shoreline sequence in which the offshore transition and lower shoreface zones are dominated by storm processes (34-17m) while the upper shoreface is dominated by longshore currents (17-4m); Cretaceous Gallup Formation, New Mexico. From McCubbin (1982).



This association of certain environments is common along prograding coastlines. The generalised model of McCubbin (1982) for a barrier island-lagoonal setting has lower shoreface sands overlain by upper shoreface sands. However, there is no evidence for lagoonal sedimentation in this sequence but the foresets observed may be a channel infill from an inlet channel. Alternatively, the sequence could be that of a progradational beach (Fig. 5.22) where there are no lagoonal sediments. In this case the foresets would be part of a small fine-grained delta system. The abundant soft-sediment deformation in this succession may be the result of syn-tectonic sedimentation, unlike passive margins where the shoreline models were developed.

A well-exposed section of the Late Miocene to Pliocene age sediment is exposed near Sutas (Fig. 4.57). Again the boundary was identified using micropalaeotology. The Upper Miocene sediments in this succession are composed of interbedded sandy mudstone and greywackes. These sediments contain abundant bivalves and gastropods (both fragmented and whole), often in discrete horizons or lags. Reworked oncolite and plant material was also occasionally observed, which could indicate a near-shore depositional environment, although the presence of planktic foraminifera (seen in thin-section) suggests a more open-marine setting. Horizontal lamination and trough cross-bedding were observed, but was often disrupted by burrowing (horizontal and vertical; specific types were not identified). Bedding planes are sharp and some beds fine-upwards occasionally with mud clasts at the base. Similarly, common features of tempestites (storm deposits) are beds with sharp, often erosional, bases that fine upwards, and have parallel and cross lamination and locally ripples present. Shell accumulations are common and are often intercalated with marl and carbonate in shallowing-upwards sequences thus suggesting deposition by storm events (Flügel 2004). The bioturbation, in contrast suggests that sedimentation was at times relatively slow allowing colonisation of the substrate.

The mixed sand and mud composition and the sedimentary structures present are characteristic of a *lower shoreface environment*. In this environment much of the deposition occurs during storm events with periods of low-sedimentation between.

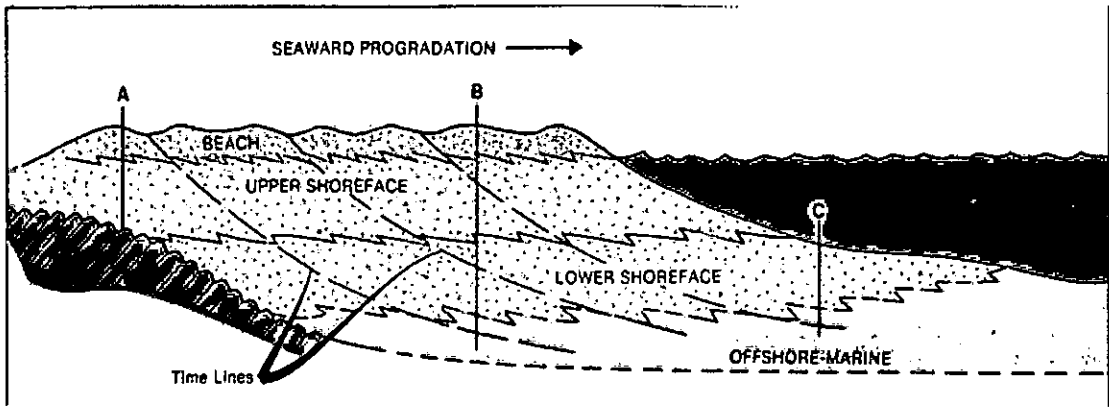


Figure 5.23. Idealised cross-section of a progradational beach to offshore environment illustrating the variation in the vertical facies sequence in a landward to seaward direction, from McCubbin 1982. The section from Location 8 is equivalent to location B on this cross-section.

Above the Miocene – Pliocene boundary the proportion of mud decreases and the sediment is lithic calcarenite. Other than in the lowest beds bioturbation is absent and rare fossil material is very fragmented. High-angle bi-directional trough cross-bedding is present (see 4.2.11.2), along with horizontal parallel lamination and very thin-bedded rippled sandstones.

‘Herringbone’ cross-bedding is typical of the *Upper Shoreface facies*, the result of oscillatory motion related to the primary onshore waves and secondary back-flow. Alternatively, the cross-bedding could be the result of tidal influences. Also, an increase in grain-size is common from the lower to the upper shore face. Bimodal palaeocurrent patterns recorded are typical of this facies (see 4.2.11.7; Fig 4.64).

The overlying beds exhibit more parallel laminations and unidirectional trough cross-bedding and two lenticular conglomerate horizons were observed. These polymictic conglomerates are clast-supported with sub-angular clasts. These coarse-grained sediments are capped by 1 m of pink palaeosol.

The progradational nature of this sequence suggests that this interval is representative of a *beach facies*. This interpretation is supported by the presence of horizontal laminations, developed by wave swash and the cross-bedding may be the result of a migrating ‘ridge and runnel’ (McCubbin 1982). The conglomerate lenses are likely to be channel fills. The palaeosol indicates sub-aerial emergence, and can be compared to an idealised cross-section of a beach (section 4.2.11.1, Fig 5.13).

The highest beds of the sequence show a return to lithic calcarenite deposition. More than 15m of medium-grained sandstone characterises the top of the Pliocene succession in many outcrops. Intense bioturbation has destroyed sedimentary structures in these sediments, apart from occasional parallel lamination. Large carbonate-cemented nodules are present, but there is little fossil material. It is likely that the lithic calcarenite deposition represents a transgression and that these sediments could be lower shoreface facies. In other locations where this is observed, there are not so many sedimentary structures present and the sediment is usually poorly lithified (See 4.2.11).

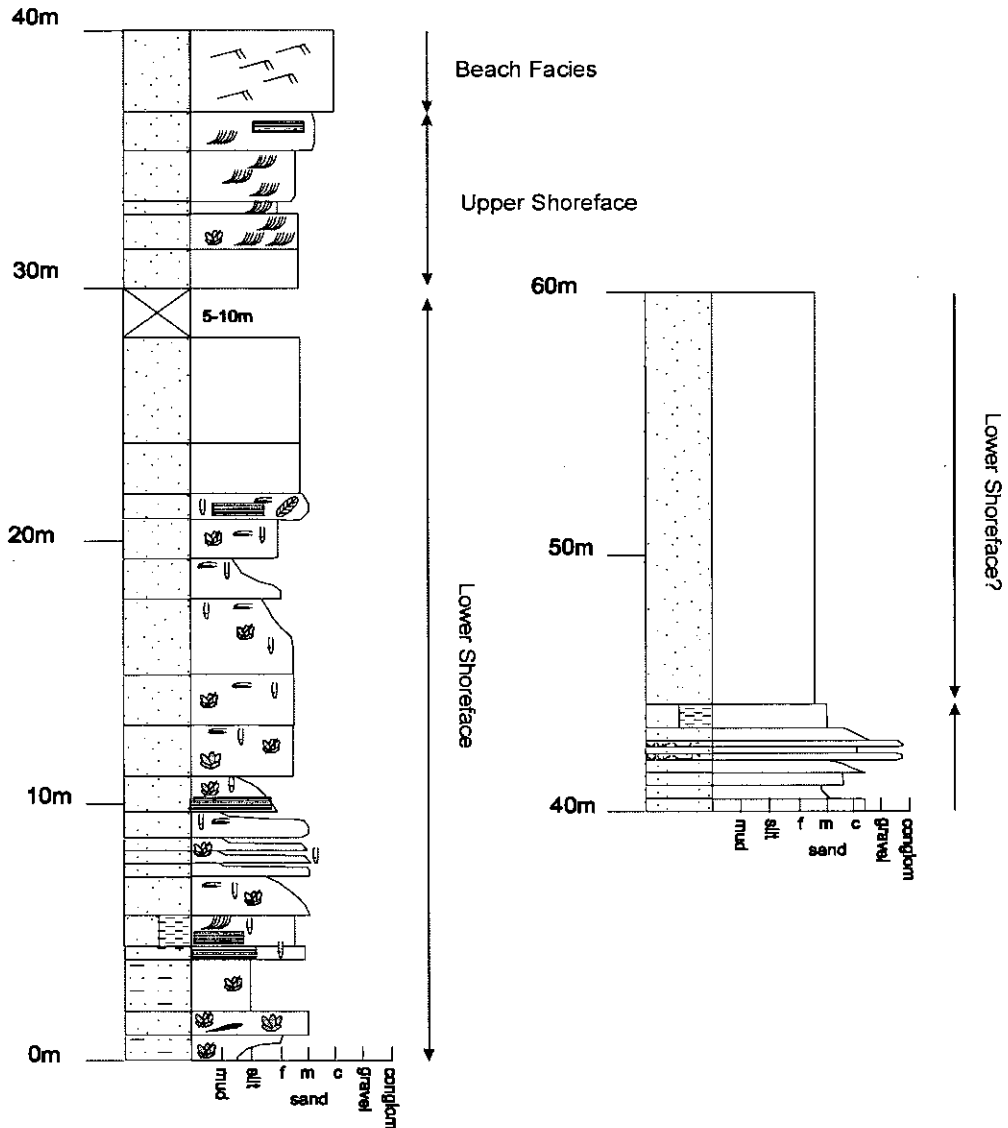


Figure 5.24. Sedimentary log showing the environmental interpretations for location 8.

A coarsening-upwards sequence was observed at location 7 (see 4.2.11.4). Medium- to coarse-grained litharenite coarsens up into pebbly sandstone and conglomerate. The litharenite is trough-cross bedded and palaeocurrents are bi-directional (See 4.2.11.7). Small bivalve fragments indicate a marine origin for the sediment. The conglomerate horizons are lenticular and composed of rounded clasts (<20cm).

Coarsening upwards sequences are classic deltaic indicators (Reading & Collinson 1996), and bi-directional currents are also very common. The lower cross-bedded sandstones may belong to the *Distributary mouth-bar facies*, while the conglomerate lenses could be channel-fill deposits. The palaeosol observed above the sandstone probably records the abandonment of the delta front.

The Pliocene Nicosia Formation of Cyprus shares some similarities with the marl dominated Pliocene facies of the Hatay Graben. The majority of the Nicosia Formation is composed of marine calcareous siltstone, fossiliferous and generally structureless. This facies was interpreted as background sedimentation on a shallow shelf below storm wave base (McCallum & Robertson 1995). Numerous channel conglomerates and sandstones fed onto this shelf from a fan-delta system.

The Kakkarista Formation of Cyprus has similarities to the coastal sediments observed in the study area. Well-sorted sandstones with a lower trough cross-laminated part, a middle part with symmetrical ripples and an upper part containing pebbles was interpreted as a shoreface – shoreline – upper shoreface/foreshore zone (McCallum & Robertson 1995). These sediments are associated with thin conglomerate horizons from the shoreline/beach and cross-bedded conglomerates from the foreshore and deltaic environs. The association of these facies was interpreted as a fan-delta system mainly due to the coarseness of the sediments and the regressive setting (McCallum & Robertson 1995). Conglomerate is less abundant in the Hatay area making this explanation for the coastal sediments unlikely.

Pliocene shallow-marine shelf and deltaic sediments have also been described in the Aksu Basin, southern Turkey (Glover & Robertson 1998), suggesting that during this time environmental conditions around the edge of the Mediterranean Sea were similar in different places.

## 5.7 Quaternary

The majority of the Quaternary sediments (section 4.2.13) are composed of conglomerates; these can be clast- or matrix-supported, are often poorly sorted with sub-rounded to rounded clasts and a maximum clast size of 0.5-1 m. Clast imbrication and cross-bedding is often observed. Pebbly and coarse-grained sandstone is often present, generally as lenses within the conglomerates, cross-bedding, parallel and cross-lamination is present within these horizons.

Quaternary sediments are often observed on the top of river terraces and appear to be similar to the sediments being deposited in the present rivers. The present river alluvium is composed of poorly sorted conglomerate with rounded clasts with a composition reflecting the various lithologies present in the field area and the Arabian shield to the south. Therefore, these sediments could be interpreted as having formed in a similar environment, i.e. coarse-grained *braided and meandering streams*. The present Asi Nehir is dominantly a meandering river with occasional bars but the Bükükaraçay and other tributaries are braided rivers.

The characteristics of these conglomerates are, for example, similar to Quaternary conglomerates (fanglomerates) of Cyprus (Poole & Robertson 1998), which were deposited in a braidplain setting fed by alluvial fans. Coarse alluvial sediments are seen in other areas around the Mediterranean, such as in the Aksu Basin from the Late Pliocene (Glover & Robertson 1998) and on Crete (Postma & Nemec 1990).

The other Quaternary sediments of most interest are tufa exposed at Harbiye and cross-bedded sandstone observed at location 406 (Section 4.2.13.1).

Flügel (2004) defines Tufa as a porous carbonate that forms in non-marine cool waters and the formation is strongly controlled by aquatic plants. Tufa at Harbiye forms a significant deposit probably exceeding 50m in thickness. Tufa is still forming in the waterfalls at the present time so it seems logical to assume that the ancient deposits formed in the same way. It is interesting to note that this location is next to one of the bounding faults of the graben, likely the reason why there is a spring here. This has been observed in similar tectonic situations such as the Hula Valley in Israel (Heimann & Sass 1989) and in the more extensive tufa deposits in the Antalya area, SW Turkey (Glover & Robertson 2003).

Well sorted, quartz-rich sandstone is exposed near the top of a Quaternary river terrace (see 4.2.13). The sandstone is variably cemented and has a honeycomb-weathering pattern. Although the evidence is slight (compositional and textural maturity) it is possible that this sandstone is *aeolian*.

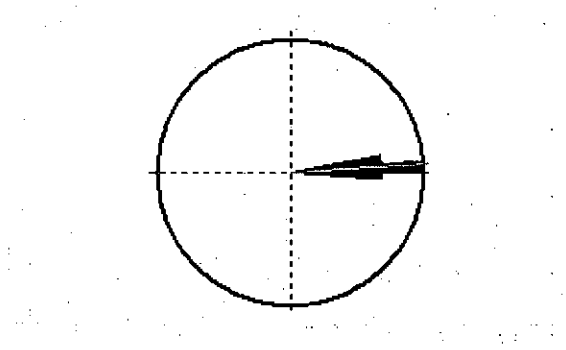


Figure 5.25 Rose diagram showing palaeocurrent data for Location 406, all data from cross-beds, N=4, mean direction = 086°

## 5.8 Summary palaeoenvironmental models.

- Upper Cretaceous** – Microbial limestone was deposited in the intertidal zone with an estimated exposure index of 40-90%. The top of the formation is composed of variable continental sediments.
- Eocene** – In the Hatay Graben, the Early Eocene sequence is composed of microbial limestones deposited in the intertidal zone; palaeosols indicate complete exposure at times. The upper part of the sequence of Nummulitic limestones indicates a shelf environment. To the north the Eocene is represented by calciturbidites, debris flows and slumps indicating a slope environment of deposition.
- Early Miocene** – In the Hatay Graben the Lower Miocene sediments are braided river sediments similar to the Scott and Donjek types of Miall (1977). In the north, the K1c1 Formation is composed of alluvial fan, braided river, pro-delta and continental sediments. These differing environments are interpreted as a fan-delta association.
- Middle Miocene** – The lower part of the Sofular Formation is composed of peritidal cyclothem at Kozkalesi and lagoonal sediments at Asi Nehir, indicating deposition on a carbonate platform. Upwards, the sediments become coarser and contain abundant reworked bioclastic material indicating deposition on a carbonate slope. Inland, numerous coralline fragments and a patch-reef suggest that reefs may have been common at this time in shallow-marine areas adjacent to a deeper water slope.
- Late Miocene** – In the Hatay Graben the Upper Miocene sediments consist of marls and interbeds of sandstone and conglomerate; these are interpreted as background sediments, turbidites and debris-flow deposits, respectively. Occasional slump horizons are also observed. These facies are considered to be representative of a fully marine basin with material being reworked down slope from the margins to the basin floor. In the latest Miocene (Messinian Stage) there were many

different environments. The most distinctive deposit is gypsum, caused by the evaporation of concentrated brine, indicating that the basin became isolated from the Mediterranean and dried up. Unconformity surfaces and incomplete Upper Miocene sequences indicate that extensive erosion took place during this stage. Near the present coastline, offshore to lower shoreface sediments were dated using microfossils as uppermost Miocene. In the north, the Gökdere Formation is interpreted as fully marine basin sediments. The lower marl-dominated sequence is interpreted as a pro-delta sequence. An overlying marl sequence contains sand-bodies, interpreted as submarine channels on a delta front. These are overlain by possibly distributary mouth bar and interdistributary bay sandstones.

**Pliocene –** Pliocene sediments are mostly shallow marine facies. The very latest Miocene/earliest Pliocene lithic greywackes are interpreted as an offshore to lower shoreface transition. These sediments are generally overlain by inferred lower-shoreface litharenites containing evidence of storm processes. Upper shoreface and beach facies commonly overlie lower shoreface sediments completing the facies association. In addition, deltaic sandstones were identified. No Pliocene sediments are present in the north perhaps due to this area being continental at this time and being an area of non-deposition. The whole area is likely to have become more continental as the present geography of the graben emerged

The following figures (Figures 5.26-5.30) show the proposed local palaeogeography of the field area for the Eocene, Early Miocene, Middle Miocene, Upper Miocene and Pliocene times, developed from the data presented in the preceding chapters.



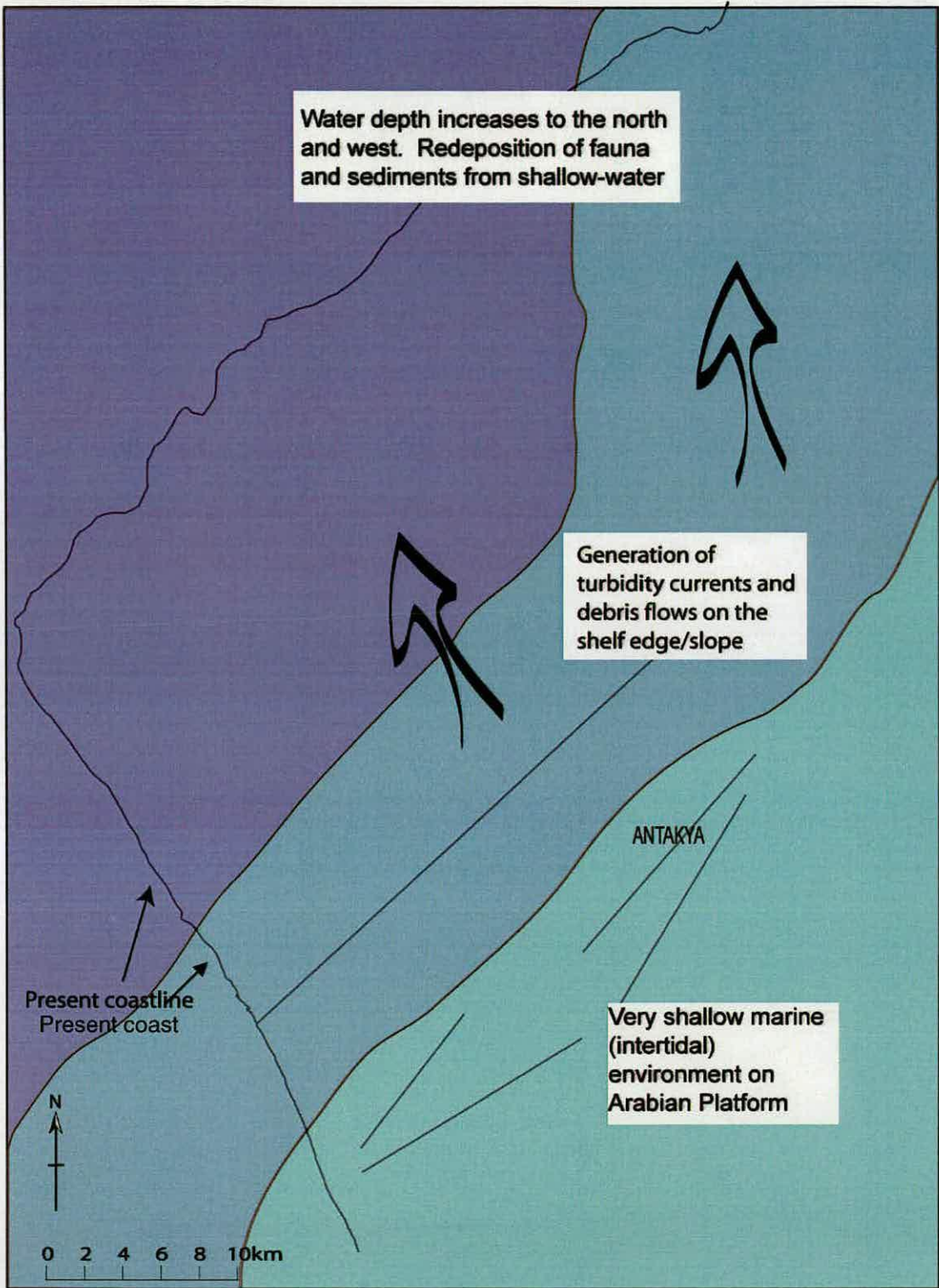


Figure 5.26. Palaeogeographic map of the field area for the Late Cretaceous to Eocene period; shallow-marine carbonate deposition dominated the region, with water depth increasing to the north (towards the Neotethys Ocean). N.B. dark blue indicates deep water, light blue indicates shallow water.

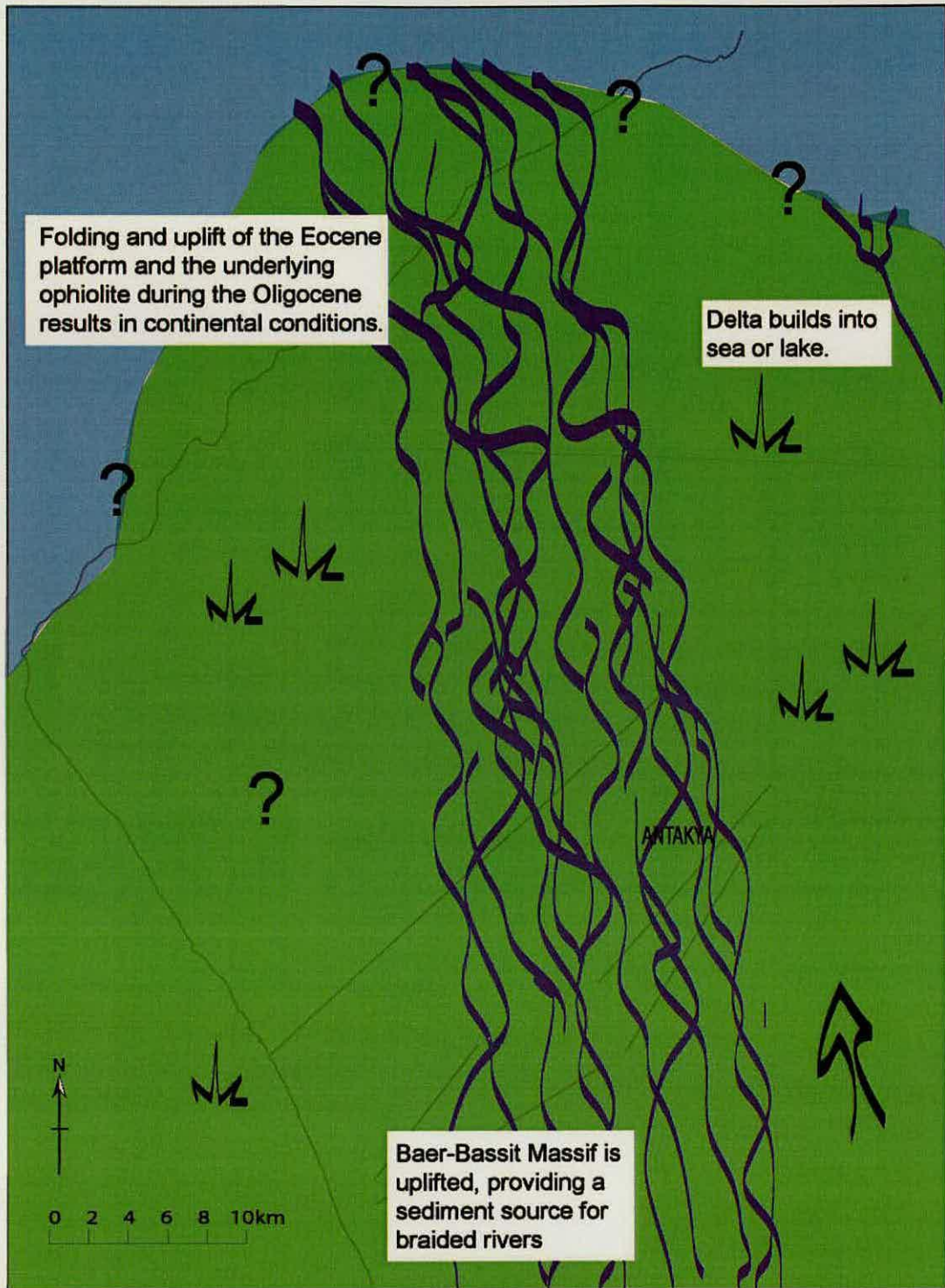


Figure 5.27. Palaeogeographic map of the field area during the Early Miocene (Burdigalian). Regional compression has caused uplift and folding of the Eocene sediments resulting in a hiatus during the Oligocene, related to a collision to the north. Sedimentation is mainly continental in nature with some sub-aerial sedimentation in the north. The Baer-Bassit Massif to the south in Syria is the source for the braided-rivers. The Amanos Mountains have not experienced as much uplift at this time.

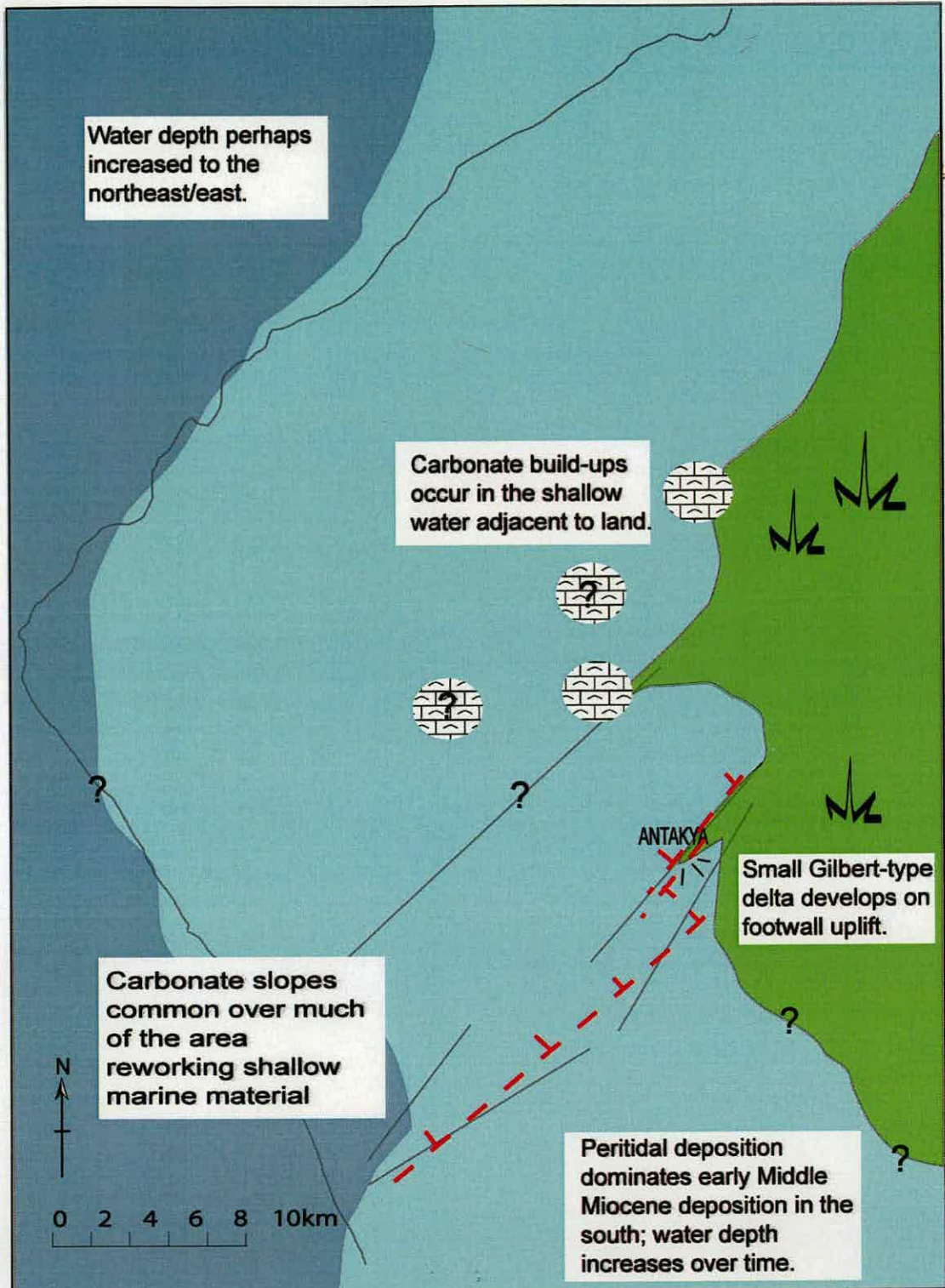


Figure 5.28. Palaeogeographic map of the field area during the Middle Miocene (Langhian). Relative sea-level rise lead to widespread shallow-marine carbonate deposition. Small carbonate build-ups developed (possibly more common than indicated). Extensional faulting had become active (section 7) affecting the distribution of facies but the main control on the depositional environment was still mostly determined by regional tectonics.

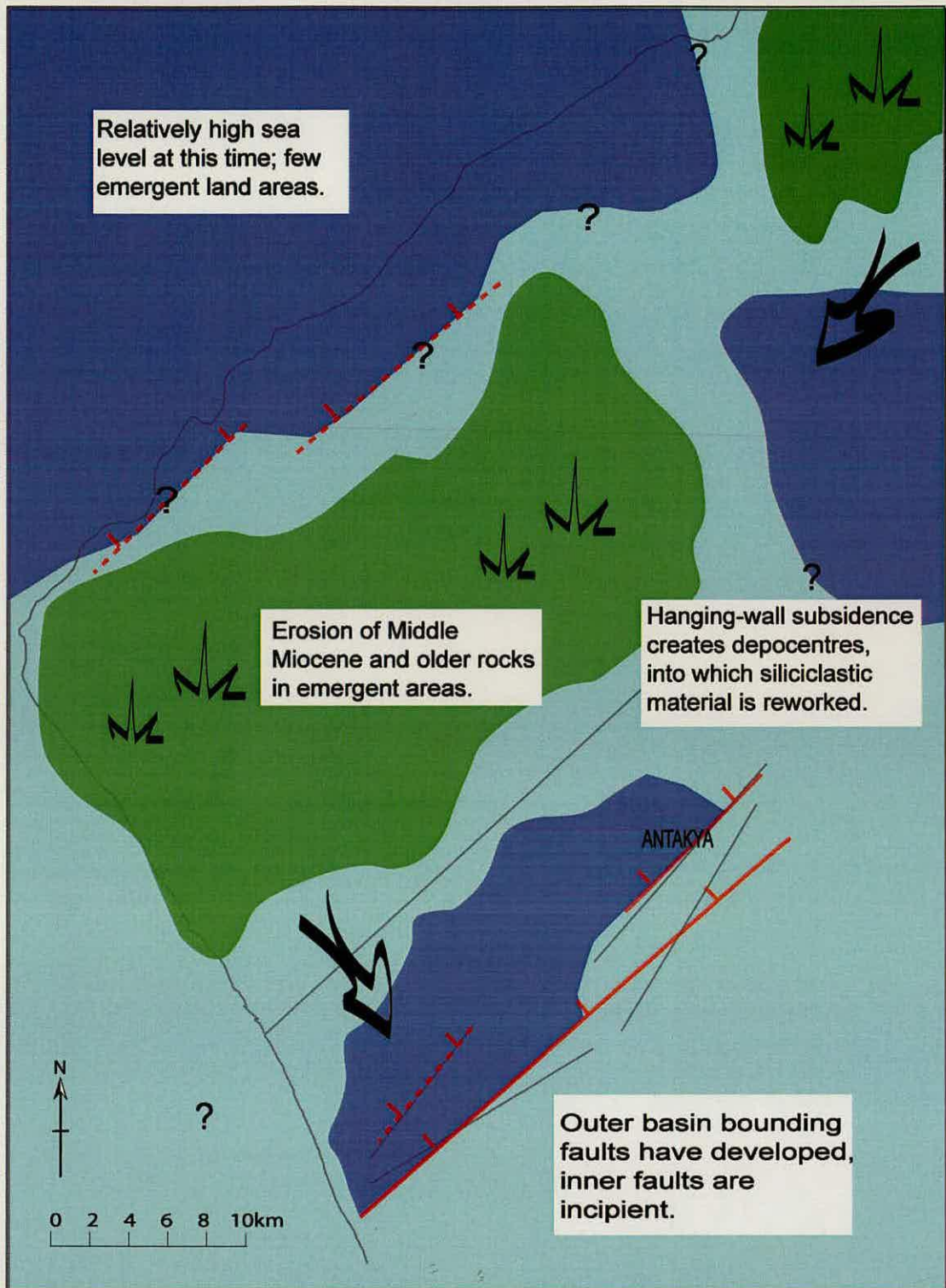


Figure 5.29. Palaeogeographic map of the field area during the Late Miocene (Tortonian). Development of the Hatay Graben is now well advanced, creating sea-floor topography; some land is emergent nearby shedding clastic material into the basin. Uplift is likely to be due to the final stages of continental collision taking place to the north (Robertson et al. 2004).

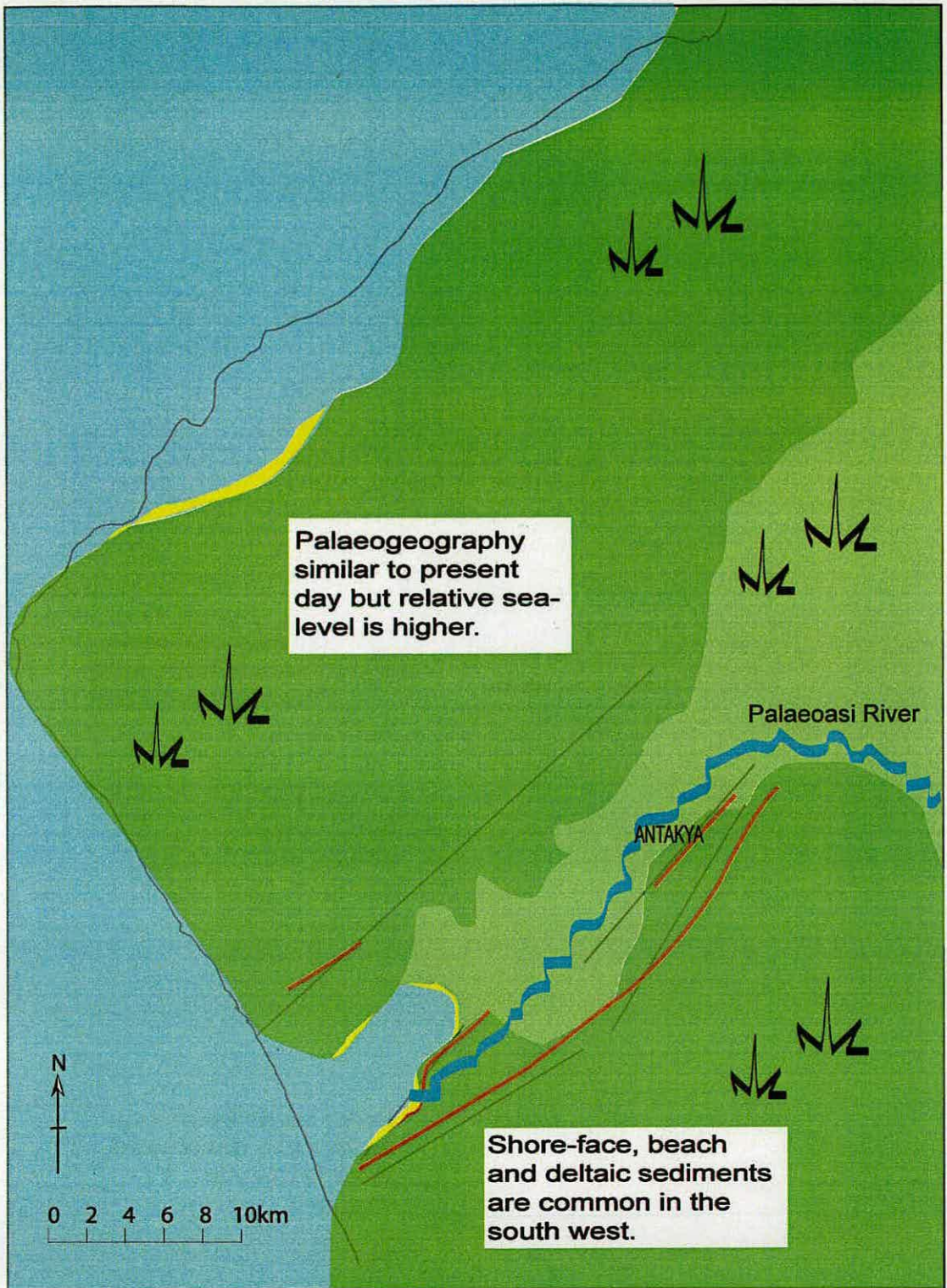


Figure 5.30. Palaeogeographical map of the field area in the Early Pliocene. At this time the area was very similar to today, but relative sea-level was higher.

## Chapter 6



The pass at Beilan [Belen] looking towards the sea.

## 6 Subsidence Curves

### 6.1 Introduction and methodology

The tectonic subsidence history of a sedimentary basin can be determined by using a technique called back-stripping (i.e. Steckler & Watts 1978). This method involves the progressive removal of the isostatic loading effect of the sediment fill of the basin, in order to calculate the subsidence that would have occurred in the absence of a sedimentary fill. The shape of a subsidence curve can be characteristic of the process of basin formation (i.e. a strike-slip pull apart will have a different shaped subsidence curve to a foreland basin; figs. 6.4 and 6.5) by calculating a curve for the Hatay Graben it can be used as another line of evidence for the determination of the tectonic controls on graben formation. The data presented in the previous chapters allow these calculations to be undertaken.

The first step to be taken when back-stripping a basin is to divide the sediments into packets of sediment where the following is known:

- The thickness of the unit
- The age of each unit
- The density of the sediment in the unit
- The water depth at the time of deposition
- The compaction history

However, there are problems with this method so the resultant curves will not be totally accurate. Errors in the calculated curves are due to uncertainties in the age of the units and in the water depth of the depositional environment. Additionally, it is not known how much material was removed from the unconformity surfaces that formed during the Oligocene and Messinian. This lack of knowledge affects the accuracy of the calculation in two ways; firstly, the original depositional thicknesses of the affected units are not known. Secondly, the compaction history for those units is more complicated than simple burial and compaction, as uplift has also occurred. Thus, there is an immeasurable error for each of the variables in this equation but this error will be the same for all analysed sections and therefore can be considered as negligible.

To calculating subsidence the oldest sedimentary unit is considered first (termed unit A). The thickness and density are known and the porosity can be calculated. Thus the original values of the density and the original thickness can be calculated for unit A using the formulae:

$$h_0 = \frac{h(1 - \phi)}{(1 - \phi_0)}$$

$$\rho_{s0} = \rho_w \times \phi_0 + \rho_s(1 - \phi_0)$$

*Equation 1*

Where;  $h_0$  = original thickness

$h$  = present thickness

$\Phi$  = present porosity

$\Phi_0$  = original porosity

$\rho_w$  = density of water

$\rho_s$  = present density of the sediment

$\rho_{s0}$  = original density of the sediment

These values can then be used to calculate the subsidence required to provide the necessary accommodation space for unit A.

$$T_A = \frac{h_0(\rho_m - \rho_{s0})}{(\rho_m - \rho_w)}$$

*Equation 2*

Where  $T_A$  = tectonic subsidence

$\rho_m$  = density of the mantle and depth of isostatic compensation

When this is known the next oldest unit (B) is then considered. The same values are calculated for unit B and secondly the values of the unit A are recalculated to take into account that it is now buried under unit B. Thus, the total subsidence for both units can be calculated using:



$$T_B = \frac{(h_{AO} + h_{BO})\rho_m - (h_{AO} \times \rho_{SA}) - (h_{BO} \times \rho_{SB})}{(\rho_m \times \rho_w)}$$

Equation 3

This process is repeated for each successive unit and the values for the previous units recalculated to give the tectonic subsidence for each unit. This can then be plotted against the mean age of the unit generating a subsidence/time plot.

In order to quickly and accurately calculate the subsidence history for the area, a computer program developed by Turner (1996) was utilised. In this program, each sedimentary layer is assigned a bulk lithology and water depth at the time of deposition. Unconformities are treated as periods of zero deposition and given a nominal thickness of 10cm, this program unfortunately does not have an option to erode material. The bulk lithology is known from the field studies; however, as the program contains only five different lithologies each unit can only be assigned one type based on the greatest percentage of each lithology present. Water depth at the time of deposition is estimated based on sedimentary facies and the ratio of benthic:planktic foraminifera (see chapter 5).

The sedimentary layers are then decompacted by removing the affect of burial; burial decreases the porosity and thus the thickness of the unit (eq. 1 and 2). The porosity/depth relationship varies depending on the lithology; in order to calculate the changing porosity the program uses the Sclater and Christie's (1980) exponential porosity/depth function. After the unit is decompacted it is then backstripped (eq. 3). This process calculates the 'total subsidence'; in order to calculate the 'tectonic subsidence' the effect of sediment loading needs to be taken into account. The effect of sediment loading is removed by isostatically unloading the remaining sediment column from the basement as each layer is removed.

The programme used for this assumes Airy isostasy; it is possible that this assumption will lead to some over compensation if the area is not controlled by simple isostatic behaviour. However, as all sections are treated the same and the distances between the sections are much shorter than flexural wavelengths the error from this should be negligible. Additionally, regional lithospheric properties are poorly constrained therefore using Airy isostasy is reasonable, this approach has been used in similar areas, i.e. Hyblean Plateau, Sicily (Yellin-Dror *et al.* 1997).

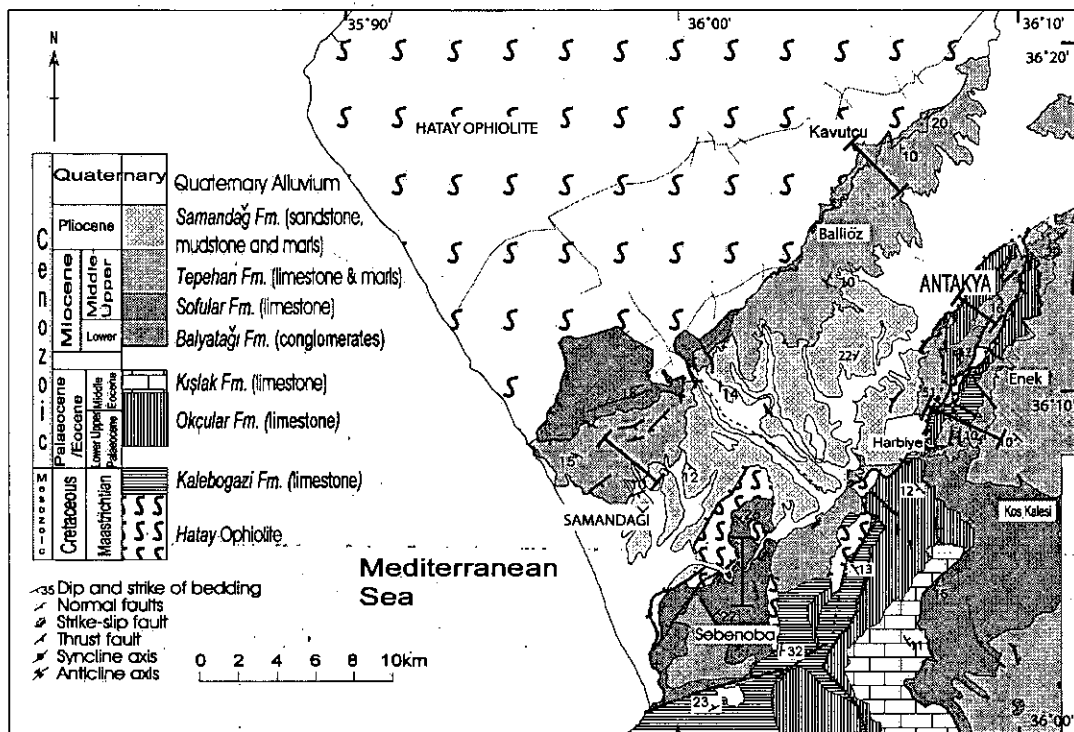


Figure 6.1. Geological map of the Hatay Graben showing the approximate location of the logs used to calculate the subsidence curves.

Five representative sections were selected for backstripping; three sites from the southeastern margin of the graben (Antakya, Harbiye and Asi Nehir; Figure 6.1) and two from the northwestern margin (Kavutcu and Nurzeytin; Figure 6.1). These sections were chosen to investigate the differences in subsidence histories of the margins and along the strike of the graben. Additionally, these sections represent complete sedimentary sections constructed either from one log or as a composite from a number in spatially close locations (the latter applies to the Antakya and Asi Nehir sections) (Fig. 6.1).

	Antakya Section	Harbiye Section	Asi Nehir Section	Kavutçu Section	Nurzeytin Section
Quaternary					10m sandstone WDB 0m WDT 0m
0.5-1.64 Ma					50m sandstone WDB 0-10m WDT 0m
Late Pliocene 1.64-3.4 Ma					50m silt WDB 50-175m WDT 10-50m
Early Pliocene 3.4-5.2Ma			5m sandstone WDB 10m WDT 10m	50m sandstone WDB 50-100m WDT 0-10m	
Messinian 5.2-6.7Ma			10m silt WDB 10m WDT 10m		10m silt WDB 0-10m WDT 0-10m
Late Miocene 10.4-6.7 Ma	300m silt WDB 0-10m WDT 300-750m	300m silt WDB 300-750m WDT 300-750m	50m silt WDB 300-750m WDT 300-750m	250m silt WDB 300-750m WDT 300-750m	300m silt WDB 300-750m WDT 300-750m
Middle Miocene 16.3-10.4 Ma	5m limestone WDB 0-10m WDT 10-50m	100m limestone WDB 0-10m WDT 50-100m	200m limestone WDB 10-50m WDT 50-100m	5m limestone WDB 0-10m WDT 10-50m	150m limestone WDB 50-100m WDT 50-175m
Early Miocene 21.50-16.3 Ma	150m sandstone WDB 0m WDT 0m	75m sandstone WDB 0m WDT 0m			
Eocene 50.0-42.1 Ma	300m limestone WDB 10-50m WDT 10-50m	60m limestone WDB 10-50m WDT 50-100m	100m limestone WDB 10-50m WDT 50-175m	100m sandstone WDB 0m WDT 0m	
Late Cretaceous 69.5-65.0 Ma		215m sandstone WDB 10-50m WDT 0-10m	100m limestone WDB 10-50m WDT 0-10m		

Table 6.1. Table of data inputted into programme to calculate the subsidence curves, WDB – Water-depth at base of the formation; WDT – Water-depth at the top of the formation.

## 6.2 Results

The subsidence curves along the northern margin show that there is a difference in the subsidence history from the northeast to the southwest. The oldest rocks in the Antakya section are Eocene in age (Fig. 6.3). The subsidence curve shows that there was rapid subsidence during this period. Following a hiatus during the Oligocene the graben continued to subside but at a slower rate than previously. The Harbiye and Asi Nehir (Fig. 6.3) sections show that subsidence began in the Late Cretaceous and the graben subsided slowly until the end of the Eocene; again there is no subsidence during the graben-wide Oligocene hiatus. The Harbiye section then subsided continuously until the Pliocene whereas the Asi Nehir section appears to have subsided rapidly until the Middle Miocene and then continued to subside slowly to the present day. On the northwestern margin of the graben, the Nurzeytin section and the Kavutcu section (Fig. 6.2) appear to have subsided quite rapidly since the Miocene.

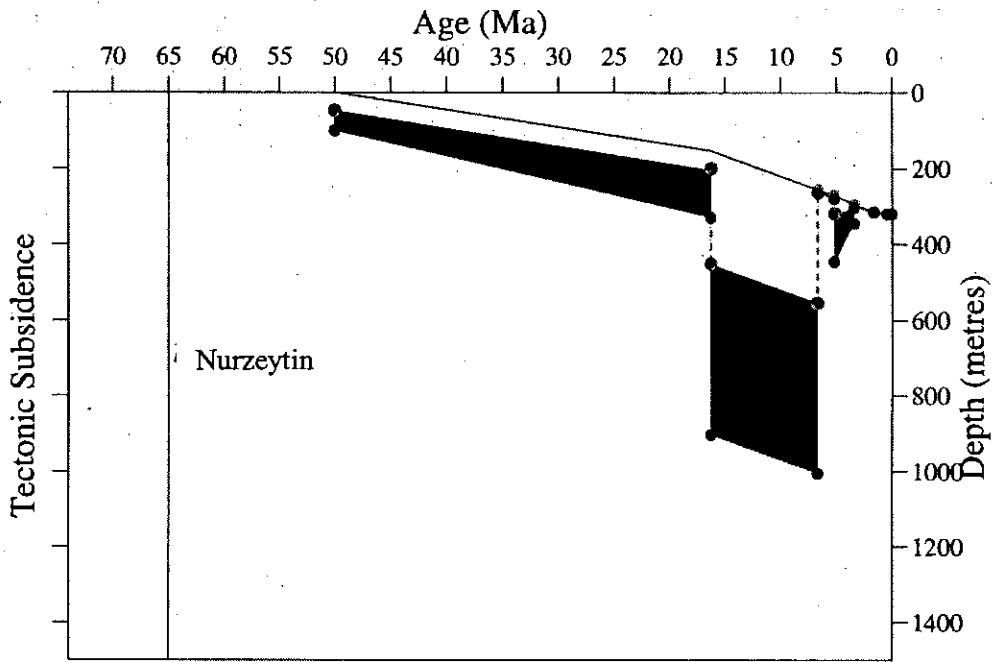
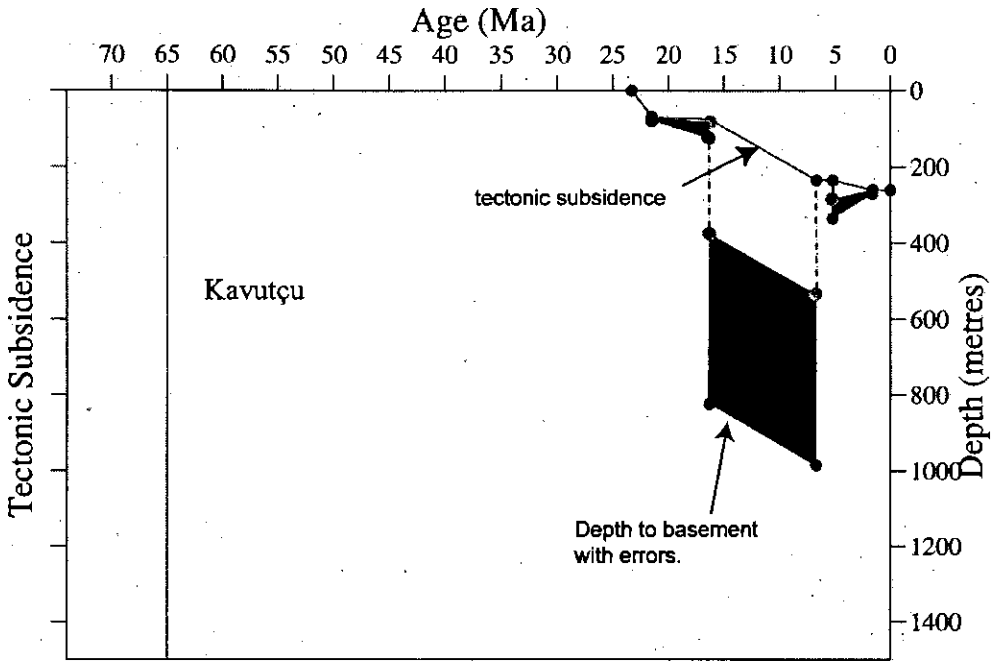


Figure 6.2. Graphs showing the tectonic subsidence (left axis and solid line) and depth to basement (right axis and shaded area)/total subsidence, true total depth to the basement lies somewhere within the shaded area. A range is given for the depth to basement as this is calculated from the depositional water depth for each unit, also given as a range) for the Kavutcu and Nurzeytin sections, see Fig. 6.1 for locations.

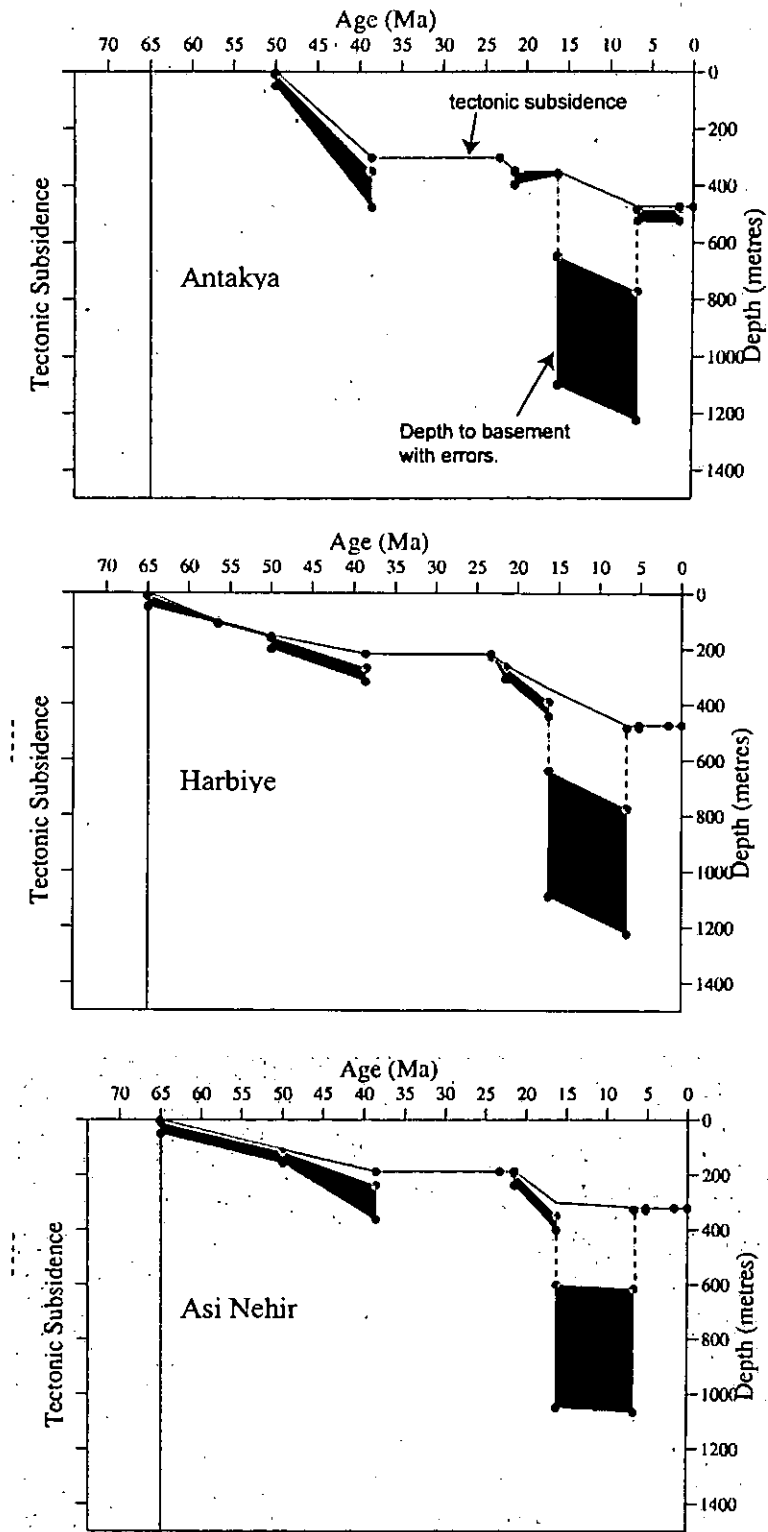


Figure 6.3. Graphs showing tectonic subsidence for Antakya, Harbiye and Asi Nehir sections. Axis as Fig. 6.2, locations shown on Fig. 6.1.

### 6.3 Discussion

Tectonic subsidence curves can be used as a tool to investigate the underlying controls on the formation of a sedimentary basin as the shape of the curve will vary depending on the regional tectonics.

Subsidence curves that have been derived for rifted continental margins, show that subsidence is initially rapid and then gradually decreases over time (McKenzie 1978b), a similar pattern is also observed for pull-apart basins and other structures controlled by normal faulting.

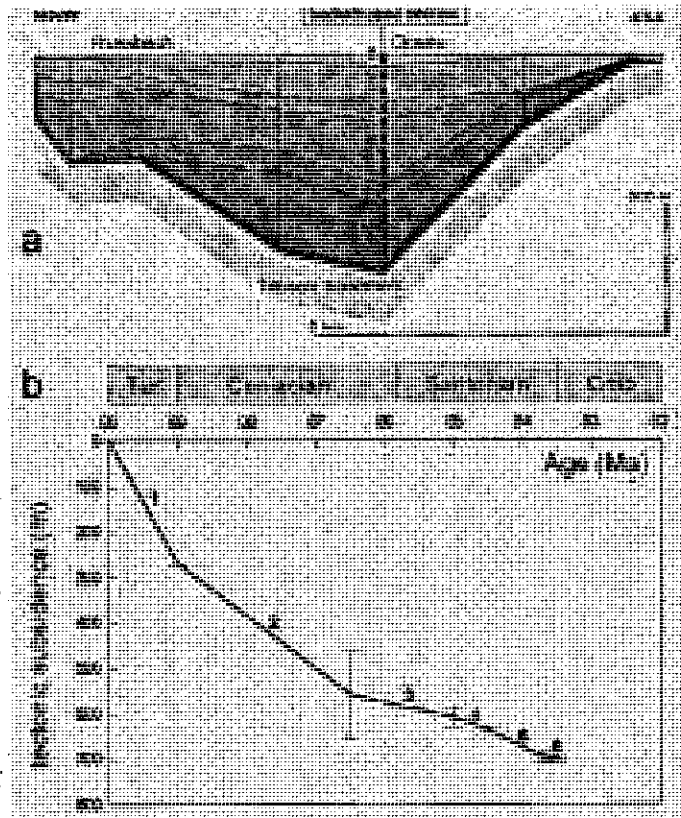


Figure 6.4. a.) WNW-ESE stratigraphic section through the Gosau Basin, Austria. Numbers refer to the lithological units used for backstripping. b.) Backstripped tectonic subsidence curve for the Gosau Subgroup of the Central Gosau Basin, error bars indicate the range in water depth estimates (from Wagreich & Decker 2001). Note the rapid initial subsidence that is dissimilar to the curves calculated for the Hatay Graben...

In contrast, subsidence curves calculated for foreland basins are characterised by a slow initial subsidence (see Figure 6.5 below), during initial loading of the continental margin, followed by accelerated subsidence as the load advances and thickens. Subsidence reaches a maximum when the basin is overridden by the emplaced load. The subsidence rate then decreases as the basin is uplifted. One of the most distinctive features of a foreland basin curve is a sharp inflection points relating to sudden increases in the rate of subsidence (Jordan *et al.* 1988; Jordan 1995; Miall 1995).

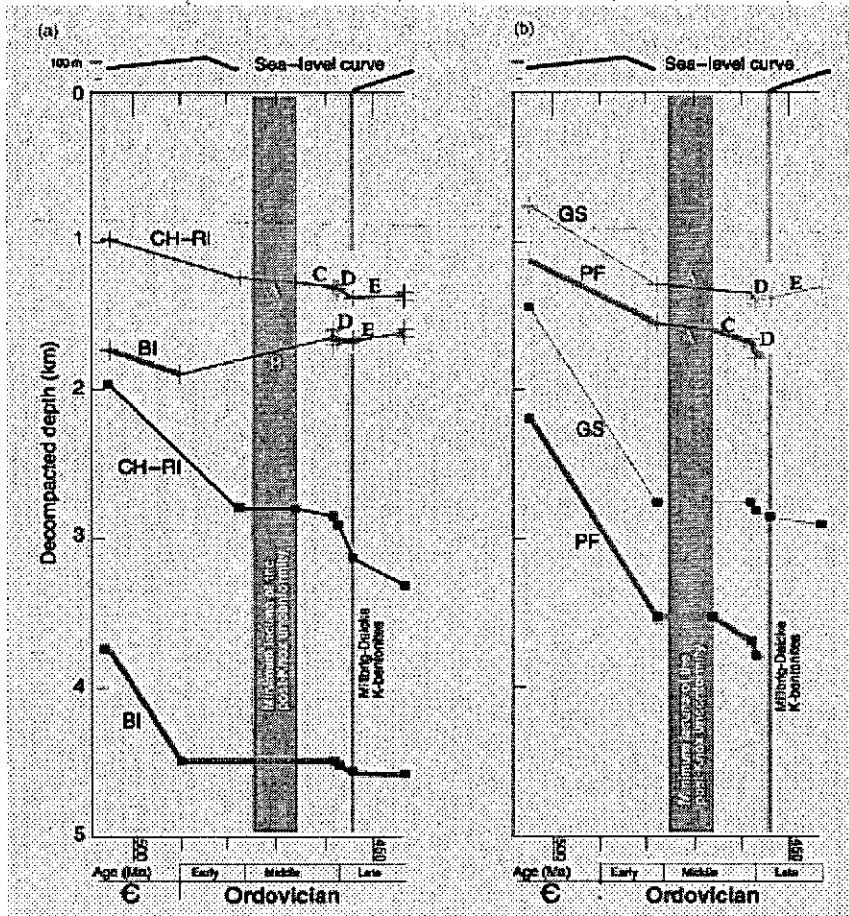


Figure 6.5. Total and tectonic subsidence curves (lower and upper curves respectively) for five sections from the Birmingham graben, situated in the peripheral Blountain Foreland Basin (Southern Appalachians, USA) from Bayona & Thomas (2003). Note the similarities of these subsidence curves derived from a foreland basin to calculated curves for the Hatay Graben, both show phases of subsidence separated by quiescent periods.

This suggests that the subsidence in the Hatay Graben area was controlled by loading of the lithosphere. Regional evidence suggests this was located to the north, along the Bitlis Suture Zone (Chapters 1 & 9) and the Hatay Graben is, therefore, part of the peripheral foreland basin to this orogen. This also may suggest that the effects of normal faulting have had little affect on subsidence until the Plio-Quaternary.



## **6.4 Conclusions**

- The subsidence curves indicate that the rate of tectonic subsidence was low from the latest Cretaceous (post-ophiolite emplacement) until the Early Miocene.
- The rate of subsidence was much greater during the Miocene.
- The Plio-Quaternary has been characterised by low to no subsidence.
- These subsidence curves have similarities with those calculated for other foreland basins but are dissimilar to extensional areas.

## Chapter 7



Remains of the Port of Seleucia near Suadeah [Samandağ?]

## 7 Structural Evolution of the Hatay Graben

### 7.1 Introduction

The aims of this chapter are to describe the structural aspects of the Hatay Graben. This will be achieved through field descriptions of faults and folds, the analysis of fault orientation data (in order to investigate fault trends), stress analysis and through the investigation of the past and present seismicity of the area. It is important to study the structural evolution of the graben in order to consider the area in the wider context of its regional plate tectonic setting.

The Hatay Graben is an asymmetrical structure (Fig. 7.1) trending 030° - 210°, ~50 x 20km in area. The SE margin is formed by large, faults striking 040° and dipping to the NW with a dominantly normal sense of movement. In contrast, the NW margin is not structurally controlled although map-scale faults are present. Normal, oblique and strike-slip faults are common on all scales and many outcrops are pervasively fractured. Compressional deformation is less common within the Miocene and younger rocks with only rare reverse faults observed and occasional folding that is probably related to normal faulting. Folding is much more common within the Eocene and older succession.

There is limited existing work on the Hatay Graben. Tinkler *et al.* (1981) considered that the Amanos Mountains and the adjacent Hatay Graben represented a mega anticline/syncline pair running NE-SW cut by later extensional faults. Tinkler *et al.* (1981) recognised five main stages of post-emplacement tectonics.

1. Folding and faulting during the Maastrichtian
2. Post Maastrichtian- Pre-Lutetian normal faults
3. Post-Maastrichtian- Pre-Miocene normal faults
4. Post-Miocene gentle folding
5. Post-Pliocene normal faulting

Although Tinkler *et al.* (1981) state that due to limited age information, the normal faulting episodes three and five could in fact belong to the same event. They attribute the formation of the topographic graben to pre-Miocene faulting with offsets of 1-2km on the normal faults. Tinkler *et al.* (1981) also recognised major unconformities at the base of the Lutetian and at the base of the Miocene.

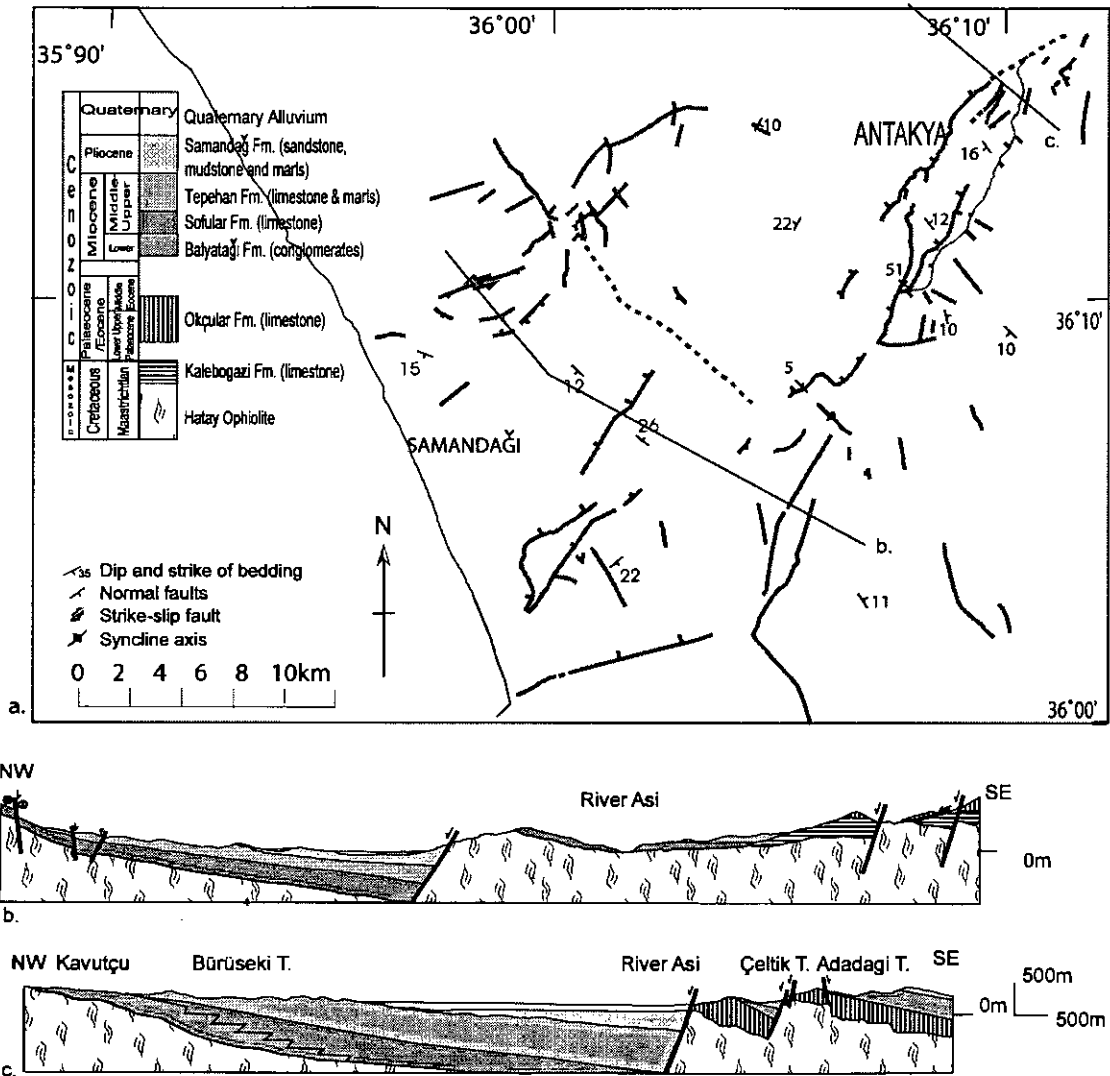


Figure 7.1. Outline fault map and cross-section of the Hatay Graben

Pişkin et al. (1986) followed the same tectonic scheme as Tinkler *et al.* (1981) but also produced a reasonably detailed map of the structure of the Hatay region, although the Neogene succession was represented as a single unit.

Rojay *et al.* (2001) appear to be the next authors to publish material on the structure of the graben; the paper focuses on the adjacent Karasu Rift, but they also took some fault measurements from the Hatay Graben. They recorded four dominant sets of faults with NE-SW strikes dipping to the NW or SE, with kinematic indicators suggesting a normal oblique-slip motion with a left-lateral component. Rojay *et al.* (2001) see the formation of the Hatay Graben or (Antakya-Samandağ depression) as representing a releasing bend on the Karasu

rift, a sinistral structure that links the DSFZ and the EAFZ. This hypothesis is erroneous as the orientation and geometry of the graben is not consistent with a pull-apart basin that would form along the DSFZ in this area (Figure 7.2) and no evidence is stated to back-up this assertion.

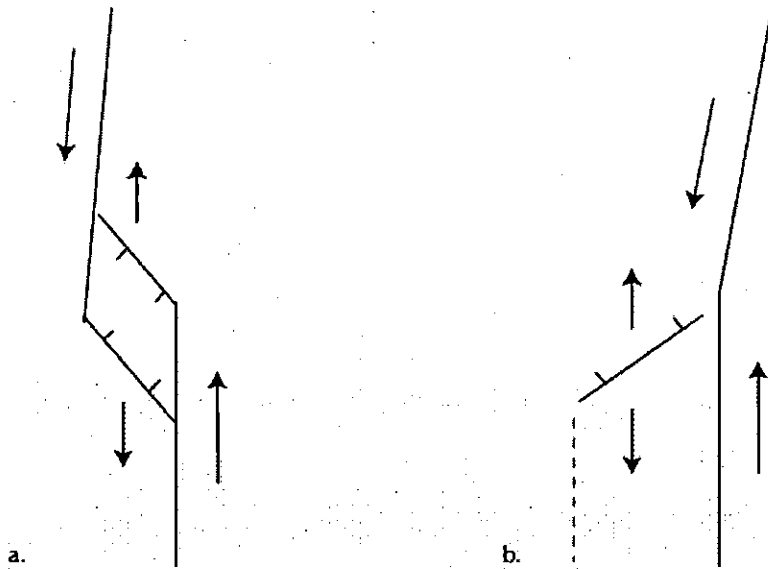


Figure 7.2. Line drawings showing; a) a releasing bend forming a pull-apart basin along an sinistral strike-slip fault – this is the proposed explanation for the formation of the Hatay Graben proposed by Rojay *et al.* (2001); b) a sketch of the actual situation of the Hatay Graben, the orientation of the graben has the characteristics of restraining bend on the DSFZ, if this fault stepped to the west at the southwestern end of the graben (indicated by a dashed line). However, this is not the case and the area is extensional and not contractional, thus Rojay *et al.*'s (2001) hypothesis does not fit the observations and an alternative explanation must be sought for the formation of this extensional structure.

Över *et al.* (2002) conducted a survey of the present-day to Plio-Quaternary stress regime of the Hatay Graben using a relatively small number of field measurements of fault planes and focal plane solutions of recent earthquakes. They identified a strike-slip stress regime ( $\sigma_3$  to NE) and two extensional stress regimes ( $\sigma_3$  to the NE and E) and observed occasionally two lineations (a high angle and a low angle lineation) on one fault plane for which they considered the normal striations to be the younger. Över *et al.* (2002) consider that the present day stress state is a dominantly normal one with a small strike-slip component. Thus they conclude that there has been a change from an older strike-slip to a younger normal fault regime that has also reactivated old faults, but they have no evidence as to when or how this may have occurred.

## 7.2 Extensional Tectonics

### 7.2.1 Basin-Scale Faults

#### 7.2.1.1 Southeastern margin

Northwest-dipping normal faults dominate on the southeastern margin of the graben. These faults form the boundary to this side of the graben, trending NE-SW parallel to the trend of the graben. Generally, fault planes are eroded but have a strong topographic expression. In the north, behind the town of Antakya, basin-scale faults are seen to place Upper Cretaceous, Eocene and ophiolitic rocks against the Plio-Quaternary basin fill. In this area two large normal faults define the edge of the graben and the width of the margin (the distance between the inner and outer boundary fault) is ~4 km. The innermost fault has the larger throw (500-1000m) but the outer fault also has a throw of >500m (Fig. 7.1). To the south, the width of the graben margin increases to about 10 km; there is a greater distance between the innermost and outermost boundary faults.

Rotated blocks of stratigraphy on fault planes were observed at a couple of localities along the boundary faults, it is thought that these formed through gravity sliding along the fault plane. There is a large block of rotated stratigraphy lying on the fault plane at location 234 (Fig. 7.4). Here, a block >1 km in length has slipped down the fault plane and rotated back into it. A small block of Miocene limestone lies on a low-angle detachment adjacent to the boundary fault behind Antakya (Fig. 7.5) and is also interpreted to have slipped down the fault plane.

#### 7.2.1.2 Northwestern Margin

Large basin-scale normal faults are not as frequent on the northern side of the graben compared to the southwestern margin (Fig. 7.1). None were observed in the northwest but a few were identified near the present-day coastline. Several normal faults were identified near the town of Çevlik. The faults are high angle and strike NE-SW. The outer faults expose Middle Miocene limestone in the footwall with Upper Miocene marl in the hanging wall. The inner faults cut Upper Miocene sediments at the surface. The magnitude of the throw on the fault is unclear but likely to be greater than 100m.

Location	Fault Plane	Foot-wall	Hanging-wall	Other features
74	036°/90 Normal	Eocene	Pliocene	Large amounts of breccia along fault plane and red conglomerate found in places
244	222°/72°N Normal	Upper Cretaceous	Eocene	Large amount of breccia along fault plane
17	354°/64°W Normal	Upper Cretaceous	Serpentinite overlain by Middle Miocene	Dry Quaternary lake on footwall of fault
12	003°56°W Normal	Middle Miocene	Middle Miocene	Breccia and slickenlines along fault plane
49	140°/75°W Normal	Middle Miocene	Quaternary	Fault scarp 10m high, lots of synthetic faults (Fig. 6-4)
20	154°/69°W Normal	Pliocene	Pliocene	Bedding very steep 075°/76°NW and extremely fractured

Table 7-1. Locations where the bounding faults were observed.



Figure 7.3. Photograph overlooking the Antakya sub-basin east of Antakya.

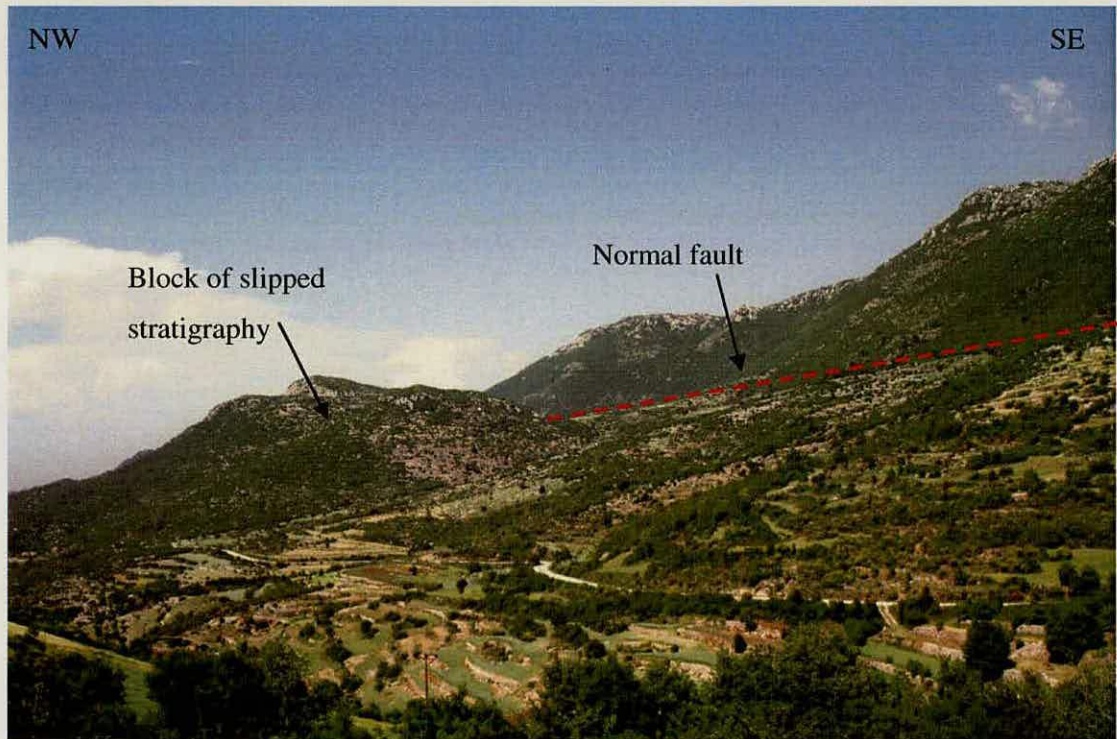


Figure 7.4. View to NE showing large block of stratigraphy lying on a fault plane this is not the hanging wall of the fault, it is thought to have formed through gravity sliding. A graben bounding normal fault has formed escarpment (footwall) on the right.





Figure 7.5. Photograph of Location 45, Miocene gravity slide block behind Antakya

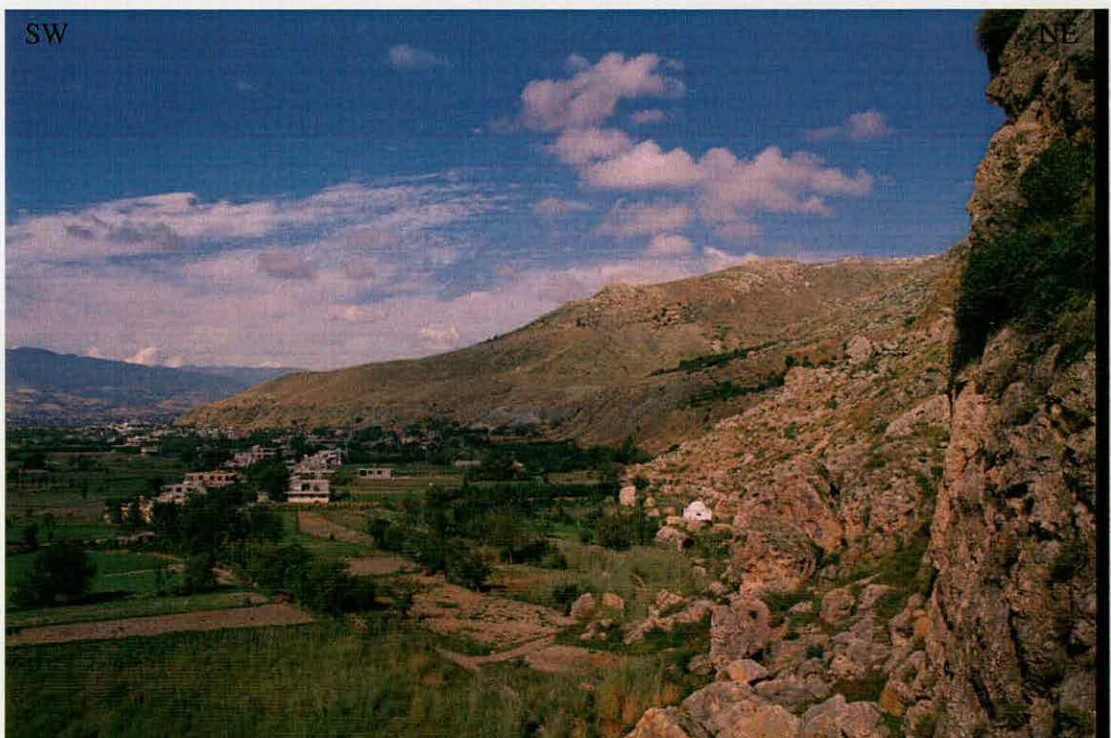


Figure 7.6. Photograph of location 49, graben boundary fault near Tekibasi.

### 7.2.2 Obliquely trending basin-scale faults.

Although the majority of large-scale faults in the graben are parallel or sub-parallel to the graben trend, a major fault strikes E-W through the Harbiye gorge and offsets the formations to either side by tens of metres; this is likely to be a dip-slip/oblique-slip fault (Fig 4.11). Potentially, there may be another large transverse fault striking along the course of the Karaçay. This is hypothesized for a number of reasons. There are numerous faults that strike NW-SE and there is a stratigraphic offset of formations on the northern margin of the graben. Additionally, there is a difference in the height of the graben margin on either side of the Karaçay in the north, and to the south one of the boundary faults appears to terminate at the Karaçay.

### 7.2.3 Map-scale Faults

There are a number of map-scale normal faults that strike at a high angle to the trend of the basin-bounding faults. These appear to be dominantly normal but some have a minor oblique component of motion shown by slickenlines orientations.

Normal faults striking at a high angle to the graben are observed from location 33 (Fig. 7.7); two major normal faults and some synthetic smaller faults are seen to dip into the graben and have caused back-rotation of the fault blocks into the fault planes. Northwards of this location NE-SW trending faults are common along the boundary. These faults appear to be dip-slip in character as they have vertically displace the lithology (Fig. 7.9 of Altinozu pass (3/41)). However, it is not clear how these relate to the timing of the major boundary faults. There are fewer map-scale NE-SW striking faults to the south of location 33. One is observed at location 182, where a normal fault offsets Miocene limestone. There is a zone of fault breccia ~5 m wide along a fault plane measuring  $143^{\circ}/70^{\circ}$  SW.

#### 7.2.3.1 *Sebenoba area*

There is a zone of intense deformation in the area around the village of Sebenoba, in the southeast of the field area (Fig. 7.8). This area is situated between two basin-bounding faults. There are two main populations of fault strike observed, NE-SW (basin parallel) and NW-SE (basin oblique); these together form a series of horst and graben structures where blocks of hard Middle Miocene limestone have been uplifted into the Upper Miocene marl succession. Slickenlines are present on many fault planes. Faults are generally planar, dip-

slip although there are a small number of reverse-slip faults. The fault populations regularly cross-cut one another but there does not seem to be any dominant trend. Granulation seams in coarse sandstone seem to indicate deformation was occurring prior to sediment lithification.



Figure 7.7. Photograph of rotated fault blocks

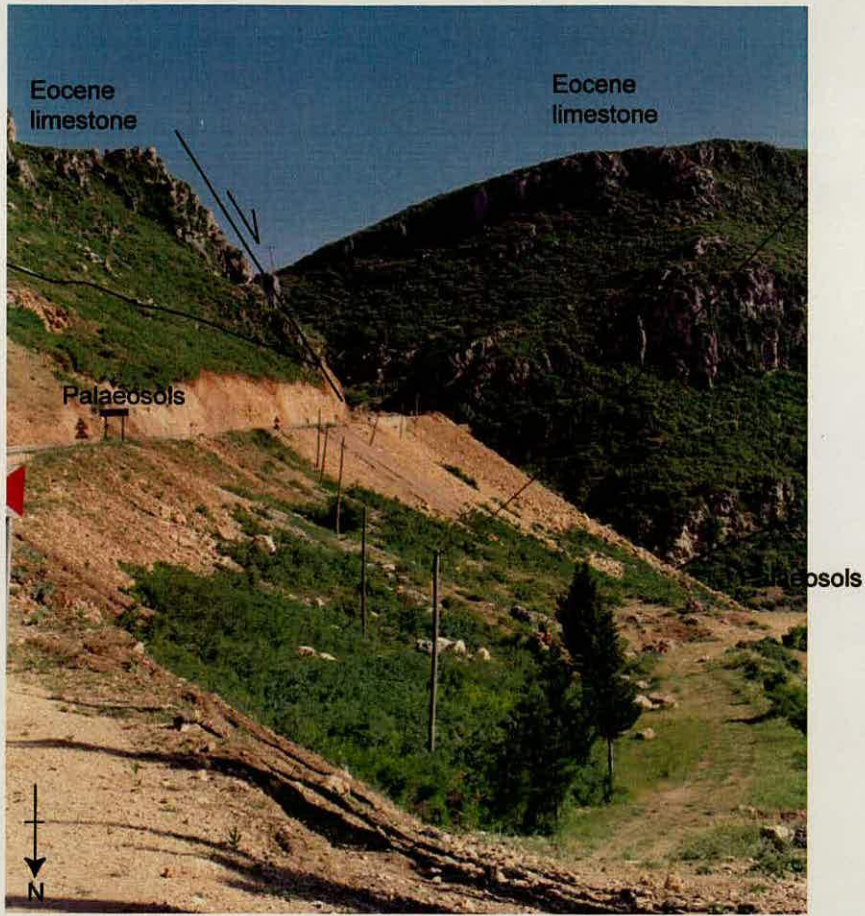


Figure 7.8. Sketch showing faulting across the Altinozu pass

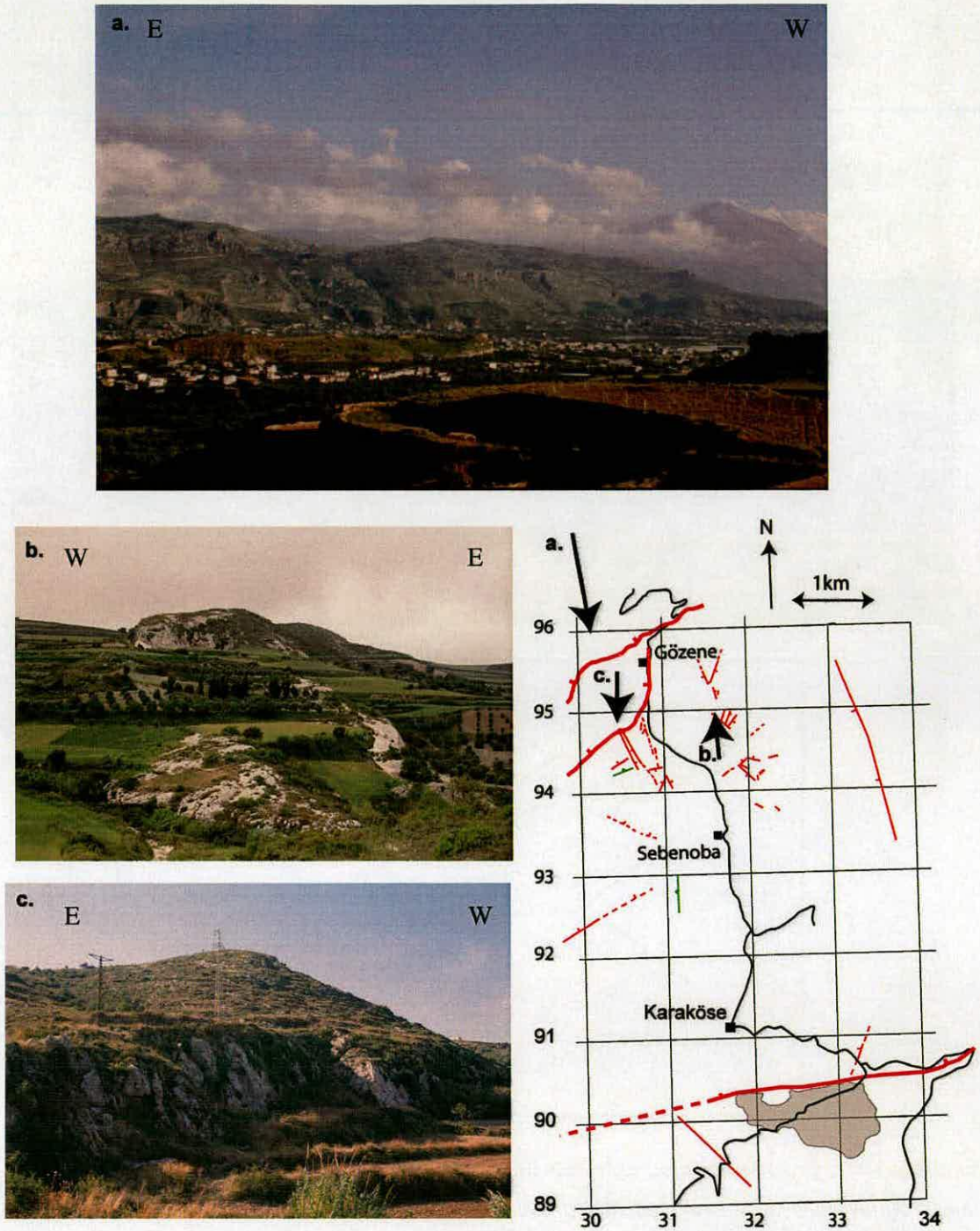


Figure 7.9. Map shows faults around the village of Sebenoba (SE of Samandağ). a) View of the southern graben margin; b) view of limestone horsts, these blocks are bounded by normal faults; c) NE-SW striking fault to south of Gözene, cut by NW-SE striking faults. Arrows on map indicate the location where the photograph was taken and the direction in which it was taken.

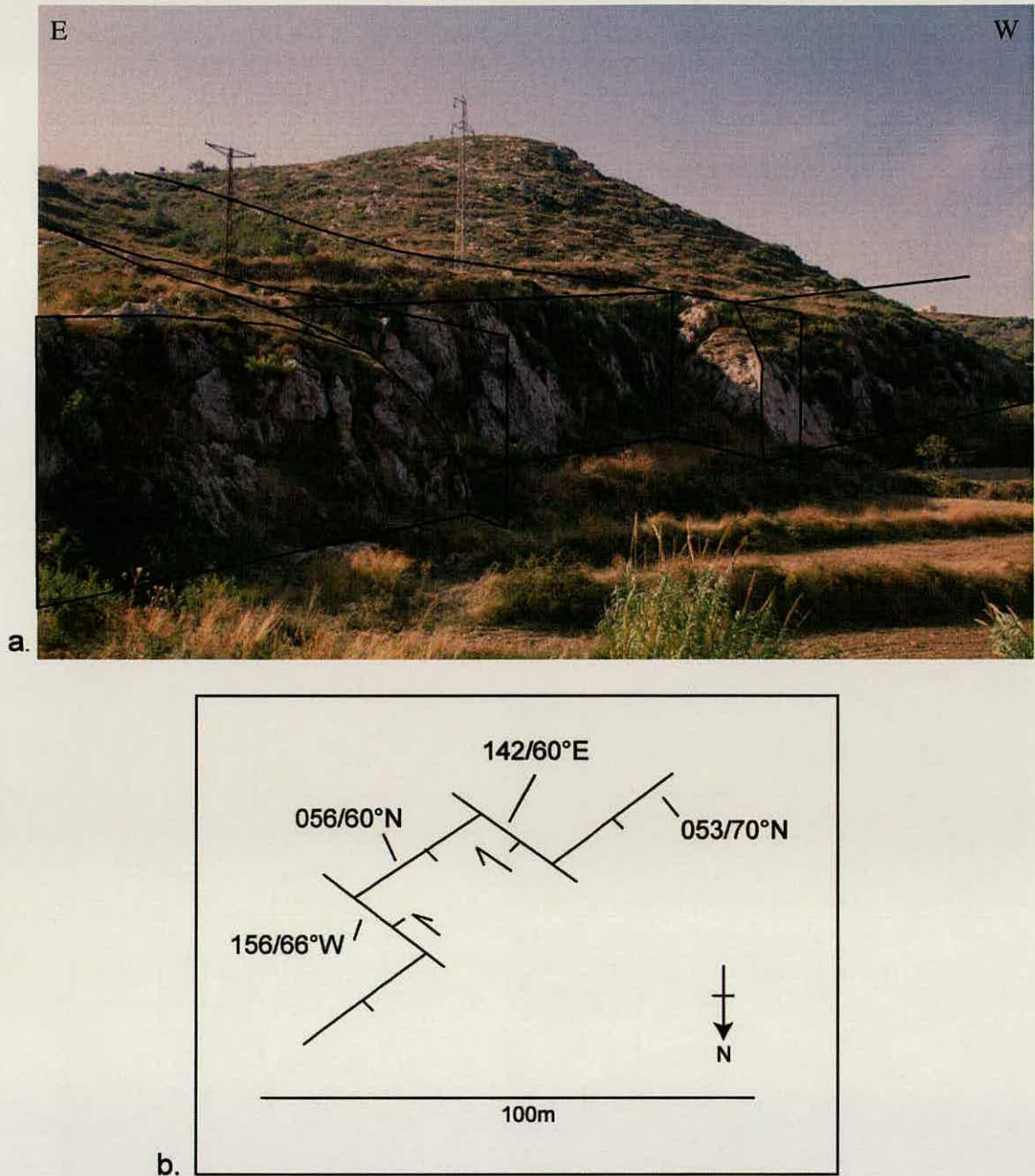


Figure 7.10. a. Enlarged photograph from Fig 7.9, showing boundary fault cross-cut by two later normal faults; b. sketch map giving structural information from the locality.

### 7.2.3.2 Antakya sub-basin

Another zone of map-scale faulting situated between to basin-bounding faults is observed in the north, to the east of the city of Antakya (Fig. 7.3; Fig. 7.11). In this area the faulting has caused back-rotation of the fault-block between the two major faults and the formation of a sub-basin between these major fault planes. Within this area a series of smaller synthetic and antithetic faults have formed mostly parallel to the boundary faults. These are planar dip-slip faults with a throw of some metres and place Eocene limestone against younger



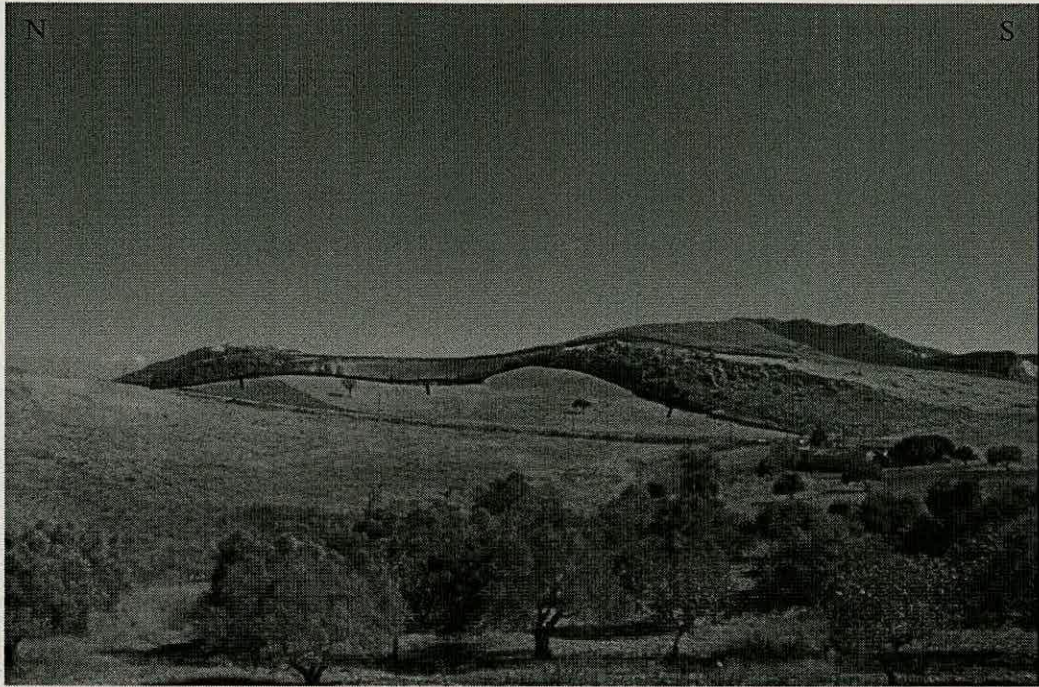


Figure 7.12. Photograph of small normal fault plane from the Antakya Basin, view ENE.

#### 7.2.4 Outcrop-scale faults

Normal faults are very common at outcrop-scale and occur in sediments of all ages. A boundary fault cuts latest Cretaceous to Eocene sediments at a quarry exposure near the village of Dursunlu, down-throwing younger sediments into the graben. The exposed fault plane has been quarried revealing a series of conjugate dip-slip and oblique-slip faults that strike at a high angle to the boundary fault; unfortunately, due to the quarrying the relationship between the boundary fault and smaller faults is unclear (Fig. 7.13). There is a significant amount of scree associated with this fault plane; within the talus are discontinuities indicating that the fault moved in discrete pulses during formation of this talus (see section 7.6 for more detail).



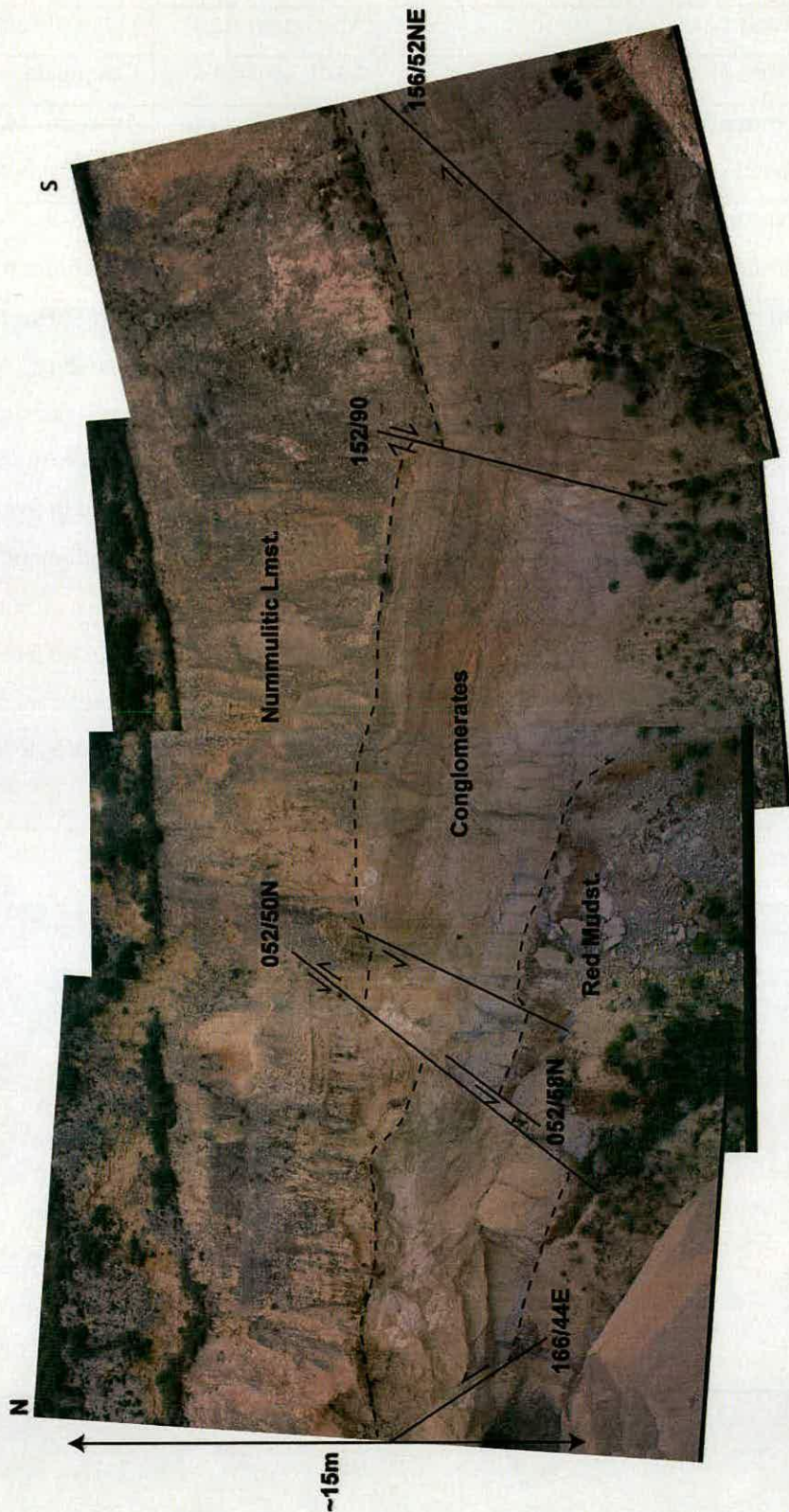


Figure 7.13. Photo-montage of the main boundary fault with a series of cross-cutting faults from the quarry located at Dursunlu. Fault breccia can be seen plastered onto the fault plane.

Location	Fault type	Lithology	Maximum Age	Other observations
439	Normal	Conglomerate	Early Miocene	Conjugate sets
336	Normal (Fig. 6-12)	Conglomerate and chalk	Middle Miocene	Lower to Middle Miocene boundary
36	Normal and strike-slip	Sandstone	Pliocene	Strike-slip faults offset normal faults
82	Normal	Conglomerate and sandstone	Quaternary	Plio-Quaternary boundary. Faulting has rotated clasts to align with the fault plane in the conglomerate
147	Normal	Sandstone	Quaternary	Series of normal faults have offset the Plio-Quaternary boundary by 20cm to 1m. (Fig.6-14)

Table 7-2. Some locations of notable outcrop-scale faults.



Figure 7.14. Photograph of normal faults observed at location 336.



Figure 7.15. Photograph of faults cutting the Plio-Quaternary boundary, one just to left of figure.

### **7.3 *Oblique-slip Faults***

#### **7.3.1 Basin-scale faults**

Major oblique-slip faults are uncommon in the Hatay Graben and one has been identified on the northwestern margin near the village of Yoğunoluk. However, there may be other oblique-slip faults present along the southeastern margin but without the presence of slickenlines this is difficult to confirm. Strike-slip motion along the fault on the NW margin plane has affected the streams that flow over it, resulting in offset streams and beheaded streams (Fig. 7.16); additionally, streams are more incised on the footwall. The direction of offset indicates that this is likely to be a dextral oblique fault with ~100-150m of offset along it. The vertical component of motion along the fault has created a noticeable difference in height between the footwall and hangingwall of 150m.

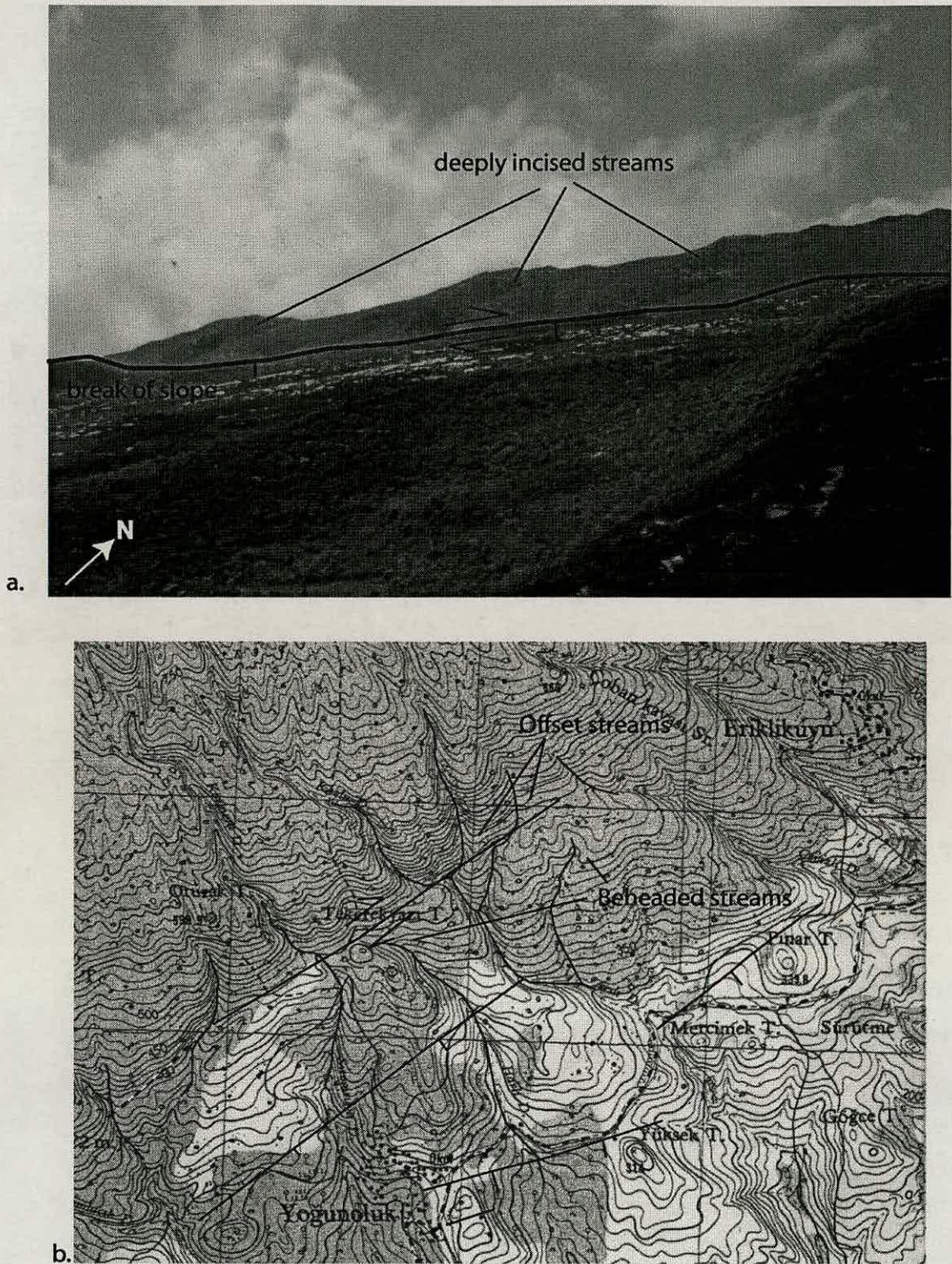


Figure 7.16. A) Photograph of the oblique-slip fault, B) Topographic map (1km squares) showing the location of the fault plane, and the effect of faulting on stream locations.

## **7.4 Strike-slip Map-scale faults**

No major strike-slip faults have been identified in the Hatay Graben and map-scale strike-slip faults are also very uncommon; however, the presence of faults with a strike-slip component of displacement is inferred from significant variations observed in the orientation of bedding in some sediments. In the central axial zone of the graben it is observed that the bedding orientations of Pliocene sandstones are variable over tens of metres. These are unlikely to be a sedimentary feature, since one would expect that the sandstones would have been deposited with the same orientation across the area. Therefore, it is likely that the sediments were faulted after deposition and that anti-clockwise block rotations may have occurred causing the variation in bedding orientation (Fig. 7.17). If sediments have indeed experienced some block rotation this implies that the faults causing the rotations were probably strike-slip in nature. Unfortunately it is impossible to quantify how much displacement has occurred and even the orientation of possible fault planes, although it is possible that the faults strike parallel to the graben margins.



### 7.4.1 Outcrop-scale faults

Strike-slip faults are relatively common at the outcrop-scale especially in sediments of Pliocene age. Good examples of strike-slip related flower structures were observed at location 41 (40401750). A small-scale positive flower structure was observed (Fig. 7.18); the main fault measured  $140^{\circ}/90^{\circ}$  and splays upwards into three faults. The sediments between these faults have been rotated and compressed. Another vertical shear zone was observed (Fig. 7.19) at the same location; the geometry is not so clear in this instance but the sediments on either side have been deformed and do not correlate across the fault plane. Normal, reverse and oblique-slip faults were recorded at this location as well as strike-slip faults.



Figure 7.18. Photograph of the positive flower structure.

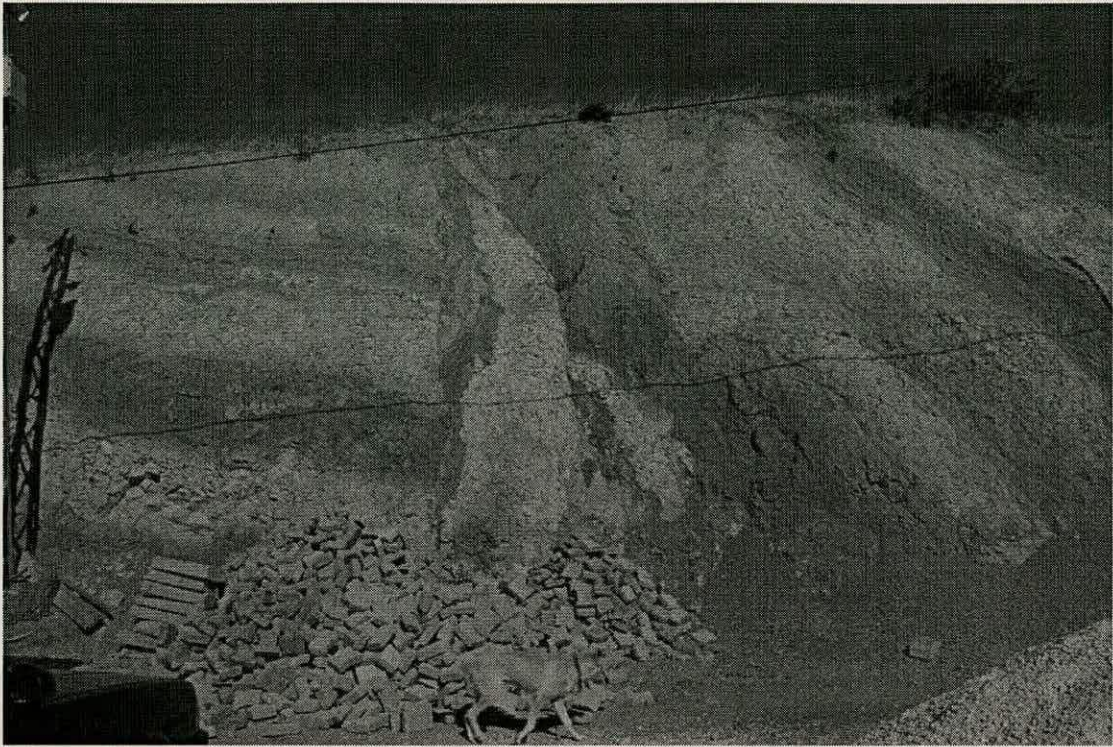


Figure 7.19. Photograph of the vertical shear zone.

Another nice example of a strike-slip fault was observed near the village of Güneysöğüt where fault cuts Pliocene marl and sandstone. The fault zone ( $117^{\circ}/90^{\circ}$ ) is  $\sim 40$  cm wide and braided. The horizontal offset could not be calculated but there was a vertical offset of  $\sim 2$  m.

## 7.5 Compressional Tectonics

### 7.5.1 Thrust faults

Thrust faults are very uncommon within the Hatay Graben. They are always small (maximum displacement  $< 10$  m) and occur along with other faults (i.e. extensional or transtensional). Small faults were observed in the Sebenoba area associated with normal faults and at location 41 associated with strike-slip faults.

A thrust fault was observed in Quaternary conglomerate at location 37. The fault plane ( $160^{\circ}/32^{\circ}W$ ) has caused two sand horizons to become displaced; however, these were not fractured indicating that the sediment was still soft when the faulting occurred (Fig 7.20).



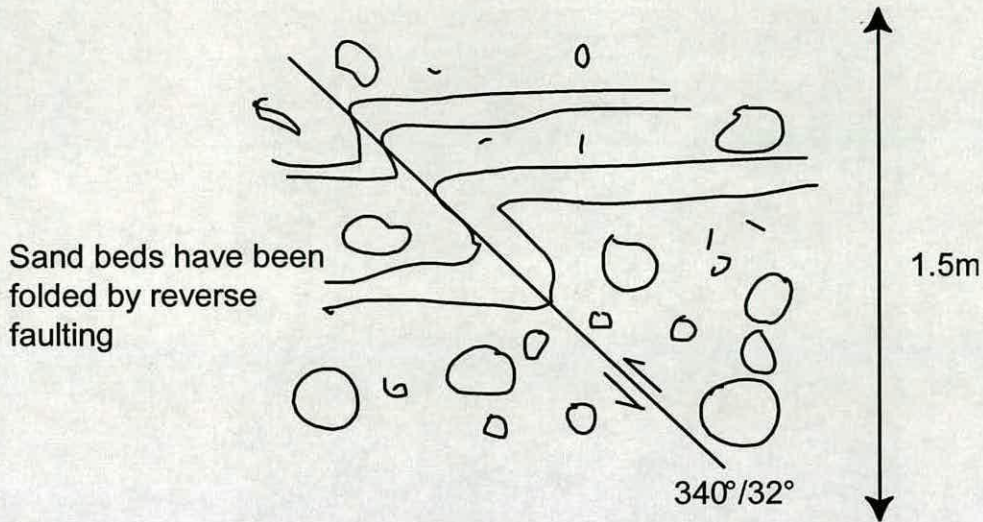


Figure 7.20. Field sketch showing the reverse structure observed at location 37.

### 7.5.2 Folding

There is little evidence of compressional deformation in the Hatay Graben. Folding was generally only observed in Eocene and older rocks. The Eocene strata are the most extensively folded; to the east of Antakya (at location 286, Fig. 7.21) medium-bedded calcarenites have been folded into disharmonic, asymmetric, gentle folds. The dip of the bedding in this area is nearly vertical in places. However, to the north, around the towns of Belen and Kırıkhan, the Eocene strata are more deformed. Folding is highly variable, but vergence was always observed as being towards the NW or W. Fold geometry ranges from open folds to tight angular folds; the axial planes are not parallel. The wavelengths of these folds are <5m.

A north-vergent monocline was observed in Upper Cretaceous limestones at location 247 (Fig.7.22).

Folding was not generally observed in sediments younger than the Eocene. Where folding is present the folds are associated with normal faulting, i.e. drag folds, as was observed at location 432 in Pliocene sediments in the graben axis.



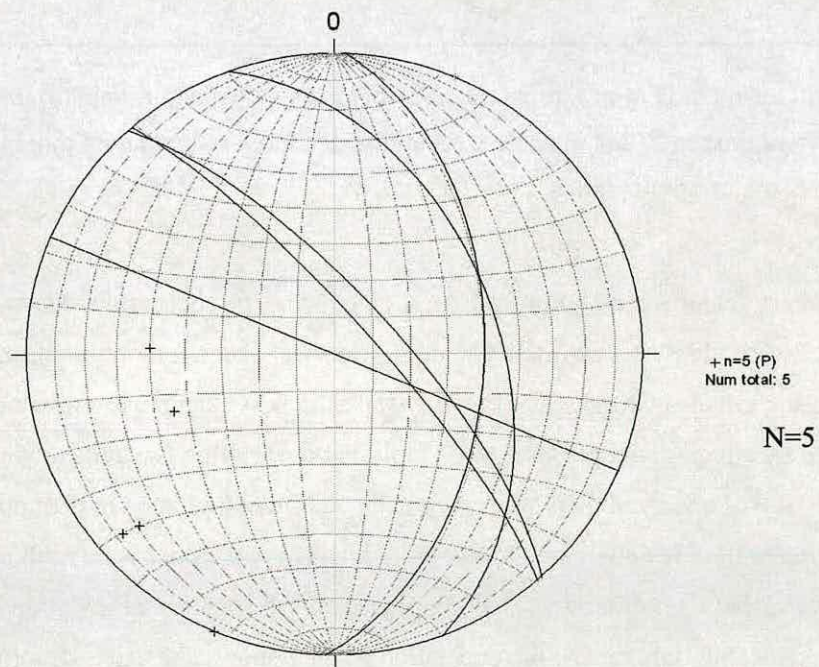
Figure 7.21 Photograph of folding in the Eocene sediments

#### 7.5.2.1 *Map-scale Folds*

Only one map-scale fold was observed in the field area, this was to the south of the village of Döver, at location 138. This is an anti-clockwise asymmetric, west-vergent syncline, which has folded the ophiolite-cover boundary.



Figure 7.22. Photograph of the monocline observed at location 247.



Equal area projection, lower hemisphere

Figure 7.23. Stereonet showing the bedding planes, the poles to those planes and position of the fold axis of the syncline observed at location 138.

## 7.6 Timing of Faulting

Tectonic-sedimentary structures can be used to determine the relative timing of faulting.

Key features are growth faults, sediment fanning, intra-formational faults and phases of fault motion as inferred from fault-derived talus.

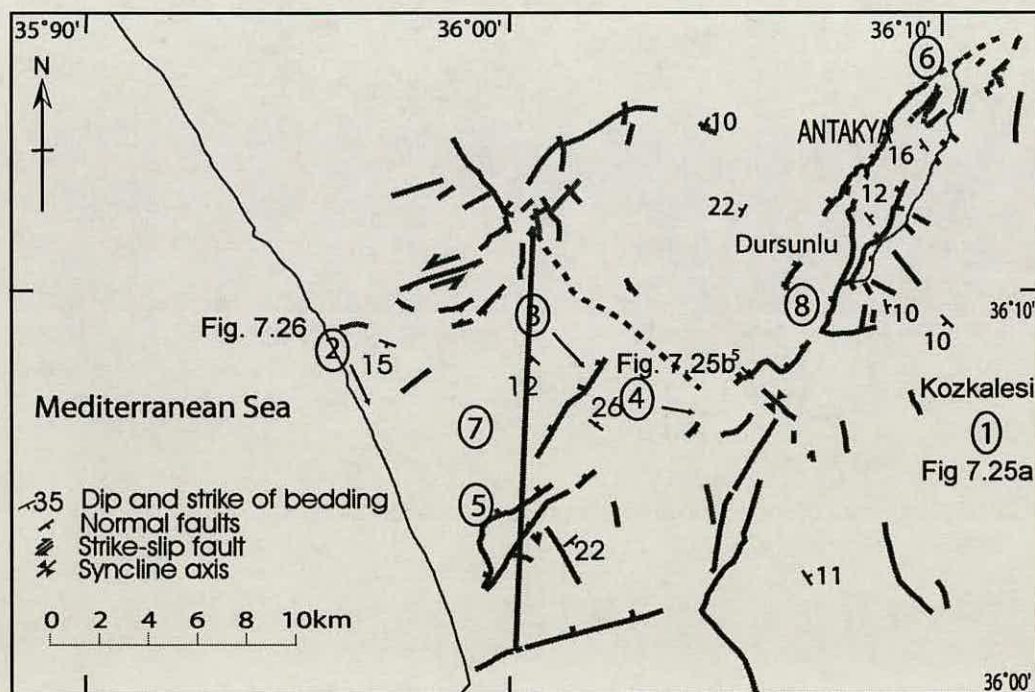


Figure 7.24. Outline fault map with the position of localities (circled numbers) referred to in the text. Arrows next to 2, 3, 4 indicate direction of sediment fanning note that in all cases this is towards major normal faults.

Syn-sedimentary features are absent from the Lower Miocene succession. However, three growth faults were identified within the Middle Miocene succession on the SE margin of the graben, near the village of Kozkalesi (Fig. 7.24/1). The best example are where limestones are displaced by a high-angle planar normal fault that dips northwestwards towards the axis of the basin. It was observed that there is a greater sediment thickness in the uppermost beds on the hanging-wall block compared to the footwall. These are cut by the fault plane (Fig 7.25) indicating that fault motion was taking place and creating accommodation space on the downthrown side, but only during the deposition of the upper beds. An undeformed horizon overlies this fault and is not cut by it showing that fault motion had ceased by the time this bed was deposited.

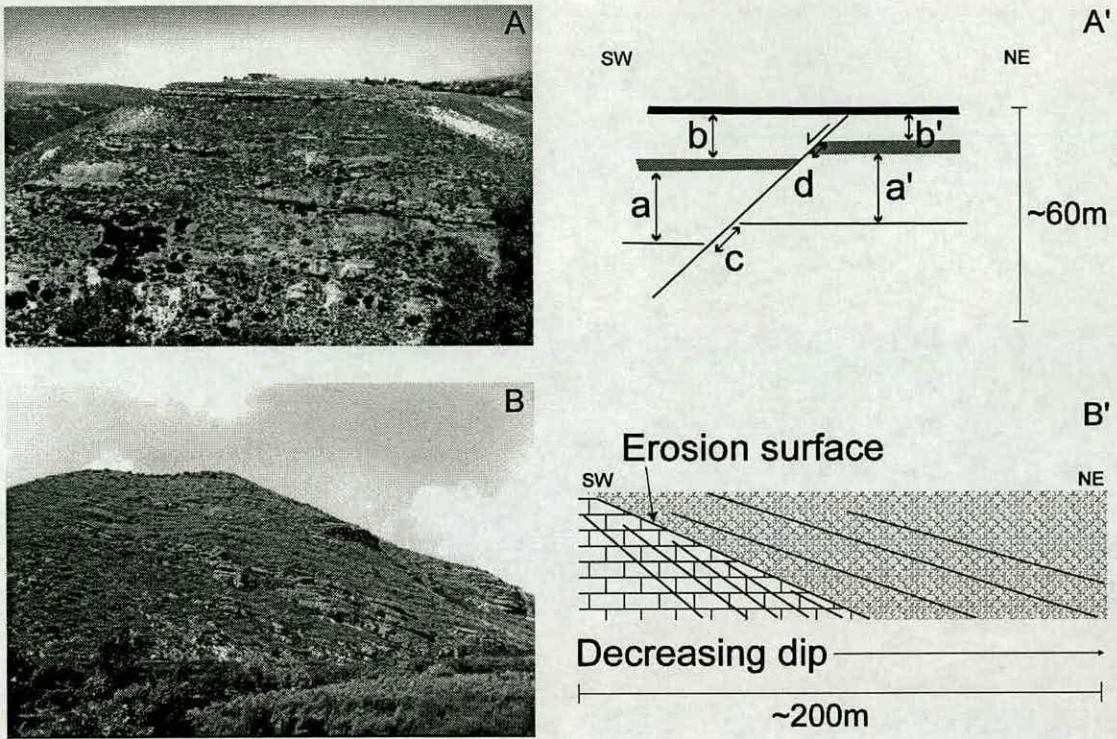


Figure 7.25. A) Photograph of a growth fault observed near the village of Kozkalesi. A') Sketch of the geometry of the fault; note that the lower interval (a and a') are displaced by the fault but are the same thickness on the footwall and hangingwall blocks. Upwards interval b has a greater thickness than b', indicating fault movement during deposition. Additionally the throw on the fault increases downwards. The upper package of strata is not cut by the fault; therefore, the fault began moving after time a, and was moving during the deposition of b yet had ceased motion when the upper layer was deposited, all within the Middle Miocene. B) Photograph showing the Middle Miocene fanning sediments exposed along the River Asi; B') Sketch of the fanning sediments; note that the dip of the bedding decreases up section. In the middle of the section is an intraformational unconformity; below are fine limestones (mudstone) above are dominantly bioclastic calcirudites with some conglomerate horizons. The surface is bored (possibly by *Lithophaga*) indicating that it was exposed for some time. There is a major normal fault to the east of this location.

Another indication of fault motion during the Middle Miocene can be observed in a cliff section on the present coast of the NW basin margin of the graben (Fig. 7.26). An upper Middle Miocene section is exposed above an unconformity with serpentinite below. The beds at the base of the exposure dip more steeply ( $35^\circ$ ) those at the top ( $25^\circ$ ) causing the sediment to 'fan' to the southeast (Fig. 7.24/2). This morphology is likely to be the result of tilting of the basin floor during sediment deposition.



Figure 7.26. Photograph showing fanning sediments observed in a coastal section.

Sediment fanning was also observed within Upper Miocene sediments at two localities: one on the basin axis (Fig. 7.24/3) and one on the southeast margin between two basin-bounding faults (Fig. 7.24/4). At the basin axis locality, the fanning (observed in a valley) is revealed by the difference in the angle of dip between the upper and lower beds ( $\sim 10^\circ$ ) exposed. The sediment fanning at location 4 (Figs. 7.24/4 and 7.25), along the Asi Nehir, is more pronounced. The lower beds are sub-vertical and the dip gradually decreases up section to  $\sim 30^\circ$ ; additionally, within the sequence there is an angular discordance between two different lithologies.

Pliocene sandstones are highly deformed adjacent to major basin-bounding faults, dipping up to  $90^\circ$  locally (Fig. 7.24/5, Table 7-1), it is not entirely clear what has caused this deformation but there are large numbers of faults suggesting that these sediments are part of the deformation zone. A steeply dipping exposure of Plio-Quaternary mudstone, sandstone and conglomerate was observed in a road cutting close to the innermost of the graben-bounding faults near the village of Narlica (Fig. 7.24/6). The bedding dips to the northeast and there are a number of angular discordances within the sequence, indicating that fault motion was probably occurring during sedimentation.

A normal fault was observed at location 418 near Samandağ. The fault strikes  $173^{\circ}/79^{\circ}\text{SW}$ , the displacement is small (tens of centimetres) and drag on the fault plane has caused slight folding of the sediments on the hanging wall (Fig.7.24/7 and 7.27). The displacement on the fault plane decreases upwards and after a couple of metres sediments are unaffected by the fault indicating the fault motion was taking place during sedimentation. Also there is evidence of slumping within the Pliocene succession at this location.

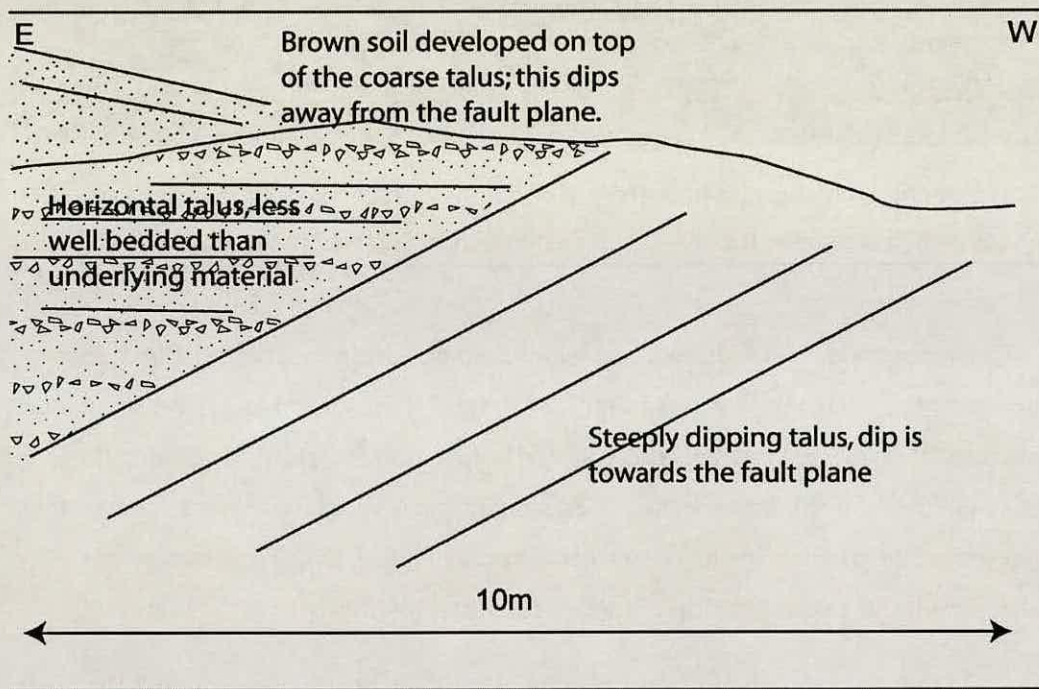
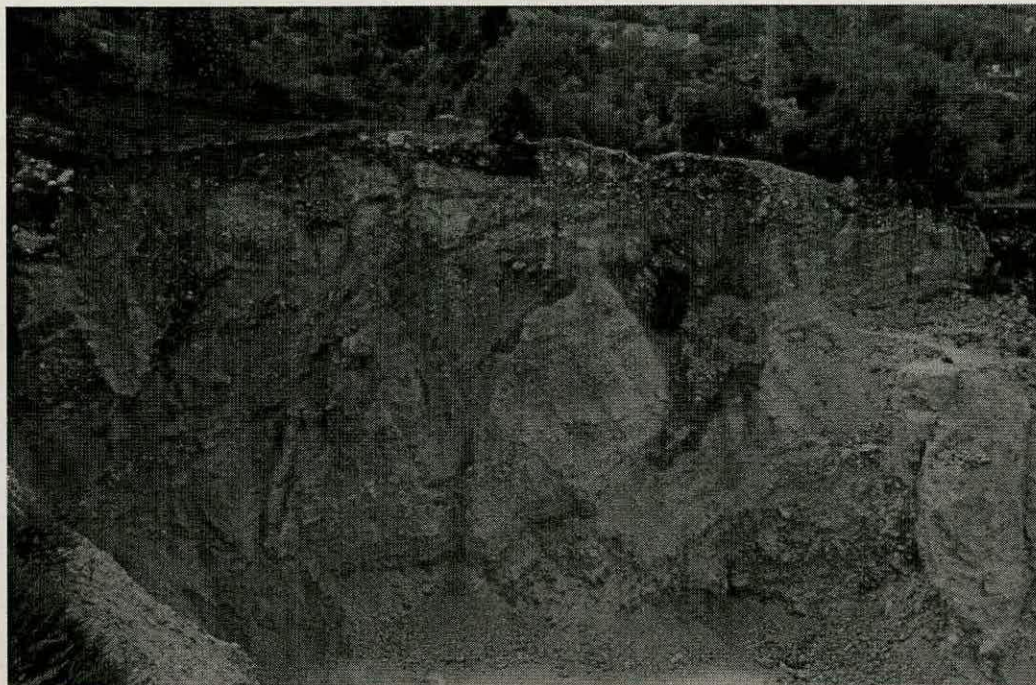


Figure 7.27. Photograph showing Pliocene growth fault. Lighter coloured bed at head height of figure thickens to the left of the picture on the hanging wall of the normal fault.

Within a Quaternary talus cone adjacent to a major fault bounding the southeast margin of the graben (near the village of Dursunlu; Fig. 7.24/8, see 7.2.4), several angular discordances were observed. It is inferred that the talus was derived from the adjacent exposed fault scarp; this fault then moved, rotating the pre-existing talus and producing more material that was deposited on top of the original along a discontinuity (Fig. 7.28). This process was repeated several times creating multiple small-scale discontinuities within the talus fan.

Only occasional faults were observed within the Quaternary deposits, probably because of the difficulty of recognition in such coarse, poorly-consolidated sediments. However, rare

faults were identified and locally the boundary between Pliocene sandstone and Quaternary conglomerate is faulted indicating that fault activity has taken place during the Quaternary.



Figur

Fig. 7.28. Photograph and fieldsketch showing the change in dip of the fault talus adjacent to the boundary fault.



The present elevation of the Messinian evaporites (Fig. 7.29) indicates that there has been significant post-Messinian fault uplift. The evaporites on the basin margin are now 190m higher in altitude than similar deposits near the basin axis, if it is assumed that all these evaporites formed in a single depocentre near the then sea-level. This would suggest that after the Messinian the graben underwent a phase of strong vertical fault movement. Using this data we can estimate the minimum rate of uplift since the Messinian of  $\sim 0.03 \text{ mmyr}^{-1}$ .

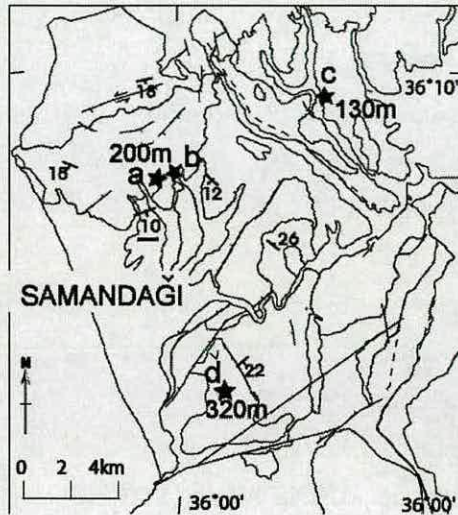


Figure 7.29. Map showing the location and altitude of Messinian evaporite deposits.

Cross-cutting relationships can be a reliable method for evaluating timing of deformation. Cross-cutting faults were observed in the field area. Two examples already mentioned are where NW-SE faults are cut by NW-SE faults. However, NW-SE faults cutting NE-SW faults were also observed. NW-SE faults crosscutting NE-SW were observed nine times, while NE-SW faults crosscutting NE-SW faults were observed seven times (Table 7-3).

Two sets of slickenlines were observed on a few fault planes (Fig. 7.30). Of these, one set of lineations on a fault plane is commonly orientated at a high angle (dip-slip) and the other at a low angle (oblique or strike-slip). However, it was not possible to determine which set of the two slickenlines was the younger, based on only a small number of measurements ( $n=13$ ) and also because of the inherent difficulty of correctly identifying the sequence of formation. In addition, Cashman and Ellis (1994) showed that variable orientations of slip data on fault planes are not necessarily the result of changing stress fields but can be explained by the

interaction of crustal scale faults in response to nearby earthquakes, as a result of highly transient local stresses in a constant regional stress field.

Location	Grid Ref.	Cross-cutting	Older	Younger	Fault plane
16	3560/0445	Fault planes	Normal 183/76SE	120/58SW(strike-slip)	N/A
20	3020/9620	Slickenlines	Dip-slip 46N	14N	150/74W
60	3560/0490	Fault planes	159/56NE	178/38W	
87	33760/96440	Slickenlines	326/24 (sinistral)	154/6 (sinistral)	154/90
87	33760/96440	Slickenlines	120/46	218/60	140/60
117	30505/94632	Fault planes	053/70N (normal)	142/60E and 156/66W	
146	38414/08826	Slickenlines	238/20	274/40	020/42W
146	38414/08826	Slickenlines	213/33	270/55	178/55W
146	38414/08826	Slickenlines	260/40	232/38	174/40W
146	38414/08826	Fault planes	151/64SW (normal)	164/90 (strike-slip)	
180	32902/08285	Fault planes	356/77NE (oblique)	046/70SE (normal)	
196	70048/89120	Fault planes	050/80SE	146/72SW	
200	31740/94762	Fault planes	023/78SE	141/73SW	
232	34888/91547	Fault planes	020/50NW and 210/68SE	076/52SE	
266	47285/10949	Fault planes	031/90NW	152/90NE	
267	47362/11012	Fault planes	031/90NW	019/77NW	
268	47498/11049	Fault planes	074/57NW	135/64SW	
281	51447/37454	Calcite vein	140/90	014/20NW	
282	51141/37099	Fault planes	026/56SE (normal oblique)	060/90 (normal)	
320	45778/05998	Calcite vein	154/70sw	160/68NW	
Q		Fault planes	108/62S	111/12SE	

Table 7-3 Cross-cutting relations data.



Figure 7.30. Photograph showing two sets of slickenlines on the same fault plane.

The syn-sedimentary features described above suggest that significant faulting related to basin formation began in the Middle Miocene, resulting, for example, in the observed growth faults.

The sediment fanning could be the result of three different processes: folding; downwarping or normal faulting. If observed fanning and intraformational angular surfaces were the result of long wavelength folding that resulted in the tilting of the basin floor, it would be expected that sediment fanning would be observed on both sides of the graben (Figure 7.31), i.e. on both limbs of the fold assuming the width of the graben is approximately the wavelength of the fold. However, field evidence does not support this hypothesis as no folds have been

observed in the Middle Miocene succession and only very rare reverse faults yet there are many normal faults suggesting an extensional regime. In addition, the fanning sediments are local features in the Middle Miocene limestones and the direction in which the fanning is variable. If folding caused the sediment fanning and unconformities, it would be expected that these would be more widespread and would have a coherent direction of fanning on both sides of the graben. Although sediment fanning is observed on both graben margins in the southeast the direction in which the fans are orientated is variable. This all suggests that folding is not the cause of the observed features.

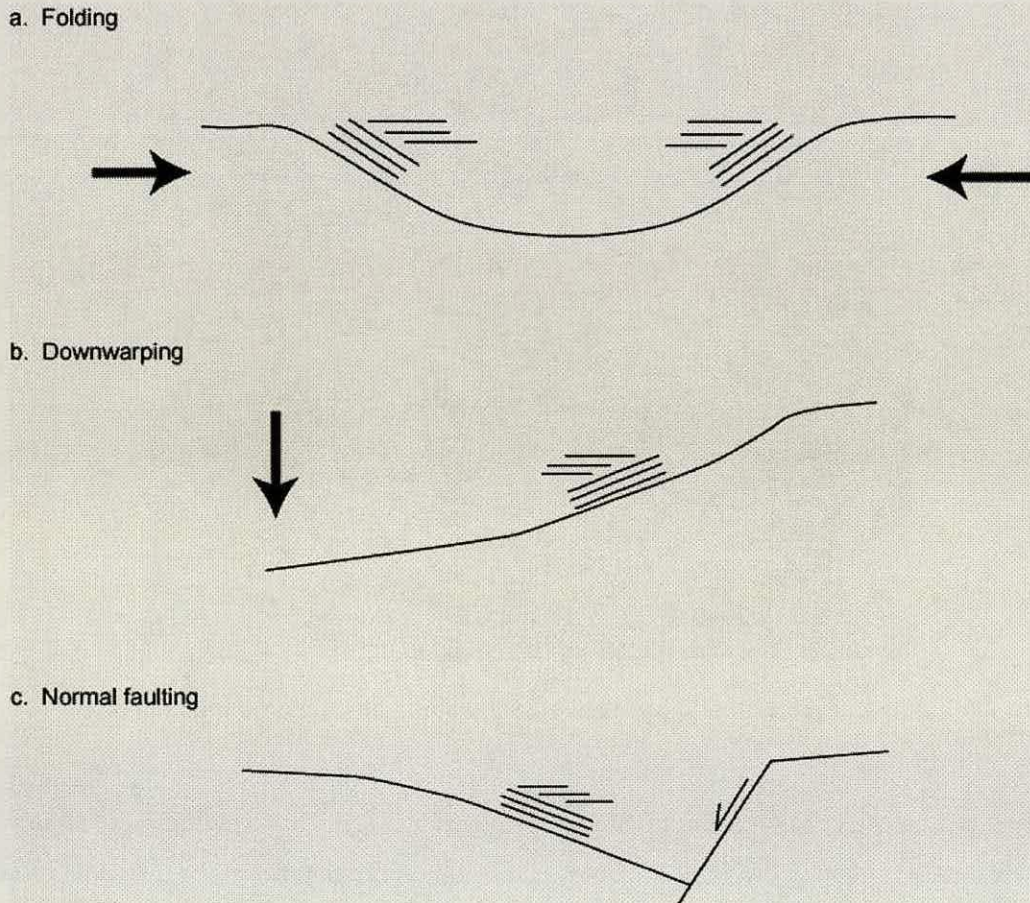


Figure 7.31. Schematic diagrams showing how: a) folding; b) down-warping and c) normal faulting could result in the formation of unconformities and sediment fanning.

Another cause of the sedimentary features observed could be down-warping of the area caused by loading of the lithosphere. Although the area would be experiencing some flexural loading due to continental collision to the north during the Miocene (Robertson *et al.* 2004), if sediment fanning was the result of this deformation only, sediment fans should all

fan to the NW (Figure 7.31). This is not what is observed in the field where fans are orientated to the SW and NE.

As the field evidence argues against folding or down-warping being the cause of the observed features it is therefore proposed that the sediment fans are the result of normal faulting tilting the basin floor and increasing accommodation space (Figure 7.31). This is corroborated by the local nature of the fans and the variable orientations relating to the fact that motion on different faults resulted in different motion of the basin floor. Thus, during the late Middle Miocene and Late Miocene significant motion on faults resulted in tilting of bedding and the creation of further accommodation space (thus resulting in the local sediment fanning).

There are no syn-sedimentary features present in the Lower Miocene sediments; although there is an unconformity between the Lower and Middle Miocene sediments this is generally very localised and often not that significant. So although this could be fault related it may well also be the result of inherited palaeotopography and thus cannot conclusively be used as evidence for fault motion at this time.

## 7.7 Fault Orientation Data

In total, over 850 measurements were made on fault planes in the field area during three field seasons. These include strike-dip and displacement measurements of the fault plane and the orientation of slickenlines present on the plane. The majority of the faults either trend parallel to the graben margins, or at a high angle to the graben (i.e. NW-SE). Normal, oblique, sinistral and dextral strike-slip faults are common, with reverse faults being rare.

When all the data are considered together, the majority of the faults strike between 60° and 320° and it is difficult to differentiate any other trends from the mass of data.

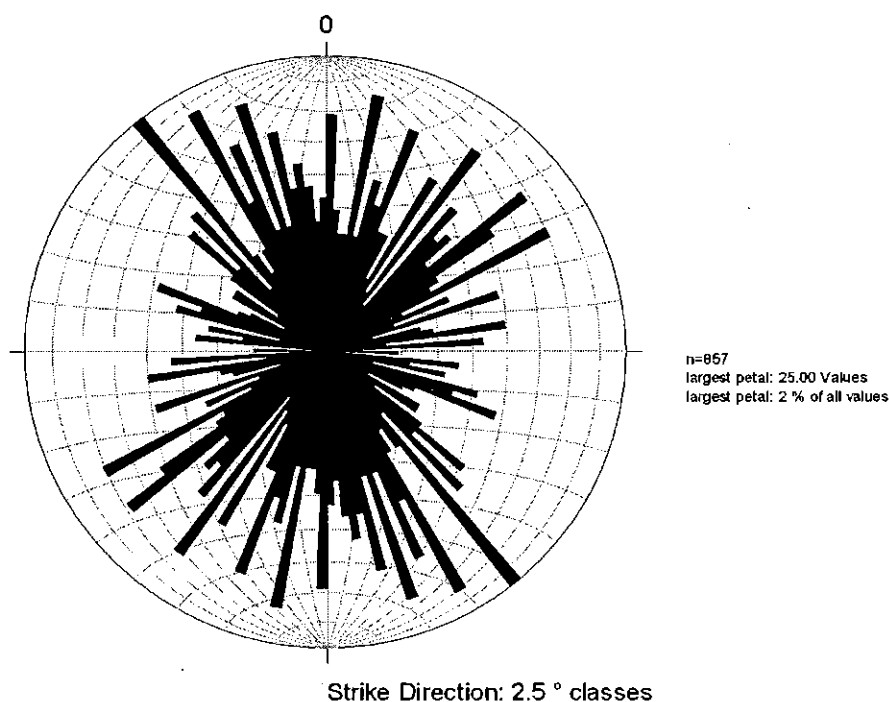


Figure 7.32. Rose diagram showing the strike of all fault planes measured in the field area.

The majority of the faults have an angle of dip greater than 50° (Fig. 7.33) and there is no apparent relationship between the fault orientation and the angle of dip. When the strike of the fault is compared to the rake of lineations on the fault plane (Fig. 7.34), there also does not seem to be any obvious trend. The rakes of the lineations are highly variable regardless of the dip of the fault plane implying that the faults do not satisfy Coulomb theory, which predicts an inverse relationship between the magnitude of the rake and dip of the fault plane (Reches & Dieterich 1983).

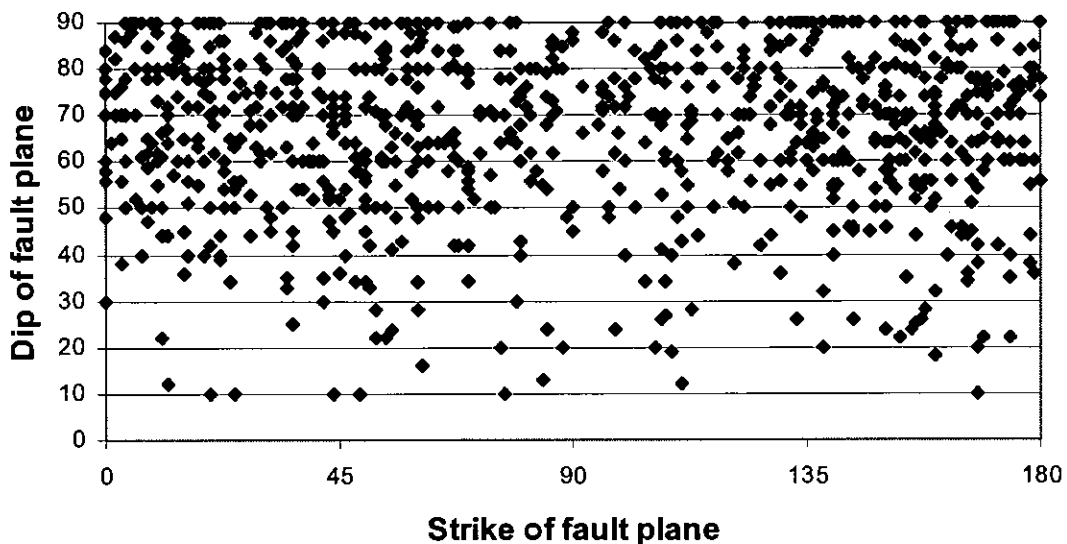


Figure 7.33. Graph showing strike of fault against the dip, for all faults measured.

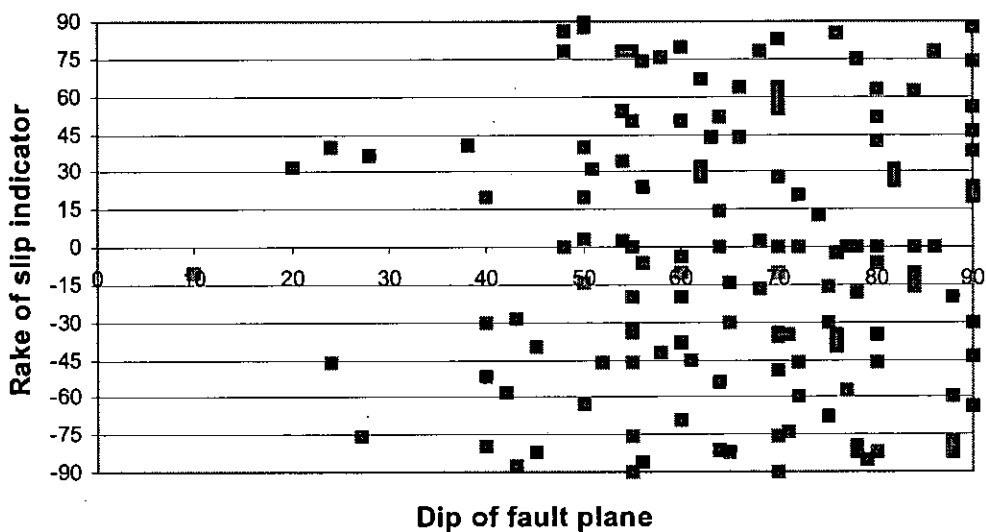


Figure 7.34. Graph showing the dip of fault plane against the rake of lineations present.

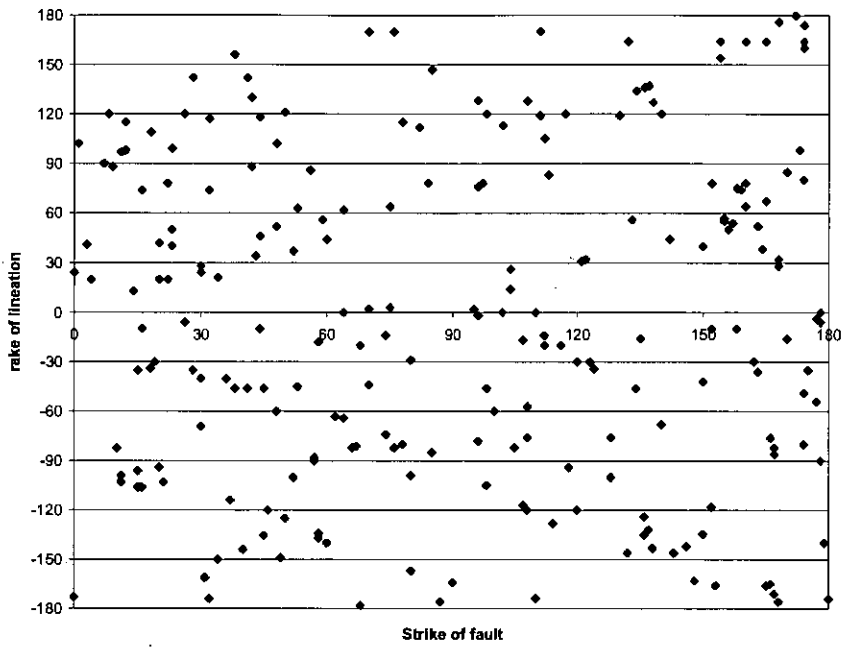


Figure 7.35. Graph showing the strike of the fault against the rake of lineations for all faults measured with lineations.

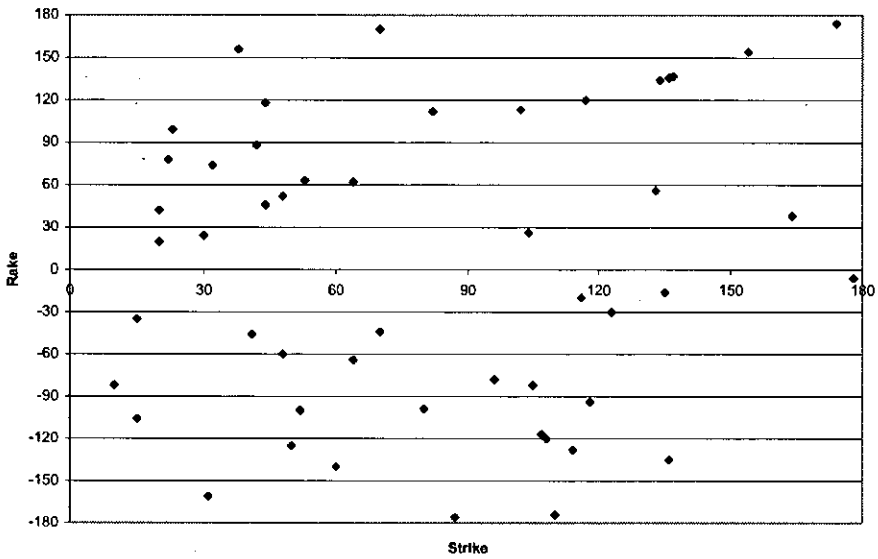


Figure 7.36. Graph showing the strike of the fault against the rake of lineations for faults with a dip of  $>80^\circ$



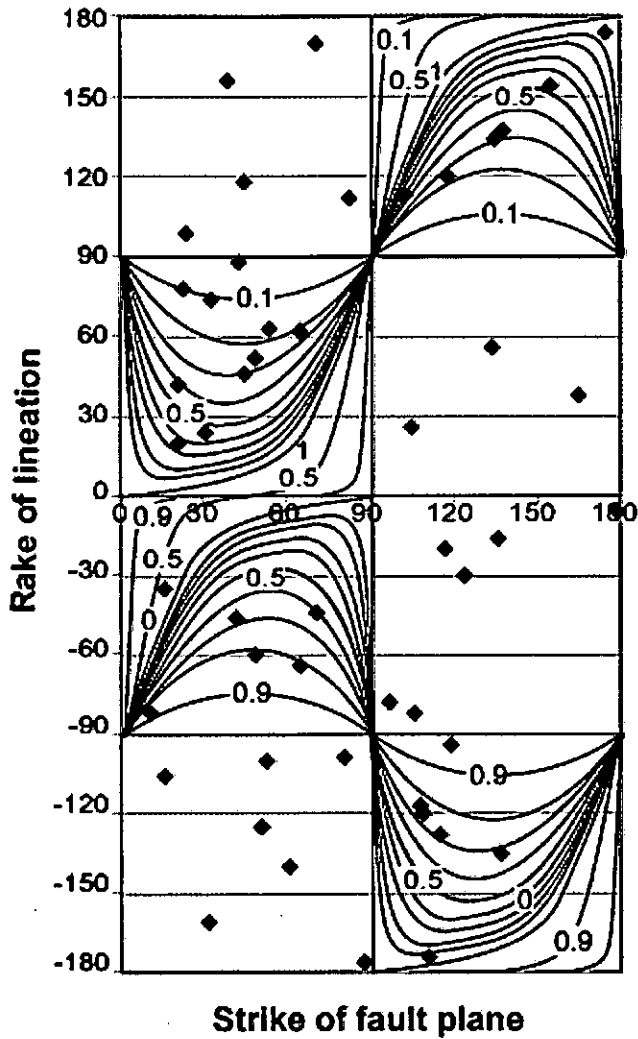


Figure 7.37. Fig. 7.35 with a superimposed Breddin's graph for tectonic regimes for planes of dip  $> 80^\circ$ , showing the relationship calculated by Célérier & Séranne (2001).

When the strike of fault plane is compared to the rake, there is great scatter in the data, probably due to the different scales and types of faults being compared. However, when only faults with dip  $> 80^\circ$ , generally normal faults, are considered there is still a wide range of rake directions recorded. When a Breddin's graph is overlaid to help infer the tectonic regime of these data there is no correspondance to the overlay suggesting that the strain field in the Hatay Graben is 3D as Breddin's graphs only work for 2D strain and one axis of the principle stress direction must be vertical.

To aid interpretation, the data were then divided into sub-groups. Firstly, in order to assess any spatial variation in fault population, the data were divided geographically into structural domains (Fig. 7.35). Six domains were defined for the Hatay Graben based on the graben margins and graben floor; additionally, data were collected from the Belen and Kırıkhan areas for comparison; these areas form a further two domains.

Secondly, the faults were considered by the age of the fault. The precise age of the fault is difficult to determine so the divisions were made on the perceived *maximum* age of the fault. This was determined by cross-cutting relationships, syn-depositional structures and the age of displaced units in which the structure occurs and the age of the sedimentary unit in which the fault was recorded. For example: a fault measured in a Middle Miocene unit is Middle Miocene or younger in age, we therefore placed this fault in the Middle Miocene age category; a fault cutting the Middle-Late Miocene boundary is younger than the Late Miocene and was therefore placed in the Late Miocene category.

7.7.1.1 Spatial distribution of faults

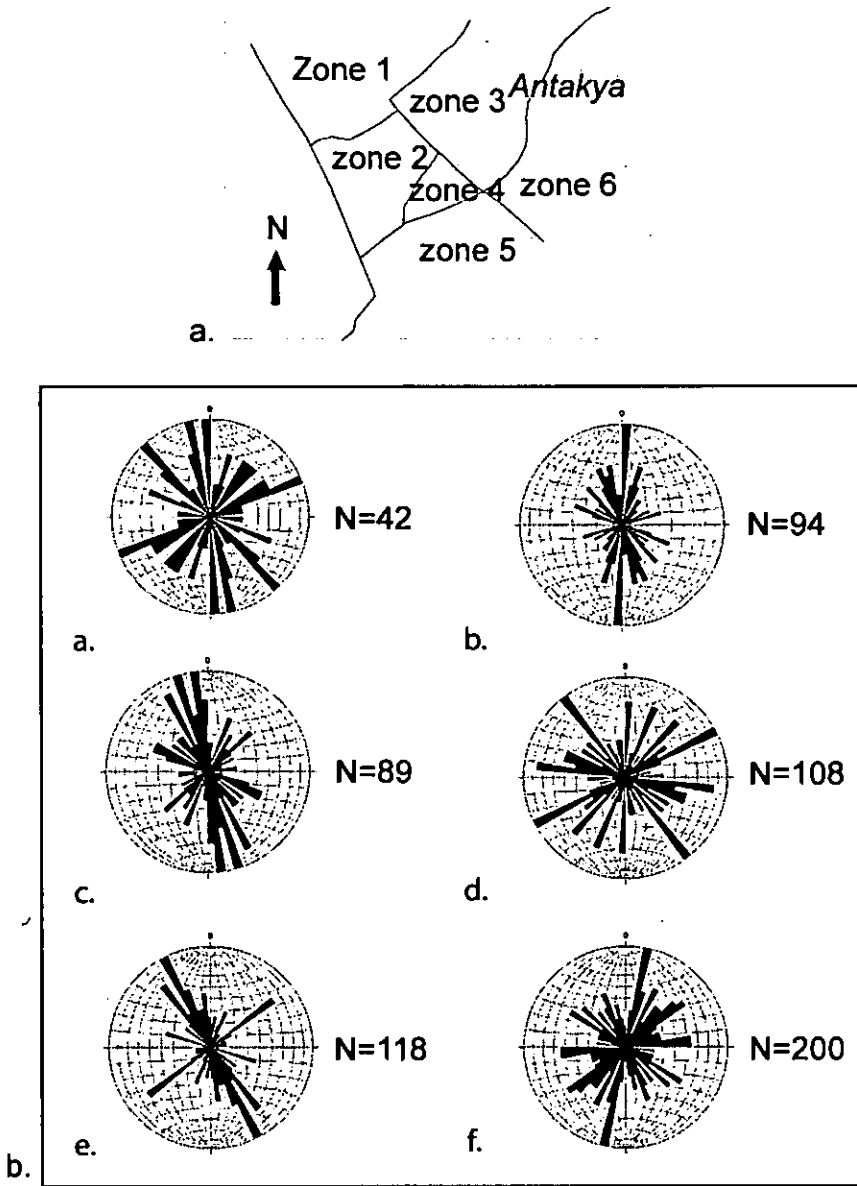


Figure 7.38. a) Sketch showing zones used to analyse spatial fault data, b) Rose diagrams showing total faults measured for each zone; a. Zone 1; b, Zone2; c, Zone 3; d, Zone 4; e, Zone 5; f, Zone 7.

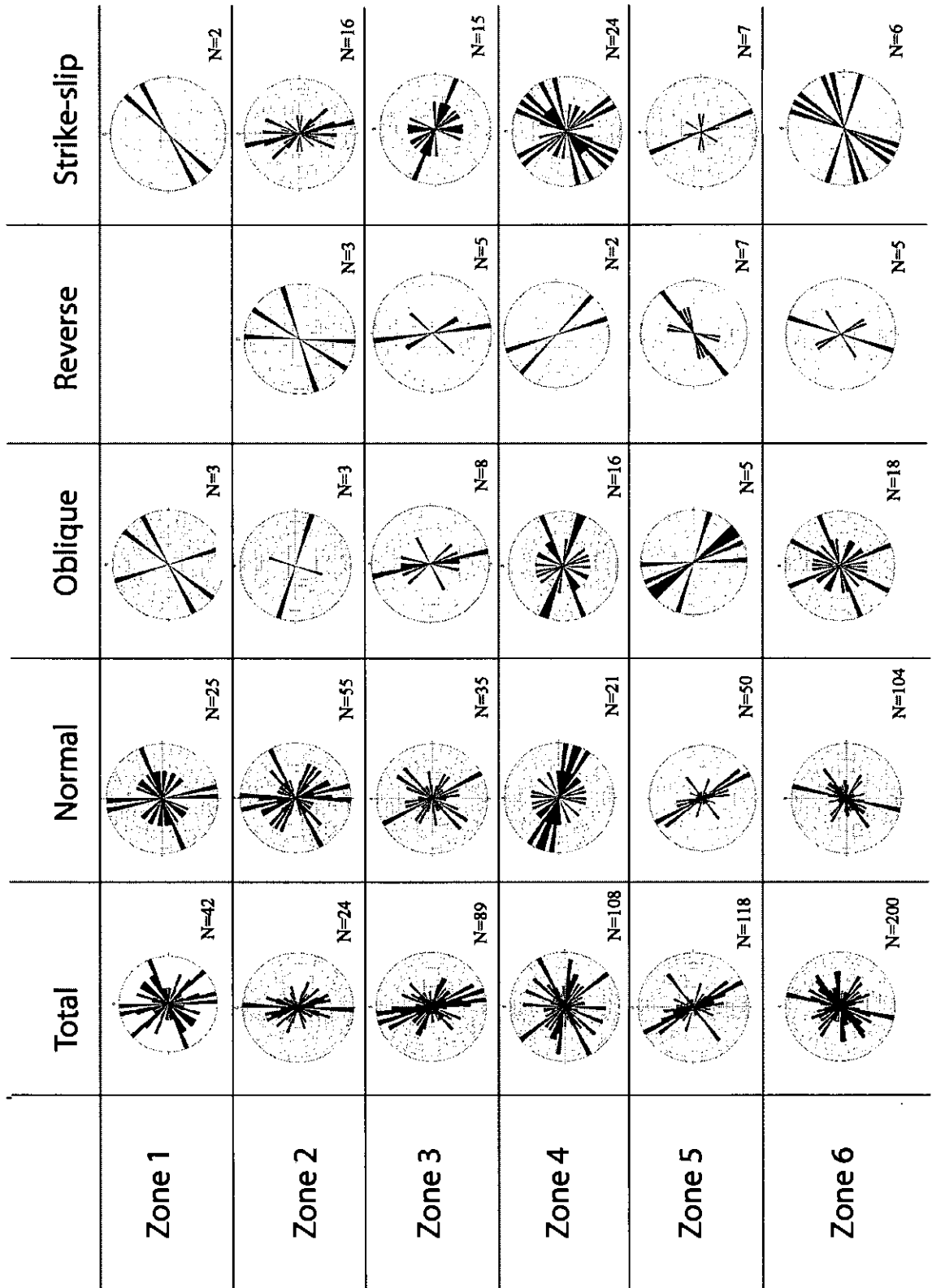


Figure 7.39. Chart showing breakdown into different fault types for each zone.

Firstly, we consider fault trends by geographical area (Fig. 7.38). Zone 1 covers the NW graben margin. This domain is dominated by normal faults striking 030-070°, 160-180° and 090-140°; a few faults are oblique-dip or strike-slip (sinistral and dextral) with strikes of 050-070° and 150-160°. In contrast, zones 2 and 3, covering the axial zone of the graben, exhibit large numbers of normal and strike-slip faults, with few oblique and rare reverse faults recorded. In both domains, the strike of normal faults show two major trends (040-060° and 150-190°) with a subordinate trend of faults striking 110°-130°, whereas strike-slip faults, although also showing a range of strikes, only have one dominant direction of faulting (in zone 2, 140-200°; in zone 3, 100-120°).

Zone 4 covers an uplifted block forming the mountain of Samandağ (Fig. 7.38) and is bounded to the south and southeast by the Asi Nehir. The faults of this domain are again normal and strike-slip, but oblique-slip faults are also common. The general trends of faults are the same as elsewhere; however, the dominant orientation of fault strike is different. Normal faults strike mostly 090-130° although there are N-S and NE-SW striking faults too. In contrast, oblique-slip and strike-slip faults have two dominant trends in orientation, 050-070°, 100-120° and 20-80°, 140-170° respectively.

Zones 5 and 6 cover the southeast margin of the graben. The division of the two areas is based on a proposed transfer fault that strikes perpendicular to the graben margins (see 7.2.2); this structure also defines the NE edge of zone 4. The majority of faults in zone 5 are normal faults, generally striking 140-180°. Additionally, there are some oblique-slip and strike-slip faults (both mainly striking 150-180°) and reverse faults (striking 050-080°). Zone 6 also has a spread in the orientation of faults; normal faults pre-dominantly strike 0-020° and 040-060°, with a sub-set striking 120-140°. Oblique faults are the next most common type, but show a dispersed fault pattern. Small numbers of reverse faults and strike-slip faults (sinistral and dextral) are also present.

Zone Number	N-S	NE-SW	NW-SE	E-W
1	✓	✓	✓	
2	✓			
3	✓	✓	✓	
4		✓	✓	✓
5		✓	✓	
6		✓		✓

Table 7-4. Summary of the main trends in fault orientation for each area of the Hatay Graben

If we compare the fault trends of the Hatay Graben to faulting around Belen (zone 8) and Kırıkhan (zone 9) there are no major differences between the areas. Zone 8 is dominated by normal faults orientated 030-080° and 160-180°. Small numbers of the other types of faults were measured but there are not enough data for trends to be identified. Additionally, in zone 8 a number of measurements were taken on striated calcite veins; the strike of these veins is mainly 000-025°. Few measurements were taken in zone 9, these were mainly normal faults striking 000-010°.

#### 7.7.1.2 *Temporal distribution of faulting*

Secondly, fault patterns can be considered according to the assumed timing of fault formation assuming a maximum age for the faults recorded (i.e. if the fault cuts Middle Miocene rocks it is considered as a Middle Miocene fault, if the fault crosses a boundary it is considered to be the age of the younger sediment). Naturally, there are some inherent problems with this method but it is hoped that trends in the youngest rocks will be clear enough in order to distinguish older fault trends. Therefore, the fault populations have been separated into classes for the Upper Cretaceous, Eocene, Early, Middle and Late Miocene and Pliocene. Few faults were identified in Quaternary deposits mainly due to the coarse and unconsolidated nature of the sediments.

The Pliocene and Quaternary exhibit three clear trends in the orientation of faults; the major trends are to the NE-SW (040°-065°) and N-S (353°-010°) with a subordinate trend at 120°-140°. Normal and strike-slip faults are the most abundant and they strike with the similar trends. There are also a few oblique and reverse faults present. Faults considered as Late Miocene or younger in age, show similar trends in fault strike as the Pliocene data set, the major difference being that the Middle Miocene sediments contain far fewer identified strike-slip faults than those of Pliocene age. This is also the case for the Middle and Early Miocene sediments, where there are three main trends (broadly NW-SE, N-S, NE-SW) dominated by normal faults.

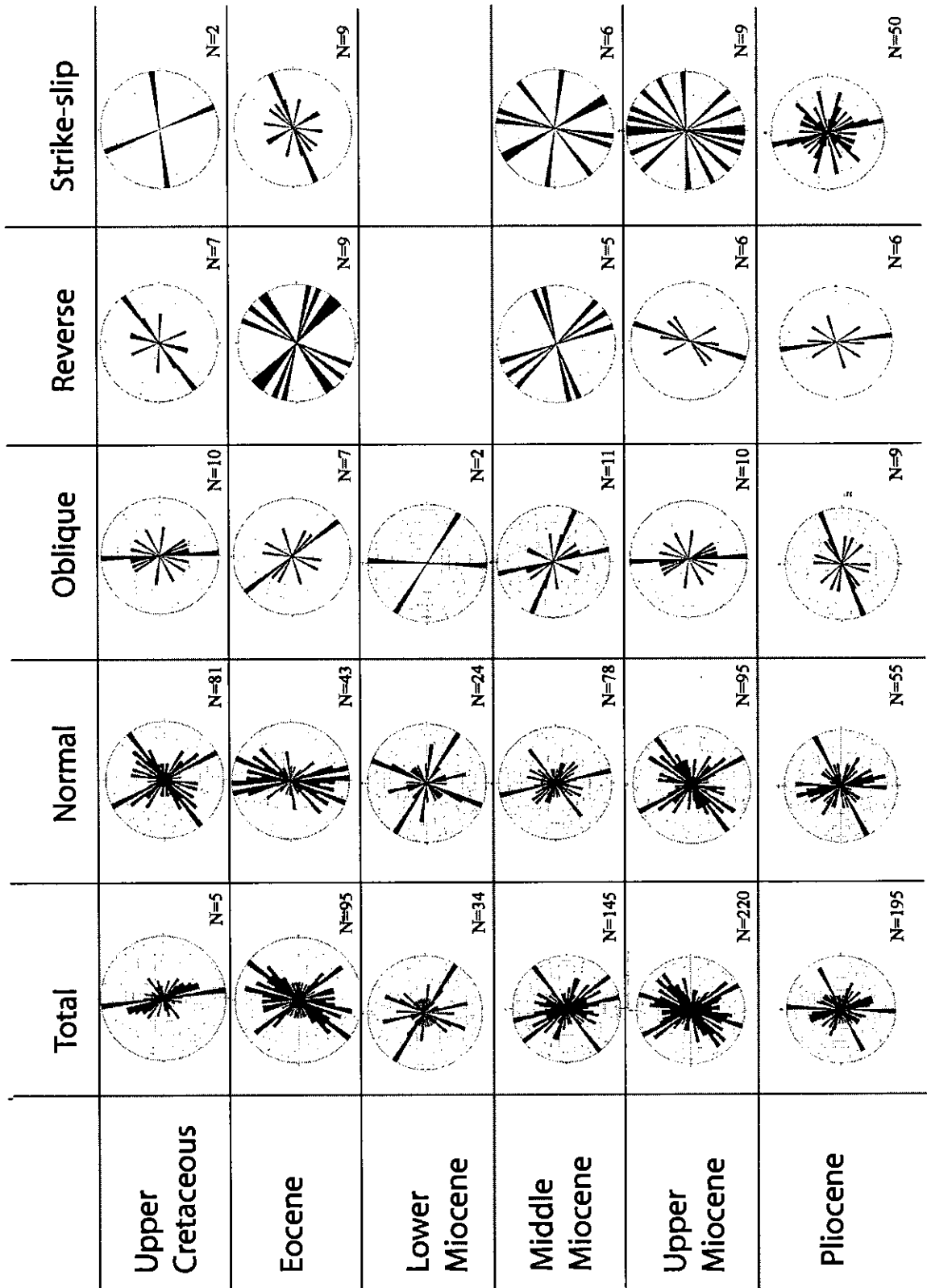


Figure 7.40. Chart showing data measured by age, and breakdown into different fault types.

However, the Eocene and the latest Cretaceous data sets are different. When all the faults measured in Eocene rocks are considered the orientation of the faults are similar to that observed in younger rocks but when the different fault types are separated, it is seen that normal faults dominate as usual but have only one main trend in strike ( $340^{\circ}$ - $040^{\circ}$ ) in contrast with two or three different trends. The Late Cretaceous data set is again different. When all faults are considered together there is one main trend orientated  $330$ - $000^{\circ}$ , this pattern is formed from oblique-slip faults trending N-S and normal faults with two dominant strike directions of  $030$ - $070^{\circ}$  and  $120^{\circ}$ - $150^{\circ}$ .

Age	N-S	NE-SW	NW-SE	E-W
Upper Cretaceous	✓		✓	
Eocene		✓	✓	
Lower Miocene		✓	✓	
Middle Miocene		✓	✓	
Upper Miocene		✓	✓	
Pliocene	✓	✓	✓	

Table 7-5. Summary of the main trends in fault strike orientation by age.

### 7.7.1.3 Discussion

When the location of the fault planes is considered, the overall pattern of fault orientation is similar for all the zones, where there are three trends in the direction of normal faulting. Zones 4 and 6 have different overall fault patterns; as there are significant numbers of E-W striking faults present and the orientation of the main fault trends is slightly different. In Zone 6, this probably reflects the presence of a large E-W trending fault observed in the Harbiye Gorge and smaller faults trending parallel to it. Zone 4 is an uplifted block and the different fault orientations could be governed by faults that bound this area.

The other important observation is that there are greater numbers of strike-slip faults present in the axial zone of the graben, whereas the graben margins are dominated by dip-slip normal faults. As the axial zone could only develop after graben formation had begun, this suggests that strike-slip faulting was not important during the initial phase of rifting and only normal faults formed; however, as time went on it appears that strike-slip faults developed perhaps suggesting that there was a change in the stress field.

Investigating the maximum age of the faulting observed in the Hatay Graben supports this conclusion. Pliocene sediments are only found within the axis of the graben and it is



sediments of this age that contain the highest number of strike-slip faults, these faults must be post-Pliocene in age. The paucity of strike-slip faults in older sediments is probably due to their off-axis location. When data sets from different aged units are compared it is not possible to identify any different fault trends; from the Late Cretaceous to Pliocene the pattern of faulting from different units appears to be similar. Allowing for the uncertainty in the fault age planes it is impossible to say whether all faults formed during the Pliocene - Quaternary or if the stress field controlling the orientation of faults has been constant since the deformation began and that any older sediment did not contain significant numbers of faults relating to prior stress-regimes.

## 7.8 $\beta$ Factor

The observations made of the structure of the Hatay Graben can be used to estimate the amount of extension (the 'beta factor') across the graben. Studies in the North Sea (White 1990) and in the South China Sea (Su *et al.* 1990) show that the initial and final dips of faults that bound tilted blocks can be used to estimate the amount of extension using a simple model and the value that is calculated is comparable to values estimated from changes in crustal thickness. This has been shown to work in Greece by Roberts & Jackson (1991) and Paton (1992). The amount of extension is calculated using the equation:

$$\beta = \sin\phi_0/\sin\phi_1$$

Where  $\phi_0$  and  $\phi_1$  are the initial and final dips of the faults and  $\beta$  is the amount of extension.

The basin bounding faults in the Hatay Graben dip at between 49° and 60°. Basin fill sediments have a dip of around 5°-20°, which suggests the dip of the faults was originally somewhat steeper maybe over 70° in places assuming domino-style fault arrays. These figures give an estimated  $\beta$  value of 1.0-1.2. This figure seems reasonable as similar numbers have been calculated for other extensional basins, i.e. Gediz and Büyük Menderes Grabens, Turkey;  $\beta \sim 1.2-1.3$  (Paton 1992); Tainan Basin, Taiwan;  $\beta \sim 1.1$  (Lin *et al.* 2003).

## 7.9 Stress Analysis

### 7.9.1 Introduction

Stress analysis was undertaken on the fault data collected in order to investigate the orientation of the principle stress axes causing faulting in the area and also to enable comparisons with previous work (Over *et al.* 2002). Slickenlines, groove marks and mineral fibre growths were measured as kinematic indicators. No kinematic information was present for the large basin-scale faults due to weathering of the fault planes; thus all data comes from smaller-scale faults.

The computation of the orientations of the axes of principle stress is based on the following assumptions:

- a) Motion on the fault plane, recorded by lineations, is parallel to the direction of resolved shear stress on the fault,
- b) There is kinematic independence between nearby faults, and
- c) The regional stress field is homogeneous (Angelier 1984; Nemock & Lisle 1995).

Although these assumptions are widely used in a number of different techniques, the results will only be meaningful in certain geological situations and must be evaluated carefully. The main limitation of these techniques is that a stress field often varies through time resulting in heterogeneous fault populations through the successive generation of faults and the reactivation and rotation of pre-existing faults. Therefore, in this situation the axes of principle stress calculated will represent an intermediate stress field between the two or more different stress regimes represented by the faults. This situation will also occur if the stress field varies spatially.

Various methods have been proposed to analyse polyphase fault data (e.g. Nemock & Lisle 1995; Liesa & Lisle 2004; Shan *et al.* 2004) for situations where there are clear-cut different data sets, since cross-cutting relationships in the field area do not demonstrate a clear temporal progression (Section 6.5) the stress inversion method based on the methods of Bott (1959) and Angelier (1984) were employed using the computer programme Daisy 2.4 (Salvini 2001). The main limitation of this method is that the sense of motion must be known for all slip data (therefore the whole data set cannot be used); the friction on the fault

is taken as zero and the method does not give a unique solution for the orientations of the principle stress axes.

In order to understand the data set fully, the data were analysed in subsets, using the same groups as before (i.e. age of faulting and geographical area) but, where possible, the data were also considered by individual outcrop location. This allows deformation to be studied for point locations; this was not possible for many locations as the size of the exposure or paucity of fault planes meant that not enough data were collected for meaningful analyses in many localities.

### 7.9.1.1 Results and discussion

Figure 6.41 shows that zones 1, 3 and 6 have  $\sigma_1$  positioned in the vertical; this is the maximum stress axis and thus relates to a normal faulting regime. Zones 2 and 5 have  $\sigma_1$  positioned sub-vertically and thus represent a more transtensional stress regime. Zone 4 differs in that the vertical axis of stress is  $\sigma_2$  and thus is dominated by strike-slip faulting. In all of these cases the minimum principal axis of stress,  $\sigma_3$ , is orientated in the 0-90° or 180-270° quadrant and faults should therefore trend 90° from this direction.

Figure 6.42 shows the fault data from zone 8 (Belen area), which fits with the general pattern observed in the Hatay Graben;  $\sigma_1$  is vertical and  $\sigma_3$  is orientated E-W. Zone 9 is different with no principle axes of stress orientated in the vertical.

When the fault data are considered by age (Fig. 7.43), the stress analysis results in  $\sigma_1$  being nearly vertical, thus corresponding to a normal stress regime, for all time slices. The orientation of  $\sigma_3$  is orientated within the 0-90° quadrant of the stereonet.

Individual data sets recorded at eleven locations are large enough to be analysed individually. These data were mostly measured in Pliocene sediments but some are from older rocks. In the northern part of the field area,  $\sigma_3$ , is orientated at a high angle to the basin margins (Fig. 7.44) in line with the direction of maximum extension. Further to the south near Samandağ,  $\sigma_3$  orientations become very variable.

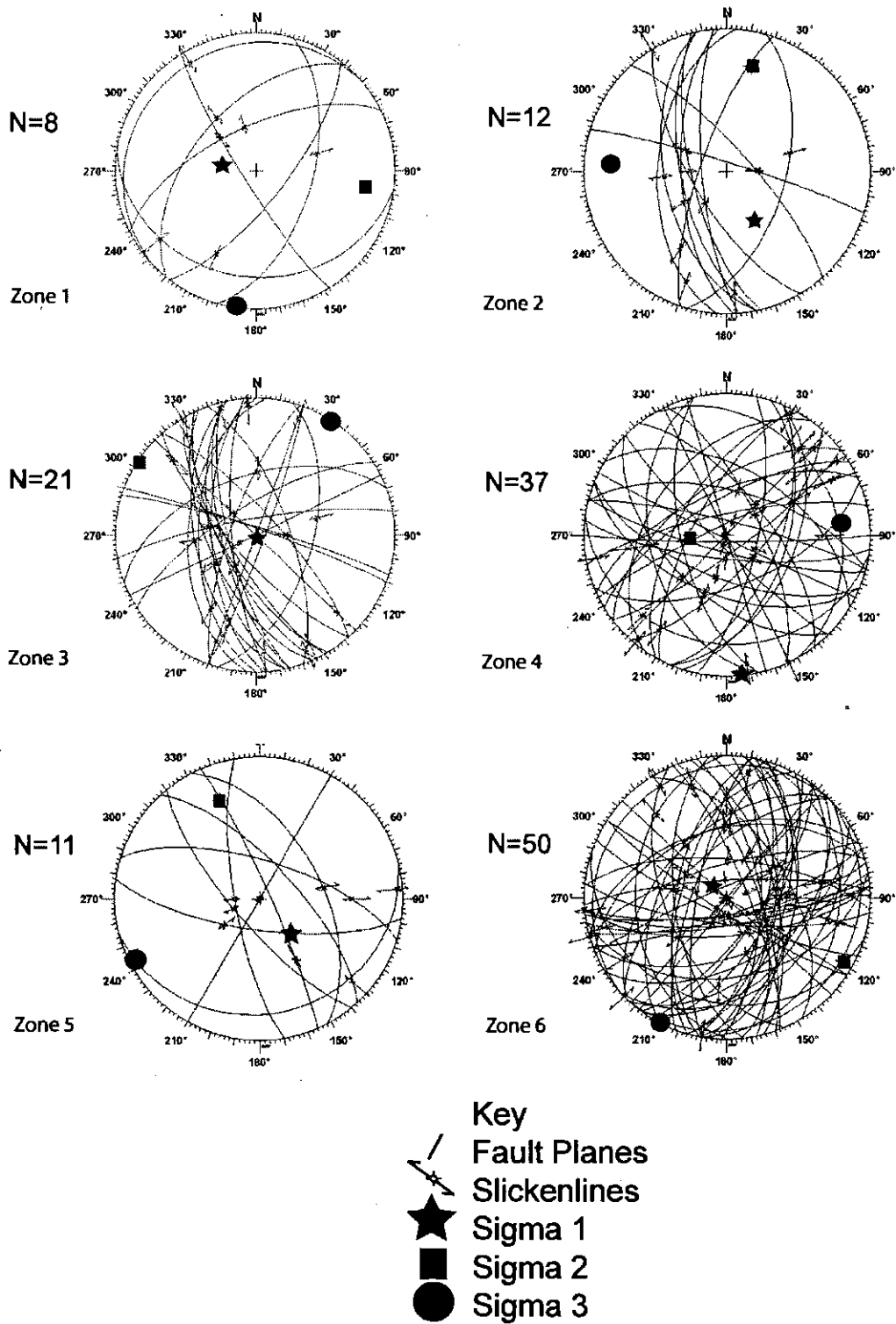


Figure 7.41. Stereonets for showing the results of the stress analysis when data are considered by zone.

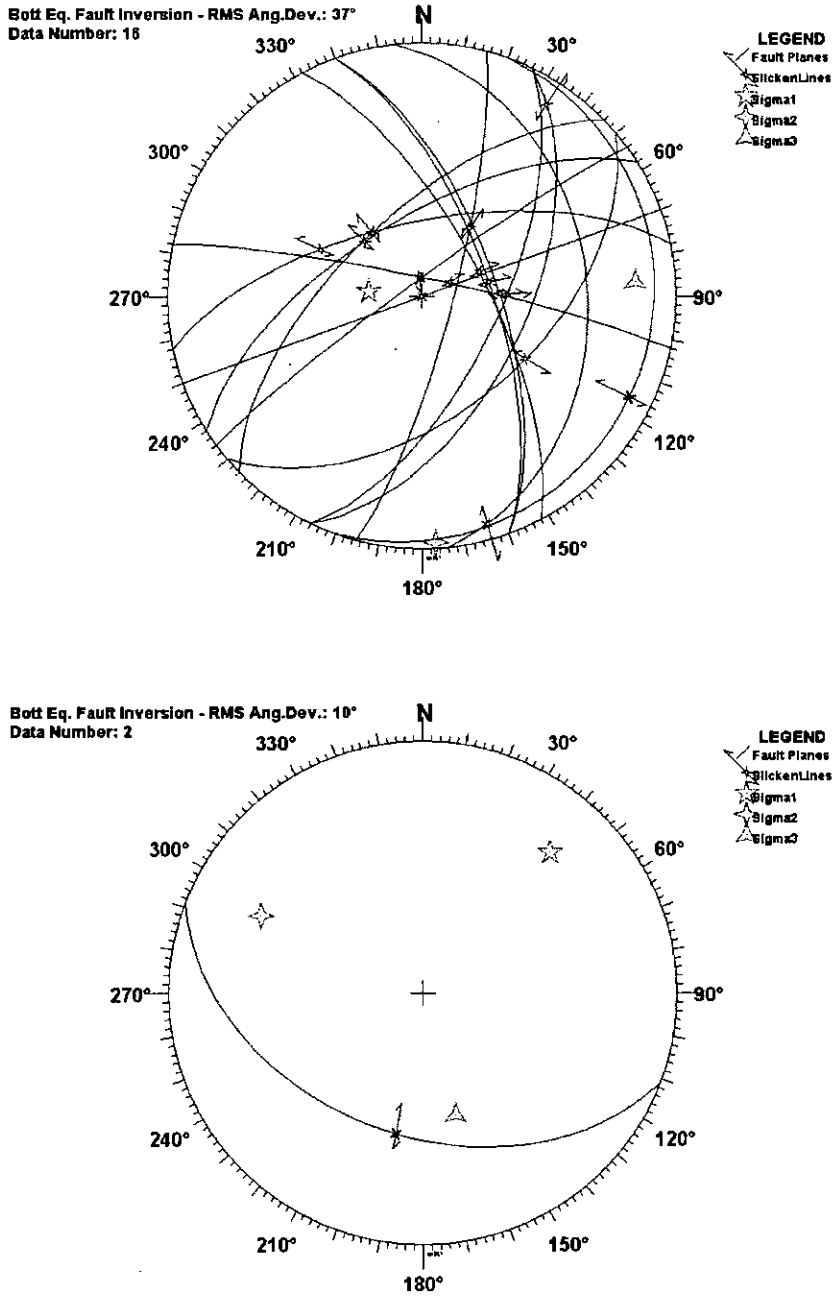


Figure 7.42. Stereonets showing the results of the stress inversion carried out on data from a) zone 8 and b) zone 9.

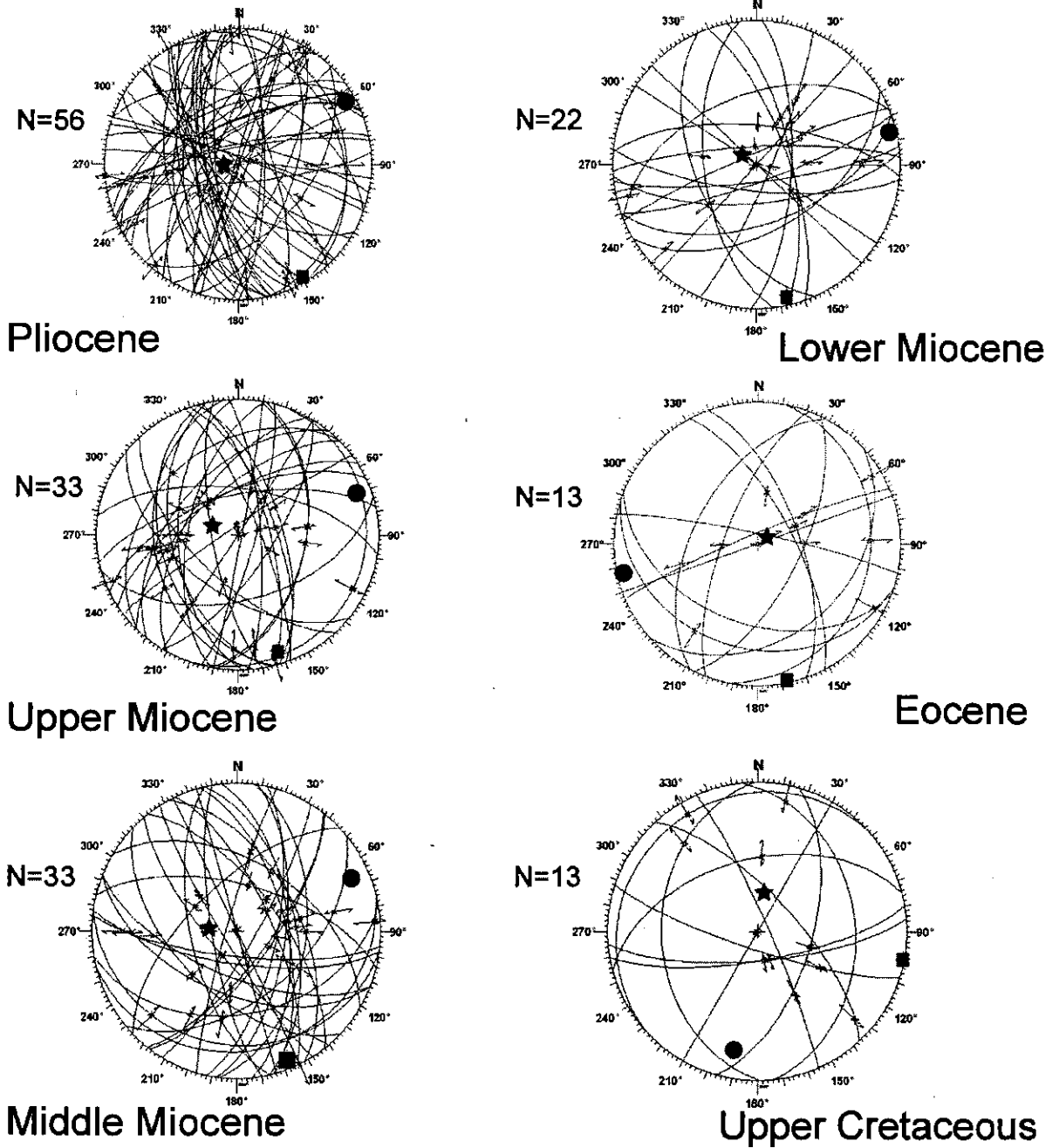


Figure 7.43. Stereonets showing the results of the stress inversion carried out when data are considered by the age of the unit they were measured in. Same key as Fig. 7.39.

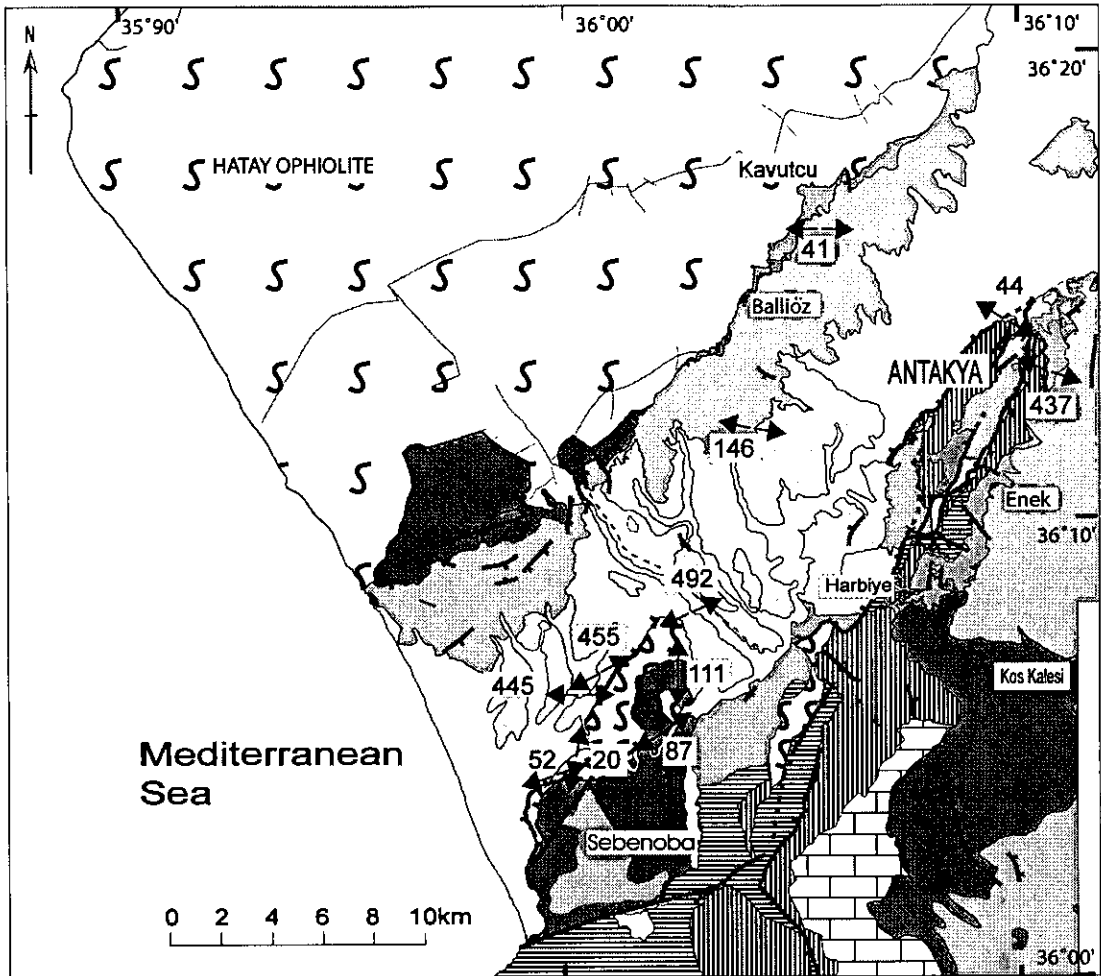


Figure 7.44. Map showing the orientation of the  $\sigma_3$  axis for the locations where individual stress analyses could be carried out.

This shows that the data for individual locations gives clearer orientations for the principle stress axis. In the northern part of the graben,  $\sigma_3$ , is orientated perpendicularly to the graben and  $\sigma_1$ , is vertical. This stress field would result in the faults observed today. Locations further to the south suggest that either the stress field in that area is very variable or that faults have been rotated after formation resulting in misaligned principle stress axes. This is the area in which it is postulated that block rotations have taken place (section 6.2.3).

When the data are treated in larger groups the results are not so clear.  $\sigma_3$  generally comes out as being orientated NE-SW, which would generate NW-SE trending faults, although these are plentiful they are not the major graben faults. This result possibly reflects the fact that most lineations were measured on small fault planes and that the large boundary fault were too eroded to retain slickenlines. This is confirmed with an experiment where lineation

values are assigned for these boundary faults are analysed; in this case  $\sigma_3$  is orientated NW-SE. It is likely that the complicated nature of the faulting in this area makes bulk analysis of the fault data for palaeostresses difficult.

In some areas it has been shown (i.e. de Paolo 2003) that stress can become compartmentalised between different lithologies. In order to investigate any possible effects that the different lithologies may have on the results of the stress inversion technique fault data were plotted according to the lithology in which it was recorded. Limestone, marl and sandstone were chosen. All three lithologies selected show similar orientations for the stress axes (this is the same as the orientation calculated for the total number of faults in the field area). Thus, there appears to be no difference in the response of different rock types in the area to the overriding stress field.

## ***7.10 Past and Present Seismicity.***

### **7.10.1 Historical Earthquakes.**

In historical times the city of Antakya was known as Antioch, one of the most important cities in the eastern world, which was established ~300 years BCE (Before Common Era; historians now use this notation instead of BC). As a result historical records are particularly good for the region and illustrate that the area has always been prone to earthquakes. Between the founding of the city and 1000 CE (Common Era (AD)) the area experienced thirteen significant earthquakes (Appendix 5 for a full list and descriptions) (Guidoboni 1994).

Particularly strong earthquakes occurred on the 13th December 115 CE “Antioch suffered the worst destruction[...]the whole earth heaved up[...]trees, with all their roots, were thrown into the air[...]even Mt. Casius [Ziyaret Dağ] was so badly shaken that its peaks seemed to lean over and break off, and to be falling right on the city” (Dio Cassius from Guidoboni 1994). On the night of the 13th-14th September 458 CE, when the city was virtually completely destroyed and many people died. “for many were burned by lightning flashes, many were swallowed up by chasms of the ground, others were engulfed by the waters of the sea or of the clouds” (Severus of Antioch, Guidoboni 1994).



The 6th century CE was a particularly active period with 5 or 6 strong earthquakes recorded in Antioch, but many towns along the NAFZ (including Istanbul) and the EAFZ also experienced higher than normal levels of seismicity. Although this maybe the result of bias in the historical record, the large volume of material from Antakya (and Istanbul) could represent a real increase in the frequency of earthquakes (Siros 2001). The earthquake of May 526 (Guidoboni 1994) or 528 CE (Erol & Pirazzoli 1992) was a particularly strong earthquake and resulted in the death of thousands of people, perhaps as many as 250,000 (Guidoboni 1994). The roman harbour of Seleucia Pieria, near modern Çevlik, was rendered unusable and Antakya suffered major destruction and a subsequent great fire, “the surface of the earth boiled and foundation of buildings were struck by thunderbolts thrown up by the earthquakes and were burned to ashes by fire” (Malalas, Guidoboni 1994).

Pirazzoli *et al.* (1991) correlate this increase in earthquake activity to a major tectonic event that took place ~1500 years ago in the eastern Mediterranean they call the ‘Early Byzantine Tectonic Paroxysm’ apparently due to a particularly active period of plate interaction in the Eastern Mediterranean. Pirazzoli *et al.* (1991) also report that there may have been another major regional tectonic event that they date to ~2500 ago that uplifted coastal features.

Daphne, modern Harbiye, was totally destroyed in 580 CE (Guidoboni 1994) and Antioch was damaged at the same time. Then, in October 587/588, Antioch was again devastated by a strong earthquake and an estimated 60,000 people lost their lives (Guidoboni 1994).

Information is more patchy between the end of the 10th century and 1899, when a seismic station was installed in the Eastern Mediterranean (al-Tarazi 1998). However, in this period at least three large earthquakes took place. One on the 20th November 1114, magnitude ~7 (al-Tarazi 1998). Then, two large earthquakes occurred in the 19th century and completely destroyed Antakya; a magnitude 7.4 earthquake on August 13th 1822 and a  $M \approx 7.2$  on April 13th 1872 (Över *et al.* 2002).

7.10.2 Present seismicity.

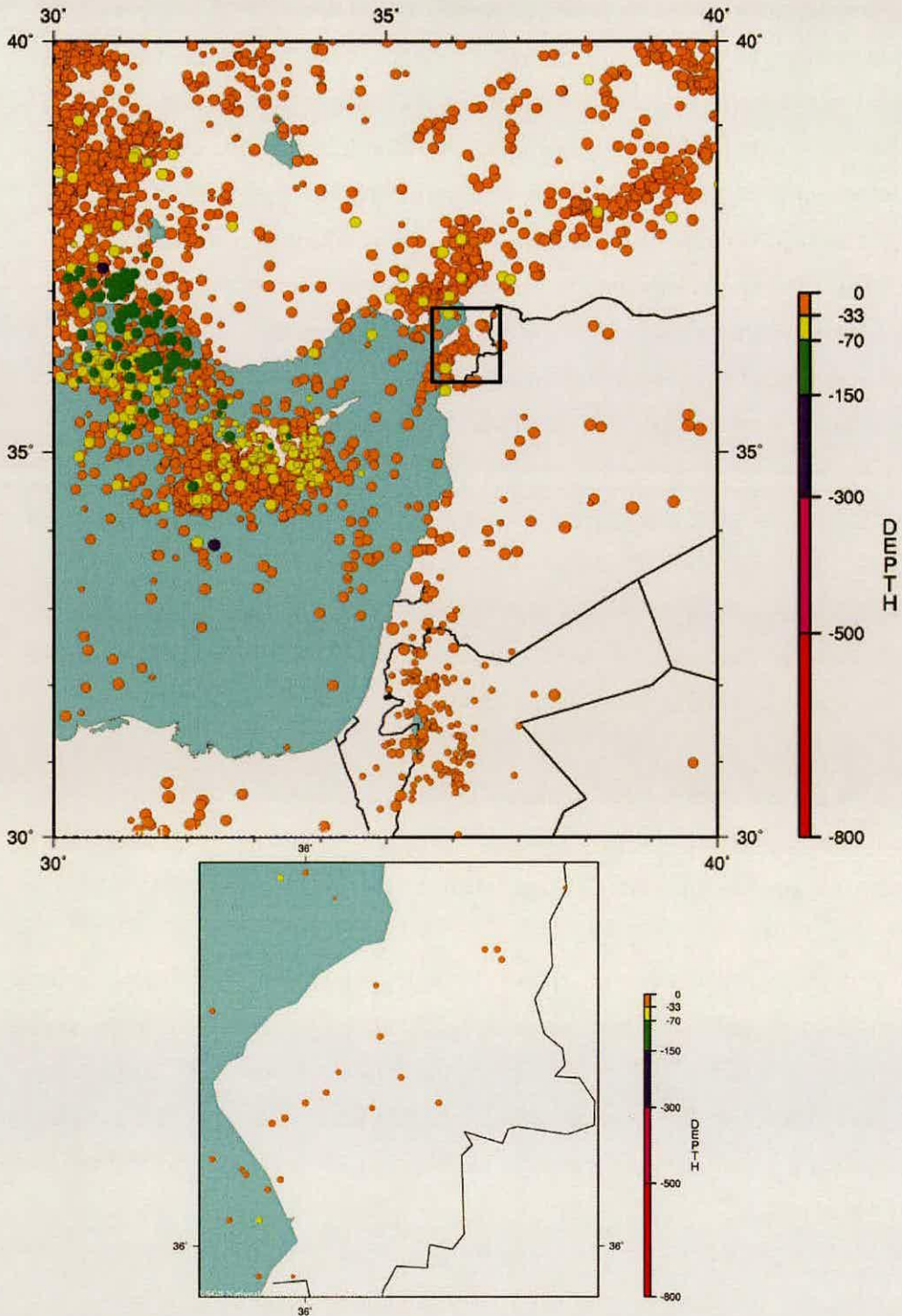


Figure 7.45. Map showing the earthquakes that have occurred between 1973 and the present day in the Eastern Mediterranean region; box shows location of inset map showing the earthquakes that have occurred in the Hatay during the same period. Maps generated by the USGS National Earthquake Information Centre (<http://www.neic.cr.usgs.gov/neis/epic/>).

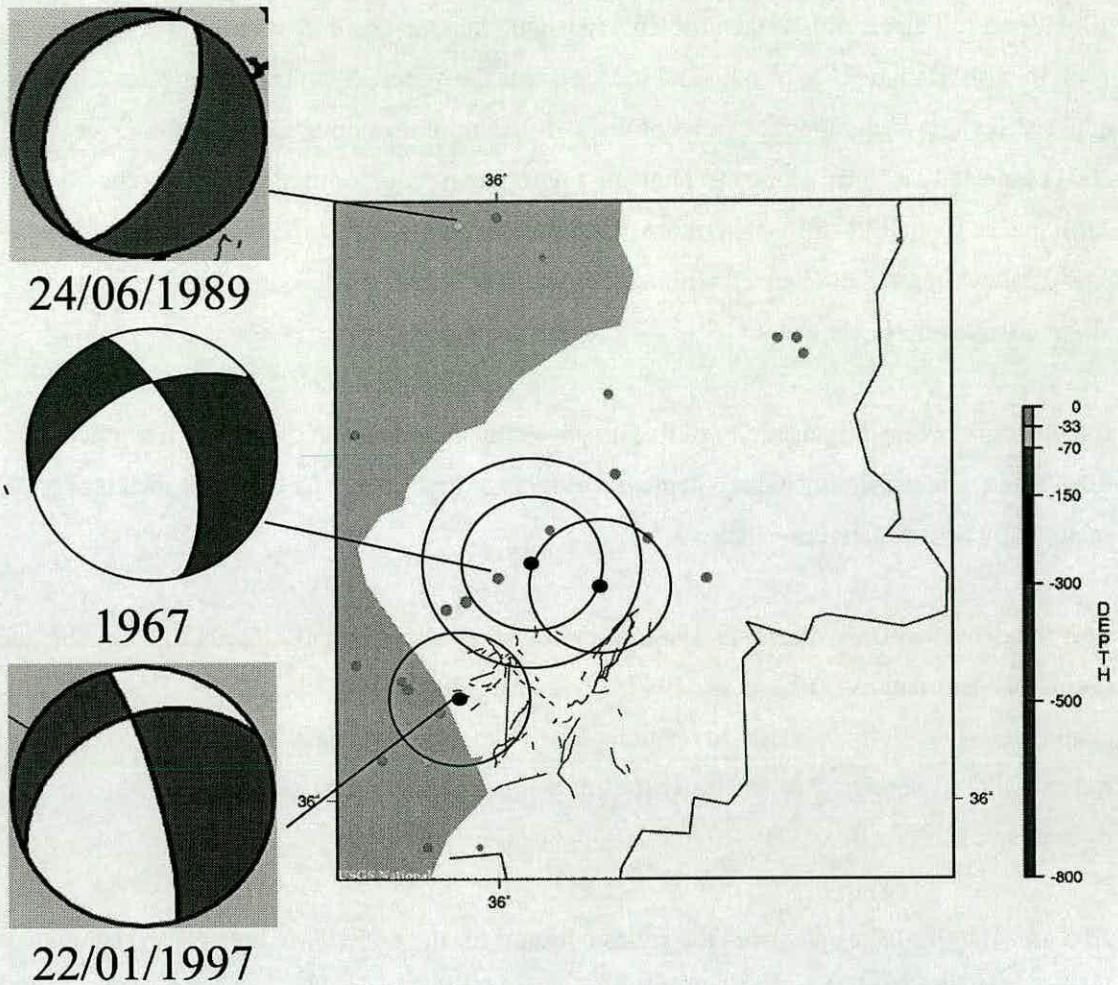


Figure 7.46. Map showing the loci of errors for some of the earthquake epicentres, inner locus is 10km, outer is 20km; focal mechanisms are shown for available data. The 1989 focal mechanism indicates normal faulting, whereas the other two earthquake focal mechanisms indicate dominantly normal oblique-slip motion.

At the present time the Hatay Graben is still tectonically active as witnessed by current seismic activity. The USGS National Earthquake Information Centre (NEIC) lists 28 earthquakes that have occurred in the last 20 years in the area from 35.9°N to 36.75°N, 35.76°E to 36.7°E. When these earthquakes are mapped out the majority of the earthquakes form a linear trend NE-SW parallel to the orientation of the basin margins (Fig 7-44). Several of the faults lie along a linear trend in the Hatay Graben with the majority of the earthquakes apparently occurring within the Hatay Ophiolite and in the coastal area. It appears that this trend also continues offshore but the orientation rotates anticlockwise towards the south. However, the epicentre location of these earthquakes should be treated with some caution, as the error in the location can be as much as 10-15km (see Jackson

2001, for a full discussion of the problems in calculating the position of epicentres). Figure 7.45, thus shows the range of potential locations for the recorded faults. The presence of a major strike-slip fault along the trend of the earthquakes it thus quite unlikely (c.f. Över *et al.* 2004) especially as focal plane mechanisms suggest an oblique-normal motion for the earthquakes (not strike-slip). Therefore, it is much more likely that the faults on which the earthquakes occurred are located within the graben or along the boundary faults and not along a strike-slip lineament.

Interestingly, when the seismicity of this area is compared to that of the northern segment of the DSFZ (in particular the Gharb depression) it is noticeable that the Hatay Graben is more seismically active than these areas.

The focal mechanisms of recent shallow earthquakes show that the faults are dip-slip to oblique-slip in nature (Erdik *et al.* 1997; Över *et al.* 2002, Över *et al.* 2004, Havard CMT catalogue) (Fig. 7.46). Stress inversion carried out on these data by Över *et al.* (2002) indicate that  $\sigma_1$  is orientated vertically thus corresponding with a normal faulting regime and  $\sigma_3$  trends  $051^\circ$ .

Al-Tarazi (1998) have calculated the seismic hazard for the eastern Mediterranean region. Interestingly the Hatay has the highest hazard value for the next 50 years indicating a maximum ground acceleration of  $5\text{ms}^{-2}$ , compared to an average value of  $\sim 3\text{ms}^{-2}$  for the rest of the region.

## **7.11 GPS Velocity Fields**

The Global Positioning System (GPS) is providing a new tool for investigating and quantifying continental plate tectonic motions on a short timescale. The Eastern Mediterranean area has been intensively investigated from this point of view for nearly 20 years; however, there is only little information for the Hatay Graben. McClusky *et al.* (2000) present the most recent data for the region. In the Hatay region there are three GPS stations; SENK (near Senköy in the far south of the field area), ULUC (near Uluçmar in the Iskenderun Basin) and DORT (near Dörtyöl also in the Iskenderun Basin), so there are actually no GPS stations within the Hatay Graben.



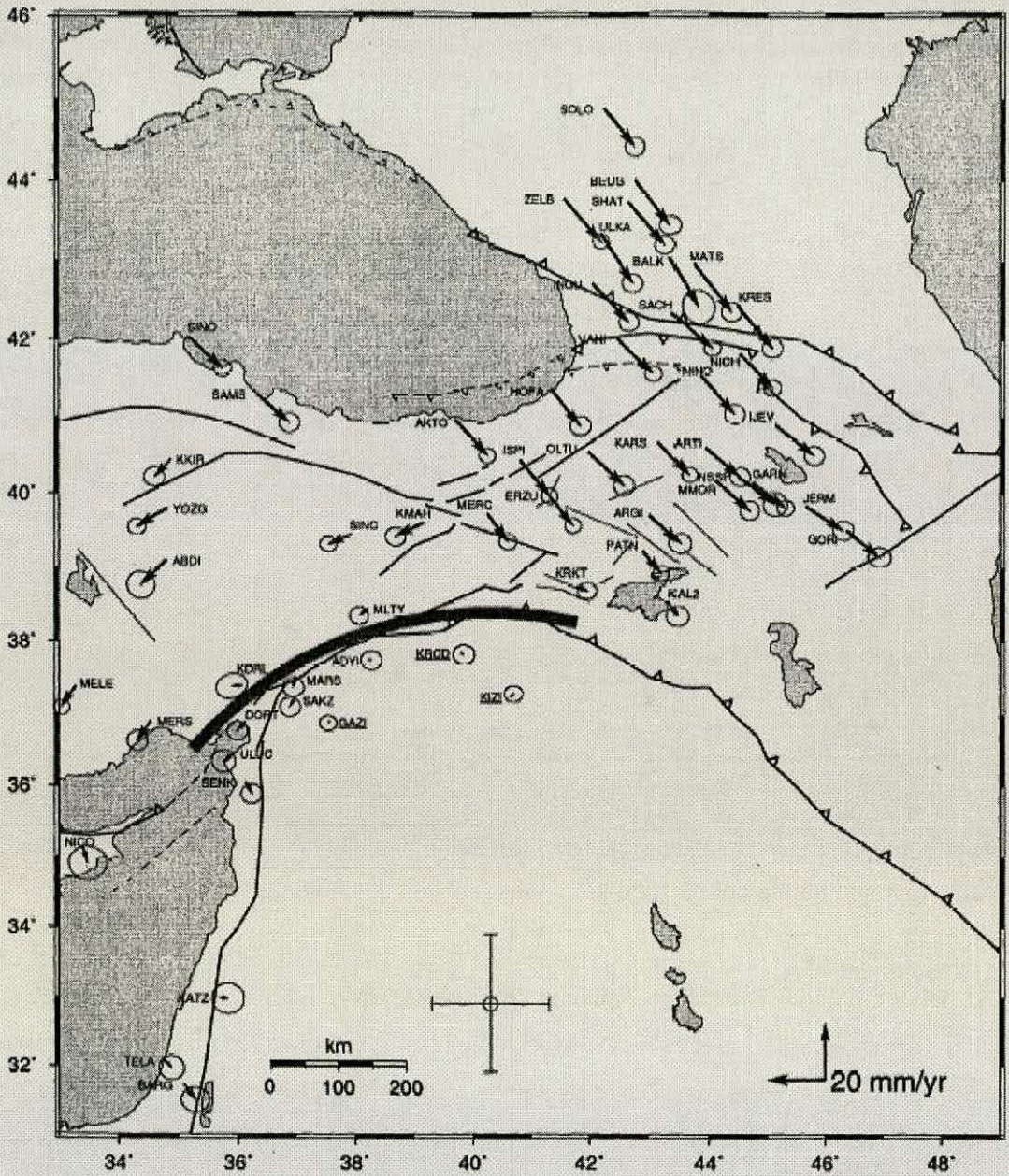


Figure 7.48. GPS horizontal velocities and their 95% confidence ellipses in a Arabia-fixed reference frame for the period 1988-1997 (McClusky *et al.* 2000). The arc represents the small-circle about the Arabia-Anatolia euler vector calculated by the authors and represents the approximate location of the EAFZ.

## 7.12 Discussion

On the southeastern margin of the graben a number of en-echelon fault segments step away from the axis of the graben, forming two arrays of sub-parallel faults (Fig. 7.1); the outer array comprises three main segments, whereas the inner array is shorter with two fault segments. This second array is possibly truncated by a transfer fault, orientated at a high angle to the graben (Fig. 7.1). The greatest throw (>500m) is on the innermost of the major faults. Near Antakya, two fault segments overlap to form a relay ramp that has relay breaching faults, indicating that fault linkage has occurred (Fig. 7.1). The relay ramp forms a small sub-graben (<10km<sup>2</sup>) on the flank of the graben and is cut by faults trending dominantly NE-SW, although NW-SE faults are seen to cross-cut these faults (Fig. 7.1). In the south (to the east of Samandağ) another sub-basin has developed on the graben flank. In this subbasin, minor faulting has dissected the topography creating a complex horst and graben system (Fig. 7.8). As to the north, the main fault strike trend is NE-SW with cross-cutting NW-SE faults. Between these two areas of sub-basin formation a large monocline is observed on the margin; the axial plane is orientated NW-SE, perpendicular to the orientation of the graben.

On the northwest margin of the graben, map-scale faults (~100-200m of displacement) dip into the graben; however, it appears that these faults are not as significant as the faults bounding the southeast margin. The majority of the faults are synthetic and antithetic normal faults parallel to the trend of the basin, with only rare faults orientated to the NW-SE. Additionally, identified along this margin is a large oblique-slip fault with a significant component of sinistral strike-slip (~150m of displacement) motion.

Faulting is observed within the axial zone of the graben, however, these are generally microfaults (displacement on faults <50cm) or outcrop scale faults (displacement <10m) with variable orientations. The presence of larger faults is inferred from significant variations observed in the orientation of bedding planes and the variable orientation of the axes of principle stress calculated from fault planes that indicate that block rotations have taken place in the Pliocene and younger sediments.

Syn-tectonic sedimentary features (growth faults; sediment fanning) indicate that fault motion had begun by the Middle Miocene. Tectonic subsidence was low and sedimentation kept pace with subsidence thus infilling the available accommodation space, resulting in a

lack of topographic expression. Fault motion may at this time have been only on the outer bounding faults and over time the deformation has localised onto the inner boundary faults that have the greatest throw. This is in line with observations made in other extensional systems, i.e. North Sea (Cowie *et al.* 2005). This motion on the inner faults was probably occurring during the Late Miocene when sediment fanning is observed in outcrop; however it is not clear if there was a pronounced topographic graben present at this time. It is possible that although normal faulting was taking place in the Middle Miocene, the majority of the faulting is later as there appears to be only one faulting event, which effects strata of all ages in a similar and thus is likely to have occurred relatively recently. Pliocene sediments are very deformed adjacent to boundary faults possibly also indicating that a lot of the fault motion has taken place recently. So it was fault motion with continued subsidence during the Plio-Quaternary that resulted in the present topographic graben, the Hatay Graben; this also confined sediments of that age to the axial zone.

Patterns of faulting are unlike those observed in areas of pure extension ( $\alpha=90^\circ$ ) where all faults are normal and strike parallel or sub-parallel to the graben margins, nor are they similar to strike-slip regimes where two dominant directions of faults occur  $\sim 45^\circ$  apart, and normal, reverse and strike-slip faults develop within the fault zone. Additionally, there appears to be a spatial difference in the style of faulting with the majority of strike-slip faults being present within the axial zone Pliocene sediments, while the graben margins are dominated by normal faults.

Graben formation is likely to be the result of transtensional tectonics, the range between the two end members of pure extension and strike-slip (where the trend of the basin is oblique to the extension direction). A number of recent studies have investigated the process of oblique extension (transtension), both experimentally (Withjack & Jamison 1986; McClay & White 1995; Tron & Brun 1991; Clifton *et al.* 2002;) and using field evidence (Umhoefer & Stone 1996; ten Veen & Kleinspehn 2002). These show that the acute angle,  $\alpha$ , between the rift trend and the direction of displacement on the plate edge is inversely related to obliquity; thus, a largely oblique regime (i.e. strike-slip basin) exhibits a low value of  $\alpha$  ( $\alpha=0^\circ$ ) and in pure extensional regimes  $\alpha = 90^\circ$ .

Analogue experiments have shown that there is a change in the style of faulting between  $\alpha=45^\circ$  and  $\alpha=30^\circ$  (Withjack & Jamison 1986; Clifton *et al.* 2002). When  $\alpha \geq 45^\circ$  all of the faults are of dip-slip type. Faults near the graben margin strike slightly obliquely to the main



trend, whereas near the axis of the graben faults strike near to the displacement-normal direction (Fig. 7.43). However, when  $\alpha \leq 30^\circ$  dip-slip, oblique-slip and strike-slip faults form and three populations of faults can develop. One population forms sub-parallel to the graben trend and two trends at a high angle to the rift and displacement direction. However, when  $\alpha = 15^\circ$  the majority of the faults are strike-slip in nature.

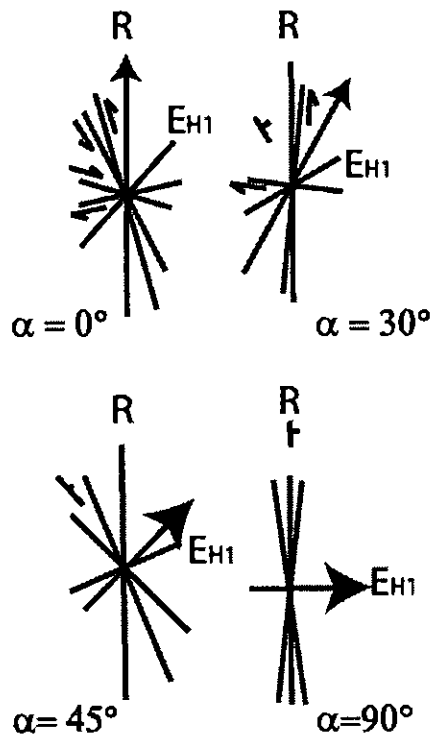


Figure 7.49. Rose Diagrams of fault trends predicted by a transtensional model (combined extension and sinistral shear). R is the rift trend; the large arrow indicates the direction of extension between the rift margins; EH1 is the direction maximum extensional strain; modified from Withjack & Jamison (1986).

Therefore, it could be inferred that the deformation in the Hatay Graben reflects oblique extension, where  $\alpha$  is approximately  $30-45^\circ$  (Fig.7.49) thus accounting for the three principle directions (N-S; NE-SW and NW-SW) of faulting observed. However, this does not explain the large number of strike-slip faults found within the Pliocene sediment fill. The concentration of faults suggests that the axial zone of the graben was an area of strike-slip faulting and related block rotations during the Pliocene to recent period.

A possible explanation for this is that the axial zone of the graben is dominated by siliciclastic sediments compared to the margins that are dominantly carbonates; however, in

section 6.7 it was shown that there is no evidence for stress compartmentalisation between lithologies and therefore, there should be no difference between the deformation style of the margins and axial zone of the graben. An alternative explanation is that the strike-slip faulting took place in the post-Pliocene times under a tectonic regime where  $\alpha \leq 15^\circ$ , thus resulting in the formation of only strike-slip faults, and was concentrated in the axial zone of the graben as it is a pre-existing zone of weakness. This would imply that the angle of extension,  $\alpha$ , has been decreasing since the Middle Miocene, resulting in a change in the style of faulting over time from normal to strike-slip faulting.

An alternative explanation could be that the strain has become partitioned, where regions of strike-slip faulting are separated from regions of normal faulting. This is common in transtensional regimes and has been recognised along the NAFZ (McNeill et al. 2002) and along the San Andreas Fault system (i.e. Schweickert et al. 2004). Strain partitioning occurs when transextensional strain is accommodated by two concurrent styles of faulting. In this case the normal component of the strain is accommodated along the graben boundary faults and the strike-slip deformation is concentrated in the graben floor and is expressed mainly as minor faulting. If this were the case for the Hatay Graben this may indicate that the strike-slip faulting is a surface expression of a major through going strike-slip fault at depth. This is somewhat corroborated by GPS vectors, when the reference frame is Arabia it appears that the areas to the north and the south of the Hatay Graben are moving independently again suggesting a major strike-slip zone. However, when the reference frame is Anatolia there is no difference in vectors. So although there is some evidence for the presence of a major strike-slip fault more evidence is needed.

The evidence of faults within the Quaternary gravels and the record of past and present seismicity show that this area is still experiencing active deformation. Calculated focal mechanisms show that earthquakes in the area are the result of oblique-slip motion, with a dominantly normal component of motion. This does not fit well with other observations made. However, only a few earthquakes have been observed and faulting in the Quaternary sediments are not all dip-slip, so it could be that the small data base of focal mechanisms is giving an erroneous impression of the style of present tectonics.

The presence of E-W trending faults is not adequately explained by this paradigm; therefore, these faults may be the surface expression of reactivated basement faults as E-W trending faults are common within the underlying ophiolite (Jenny Inwood pers. com.).

### **7.13 Conclusions**

- Growth faults indicate that normal faults were active from the Middle Miocene time onwards.
- Present seismicity shows that motion on faults is still occurring at the present time.
- Normal and strike-slip faults are the most common faults observed in the Hatay Graben, but oblique and reverse faults are also present.
- Cross-cutting relationships are inconclusive.
- Prior to the Late Miocene/Early Pliocene there was no topographic graben present in this area during this period the area was in a foreland basin setting; however, some normal faulting was taking place but did not form significant topographic relief.
- We propose that the present topographic Hatay Graben formed as a result of transtensional stress since the Pliocene.

## Chapter 8



Scene on the river Orontes near Suadeah.

## 8 Tectonic Geomorphology of the Hatay Graben

### 8.1 Introduction

As shown in the previous chapter (Chapter 7) the Hatay area at the present time is tectonically active with earthquakes recorded in the region. Fault motion will affect the geomorphology of a given area; therefore, it seems likely that if faults controlling the Hatay Graben are still active then this will be reflected by observable features. The aims of this chapter are to demonstrate that faulting is still active at the present time and, if possible, to identify which faults are currently active by looking at various geomorphological aspects of the Hatay Graben.

In recent years there has been increased interest in using geomorphology to investigate the neotectonics of actively deforming regions (Leeder & Alexander 1987; Merritts & Vincent 1989; Leeder & Jackson 1993; Collier *et al.* 1995; Goldsworthy & Jackson 2000) through the use of a number of different methods, e.g., stream profiles, drainage patterns.

Here, observations on river terraces and landforms related to the Plio-Quaternary uplift of the graben will be described, but the main focus of the chapter is on the drainage patterns of the study area and the longitudinal profiles that have been constructed for a number of specific streams. Both of these methods can lead to a greater understanding of the relative timing of recent tectonic events. In addition, terrace levels can provide information on the rate of uplift taking place in the area.

The Hatay Graben is orientated NE-SW and is bounded to the NW by the Kızıl Dağ, a range of mountains that extends northwards for about 80km and rises sharply from the Mediterranean Sea and the Gulf of Iskenderun to ~1800m in height. To the SE the basin is bounded by the Ziyaret Dağ, which rises to ~1300m. The Hatay Graben, situated between these mountains ranges, is a topographic low formed due to transtension along dominantly normal faults forming an asymmetrical graben. The basin floor in the northeast is relatively smooth and level linking with the Amik Plain, at 160m in altitude. The surface dips at ~0.001° (calculated using the difference in elevation between the coast and the Amik Plain) towards the present coastline. Towards the coast the Asi Nehir and smaller streams

increasingly erode into the Neogene sedimentary fill resulting in significant dissection and irregularity of the topography.

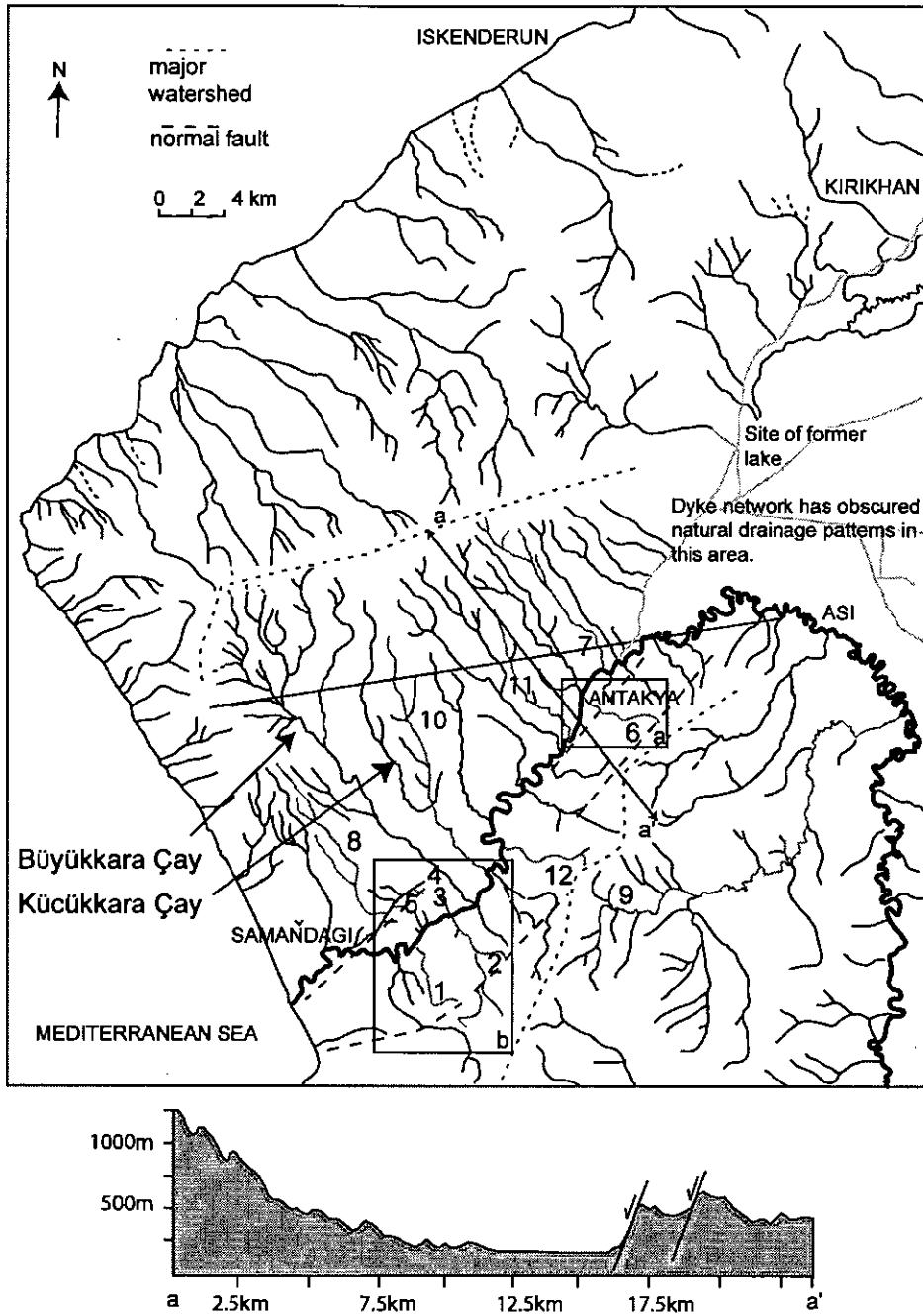


Figure 8.1. Map of the Hatay region of Southern Turkey showing the location of some of the places and features referred to in the text and the drainage pattern of the area. Numbers refer to the streams discussed in section 8.3 and the boxes show the locations of a. Fig. 8.4 and b. Fig. 8.5. Line a-a' is a topographic profile across the north of the graben showing the difference between the northern and southern margins, only graben-boundary faults are shown.

### 8.1.1 Coastal terraces

Coastal terraces have been documented in the Hatay Graben (Pirazzoli *et al.* 1991; Erol & Pirazzoli 1992) and wave cut notches were taken as evidence for former sea-levels. Pirazzoli *et al.* (1991) found evidence of two former sea-levels at 0.7-0.8m asl (above present sea level) and 2.0-2.2m asl to the south of the Asi Nehir and at  $1.0\text{m} \pm 0.3\text{m}$  and  $2.5\text{m} \pm 0.3\text{m}$  near the town of Çevlik.

Pirazzoli *et al.* (1991) additionally sampled biogenic material from some of these features and dated them by the radiocarbon method. Assuming these dates are accurate, this places the highest notch ( $\sim 2.5\text{m}$  asl) as having formed at  $5170 \pm 190$  to  $2595 \pm 100$  yrs B.P and the lower ( $\sim 0.75\text{m}$  asl) at  $2910 \pm 95$  to  $1345 \pm 70$  yrs B.P (radiocarbon dating; Pirazzoli *et al.* 1991). From these figures rates of uplift relative to sea-level can be calculated. The higher notch has been uplifted at  $0.4 - 1 \text{ mmyr}^{-1}$ , whereas the lower notch has been uplifted at  $0.25 - 0.55 \text{ mmyr}^{-1}$ , suggesting an average rate of uplift in the order of  $0.55 \text{ mmyr}^{-1}$ . Interestingly this figure is very similar to the rate of displacement on the Karasu Fault zone estimated near Kırıkhan of  $0.69 \text{ mmyr}^{-1}$  (Rojay *et al.* 2001). It has been suggested that the two notches correspond to discrete uplift events (Erol & Pirazzoli 1992) although the overlap in the ages of the two notches may cast some doubt on this idea.

The remains of the Roman harbour of Seleucia Pieria have also been used to document recent uplift (Pirazzoli *et al.* 1991; Erol & Pirazzoli 1992). The remains of the Roman structure now lie on the coastal plain  $<10\text{m}$  asl near the town of Çevlik. Pirazzoli *et al.* (1991) identified *Lithophaga* boring and attached oyster shells at a maximum elevation of  $0.75\text{m}$  asl, which they dated at  $1345 \pm 70\text{yrs}$  B.P. However, when I visited the harbour it was not clear if these blocks were *in situ*. Seleucia Pieria ceased to be used as a port after 596 C.E. (Common Era) following a destructive earthquake (section 7.10.1.; Guidoboni 1994). This date is within error of the age obtained for the oyster sample perhaps indicating a link between these events.

Pleistocene shorelines have also been described from the field area (Erol 1963; Pirazzoli *et al.* 1991; Erol & Pirazzoli 1992). Although I attempted to locate these features, the grid references given in Pirazzoli *et al.* (1991) proved to be inaccurate. Erol (1963) documented a marine notch in an uplifted marine cliff at  $45\text{m}$  asl. They considered the base of the cliff to be a shoreline of Tyrrhenian age ( $\sim 260 - 10 \text{ ka}$ ), but the age of the shoreline is not further constrained. Due to the large age range given for the terrace and the fluctuations in the

eustatic sea-level due to glaciation, it is impossible to calculate a valid rate of uplift for this feature. Using average values a rough figure of  $0.45 \text{ mmyr}^{-1}$  can be gained and although this is similar to rates calculated for the younger notches it is questionable how accurate this is. Pirazzoli *et al.* (1991) also document a beach deposit at 60m asl and a wave cut notch at  $12.2 \pm 0.3\text{m}$ . There is no dating evidence for these features.

### 8.1.2 River Terraces

The Neogene sedimentary fill of the Hatay Graben has undergone significant Quaternary river incision that has resulted in the formation of river terraces, which form distinct planar surfaces. The tops of these terraces are capped by Quaternary alluvium (sections 4.2.12 and 5.7). To the NE of the Büyükkaçay valley (Fig. 8.1) there are four terrace levels: T0 is the highest and oldest terrace level and T3 the present river level. F0 is the highest terrace level observed and forms the top of linear ridges formed through river incision towards the Asi Nehir. These ridges generally trend N-S from ~290-200m with some trending NE-SW from ~250-150m in height. There is some variability in the height of the terraces but in general the height of each ridge is similar along the strike of the graben. T1 is at ~150-100m and T2 at ~130-90m. T0 may represent an older (Late Pliocene?) land surface that has been fluviially incised forming river terraces T1-T3.

To the SW of the Büyükkaçay valley terraces are found within a bowl-shaped erosion surface (~150m) eroded into the Pliocene and Upper Miocene sediments; aeolian sandstone were observed plastered onto this surface (Section 4.2.12). There are five distinct planar surfaces: T0 into which the bowl shaped erosion surface has been cut; T1 at ~100-130m elevation, T2 at ~70-90m, T3 at ~60m and T4, the present delta plain at 20-0 m. This area of incision extends to the end of the central graben high (Fig. 8.3).



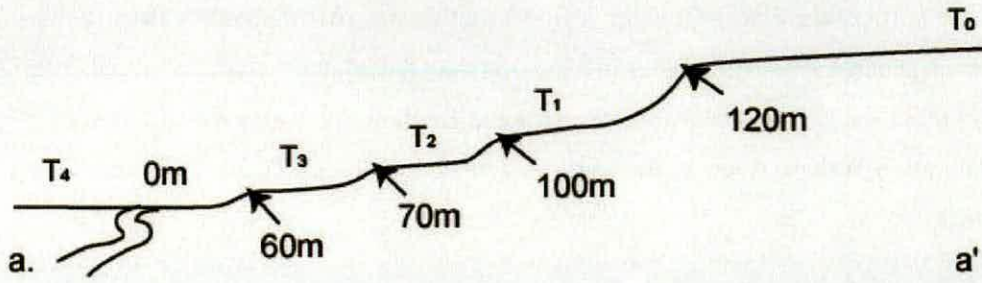


Figure 8.2. Profile showing the form of the river terraces observed in the Hatay Graben, terrace heights are variable and given in the text but the approximate height of the inflection points are given for the different terraces. The line of the section is shown on Fig. 8.3 below.

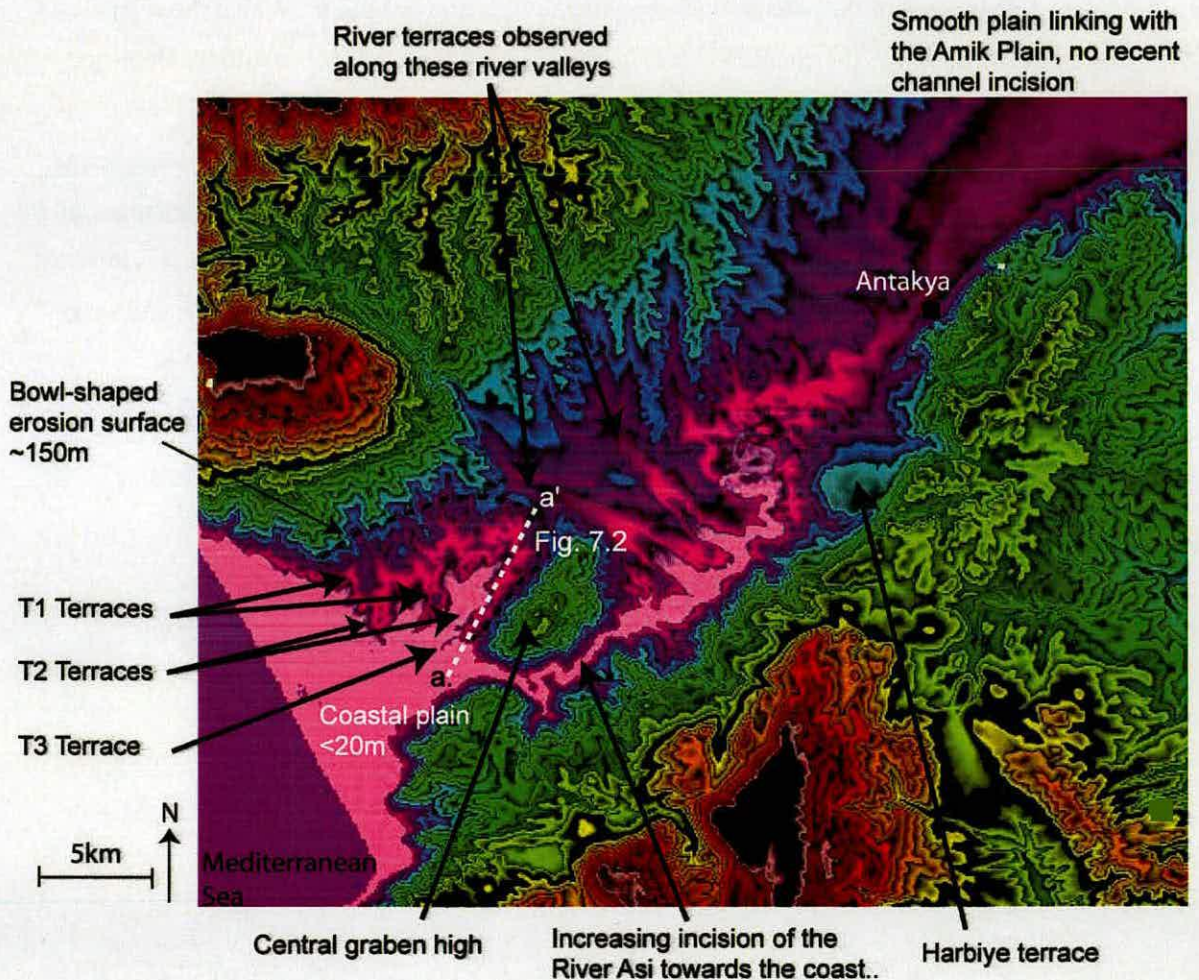


Figure 8.3. Digital topographic image of the Hatay Graben showing some geomorphic features. Black lines indicate 10m contour lines.

The Büyükkaraçay is an interesting feature; this is a river that drains a large area of the ophiolite to the north of the Hatay Graben. It flows southeast across the graben floor to the Asi Nehir but is generally 10-30m higher in elevation than the adjacent river, the Küçük kara Çay. Both of these rivers have steep southwestern and gentle northeastern margin, possibly indicating migration of these rivers to the southwest towards the present coast and parallel to the graben margin.

On the gentle northeast margin of the Büyükkaraçay a series of three river terraces can be observed above the present level of the river; the original erosion surface sloped to the southeast towards the Asi Nehir (170-90m), T1 20m below this level and T3, the modern river level, 10m below this. River terraces are only observed where the river cuts through the soft sediments of the graben floor, creating a wide alluvial plain. Where the river flows through the ophiolite the channel is very narrow and no terrace levels could be identified.

These terrace levels observed in the Hatay Graben may be equivalent to those observed in Cyprus, as these areas are geographically close such that the eustatic sea-level changes might be similar; although the tectonics effecting the areas are not the same i.e. Cyprus is affected by uplift of the Troodos Ophiolite versus the Hatay Graben is affected by uplift and strike-slip, so it is unlikely that this would be the case.

## 8.2 Drainage Patterns

The drainage evolution of tectonically active regions has attracted much attention in recent years; for example, drainage evolution has been studied in fold and thrust belts (Burbank *et al.* 1986; Jackson *et al.* 1996; Keller *et al.* 1999) and in extensional grabens (Paton 1992; Leeder & Jackson 1993; Goldsworthy & Jackson 2000; Zelilidis 2000) in order to understand how active tectonics affects drainage patterns but also how drainage patterns can be used to document the evolution of fault propagation over time. In this section the drainage pattern of the Hatay Graben will be described, mainly through the use of topographic maps, and then related to the development of the large basin-bounding faults in order to try and identify active faults.

In general, streams can be classified into four types (redefined by Seger & Alexander 1993): antecedent, reversed, captured and juvenile. Antecedent drainage is when a river has maintained its original direction of flow across later tectonic topography. Reverse drainage is when the flow direction along part of a river is reversed, caused by tectonic deformation of the riverbed. Reversed drainage consists of two opposing drainage components: a misfit and a reversed element; the area between these two elements, termed a 'wind-gap', is a dry valley. Capture is used for drainage when the flow direction of the reverse drainage elements returns to the original flow direction. Juvenile drainage basins consist of small incising and headward eroding streams.

### 8.2.1 General Characteristics

The Hatay Graben exhibits many of the characteristics of an asymmetric block-faulted terrane, i.e. steep footwall slopes and long, gentle hangingwall slopes (Leeder & Jackson 1993). Thus, the streams on the hanging wall are long with a well-developed network of tributaries, but the general morphology of the valleys is linear. These streams are well incised forming steep narrow valleys within the ophiolite but opening out and forming broader valleys in the softer Neogene sediments of the basin floor. The topographic profile shows that the soft Neogene sediments have undergone greater erosion than the harder ophiolitic ones (Fig. 8.1). The valleys on the hangingwall of the graben, cut far to the northwest with the drainage divide being 12-24km (Fig. 8.1) from the confluence with the River Asi. The length of these streams and the number of tributaries decreases towards the NE (Fig 8.1).

In contrast, footwall streams are shorter (by 4/5 to 2/3) and do not have as many tributaries but have incised deeply into the sediments, although the amount of incision does vary along the margin probably due to the different lithologies present in the footwall. Serpentinite and limestone are the most common lithologies present; in these areas juvenile streams are generally much shorter than those in softer marls probably due to the difference in hardness. The drainage divide is much nearer to the southeast margin of the graben (Fig. 8.1), on average 4-8km, than it is on the hangingwall. Although there are numerous footwall catchments, alluvial fans are not developed in this area. This may be due to low sediment flux preventing fans from forming or the erosive power of the River Asi, removing the sediments before a fan could form. As there is no evidence for the presence of alluvial fans in the Hatay Graben, the former seems likely.

The River Asi enters the Hatay Graben east of Antakya at the end of the graben (Fig. 8.1), at the termination of a number of fault segments, and then flows along the southeast side of the graben occupying an asymmetrical position within the valley close to the boundary faults. This is because the position of the river is determined by the area where the rate of subsidence is greatest. A similar relationship has been observed in other regions of active normal faulting, such as the Basin and Range province of the USA (Leeder & Alexander 1987; Leeder & Jackson 1993), where the valley floor is tilted towards the main fault(s). The river flows within the graben floor until the area of the Karaçay, where the boundary faults overlap and step into the graben. Here the river flows into a gorge that has been incised into the uplifting footwall of the fault block. This suggests that the river is following its original course and the rate of erosion is greater than the rate of footwall uplift (Fig. 8.8).

Many of the larger streams enter the graben at the end of fault segments. For example, the Karanlık Dere (Fig. 8.8) enters the graben at the end of two fault segments. The southerly fault there is a break of ~1.5km, and to the north near the River Asi there is a fault offset of ~2km. Other large streams that enter the graben at the end of fault segments include Harrup Dere (Fig. 8.8) and catchment B on Figure 8.5. Rarely streams cut across faults, i.e. the stream to the east of Antakya (Fig. 8.5).

Dry valleys were observed in a number of different locations along the south-eastern margin of the graben. These dry valleys, along with the upper reaches of some active streams, have a broad U-shaped profile. Whereas active streams in this area generally have a steep V-shaped profile. The transition between these two profiles when observed is often marked by the presence of a waterfall (Fig. 8.4). This change to greater incision of channels may reflect increased rates of uplift causing the streams to erode faster or a change in climatic conditions.

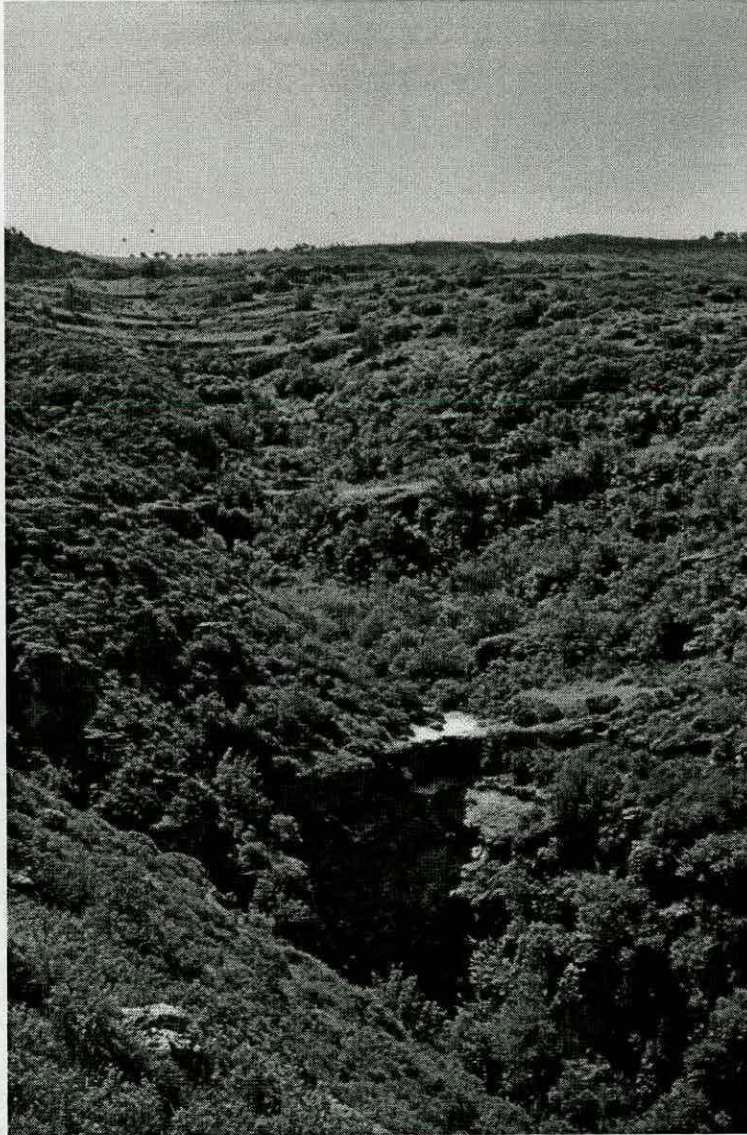


Figure 8.4. Photograph of seasonal valley to the east of Antakya. The upper part of the stream course has a broad U-shaped profile, while the lower reaches are more deeply incised. View is to the southeast.

### 8.2.2 Antakya Basin

There is a small basin (<25 km<sup>2</sup>) present to the east of Antakya, 250-400m above sea-level in the footwall of the innermost boundary fault of the Hatay Graben (Fig. 8.5). Eocene limestones form the crests of the rotated fault blocks. These limestones are unconformably overlain by Lower Miocene and younger sediments. The Lower Miocene sediments dip to the SE (towards the outer graben boundary fault) at 10-20°. In contrast, the younger sediments dip to the southwest at ~15°. This suggests that the Lower Miocene sediments pre-date block rotation, whereas the younger sediments post-date fault motion causing rotation into the outer fault. The age of the younger sediments is poorly constrained but may be Late Miocene.

These Neogene sediments are being eroded by a series of drainage networks; in particular, the central part of the basin is being drained by two catchments, A and B (Fig. 8.5), whose tributaries are eroding the basin fill and extending back into the footwall of the outer fault. The tributaries of these catchments flow axially until they find their escape across the innermost graben-bounding faults. Catchment A goes through a gorge cut into the limestone, coincident with a dogleg in the strike of the fault that maybe a small offset. By contrast, catchment B escapes at a prominent offset zone in the innermost graben boundary faults at the end of the Antakya Basin.

This drainage pattern in an uplifted footwall basin is similar to that recorded for the Renginon Basin (Fig. 8.6), central Greece (Leeder & Jackson 1993; Collier et al. 1995). Similarities between the two areas are that both are Miocene-Quaternary aged half-grabens, which have been formed due to normal faulting and block rotations. These areas are being drained by streams some of which are eroding into the footwall of the outermost fault, and then escape through the innermost fault at a fault offset. The major difference between the two areas is the scale; the Renginon Basin is almost an order of magnitude larger than the Antakya Basin. In the Renginon Basin, the outermost fault has been shown to be inactive. The similarities between the Renginon and Antakya Basin suggest that the outermost faults of the Antakya Basin, and therefore the Hatay Graben, may be inactive too.

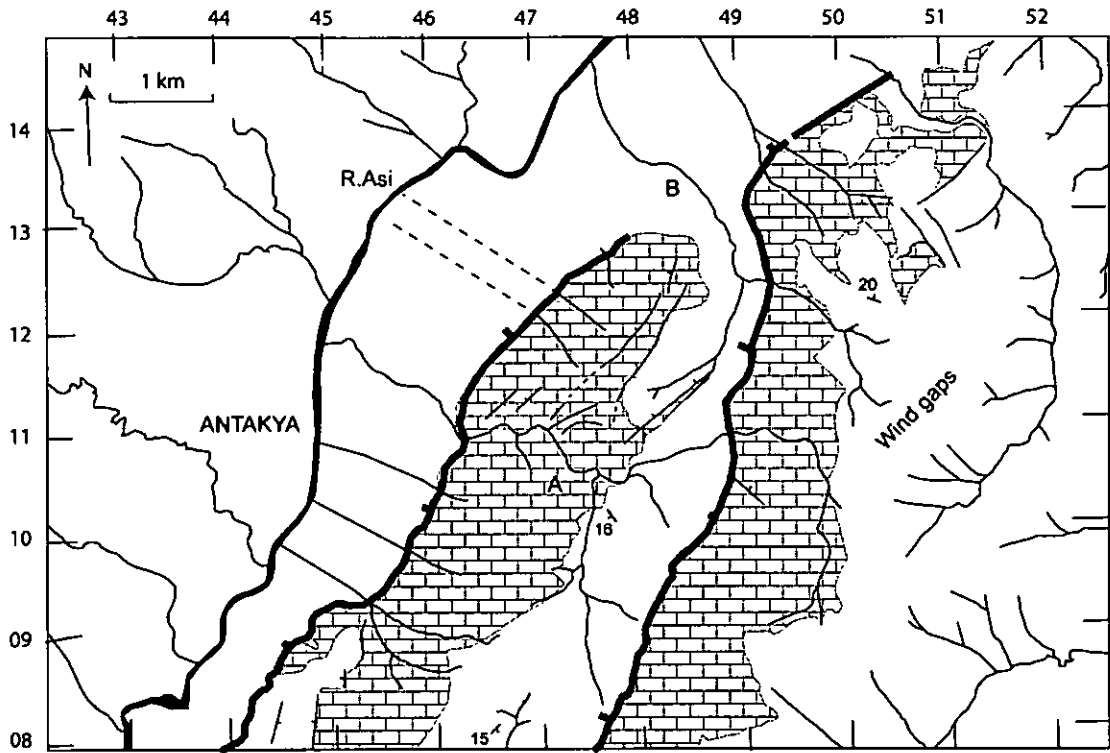


Figure 8.5. Drainage patterns of the Antakya Basin. Brick pattern indicates location of Eocene and older basement; white indicates Neogene sediments. From map sheet Antakya P33-d2.

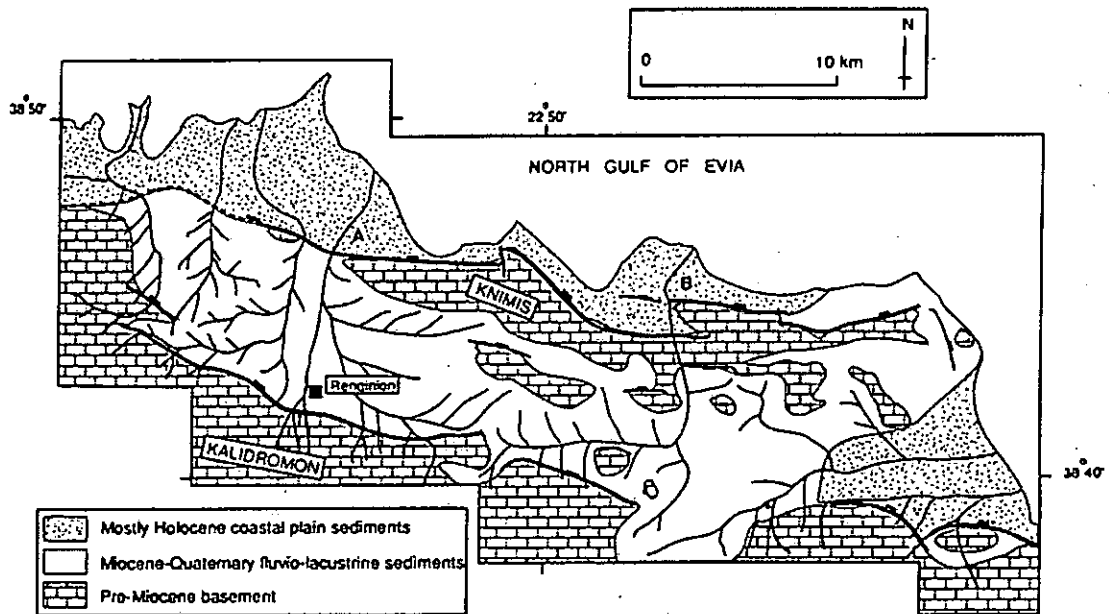


Figure 8.6. Faulting, geology and drainage in the Renginion and northern Gulf of Evia graben (from Leeder & Jackson 1993). Note the similarity in the morphology and drainage between this and the Antakya Basin but the difference in scale.

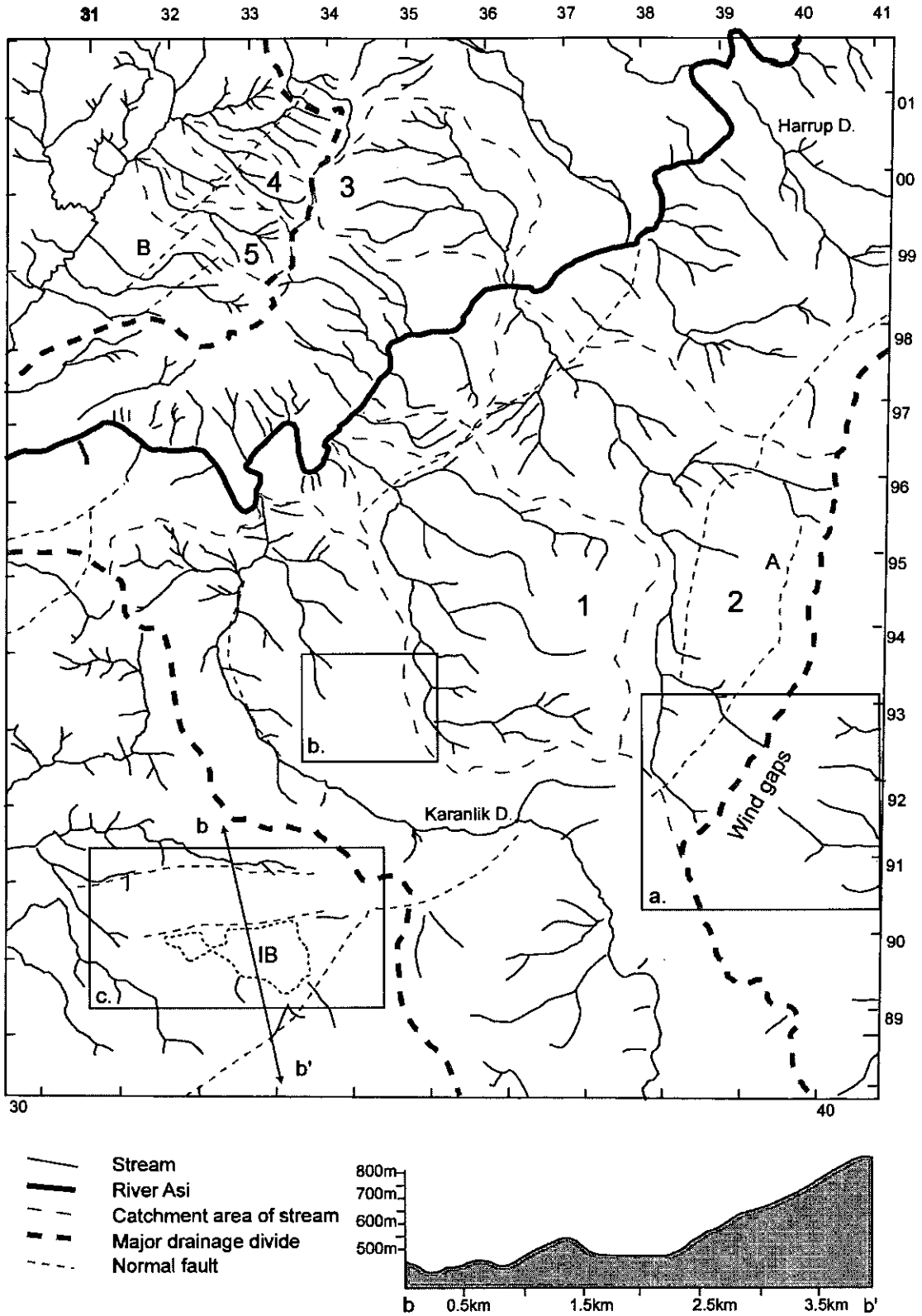


Figure 8.7. Streams, drainage divides and faults for map sheet Antakya P36-d4 (for location see Fig. 7.1). Numbers refer to streams discussed in section 7.3; boxes show location of a) Fig 7.9, b) Fig 7.12d and c) Fig. 7.11. Map sheet Antakya P36-d4.



## 8.2.3 Wind gaps and dry valleys

### 8.2.3.1 *Wind gap formation*

Wind gaps can develop when normal faulting cuts across the path of existing streams, the antecedent drainage. The stream will continue along the same route as long as footwall uplift is not greater than the erosive power of the stream. If this is the case then the part of the stream on the footwall will no longer be able to continue along the same course and will be diverted (reverse drainage). This will create a “dry valley”, the part of the valley between the part of the stream still following the original course and the reversed section, on the crest of the footwall; this is commonly called a wind gap (Burbank & Anderson 2001).

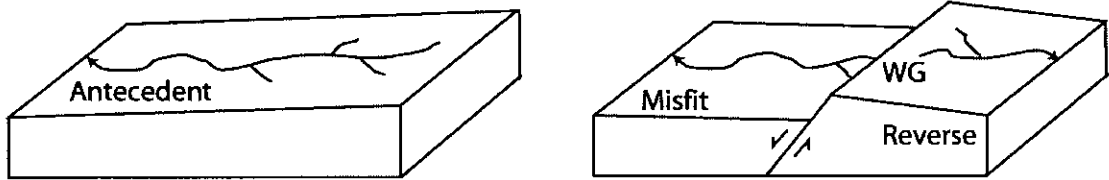


Figure 8.8 Block diagrams illustrating how a wind gap may form.

There are a number of places in the field area where dry valleys on the footwalls of normal faults can be observed. These topographic features often link valleys with streams flowing in opposite directions away from the dry valley; these are therefore considered to be wind gaps, although further fieldwork to confirm this would be beneficial. Many wind gaps are present along the drainage divide of Fault A (Figs. 8.7, 8.10) and are present on other fault segments on the same array. This array of faults forms the outer tectonic boundary of the Hatay Graben. Presently, the streams showing reversed drainage have the reversed element of the stream flowing dominantly to the east and into the Gharb depression. While the misfit part of the stream flows westwards into the Hatay Graben. The wind gaps are orientated perpendicular to the strike of the fault. In the north near Antakya (Fig. 8.5) wind gaps are generally orientated E-W while further to the south (Fig. 8.7) the wind gaps are more often orientated NW-SE reflecting the difference in the strike of the faults.

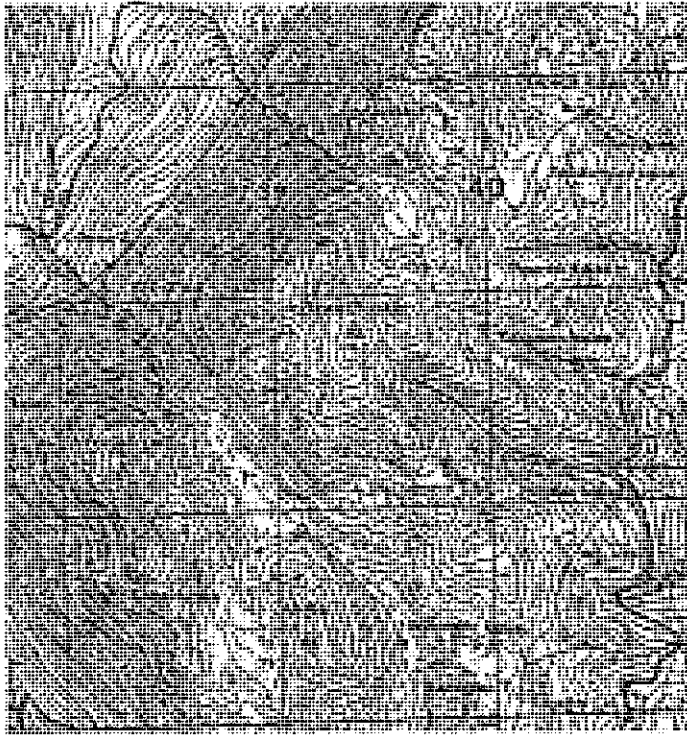


Figure 8.9. Topographic map with fault and stream lines highlighted. The dashed line indicates possible paths of antecedent drainage along dry valleys in the footwall of the fault. For the location of the map see Figure 8.7. Grid is 1km.

A striking feature related to the formation of wind gaps can be observed in the south of the field area (for location see Fig. 8.7, enlargement Fig. 8. 10). A flat area can be seen located between several large normal faults with three streams draining into the area. This is interpreted as a dry lake bed. It may have formed when footwall uplift (of the fault shown as a dashed line on figure 8.7) caused the drainage pathway of possibly three streams (two minor, one major) to become blocked due to the beheading of the antecedent drainage. The presence of another normal fault dipping northwards to the south of this fault prevented these streams from flowing to the south, resulting in the formation of an interior drainage basin as water could not drain away. The location of the lake was possibly controlled by the area of maximum subsidence on the fault. The floor of this basin is composed of terra rossa soil suggesting a Quaternary age for this feature. Similar internal basins have been described in the Gulf of Conrinth region, Greece (Morewood & Roberts 2002).

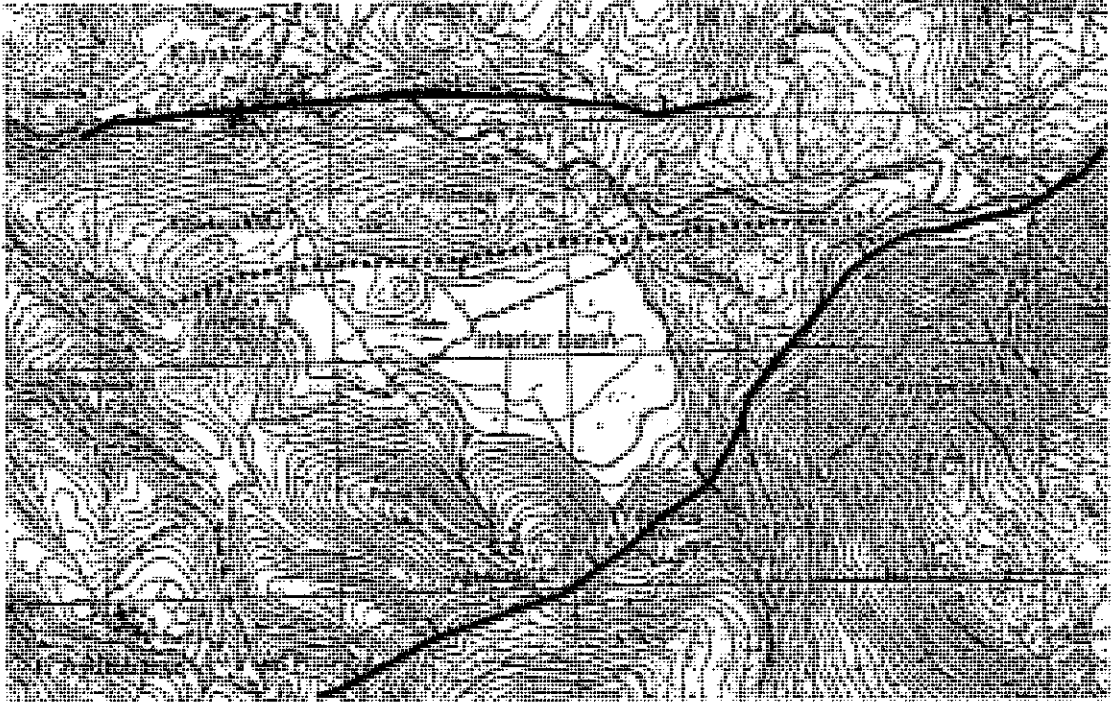


Figure 8.10. Topographic map showing faults and drainage around the interior basin described above; note location of basin next to faults. Thick lines are normal faults with direction of throw indicated; thin lines show drainage pattern; WG = wind gap.

#### 8.2.3.2 *Dry valley formation.*

In the south of the field area (Figs. 8.1 and 8.7), there are a number of faults within close proximity. In general, faulting creates stream systems that run perpendicular to the fault (Goldsworthy & Jackson 2000), and this can be seen on the large scale for the basin as a whole (Fig. 7.1). However, the hangingwall drainage in this area shows some modification, with several of the streams having a prominent asymmetrical shape to the drainage network. NNW-SSE streams receive all their catchments from the eastern side of the stream, perhaps suggesting that one set of streams has been superimposed upon the other.

Topographic maps indicate that there are a number of east-west orientated dry valleys present on the west side of the NNW-SSE streams, thus suggesting that these NNW-SSE streams are younger and have cross-cut and captured an older SE-NW drainage. The presence of a NNE-SSW trending graben-bounding fault to the east (Fig. 8.7, fault A), suggests that these older streams were influenced by a regional tilt to the west/northwest caused by motion on this and related faults. This suggests that at that time these streams

flowed axially down the basin and into the sea, as the streams on the far west of Figure 8.7 still do at the present time.

However, subsequent faulting has uplifted the eastern streams and blocked the route to the sea. As a response to this, the River Asi began downcutting into the sediments and the streams that originally flowed westwards were diverted to the north. See Fig 8.11a-c for illustrations showing the reconstruction of the formation of the drainage pattern.

Asymmetric drainage patterns have been observed in other areas, such as Greece (e.g. Goldsworthy & Jackson 2000); however, in this case the drainage had developed in the footwall drainage system and was the result of two successive phases of fault motion on faults with different orientations (see Goldsworthy & Jackson (2000) their Fig. 8).

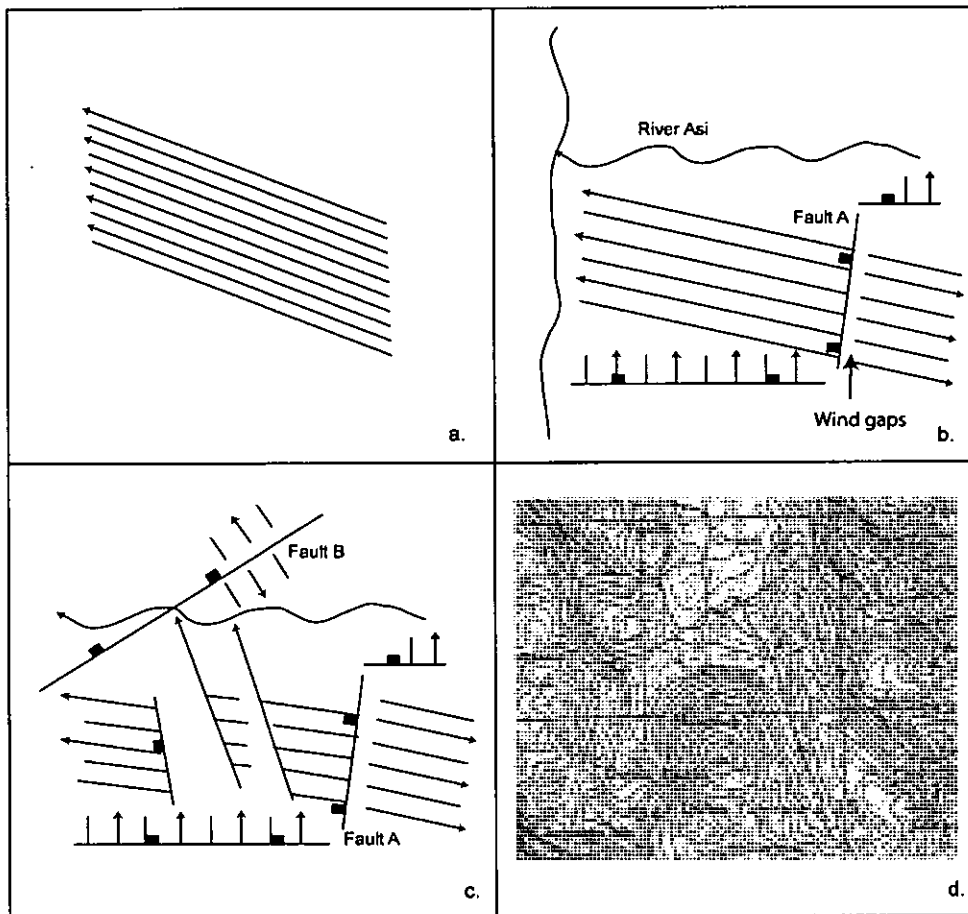


Figure 8.11. (a)-(c) Schematic cartoon showing a possible evolution to form the asymmetrical drainage patterns observed (Fig. 8.7), resulting from the superposition of a N-S stream network on a NW-SE one as a result of a change in the regional tilt of the land surface caused by a change in the orientation of active faulting. (d) Example of E-W orientated wind gap for location, see Fig. 8.7.

### 8.3 Karasu Rift

To the northeast of the Hatay Graben is the Karasu Rift, the geomorphological characteristics of this area are different to the Hatay Graben. The floor of the basin is relatively smooth with outcrop of Quaternary basalts, dated as between 2.10 to 0.05 Ma (Rojay et al. 2001; Parlak et al. 1998) and often the lavas infill pre-existing Quaternary valleys. The thickness of the basin floor sediments varies from <50m to >360m (Fig. 8.12), the sediment thickness generally increases towards the centre of the Amik Plain but sudden changes in the sediment thickness have been observed and interpreted as the result of buried faults (Rojay et al. 2001) probably normal (Tatar et al. 2004). The sediments are fluvial and lacustrine (Rojay et al. 2001) and interfinger with the lavas. No terrace levels were observed.

The flanks of the Karasu Rift are uplifted but the eastern and western margins are morphologically different. The western margin has high relief and an elevation of up to 2250m. In contrast, the eastern margin is lower, a maximum height of 800m. Along the western margin a series of large alluvial fans can be observed (Fig. 12), most are fan-shaped and unaffected by faulting. The morphology only one fan was observed to have been affected by faulting. The fan is situated next to a fault; uplift on the footwall has apparently caused the fan to have an asymmetrical shape due to topographic control on sediment dispersal. This is dissimilar to observations from other major strike-slip faults (i.e. Karakoram Fault; Burgess & Murphy 2003) where alluvial fans are offset by lateral motion along the faults. Slopes of 4° to 0.4° have been reported for the surfaces of these fans (Rojay et al. 2001).

The western margin of the Karasu Rift is controlled by the Amanos Fault, a sinistral strike-slip fault. A number of geomorphological features have been observed along its length including shutter ridges, beheaded streams, sag ponds and small-scale pull-apart basins (this study; Rojay et al. 2001).

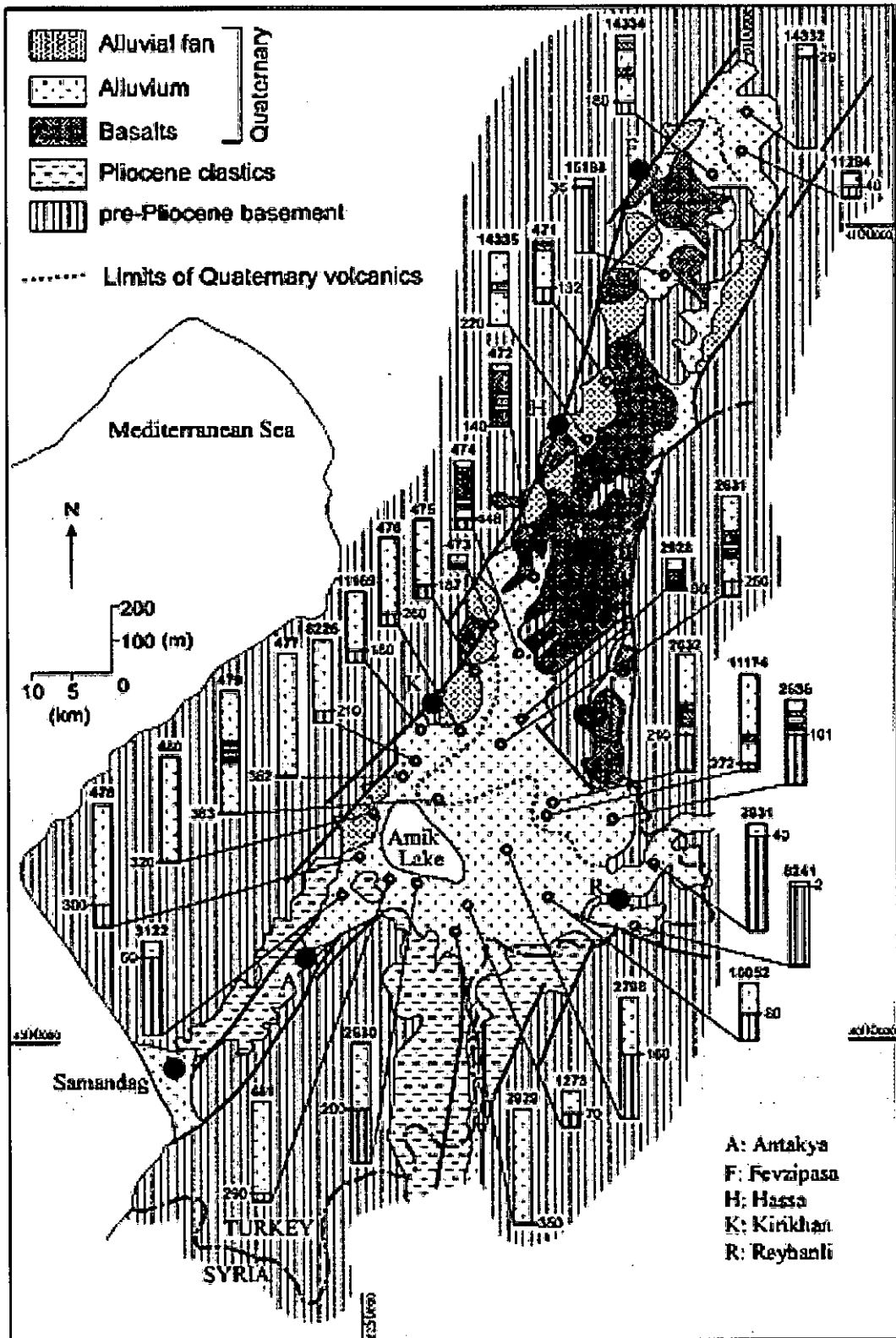


Figure 8.12. Borehole data from Karasu Rift. Number on top of sections refers to borehole number; number at the side of the section refers to the depth. Note that a simplified stratigraphy has been used (in Rojay et al. 2001 from a DSI report).

## 8.4 Stream Profiles

Longitudinal stream and river profiles have attracted the attention of a number of studies in recent years (Merritts & Vincent 1989; Demoulin 1988; Snyder *et al.* 2000; Tucker & Whipple 2002; Radoane *et al.* 2003). These have mostly been undertaken in areas of active tectonics where uplift rates are relatively well known, e.g. Mendocino triple junction area (Merritts & Vincent 1989). The rationale behind the study of stream profiles is that over time, rivers will equilibrate and form an 'ideal' river profile; a smooth concave longitudinal profile (Fig. 8.13). This smooth profile will develop in an unperturbed system due to the stream-gradient index (the progressive reduction in gradient linked to a progressive increase in discharge) remaining approximately constant.

Streams may not achieve an equilibrium profile for a number of reasons, such as variation in rock type and therefore hardness, contact with alluvial fans and incoming tributaries, base-level changes in short lived (fault-controlled) basins, climatic variations, neotectonics, i.e. zones of differential uplift or subsidence, etc. Therefore, when these variables are known, longitudinal profiles can prove useful in highlighting recent regional or local tectonic activity, as these will create irregularities in the profile known as 'knick-points' (Burbank & Anderson 2000).

Most work using this technique has focussed on tectonically active areas where uplift rates (Merritts & Vincent 1989), or the rates of slip on individual faults are known (Whittaker *pers. com.* 2005), and can then be used to determine how the fault motion has affected the river profiles. By contrast, the rates of motion on the faults are not known in this case and only approximate rates of uplift have been calculated; however, by constructing rivers profiles we can try to determine if known faults are still active and potentially identify faults that have not been identified in the field.

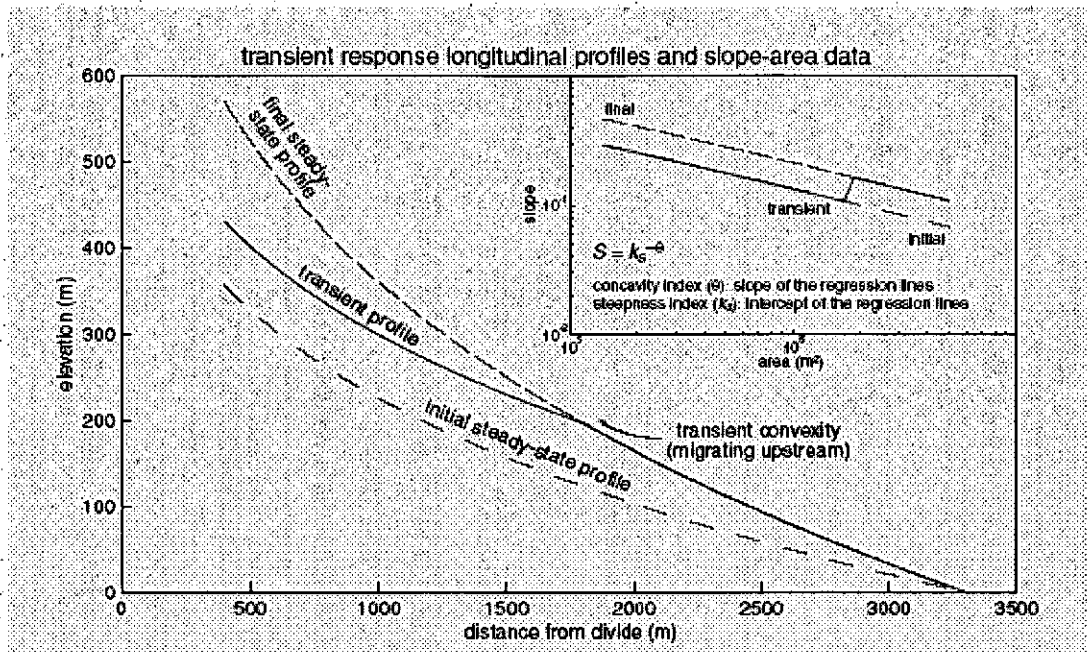


Figure 8.13. Example of a transient-state profile between initial low-uplift and final high-uplift zone conditions. Note the prominent convexity at the midprofile position. This knick zone migrates upstream as the channel responds to the uplift-rate change. Inset shows the slope-drainage area data for the three longitudinal profiles. Note that the channel concavity is the same for both the initial and final profiles, while the steepness is considerably higher for the final profile, from Snyder *et al.* (2000).

#### 8.4.1 Methodology

Twelve streams were selected for stream profile analysis (Fig. 8.1). These streams flow over potentially active normal faults, a strike-slip fault and an area presumed to have no faults present, representative of the different tectonic regimes of the Hatay Graben. Streams 1-8, 10-12 flow into the Hatay Graben either from the southeast or the northwest, with four on the hanging wall of the half-graben and eight in various locations along the footwall. Stream 9, by contrast, flows eastwards into the Dead Sea Fault Zone, and captures the drainage from the footwall of the faults. All streams flow into the River Asi, the major river in the area, which flows northwards through the Dead Sea Fault zone and then swings to the southwest and flows to the southwest through the Hatay Graben to the Mediterranean Sea.

Many studies of river profiles use DEMs (digital elevation models) of the field area to extract pertinent topographic data. However, it was not possible to obtain a high resolution DEM for the Hatay region. Therefore, longitudinal profiles were generated using detailed



1:25000 topographic maps. For all twelve streams, downstream distance was measured from the map and the elevation read off at each 10m contour. This length and height data were then used to calculate the change in height between each contour, thus giving reasonably accurate measurements of the gradients of the slopes.

The other important variable when considering stream profiles is the drainage area of the streams. For streams 1,7 and 8 the drainage area was measured from the map at points downstream by drawing lines around the catchment areas based on where watersheds are located and then measuring the incremental increase in area at regular intervals.

## 8.4.2 Results

River	Length (m)	Z <sub>0</sub> (m)	Z <sub>1</sub> (m)	ΔH (m)
1	6550	690	20	670
2	7975	950	20	930
3	4475	320	25	295
4	2050	365	45	340
5	2350	360	37	323
6	3812.5	300	90	210
7	10350	900	85	815
8	7625	900	40	860
9	6025	440	120	320
10	19875	650	30	620
11	12387.5	400	100	300
12	6962.5	490	50	440

Table 8.1. Longitudinal data for the nine rivers investigated, where Z<sub>0</sub> is the initial elevation of the stream absl, Z<sub>1</sub> is the elevation of the stream when it enters a major stream, ΔH is the change in height between Z<sub>0</sub> and Z<sub>1</sub>.

River	C	Θ	R <sup>2</sup>
1 – total	0.0869	0.4951	1
1 – oversteepened	38.744	2.922	0.8939
1 – above fault	0.1556	0.1213	0.4497
7 – total	0.252	0.9073	0.7689
8 – total	0.0109	0.8389	1
8 – oversteepened	0.6016	1.608	0.7729
8 – above fault	0.1831	0.0345	0.0101

Table 8.2. Data on the catchment areas for the three streams studied. C is the intercept with the x axis ;θ is the concavity of the stream; R<sup>2</sup> is measure of how well the line fits the data.

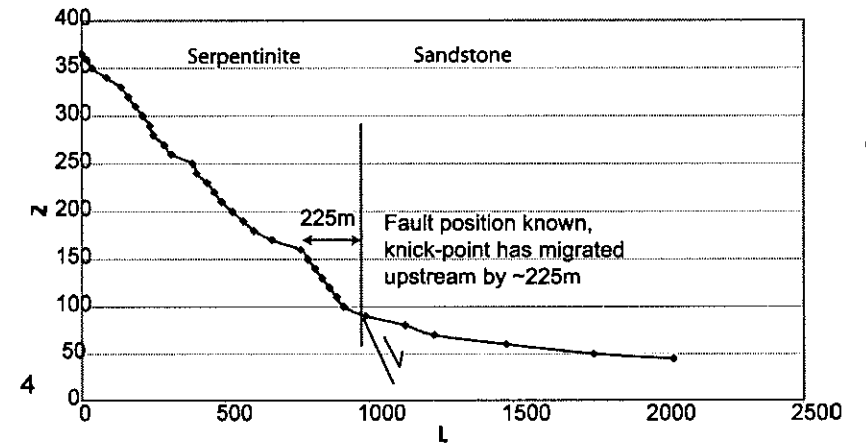
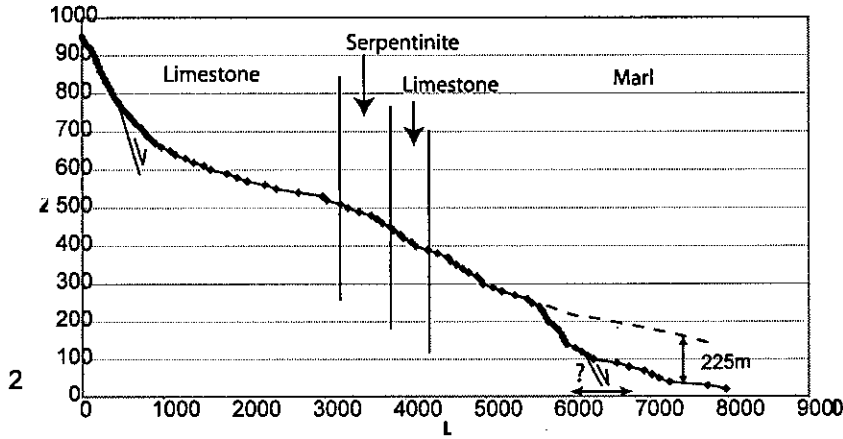
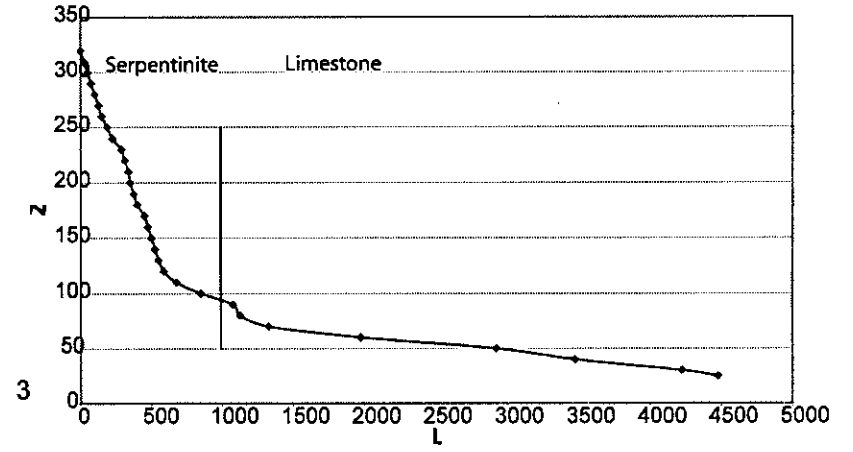
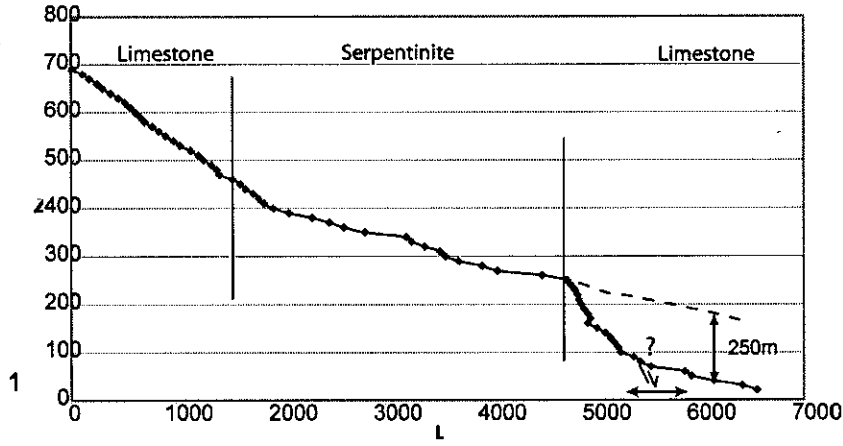
The form of the river profiles in the study area varies from those that are smoothly concave to relatively linear (Fig.7.14). Streams 7, 10 and 11 exhibit a smooth concave profile, whereas streams 8 and 9 are almost smooth curves but with some perturbations in the upper reaches. Streams 3, 4, 5 and 6 have steep linear upper reaches to the profile. These streams are quite short and probably represent debris-flow processes (Stock et al. 2005). Streams 1, 2, 5, 6 and 12 have a more irregular shape due to the presence of knick-points. When the position of lithological boundaries and confluences with tributaries are considered there is no apparent correlation. However, there does appear to be a correlation with the position of known faults. There are a few knick points that do not correlate with known features. Therefore, it is suggested that these knick points are surface expression of faults that have no escarpment, due to either weathering of the fault plane or they are blind faults.

A graph of drainage area versus slope gradient for stream 7 shows an inverse trend with little scatter,  $\theta = 0.91$ . It is important to note that although stream 7 has lithological variations present there are no knick points, indicating that lithology is not exerting a control on the formation of these features. When streams 1 and 8 are considered these too show an inverse trend with a  $\theta$  of 0.50 and 0.84, respectively. These data can be split into two sets corresponding to the slope of the profile above and below the knick point. This shows that the concavity ( $\theta$ ) above the knick point is small (stream 1  $\theta=0.12$ , stream 8  $\theta=0.03$ ), whereas below the knick point in the oversteepened area  $\theta>1.5$ . The variation in  $R^2$  indicates some variability in these relationships.

Dividing the data into two sets when considering the area-slope data for streams 1 and 8 seems to be justified due to significant difference in concavity between the two sets; this can also be seen when length-slope plots are considered. These show a considerable spread of data to which one straight line cannot be fitted; this is in contrast with the length-slope plot from stream 7 where the data do plot as a straight line. Catchment area-length plots show a normal relationship with catchment area increasing downstream.

Following three pages; Figure 8.14. Downstream length (L) against altitude (Z) for the twelve streams investigated in the field area (graphs numbered 1-12). Lithological changes and fault locations are marked on the graphs. Faults marked with a question mark indicate knick points that may be fault-controlled but no fault was directly observed at that location. Stream 9 is the river which is capturing drainage around the footwall of the southeastern basin margin.

Fig. 7.14



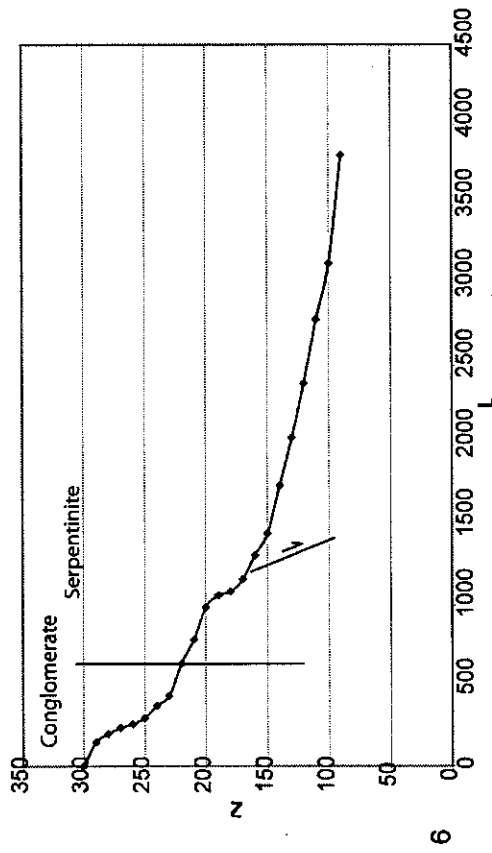
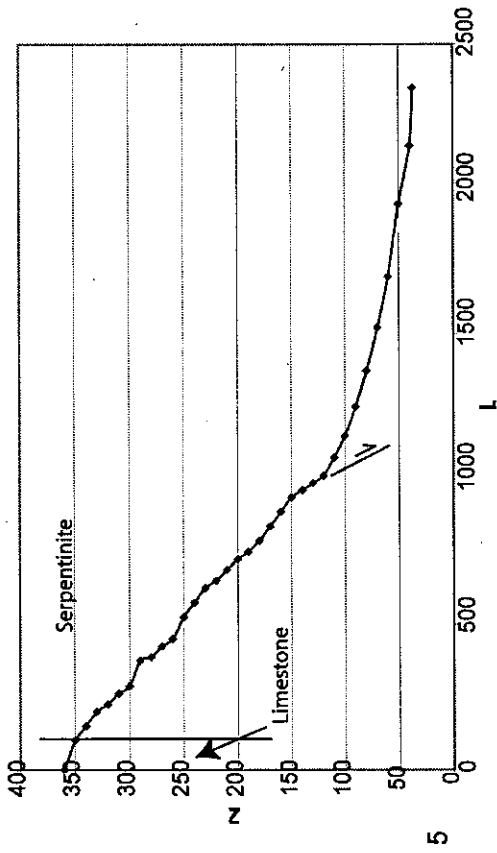
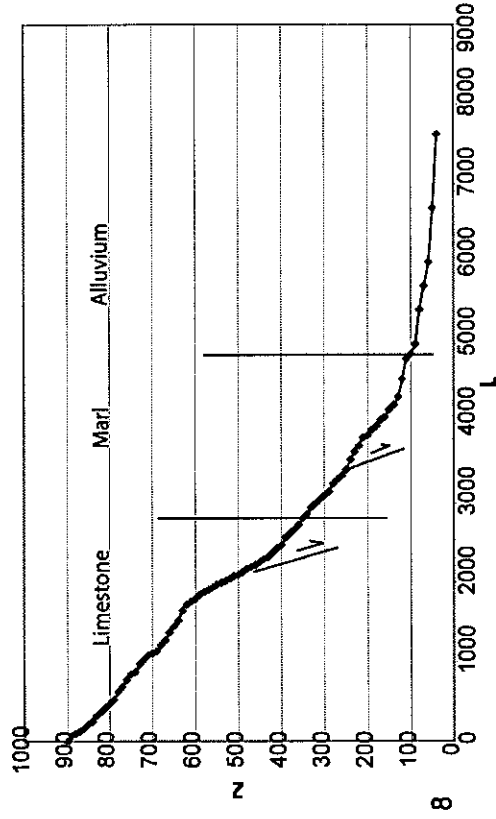
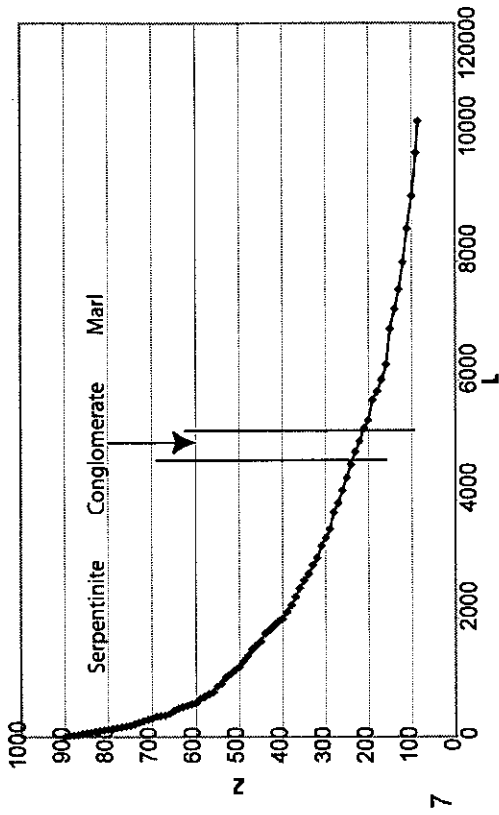


Fig. 7.14 cont.

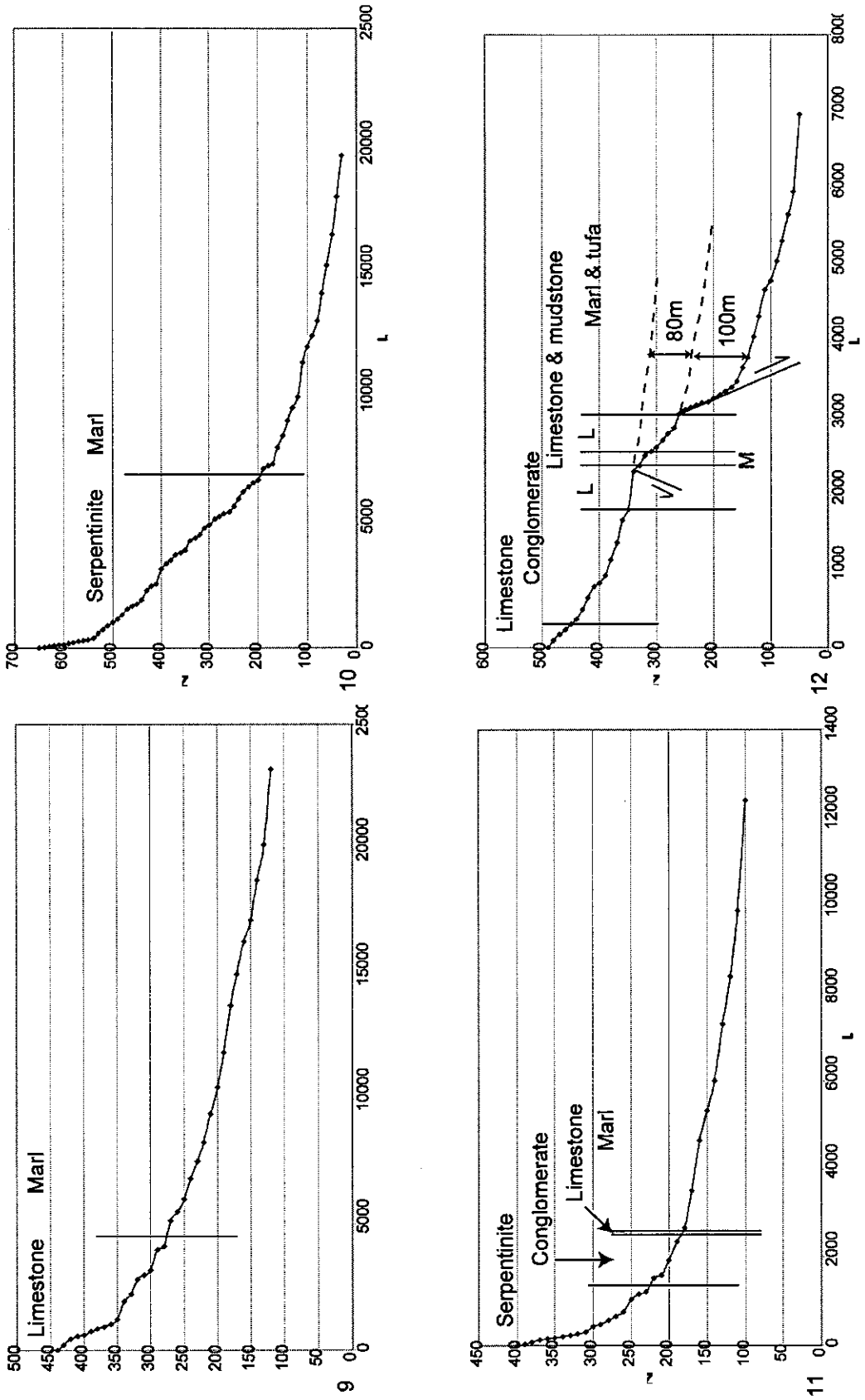


Fig. 7. 14 cont.

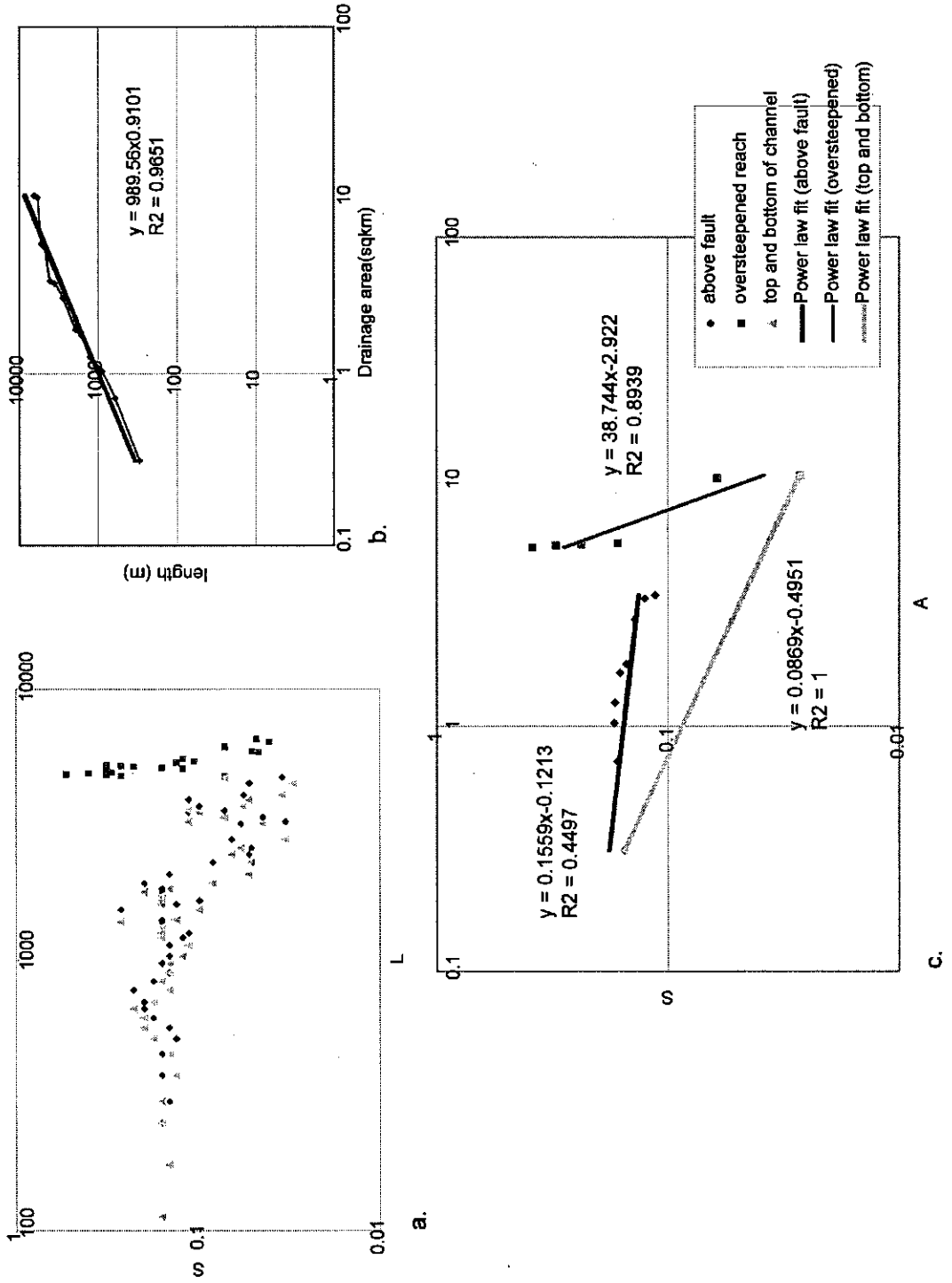


Figure 8.15. Stream 1: a) length vs. slope, b) drainage area vs. length, c) drainage area vs. slope.

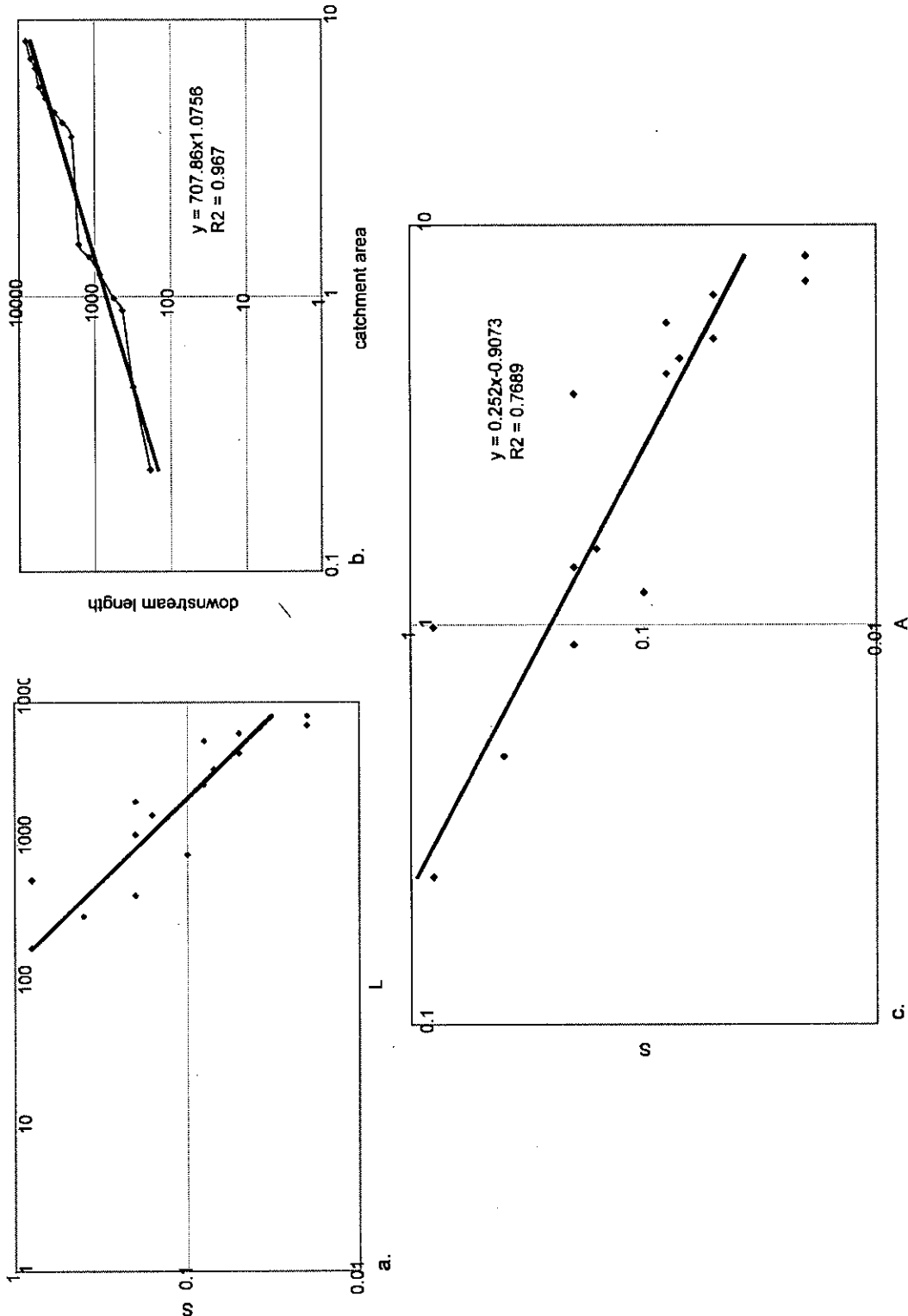


Figure 8.16. Stream 7: a) length vs. slope, b) drainage area vs. length, c) drainage area vs. slope.

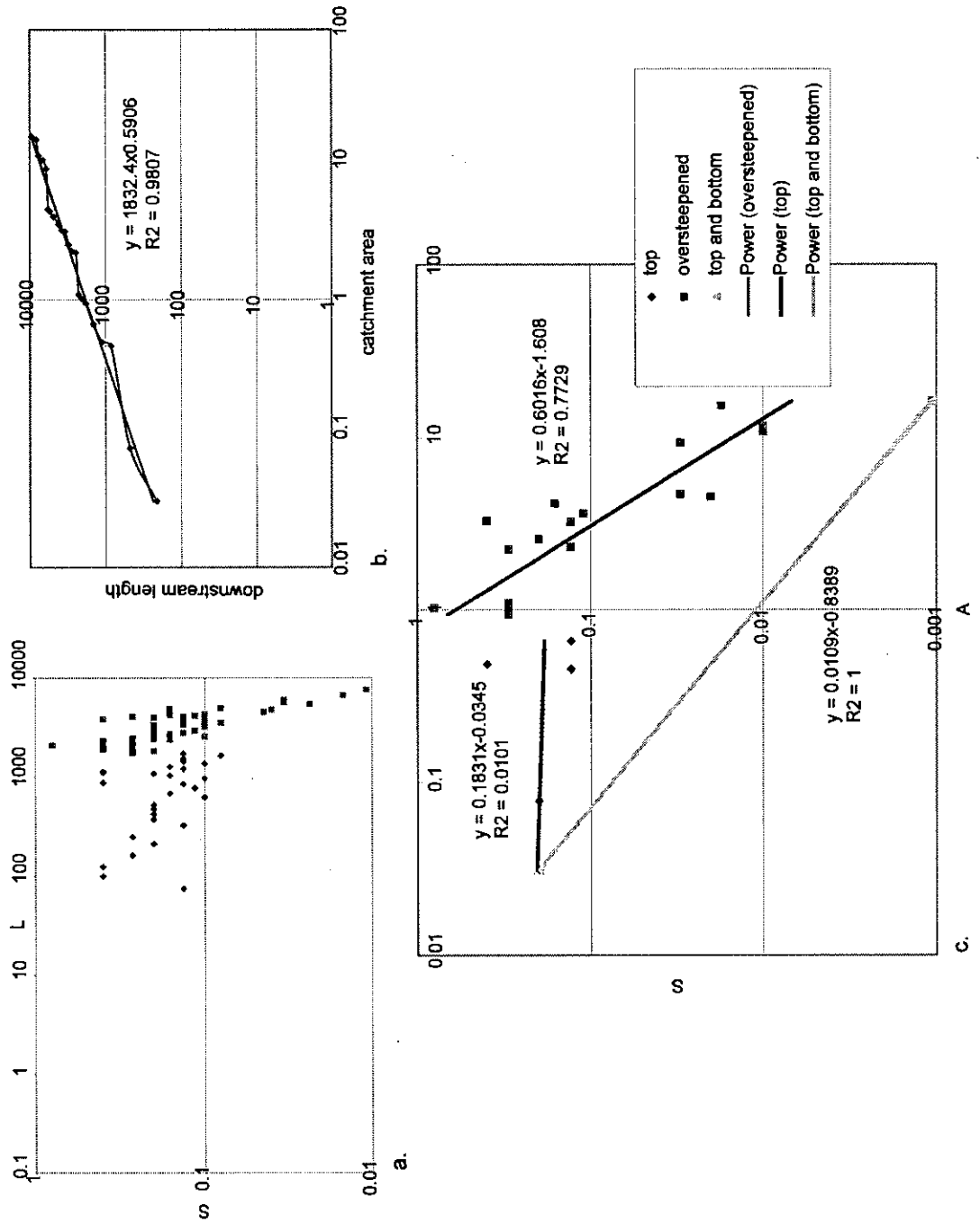


Figure 8.17. Stream 8: a) length vs. slope, b) drainage area vs. length, c) drainage area vs. slope.



## 8.5 Discussion

There is a plethora of evidence indicating that at the present time the Hatay Graben is still undergoing active deformation along the major fault zones (this study section 7.8.2; Över et al. 2000; 2004). The drainage patterns are well developed and can be used to try to interpret the recent structural evolution. In the Antakya Basin (Fig. 8.5) streams are actively incising the basin fill and are cutting back into the footwall of the eastern fault. This suggests that the uplift on the western fault is relatively recent and has uplifted the basin fill. To the east headward erosion of streams is cutting back into a major fault; this fault is likely to be older than the one that has uplifted the basin.

The evidence from proposed wind gaps and dry valleys supports this idea, as a series of wind gaps can be found along the easternmost faults that have an NW-SE orientation. This may have been the orientation of antecedent drainage before footwall uplift on this fault caused the direction of flow to become reversed. In the hanging wall of this fault, NW-SE streams are still present but now flow into northward flowing streams that have captured the drainage in the area. Cross-cutting relationships indicate that the N-S streams are younger and may have developed due to a change in the orientation of the faults causing the dip of the land surface to change. Again, this implies that the outermost faults are the oldest and the innermost faults of the graben are younger.

Longitudinal stream profiles are sensitive to a number of factors (e.g. lithological changes, tributaries, climate) including tectonic uplift and subsidence. When the profiles are studied it is seen that in the majority of cases there is no significant change when the nature of the underlying bedrock changes, and thus it seems likely that the lithology in this area does not have a great effect on the shape of the stream profile. Climate has varied through the Holocene this is assumed to be on a timescale shorter than that of fault growth and thus can be considered as relatively constant. Although climate change would also have an effect on drainage patterns, a lack of age control on land surfaces makes it impossible to determine how great this is. The positions of major tributaries intersecting the stream profile also do not appear to have an appreciable effect, this leads to the conclusion that the knick points observed on the profiles are the result of fault-controlled subsidence, causing the river to disequilibrate and form a knick point that then migrated up-stream with time.

Most of these knick points are in the lower part of the stream close to the basin floor and are probably related to movement on the innermost bounding faults of the graben. What is

interesting is that in two of the profiles (streams 1 and 2) no faults were identified in the field as crossing those streams but knick points are clearly visible on the profiles. This may have a several causes: that the knick point was not caused by a fault; the fault has been eroded, or the fault does not have a surface expression (i.e. it is a blind fault). If the knick point is not fault controlled, a change in lithology or a tributary must be the cause. In stream 1 there is a change in lithology from limestone to serpentinite, but these lithologies are commonly juxtaposed in the field area and do not cause knick points on any other of the profiles, suggesting that this is not the cause. However, there are tributaries joining the stream in the area of the knick point, but these are small and unlikely to have had a big effect on the profile. Instead, I propose that the knick point is fault controlled and the footwall uplift has prevented small streams from continuing along the antecedent drainage, diverting them instead into larger streams that could down cut through the fault. This ended with a knick point caused by fault motion associated with a tributary (Fig. 8.18).

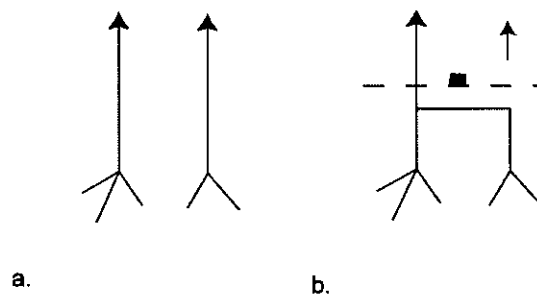


Figure 8.18. Diagram showing the evolution of streams 1 and 2 in two stages: a) antecedent drainage, b) reversed drainage due to fault motion. This drainage pattern can be seen for these streams in Figure 7.7.

Faults observed in the field when marked onto the stream profiles often coincide with the position of a knick point (streams 4, 5, 6, 12) which implies that these faults have been active recently; these are faults that form the inner boundary of the graben. On the profile for stream 4, the position of the fault is not located at the knick-point indicating that the knick-point has migrated backwards with time. The top of the knick-point is ~225m back from the fault. Published values of average long term knick-point retreat rates vary from  $0.4 \text{ mmyr}^{-1}$  to  $2 \text{ mmyr}^{-1}$  (Seidl et al. 1997; Weissel & Seidl 1998) using these values the age of this fault can be calculated as  $225,000 \text{ yrs} \pm 225,000$ .

In contrast, some of the faults, when marked on the stream profiles, have no associated knick points (streams 2 and 8). The fault on stream 2 is located in the south (Fault A on Fig 7.7)

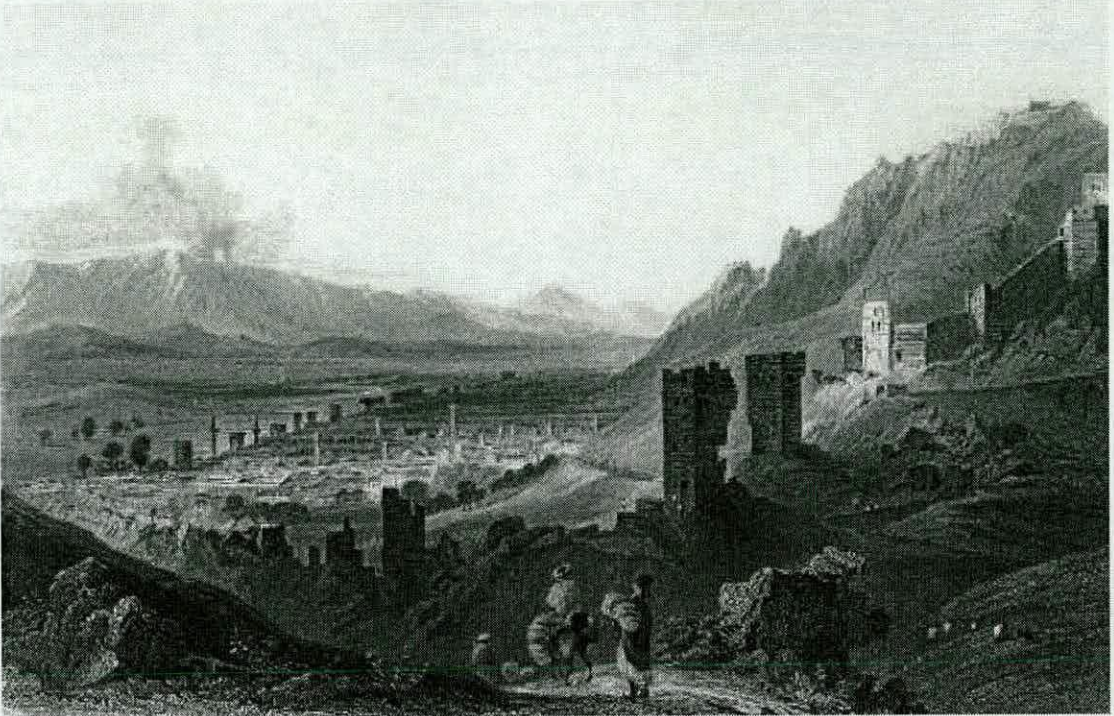
and is probably inactive. Stream 8 flows across a strike-slip fault with a small vertical component and so there would be negligible subsidence, perhaps not enough to form of a knick point.

Stream 7 is the only stream profile showing a classic concave profile, and is thus the only stream in equilibrium. Interestingly there is often a fault drawn on previous maps in this area (Pişkin 1985). This stream profile indicates that there is unlikely to be active faulting along the path of this stream and field observations do not support the presence of a fault. Streams 9, 10, 11 have profiles that also exhibit a nearly concave profile but with some irregularities, it is not clear whether these are small knick-point or an affect of the data acquisition method.

## 8.6 Conclusions

- There are a series of fluvial (T0-T4) terraces that document the progressive down cutting of the river systems in response to base level change due to relative sea-level fall probably as the result of tectonic uplift.
- Marine terraces also record phases of uplift.
- Drainage patterns indicate that the antecedent drainage has been affected by faulting. Resulting in increased relief and the formation of windgaps along the crest of uplifted footwall blocks. Cross-cutting stream patterns suggest that there has been a change in the dip direction of the land surface likely to be due to faulting.
- Knick-points along stream profiles are a response to active faulting and observed along several streams along the south-eastern margin.
- The innermost boundary faults of the graben have been recently active; however, it is likely that the outer graben boundary faults are inactive due to a lack of expression on river profiles and by analogy to similar areas.

## Chapters 9 and 10



Antioch from the west [actually from the east].

## **9 Regional comparisons and discussion of the geological evolution of the Hatay Graben.**

In this chapter the results from the previous chapters will be drawn together to develop an integrated history of the geological evolution of the Hatay Graben. This will then be compared to published models of graben formation. The sedimentology and tectonic models of six areas in the Eastern Mediterranean will then be described briefly, to compare and contrast the geological evolution of the region around the Hatay Graben. Finally, existing models for basin evolution will be discussed and a new model proposed to explain the data gathered in this research project.

### ***9.1 Geological history of the Hatay Graben and the Kırıkhan area.***

The oldest sediments in the field area date from the uppermost Cretaceous (Kaleboğazi Formation), deposited after the emplacement of the Kızıldağ ophiolite. East of Antakya (Figure 9.1), these sediments are composed of shallow-marine (intertidal) carbonates that are overlain by palaeosols and occasional conglomerate horizons (section 4.2.1), indicating this area was emergent in the Latest Cretaceous/Palaeocene. This implies that a regression had occurred due to either sea-level fall or uplift (section 5.2.2). Sandstones of probable Late Cretaceous age (based on field relationships) are present near the town of Serinyol (section 4.4.1.1 & Figure 9.1) composed dominantly of sedimentary lithic fragments and representing a shallow-marine environment, suggesting that in the north there was a more open marine setting at that time.

Marine conditions returned to the area during Palaeocene/Eocene time (Okçular Formation, section 4.2.1). On the flanks of the Hatay Graben these sediments form a transgressive sequence of shallow-marine intertidal carbonates, similar to the Upper Cretaceous limestones. These sediments pass upwards into deeper marine nummulitic limestones of shelf depths (section 5.2.2.1). To the north, limestones of a similar age are composed of calciturbidites, debris flows and slumps, implying an unstable shelf-edge position (section 5.2.4). This suggests that water depths increased northwards, probably towards the shelf margin. Outcrops of Cretaceous-Eocene sediments were observed high up (1000m) in the

Kızıldağ, this combined with a lack of siliciclastic material in the limestones indicates that the ophiolitic massifs can not have had significant relief during this time and as a result limestone deposition was able to take place over the whole area.

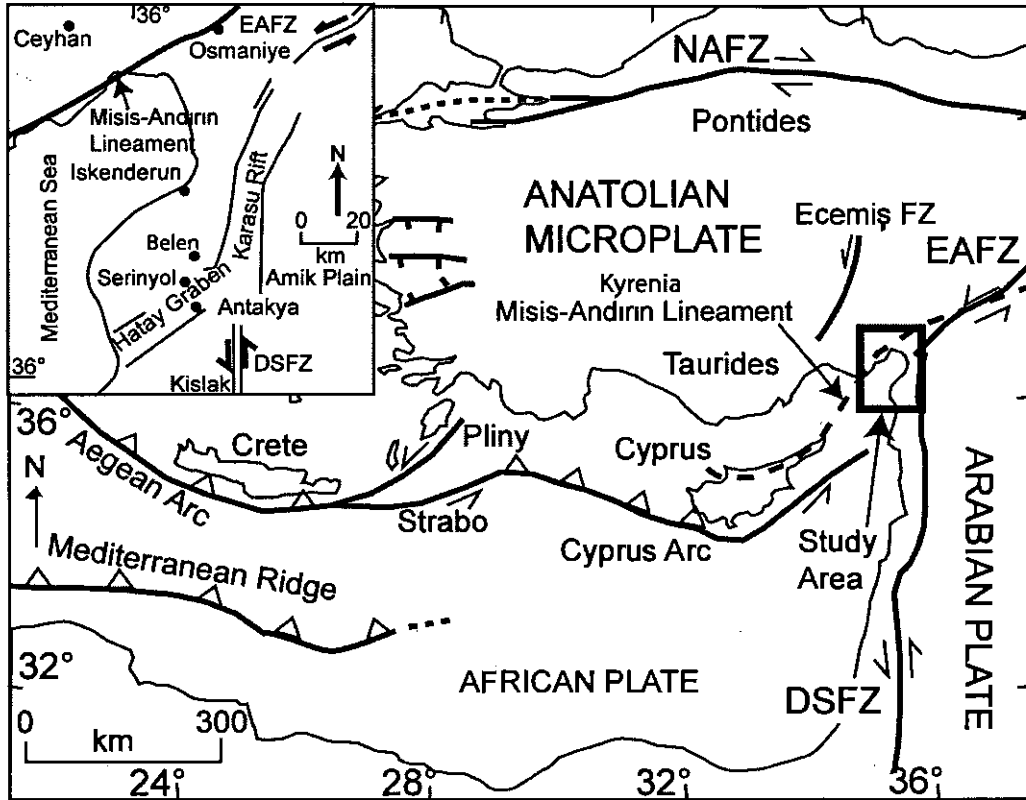


Figure 9.1. Map showing the regional Neotectonic setting of the Eastern Mediterranean; insert: the region around the study area, showing some of the places mentioned in the text.

The top of the Eocene succession is marked by an angular unconformity. The Eocene strata have been folded into disharmonic folds and dips reach  $90^\circ$  in places (section 7.4.2). The top surface of the limestones is often karstified. No Oligocene sediments were identified in the field area. This, combined with the fact that the overlying Early Miocene sediments are unfolded, implies that this episode of folding took place during the Oligocene. The area may also have been emergent and eroding at that time. This deformation was probably related to the initial diachronous continental collision of the Tauride micro-continent to the northeast (Robertson 1998) and to Syrian Arc II deformation that began in the Early Eocene and culminated in the Late Oligocene and is also generally related to the formation of the Bitlis Suture Zone (Hempton 1985; Walley 1998).

Sedimentation recommenced in the Aquitanian to Burdigalian (Early Miocene; Balyatağı Formation, section 4.2.3) with a thin, localised shallow-marine limestone horizon. This represents a brief marine incursion that is overlain by a considerable thickness of braided-river sediments (section 5.3.1). These sediments are rich in ophiolitic material and exhibit palaeocurrent directions towards the north suggesting transport of ophiolitic material from the south, possibly from the ophiolitic Baer-Bassit Massif (Syria; Al-Riyami et al. 2002). This further indicates that uplift and erosion were taking place to the south of the field area during the Early Miocene, as prior to this time carbonates were deposited over the whole of the Arabian Platform. These braided-river sediments are only found along the graben margins in the northwest of the Hatay Graben.

Along the northwestern margin and near the town of Seriyol (sections 4.3.3 & 4.4.1.3), Early Miocene sediments contain more palaeosols but braided river deposits are still present. The appearance of palaeosols perhaps indicates more stable bar-forms or fewer channels in the river system. However, coarse-grained conglomerates (alluvial fans) and fine-grained sediments, interpreted as fan-delta deposits, are present to the southeast of the braided river deposits. These fan-delta sediments are found at the base of Middle Miocene limestone sequence.

Early Miocene sediments, near Kırıkhan, have also been interpreted to represent fan-delta sedimentation (section 5.3.2). Although these sediments are composed dominantly of serpentinite, limestone clasts are also present, showing that both the ophiolite and the platform carbonates in this area were undergoing erosion at this time. Palaeoflow is easterly (i.e. towards the braided-river sediments) suggesting that the palaeogeography was complex and a lake/marine embayment may have existed in the Amik Plain area (Fig. 5.10). This, in turn, suggests that the range of different depositional environments is likely to have been controlled by topographic factors at this time. Although faulting is observed in sediments of Early Miocene age there is no evidence to indicate if these faults are syn- or post-sedimentary.



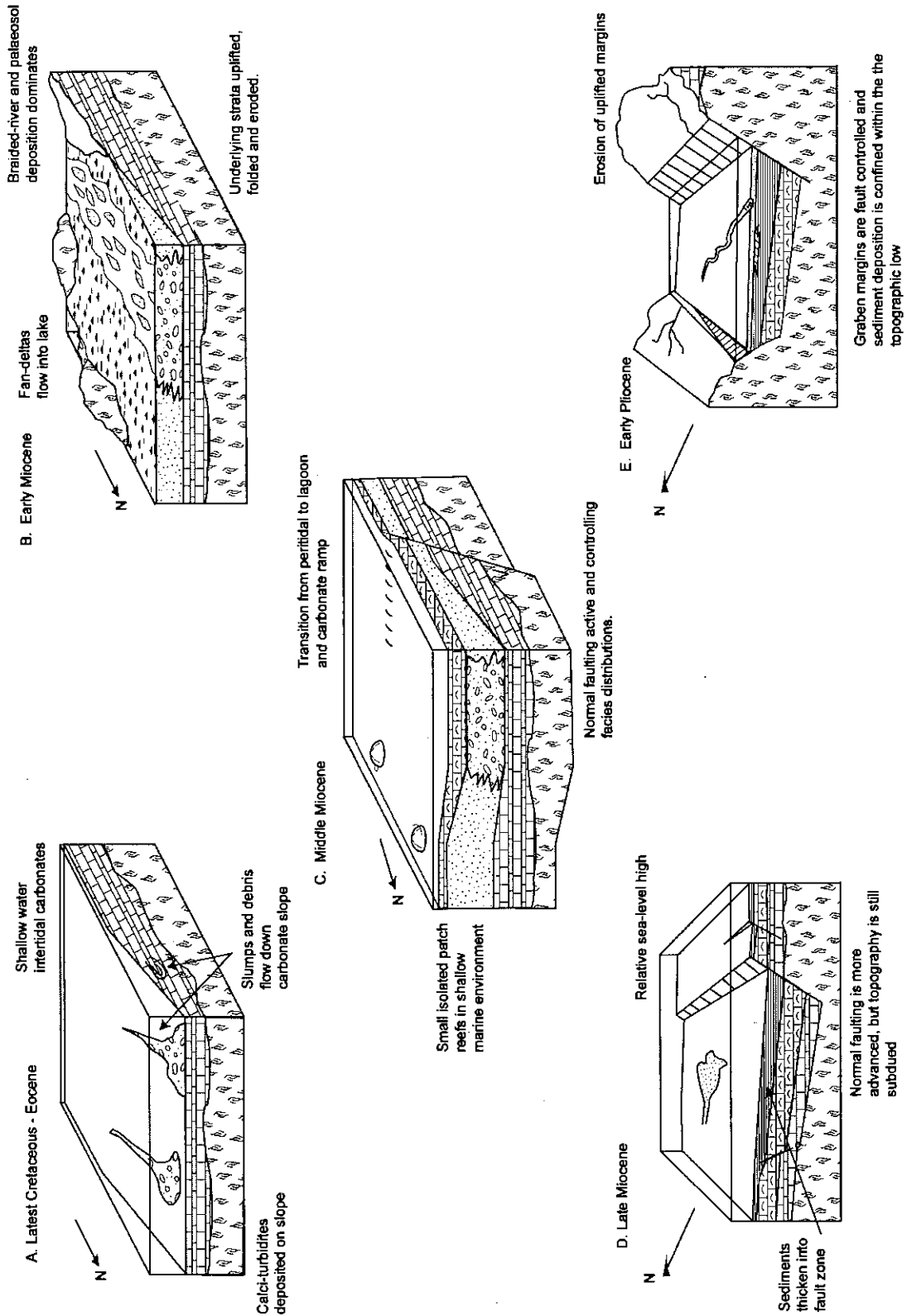


Figure 9.2. Simplified block diagrams illustrating the local geological evolution of the Hatay Graben. See text for explanations.

Middle Miocene sediments (Sofular Formation, section 4.2.5) show a great variety of sedimentary facies. Shallow-marine limestones dominate, showing that relative sea-level was higher than in the Early Miocene. The sediment thickness is greatest in the southeast indicating that there was greater accommodation space in this area, perhaps due to higher amounts of extension in this area. Interestingly, in the southeast the limestones directly overlie ophiolitic rocks, whereas in the northeast limestones overlie Early Miocene and older sediments. This may be because the southwest was mainly an area of non-deposition and erosion during Oligocene to Early Miocene times, whereas sedimentation was ongoing to the northeast, until higher sea-levels in the Middle Miocene submerged the whole area.

In the southwest, where the sediments are the thickest, there is a progression from peritidal facies, to lagoonal, to shelf limestones over time; there may also have been a progressive deepening to the northwest along a carbonate ramp (section 5.4.1). This suggests that overall basin topography had not changed significantly since the Eocene. The peritidal carbonates are composed of many transgressive cycles; this may have been due to eustatic sea-level fluctuations superimposed onto a slow (continuous) subsidence. Locally developed hard-grounds suggest that rates of sedimentation were low at times.

Reef material and rare patch reefs are more common in the northeast (section 4.2.5.7), indicating that the environment there was energetic or there was greater topography. The resulting removal of sediment allowed the reefs to thrive. The southeast was, therefore, marked by lower energy environments with less topography.

The Sofular Formation contains some ophiolitic material as well as limestone clasts suggesting that the underlying limestone formations (Kaleboğazı and Oçkular Formations.) and the ophiolite were being eroded. There is evidence that most of the study area was submerged at this time and so the clastic material was probably eroded from the hinterland to the south. Additionally, on the northwest margin a large area of carbonate (dipping SE) overlies the ophiolite (Fig. 9.3) with a flat-topped topography. This was possibly more extensive; if so, the Kızıldağ was not then uplifted and a carbonate ramp existed over a large area.

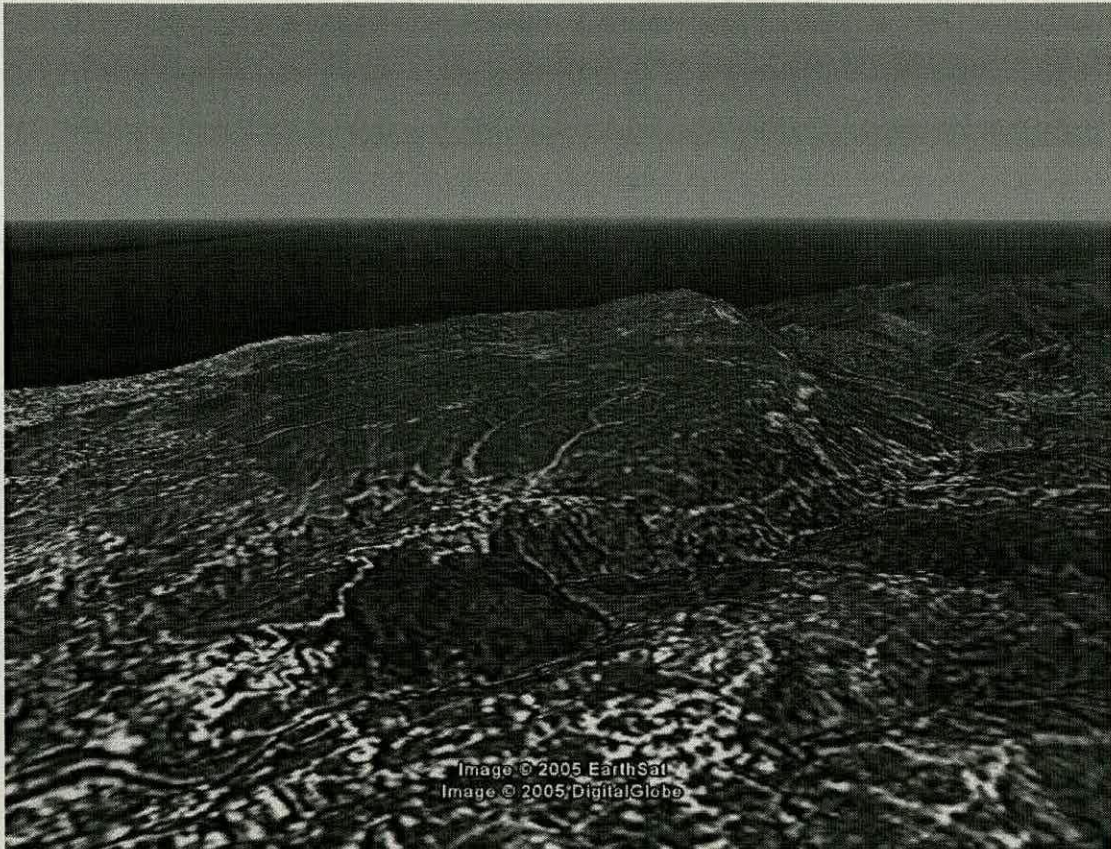


Figure 9.3. Low-resolution DEM showing the relatively flat top of the Middle Miocene carbonates. It is proposed that these limestones once covered a larger area but were eroded due to uplift of the Kızıldağ that exposed the underlying ophiolite. View to northwest, field of view ~10km; the town of Samandağ is to the right. Image from Google Earth.

There is evidence that fault activity was taking place during the Middle Miocene (section 7.5). Growth faults, intraformational discordances and sediment fanning all point to fault activity. Additionally, rare palaeocurrents indicate flow to the southwest, axially along the present graben and there is a small Gilbert-type delta of Middle Miocene age that would have needed significant topography to form (section 5.4.1). This suggests that faulting was already playing a role in controlling the spatial distribution of facies.

The Upper Miocene marls (Nurzeytin Formation, section 4.2.7) are concordant with the underlying limestone. Strontium dating of the basal sediments indicates that the boundary is diachronous, with older sediments in the north (section 3.4). Planktonic foraminiferal ratios indicate that the water depth was also deeper in the north. The large thickness of marls (~300m) indicates that from ~9.5 Ma to the Messinian (7.25-5.33 Ma; Gradstein et al. 2004) the Hatay Graben experienced relatively deep (>200m) conditions. There is evidence for

gravity reworking of sediments, clearly indicating the presence of a topographic graben at this time (section 5.5.1). The composition of the marl and the reworked sediments exhibits a mixed provenance indicating erosion of ophiolitic and sedimentary rocks. This is supported by the basal sediments unconformably overlying ophiolitic and sedimentary cover units. This also implies that there must have been subaerial and shallow-marine areas to supply the siliciclastic material to the basin. Mica first appears in this unit. There are no micaceous rocks in the basement of this area; therefore, this material must have been sourced from outside the graben and it was not a closed system. Mica first appears in Lower Miocene sediments in the Kırıkhan area along with a high concentration of quartz (section 4.5), suggesting that this area was closer to the source of the mica and quartz, which possibly lay to the north.

In the Kırıkhan and Belen areas, the Upper Miocene succession (Gökdere Formation, section 4.3.8) is dominated by deep-marine sediments with a deltaic influence in the north, suggesting that the depth of the basin decreased from the southwest to the northeast. Horizons within the formation near Kırıkhan contain abundant *Ostrea* and other bioclastic material, indicating that the water depth in this area was very shallow or even restricted at times (section 5.5.2). Palaeocurrents were southwesterly across what is now the Kızıldağ. There appears to be no deflection of current direction around the uplifted ophiolitic massif, implying that no mountainous relief then existed and uplift had not yet begun. Although, there was probably some basin topography this was not significant in the north, suggesting that faulting was only active at this time along the southeast margin of the basin.

During the Messinian, the Mediterranean as a whole was affected by a dramatic decrease in sea-level and consequent evaporite deposition (Hsü 1978). Evaporites are present in a few areas of the Hatay Graben (section 4.2.8). These locations are assumed to represent local depocentres; this is suggested by evidence of reworking and gravity flows (section 5.5.3). These evaporitic sediments are now at different elevations; assuming the evaporites were formed at approximately the same levels, this would suggest that there has been substantial post-Messinian fault motion and flank uplift. However, evidence from Sicily (Butler et al. 1995) suggests that evaporites in marginal basins may form in a number of 'perched basins' at different elevations and at different times, which if this were true for the Hatay Graben could suggest that there has been less (but still substantial) post-Messinian uplift. Poor exposure and dating means that the difference between these two cases cannot be

satisfactorily resolved; however, the similarity of facies in the different localities is suggestive of contemporaneous deposition.

There is also evidence that some erosion took place at this time; for example, the upper surface of the Middle Miocene Sofular Formation is a bored unconformity surface overlain by Pliocene cross-bedded sandstones (section 4.2.10.4). In contrast, some locations show a complete Upper Miocene to Pliocene sedimentary sequence apparently without a break in sedimentation (section 4.2.10.1).

Pliocene sediments were deposited in a range of different depositional environments, indicating a complicated palaeogeography during this time (section 5.6.1). Inland, sediments are dominated by marl with channel structures representing an Early Pliocene transgression, whereas towards the margins of the graben, near the present coastline and higher in the succession, sandstones are the main lithology present. This suggests that in the Pliocene the centre of the graben was marine or lagoonal following an Early Pliocene sea-level rise that resulted in marl deposition. By contrast, on the edge of this body of water shore-face deposition took place. As sea-level fell coastal and non-marine environments became more prevalent resulting in widespread sandstone deposition.

Pliocene sedimentation was strongly affected by faulting; near the major graben boundary faults (section 7.2.1), sandstones have been caught up in this deformation and have high angles of dip. Evidence for block rotation has been observed in the centre of the graben (section 6.3.2). During the Late Pliocene and Quaternary faulting was active, uplifting the graben margins and probably affecting the distribution of facies within the graben. Normal faulting was observed to cut the Pliocene – Quaternary boundary and Quaternary sediments showing that faulting continued into the recent period.

Several factors show that active faulting is still occurring in the graben at the present time (section 7.8.2). Seismic activity has been recorded recently and there were many earthquakes in the historical times (section 7.8.1). A number of marine terraces are present, formed due to changes in relative sea-level, usually attributed to discrete tectonic events (i.e. Pirazzoli et al. (1991)). Although the majority of Quaternary sediments are fluvial, these show evidence of periods of incision forming series of river terraces, indicating that the basin floor has been uplifting causing the rivers to incise downwards towards sea-level. Analyses

of drainage patterns and stream profiles have also shown that faulting has affected the morphology of the streams in the more recent period (chapter 8).

There are some similarities in the development of the Plio-Quaternary Hatay Graben with conceptual models of rift basin development (Leeder & Gawthorpe 1987; Gawthorpe & Leeder 2000). The Hatay Graben, *sensu stricto*, in the Early Pliocene was a coastal-marine basin. In models for this setting, when faults break the surface, strata forms a 'divergent wedge' that is rotated and thickened into the fault (Gawthorpe & Leeder 2000). This can be actually observed for the Late Miocene marls, which were probably deposited prior to the development of significant topographic relief in the field area; this fits well with an early stage of basin formation.

As fault growth continues, fault linkage occurs causing some faults to become inactive, and motion to become focussed on inner faults. Depocentres associated with these faults may become filled in or incised and reworked. This can be seen in sub-basins on the southwest margin of the Hatay Graben that have been uplifted since the Messinian. In Gawthorpe & Leeder's (2000) model, a pronounced footwall topography and graben forms during this stage; this is due to increased displacement rates on major faults compared to during the initiation of faulting.

These models predict that during highstands hemipelagic sediments are deposited; these are cut by subaqueous channels derived from alluvial fans and fan deltas and that feed basinal turbidite systems. A plethora of slump scars, slumps and debris flows can also be observed (Gawthorpe & Leeder 2000). During lowstands fluvial incision and shallow-marine sedimentation takes place; some depocentres may then become isolated and form lakes. Some of these features can also be observed in the Hatay Graben in the Pliocene sediments.

In the Mid-Late Pliocene the basin became continental in character. Gawthorpe and Leeder (2000) also developed conceptual models for continental rift basins. These basins feature antecedent drainages that cut through uplifted fault blocks, lakes, deep-water deposition in basin depocentres and the reworking of alluvial and shoreline sands by the wind into ergs. Similar features (i.e. deep-marine sediments with channels, shoreface sediments, and aeolian sandstone) can be observed in the Hatay area but one feature that is not present is recent alluvial fans. These are a major feature of the edges of grabens in these models and although are observed further to the north in the Karasu Rift are not present in the field area. This

may be due to a number of different reasons; low rates of erosion and, therefore, sediment supply, the dominance of karstified carbonate on the flanks generating little runoff, the graben may have been submerged, the sides of the graben too steep for fans to develop, or alluvial fans were developed but are now buried.

## 9.2 Regional Comparisons

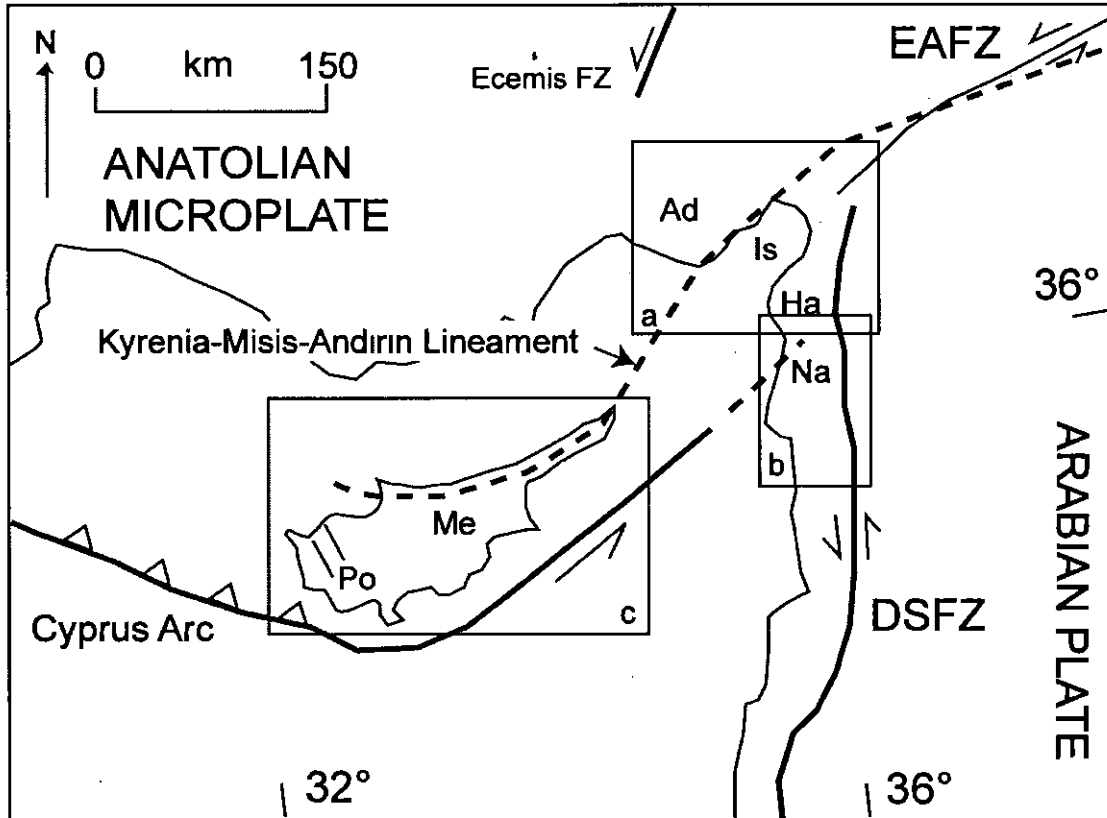


Figure 9.4 Simplified map of the Eastern Mediterranean showing the location of the basins discussed in this section. a. Location of figure 8.2; b. Location of figure 8.6; c. Location of figure 8.7. Ad = Adana Basin, Ha = Hatay Graben, Is = Iskenderun Basin, Me = Mesaoria Basin, Na = Nahr El-Kabir Graben, Po = Polis Graben.

### 9.2.1 Adana Basin, Southern Turkey

The Adana Basin is situated in southern Turkey to the northeast of the Hatay Graben (Figure 9.4). To the north, the Adana Basin is bounded by the Taurus Mountains, to the west by the Ecemiş Fault zone and to the east by the Misis Mountains. The Adana Basin is separated

from the Iskenderun Basin by the Misis-Andırın structural high (Kelling *et al.* 1987; Gökçen *et al.* 1988).

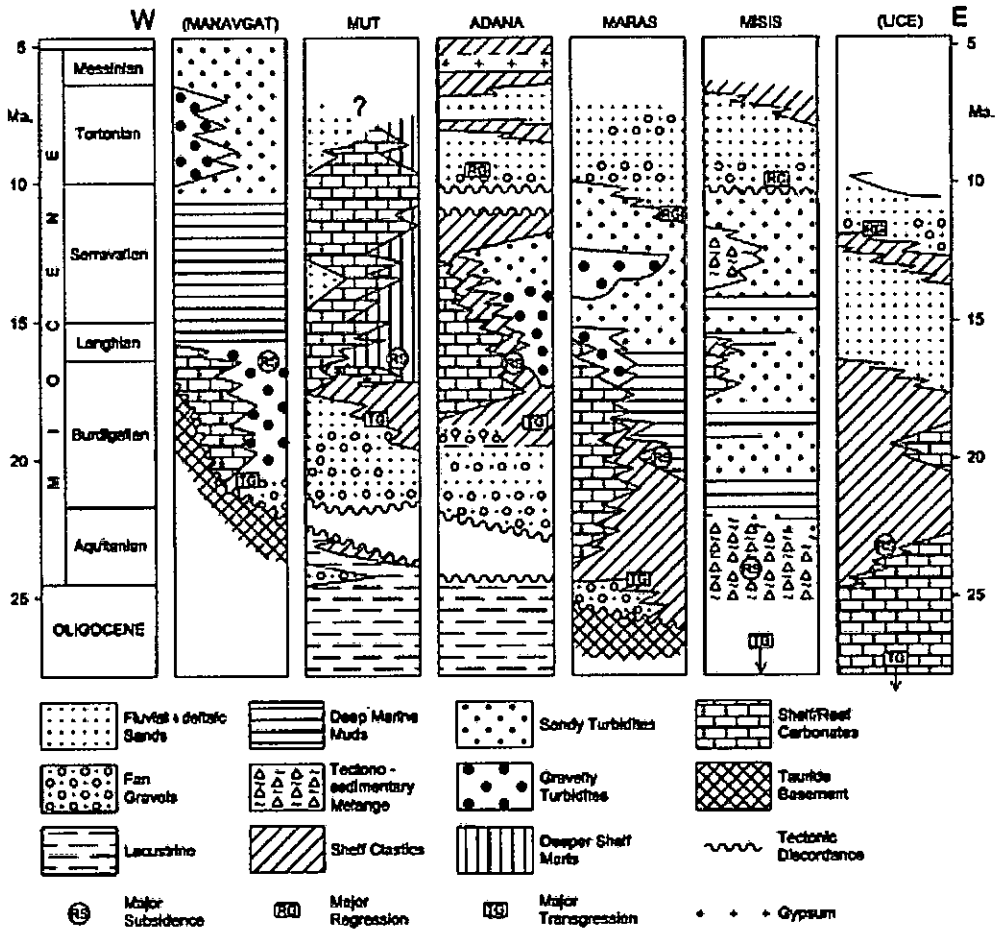


Figure 9.5. Stratigraphic columns summarising the sedimentary successions and tectono-stratigraphic events identified in the main Neogene basins in southern Turkey, from Kelling *et al.* (2005).

9.2.1.1 Stratigraphy and sedimentology of the Adana Basin

The basement of the Adana Basin is composed of Palaeozoic and Mesozoic rocks overlain by an ophiolitic melange that was emplaced during and after the Late Maastrichtian (Schmidt 1961; Ünlügenç 1993). The Cenozoic basin-fill comprises Tertiary units on the northern margin of the basin unconformable overlying the basement (Figure 9.6), while to the south Quaternary units outcrop; the strata generally dips to the south (Görür 1979; Yetiş 1988; Williams *et al.* 1995; Cronin *et al.* 2000). The sedimentary succession has been divided into nine stratigraphic units (Figure 9.7), each of which will be briefly summarised here.



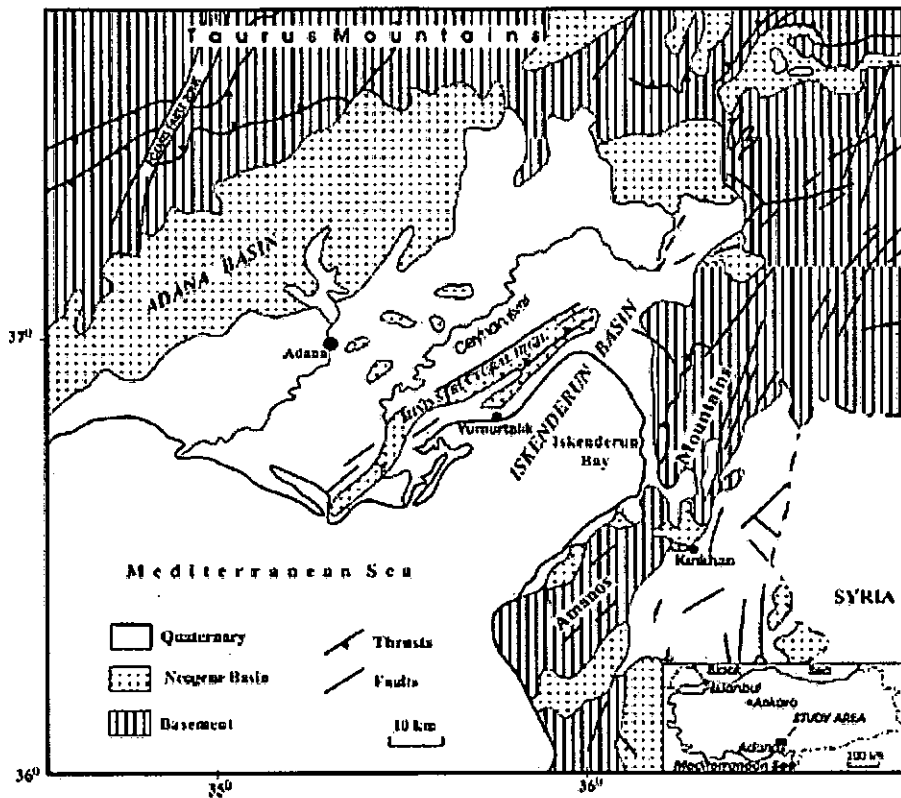


Figure 9.6. Geological map of the northeast Mediterranean area showing the Adana and Iskenderun Basins, and Hatay Graben. From Nazik (2004).

AGE	FORMATION	LITHOLOGY		PLANKTONIC FORAMINIFERAL ZONES OF THIS STUDY	ENVIRONMENT
Pliocene	HANDERE		Fine grained sandstone & siltstone	<i>Sphaerodentopis Acme Zone</i>	SHALLOW MARINE
Messinian			Gypsum & conglomerate	Non-distinctive Zone	FLUVIAL/LAGOONAL
Tortonian	KUZGUN		Turfite Sandstone & conglomerate	First occurrence <i>Globorotalia suterae</i>	SHALLOW MARINE DELTAIC FLUVIAL
Serravallian	GÜVENÇ		Sandstone and shale alternation	<i>Globorotalia mayeri</i>	SHALLOW MARINE DEEP MARINE
Langhian	CİNGÖZ		Turbiditic sandstone Conglomerate	<i>Orbulina suturalis</i>	SUBMARINE FANS
Burdigalian	KARASALI		Reefal carbonate	<i>Procaribulina glomerata curva</i>	SHALLOW MARINE/ SLOPE DEPOSITS
	KAPLANKAYA		Pebbly sandstone	<i>Globigerinoides trilobus</i>	REEFAL CARBONATES
Aquitanian-Late Oligocene	GILDIRLI		Conglomerate	Non - fossils	FLUVIAL

Figure 9.7. Correlation of lithologic, biostratigraphic and environmental features of the Adana Basin (Nazik 2004).

**Oligocene to earliest Miocene Gildirli Formation:** This formation is composed of red-beds, including conglomerates, sandstones, siltstones and mudstone. These sediments are

interpreted as representing alluvial-fan to fan-delta deposition that took place during a rapid Early Miocene transgression (Görür 1992). No microfossil evidence has been found but the formation is probably Oligocene to Early Miocene in age. The formation passes vertically and laterally into the Kaplankaya Formation and is concordantly overlain by the Karaisali Formation (Gürbüz & Kelling 1993; Yetiş et al. 1995; Nazik 2004).

**Early Miocene Kaplankaya Formation:** This is composed of pebbly sandstones, sandstones, sandy limestones and silts. This formation represents a range of environments ranging from shallow-marine sediments that are transitional to the reefal Karaisali Formation, to deep-marine turbidites to the north of Adana basin, which are transitional to the basal Cingöz Formation (Cronin et al. 2000). The formation is considered to represent a carbonate slope environment and has been dated to Late Burdigalian to Langhian (Cronin et al. 2000; Nazik 2004).

**Burdigalian to Langhian Karaisali Formation:** This formation is composed of reefal carbonates (Görür 1979). The main reef was deposited on structural highs and is composed of coral packstone and boundstone and small benthic foraminifera-algal packstone. By contrast, coral wackestone and packstone and large benthic foraminiferal biofacies formed talus deposits on submarine fore-reef slopes. This formation is transitional to the Kaplankaya Formation and the Cingöz Formation and is of Burdigalian to Langhian in age (Görür 1979; Nazik 2004). It is thought that these reefs formed on the top of tilted fault blocks (Williams et al. 1995).

**Late Burdigalian to Serravalian Cingöz Formation:** The siliciclastic Cingöz Formation is composed of turbidites (mainly sandstone and conglomerate) that form a large axial deep-water submarine fan system where palaeocurrents flow to the east and southeast. The formation is interpreted as either consisting of two distinct submarine fans (Gürbüz & Kelling 1993) or as one system with two major axial conduits and smaller tributaries (Cronin et al. 2000) that bypasses the shallow-marine realm. Cronin et al. (2000) proposed that the Cingöz Formation was a deep-water facies contemporaneous with the Kaplankaya slope system and the Karaisali reef limestones.

**Langhian to Serravalian Güvenç Formation:** This formation is composed of olive grey sandstones and interbedded shales, and is laterally and vertically transitional to the Cingöz

Formation. It is dated as Langhian to Serravalian (Nazik 2004) in age and is considered to have been deposited in deep-marine to offshore environment.

**Tortonian Kuzgun Formation:** The Kuzgun Formation is composed of siliciclastics, detrital carbonates and other carbonates (Nazik 2004). There are lateral and vertical facies changes between meandering river deposits, deltaic sediments, shallow-marine deposits and lagoonal limestones containing *Ostrea*.

**Upper Miocene to Pliocene Handere Formation:** The Handere Formation is composed of sandstone and mudstone with occasional conglomerate horizons. The environment of deposition is probably similar to the Kuzgun Formation. Some Messinian gypsum is present in this formation; the principle gypsum level is named the Gokkuyu Gypsum Member (Yetiş 1988).

**Quaternary:** Onshore the Quaternary of the Adana Basin is composed of alluvium, terrace conglomerates and caliches. Offshore, the Adana and Iskenderun Basins share their Quaternary sedimentary history; there are at least eleven stacked, progradational depositional sequences revealed by seismic reflection (Aksu et al. 1992). These are deltaic sequences separated by regional seismic unconformities. Each deltaic system appears to have been terminated during the beginning of a glacial period, thus reflecting a fall in sea-level. Drilling shows that a wedge of Quaternary deposits blankets the Adana Basin and thickens towards the present shoreline. This combined with dating indicates the basin has experienced relatively continuous subsidence since ~ 0.6 Ma (Aksu et al. 1992).

#### 9.2.1.2 *Tectonic setting of the Adana Basin*

Subsidence in the Adana Basin started in the Early Miocene (Kelling et al. 1987; Williams et al. 1995) due to the initiation of extensional faulting. Thus, basin formation predates the development of the EAFZ. Deposition of the Early Miocene sediments took place within a half graben. Ünlügenç (1993) proposed that the basin formed as a peripheral foreland basin due to the collision of the Arabian and Anatolian plates, causing the Tauride Orogeny and loading of the lithosphere. Subsequently the basin behaved as a transpressional basin complex related to the creation of the Kahramanmaraş triple junction to the east. This interpretation is also favoured by Williams *et al.* (1995) and the recent work of Aksu *et al.* (2005) suggests that the basin during the Miocene was part of the foredeep to the Tauride

orogeny, which by the Plio-Quaternary had developed into an asymmetric 'piggy-back' basin on the hanging wall of the Misis-Andirın thrust culmination. However, as the Adana Basin lies to the north of the collision zone it cannot form part of the foreland basin as there was no overthrust load on the western, northern or eastern margins of the basin. Instead Robertson (1998) proposes that basin formation was due to regional extension originating to the south of the area rather than crustal loading. This crustal extension is proposed to be the result of subduction zone roll-back, situated to the south of Cyprus.

### 9.2.1.3 *Comparisons to the Hatay Graben*

- Both the Adana Basin and Hatay Graben seem to have developed around the same time (Early Miocene). However, in the Adana area Oligocene rocks are present unlike in the Hatay Graben.
- The Lower Miocene of the Adana Basin is composed of alluvial and fluvial sandstones and conglomerates, possibly contemporaneous with the Balyatağı and Kıcı Formations.
- These terrestrial sediments are overlain by three associated formations of siliciclastic and carbonate composition that are dated as Burdigalian to Serravalian. These represent a shallow-marine reef with associated slope and basin floor facies in the Adana Basin. These sediments share some similarities with the Sofular and Kepez Formations that are dated similarly. Although similar environments are represented the Sofular formation is almost completely composed of shallow-marine carbonates, and deep-water sediments were not identified in the Hatay region.
- The Tortonian sediments in the Adana Basin represent a much shallower environment than the sediments of the study area for the same time period.
- The Messinian to Recent sediments seem to be similar in nature in both the Adana Basin and the Hatay Graben.

## 9.2.2 **The Misis-Andırın Complex.**

The Misis-Andırın lineament is the suture zone that runs through SE Turkey to Cyprus (Kyrenia Range) it is a structurally high area that separates the Adana and Iskenderun Basins in south central Turkey. The zone is comprised of a complex assemblage of Mesozoic-Early Cenozoic rocks (Fig. 9.5) preserved as melange, broken formation and thrust sheets termed the Misis Complex (Gökçen et al. 1988) or Misis-Andırın Complex (Robertson et al. 2004). Overthrusting along this lineament caused loading of the lithosphere and the development of

a peripheral foreland basin to the south (Kelling et al. 1987; Gökçen et al. 1988; Robertson et al. 2004). This complex documents the tectono-sedimentary processes that effected the active, northern, margin of the Neotethys Ocean (Robertson et al. 2004); it is interpreted variously as an accretionary prism related to the last stages of diachronous continental collision (Yılmaz et al. 1984; Robertson et al. 2004); as olistostromes reflecting motion along the plate margin (Kelling et al. 1987) or as having a post-collisional origin involving extension in the Late Eocene-Oligocene or transtension following the final closure of the Neotethys in the Latest Cretaceous (Karig & Kozlu 1990).

Present within the Misis-Andırın Complex are units of Miocene age that have been folded and thrust from the Early-Middle Miocene to the Quaternary (Gökçen et al. 1988). These sediments structurally underlie the melange and volcano-sedimentary units that make up the majority of the complex (Robertson et al. 2004) and have been interpreted as sediments from the foreland basin to the orogenic front (Gökçen et al. 1988; Robertson et al. 2004); as extensional or transtensional basin sediments (Karig & Kozlu 1990), or as also being part of the accretionary prism (Yılmaz & Gürer 1995).

**Lower to Middle Miocene Karatas Formation:** The Karatas Formation is dated as Burdigalian to Serravallian in age (Gökçen et al. 1988) and overlies the Aquitanian Isali Formation, which is an olistostrome unit. The formation is composed of sandstone and marl facies that are interpreted as dominated by basin-plain deposits with minor submarine fans during the Burdigalian to Langhian, whereas the Serravallian a range of environments from basin plain to outer-middle shelf sediments are present (Gökçen et al. 1988) indicating a shallowing over time.

**Upper Miocene Kizildere Formation:** The Tortonian Kizildere Formation is composed of mudstones, sandstones and minor conglomerates that represent a shallowing upwards sequence from fluvio-deltaic to shallow-marine siliciclastics (Gökçen et al. 1988).

The sediments observed in this area are somewhat different to those observed within the Hatay Graben. During the Lower to Middle Miocene the Hatay Graben is continental to shallow-marine compared with deep marine in the Misis-Andırın area. Then in the Upper Miocene when this area is experiencing shallowing and deltaic to shelf sedimentation, the Hatay Graben is subsiding and relatively deep marine conditions predominate.

### 9.2.3 Iskenderun Basin, Southern Turkey

The Iskenderun Basin at the present time is a marine embayment situated ~20km north of the Hatay Graben (Figure 9.4) on the northern side of the Kızıldağ Mountains, which form the southern margin of the basin. To the east the basin is bounded by the EAFZ/DSFZ and to the north by the Misis-Andırın lineament. There is a sparse literature on the onshore sediments of the Iskenderun Basin and there are few published papers on the offshore sediments (Aksu *et al.* 1992; Koral *et al.* 2001; Calon *et al.* 2005) and the area has been extensively drilled for hydrocarbon exploration by the Turkish Petroleum Company (TPAO unpublished data).

During this work, some time was also spent on studying the southern margin of the Iskenderun Basin in order to identify the nature of the sediments and the structures present.

The southern margin of the basin appears to be controlled by a number of large normal faults (dominantly dipping northwards) that have affected the Miocene and Pliocene sediments. Generally, the sediments dip to the north (seawards) but near major faults sediments can be seen dipping to the south. This is interpreted as back-rotation of fault blocks. Faulting was observed in sediments of Early Miocene age and younger. Unfortunately, due to the small amount of time spent in the area the precise age of many of the sediments is not known; this is an area that would benefit from future research. Normal faults have also been observed in offshore seismic lines (Aksu *et al.* 2005).

**Miocene:** Sediments of probable Miocene age are made up of two sedimentary facies. The lower facies is composed of fine-grained pinkish white carbonate with small (<10cm) sub-rounded to sub-angular clasts composed mostly of limestone and serpentinite, with minor chert, quartz and sandstone. The texture is clast- and matrix-supported and there is rare pebble imbrication indicating that palaeoflow was approximately northwards. This lithology shares similarities with the Balyatağı Formation and could be Early Miocene.

The upper facies is dominantly composed of marl. Thin micaceous sandstone beds can be observed within this background sedimentation. Some sandstone beds fine upwards, have flutes and grooves on the base of the beds and exhibit parallel lamination. These are interpreted as turbidites but some thinner beds may be storm deposits. In other places thin, lenticular sandstone beds are observed to have slumped (Figure 9.8). The direction of the slumps suggests the slope dipped toward the east. These sediments are probably Middle to

Upper Miocene in age. It is likely that deposition took place in a relatively deep-marine environment, possibly a slope setting, as suggested by the presence of slumps and turbidites. This is similar to the depositional environments seen to the south and east in the main study area. If the slope was orientated to the east, as suggested by the slumps, this would indicate that the basin organisation was not the same as at the present time.

Drilling in the Iskenderun Basin shows that the Middle Miocene sediments are composed of turbiditic sequences (Gökçen *et al.* 1988) overlain by limestones that are correlated with the Karaisali Formation of the Adana Basin (Aksu *et al.* 2005).



Figure 9.8. Photograph showing slumped sandstone beds in background marl, these may be of Middle to Late Miocene age.

**Messinian:** Messinian evaporates were identified at several localities. Massive selenitic gypsum crystals with no consistent orientation suggest reworking of primary crystals. Elsewhere alabastrine gypsum is seen partly altered to selenite and this is interbedded with marl. Offshore, the Messinian is represented by halite with minor anhydrite and limestone (Uffendorfer *et al.* 1990) but an unconformity of this age within the succession is reported to the southeast.

**Pliocene:** Sediments of presumed Pliocene age are exposed in coastal sections. These sediments are conglomerates, sandstones and silty sandstone, cream to grey in colour. These facies contain fragmentary fossil material and are micaceous. Sedimentary structures are common and include parallel laminations, cross-bedding (indicating an easterly palaeoflow) and pebble lags (Figure 9.9). Conglomerates are often clast supported, composed of sub-angular to rounded poorly sorted clasts; pebble imbrication is present in some horizons. The base of these beds is usually erosive and there is no grading. The composition of these sediments is dominated by Nummulitic limestone and serpentinite clasts but other lithologies are also present. These sediments are interpreted as shallow-marine, possibly shoreface sediments.

The offshore Plio-Quaternary sequence is very similar to that observed in the Adana Basin and is composed of stacked progradational deltaic systems (Aksu et al. 1992).

**Quaternary:** Quaternary soils and conglomerates are present along the southern margin of the Iskenderun Basin. Additionally, three terrace levels of presumed Quaternary age have been identified. Near the city of Iskenderun alkaline lava flows of Quaternary age are found (Yurtmen et al. 2000).

It appears that the sediments of the Iskenderun Basin are similar to those observed in the Hatay Graben, although Middle Miocene limestones were identified only on seismic lines in the Iskenderun Basin, suggesting that this area was experiencing deeper marine conditions at this time. However, the general similarity between the two areas indicates that the basins experienced a related geological history. However, it is not clear whether the basins were connected at any time in the past, although the conglomerate facies does have northward-directed palaeocurrents possibly indicating that during the Early (?) Miocene this may have been the case. The margin of the Iskenderun Basin appears to have been controlled by large normal faults resulting in block rotations, akin to the Hatay Graben, and may indicate a similar mode of formation for the two basins.





Figure 9.9. Photograph of (Pliocene?) coarse-grained sandstone and conglomerate in the Iskenderun Basin. Note that the pebbles usually form discrete horizons although there are occasional pebbles present on the foresets of the cross-bedding in the upper half of the picture. Lens cap for scale.

#### 9.2.4 Latakia, Northern Syria

The area around the city of Latakia is situated ~45km directly to the south of the Hatay Graben (Figure 9.4 and Figure 9.10), although there is a paucity in the literature on the sedimentology and structural development of the region. Mat Hardenberg completed his Ph.D thesis on the area in 2004 detailing sedimentological and tectonic data from the region. The main depositional feature in the area is the Neogene Nahr El-Kabir Valley, a graben

controlled by a major sinistral strike-slip fault, the Nahr El-Kabir Lineament, along the northern margin of the basin. The graben is bounded to the east by the DSFZ and to south by small normal faults.

#### 9.2.4.1 *Sedimentology of the Latakia Region.*

**Upper Cretaceous to Eocene Limestones:** Upper Cretaceous (Maastrichtian) sediments are composed of conglomerates and sandstone overlain by limestones. These are interpreted as transitional from sub-aerial (fluvial) to fully marine conditions. The limestone fauna indicate a deep-water platform setting. Palaeocene to Eocene rocks are generally foraminiferal limestones that indicate neritic marine conditions that possibly became shallower through time. There was some relief and erosion of the Baer Bassit Massif as clastic material is present in some locations. Middle Eocene limestones contain a higher proportion of marl and are interpreted as stacked channel sequences in a shelf environment.

**Lower Miocene (Aquitainian):** There was a regional hiatus during the Mid-Late Eocene to Oligocene. Aquitainian sediments are unconformable on older strata; the base of the formation is locally a bioclastic conglomerate overlain by a conglomerate composed of sparite clasts. Ophiolitic material is generally absent, although present in some sections. Upwards, there is a transition to marls and chalky foraminiferal limestone that compose the majority of the unit. This unit is interpreted as a very shallow-marine environment that rapidly deepened to shelf depths but probably only in the Nahr El-Kabir Graben (Figure 9.10).

**Lower Miocene (Burdigalian):** Burdigalian-age rocks are siltstones, sandstones, limestones and conglomerates with abundant chert, bioclastic and mafic clasts. Wackestones are the most common lithology and the unit can be seen to prograde from the margins of the Nahr El-Kabir Graben as a series of stacked beds. The centre of the valley is dominated by marl deposition probably from shelf water depths. Hardenberg (2004) considers that the Baer-Bassit Massif may have been partly subaerial at this time.

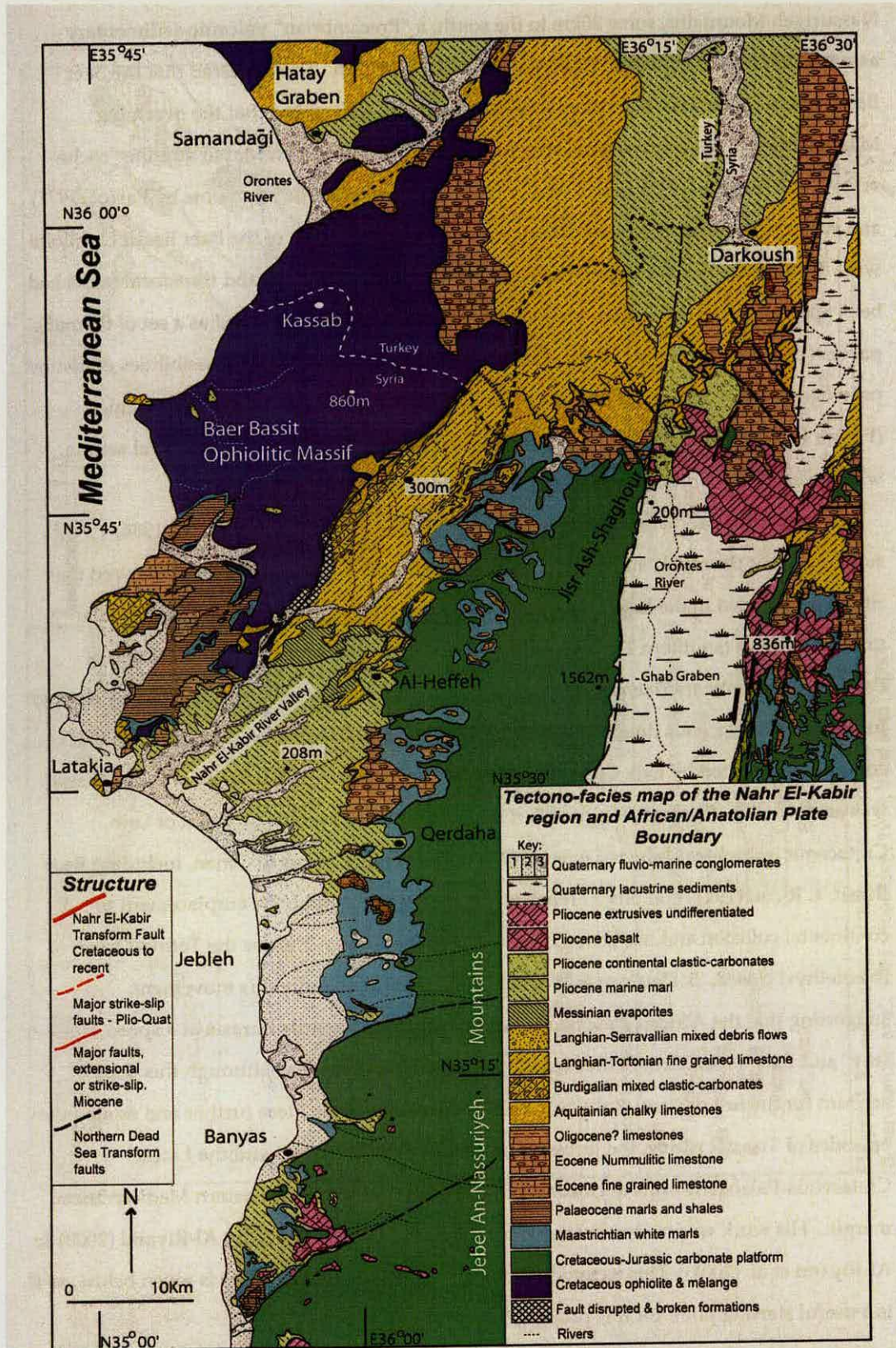


Figure 9.10. Geological map of the Latakia area (from Hardenberg 2004).

**Middle Miocene (Langhian - Serravallian):** Langhian bioclastic limestone is preserved on the western margin of the Bear-Bassit Massif. These sediments were formed in a very shallow-marine environment and probably represent small patch reefs. These limestones are overlain by a variable unit of Langhian to Serravallian age, composed of marl, limestone and conglomerate, probably deposited in shelf water depths within the Nahr El-Kabir Graben and in shallow water along the margins with debris flows transporting material downslope.

**Upper Miocene (Serravallian – Messinian):** A small unit of thin bedded, foraminiferal wackestones was dated as Serravallian (Hardenberg 2004) but no rocks of Tortonian age were identified. The Serravallian limestones are possibly lagoonal. Messinian evaporites crop out locally in the axis of the Nahr El-Kabir Graben. Gypsum is present as selenite and alabastrine with variable thickness generally <100m.

**Pliocene:** The Pliocene is divided into three units. An Lower Pliocene transgressive marl sequence indicates a return to fully marine conditions after the Messinian. Pliocene basalts are present to the south near Banyas (Fig. 9.10), closely associated with marls. This association is interpreted as shallow marine sedimentation with basaltic magma being erupted into this environment. The basalts are dated at  $4.35 \pm 0.22$  Ma (Devyatkin et al. 1996). The marls are overlain by yellow sandstones, rich in shallow marine bioclastic material and are interpreted as a very shallow marine, probably shoreface environment.

**Quaternary:** Quaternary deposits of calciche, palaeosol, conglomerate and coastal bioclastic packstones are present in Latakia area. Terraces are well developed along the coast and associated with rivers.

#### 9.2.4.2 *Tectonic setting of the Latakia region.*

Fault motion in the area is inferred to have taken place in the Middle to Late Eocene, in the Plio-Quaternary and also possibly during the Middle Miocene. Hardenberg (2004) considers that the Nahr El-Kabir Graben probably began to form during the Aquitanian as a half-graben and developed through the Burdigalian to Serravallian into a graben. The presence of this tectonic feature is related to the development of a graben boundary fault (the Nahr El-Kabir lineament) that links the Latakia ridge to the DSFZ.

### 9.2.4.3 Comparisons to the Hatay Graben

- Palaeogene and Eocene strata are widely developed in the Latakia region and are broadly similar to those seen in the south of the Hatay Graben but deep water environments, such as around Belen, are not present. An Oligocene hiatus is present in both areas.
- The Lower Miocene facies are very different in Syria to those further to the north. The marine carbonates with rare input from the ophiolitic massifs in the area compared to terrestrial facies in the Hatay Graben suggest that at this time either subsidence was greater in the south or uplift was greater in the north.
- The Middle Miocene sediments contain a much higher proportion of clastic material and marl and less bioclastic material than the Sofular and Kepez Formations, perhaps suggesting that the Latakia region experienced deeper water sedimentation during this time.
- Tortonian sediments appear to be absent from the Latakia area.
- Messinian-age sediments (both gypsiferous marls and gypsum) are much more common in Syria; outcrop thicknesses are much greater too. This perhaps indicates a higher influx of brine into the Nahr El-Kabir Graben.
- Pliocene facies are very similar suggesting a common environment across the region.
- The timing of tectonic events is similar in the two areas.
- Although the two areas are in close proximity to each other there are some major differences in the sedimentary and tectonic history of the basins.

### 9.2.5 Cyprus – Polis Graben and Mesaoria Basin.

The island of Cyprus lies <150km to the southwest of the Hatay Graben (Figure 9.4). The geology of Cyprus has been extensively studied and many Ph.D projects have been undertaken there, including Eaton (1987), McCallum (1989), Follows (1990), Poole (1992) and Payne (1995). Tim Kinnaird is currently researching the sedimentology and neotectonics of Southern Cyprus for his Ph.D project.

The sedimentary cover of the island is relatively uniform, although there are several depositional basins present on Cyprus. The sedimentology will be considered generally and the tectonics of two basins, the Polis Graben and the Mesaoria Basin (Figure 9.11), will be described and compared to the Hatay Graben.

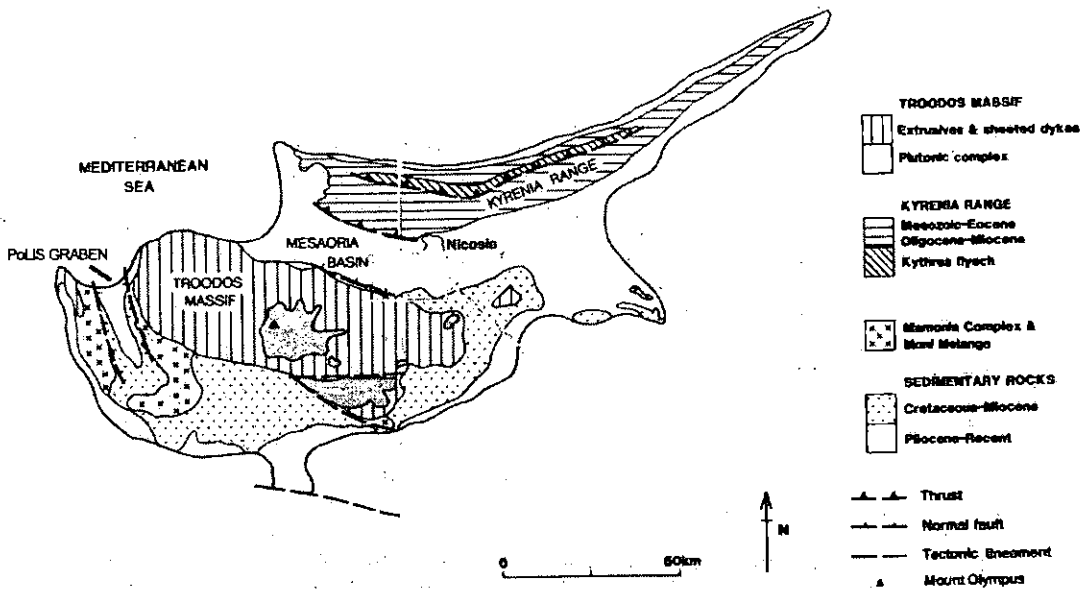


Figure 9.11. Map of Cyprus showing the main stratigraphic and structural units of the island, adapted from Robertson et al. 1995.

#### 9.2.5.1 General Sedimentology of Cyprus

**Cretaceous – Oligocene Lefkara Formation:** The Lefkara Formation overlies the Perapedhi Formation (Campanian – Maastrichtian umbers, radiolarites, volcanogenic clay and sandstone) and the Kannaviou Formation (Maastrichtian bentonitic clays; Robertson and Hudson, 1974) which form the base of the sedimentary cover sequence of the Troodos ophiolite. The Lefkara Formation is composed of pelagic carbonates, mainly chalk. Sediments higher in the succession are mainly calciturbidites (Robertson 1976) and contourites (Stow et al. 1998), which have been extensively altered to chert (Robertson 1977). These carbonates are Palaeocene to Eocene in age (Mantis 1970). The uppermost part of the formation is composed of a massive unit containing slumped horizons.

**Miocene Pakhna Formation and Messinian Kalavassos Formation:** The Pakhna Formation covers the whole of the Miocene Period and is dominantly composed of chalks and marls (Eaton & Robertson 1993). There are two members within the marl succession that represent two phases of reef growth in the Aquitanian-Burdigalian (Terra Mb) and in the Tortonian (Koronia Mb) (Follows 1992). The Terra Member is exposed in the west and southeast of Cyprus. Tectonic controls had little influence on the growth patterns of the reefs in this member. In contrast, the Koronia Member reefs are exposed around Troodos

and are developed on the top of tilted fault blocks (Follows 1992). The rest of the Pakhna Formation represents basinal deposition and the material that was shed from the reefs.

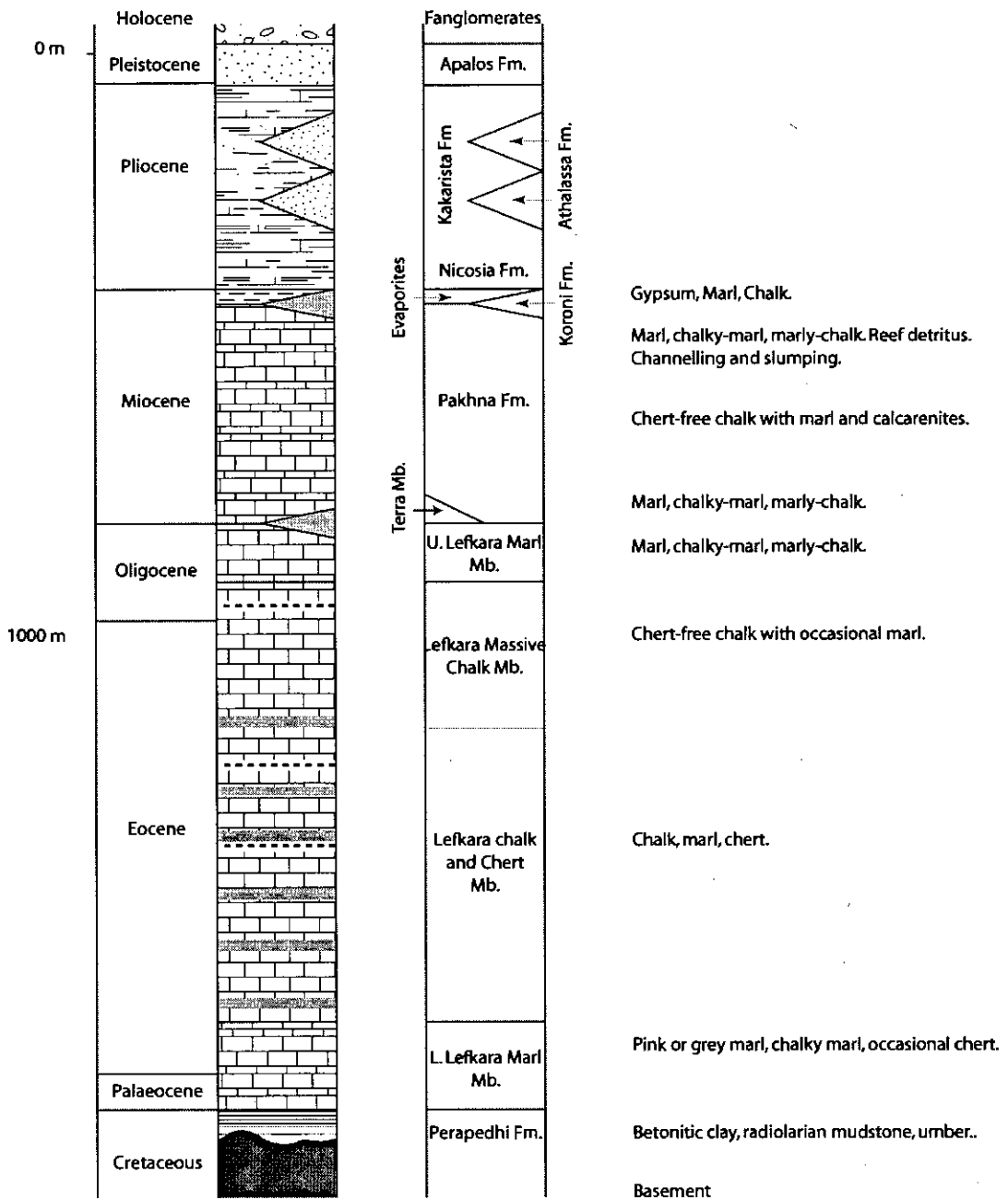


Figure 9.12. Stratigraphic column showing the sedimentary succession on Cyprus (T. Kinnaird, pers. com. 2005).

The Kalavassos Formation is composed of alabastrine and selenitic gypsum; outcrops are generally observed within Late Miocene basins i.e. Khalassa, Maroni (Robertson *et al.*

1995). Deposits are generally thick (>10m) and have often been cut by high-angle extensional faults, not observed in younger sediments (Robertson 2000). The evaporites are overlain by lagoonal – lacustrine deposits of the Late Messinian Lago Mare facies.

**Pliocene Nicosia Formation:** The basal Nicosia sediments record the Early Pliocene transgression (McCallum & Robertson 1990). The sediments are unconformable upon older rocks. In the Mesaoria Basin the basal sediments of the Nicosia Formation are conglomerates interpreted as mass-flow deposits of fan-delta systems that built across a narrow, fault-controlled basin margin. The majority of the Nicosia Formation is dominantly composed of marine calcareous siltstones. But also on the margins of basins the formation is composed of shallow-marine fine-grained carbonates.

**Late Pliocene – Early Pliocene Athalassa and Kakkarista Formations:** These formations are found within the Mesaoria Basin. The Athalassa Formation is composed of bioclastic sandstones that are interpreted as shallow-marine carbonate sandbodies (McCallum & Robertson 1995a). These sandbodies are separated by finer grained mud facies.

The Kakkarista Formation, in contrast, is composed of coarse conglomeratic material and is interpreted as a fan-delta system that developed when the Mesaoria Basin had virtually ceased subsiding (McCallum & Robertson 1995b); this fan-delta sedimentation was triggered by uplift of the Troodos Massif. Shoreface and beach facies have also been recognised in this formation.

Pliocene sediments in the Polis Graben are composed of marginal to shallow-marine sandstones and conglomerates.

**Quaternary:** Quaternary uplift of Cyprus due to the underthrusting the African plate and serpentinite diapirism in the Troodos Massif has resulted in the formation of a series of marine terraces around the island (Poole & Robertson 1991; Poole & Robertson 1998). Associated with these terraces are siliciclastic sediments deposited in a variety of environments; including fluvial, alluvial fan, beach and braid-delta environments.



### 9.2.5.2 *The Polis Graben and Mesaoria Basin*

The Polis Graben is a Late Miocene - Pliocene basin situated in the west of Cyprus. It is a graben formed by extension with perpendicular transfer faults linking graben-bounding normal faults. The largest normal faults are those bounding the margin of the graben and forward-rotated fault blocks are common along these margins. The graben is inferred to have formed due to extension caused by subduction zone roll-back that was probably most active in the Tortonian to Messinian (Payne & Robertson 2000).

Mesaoria Basin is situated in the northern and eastern Cyprus between the Troodos Massif and the Kyrenia Range. Two models exist for the evolution of the Mesaoria Basin. In the first the formation of the half-graben is related to a phase of extension in the forearc region, possibly due to roll-back of the subduction zone (Robertson 1998; Robertson et al. 1991; McCallum & Robertson 1990). The basin probably formed during the Late Miocene (McCallum 1989) bounded to the north by large normal faults now forming the edge of the Kyrenia Range. The southern margin is defined by smaller antithetic faults but the basin morphology is that of a half graben. Extension and subsidence continued until the Late Pliocene. At the end of the Pliocene the Troodos Massif experienced a pulse of uplift (Robertson 2000) resulting in the emergence of the basin in the Pleistocene.

The second model explains the formation of the Mesaoria Basin as a large piggy-back basin between the Kyrenia fold/thrust belt and the Troodos within a crustal scale thrust system encompassing the whole of a forearc region north of the Cyprus Arc (Calon et al. 2005). The basin formed from the Eocene-Oligocene to Recent times and thrusting has been active during the whole of that period in this model. These two alternatives are currently being studied by Tim Kinnaird (Ph.D. Edinburgh University).

### 9.2.5.3 *Comparisons to the Hatay Graben*

- The Palaeocene is characterised in both areas by carbonate deposition. Generally the environment of deposition in Cyprus appears to be deeper than that of the Hatay area, apart from the area around Belen where Eocene calciturbidites were observed.
- The Pakhna Formation is similar to the sediments in the study area. Both regions experienced reef deposition during the Burdigalian, but in Cyprus this also occurred in the Late Miocene indicating that at this time Cyprus experienced shallower water conditions than southern Turkey. The bulk of the formation, being composed of marls, is very similar in both areas.
- Similar evaporites are developed in both Cyprus and the Hatay Graben.

- The Pliocene to Pleistocene units in Cyprus are mostly controlled by local tectonics within a syn-collisional regional plate-tectonic setting, in contrast to the more collisional setting in the Hatay and areas to the east. However, basinal sediments and evidence of Quaternary uplift are similar probably due to similar climatic conditions and eustatic sea-level changes.
- The Polis and Mesaoria Basins appear to have formed at a similar time to the Hatay Graben.

<i>Epoch</i>	<i>Structural event in the Hatay area.</i>	<i>Sedimentary environments in the Hatay area.</i>	<i>Comparisons to regional environments as described previously</i>	<i>Regional tectonic events</i>
Late Cretaceous	Emplacement of ophiolitic material southwards onto the Arabia	Post-emplacment very shallow-marine (intertidal) carbonates – carbonate platform.	Regional carbonate platform; deeper water environment to the south.	Ophiolite obduction. Late Phase of Syrian Arc I deformation.
Palaeocene-Eocene	?	Transgressive limestone sequence from intertidal sediments into those deposited at shelf depths. Calciturbites in the north.	Regional carbonate platform. Latakia region shows regression. Pelagic limestones and calciturbidites in Cyprus.	Initial fold and thrusting along the Bitlis-Zagros suture zone.
Oligocene	Folding of Eocene and older rocks.	No sediments of this age – unconformity.	Regional unconformity on Arabian Platform. To the north terrestrial deposition; to the west deep marine. Syrian Arc II deformation.	Regional uplift associated with collision
Early Miocene	Early faulting?	Brief marine incursion followed by braided rivers flowing to the north (near Antakya). To the north deposition took place on an fan delta.	Shallow-marine conditions prevailed to the south and west, while to the north there was a transition from non-marine to marine environments.	Dead Sea Fault Zone forms in Dead Sea region ~25 Ma; initiation of subduction along the
Middle Miocene	Normal faults active – thickening of strata into faults.	Various shallow-marine carbonate environments, including peritidal platform, lagoon, ramp and reefs.	Widespread reef formation and shallow-marine environs at this time. Some areas have deeper water facies and turbidites (north and west).	Northward propagation of DSFZ. Terminal closure and uplift of the Bitlis suture in Mid-Late Miocene time.

<i>Epoch</i>	<i>Structural event in the Hatay area.</i>	<i>Sedimentary environments in the Hatay area.</i>	<i>Comparisons to regional environments</i>	<i>Regional tectonic events</i>
Late Miocene	Continued normal faulting, significant basin subsidence.	Relatively deep marine sedimentation.	Regional deep-marine environments, some reef growth in Cyprus. Non-marine conditions only to north in Adana area	Possible subduction zone roll-back results in basin formation in Cyprus.
Messinian	Continued subsidence and faulting.	Evaporite formation and marl deposition in depocentres. Erosion of exposed areas. Some areas with no break in beach deposits	Regional evaporate formation and erosion.	
Pliocene	Continued normal faulting, initiation of strike-slip faulting along basin axis.	Shoreface sediments and marl deposition.	Early Pliocene transgression followed by regional regression	Initiation of EAFZ and NAFZ, DSFZ reaches southern Turkey.
Quaternary	Continued fault activity – still seismically active.	Quaternary river deposits and terraces, tufa, scree and marine notches.	Various continental deposits, marine terraces common. Deltas offshore, some basaltic magmatism.	Uplift of the Troodos Massif.

Table 9.1. Table showing the timing of structural and sedimentary events in the Hatay Graben compared to other basins in the Eastern Mediterranean; these areas were discussed in the previous section and include Cyprus, Adana and Iskenderun Basins and the Latakia area.

### 9.3 Tectonic Models for the formation of the Hatay Graben

In the introduction to this thesis a number of tectonic models from the literature were outlined, with the Hatay Graben as either:

- a) A pull-apart basin (Perinçek et al. 1990), half-graben (Lyberis et al. 1992), or graben (Muehlberger 1981; Perinçek & Çemen 1990) formed as the result of extension at a divergent flexural bend in a strike-slip controlled fault system.
- b) A graben resulting from the westward escape of Anatolia (Yürür & Chorowicz 1998).
- c) A strike-slip or transtensional basin related to the Cyprus arc to the west (Ben-Avraham et al. 1995; Kempler & Garfunkel 1994).

These models will now be evaluated in light of the new data and interpretations gained from this research and a new model for the formation of the Hatay Graben will be presented.

#### 9.3.1.1 Strike-slip related models

The Hatay Graben is interpreted as a pull-apart basin (Perinçek et al. 1990), half-graben (Lyberis et al. 1992), or graben (Muehlberger 1981; Perinçek & Çemen 1990) formed as the result of extension at a divergent flexural bend in a strike-slip controlled fault system (Arpat & Şaroğlu 1972; Şengör et al. 1985; Lyberis et al. 1992; Şaroğlu et al. 1992; Parlak et al. 1998)

The majority of published models considered that graben formed in response to stresses caused by the propagation of the EAFZ, the DSFZ, or both. In some interpretations the Hatay Graben is a direct extension of the EAFZ (Şengör et al. 1985; Lyberis et al. 1992; Şaroğlu et al. 1992). Others (Arpat & Şaroğlu 1972; Parlak et al. 1998) trace the extent of the DSFZ further north through the Amanos Mountains to the Turkish coastal area and relate basin formation to this structure.

Evidence from syn-depositional faults within the Hatay Graben, however, indicates that normal faulting parallel to the basin was active during the Middle Miocene, around 13-15Ma. But the inception of the EAFZ is dated as *Late Miocene to Pliocene* (Şengör et al. 1985; Dewey et al. 1986; Hempton 1987; Şaroğlu et al. 1992; Westaway & Arger 1998; Yürür & Chorowicz 1998). Although the DSFZ formed synchronously with the opening of

the Red Sea around 18-20 Ma (Garfunkel *et al.* 1981; Hempton 1987; Lyberis 1988; Rojay *et al.* 2001), studies of the more northerly strands of the DSFZ indicate that the fault did not propagate northwards into northern Syria and southern Turkey for another 15 Ma during a second phase of fault motion at 4.5 Ma (Freund *et al.* 1968; Girdler & Styles 1978; Zanchi *et al.* 2002).

Therefore, the timing of these events *postdates* the initiation of faulting in the Hatay Graben. Hence, the initiation of the Hatay Graben cannot be linked with either the inception of the EAFZ or the DSFZ. The formation of these large strike-slip faults is a result of the westward escape of Anatolia after continental collision in the Late Miocene; thus, the timing of the faulting also shows that faulting in the field area was not initially as a result of the tectonic escape of Anatolia (model b).

Strike-slip faults are common within the axis of the present topographic graben. The present tectonic regime is transtensional possibly with a dominantly strike-slip character and appears to be a recent or stable stress field. So that although initial deformation was not directly related to the EAFZ or DSFZ, during the Plio-Quaternary transtensional tectonics have resulted in strike-slip controlled faulting within the significant topographic graben (the Hatay Graben, *sensu stricto*) that could be related to the EAFZ or DSFZ (see below).

## 2. Extension related to subduction roll-back (model c).

During the Early Miocene, the Southern Neotethys to the north and east of the study area was in the final stages of subduction and incipient collision of the Tauride microcontinent with the Arabian microplate; whereas to the west, ocean crust still existed. At this time the subduction zone that existed along the Misis-Andırın lineament moved southwards initiating a subduction zone south of Cyprus (Kempner & Ben-Avraham 1987; Robertson 1990; Robertson *et al.* 2004). Thus initiation of faulting on the subducting Arabian slab could be related to stresses associated with the southward retreat of the subduction zone, e.g. trench roll-back.

There is evidence that the over-riding plate was strongly extended during the Early-Mid Miocene, with the formation of thrust-top (piggy-back) basins within the Misis-Andırın lineament to the north (Robertson *et al.* 2004) and faulting associated with graben formation was active. This extension could be related to roll-back of the down going slab during the final stages of subduction when old, dense oceanic crust was being subducted. This model is

proposed for a number of other extensional basins in the Eastern Mediterranean (i.e. Polis Graben, Payne & Robertson 2001; Mesaoria Basin, Robertson 1998; Robertson *et al.* 1991; McCallum & Robertson 1990; Crete, ten Veen & Kleinspehn 2002; Peterek & Schwarze 2004). Here these basins are situated within the “forearc” of the subduction zone, not the foreland like the Hatay Graben. Additionally, roll-back effectively ceases (or becomes much less active) when all the ocean crust is subducted and continental crust enters a trench; this is thought to have occurred along the Bitlis Suture Zone in the Early Miocene (Robertson *et al.* 2004), therefore pre-dating the initiation of faulting in the Middle Miocene. So although roll-back probably played a role in the evolution of the region it does not appear likely that the process was important in the geological development of the field area.

### *3. Foreland basin mode followed by tectonic escape – preferred hypothesis (Fig. 9.13)*

In this two-stage model the pre-Messinian sediments in the Hatay area formed part of the basin fill of the foreland basin that developed ahead of the Bitlis-Zagros suture zone; then during the Late Miocene/Pliocene a topographic graben developed due to transtensional stresses related to the extrusion of Anatolia.

Peripheral foreland basins develop in response to the loading of the lithosphere of the down-going plate during continent-continent collision. The sedimentary fill of unfilled basins forms a classic sequence that has been termed the “unfilled trinity” (Sinclair 1997). Unfilled forelands are composed of dominantly deep-marine sediments (Tankard 1986), as opposed to filled forelands with a fill of shallow-marine to continental sediments. This underfilled trinity is composed of three units that are diachronous and often superimposed on top of one another due to the migration of facies away from the orogen (Fig. 9.14). The three units generally overlie the underlying basement and passive margin sediments along an unconformity (e.g. Allen *et al.* 1991; Coakley & Watts 1991; Sinclair 1997); these are composed of a lower unit of shallow-marine limestones and sandstones, a middle unit of pelagic mudstones and an upper unit of sandstone turbidites classically termed “flysch”.

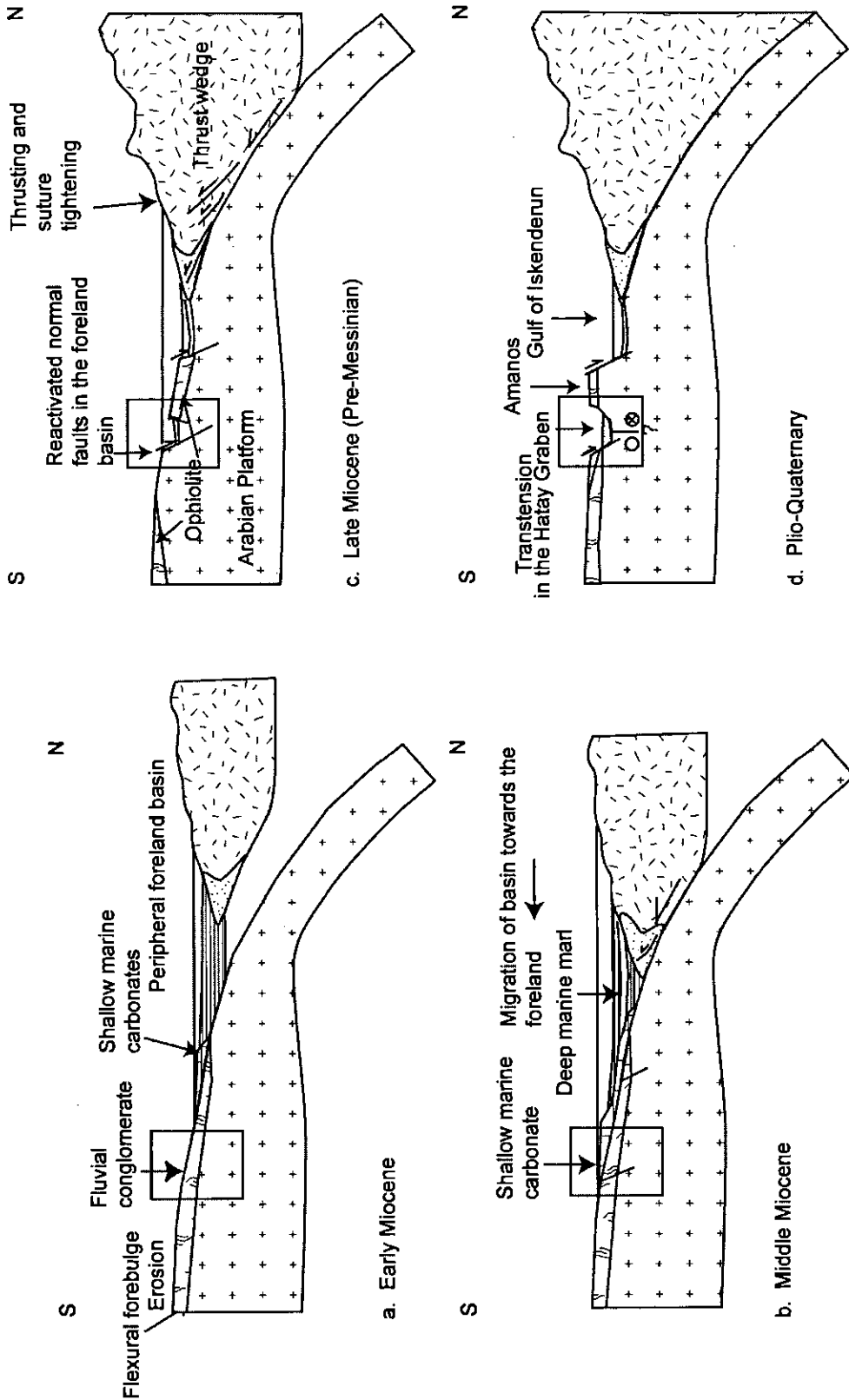


Figure 9.13. Schematic Cross-sections for the Northern Arabian Platform to the margin of Anatolia showing structure for: a) Early Miocene; b) Middle Miocene; c) Late Miocene and d) Pliocene times. The box indicates the position of the field area.



The underfilled trinity represents sedimentation in three different areas of an underfilled peripheral foreland basin. The lower unit reflects shallow-marine sedimentation on the cratonic margin of the foreland basin, deposited on top of the passive margin succession along an unconformity. The basal deposits record the initiation of subsidence at a given location. The middle unit records the period when relative sea-level rise linked to flexural subsidence outpaces the growth of shallow-marine carbonates. The upper part of this unit represents the deepest part of the basin and records the position of the basin axis at that time. The upper unit is dominated by siliciclastic material derived from the thrust wedge.

This pattern of sedimentation is similar to that observed in the study area. The passive margin sediments are composed of the Eocene and older platform carbonates of the Arabian Platform and the fluvial conglomerates and sandstones of the Balyatağı Formation. The top of the platform carbonates (Eocene) is a regional unconformity and there are local unconformities at the top of the Balyatağı Formation. The unconformity at the top of the Eocene may also be related to Syrian Arc, phase II, deformation that can be recognised as a factor in the development of the Eocene/Oligocene unconformity to the south in Lebanon and Syria (Walley 1998). The basal Balyatağı Formation unconformity is likely to represent more local conditions in the foreland basin and probably represents river systems that were draining the cratonic margin of the emergent foreland (the Baer-Bassit Massif) that was undergoing erosion due to uplift, perhaps associated with a peripheral bulge.

The lower unit of the underfilled trinity could be represented by the Sofular Formation, composed of peritidal, lagoonal, reef and ramp carbonates. Similar limestones are observed in Papua New Guinea (Pigram *et al.* 1989), the Persian Gulf (Murriss 1980) and especially the Alps (Sinclair 1997) where there are rapid along-strike facies variations. The middle unit of the trinity could be represented by the Nurzeytin Formation, foraminiferal rich marl, very similar to carbonate pelagic-hemi-pelagic sediments from other foreland basins (Sinclair 1997). An equivalent of the upper unit does not appear to be present in the Hatay Graben for several possible reasons that will be explored further below.

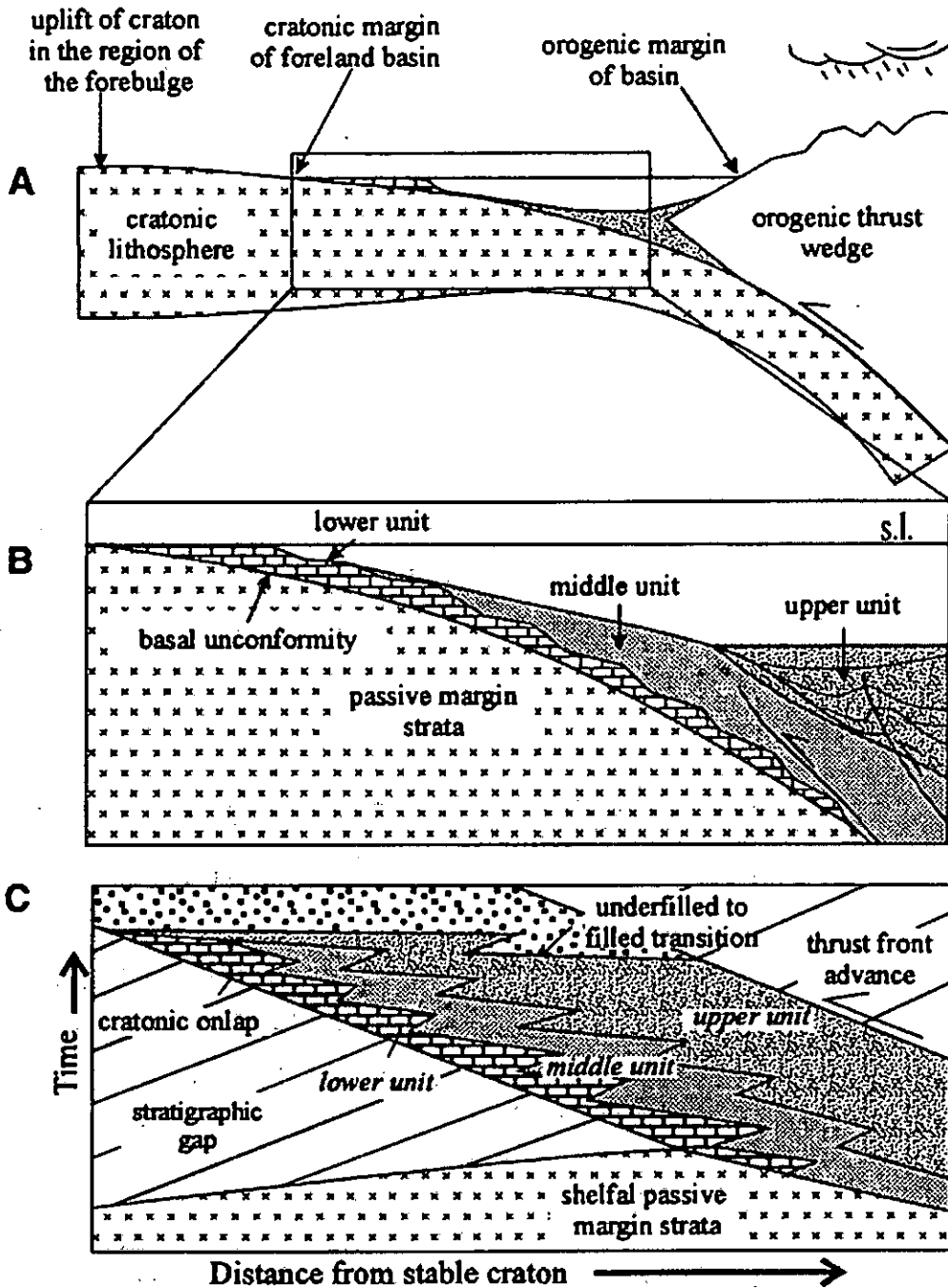


Figure 9.14. A) Basinal setting of the underfilled trinity in a peripheral foreland basin. As the thrust load thrusts over the craton, so the foreland basin migrates at approximately the same rate. B) This migration results in a superposition of the three units of the trinity with a basal unconformity resulting from the uplift and erosion of the flexural forebulge. C) Chronostratigraphic representation of the underfilled trinity, all three units are diachronous in response to basin migration. From Sinclair (1997).

Normal faulting has been documented in many foreland basins. Normal faults with throws of up to 150m are present on the Sahul shelf of Timor (Veevers *et al.* 1978) in the lower limestone unit. Normal faults have also been documented in the middle unit of the Taconic foreland basin (Utica Shale) of New York (Fig. 9.15; Bradley & Kidd 1991), the Pliocene of the Timor Trough (Veevers *et al.* 1978), the French Alps (Sinclair 1997), the Pelagian Shelf, the central Mediterranean, Italy (Argani & Torelli 2001) and the Muti Formation of Oman (Robertson 1987).

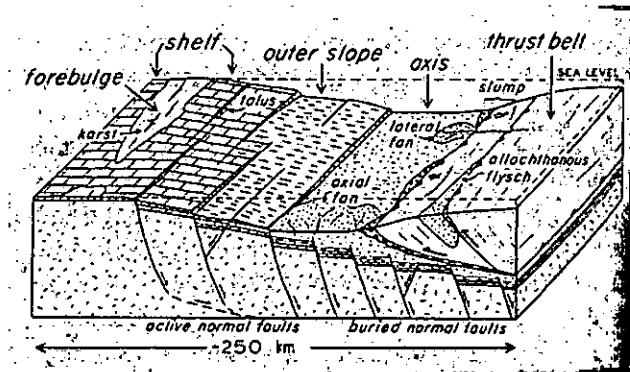


Figure 9.15. Schematic block diagram of Taconic foredeep, New England, showing structural regime and facies belts shortly before plate convergence ended. From Bradley & Kidd (1991).

Normal faulting in the foreland basin fill can be related to two things. Firstly, the underlying passive margin is likely to have normal faults that formed during continental break-up. These form deep seated weaknesses in the lithosphere that could be reactivated later. Secondly, Bradley & Kidd (1991) suggest that active faulting in the foreland maybe due to extensional stresses generated on the outer arc of the fixed lithosphere. Therefore, I suggest that the faulting in the early Hatay Graben, prior to the formation of significant topographic relief, was due to extensional stresses caused by the flexure of the foreland reactivating deep-seated normal faults in the Arabian passive margin. It is unlikely that this faulting resulted in significant topographic relief, as syn-tectonic sediments appear to have been contemporaneously in-filled as accommodation space was created.

Peripheral foreland basins have distinctive patterns of subsidence (Burbank *et al.* 1986; Cross 1986; Homewood *et al.* 1986; Johnson *et al.* 1986; Miall 1995), where the initial subsidence rate is slow due to the emplacement of the supracrustal load. The rate of

subsidence increases as the wedge thickens and impinges on the continental margin and reaches a maximum when the basin is overridden by the emplaced load. The rate of subsidence then decreases as uplift and tectonic rebound occur. Foreland basin subsidence curves have sharp inflection points that may represent flexural response to specific thrust loading events. The subsidence curves calculated for the Hatay Graben, although likely to contain errors, show this pattern of initial low, then fast subsidence, further supporting the foreland basin hypothesis.

Uplift to the south in the Baer-Bassit Massif may be due to forebulge uplift, shedding sediments to the north from the Lower Miocene onwards, although the massif was possibly drowned in the Middle Miocene due to relative sea-level rise. Robertson *et al.* (2004) suggest that during the Mid-Miocene there was a re-advance of the thrust load overriding the foreland and causing the forebulge to collapse, which may account for this drowning in the Mid-Miocene. Also, models of continental collision suggest that the position of the flexural forebulge could be ~400km from the thrust front (Stockmal *et al.* 1986) making this feasible.

Mica and other extrabasinal sediments are assumed to have been derived from the north, as there are no suitable source lithologies locally, possibly from the Tauride Mountains or from the Misis-Andırın lineament where mica schists and other micaceous sediments are exposed (Robertson *et al.* 2004). Mica is first observed in the northeast of the area (near Belen) during Late Miocene suggesting that before that time the axis of the foreland basin prevented northward-derived material from being transported as far south as the Hatay, therefore, this may indicate when the foredeep to the Bitlis suture was in filled and bypassed.

When marine conditions returned to the basin in the Early Pliocene the overriding tectonic controls on the area had changed from a zone of continent-continent collision to one of tectonic escape (Şengör *et al.* 1985). Large strike-slip faults were by then dominating the plate tectonics of the area (i.e EAFZ/DSFZ; Arpat & Şaroğlu 1972, Şengör *et al.* 1985; Mart & Rabinowitz 1986; Barka & Kadinsky-Cade 1988; Lyberis 1998). The boundary faults that controlled the development of the Plio-Quaternary Hatay Graben were superimposed on existing structures resulting from extension within the foreland basin or reactivation of basement faults. Structural data indicate the area is transtensional, as several populations of faults are present with no clear age relationship (section 7.5). There are no consistent cross-cutting relationships and also fault patterns in rocks of Upper Cretaceous to Quaternary age are very similar suggesting only one on-going event has taken place recently. The area may

be experiencing oblique extensional strain due to a difference in the orientation of basement faults and the present direction of maximum extension controlled by continental escape towards the deep Eastern Mediterranean Basin.

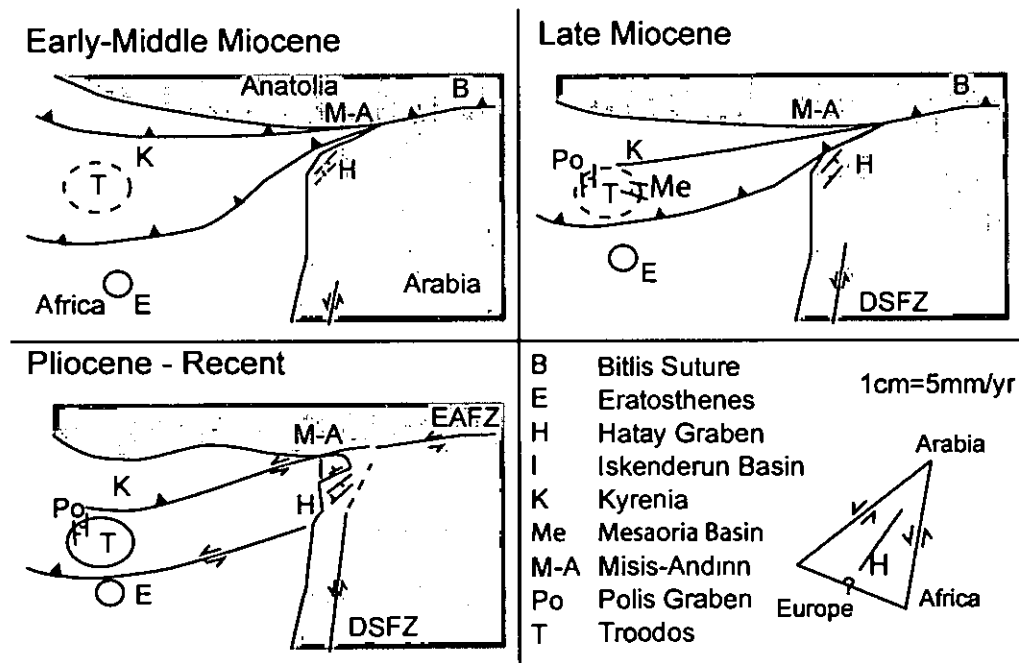


Figure 9.16. Maps illustrating the tectonic evolution of the Eastern Mediterranean from the Early-Middle Miocene to the present day. The Early-Middle Miocene is a time of subduction near the coast of Anatolia, subsequently migrating to the south to near its present position. Thrusting occurs along the Arabian margin forming a foreland basin. Faulting is initiated in the Hatay Graben. By the Late Miocene roll-back of the subduction zone has given rise to extensional basins on the overriding plate and thrust emplacement is complete in southern Turkey. The DSFZ is propagating northwards. Faulting in the Hatay Graben is advanced. In Pliocene to Recent times, collision has resulted in the westward escape of Anatolia, initiating the EAFZ, and the DSFZ has propagated northwards into southern Turkey. The Eratosthenes Seamount is being thrust under Cyprus and the Troodos Massif is uplifting in response. The vector diagram illustrates the orientation and motion of the DSFZ and EAFZ with the orientation of the Hatay Graben shown between them.

The upper unit of the ‘unfilled trinity’ is not present in the field area. This may be the result of a number of factors. Most importantly by the Mid-Late Miocene active subduction of the continental lithosphere had ceased (Robertson *et al.* 2004), but continuing N-S directed compression was ongoing along the Bitlis Suture, leading to uplift and crustal thickening of Anatolia during the Late Miocene/Early Pliocene time (Şengör & Kidd 1979). As further

loading of the lithosphere ceased after this time, isostatic rebound of the foreland basin would have taken place leading to uplift and shallowing of marine environments. By the Late Miocene, uplift in the Betics (Southern Spain) resulted in the Straits of Gibraltar no longer being a marine connection and as a result the Mediterranean became isolated and sea-level fell within marginal basins (Hsu *et al.* 1987). Accordingly evaporites were deposited in the field area.

No large discrete strike-slip faults have been identified in the field area, but there is potentially a zone along which strike-slip motion may have occurred (with evidence of block rotations, section 7.3.2). There is no definite evidence for the offset on this zone. However, the deformation of the sediments is limited to minor folding and differences in the orientation of bedding. This is much less than seen in sediments of similar age that are adjacent to graben boundary faults, where bedding has been rotated to vertical in places and is heavily faulted. This relatively minor deformation suggests that the Anatolian-African plate boundary does not run through this area as previously suggested (Şengör *et al.* 1985; Girdler 1990; Şaroğlu *et al.* 1992; Lyberis *et al.* 1992; Över *et al.* 2004). It is more likely that the Kyrenia-Misis Lineament or the Al-Nakib Graben in Syria represents the plate boundary between the African and Anatolian plates (assuming the boundary is a discrete structure). Alternatively the boundary is diffuse and distributed throughout the area as inferred by Kempler & Garfunkel (1994).

If we compare the tectonic and stratigraphic evolution of this area to the wider region we can integrate the geological evolution of the Hatay Graben into the regional picture. The Miocene sediments to the north of the Hatay Graben are buried beneath the Iskenderun Basin.

Exploration oil wells offshore in the Iskenderun Basin indicate that, in general, Late Oligocene to Early Miocene turbidites overlie ophiolitic rocks (Kempler & Garfunkel 1994), these were then overlain by Messinian evaporites and Plio-Quaternary clastic sediments that prograded from the Misis-Andırın thrust front to the north (Aksu *et al.* 1992). On land, the Iskenderun Basin was marked by extensional faulting especially around the northern margin of the Hatay ophiolite, opening a basin that was partially filled with a relatively deep-marine marl sequence of the Middle Miocene, overlain by evaporites and shallow-marine clastic sediments. No limestone was observed in the area but it is possible that limestone is

present offshore (Aksu *et al.* 2005). If this is the case then the three units of the “underfilled trinity” of the foreland basin are also present in this area. The greater thickness of the middle/upper unit may indicate a deeper water setting and more proximal location to the thrust front and/or greater subsidence in the foreland basin axis. Palaeocurrent directions indicate that in the Lower (?) Miocene flow was to the north, indicating that at this time the Hatay and Iskenderun basins were not separated by a high. Late Miocene palaeocurrents in the Iskenderun area indicate flow to the east, while in the Hatay Graben flow was mainly westerly, suggesting that by the Mid/Late Miocene some topography existed. Aksu *et al.* (2005) propose the presence of a thrust culmination (cored with ophiolite) in Iskenderun Bay that was active until the Pliocene. This feature could result in basin floor topography. However, thrust faults are rare in the sedimentary cover, and those that are present have throws of <10's of centimetres and no post-emplacement thrusts have been identified in the Kızıldağ ophiolite (J. Inwood, pers. com. 2005). Therefore, it seems more likely that basin floor topography resulted from normal fault motion.

To the north of Iskenderun, Miocene sediments are exposed structurally underlying the Misis-Andırın lineament. Interpreted as peripheral foreland basin sediments by Gökçen *et al.* (1988) and Robertson *et al.* (2004), Early - Middle Miocene deep-marine turbiditic sediments are present with associated slope deposits at the base of the succession, as would be expected from the areas proximal to the thrust front where loading and, therefore, subsidence are greatest. Similar facies can be observed elsewhere in southeastern Turkey (i.e. Lice Formation; Aksu & Robertson 1984; Gökçen *et al.* 1988).

Deep-water conditions persisted through the Middle Miocene, although there was shallowing the east during the Serravallian into shelf and submarine fan deposits; palaeocurrents were directed towards the west (Gökçen *et al.* 1988). These effects were perhaps due to the effects of diachronous continental collision that occurred first in the east. The shallower water conditions experienced in the Late Miocene suggest infilling of the foreland, and a transition from unfilled to filled foreland basin. Deep-water conditions were still present to the south (Iskenderun and Hatay) suggesting that the foreland basin subsidence migrated southwards and the Misis area was shallowing due to collision related folding, thrusting and uplift. Palaeocurrents in the Misis area are directed to the south away from the suture zone and not along the trench supporting this idea.

To the northwest, the Adana Basin contains a transgressive sequence of continental siliciclastics, followed by shallow-marine limestone into basinal turbidite sequences. Although this basin has been interpreted as a foreland basin in the past (e.g. Ünlügenç 1993), the position of the basin behind the Misis-Andırın lineament, not in front means that it is on the over-riding plate not the subducting plate. So although there are similarities between the sedimentary fills of the two areas, the tectonic controls were different and similarities are likely to be related to climatic and eustatic controls.

On Cyprus, there are a couple of basins whose formation has been linked to subduction zone roll-back and there are similarities between the sedimentary successions of the Hatay Graben and Cyprus. But generally, the sediments observed in Cyprus represent much deeper water conditions than in the Hatay Graben. The exceptions to this are the Miocene reefs that are much more common in Cyprus. But, the Plio-Quaternary sediments are very similar due to both areas becoming sub-aerial at this time. The similarities between the areas are also likely to be due to the closeness of the two areas, and so are affected in a similar way by eustatic sea-level changes and regional tectonic events. However, the position of Cyprus in a location of pre-continental collision is quite different to the Hatay, suggesting that the controls of sediment facies and basin formation would be significantly different.

In contrast, the Latakia region has a different stratigraphy and although there are some similarities during most of the Neogene the Nahr El-Kabir Graben experienced much deeper water conditions than the Hatay Graben (Hardenberg 2004). If this area was also part of the foreland basin it would be expected that this area would have experienced generally shallower water conditions than the Hatay as the Nahr El-Kabir Graben is in a more distal position. This indicates that either this area was not affected by the orogen, unlikely due to the areas proximity, or that the Nahr El-Kabir Graben had a significant effect on the distribution of sedimentary facies.

All these areas have experienced the effects of the Messinian Salinity Crisis and Plio-Quaternary uplift. Pliocene facies are variable but the Quaternary of the region has mainly seen fluvial deposition and terrace formation. The similarities in the Plio-Quaternary sedimentation between the different areas reflect regional uplift in Turkey and unrelated uplift of the Troodos Massif resulting in widespread non-marine conditions at the present time.



## 9.4 Wider Implications

Irregular and diachronous continental collision is common along convergent plate boundaries past and present due to the irregular shapes of continents. The Hatay Graben is located at the transition from a post-collisional to pre-collisional setting and thus represents a natural laboratory for studying the affects of irregular continental collision. Due to the distal position of the area in the foreland basin the Miocene and younger stratigraphy has not been deformed by thrusting and folding, and therefore stratigraphic and structural relationships of a distal foreland basin are relatively easy to unravel. The later formation of the Hatay Graben, *sensu stricto*, related to the post-collision extrusion of Anatolia gives insights into how transtension related to extrusion tectonics can affect adjacent areas. Additionally, recently multi-phase models for sedimentary basin formation are being proposed for other basins in the Eastern Mediterranean (i.e., the Isparta Angle area, Turkey; Flecker *et al.* 2005) suggesting that many basins in this area do not form due to a single event but may have more complicated origins than previously understood. This may also be the case for other basins in different regions. In addition, not only is the two-phase development of the Hatay Graben important for understanding the geology of the Eastern Mediterranean region, these results will also be of interest for people working in other collision zones. For example; in the Himalayas where the processes of continental collision and extrusion tectonics are more advanced, and in the western Pacific where full continental collision has yet to occur, but the numerous microplates will result irregular and diachronous collisions.

## 9.5 *Future Work*

There are a number of outstanding questions that have not been satisfactorily answered in regard to the Hatay Graben, mainly due to fieldwork constraints. These would warrant further investigation and include:

- Is the block faulting inferred in the graben floor significant? What is the extent of this feature? This could be resolved through careful field mapping combined with sampling for palaeomagnetic investigation.
- There are several outstanding issues with regard to the geomorphological evolution of the area. Are buried faults causing the knick-points observed on several of the river profiles? Are all the features interpreted as windgaps actually wind gaps? If so, when were these features formed? Further field work and cosmogenic isotope dating of surfaces would contribute significantly to the understanding of the geomorphology.
- How does the Hatay Graben relate structurally to the Karasu Rift and Dead Sea Fault Zones?

Finally, there is still a question mark over the location of the Anatolian/Arabian/African triple junction until this is resolved there is much field work to be undertaken in the Eastern Mediterranean area.

## 10 Conclusions

A number of important conclusions drawn from this research project can be summarised from the preceding chapters:

- The sedimentary evolution of the Hatay Graben and the area of the Karasu Rift around Belen and Kırıkhan share many similarities and have a shared history.
- The Palaeogene units of moderate deep-water shelf carbonates (the Cona and Hacıdağ Formations) in the north correlate with shallow-marine platform carbonates (the Okçular and Kışlak Formations) in the Hatay Graben.
- The Neogene units: The Early Miocene braided-river conglomerates (Balyatağı Formation) of the Hatay Graben are equivalent to the fan-delta sediments (Kııcı Formation) of the north; the Middle Miocene shallow-marine to shelf carbonates (Sofular Formation) of the Hatay Graben are equivalent to the shallow marine carbonates of the Kepez Formation and the relatively deep-marine Late Miocene marls across the field area are equivalent (Nurzeytin Formation and the Gökdere Formation).
- Samples from the relatively deep-marine marls (Nurzeytin Formation) yielded ages of between 13.25 Ma and 8.33 Ma, i.e. Serravallian to Tortonian in age (Late Miocene), by strontium dating. The base of the Nurzeytin Formation is likely to be diachronous and top of the formation has probably been differentially eroded
- Samples from Pliocene sediments yielded ages of 5.35 Ma and 5.61 Ma.
- Prior to the Lower Miocene some erosion of ophiolite took place but this was confined to periods of relative low sea-level, whereas it seems that the sedimentary cover was generally more eroded. From the Early Miocene to present day there has been continual erosion of the ophiolite and cover sediments.
- Mica has an extrabasinal source, the appearance of this mineral in the Hatay Graben may indicate the time when the foredeep to the Bitlis suture was bypassed.
- Growth faults indicate that faults were active from the Middle Miocene time (Sofular Formation) onwards. Present and historical seismicity shows that motion on faults is still occurring at the present time. Geomorphic features indicate that the innermost boundary faults of the graben have been recently active; however, it is likely that the outer graben boundary faults are inactive.
- Normal and strike-slip faults are the most common faults observed in the Hatay Graben, but oblique and reverse faults are also present.

- Cross-cutting relationships are inconclusive; therefore, it is proposed that the Hatay Graben formed as a result of transtensional stresses that may have become more oblique over time.
- There are a series of fluvial (T0-T4) that document the progressive down cutting of the river systems in response to base level change due to relative sea-level fall probably as the result of tectonic uplift. Marine terraces also record uplift.

These conclusions have lead to the development of a two-stage model for the evolution of the area. Initially, prior to the Pliocene, the Hatay Graben, *sensu stricto*, did not exist. The area was part of the distal foreland to the Tauride allochthon to the north. Normal faulting was occurring and influencing facies distribution, probably as a result of reactivation of basement faults. Since the Pliocene, diachronous continental collision has lead to the westward extrusion of Anatolia and the formation of large strike-slip faults. This has lead to transtension in the field area, reactivating basement normal faults forming the present Hatay Graben.

## References

- Aksu, A. E., Ulug, A., Piper, D. J. W., Konuk, Y. T. & Turgut, S. 1992. Quaternary sedimentary history of Adana, Cilicia and Iskenderun Basins: northeast Mediterranean Sea. *Marine Geology*, 104, 55-71.
- Aksu, A. E., Calon, T. J., Hall, J., Mansfield, S. & Yaşar, D. 2005. The Cilicia-Adana basin complex, Eastern Mediterranean: Neogene evolution of an active fore-arc basin in an obliquely convergent margin. In press.
- Aktaş, G. & Robertson, A. H. F., 1984. The Maden Complex, SE Turkey: evolution of a Neotethyan continental margin. *Geological Society of London, Special Publication 17*, 375-402.
- Allen, P. A., Crampton, S. L. & Sinclair, H. D., 1991. The inception and early evolution of the North Alpine foreland basin, Switzerland. *Basin Research*, 3, 143-163.
- Al-Riyami, K., Robertson, A. H. F., Dixon, J. & Xenophontos, C., 2002. Origin and emplacement of the Late Cretaceous Baer-Bassit ophiolite and its metamorphic sole in NW Syria, *Lithos*, 225-260.
- Al-Tarazi, E. A. 1998. Regional seismic hazard study for the Eastern Mediterranean Trans-Jordan, Levant and Antakia and Sinai region. *Journal of African Earth Sciences*, 28-3, 743-750.
- Alvarez, G., Busquets, P., Permanyer, A. & Vilaplana, M. 1977. Growth dynamic and stratigraphy of Sant Pau d'Ordal Miocene patch reef Province of Barcelona, Catalonia. *Second International Symposium of Corals and Fossil Coral reefs, Paris, 1975. Bureau de recherches Geologiques et Minieres, Memoires 89*, 367-377.
- Angelier, J. 1984. Tectonic analysis of fault slip data sets. *Journal of Geophysical Research*, 89, 5835-5848.
- Argani, A. & Torelli, L., 2001. The Pelagian Shelf and its graben system (Italy/Tunisia). In: Ziegler, P. A., Cavazza, W., Robertson, A. H. F. & Crasquin-Soleau, S. (eds), *Peri-Tethys Memoir 6: Peri-Tethyan Rift/Wrench basins and Passive margins, Mémoires du Museum Nationale d'histoire naturel*, 186, 529-544.
- Arpat, E. & Şaroğlu, F. 1972. The East Anatolian Fault System; thoughts on its development. *Bulletin of the Mineral Research and Exploration Institute of Turkey*, 78, 33-39

- Atan, O. R. 1969. Eğribucak Kırıkhan bölgesindeki ofiyolilerin jeolojisi ve petrografisi M.T.A yayını no 150, pp71, Ankara.
- Barka, A. A. & Kadinsky-Cade, C., 1988. Strike-slip geometry in Turkey and its influence on earthquake activity. *Tectonics*, 7, 663-684.
- Bayona, G. & Thomas, W. A., 2003. Distinguishing fault reactivation from flexural deformation in the distal stratigraphy of the Peripheral Blountian Foreland Basin, southern Appalachians, USA. *Basin Research*, 15, 503-526.
- Ben-Avraham, Z., 1978. The structure and tectonic setting of the Levant Continental margin, eastern Mediterranean. *Tectonophysics*, 48, 313-331.
- Ben-Avraham, Z., Tibor, G., Liminov, A. F., Leybov, M. B., Ivanov, M.K., Tokarev, M. Y. and Woodside, J. M. 1995. Structure and tectonics of the Eastern Cyprean Arc. *Marine Petrology and Geology*, 12, 263-271.
- Bentham, P.A., Talling, P.J. & Burbank, D.W. 1993. Braided stream and flood-plain deposition in a rapidly aggrading basin: the Escanilla formation, Spanish Pyrenees. In: Best J.L. & Bristow, C. S. eds, 1993, *Braided Rivers*, Geological Society of London Special Publication No 75, pp. 177-194.
- Bossio, A., Bradley, F., Esteban, M., Giannelli, L., Landini, W., Mazzanti, R., Mazzei, R., Ricci Lucci, F. & Slavatorini, G. 1978. Some aspects of the Upper Miocene in Tuscany. Pisa, Messinian Seminar number 4. *International Geological Correlation Project n. 96*, 88pp.
- Bott, M. H. P. 1959. The mechanics of oblique slip faulting. *Geological Magazine*, 96, 109-117.
- Bouma, A. H. 1962. *Sedimentology of some Flysch Deposits: A Graphic approach to Facies interpretation*, 168 pp. Elsevier, Amsterdam.
- Boulton, S. J. & Robertson, A. H. F. In press. Tectonic and sedimentary evolution of the Cenozoic Hatay Graben, Southern Turkey: A two-phase, foreland basin then transtensional basin model. *Special Publication of the Geological Society of London*.
- Bozkurt, E. 2001. Neotectonics of Turkey – a synthesis. *Geodynamica Acta*, 14, 3-30.

- Bradley, D. C. & Kidd, W. S. F., 1991. Flexural extension of the upper continental crust in collisional foredeeps. *Geological Society of America Bulletin*, 103, 1416-1438.
- Brass, G. W. 1976. The variation of marine  $^{87}\text{Sr}/^{86}\text{Sr}$  ration during Phanerozoic time: Interpretation using a flux model, *Geochemical Cosmochemical Acta*, 40, 721-730.
- Broecker, W. S. & Peng, T. H. 1982. *Tracers in the Sea*, Eldigio, Pallisades, N. Y., 690pp.
- Bryant, G. 1960. Stratigraphic report Hassa area, Petroleum District VII, southeast Turkey. American Overseas Petroleum Ltd., Report number 506.
- Buchbinder, B. 1996. In: Franseen, E. K., Esteban, M., Ward, W. C. & Rouchy, J-M. eds, *Models for Carbonate stratigraphy from Miocene Reef complexes of Mediterranean regions*. Society for Sedimentary Geology, *Concepts in Sedimentology and Palaeontology* volume 5. Tulsa, Oklahoma, USA. 391pp.
- Bull, W. B., 1972. Recognition of alluvial fan deposits in the stratigraphic record. In: Rigby, J.K. & Hamblin, W. K. (eds) *Recognition of ancient sedimentary environments*. Society of Economic Palaeontology and Mineralogy Special Publication, 16, 63-83.
- Burbank D.W., Raynolds R.G.H. & Johnson G.D., 1986. Late Cenozoic tectonics and sedimentation in the north-western Himalayan foredeep: II. Eastern limb of the Northwest Syntaxis and regional synthesis ( India, Pakistan). In: Allen, P. A. & Homewood, P. (eds) *Foreland basins*. International Association of Sedimentologists Special Publications, 8, 293-306.
- Burbank, D. W. & Anderson, R. S. 2001. *Tectonic Geomorphology*. Blackwell Science, 274 p.
- Burgess, P. & Murphy, M. A., 2003. Geometry and kinematics of Recent deformation of the Himalayan hinterland, southwest Tibet and northwest Nepal. *Geological Society of America, 2003 annual meeting; Abstracts with Programs - Geological Society of America*, 35(6), 548
- Butler, R. W. H., Lickorish, W. H., Grasso, M., Pedley, H. M. & Ramberti, L. 1995. Tectonics and sequence stratigraphy in Messinian basins, Sicily: Constraints on the initiation and termination of the Mediterranean salinity crisis. *GSA Bulletin*, 107(4), 425-439.
- Calon, T. J., Aksu, A. E. & Hall, J. 2005. The Oligocene-recent evolution of the Mesaoria Basin Cyprus and its western marine extension, Eastern Mediterranean. *Marine Geology*, in press

- Cant, D.J. 1982. Fluvial Models. In: Sandstone Depositional Environments, Ed. P.A. Scholl & D. Spearing. Pp115-137. AAPG Memoir 31.
- Cashman, P. H. & Ellis, M. A. 1994. Fault interaction may generate multiple slip vectors on a single fault surface. *Geology*, 22, 1123-1126.
- Catalano, R. & Esteban, M. 1978. Messinian Reefs of western and central Sicily abs. Rome, Messinian Seminar 4, 1pp.
- Clifton, A. E., Schlische, R. W., Withjack, M. O. & Ackermann, R. V. 2002. Influence of rift obliquity on fault-population systematics: results of experimental clay models. *Journal of Structural Geology*, 22, 1491-1509.
- Coakley, B. J. & Watts, A. B., 1991. Tectonic controls of the development of unconformities: The North Slope, Alaska. *Tectonics*, 10, 101-130.
- Çoğulu, E., 1974. Ultrabasic tectonites and layered periodites of the Hatay area (Turkey). *Bulletin of the Maden Tektik Arama*, 83, 139-147.
- Coleman, J. M. & Wright, L. D. 1975. Modern river deltas: variability of processes and sand bodies. In: Broussard, M. L. eds *Deltas, models for exploration*. Houston Geological Society, Houston, 99-149.
- Coliaticchi, R., Passeri, L. & Pialli, G. 1975. Evidence of tidal environment deposition in the Calcave Massiccio Formation Central Appenines, Lower Lias, In: *Tidal Deposits* Ed, R. N. Ginsburg, pp 345-353. Springer-Verlag, Berlin.
- Collier, R. E. Ll., Leeder, M. R. & Jackson, J. A. 1995. Quaternary drainage development, sediment fluxes and extensional tectonics in Greece. In: Lewin, J., Macklin, M. G. & Woodward, J. C. *Mediterranean Quaternary Environments*. Refereed proceedings of an international conference, University of Cambridge, UK, 28-29 Spetember 1992. A. A. Balkema, Rotterdam, Brookfield.
- Collinson, J. D., Martinsen, O.J., Bakken, B. & Kloster, A. 1991. Early fill of the Western Irish Namurian Basin: A complex relationship between turbidites and deltas. *Basin Research*, 3, 223-242.
- Collinson, J. D., Holdsworth, B. K., Jones, C. M. & Martinsen, O. J. 1992. Discusson of: 'The Millstone Grit Namurian of the southern Pennines viewed in the light of eustatically controlled sequence stratigraphy' by Read, W. A. *Geological Journal*, 27 173-180.



- Collinson J.D. 1996. Alluvial Sediments. In: Sedimentary Environments: Processes, Facies and Stratigraphy, 3<sup>rd</sup> edition Ed: H.G. Reading. Pp37-82. Blackwell Science.
- Coniglio, M., James, N. P. & Aissaoui, D. M. 1996 In: Franseen, E. K., Esteban, M., Ward, W. C. & Rouchy, J.-M. eds, Models for Carbonate stratigraphy from Miocene Reef complexes of Mediterranean regions. Society for Sedimentary Geology, Concepts in Sedimentology and Palaeontology volume 5. Tulsa, Oklahoma, USA. 391pp.
- Cowie, P., Underhill, J.R, Behn, M., Lin, J. & Gill, C. M. 2005. Spatio-temporal evolution of strain accumulation derived from multi-scale observations of Late Jurassic rifting in the northern North Sea: A critical test of models for lithospheric extension. *Earth and Planetary Science letters*, 234, 401-419.
- Cronin, B. T., Gürbüz, K., Hurst, A. & Satur, N. 2000. Vertical and lateral organisation of a carbonate deep-water slope marginal to a submarine fan system, Miocene, southern Turkey. *Sedimentology*, 47, 801-824.
- Cross, T. A., 1986. Tectonic controls of foreland basin subsidence and laramide style deformation, western United States. In: Allen, P. A., & Homewood, P. eds Foreland basins. International Association of Sedimentologists Special Publications, 8, 15-39.
- Decrouez, D. & Selçuk, H., 1981. Les Nummulites de la craie de la Formation d'Okçular (Hatay, unite tectonique des plis bordiers, sud de la Turquie). *Notes du laboratoire de palaeontology de l'universite de geneve*, 8 (2), 7-18.
- Deer, W. A., Howie, R. A. & Zussman, J. 1992. An Introduction to the rock-forming minerals - 2<sup>nd</sup> Edition. Longman Scientific & Technical, UK.
- Delaloye, M., Piskin, Ö., Selçuk, H., Vuagnat, M. & Wagner, J-J. 1980. Geological section through the Hatay ophiolite along the Mediterranean coast, southern Turkey. *Ofiliti*, 52/3, 205-216
- Demoulin, A. 1998. Testing the significance of some parameters of longitudinal river profiles: the case of the Ardenne Belgium, NW Europe. *Geomorphology*, 24, 189-208.
- Derman, A. S. 1979. Antakya Hatay civarı stratigrafi ve jeolojisi, TPAO report no. 1513.

- Derman, A. S., Akdağ, K., Gül, M. A. & Yeniay, G. 1996. Relationship between sedimentation and tectonics in the Maraş Miocene basin. Turkish Association of Petroleum Geologists, 11<sup>th</sup> Petroleum Congress, Turkey, 91-102.
- De Paola, N., Holdsworth, R. E. & McCaffery K. J. W., 2004. The recognition of transtension, strain partitioning and reactivation in the Northumberland Basin: An alternative to basin inversion models. Abstract, Tectonics Studies Group AGM, Durham.
- Dewey, J. F. & Şengör, A. M. C., 1979. Aegean and surrounding regions: complex multiple and continuum tectonics on a convergent zone. Geological Society of America Bulletin, 90, 71-91.
- Devyatkin, E. V., Dodonov, A. E., Gablina, S. S., Golovina, L. A., Kurenkova, V. G., Simakova, A. N., Trubikhin, V. M., Yasamanov, N. A., Khatib, K. & Nseir, H. 1996... Upper Pliocene – Lower Pleistocene marine deposits of Western Syria: stratigraphy and palaeogeography. Stratigraphy and geological correlation translation from Russian, 41, 67-77.
- Dewey, J. F., Hempton, M. R., Kidd, W. S. F., Şaroğlu, F., Şengör, A. M. C. 1986. Shortening of continental lithosphere: the neotectonics of eastern Anatolia – a young collision zone, in: COWARD, M. O. & REIS, A. C. eds. Collisional Tectonics, Geological Society, London, Special Publication, 19, 3-36.
- Dickinson, W. R. 1983. Interpreting province relations from detrital modes of sandstones. In: Zuffa, G. G. ed, Provenance of Arenites, Riedel, Dordrecht, 333-361.
- Dubertret, L. 1939. Sur la genèse et l'âge des roches vertes syriennes On the genesis and age of the green rocks of Syria. Comptes Rendus de l'Academie des Sciences, Paris, 209 P763.
- Dubertret, L. 1953. Géologie des roches vertes du nord-ouest de la Syrie et du Hatay Turquie. The Geology of the green rocks of Northwest Syria and Hatay Turkey. Notes et Mémoires sur le Moyen-Orient, Museum National d' Histoire Naturelle, 5, 5-179, Paris.
- Dunham, R. J. 1961. The Classification of carbonate rocks according to depositional texture. In: Ham, W. E. ed, Classification of carbonate rocks, Memoir of the American Association of Petroleum Geologists, 1, 108-121.
- Eaton, C. 1987. The sedimentology of mid to late Miocene carbonates and evaporites in Southern Cyprus. School of Geosciences. Edinburgh, University of Edinburgh [Unpublished Ph.D thesis]

- Eaton, S. & Robertson, A. H. F., 1993. The Miocene Pakhna Formation, Cyprus, and its relationship to the Neogene tectonic evolution of the Eastern Mediterranean. *Sedimentary Geology*, 86, 273-296.
- Einsele, G. 1992 *Sedimentary Basins: Evolution, Facies, and Sediment budget*. Springer-Verlag Berlin, pp 628.
- Elderfield, H. 1986. Recent trends in Strontium isotope stratigraphy. *Terra Nova*, 6 4, 331-358.
- Erdik, M., Aydınoglu, N., Pinar, A. & Kalafat, D. 1997. Report of Hatay Earthquake, Kandilli Observatory, Istanbul.
- Erol, O. & Pirazzoli, P. A. 1992. Seleucia Pieria: an ancient harbour submitted to two successive uplifts. *The international journal of Nautical Archeology*, 21-4, 317-327.
- Esteban, M. 1996. An overview of Miocene reefs from Mediterranean areas. In: Franseen, E. K., Esteban, M., Ward, W. C. & Rouchy, J-M. eds, *Models for Carbonate stratigraphy from Miocene Reef complexes of Mediterranean regions*. Society for Sedimentary Geology, Concepts in Sedimentology and Palaeontology volume 5. Tulsa, Oklahoma, USA. 391pp.
- Eyal, Y. 1996. Stress field fluctuations along the Dead Sea Rift since the Middle Miocene. *Tectonics* 15, 157-170.
- Flecker, R. 1995. Miocene Basin Evolution of the Isparta Angle, Southern Turkey. [Ph.D Thesis] University of Edinburgh.
- Follows, E. 1990. Sedimentary and tectonic setting of Miocene and related sediments in Cyprus. School of Geosciences. Edinburgh, University of Edinburgh [Unpublished Ph.D thesis].
- Follows, E. J. 1992. Patterns of reef sedimentation and diagenesis in the Miocene of Cyprus. *Sedimentary Geology*, 79, 225-253.
- Follows, E. J., Robertson, A. H. F. & Scoffin, T. P., 1996. Tectonic controls of Miocene reefs and related carbonate facies in Cyprus. In: Franseen, E. K., Esteban, M., Ward, W. C. & Rouchy, J-M. eds, *Models for Carbonate stratigraphy from Miocene Reef complexes of Mediterranean regions*. Society for Sedimentary Geology, Concepts in Sedimentology and Palaeontology volume 5. Tulsa, Oklahoma, USA. 391pp.
- Folk, R. L. 1959. Practical petrographic classification of limestones. *Bulletin American Association of Petroleum Geologists*, 43, 1-38.

- Flügel, E. 2004. *Microfacies of Carbonate rocks: analysis, interpretation and application*. Springer, New York. 976 pp.
- Freund, R., Zak, I., & Garfunkel, Z. 1968. On the age and rate of sinistral movement along the Dead Sea rift, *Nature*, 220, 253-255.
- Garfunkel, Z. 1981. Internal structure of the Dead Sea leaky transform rift in relation to plate kinematics. *Tectonophysics*, 80, 81-108.
- Garfunkel, Z. & Ben-Avraham, Z., 1996. The structure of the Dead Sea Basin. *Tectonophysics*, 255, 155-176.
- Gawthorpe, R. L. & Leeder, M. R., 2000. Tectono-sedimentary evolution of active extensional basins. *Basin Research*, 12, 195-218.
- Ginsburg, R. N. 1975. *Tidal Deposits: A Casebook of recent examples and fossil counterparts*, 428 pp. Springer-Verlag, New York.
- Ginsburg, R. N., Hardie, L. A., Bricker, O. P., Garret, P. & Wanless, H. R. 1977 Exposure index: a quantitative approach to defining position within the intertidal zone. In: L. A. Hardie (ed) *Sedimentation on the Modern Carbonate tidal Flats of Northwest Andros Island, Bahamas*, 7-11. John Hopkins University Press, Baltimore.
- Girdler, R. W., 1990. The Dead Sea transform fault system. *Tectonophysics*, 180, 1-13.
- Girdler, R. W. & Styles, P. 1978. Seafloor spreading in the western Gulf of Aden, *Nature*, 271, 615-617.
- Gleason, J. D., Moore, T. C., Rea, D. K., Johnson, T. M., Owen, R. M., Blum, J. D., Hovan, S. A., Jones, C. E. 2002. Ichthyolith strontium isotope stratigraphy of a Neogene red clay sequence: calibrating aeolian dust accumulation rates in the central North Pacific. *Earth and Planetary Letters*, 202, 625-636.
- Glover, C. P. & Robertson, A. H. F. 1998. Role of regional extension and uplift in the Plio-Pleistocene evolution of the Aksu Basin, SW Turkey *Journal of the Geological Society, London*. 155, 365-387.

- Glover, C. P. & Robertson, A. H. F. 2003. Origin of tufa (cool-water carbonate) and related terraces in the Antalya area, SW Turkey. *Geological Journal*, 38, 329-358.
- Goldsworthy, M. & Jackson, J. A. 2000. Active normal fault propagation in Greece revealed by geomorphology and drainage patterns. *Journal of the Geological Society, London*. 157, 967-981.
- Gökçen, S. L., Kelling, G., Gökçen, N. & Floyd, P. 1988. Sedimentology of the Late Cenozoic collisional sequence: the Misis Complex, Adana, Southern Turkey. *Sedimentary Geology*, 59, 205-35.
- Görür, N. 1979. Karaisalı kireçtaşının sedimentolojisi Türkiye Jeoloji Kurumu Bülteni, 22, 227-235 in Turkish.
- Görür, N. 1992. A tectonically active controlled alluvial fan which developed into a marine fan-delta at a complex triple junction: Miocene Gildirli Formation of the Adana Basin, Turkey. *Sedimentary Geology*, 81, 243-252.
- Gradstein, F.M., Ogg, J.G., and Smith, A.G., Agterberg, F.P., Bleeker, W., Cooper, R.A., Davydov, V., Gibbard, P., Hinnov, L.A., House, M.R., Lourens, L., Luterbacher, H.P., McArthur, J., Melchin, M.J., Robb, L.J., Shergold, J., Villeneuve, M., Wardlaw, B.R., Ali, J., Brinkhuis, H., Hilgen, F.J., Hooker, J., Howarth, R.J., Knoll, A.H., Laskar, J., Monechi, S., Plumb, K.A., Powell, J., Raffi, I., Röhl, U., Sadler, P., Sanfilippo, A., Schmitz, B., Shackleton, N.J., Shields, G.A., Strauss, H., Van Dam, J., van Kolfschoten, T., Veizer, J., and Wilson, D., 2004. *A Geologic Time Scale 2004*. Cambridge University Press, 589 pages.
- Guidoboni, E. 1994. *Catalogue of Ancient Earthquakes in the Mediterranean area up to the 10<sup>th</sup> Century*. Istituto Nazionale Geofisica. Italy.
- Günay, Y. 1984. Amanos dağlarının jeolojisi ve Karasu-Hatay grabeninin petrol olankları. TPAS Harrakri-Sariyaj prjct, TPAO-1984, Ankara.
- Gürbüz, K. & Kelling, G. 1993. Provenance of Miocene Submarine fans in the Northern Adana Basin: A test of discriminant function analysis. *Geological Journal*, 28, 277-95.
- Gvirtzman G. ; Honigstein A. ; Reiss Z. ; Almogi-Labin A. ; Moshkovitz S. ; Lewy Z. Upper Cretaceous high-resolution multiple stratigraphy, northern margin of the Arabian platform, central Israel *Cretaceous Research* 10, no.2 (1989) p. 107-135

- Haq, B. U., Hardenbol, J. & Vail, P. R., 1987. Chronology of fluctuating sea-levels since the Triassic, *Science*, 4793, 1156-1167
- Hardenberg, M. F. 2004. Tectonics and sedimentation of early continental collision in the Eastern Mediterranean Northwest Syria. [Ph.D thesis], University of Edinburgh.
- Hayward A. B., Robertson, A. H. F. & Scoffin, T. P. 1996. Miocene patch reefs from a Mediterranean terrigenous setting in southwest Turkey. In: Franseen, E. K., Esteban, M., Ward, W. C. & Rouchy, J-M. eds, *Models for Carbonate stratigraphy from Miocene Reef complexes of Mediterranean regions*. Society for Sedimentary Geology, *Concepts in Sedimentology and Palaeontology* volume 5. Tulsa, Oklahoma, USA. 391pp.
- Heimann, A. & Sass, E. 1989. Travertines in the northern Hula Valley, Israel. *Sedimentology*, 36, 95-108.
- Hempton, M. R. 1987. Constraints on Arabian Plate motion and extensional history of the Red Sea. *Tectonics* 6, 687-705.
- Hodell, D. A. 1994. Progress and paradox in strontium isotope stratigraphy. *Palaeoceanography*, 9 3, 395-398.
- Hodell, D. A. & Woodruff, F. 1994. Variations in the strontium isotopic ratio of seawater during the Miocene :Stratigraphic and geochemical implications. *Palaeoceanography*, 9 3, 405-426.
- Holmes, A. 1965. *Principles of Physical Geology*, 2<sup>nd</sup> Edition. Nelson, London. Pp 1288.
- Homewood, P., Allen, P. A. & Williams, G. D., 1986. Dynamics of the molasses basin of western Switzerland. In: Allen, P. A. & Homewood, P. eds *Foreland basins*. International Association of Sedimentologists Special Publications, 8, 199-217.
- Howarth R.J. & McArthur, J.M. 1997 Statistics for strontium isotope stratigraphy: a robust LOWESS fit to the marine Sr-isotope curve for 0-206 Ma, with look-up table for derivation of numeric age. *J. Geol.* 105, 441-456.
- Howell, D. G. & Normark, W. R. 1982. Fluvial Models. In: P.A. Scholl & D. Spearing (eds) *Sandstone Depositional Environments*, 365-404. AAPG Memoir 31.

- Hsü, K. J. 1972. The desiccated deep-basin model for the Messinian events  
In: Drooger, C. W. (ed) Messinian events in the Mediterranean, North-Holland Pub. Co, Amsterdam.  
60-67.
- Hubbard, J. A. E. B. & Pocock, Y. P. 1972. Sediment rejection by Scleractinian corals: a key to  
palaeoenvironmental reconstruction. *Geologisches Rundschau*, 61, 598-626.
- Jackson, J. 2001. Living with Earthquakes: Know your faults. *Journal of Earthquake Engineering*, 5,  
special issue 1, 5-123.
- Jackson, J. A., Norris, R. & Youngson, J. 1996. The structural evolution of active fault and fold  
systems in central Otago, New Zealand: evidence revealed by drainage patterns. *Journal of Structural  
Geology*, 18, 217-234.
- Jaffey, N. & Robertson, A. H. F. 2001. New sedimentological and structural data from the Ecemiş  
Fault Zone, southern Turkey: implications for its timing and offset and the Cenozoic tectonic escape  
of Anatolia. *Journal of the Geological Society, London*, 158, 367-378.
- Johnson G.D.; Raynolds R.G.H.; Burbank D.W., 1986. Late Cenozoic tectonics and sedimentation in  
the north-western Himalayan foredeep: I. Thrust ramping and associated deformation in the Potwar  
region ( India, Pakistan). In: Allen, P. A. & Homewood, P. eds Foreland basins. International  
Association of Sedimentologists Special Publications, 8, 273-291.
- Jordan, T. E., 1995. Retroarc foreland and related basins. In: Busby, C. J. & Ingersoll, R. V. (eds),  
*Tectonics of Sedimentary Basins*. Blackwell Science, 579pp
- Jordan, T. E., Flemings, P. B. & Beer, J. A., 1988. Dating of thrust-fault activity by use of foreland  
basin strata. In: Kleinspehn, K. & Paola, C. (eds). *New perspectives in basin analysis*. Springer-  
Verlag, New York, 307-330.
- Karig, D. E. & Kozlu, H., 1990. Late Palaeogene evolution of the triple junction region near Maraş,  
south-central Turkey. *Journal of the Geological Society of London*, 147, 1023-1034
- Keller, E. A., Gurrola, L., & Tiernay, T. E. 1999. Geomorphic criteria to determine direction lateral  
propagation of reverse faulting and folding. *Geology*, 27, 515-518.
- Kelling, G., Gökçen, S. L. Floyd, P. A. & Gökçen, N. 1987. Neogene tectonics and plate convergence  
in the Eastern Mediterranean: new data from southern Turkey. *Geology* 15, 425-429

- Kelling, G., Robertson, A. H. F. & Van Buchem, F. 2005 Cenozoic sedimentary basins of southern Turkey: an introduction. *Sedimentary Geology*, 173, 1-13.
- Kempler, D. & Ben-Avraham, Z., 1987. The tectonic evolution of the Cyprean arc. *Annales Tectonicae*, 1, 58-71.
- Kempler, D. & Garfunkel, Z., 1994. Structure and kinematics in the northeastern Mediterranean: a study of an irregular plate boundary. *Tectonophysics*, 234, 19-32.
- Koçayığıt, A. & Beyhan, A. 1998. A new intracontinental transcurrent structure: the Central Anatolian Fault Zone, Turkey. *Tectonophysics*, 284, 317-336.
- Kop, A., 1996. Kırıkhan ve Kuzeyinin tektono-stratigrafik incelemesi (Tectono-stratigraphic investigations of Kırıkhan and its northern area. Masters Thesis, University of Çukurova.
- Koral, H., Kronfield, J., Avsar, N., Yanko, V. & Vogel, J. C. 2001. Major recent tectonic uplift in Iskenderun Bay, Turkey. *Radiocarbon*, 43, 957-963.
- Kozlu, H. 1982. Iskenderun Baseni Anadolu nun Kambrien teşekkülleri ve bunların Doğu İran Kambrieni ile mukayesesi. MTA periodical no 66, Ankara.
- Kozlu, H., 1997. Tectono-stratigraphic units of the Neogene basins (Iskenderun, Misis-Andırın) and their tectonic evolution in the eastern Mediterranean region. [Ph.D Thesis] Natural Science Institute, Cukurova University, Turkey.
- Kraus, M. J. & Middleton, L.T. 1987. Contrasting architecture of two alluvial suites in different structural settings, In: Etheridge, F. G., Flores, R. M. & Harvey, M. D. (eds). *Recent developments in Fluvial Sedimentology*. Society of Economic Palaeontologists and Mineralogists Special Publications, 39, 253-262.
- Krenkel, 1924. Der Syrische Bogen. *Zentralbl. Mineral*, 9, 274-281.
- Leeder, M. R. & Alexander, J., 1987. The origin and tectonic significance of asymmetrical meander belts. *Sedimentology*, 34, 217-226.



- Leeder, M. R. & Gawthorpe, R. L. 1987. Sedimentary models of extensional tilt-block/half graben basins. In: Coward, M. P. Dewey, J. F & Hancock, P. L. (eds) Continental extensional tectonics. Geological Society of London Special Publication 28, 139-152.
- Leeder, M. R. & Jackson, J. A. 1993. The interaction between normal faulting and drainage inactive extensional basins, with examples from the western United States and Central Greece. *Basin Research*, 5, 79-102.
- Le Pichon, X. & Angelier, J., 1979. The Aegean Arc and trench system: a key to the neotectonics evolution of the eastern Mediterranean area, *Tectophysics*, 60, 1-42
- Liesa, C. L.. & Lisle, R. J. 2004. Reliability of methods to separate stress tensors from heterogeneous fault-slip data. *Journal of Structural Geology*, 26, 559-572.
- Lin, A. T., Watts, A. B. & Hesselbo, S. P. (2003). Cenozoic stratigraphy and subsidence history of the South China Sea margin in the Taiwan region. *Basin Research*, 15, 453-478.
- Lort, J. M., 1971. The tectonics of the eastern Mediterranean: a geophysical review. *Reviews of Geophysics and Space Physics*, 9, 189-216.
- Lovelock, P. E. R. 1984. A review of the tectonics of the northern Middle East region. *Geological Magazine*, 121, 577-587.
- Lyberis, N. 1988. Tectonic evolution of the Gulf of Suez and the Gult of Aqaba. *Tectonophysics*, 153, no. 1-4, 209-220.
- Lyberis, N., Yürür, T., Chorowicz, J., Kasapoğlu, E., & Gündoğdu, N. 1992. The East Anatolian fault: an oblique collisional belt. *Tectonophysics*, 204, 1-15.
- Mantis, M. 1970. Upper Cretaceous-Tertiary Foraminiferal Zones in Cyprus. *Science Research Cent. Cyprus. Epithris*, 3, 227-241.
- Manzi, V., Lugli, S., Ricci Lucchi, F. & Roveri, M. 2005. Deep-water clastic evaporites deposition in the Messinian Adriatic foredeep northern Apennines, Italy: did the Mediterranean ever dry out? *Sedimentology*, 52, 4, 875-902

- Mart, Y. & Rabinowitz, P. D., 1986. The northern Red Sea and the Dead Sea Rift. *Tectonophysics*, 124, 85-113.
- Martinsen, O. J. 1990. Fluvial, inertia-dominated deltaic deposition in the Namurian Carboniferous of northern England. *Sedimentology*, 37, 1099-1113.
- McArthur, J. M. 1994. Recent trends in strontium isotope stratigraphy. *Terra Nova*, 6 4, 331-358
- McCallum, J. E. & Robertson, A. H. F. 1990. Pulsed uplift of the Troodos Massif-evidence from the Plio-Pleistocene Mesaoria Basin. In: Malpas, J., Moores, E. M., Panayiotou, A. & Xenophontos, C. eds. *Ophiolites, Orogenic Crustal analogues. Proceedings of the Symposium "Troodos 1987"*. Geological Survey Department, Ministry of Agriculture and Natural Resources, Cyprus, 217-229.
- McCallum, J. E. & Robertson, A. H. F. 1995a. Late Pliocene-early Pleistocene Athalassa Formation, north central Cyprus: carbonate sand bodies in a shallow seaway between two emerging landmasses. *Terra Nova*, 7, 255-264.
- McCallum, J. E. & Robertson, A. H. F. 1995b. Sedimentology of two fan-delta systems in the Pliocene-Pleistocene of the Mesaoria Basin, Cyprus. *Sedimentary Geology*, 98, 215-244.
- McCallum, J. E. 1989. Sedimentation and tectonics of the Plio-Pleistocene of Cyprus. Ph.D Thesis, University of Edinburgh.
- McClay, K. R. & White, M. J. 1995. Analogue modelling of orthogonal and oblique rifting. *Marine and Petroleum Geology*, 12, 147-151.
- McClusky, S., Balassanian, S., Barka A.A., Demir, C., Ergintav, S., Georgiev, I., Gurkan, O., Hamburger, M., Hurst, K., Kahle, H., Kastens, K., Kekelidze, G., King, R., Kotzev, V., Lenk, O., Mahmoud, S., Mishin, A., Nadariya, M., Ouzuinis, A., Paradissis, D., Peter, Y., Prilepin, M., Reilinger, R., Sanli, I., Seeger, H., Tealab, A., Toksoz, M. N. & Veis, G. 2000. Global Positioning System constraints on plate kinematics and dynamics in the Eastern Mediterranean and Caucasus. *Journal of Geophysical Research*, 105 (B3), 5695-5719.
- McCubbin, D. G. 1982. Barrier Island and strand-plain facies. In: Scholle, P. A. & Spearing, D. eds *Sandstone depositional environments. Memoir of the American Association of Petroleum Geologists*, 31, 247-279.

- McKenzie, D. P. 1978a. Active tectonism in the Alpine-Himalayan belt: the Aegean Sea and the surrounding regions (tectonics of the Aegean region). *Geophysics Journal of the Royal Astronomical Society*, 55, 217-254.
- McKenzie, D. P., 1978b. Some remarks on the development of sedimentary basin. *Earth and Planetary Science Letters*, 40, 25-32.
- McNeill, L. C., Mille, A., Minshull, T. A., Bull, J. M. & Kenyon, N. H. 2004. Extension of the North Anatolian Fault into the North Aegean Trough: Evidence for transtension, strain partitioning, and analogues of Sea of Marmara basin models. *Tectonics*, 23, TC2016.
- Merritts, D & Vincent, K. R. 1989. Geomorphic response of coastal streams to low, intermediate, and high rates of uplift, Mendocino junction region, northern California. *Geological Society of America Bulletin*, 101 1373-1388.
- Meschede, M., Weiss, R., Schmiedl, G. & Hemleben, C. 2002. Benthic foraminiferal distribution and sedimentary structures suggest tectonic erosion at the Costa Rica convergent plate margin. *Terra Nova*, 14, 388-396.
- Miall, A. D., 1977. A review of the braided river depositional environment. *Earth Science Review*, 13, 1-62.
- Miall, A. D. 1978. *Fluvial Sedimentology*. Canadian Society of Petroleum Geologists Memoir 5, pp 859.
- Miall, A. D., 1985. Architectural element analysis: a new method of facies analysis applied to fluvial deposits. *Earth Science Review*, 22, 261-308.
- Miall, A. D., 1995. Collision-related foreland basins. In: Busby, C. J. & Ingersoll, R. V. (eds), *Tectonics of Sedimentary Basins*. Blackwell Science, 579pp
- Miall, A. D. 1996. *The Geology of Fluvial Deposits: Sedimentary facies, basin analysis and Petroleum geology*. Springer-Verlag, Berlin, 582 pp.
- Miller, K. G, Feigenson, M. D., Wright, J. D. & Clement, B. M. 1991. Miocene isotope reference section, Deep Sea Drilling Project site 608: An evaluation of isotope and biostratigraphic resolution. *Palaeanography*, 6, 33-52.

- Mistik, T. 2002. Samandağı Antakaya Tektono-Stratigrafik incelemesi. Masters Thesis, Adana University.
- Montgomery, D. R. & López-Blanco, J. 2003. Post-Oligocene river incision, southern Sierra Madre Occidental, Mexico. *Geomorphology*, 55, 235-247.
- Morewood, N. C. & Roberts, G. P. 2002. Surface observations of active normal fault propagation: implications for growth. *Journal of the Geological Society, London*. 159, 263-272.
- Muehlberger, R. W., 1981. The splintering of the Dead Sea Fault Zone in Turkey. *Hacetepe University Earth Sciences*, 8, 123-130.
- Muehlberger, R. W. & Gorbon, M. B., 1987. Observation on the complexity of the East Anatolian Fault, Turkey. *Journal of Structural Geology*, 9, 899-903.
- Murris, R. J., 1980. Middle East: Stratigraphic evolution and oil habitat. *American Association of Petroleum Geologists Bulletin*, 64, 597-618.
- Nazik, A. 2004. Planktonic foraminiferal biostratigraphy of the Neogene sequence in the Adana Basin, Turkey, and its correlation with standard biozones. *Geological Magazine*, 1413, 379-387.
- Nemcock, M. & Lisle, R. J. 1995. A stress inversion procedure for polyphase fault/slip data sets. *Journal of Structural Geology*, 17 10, 1445-1453.
- Nemec, W. 1990. Deltas – Remarks on terminology and classification. In: Colella, A & Prior, D. B. (eds), *Coarse-grained Deltas*. Special Publication of the International Association of Sedimentologists, 10, 3-12.
- Nemec W. & Steel R. J. 1988. Alluvial and coastal conglomerates: flow deposits. In: *Sedimentology of Gravels and Conglomerates* Ed. E.H. Koster and R. J. Steel pp.1-31. *Memoires of the Canadian Society of Petroleum Geology*. 10, Calgary.
- Nilsen, T. H. 1982. Fluvial Models. In: *Sandstone Depositional Environments*, Ed. P.A. Scholl & D. Spearing. pp115-137. *AAPG Memoir* 31.
- Oslick, J. S., Miller, K. G., Feigenson M. D. & Wright, J. D. 1994. Oligocene – Miocene stontium isotopes: Stratigraphic revisions and correlations to an inferred glacioeustatic record. *Palaeoceanography*, 9 3, 427-443.

- Över, S., Ünlügenç, U. C. & Bellier, O. 2002. Quaternary stress regime change in the Hatay region SE Turkey. *Geophysics Journal International*, 148, 649-662.
- Över, S., Kavak, K.Ş., Bellier, O. & Özden, S. 2004. Is the Amik Basin SE Turkey a triple junction area? Analyses of SPOT XS imagery and seismicity. *International Journal of Remote Sensing*, 25 19, 3857-3872.
- Parlak, O., Kop, A., Ünlügenç, U. C., & Demirkol, C. 1998. Geochronology and geochemistry of basaltic rocks in the Karasu graben around Kırıkhan Hatay, S. Turkey. *Turkish Journal of Earth Sciences*, 7, 53-61.
- Paton, S. 1992. Active normal faulting, drainage patterns and sedimentation in southwestern Turkey. *Journal of the Geological Society, London*. 149, 1031-1044.
- Payne, A. S. 1995 Neogene tectonic and sedimentary evolution of the Polis Graben system, West Cyprus [Ph.D thesis], University of Edinburgh.
- Payne, A. S. & Robertson, A. H. F. 2000. Structural evolution and regional significance of the Polis Graben system, western Cyprus. In: Panayides, I., Xenophontos, C. & Malpas, J. eds, *Proceedings of the third international conference on the geology of the Eastern Mediterranean*. 45-59.
- Pedley, H. M. 1990. Classification and environmental models of cool freshwater tufas. *Sedimentary Geology*, 68, 143-154.
- Perinçek, D., & Çemen, İ., 1990. The structural relationship between the East Anatolian and Dead Sea fault zones in Southeastern Turkey. *Tectonophysics*, 172, 331-340.
- Permanyer, A. & Esteban, M. 1973. El arrecife mioceno de Sant Pau d'Ordal provinca de Barcelona. *Barcelona, Institut d'Investigacions Geologiques*, 28, 45-72.
- Peterek, A. & Schwarze, J., 2004. Architecture and Late Pliocene to recent evolution of outer-arc basins of the Hellenic subduction zone (south-central Crete, Greece). *Journal of Geodynamics*, 38, 19-55.
- Pickering, K. T., Stow, D. A. V., Watson, M. & Hiscott, R. N. 1986. Deep-water facies processes and models: a review and classification scheme for modern and ancient sediments. *Earth Science Review*, 23, 75-174.

- Pigram, C. J., Davies, P. J., Feary, D. A. & Symonds, P. A., 1989. Tectonic controls on carbonate platform evolution in southern Papua New Guinea: Passive margin to foreland basin. *Geology*, 17, 168-161.
- Pirazzoli, P. A., Laborel, J., Saliège, J. F., Erol, O., Kayan, I., & Person, A., 1991. Holocene raised shorelines on the Hatay coasts Turkey: Palaeoecological and tectonic implications. *Marine Geology*, 96, 295-311.
- Pişkin, O., Delaloye, M., Selçuk, H., Wagner, J. 1986. Guide to Hatay Geology SE Turkey. *Ofioliti*, 11, 87-104.
- Poole, A. J. 1992. Sedimentology, neotectonics and geomorphology related to tectonic uplift and sea-level change: Quaternary of Cyprus [Ph.D thesis], University of Edinburgh.
- Poole, A. J. & Robertson, A. H. F. 1991. Quaternary uplift and sea-level change at an active plate boundary, Cyprus. *Journal of the Geological Society of London*, 148, 909-921.
- Poole A. J. & Robertson A. H. F. 1998. Pleistocene fanglomerate deposition related to uplift of the Troodos ophiolite, Cyprus. *Proceedings of the Ocean Drilling Program: Scientific Results*, 160, 545-568.
- Postman, G. & Nemeç, W. 1990. Regressive and transgressive sequences in a raised Holocene gravelly beach, southwestern Crete. *Sedimentology* 37 (5), 907-920.
- Pratt, B. R., James, N. P. & Cowan, C. A. 1992 Peritidal Carbonates. In: *Facies, Models and response to sea-level change* Eds; R. J. Walker & N. P. James, pp 303-322. Geological Association of Canada, St John's, Newfoundland.
- Purser, B. H., Plaziat, J-C. & Rosen, B. R. 1996. In: Franseen, E. K., Esteban, M., Ward, W. C. & Rouchy, J-M. eds, *Models for Carbonate stratigraphy from Miocene Reef complexes of Mediterranean regions*. Society for Sedimentary Geology, *Concepts in Sedimentology and Palaeontology* volume 5. Tulsa, Oklahoma, USA. 391pp.
- Rădoane, M., Rădoane, N. & Dumitriu, D. 2003. Geomorphological evolution of longitudinal river profiles in the Carpathians. *Geomorphology*, 50, 293-306.
- Reading, H. G. & Collinson, J. D. 1996. Clastic coasts. In: *Sedimentary Environments: Processes, Facies and Stratigraphy*, 3<sup>rd</sup> edition. Ed: H.G. Reading. Blackwell Science. 154-231.

- Reches, Z., Hoexter, D. F. & Hirsch, F. 1981. The Structure of a monocline in the Syrian Arc System, Middle East – Surface and subsurface analysis. *Journal of Petroleum Geology*, 3, 413-425.
- Reches, Z. & Dieterich, J. H. 1983. Faulting of rocks in three-dimensional strain-fields, I, failure of rocks in polyaxial, servo-control experiments. *Tectonophysics*, 95, 111-132.
- Richter, F. M. & DePaulo, D. J. 1988. Diagenesis and strontium isotope evolution of sea-level using data from DSDP 590B and 575. *Earth and Planetary Science Letters*, 90, 382-394.
- Roberts, S. & Jackson, J., 1991. The Borah Peak, Idaho earthquake and its aftershocks. *Geological Society of America Bulletin*, 77, 694.
- Robertson, A. H. F. 1976. Pelagic chalks and calciturbidites from the Lower Tertiary of the Troodos, Massif. Cyprus. *Journal of Sedimentary Petrology*, 4, 1007-1016.
- Robertson, A. H. F. 1977. The origin and diagenesis of cherts from Cyprus. *Sedimentology*, 24, 11-30.
- Robertson, A. H. F. 1987. Upper Cretaceous Muti Formation; transition of a Mesozoic carbonate platform to a foreland basin in the Oman Mountains. *Sedimentology*, 34 (6), 1123-1142
- Robertson, A. H. F. 1998. Mesozoic-Tertiary Tectonic evolution of the easternmost Mediterranean area: intergration of marine and land evidence. In: Robertson, A. H. F., Emeis, K. -C., Richter, C. & Camerlenghi, A. eds. *Proceedings of the Ocean Drilling Program, Scientific Results*, 160, 723-782.
- Robertson, A. H. F. 2000. Tectonic evolution of Cyprus in its Eastern Mediterranean setting. In: Panayides, I., Xenophontos, C. & Malpas, J. eds, *Proceedings of the third international conference on the geology of the Eastern Mediterranean*. 11-44.
- Robertson, A. H. F., Eaton, S., Follows, E. J. & McCallum, J. E. 1991. The role of local tectonics versus global sea-level change in the Neogene evolution of the Cyprus active margin. *International Association of Sedimentologists, Special Publications*, 12, 331-369.
- Robertson, A.H.F., Eaton, S., Follows, E.J. and Payne, A.S. 1995 Depositional processes and basin analysis of Messinian evaporites in Cyprus. *Terra Nova*, 7, 233–253
- Robertson, A. H. F., Ünlügenç, U. C., İnan, N. & Taşlı, K. 2004. The Misis-Andırın Complex: a Mid-Tertiary melange related to late-stage subduction of the Southern Neotethys in S Turkey. *Journal of Asian Earth Sciences*, 22, 413-453.

- Rojay, B., Heimann, A., & Toprak, V. 2001. Neotectonic and volcanic characteristics of the Karasu fault zone Anatolia, Turkey: The transition zone between the Dead Sea transform and the East Anatolian fault zone. *Geodinamica Acta*, 14, 197-212.
- Şafak, Ü. 1993a. Antakya Havzası planktonic foraminifer biyostratigrafisi Planktonic foraminifera biostratigraphy of Antakya Basin. A.Suat Erk jeoloji simpozyumu, 143-156.
- Şafak, Ü. 1993b. Antakya Havzası ostrakod foraminifer biyostratigrafisi The ostracode biostratigraphy of the Antakya Basin in Turkish, with English abstract. *Geological Bulletin of Turkey*, 36, 115-137.
- Saller, A., Armin, R., Ichram, L. O. & Sullivan, C. 1993. Sequence stratigraphy of aggrading and backstepping carbonate shelves, Oligocene, Central Kalmantan, Indonesia. In: Carbonate sequence stratigraphy: recent developments and applications AAPG Memoir, 57, 267-290
- Salvini, F. 2001. Daisy 2.4: the structural data integrated system analyser. University 'Roma Tre', Italy
- Şaroğlu, F., Emre Ö., & Kusçu, İ. 1992. The East Anatolian fault zone of Turkey. *Annales Tectonicae*, 6, 99-125.
- Sartorio, D. & Venturini, S. 1988. Southern Tethys Biofacies. AGIP, Italy. 235pp.
- Schmidt, G. C. 1961. Stratigraphic nomenclature for the Adana region petroleum distric 7. *Petroleum Administration Bulletin*, 6, 47-63.
- Schreiber, B. C., Friedman, G. M., Decima, A. & Schreiber, E. 1976. Depositional environments of the Upper Miocene Messinian evaporate deposits of the Silician Basin. *Sedimentology*, 23, 729-760.
- Schweickert, R. A., Lahren, M. M., Smith, K. D., Howle, J. F. & Ichinose, G. 2004. Transtensional deformation in the Lake Tahoe region, California and Nevada, USA. *Tectonophysics*, 392, 303-323.
- Sclater, J. G. & Christie, P. A. F. 1980. Continental stretching: an explanation of the Post Mid-Cretaceous subsidence of the central North Sea basin. *Journal of Geophysics research*, 85, 3711-3739.
- Seidl M.A. Dietrich W.E. & Finkel R.C. 1997. Cosmogenic isotope analyses applied to river longitudinal profile evolution: problems and interpretations. *Earth Surface Processes and Landforms* 22, 195-209.



- Seger M.; & Alexander J, 1994. Distribution of Plio-Pleistocene and modern coarse-grained deltas south of the Gulf of Corinth, Greece. In: Frostick L.E (ed), Tectonic controls and signatures in sedimentary successions. IAS Special Publication, 20, 37-48
- Selçuk, H. 1981. Étude géologique de la partie meridionala du Hatay Türkiye: Doctoral thesis, University of Genève. Pp116.
- Şengör, A. M .C., Görür, N., & Şaroğlu, F. 1985. Strike-slip faulting and related basin formation in zones of tectonic escape: Turkey as a case study. Society of Economic Palaeontology and Mineralogy Special Publication, 37, 227-264.
- Şengör, A. M. C. & Yılmaz, Y. 1981. Tethyan evolution of Turkey: a plate tectonic approach. Tectonophysics, 75, 181-241.
- Şengör, A. M. C. & Kidd, W. S. F. 1979. Post-collisional tectonics of the Turkish-Iranian plateau and a comparison with Tibet. Tectonophysics, 55, 361-376.
- Shan, Y., Li, Z. & Lin, G. 2004. A stress inversion procedure for automatic recognition of polyphase fault/slip data sets. Journal of structural geology, 26, 919-925.
- Sinclair, H. D 1997. Tectonstratigraphic model for underfilled peripheral foreland basins: An Alpine perspective. GSA Bulletin, 109, 324-346.
- Snyder, N. P., Whipple, K. X., Tucker, G. E. & Merritts, D. J. 2000. Landscape evolution to tectonic forcing: Digital elevation model analysis of stream profiles in the Mendocino triple junction region, northern California. GSA Bulletin, 112, 1250-1263.
- Steckler, M. S., Berthelot, F., Lyberis, N. & Le Pichon, X. 1988. Subsidence in the Gulf of Suez: implications for rifting and plate kinematics. Tectonophysics, 153, 249-270.
- Steckler, M. S. & Watts, A. B. 1978. Subsidence of the Atlantic-type continental margin of New York. Earth and Planetary Science Letters, 41, 1-13.
- Stock, J.D., Sklar, L., Montgomery, D.R., Collins, B.D. & Dietrich, W.E. 2005. Field measurements of incision rates following bedrock exposure: Implications for process controls on the long profiles of valleys cut by rivers and debris flows Bulletin of the Geological Society of America 117, 174-194

- Stockmal, G. S., Beaumont, C. & Boutilier, R. 1986. Geodynamic models of convergent margin tectonics: Transition from rifted margin to overthrust belt and consequences for foreland basin development. *American Association of Petroleum Geologists Bulletin*, 70 (2), 181-190.
- Stow, D. A. V., Kahler, G. & Panayides, I. 1998. Fossil Contourites: the section from the Palaeogene slope system of southern Cyprus. In: Panayides, I. & Xenophontos, C. eds *Tidr International Conference on the Geology of the Eastern Mediterranean, Abstracts*, Cyprus Geological Society, 66.
- Su Daquan, White, N. & McKenxie, D. (1990). Extension and subsidence if the Pearl River Mouth basin, northern South China Sea. *Basin Research*, 2, 205-222.
- Svela, K. E., 1998. Sedimentology of the Lower and Middle Coal measures Westphalian A and B in the Broadhaven-Little Have Coalfield, Pembrokeshire, SW Wales.
- Tankard, A. J., 1986. On the depositional response to thrusting and lithospheric flexure: Examples from the Appalachian and Rocky Mounatin basins. In: Allen, P. A. & Homewood, P. eds *Foreland basins*. International Association of Sedimentologists Special Publications, 8, 369-392.
- Tatar, O., Piper, J. D. A., Gürsoy, H., Heimann, A. & Koçbulut, F., 2004. Neotectonic deformation in the transition zone between the Dead Sea Transform and the East Anatolian Fault Zone, Southern Turkey: a palaeomagnetic study of the Karasu Rift volcanism. *Tectonophysic*, 385, 17-43.
- Tinkler, C., Wagner, J. J., Delaloye, M. & Selçuk, H. 1981. Tectonic history of the Hatay Ophiolites South Turkey and their relationship with the Dead Sea rift. *Tectonophysics*, 72, 23-41.
- Temizkan, N. 2003. Harbiye Antakaya Tektono-Stratigrafik incelemesi. Adana University.
- ten Veen, J. H. & Kleinspehn, K. L. 2002. Geodynamics along an increasingly curved convergent plate margin: Late Miocene-Pleistocene Rhodes, Greece. *Tectonics*, 21, 3, 1017-1038.
- Tron, V. & Brun, J-P. 1991. Experiments on oblique rifting in brittle-ductile systems. *Tectonophysics*, 188, 71-84.
- Tucker, M. E. 1991. *Sedimentary Petrology: An Introduction to the Origin of Sedimentary Rocks*. 2<sup>nd</sup> Edition, Blackwell Science, Oxford. 253pp.
- Tucker, G. E. & Whipple, K. X. 2002. Topographic outcomes predicted by stream erosion models: Sensitivity analysis and intermodel comparison. *Journal of Geophysical Research*. 107 B9 2179, doi:10.1029/2001JB000162.

- Turner, J. 1996. The subsidence of sedimentary basins. Ph.D Thesis, University of Edinburgh.
- Uffendorfer, H., Lund, J. J. & Georgi, K. H. 1990. Biostratigraphy of the Neogene in the Iskenderun Basin. Turkish Association of Petroleum Geologists. Proceedings of the 8th Petroleum Congress of Turkey, 363-370.
- Umhoefer, P. J. & Stone, K. A. 1996. Description and kinematics of the SE Loreto basin fault array, Baja California Sur, Mexico: a positive field test of oblique-rift models. *Journal of Structural Geology*, 18, 595-614.
- Ünlügenç, Ü. C., 1993. Controls on Cenozoic sedimentation in the Adana Basin, Southern Turkey, Unpublished Ph.D Thesis, University of Keele.
- Veevers, J. J., Falvey, D. A. & Robins, S., 1978. Timor Trough and Australia: Facies show topographic wave migrated 80km during the past 3myr. *Tectonophysics*, 45, 217-227.
- Vidal, N., Alvarez-Marron, J. & Klaeschen, D., 2000. The structure of the Africa-Anatolia plate boundary in the eastern Mediterranean, *Tectonics*, 19, 723-739.
- Wagreich, M. & Decker, K., 2001. Sedimentary tectonics and subsidence modelling of the type Upper Cretaceous Gosau basin (Northern Calcareous Alps, Austria). *International Journal of Earth Sciences (Geologische Rundschau)*, 90, 714-726.
- Walley, C. D. 1998. Some outstanding issues on the geology of Lebanon and their importance in the tectonic evolution for the Levantine region. *Tectonophysics*, 298, 37-62.
- Watts, K. F. 1990. Mesozoic carbonate slope facies marking the Arabian platform margin in Oman: depositional history, morphology and palaeogeography. In: Robertson, A. H. F., Searle, M. P & Reis, A. C (eds). *The Geology and Tectonics of the Oman Region*. Geological Society Special Publication, 49, 139-159.
- Watts, K. F. & Garrison, R. E. 1986. Sumeini Group, Oman – Evolution of a Mesozoic carbonate slope on a south Tethyan continental margin. *Sedimentary Geology*, 48, 107-168.
- Weissel, J. K. & Seidl, M. A., 1998. Inland propagation of erosional escarpments and river profile evolution across the Southeast Australian passive continental margin. In: Tinkler, K. J. & Wohl, E. E. (eds). *Rivers over rock; fluvial processes in bedrock channels*, AGU Geophysical Monograph, 107, 189-206

- Westaway, R. 1994. Present day kinematics of the Middle East and Eastern Mediterranean. *Journal of Geophysics Research*, 99, 12071-12090.
- Westaway, R. & Arger, J. 1998. The Gölbaşı basin, southeastern Turkey: A complex discontinuity in a major strike-slip zone, *Journal of the Geological Society, London*, 153, 729-743.
- Westcott, W. A. & Ethridge, F. G. 1990. Fan-deltas: alluvial fans in coastal settings. In: Rachocki, A. H. & Church, M. eds. *Alluvial Fans: a field approach*. Wiley, Chichester, 195-211.
- White, N. (1990). Resolving the extension discrepancy in the North Sea. In: Blundell, D. J. & Gibbs (eds). *Tectonic evolution of the north sea rifts*. Oxford University Press, 217-239.
- Williams, G. D., Ünlügenç, U. C., Kelling, G. & Demikol, C. 1995. Tectonic controls on stratigraphic evolution of the Adana Basin, Turkey. *Journal of the Geological Society of London*, 152, 873-882.
- Wilson, M., 1989. *Igneous Petrogenesis: A Global Tectonic approach*. Unwin Hyman, 466p.
- Withjack, M. O. & Jamieson, W. R. 1986. Deformation produced by oblique rifting. *Tectonophysics*, 126, 99-124.
- Wright V. P & Burchette, T. P. 1996. Shallow water carbonate environments. In: *Sedimentary Environments: Processes, Facies and Stratigraphy*, 3<sup>rd</sup> edition Ed: H.G. Reading. Pp. 325-394. Blackwell Science.
- Yetiş, C. 1988. Reorganisation of the Tertiary stratigraphy in the Adana Basin, Southern Turkey. *Stratigraphy newsletters*, 201, 43-58.
- Yetiş, C., Kelling, G., Gökçen, S. I., & Baroz, F. 1995. A revised stratigraphic framework for Late Cenozoic sequences in the northeast
- Yılmaz, Y. 1982. Amanos dağlarının tektoniği. TPAS report, project number YDP-35.
- Yılmaz, Y. 1993. New evidence and model on the evolution of the southeast Anatolian orogen. *Geological Society of America Bulletin*, 105 (2), 251-271.

Yılmaz, Y., Demirkol, C., Yalçın, N., Yetiş, C., Yiğitbaş, E., Günay, Y., Sarıtaş B. 1984. Amanos dağlarının jeolojisi: TPAS Report No 1920.

Yılmaz, Y. & Güner, O. F., 1995. The geology and evolution of the Misis-Andırın belt, around Andırın (Kahramanmaraş). Turkish Journal of Earth Sciences 5, 39-55.

Yurtmen, S., Rowbotham, G., Isler, F. & Floyd, P. A., 2000. Petrogenesis of basalts from southern Turkey: The Plio-Quaternary volcanism to the north of Iskenderun Gulf. Geological Society Special Publication, 173, 489-512

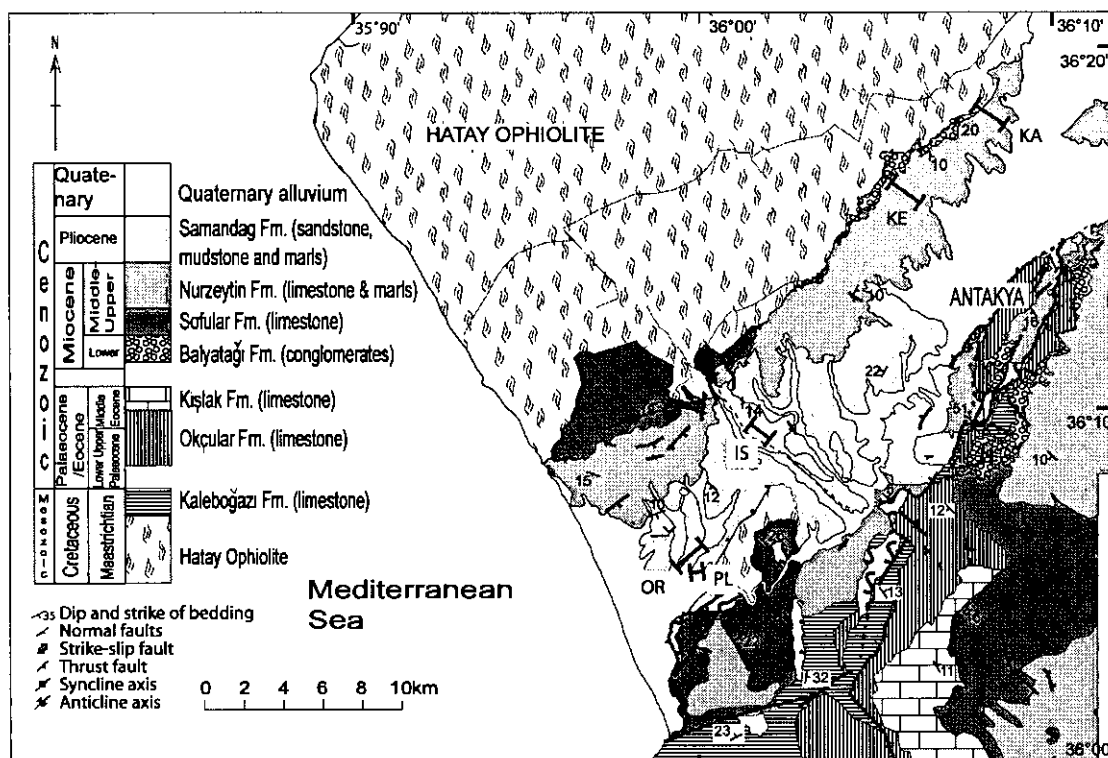
Yürür, T., & Chorowicz, J. 1998. Recent volcanism, tectonics and plate kinematics near the junction of the African, Arabian and Anatolian plates in the Eastern Mediterranean. Journal of Volcanology and Geothermal research, 85, 1-15.

Zanchi, A. Crosta, G. B. & Darkal, A. N. 2002. Paleostress analysis in NW Syria: constraints on the Cenozoic evolution of the northwestern margin of the Arabian plate. Tectonophysics, 357, 255-278.

Zelilidis, A. 2000. Drainage evolution in a rifted basin, Corinth graben, Greece. Geomorphology, 35, 69-85.

# Appendix 1

## Microfossil Data



A geological map showing the location of sections where samples micropalaeontological research were taken. Serinyol section is not on this please refer to Fig. 2.5 for the location of the town of Serinyol. OR – Ortatepe, PL – Pliocene section, IS – Iskendertepe, KE – Kesecik, KA – Kaaralı. Samples were taken at other localities but age determinations could not be made for these locations.

On all graphs the numbers along the sides indicate the sample number and not the distance along the section.

Tertiary										SYSTEM	IS
Neogene										SERIES	
Miocene					Late					SAMPLE NUMBER	
1	2	3	4	5	6	7	8	9	10		
										OSTRACODS	Planktic Forams
	+									Globigerinoides tribbus (Reuss)	
						+	+	+	+	Globigerinoides sacculifer (Brady)	
									+	Globigerinoides bisphericus Todd	
	+		+		+					Globigerinoides ruber (d'Orbigny)	
			+							Globigerinoides obliquus Bolli	
			+							Globigerinoides extremus Bolli&Bermudez	
						+	+	+	+	Orbulina suturalis Brönnimann	
							+			Globoquadrina dehiscens <small>(Chapman, Parr &amp; Collins)</small>	
							+			Globigerinella obesa (Bolli)	
											SR
											SERINYOL SECTION
											Globigerinoides tribbus (Reuss)
											Orbulina suturalis Brönnimann
											Orbulina bilobata (d'Orbigny)

IS – Iskender Tepe (0232850/4005582), sandstone, silt and marl. Section length is 30m.

SR – Serinyol section (not on location map), whole of sedimentary cover sequence sampled, only Late Miocene marl samples contained microfossils. Section length is ~250m.

Tertiary																SYSTEM	KA					
Neogene																						
Late Miocene											Early Pliocene					SERIES						
1	2	3	4	5	6	7	8	9	10	11	12	13	14	15	16	17	18	19	20	21	SAMPLE NUMBER	
																					OSTRACODS	Planktic Forams
						+							+									<i>Cytherelloidea glypta</i> Doruk
	+				+																	<i>Bairdia subdeltoidea</i> (Muenster)
	+																					<i>Cyprideis torosa</i> (Jones)
																						<i>Krithe monosteracensis</i> (Sequenza)
																						<i>Acanthocythereis hystrix</i> (Reuss)
																						<i>Costa edwardsii</i> (Roemer)
																						<i>Incongruella rotundata</i> (Ruggieri)
	+																					<i>Keijella hodgii</i> (Brady)
																						<i>Procythereis sulcatopunctatus</i> (Reuss)
	+																					<i>Aurila convexa</i> (Baird)
																						<i>Aurila speyeri</i> (Brady)
																						<i>Aurila freudenthali</i> Sissingh
																						<i>Aurila</i> sp. B Bassiouni
	+																					<i>Aurila soummamensis</i> Coutelle&Yassini
																						<i>Pokornyella deformis</i> minor (Moyes)
	+																					<i>Hermanites haidinger</i> minor Ruggieri
																						<i>Tenedocythere mediterranea</i> Ruggieri
																						<i>Tenedocythere prava</i> (Baird)
																						<i>Loxocorniculum quadricomis</i> (Ruggieri)
	+																					<i>Xestoleberis ventricosa</i> Müller
																						<i>Xestoleberis communis</i> Müller
																						<i>Xestoleberis glabrescens</i> (Reuss)
																						<i>Globigerinoides trilobus</i> (Reuss)
																						<i>Globigerinoides sacculifer</i> (Brady)
																						<i>Globigerinoides obliquus</i> Bolli
																						<i>Globigerinoides extremus</i> Bolli&Bermudez
																						<i>Globigerinoides bisphericus</i> Todd
																						<i>Globigerinoides ruber</i> (d'Orbigny)
																						<i>Globigerinoides subquadratus</i> Brönnimann
																						<i>Praeorbulina glomerosa curva</i> (Blow)
																						<i>Praeorbulina glomerosa glomerosa</i> Blow
																						<i>Orbulina suturalis</i> Brönnimann
																						<i>Orbulina universa</i> d'Orbigny
																						<i>Orbulina bilobata</i> (d'Orbigny)
																						<i>Globigerinella obesa</i> (Bolli)
																						<i>Paragloborotalia mayeri</i> Cushman&Ellisor
																						<i>Neogloboquadrina acostaensis</i> (Blow)
																						<i>Neogloboquadrina dutertrei</i> (d'Orbigny)
																						<i>Globoquadrina venezuelana</i> Hedberg
																						<i>Globigerina ouachitaensis</i> Howe&Wallece
																						<i>Globoturborotalita euapertura</i> Jenkins
																						<i>Pulleniatina finalis</i> Banner&Blow
																						<i>Dentoglobigerina altispira altispira</i> <sup>Cushman</sup> & <sup>Jarvis</sup>

KA – Kaarali. Base of section is composed of conglomerate and red mudstone. Length of the section is 100m.



Tertiary				SYSTEM	KE
Neogene					KESECIK VILLAGE
Miocene		Middle		SERIES	
+	+	+	+	SAMPLE NUMBER	
				OSTRACODS	Planktic Forams
		+	+	<i>Cytherella vulgata</i> Ruggieri	
		+		<i>Bairdia subdeltoidea</i> (Muenster)	
+				<i>Cnestocythere truncata</i> (Reuss)	
+				<i>Krithe monosteracensis</i> (Sequenza)	
+				<i>Acanthocythereis hystrix</i> (Reuss)	
	+			<i>Costa edwardsii</i> (Roemer)	
+	+			<i>Chrysocythere paradisi</i> Doruk	
	+			<i>Cistocythereis pokorny</i> (Ruggieri)	
+				<i>Keijella hodgii</i> (Brady)	
+		+		<i>Ruggieria tetraptera</i> (Sequenza)	
+				<i>Procythereis sulcatopunctatus</i> (Reuss)	
+				<i>Echinocythereis scabra</i> (Muenster)	
+				<i>Aurila convexa</i> (Baird)	
+				<i>Aurila albicans</i> (Ruggieri)	
+				<i>Aurila</i> sp. B Bassiouni	
+				<i>Pokomyella deformis minor</i> (Moyes)	
+	+			<i>Hermanites haidingeri minor</i> Ruggieri	
+				<i>Xestoleberis ventricosa</i> Müller	
+				<i>Xestoleberis communis</i> Müller	
		+	+	<i>Globigerinoides trilobus</i> (Reuss)	
	+		+	<i>Globigerinoides sacculifer</i> (Brady)	
+				<i>Globigerinoides immaturus</i> Le Roy	
			+	<i>Globigerinoides ruber</i> (d'Orbigny)	
			+	<i>Globoquadrina dehiscens</i> <small>(Chapman, Parr &amp; Collins)</small>	
		+	+	<i>Praeorbulina glomerata curva</i> (Blow)	
		+	+	<i>Orbulina bilobata</i> (d'Orbigny)	
+	+	+	+	<i>Orbulina suturalis</i> Brönnimann	
+			+	<i>Orbulina universa</i> d'Orbigny	
		+		<i>Globigerinella obesa</i> (Bolli)	

KE – Kesecik section. Interbedded marl and thin limestone beds. Length of section is 24m.

Tertiary															SYSTEM	OR ORTATEPE SECTION
Neogene																
Late Miocene					Early Pliocene										SERIES	
1	2	3	4	5	6	7	8	9	10	11	12	13	14	15	SAMPLE NUMBER	
															OSTRACODS	Planktic Forams
														+		<i>Cyprideis anatolica</i> Bassiouni
					+											<i>Cyprideis torosa</i> (Jones)
														+		<i>Pontocythere elongata</i> (Brady)
					+	+							+			<i>Ruggieria tetraptera</i> (Sequenza)
					+											<i>Heterocythereis albomaculata</i> (Baird)
					+									+		<i>Aurila speyeri</i> (Brady)
														+		<i>Aurila</i> sp. (B) Bassiouni
														+		<i>Aurila convexa</i> (Baird)
					+											<i>Urocythereis favosa</i> (Roemer)
														+		<i>Loxoconcha turbida</i> Müller
														+		<i>Loxoconcha tumida</i> Brady
																<i>Xestoleberis plana</i> Müller
																<i>Globigerinoides ruber</i> (d'Orbigny)
									+	+		+				<i>Globigerinoides obliquus</i> Bolli
										+		+				<i>Globigerinoides extremus</i> Bolli&Bermudez
													+			<i>Globigerinoides sacculifer</i> (Brady)
																<i>Globigerinoides immaturus</i> Le Roy
														+		<i>Globorotalia margaritae</i> Bolli&Bermudez

OR – Ortatepe section (0230398/3999093). Sandy marl and sandstone. Length of section 28m.

Tertiary														SYSTEM	
Neogene															
Late Miocene							Early Pliocene							SERIES	
1	2	3	4	5	6	7	8	9	10	11	12	13	14	SAMPLE NUMBER	
														OSTRACODS	Planktic Forams
						+							+		<i>Cyprideis torosa</i> (Jones)
		+					+	+							<i>Cyprideis anatolica</i> Bassiouni
										+					<i>Miocyprideis goekcenae</i> Bassiouni
													+		<i>Cytheridea acuminata acuminata</i> Bosquet
							+								<i>Ruggieria tetraptera</i> (Sequenza)
	+	+					+								<i>Heterocythereis albomaculata</i> (Baird)
	+	+					+	+							<i>Aurila skalae</i> Uliczny
		+					+	+							<i>Aurila convexa</i> (Baird)
		+													<i>Aurila speyeri</i> (Brady)
		+													<i>Urocythereis favosa</i> (Roemer)
										+					<i>Urocythereis margaritifera</i> (Mueller)
													+		<i>Cytheretta semiomata</i> (Egger)
								+							<i>Hirschmannia viridis</i> (Müller)
		+													<i>Xestoleberis reymonti</i> Ruggieri
		+						+							<i>Xestoleberis communis</i> Müller
		+													<i>Xestoleberis plana</i> Müller
													+		<i>Candona</i> (C) <i>parallela pannonica</i> Zalaný

Pliocene Section – location 8. Mostly sandstone, some marl and limestone. Length of the section ~100m long.

- Opaque
- Plagioclase

Quartz ~5%

Feldspars ~5%

Lithics ~90%

Litharenite

- Monocrystalline quartz
- Bioclastic material (mainly bivalves)

This is a highly altered rock, it has a very high secondary porosity where clasts (probably mostly biogenic, but not necessarily so) have been leached from the rock, leaving gaps behind. There is minor infilling of this secondary porosity.

### **SB176A**

Location 205

Conglomerate

Micritic matrix, sparite in fills porosity. Abundant clasts of serpentinite that are sub-angular. Also present are quartz, Clinopyroxene and plagioclase. There is no bioclastic material present.

### **SB177A**

Location 205

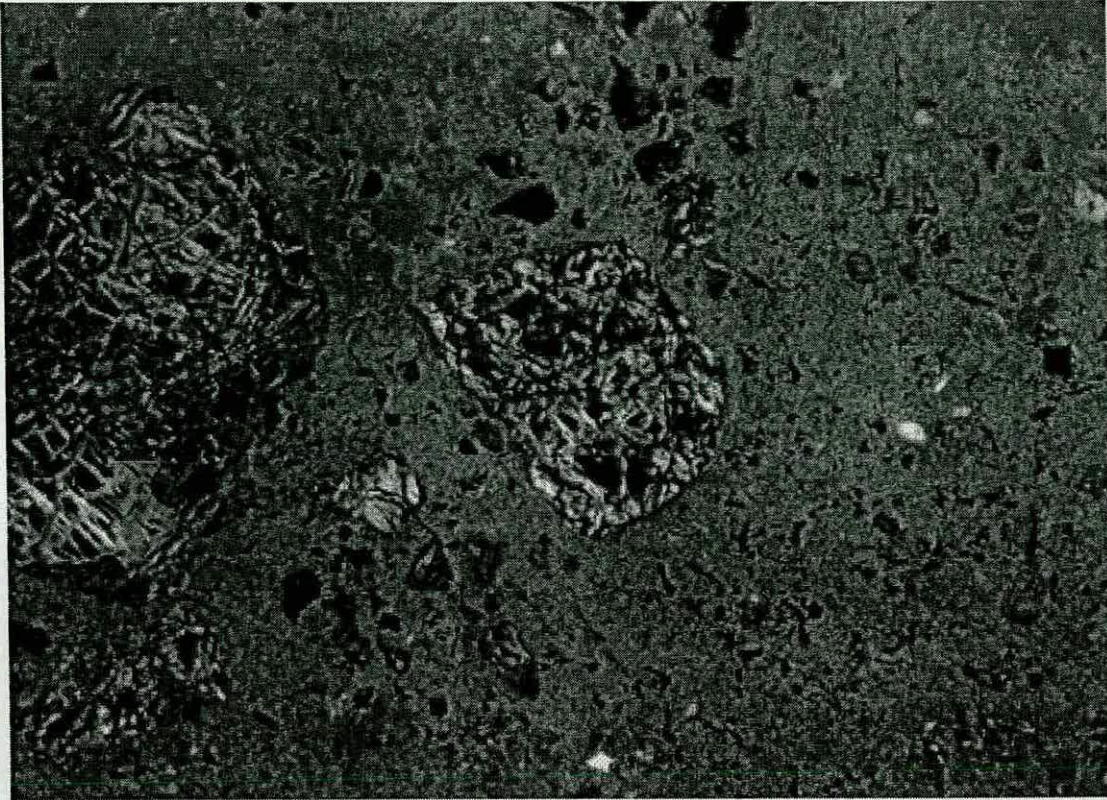
Grainsize <1mm, moderately well sorted and grains are sub-angular to sub-rounded and matrix supported. There is no micrite cement, but the rock has been cemented by sparite creating a poikiliptic texture. Around some of the clasts is an iron oxide crust. No bioclastic material present and no porosity.

Lithic Clasts

- Serpentinite
- Clinopyroxene and plagioclase
- Chlorite rich clast
- Ferruginous and radiolarian cherts
- Micritic mudstone
- Basalt
- Ferruginous chert and radiolarian chert
- Altered volcanic glass

Grains

- Olivine
- Monocrystalline and polycrystalline quartz
- Clinopyroxene



**SB13A** – Lower Miocene conglomerate in XPL. Note large clasts of serpentinite in micrite matrix. Quartz grains are also present. Magnification x2.

### **SB65A**

Location 218

Conglomerate

Micrite matrix. Contains large angular to sub-angular clasts of serpentinite and small clasts of monocrystalline quartz and plagioclase. There is no bioclastic material. There is some pore space (inter-particle vugs), which are partly in filled by sparite. Occasional peloids.

### **SB165A**

Rubbish tip at Harbiye

Sample is from a large block of limestone found within the conglomerates. Micritic matrix, with sub-rounded to rounded clasts.

Clasts

- Serpentinite

- Opaque minerals
- Iron rich pellets

~10%

## Clast composition

- Serpentinite
- Limestone – mudstone; similar to SB70 but contains more opaque material
- Feldspar
- Calcite

Contains no bioclastic material

Grains are poorly sorted and angular to sub-rounded.

After Folk – Intramicrite

After Dunham – wackestone

Sst classification – greywacke

**SB13A**

Location 163

Conglomerate

Micrite groundmass, this has a blotchy appearance indicating that this could be partly microbial, peloidal or maybe reworked in some way.

Clasts are sub-angular to sub-rounded.

- Serpentinite
- Partly recrystallised limestone
- Intramicrite
- Quartz (rare)
- Plagioclase
- Opaques
- Altered basic volcanic glass (pseudotachylite)

No bioclastic material

Most of material is derived from the ophiolite.

## **Lower Miocene**

### **SB15**

Location 42

Chalk

Composed mainly of micrite matrix with some secondary sparite. Contains minor angular to sub-rounded clasts.

- Opaques
- Quartz
- Serpentine
- Micrite
- Palagonite (altered glass)

The matrix has a curious texture, which maybe due to microbial action. There is present wavy iron-rich micrite. Maybe due to lithification and then being reworked.

### **SB59**

Location 92

Conglomerate; poorly sorted.

Clasts are mostly serpentinite, a few clasts of micritic limestone (pos peloids). The matrix is a mixture of calcite and serpentinite. There is a small amount of quartz, but the rock is dominated by serpentinite.

### **SB61**

Location 93

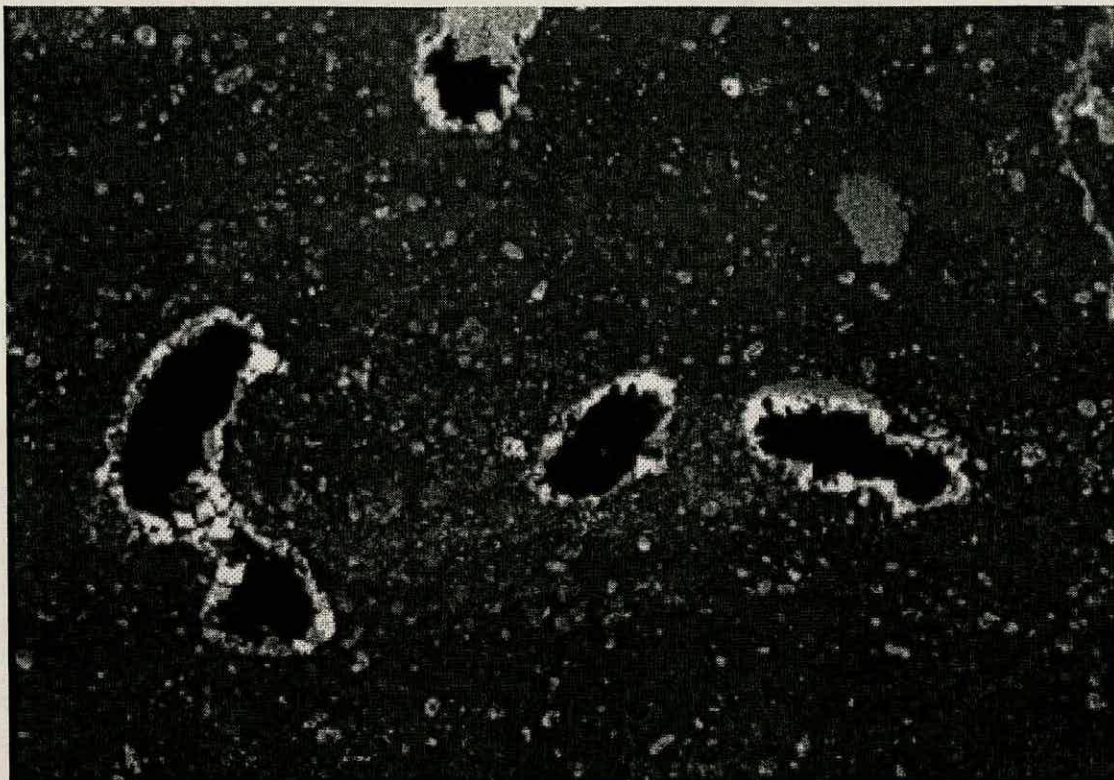
Limestone contains clasts up to 7-8mm

Brown in colour

Matrix

Very fine micrite matrix contains some siliciclastic material;

- Calcite grains ~40%
- Serpentine
- Quartz
- Feldspar



**SB81A** – Dense micritic limestone (lime mudstone) with fenestral porosity beginning to be infilled with sparite cement.

### **SB100A**

Location 288

Eocene limestone

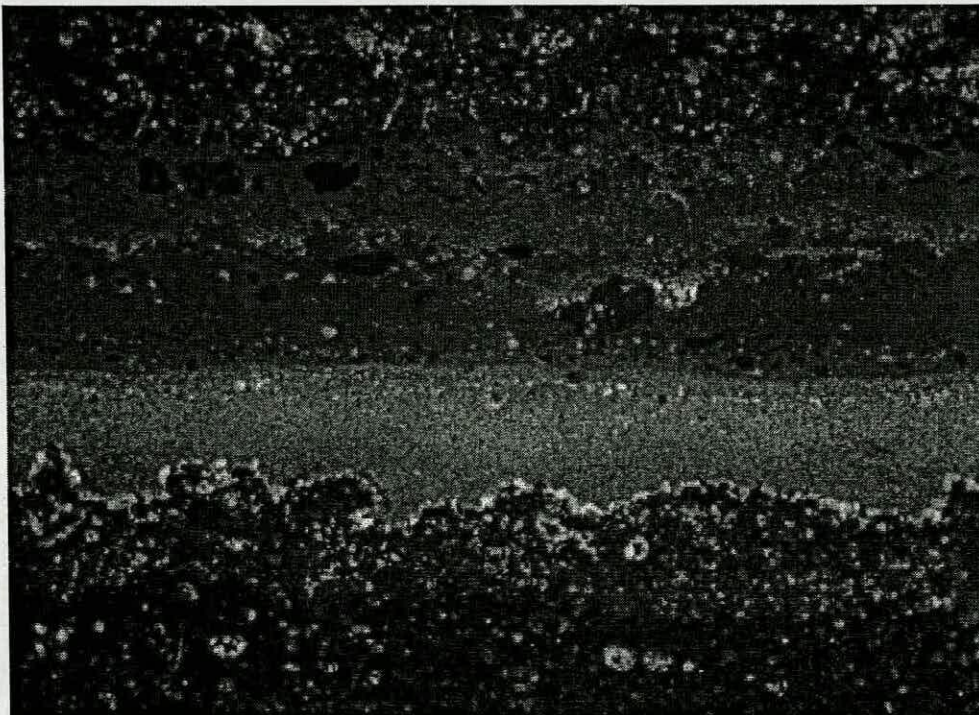
Extremely rich in bioclastic material

- Benthic and planktic forams (including *Nummulites* sp. and *Milliolid* sp.)
- Echinoid fragments with calcite overgrowths
- Coralline algae (possibly reworked)
- Coral
  
- After Dunham – Packstone





SB58 – PPL light showing different large benthic foraminifera species *Nummulites*, *Discocyclina*, *Miliolidae*, most show evidence of reworking. Also note fragment of echinoid in top left corner with an optically continuous overgrowth of calcite cement.



SB81A – Microbial limestone in PPL showing the dense micritic fabric, note layering within the micrite and clasts of micrite that may be due to drying of the sediment. Magnification x2.

- Ostracods.
- Calcispheres

More planktic foraminifera present than benthic in this sample.

Also there is some siliciclastic material

- Iron-rich clasts
- Serpentine (sub-angular)
- Monocrystalline quartz

Heamatite infilling some of bioclastic material

- After Folk – foraminiferal biomicrite
- After Dunham – Wackestone



**SB58** – Photomicrograph in XPL of packstone. Features to note are the large reworked and abraided benthic foraminifera (*Miliolidae*) and abundant other bioclastic material including *Nummulites*. Magnification x 2.

## Bioclasts

- Algal material, including red coralline algae
- Coral
- Gastropod
- Bivalves (inc. oysters)
- Echinoid plates, crinoid ossicles
- Planktic forams
- Benthic forams
- Bryozoa?
- Calcispheres
- Rare ostracod fragments

## Rare silt and limestone clasts

## Micrite matrix with sparite infilling porosity

- Calcirudite
- After Folk – biomicrite
- After Dunham - packstone

**SB81A**

## Location 250 - UK

This sample is an algal limestone with fenestral porosity.

The matrix is composed of dense micrite and the pore-spaces have a minor infill of sparite or possibly dolomite as crystals have distinctive diamond shape.

There is no siliciclastic material, but there is evidence that there may have been some bioclastic material that has subsequently been replaced.

Appears to contain planktic foraminifera and ostracod fragments

**SB98A**

## Location 286

The sample is from the Eocene boundary limestone.

Composed of very dense micrite it is rich in bioclastic material

- Planktic forams, including *Morozovella* sp, *Globergerinidae* and *Globorotalilidae*.
- Benthic forams including fragments of *Discocyclina*.
- Shell fragments

**SB56**

Dursunlu Quarry

Conglomerate – Palaeocene?

## Clasts

- Serpentinite
- Opaques
- Limestones (micritic and sparite)
- Siltstones

The matrix is composed to subhedral calcite crystals (~0.1mm) set in a poikilotopic sparry calcite cement.

**SB58**

Dursunlu Quarry - Eocene

## Bioclastic material

- Forams (Benthic inc. Nummulites, discocyclinids, miliolids, and planktic sp.)
- Bryozoa
- Echinoid fragments

There are clasts of limestone containing bioclastic material, forams, and coral. Some micrite present also lots of sparry calcite cement, equant overgrowths of echinoid plates. Also poikilotopic sparite.

- Calcirudite
- After Folk – biosparite/biomicrite
- After Dunham – grainstone/packstone

**SB65**

Location 97 - UK

Cream microbial limestone

## ***Upper Cretaceous and Eocene***

### **SB9**

Location 29 – Harbiye Gorge, Upper Cretaceous

Bright red colour

Lots of iron rich pellets – opaque but rounded, leaching from these clasts has stained surrounding micrite. Texture of the rock varies across the section, concentration of clasts varies across the slide and an area of wavy laminations, possibly algal in origin, separate areas of high and low concentration. In addition to the opaque material there are microcrystalline quartz clasts (chert possibly) and rarer mono and polycrystalline quartz clasts.

It is likely that this sample is a ferruginous soil, the Fe clasts could be some sort of pesoid. The micrite could be derived from calcrete.

### **SB18**

Location 46 - Eocene

White limestone containing large bioclasts.

Very similar to SB58

#### **Bioclasts**

- Benthic forams (Nummulites, miliolids, discocyclinids)
- Planktic forams
- Echinoid spines
- Bivalves
- Coralline algae

Contains also clasts of older limestone containing bioclastic material (gastropods, algae, forams). Drusy sparite cement with some micrite, sparite overgrowths and poikilotopic textures.

- Calcirudite
- After Folk – foraminiferal biosparite
- After Dunham – grainstone/packstone

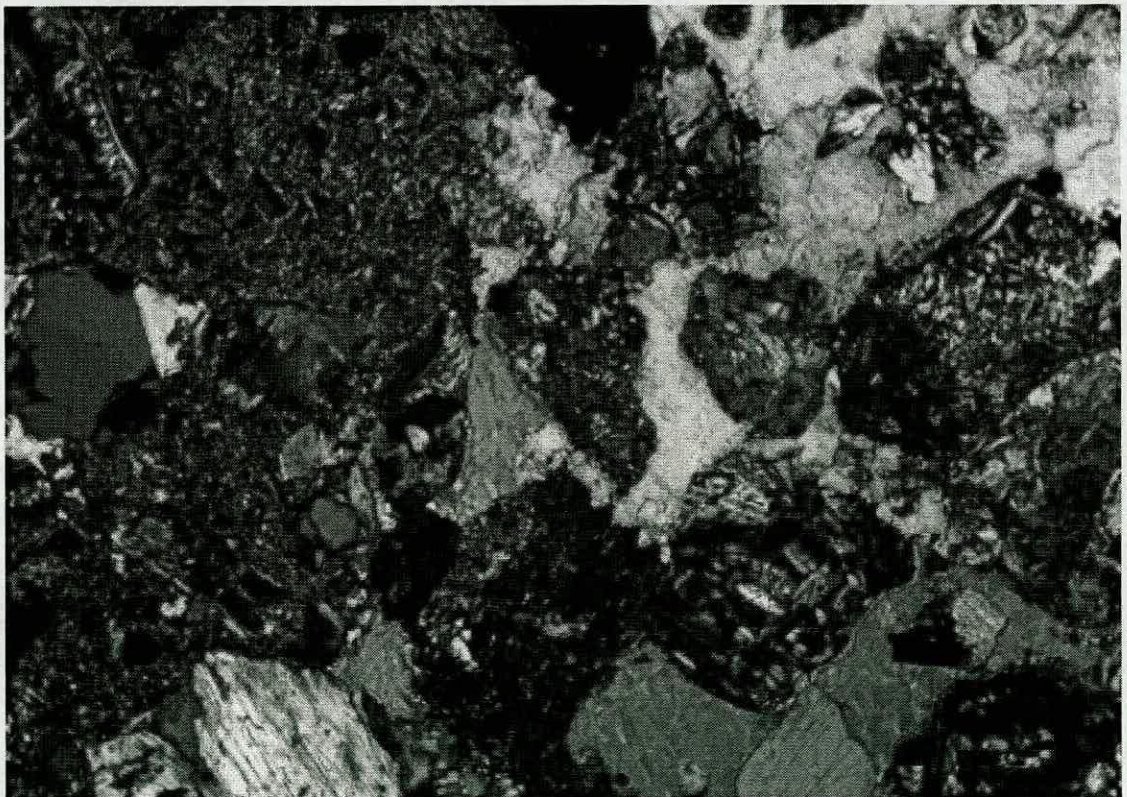
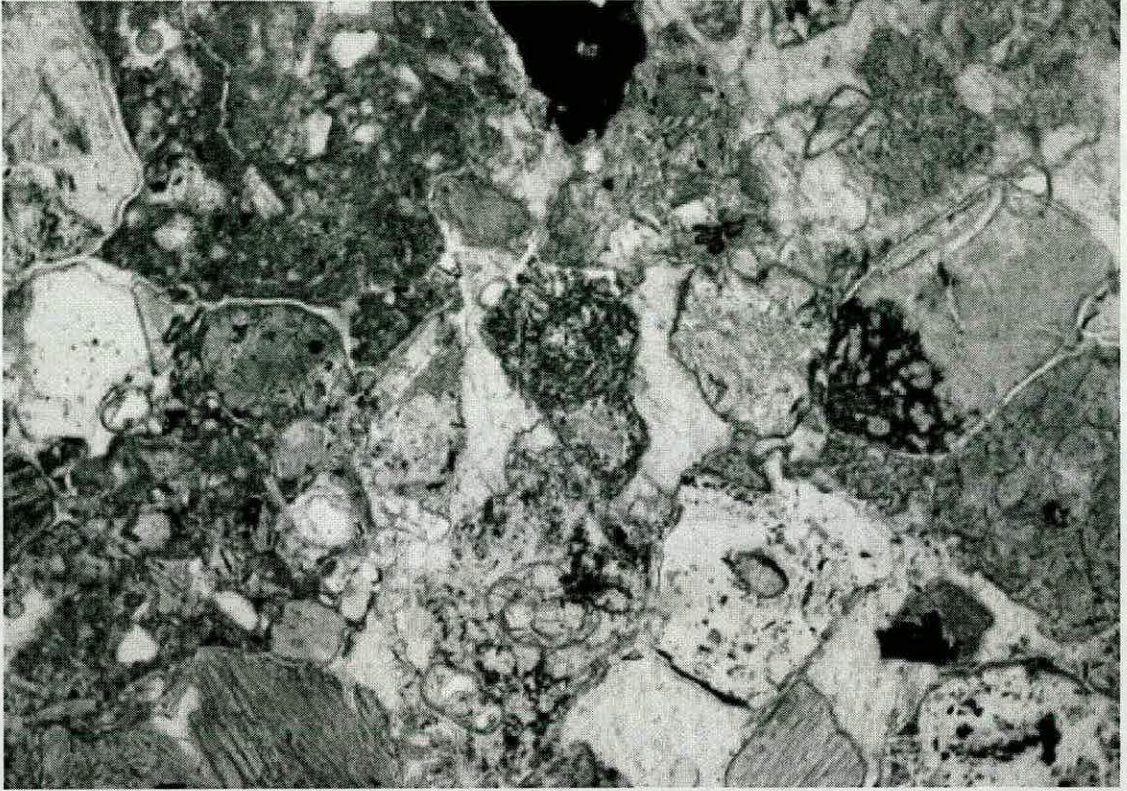
Sample	SB146A	SB140A	SB137A	SB135A	SB133A
Quartz	26	32	26	38	19
Calcite	31	41	57	59	79
Smectite	0	0	0	0	0
Illite	0	0	0	0	0
Clinochy	0	0	0	3	0
Albite	27	10	10	0	2
Dolomite	4	0	0	0	0
Heamatite					
Muscovite			6		
Others	12	17	1		
Total	100	100	100	100	100

Sample	SB128A	SB126A	SB115A	SB104A	SB98A	SB95A	SB87A	SB76A	SB72A	SB57A	SB43A	SB28A
Quartz	20	17	5	15	14	28	35	20	29	34	0	25
Calcite	78	61	55.5	56	57	49	0	5	51	9	0	39
Smectite	0	0	0	0.1	0	0	0	16	0	0	0	0
Illite	0	0	0	0	0	0	0	0	0	0	0	0
Clinochy	0	1	30.5	22	8	0	0	39	0	0	28	0
Albite	2	0	0	5	2	0	0	0	12	15	0	16
Dolomite	0	0	0	0	0	2	56	0	2	6	72	0
Heamatite										12		
Muscovite		14			16	5		20				17
Others		7	9	1.9	3	16	9		6	24		3
Total	100	100	100	100	100	100	100	100	100	100	100	100

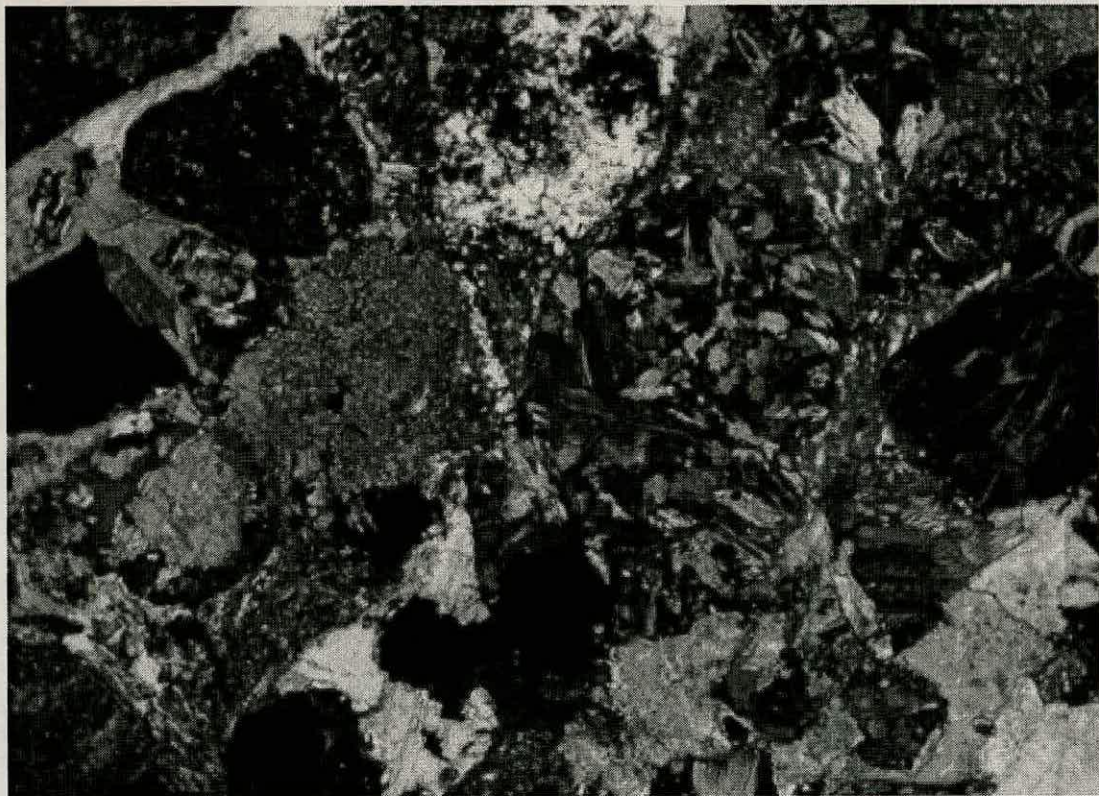
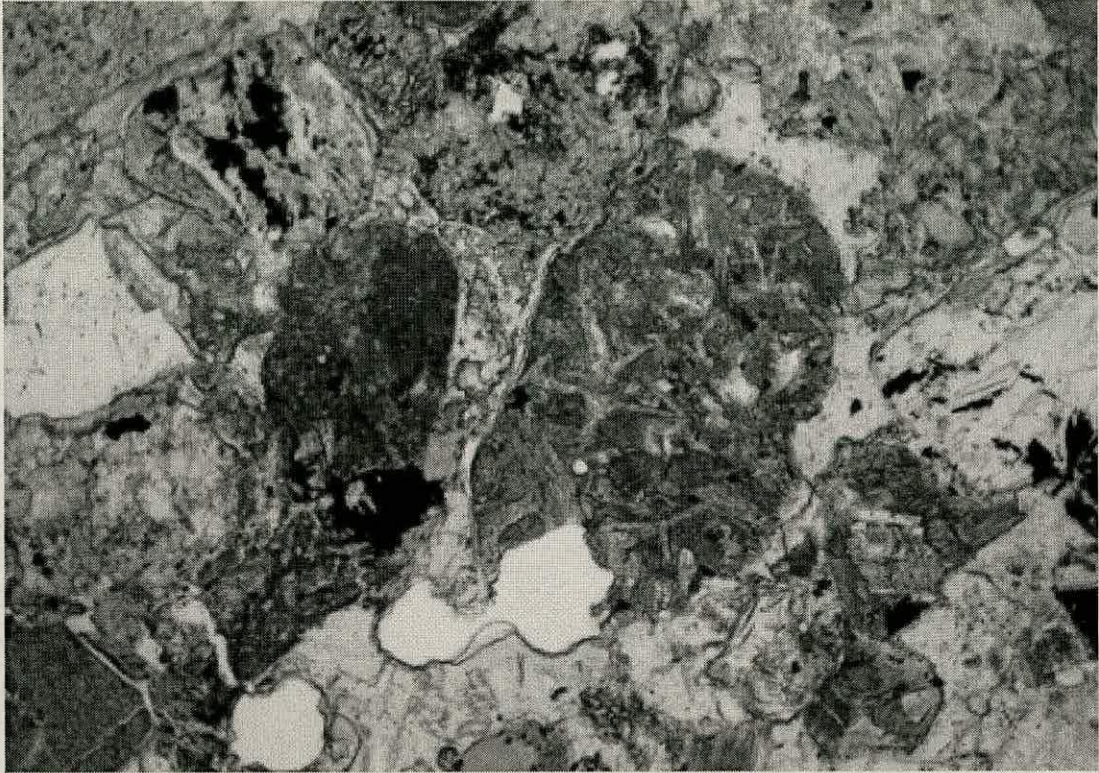
Sample	SB04A	SB01A	SB82	SB81	SB80	SB77	SB75	SB72	SB71	SB67	SB66	SB50	SB48	SB44
Quartz	0	64	10	10	7	5	5	7	17	5	17	8	13	10
Calcite	0	0	60	37	70	42	0	67	40	80	36	53	54	66
Smectite	0	0	10	30	17	11	0	24	0	10	11	18	13	17
Illite	0	0	3	3	3	3	70	0	18	0.1	28	4	2	3
Clinochy	12	6	3	3	0	0	0	0	2	0	1	2	4	3
Albite	7	19	3	7	3	1	0	2	11	0.1	6	5	2	0
Dolomite	16	4	0	2	0	0	0	0	5	0	1	0	0	0
Heamatite	16						24							
Muscovite	49													
Others		7	11	8		38	1		7	4.8		10	12	1
Total	100	100	100	100	100	100	100	100	100	100	100	100	100	100



Sample	SB44	SB42	SB38	SB36	SB35	SB34	SB33	SB32	SB31	SB30	SB25	SB22	SB16	SB07
Quartz	10	7	6	7	9	7	7	11	10	3	4	21	3	6
Calcite	66	74	53	39	58	55	40	37	48	95	93	37	16	57
Smectite	17	13	13	15	22	17	30	31	29	0	0	15	63	22
Illite	3	4	0	0	5	3	3	0	0	2	2	9	7	3
Clinochy	3	0	0.1	2	3	3	5	8	7	0	0	2	0.1	1
Albite	0	2	3	0	2	7	5	8	4	0.1	0	8	6	3
Dolomite	0	0	0	36	0	0	0	1	0	0	0	3	4	0
Heamatite														
Muscovite												5		
Others	1		24.9	1	1	8	10	4	2		1		0.9	8
Total	100	100	100	100	100	100	100	100	100	100.1	100	100	100	100



**SB177A** – Litharenite in PPL (top) and XPL (bottom), note high amount of serpentinite clasts with a calcite cement forming a poikiloblastic texture. Magnification x 10.



SB177A – Litharenite in PPL and XPL (top and bottom respectively), note large serpentinite clast showing alteration to chlorite, probably originally a plagioclase rich lithic clast.

Magnification x 10.

**SB30.3**

Enek Log/ Balyatagi type section.

Pale coloured litharenite, which is poorly sorted with sub-angular clasts of 0.5-2mm in size.

The matrix is composed of micrite and mud.

- Serpentinite >85%
- Feldspar <5%
- Opaques

Some pinky brown fine-grained clasts that are possibly basalt but very hard to identify.

***Middle Miocene*****SB5**

Location 24 (ophiolite/cover boundary)

Limestone

Peloids

Bioclasts

- Benthic and Planktic forams
- Coralline algae and encrusting algae
- Gastropods
- Bivalves

Siliciclasts

- Olivine
- Quartz
- Feldspar
- Serpentinite
- Chert

Is quite porous although some of the porosity has been in filled by secondary sparite.

- Calcirudite
- Biomicrite
- wackestone

## SB6

Location 25

White limestone

Micrite matrix with isopachous fringes developed around some grains. Porosity has mostly been in filled by sparry calcite cement.

Bioclasts

- Coral
- Forams, including *Operculina*.
- Bivalves inc. oysters
- Algal material (reworked)
- Echinoid spine
- Ostracodes?

Clasts of micrite

- Calcirudite
- After Folk – biomicrite
- After Dunham wackestone

## SB11

Location 34

Large benthic forams in a fine grained matrix Matrix is composed mostly of micrite, little primary pore space remains as pores have been in filled by sparite.

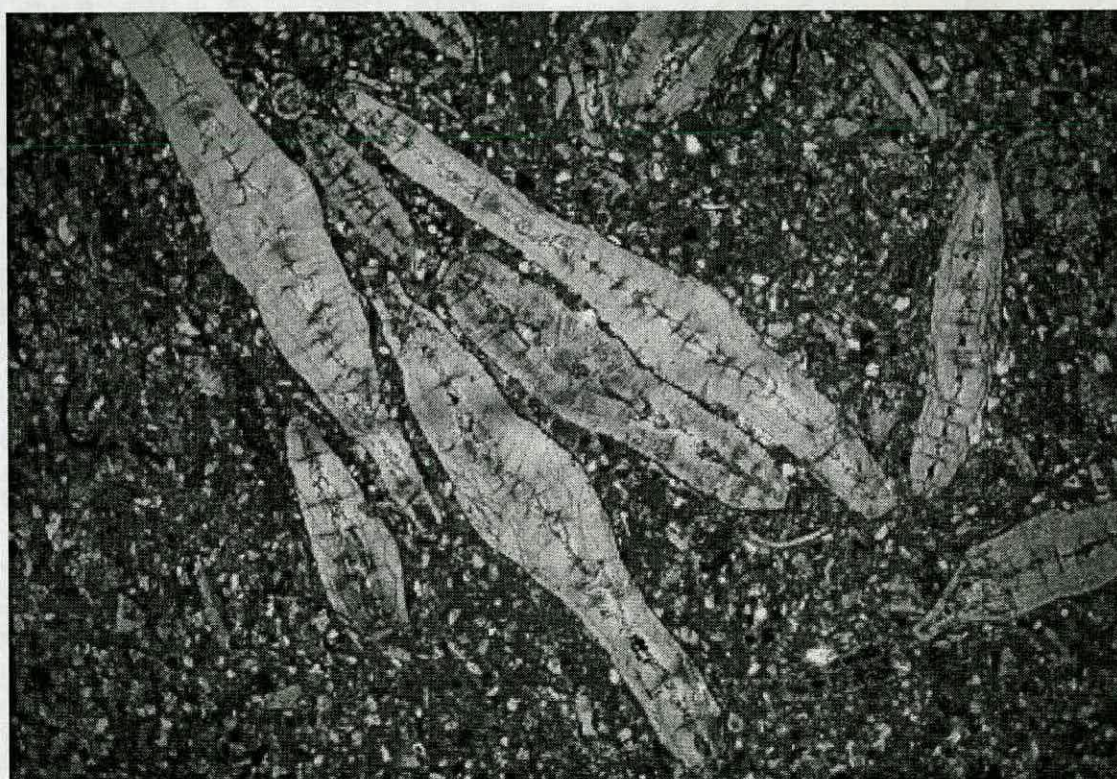
Bioclasts

- Benthic and planktic forams
- Coccoliths (?)
- Oyster

- Other bivalve fragments
- Gastropod
- Algae
- Echinoid and crinoid debris

Siliciclasts (this material forms part of the fine grained matrix, <0.1mm)

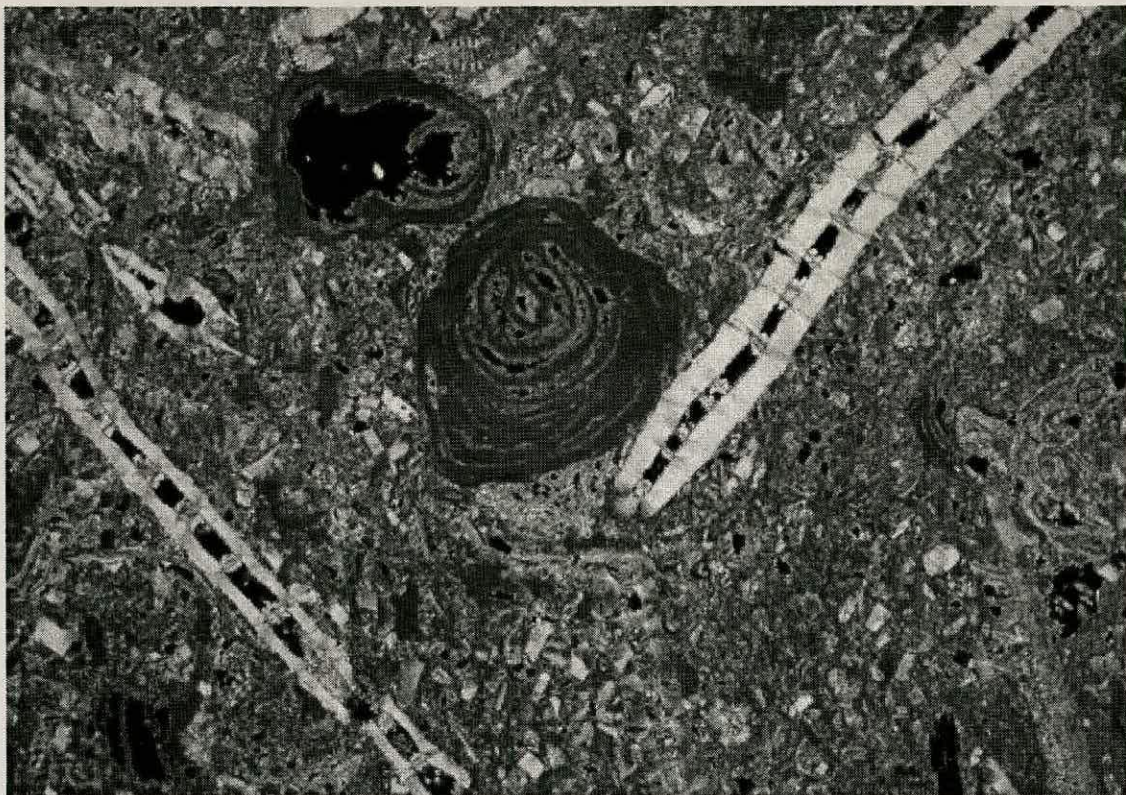
- Quartz
- Olivine
- Serpentine
- Clinopyroxene
- Plagioclase



**SB11** – PPL showing large partially aligned *Operculina* in a matrix of micrite and small siliciclastic material. Magnification x2.



**SB11** – XPL showing aligned *Operculina*.



**SB41** – Bioclastic calcarenite with *Operculina* and oncolite (algal balls), primary porosity is preserved within bioclastic cavities. Magnification x 10.



SB41 – PPL of same sample other bioclastic material present included crinoid ossicle, planktic foraminifera and *Amphistegina*.

### SB41

Location 68

Bioclasts;

- Algal material
- Benthic forams including *Operculina*.
- Planktic forams
- Ostracods
- Echinoid spines and plates
- Bivalve (oyster and others)
- Crinoid ossicle
- Gastropods
- Bryozoan
- Coral

Micrite forms the matrix and there is very little cement infilling porosity (high). Some pore spaces in bioclasts are semi-filled with micrite.



Operculina biomicrite  
Operculina wackestone

### **SB45**

Location B Teknepinar gorge  
Microbial limestone

Bioclasts;

- Algal material; oncolite and coralline algae. Large pieces so have not travelled far down slope.
- Planktonic forams
- Benthic forams
- Echinoid spines
- Bivalve fragments inc. oysters.
- Ostracodes
- Bryozoa

Micrite matrix, some of original porosity has been in-filled by sparry calcite but still porosity ~10%. Some isopachous fringes.

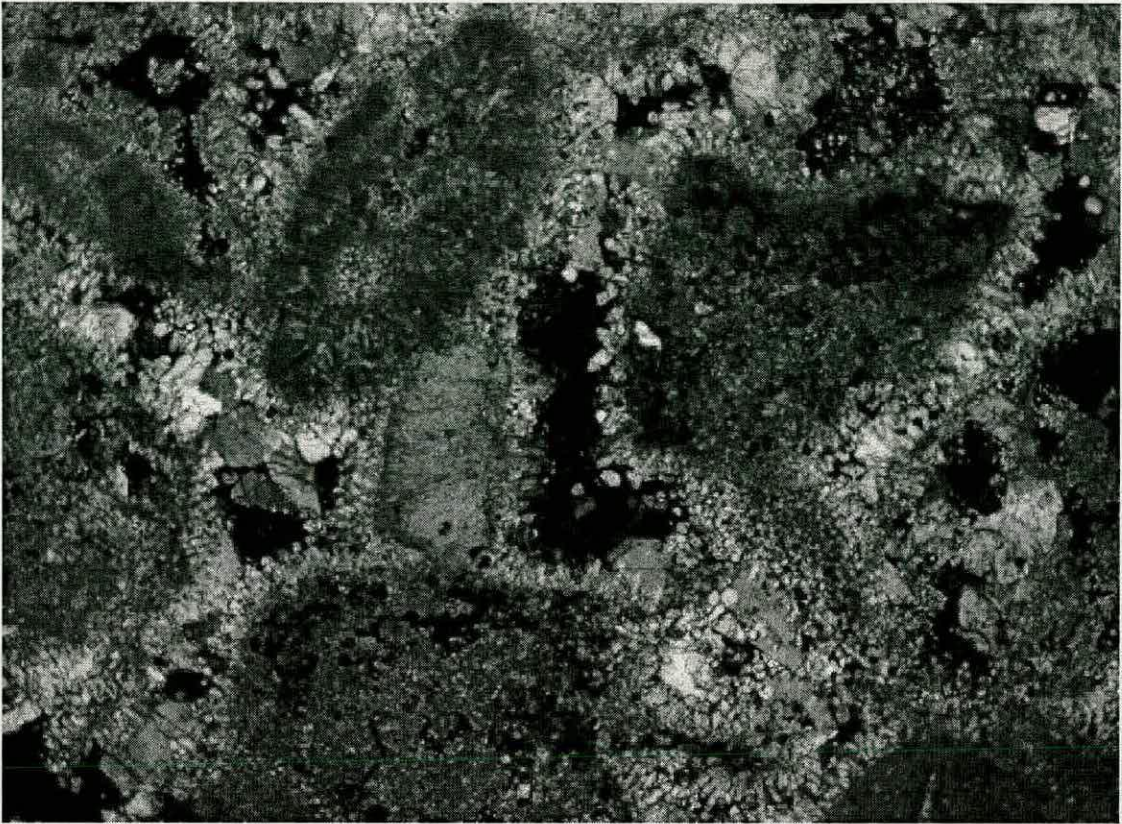
- Calcirudite
- After Folk – biomicrite
- After Dunham – wackestone

### **SB47**

Location 76

Bioclastic Packstone/ biosparite

Grainsize 1-2mm and a micrite matrix; the rock has a high porosity that is beginning to be in-filled by sparite, which is forming radial fringes to the grains. Clasts are well rounded and bioclasts are fragmented.



SB47 – XPL grainstone, note primary intergranular porosity beginning to be infilled with sparite forming acicular crystal fringes around the clasts.

#### Bioclasts

- Red algae Algae (coralline, possibly lithostratium) forms majority of the clasts
- Bivalves also Ostrea (unaltered calcite shell)
- Benthic forams
- Planktic forams
- Echinoid fragments with optically continuous overgrowths

#### Lithics

- Quartz rich silt
- Serpentinite
- Chloritised Basalt
- Bioclastic limestone rich in planktic forams

#### Grains

- Monocrystalline quartz (medium sized fluid inclusions, not fine like arkose)
- Olivine

- Peloids
- Intraclasts

Pore space ~25%

Grains ~50%, matrix/pore-space ~50%

90% of clasts are bioclasts.

### **SB49**

Karacay log

Cream limestone

Forams up to 5mm

Bioclastic material;

- Foraminifera (benthic and planktic) lots of large *Operculina*.
- Bivalves, including oysters
- Gastropods
- Coral
- Red algae

Calcite cement in-fills come of the porosity in the bioclasts but generally little cementation and lots of micrite. Siliciclastic material is rare although there are a few small quartz grains.

- After Folk – biomicrite
- After Dunham - wackestone

### **SB52**

Location 85

Mudstone – 99% micrite

Contains no bioclastic material

There are rare and very small grains of polycrystalline quartz.

### SB53

Location 85

Micrite matrix, some sparite infilling pore-spaces

Clasts

- Serpentine
- Palagonite
- Quartz (monocrystalline)
- Peloids
- Rare benthic forams

Intramicroite/pelmicrite

### SB54

Location 87

Limestone

Cream colour, foraminifera visible to naked eye average 1mm in size

Almost completely composed of bioclastic material

- Benthic forams inc. *Alveolina* sp.
- Planktonic forams inc. *Globigerina* sp.
- Bivalve fragments
- Gastropods
- Ostracods

Mostly large benthic foraminifera but significant numbers of planktics present.

Also present are trace amounts of siliciclastic material:

- Serpentine
- Quartz
- Chlorite
- Epidote?

Clast supported fabric, poorly sorted. Bioclasts are generally primary calcite however some alteration has taken place in some clasts these possibly are reworked.

- Calcarenite- calcirudite
- After Folk – biomicrite
- After Dunham - Packstone

### **SB63**

Location 96

Limestone

Bioclasts

- Benthic forams
- Planktic forams
- Algae and coralline algae
- Ostracode
- Bivalves
- Echinoid and crinoid fragments
- Oyster
- Gastropod
- Polyzoan

Very small (0.01mm) grains of quartz and hematite grains (these are staining surrounding material)

Shallow water material, some reworking but probably not very far.

### **SB64**

Location 97

White limestone with large benthic forams, grain supported.

Bioclasts;

- Discocyclinids
- Nummulites
- Other forams

- coralline algae
- Echinoid bits
- Reworked limestone material

There is almost no cement present, there rare calcite overgrowths in optical continuity with echinoid plates. No porosity

- Calcirudite
- After Folk – biomicrite
- After Dunham – packstone

## **SB70**

Location 112 - Limestone

Medium – coarse grained

White in colour with a few opaque grains

Composed almost entirely of very fine micrite cement (>80%), contains a component of siliciclastic material including;

- Detrital quartz grains, showing some evidence of sub-grain rotation (1-5%)
- Clinopyroxene
- Epidote
- Chlorite
- Serpentine

Rare calcite crystals and there is a small bioclastic component (mainly planktic foraminifera).

The bulk of the rock is micrite, possibly of peloidal original. Sparite is also present, in filling pore spaces (coarsens into the centre) and also sparry calcite occurs around the clasts and is noticeably coarser around them.

Possibly pelagic in origin

- Calcarenite
- After Folk – Intramicrite
- After Dunham – Mudstone/wackestone

The sample is from basal limestone overlying the ophiolite on the central graben high.  
Small siliciclastic input mostly derived from ophiolite (only small amount so no significant erosion at this point)

## **SB76**

Location 125

Grainsize ~1mm, clast supported, grains sub-angular to sub-rounded and poorly supported.  
Little micrite, carbonate cement <15%

### Clasts

- Serpentinite (>70%)
- Micritic limestone
- Reworked forams
- Siltstone

### Grains

- monocrystalline qtz
- Feldspars
- Chlorite
- Calcite
- Forams
- Bivalves
- Clinopyroxene

Calcite cement overgrowths on some grains. Dominantly ophiolite derived  
Litharenite/calcarenites

Qtz <1%

Feld <1%

Lithics >98%

**SB102A**

Location 297 - Limestone

Bioclasts

- Algal material (50-60%)
- Benthic forams (20%)
- Echinoid fragments (5%) with optically continuous overgrowths
- Micrite clasts (peloids?)

The whole rock is totally reworked, darker materials are remains of microbial mats reworked down slope, and these are well rounded.

Marginal microbial mat and offshore benthics reworked down-slope.

- Biosparite
- Grainstone



**SB160A**

Location 307

Grainsize 1-3mm, well rounded and moderately well sorted. Matrix supported. Micrite matrix composes ~10% of the rock, with sparite in filling porosity and forming overgrowths on bioclastic material.

Clasts

- Peloids/micrite
- Biomicrite limestone
- Serpentinite
- Ferruginous chert
- Rare quartz

Bioclasts (~90%, the majority appear to have undergone some reworking)

- Coralline algae, probably reworked
- Echinoid fragments with optically continuous overgrowths of sparite
- Forams both fresh and apparently reworked, benthic and planktic.
- Bivalve fragments

Litharenite/calcarenite

**SB12.3**

Location – kozkalesi log

White calcirudite, lots of oncolite.

Pores infilled with micrite and sparite, algal balls relatively whole, but broken in places – reworked. Micrite and sparite matrix.

- Forams
- Gastropods
- Bivalve shells
- Ostracodes
- Polyzoan
- Crinoid ossicles (disc with calcite fringe)

Most original porosity has been infilled with sparite, there is a little residual porosity left in some cavities.

- Biomicrite
- Wacke-packstone

### **SB13.3**

Kozkalesi log - Coarse calcirudite

Lots of coarse sparite, micrite is original matrix.

All bioclastic material seems to be recrystallised and/or bleached. The gaps are infilled with coarse sparite.

Some clasts are siliciclastic (heamatite, serpentinite)

### **SB14.3**

Kozkalesi log - Calcilitharenite

Coarse sandstone, orange colour, poorly sorted with subangular to rounded clasts.

>75% of clasts are serpentinite. Lots of micrite matrix.

Bioclasts

- Ostrea
- Benthic foram
- Reworked clasts (coralline algae, benthic and planctic forams)

Possibly 2 limestone sources, some reworked limestone are micrite some are sparite.

Some original porosity ~5%, now reduced to ~2%, sparite in pore spaces, micrite envelopes around clasts.

Mixed ophiolite and carbonate source ~75% serpentinite; 25% carbonate (~10% matrix).

### **SB15.3**

Kozakalesi log - Mudstone/calculutite

Brown, very fine grained but contains some rare clasts <0.5cm, very poorly sorted.

Micrite (>75%) with clasts (subangular).

Clasts are generally very small included quartz, serpentinite (greatest), basalt.

There is no texture, no microfossils.

### **SB17.3**

Kozkalesi log

White limestone – calcirudite/biomicrite

Aswell as lots of bioclastic material there are lots of diamond shaped crystals – dolomite rhombs? Many appear to have a nucleus of micrite or opaque material.

Also

- Ostrea
- Forams (benthic and planktic)
- Algae
- Echinoid
- Coral
- polyzoans

### **SB31.3**

Enek Log

Calcirudite containing large shell fragments, with a micritic matrix.

Shell fragments:

- bivalves including ostrea.
- Gastropods
- Foraminifera (benthic and planktic) these are whole.
- Crinoid ossicle
- Polyzoan

Rare siliciclastic material is present

- Serpentinite

- Haematite
- Chlorite
- Quartz

Pyrite infills some shell cavities.

The majority of the original porosity is infilled with fine-grained sparite.

### **SB43.3**

Location 486

Pale coloured, medium-grained poorly sorted sandstone. Matrix <15%. Sparite cemented.

Clast types-

- Serpentinite some of which is chloritised
- Limestone/micrite
- Polycrystalline quartz

Litharenite with a mixed limestone serpentinite source.

### **SB46.3**

Location 489

Coarse-grained orange sandstone, clasts well-rounded but not well sorted. The clasts are matrix supported, this is composed of micrite and sparite. The majority of clasts have a micritic envelope.

Clast types-

- >90% serpentinite
  - bioclastic limestone
  - sparite
  - micrite
  - chert
  - haematite
- Litharenite/calcareous sandstone.

**SB47.3**

Location 489

Micritic mudstone.

There is some porosity that occurs in lines and as blobs. However, it is unclear whether this is primary or related to thin-section creation.

There appears to be peloids and there are rare small serpentinite clasts.

***Upper Miocene*****SB4**

Location 23

Grainsize ~0.5mm, poorly sorted, grains angular to sub-rounded, clast supported. Matrix composed not of calcite but a very fine grained black siliciclastic material.

**Clasts**

- Serpentinite
- Micrite/peloids
- Limestone (micrite and sparite)
- Chert (normal and radiolarian)
- Basalt (laths of plagioclase)
- Bioclastic limestone
- Silt

**Grains**

- Monocrystalline quartz (some contain thin lines of fluid inclusions)
- Polycrystalline quartz
- Muscovite mica
- Plagioclase (altering to sericite and epidote)
- Calcite crystals
- Biotite

**Bioclasts**

- Benthic and Planktic forams
- Rare bivalve fragments

Some porosity remains

Qtz ~10%

Feldspars ~5%

Lithics ~85%

Litharenite

### **SB39**

Location 14

Mudstone – mostly composed of micrite

Clasts

- Planktic and benthic (rare) forams
- Very small quartz crystals
- Muscovite
- Ostracods
- Small hematite grains

Diamond shaped crystals could be evaporite pseudomorphs or dolomite

### **SB43**

Location 69 - Graded calcarenites

Grainsize <1mm

Mixture of micrite and sparite

Bioclasts

- Echinoid plates (calcite overgrowths in optical continuity)
- Planktonic forams
- Bivalve fragments

Lithoclasts

- Micrite
- Cherty mudstone
- Siltstone
  
- Biosparite

## **SB46**

### Location 75

Fine grained, sub-angular to sub-rounded, moderately well sorted. Clast supported, matrix is not calcite but instead composed of very fine dark siliciclastic material, this makes up only 1-2%.

### Clasts

- Micritic limestone
- Serpentine
- Calcite (peloids)
- Feldspar and hypersthene (?) clast

### Grains

- Opaques
- Plagioclase (relatively fresh)(some feldspar have strain twinning)
- Monocrystalline quartz (fluid inclusions and occasional undulose extinction)
- Microcline
- Biotite
- Hornblende
- Polycrystalline quartz
- Muscovite
- Chlorite

### Mixed provenance Litharenite

Qtz ~20%

Feld ~5%

Lithics ~75%

**SB51**

Location Karacay log

*Mudstone* composed mostly of micrite but contains lots of bioclastic material.

**Bioclasts**

- Bivalve fragments
- Planktic forams including *Orbulina universa*, *Globergerina sp.*
- Benthic forams (inc *Milliolid sp*)
- Gastropods
- Crinoid ossicle

Also contains small quartz and haematite grains.

There is replacement of microfossils by pyrite.

~50/50 planktic to benthic foraminifera.



**SB51** – PPL of bioclastic wackestone. Note bivalve fragments, planktic foraminifera (including *Orbulina*) and calcispheres.



## **SB68**

Location 104 - Cream limestone

>90% bioclastic material

- Forams (benthic and planktic)
- Gastropods
- Ostracodes?
- Bryozoa
- Bivalve

Clasts of older limestone

No siliciclastic material

Micrite matrix with some sparite infilling porosity in bioclasts.

- Calcilutite/calcarenites
- After Folk – biointramicrite
- After Dunham – packstone

## **SB73**

Location 115

V fine grained sandstone, angular to sub-rounded grains, poorly sorted with a calcite matrix

>15%

Clasts

- Bioclastic limestone
- Serpentinite
- Micritic limestone

Grains

- Plagioclase
- Monocrystalline quartz (undulose extinction, fluid inclusions and subgrain rotation all observed)
- Biotite

- Muscovite
- Hypersthene (?)
- Opaques
- Chlorite
- Glauconite
- Polycrystalline quartz
- Bioclasts (forams)

Lithicwacke

Qtz 10-15%

Feld 1-5%

Lithics ~80%

### **SB79**

Location 140

Sandstone

Angular to sub-rounded grains, quite poorly sorted. Clast supported. Grainsize ~0.1-2mm  
Minimal micrite but >15% calcite cement that has replaced the original porosity.

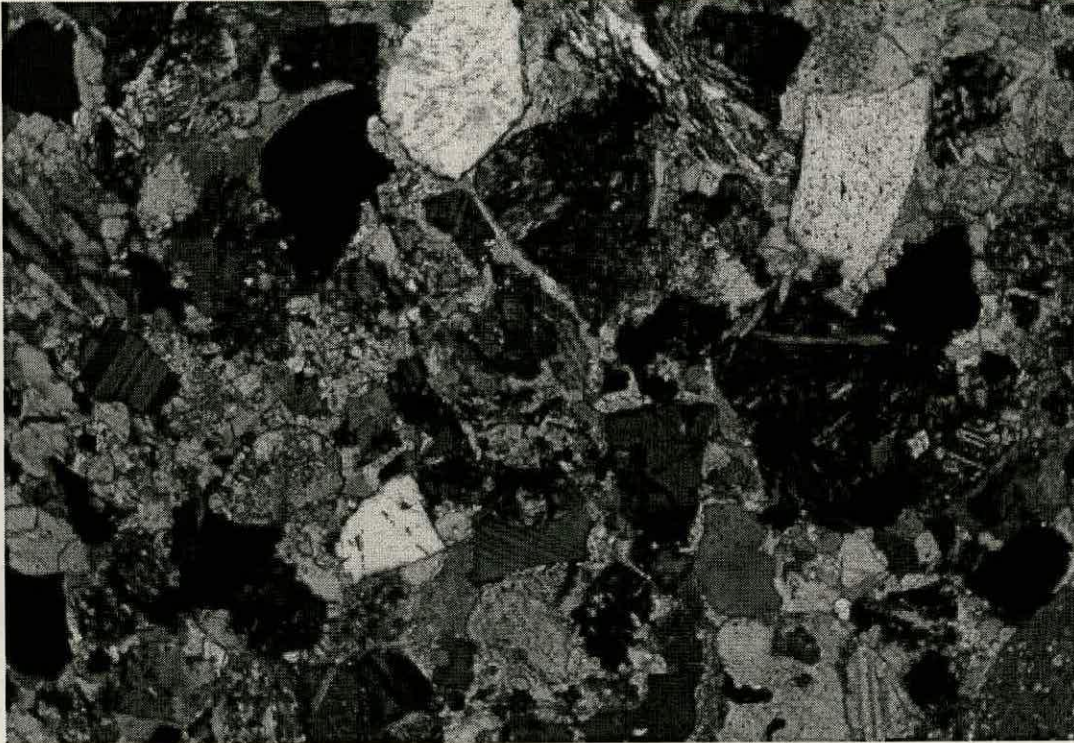
Grain types

- Muscovite mica
- Quartz (mono-crystalline, with occasional fluid inclusions and polycrystalline with sutured grain contacts, undulose extinction and subgrain formation.)
- Feldspar (some alteration to sericite)
- Pyroxene
- Biotite
- Single crystals of calcite
- Chlorite
- Glauconite

Clast types

- Micritic limestone
- Serpentinite

- Silt
- Red chert
- Multiple calcite grains
- Quartz and calcite clasts
- Altered feldspathic rock
- Minor bioclastic material (bivalves, forams)



**SB79** – XPL of litharenite with sparite cement. Clasts visible in field of view include plagioclase, serpentinite, quartz and mica. Magnification x 10.

Mixed sedimentary and igneous source

Quartz ~60%

Feldspars ~1%

Lithics ~39%

Lithic-arenite

**SB82**

Location 143

Very fine grained ~0.1mm, micrite and sparite matrix/cement. Grains are sub-angular to sub-rounded, matrix supported.

## Clasts

- Serpentine
- Chert
- Micritic limestone

## Grains

- Plagioclase
- Monocrystalline and polycrystalline quartz
- Clinopyroxene
- Opaques

## Bioclasts

- Benthic and planktic forams

Quartz ~5%

Feldspars ~20%

Lithics ~75%

Lithic greywacke

**SB84**

Location 145

Cream in colour with some opaque material. Grainsize <1mm, grains are angular – sub-rounded and poorly sorted, the fabric is clast supported. There is some carbonate matrix present <<15%, however sparry calcite cement has extensively in-filled the original porosity (>15%).

## Grains

- Monocrystalline quartz (contains fluid inclusions, often occurring in straight trails)
- Polycrystalline quartz (some undulose extinction extensive evidence for strain)

- Feldspars (plagioclase and K-feld) altering to sericite
- Biotite
- Muscovite
- Chlorite
- Clinopyroxene

Clasts

- Chert (normal, ferruginous and radiolarian)
- Mudstone/silts
- Rare reworked bioclasts
- Serpentine
- Altered glass

No bioclasts

Lithicwacke

Main sources appear to be sedimentary, with some ophiolitic input

Qtz ~25%

Feld ~5%

Lithics ~70%

**SB29A**

Location 173

Grainsize <0.5mm, slight greenish tinge to the thin section. Grains are angular to sub-rounded, it is poorly sorted and clast supported. The sample is calcite cemented infilling original porosity (>15%) but there is minimal micrite matrix.

Clasts

- Micritic limestone
- Serpentine
- Quartz-rich silt
- Chert
- Basalt (plagioclase rock)
- Quartz and epidote
- Quartz and plagioclase

Grains

- Monocrystalline quartz (thin lines of fluid inclusions)
  - Polycrystalline quartz
  - Epidote
  - Plagioclase (some grains beginning to alter to sericite)
  - Clinopyroxene
  - Chlorite
  - Opaques
  - Rare muscovite
- 
- Bivalve fragments

Quartz ~60%

Feldspars ~15%

Lithics ~25%

Litharenite

**SB50A**

Location 190

Grain size <0.5mm, clast supported, poorly sorted and has sub-angular to sub-rounded grains. There is no primary matrix, but there is extensive sparry calcite cement that composes >15% of the rock.

Clasts

- Serpentinite
- Micrite
- Plagioclase and epidote
- Biosparite and sparite
- Basalt
- Ferruginous and radiolarian chert

Grains

- Monocrystalline and polycrystalline quartz
- Epidote
- Muscovite

- Biotite
  - Plagioclase and minor k-feldspar (some alteration to sericite)
  - Clinopyroxene
  - Chlorite
  - Sparite with optically continuous sparite overgrowths.
- 
- Planktic foraminifera

Quartz ~35%

Feldspar ~10%

Lithics ~55%

Litharenite

### **SB53A**

Location 53 - Bone

Composed entirely of phosphate, the fabric of the phosphate curves around pores that are wholly to partially in-filled with micrite and sparite. The pores are rounded and have a semi-regular pattern.

Calcite veins cut the thin section in places, one of them appears to have experienced a shear. There is a small amount of the surrounding sediment plastered onto the edge of the bone, this is micritic and contains echinoderm plates, shell fragments and forams.

### **SB60A**

Location 120

Composed mainly of coralline algae 1-10mm in size. There is a primary micrite matrix and original porosity has been in-filled by sparite cement.

There are small bioclast fragments in between the algal material; bivalves, planktic forams and benthic forams.

- Packstone

**SB21.3**

Kozkalesi - Cream bioclastic limestone.

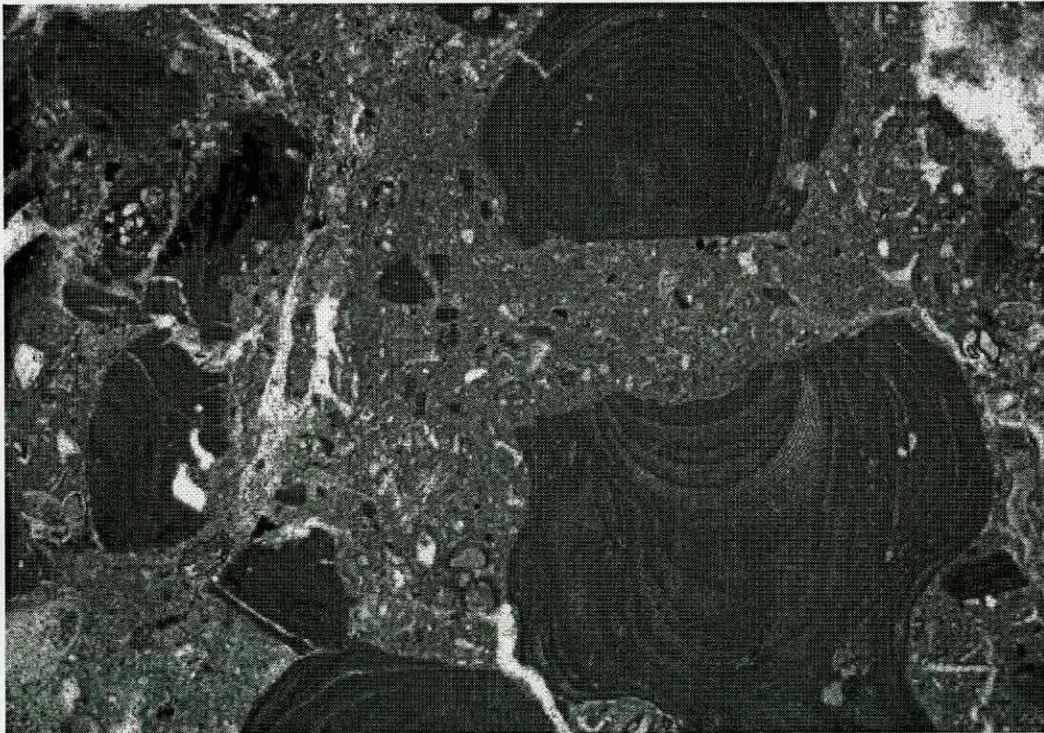
Micrite matrix rich in fauna.

- Benthic (mostly reworked) and planktic (inc Orbulina) forams
- Echinoid fragments
- Bivalve fragments
- Crinoid ossicles
- Ostrea
- Ostracods
- Coralline algae

Rare biotite clasts and other siliciclastic material (mostly serpentinite).

Primary porosity in bioclasts filled with sparite, some secondary porosity where skeletal fragments are missing. Present porosity ~5%, original <1%

- Biomicrite
- Wackestone



SB60A – PPL view of coralline algal boundstone. Magnification x 2.



## **Pliocene**

### **SB8**

Location 27

Khaki coloured limestone

Very fine grained

Clasts;

- Forams - planktic
- Chlorite
- Quartz
- Calcite crystals
- Serpentinite
- Dolomite/gypsum?
- Opaque minerals

Micrite matrix >>15%

- Calcilutite
- After Folk – Intramicrite/biointamicrite
- After Dunham – Mudstone

### **SB17**

Location 44

Mudstone dominated by micrite. Possible examples of faecal pellet as in some places there are lots of shell fragments all crammed together. Compared to other very fine limestone this sample is rich in both bioclastic and siliciclastic debris.

Very rare small clasts of:

- Quartz
- Plagioclase
- Epidote
- Clinopyroxene
- Biotite
- Opaque

## Bioclasts

- Planktic forams
- Benthic forams
- Bivalve fragments
- Ostracods
- Radiolarian

**SB23**

Location 53 - Sandstone, grainsize ~0.5mm

Grains are sub-angular to sub-rounded, matrix supported. No micrite, porosity in-filled by calcite (sparite) cement >15%. Moderate – poor sorting.

## Grains (~40%)

- Feldspar (some alteration to sericite (<10%))
- Quartz (monocrystalline and polycrystalline; evidence for grain boundary rotation, sutured contacts and some undulose extinction. Additionally some qtz have vacuoles, likely to be mixed sed, meta and hydrothermal source for qtz)
- Calcite
- Chlorite

## Lithic Clasts (~40%)

- Serpentinite
- Mudstone
- Red chert
- Micrite
- Quartz-feldspathic clasts
- Feldspar laths in fine matrix (igneous origin)
- Schist (quartz and orientated mica)

Very rare planktic forams

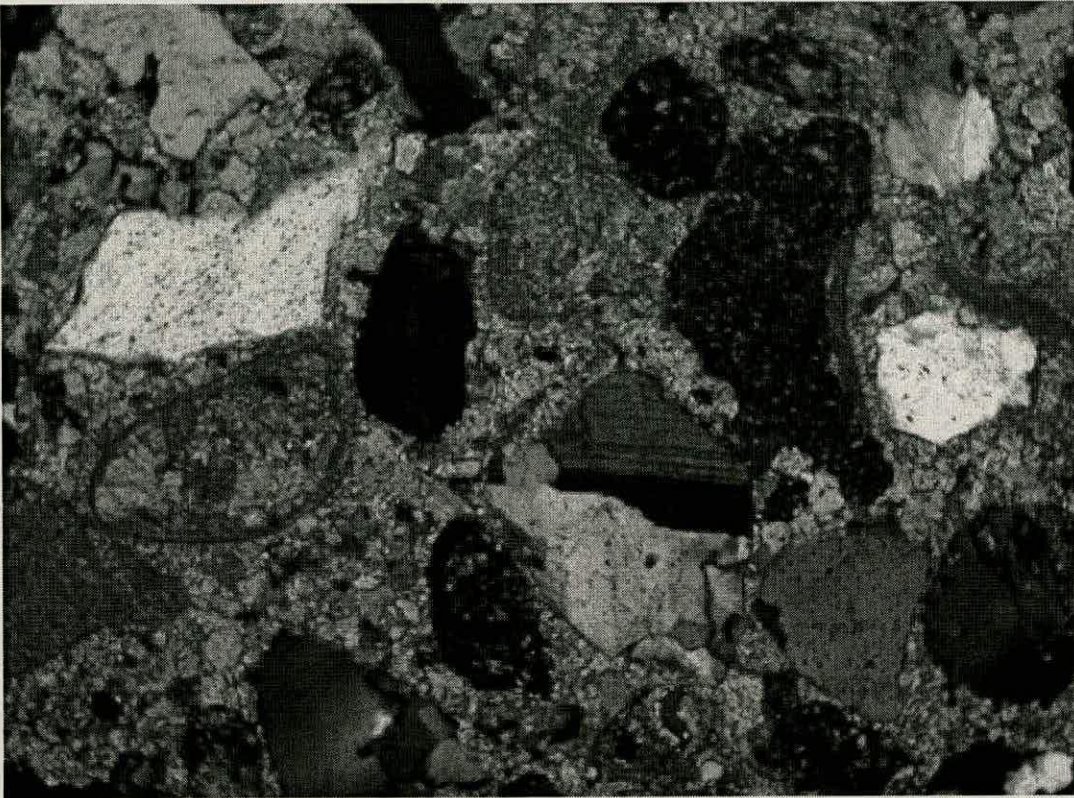
Mixed provenance

Litharenite

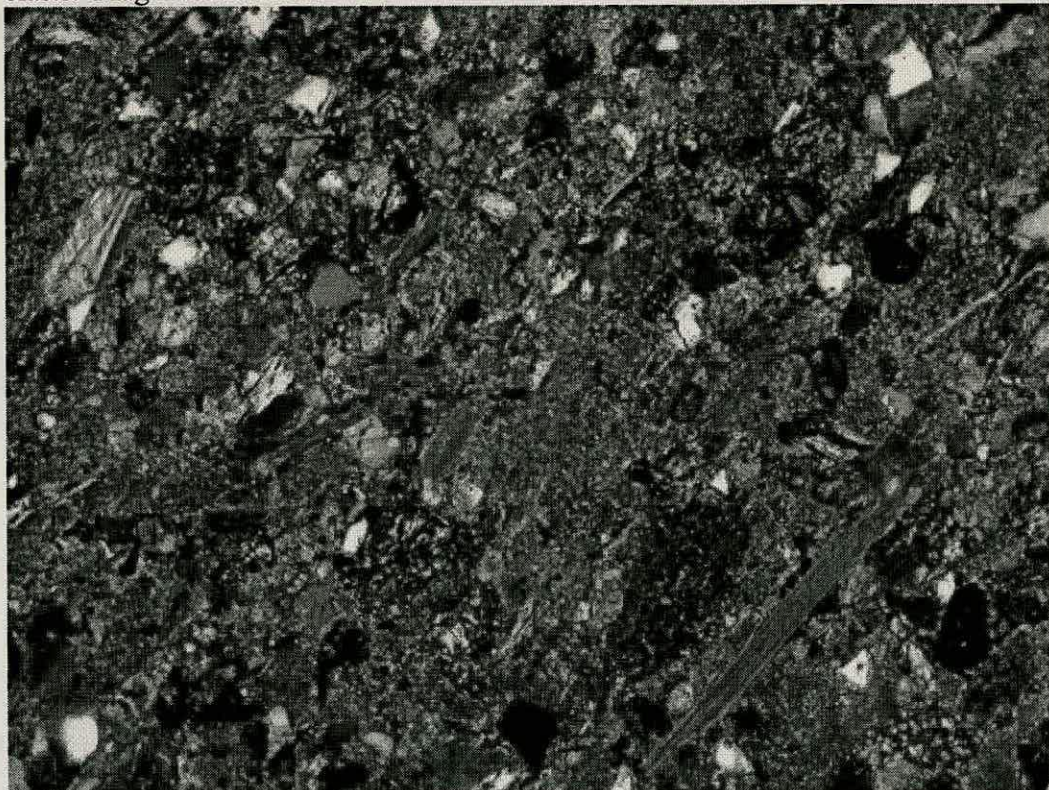
Quartz ~ 35%

Feldspar ~5%

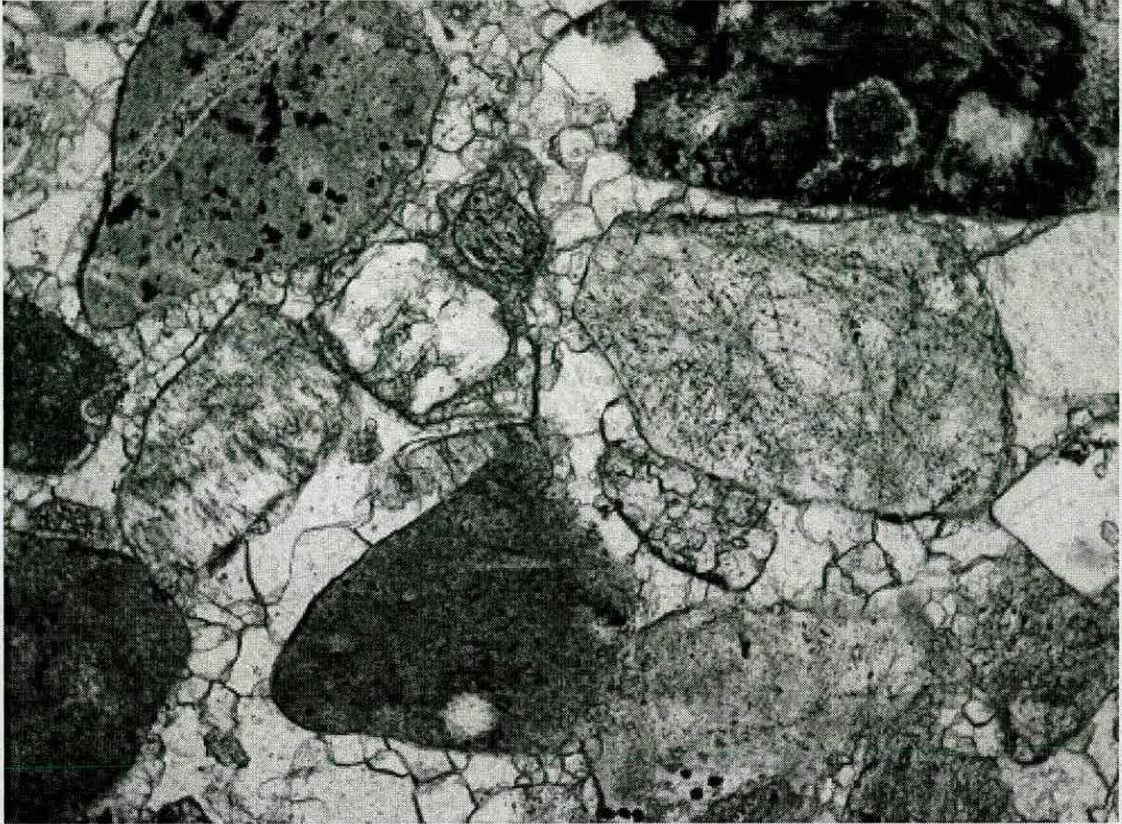
Lithics ~60%



**SB23** – XPL view of litharenite. Note mixture of siliciclasts (quartz, feldspar) and carbonate clasts. Magnification x10.

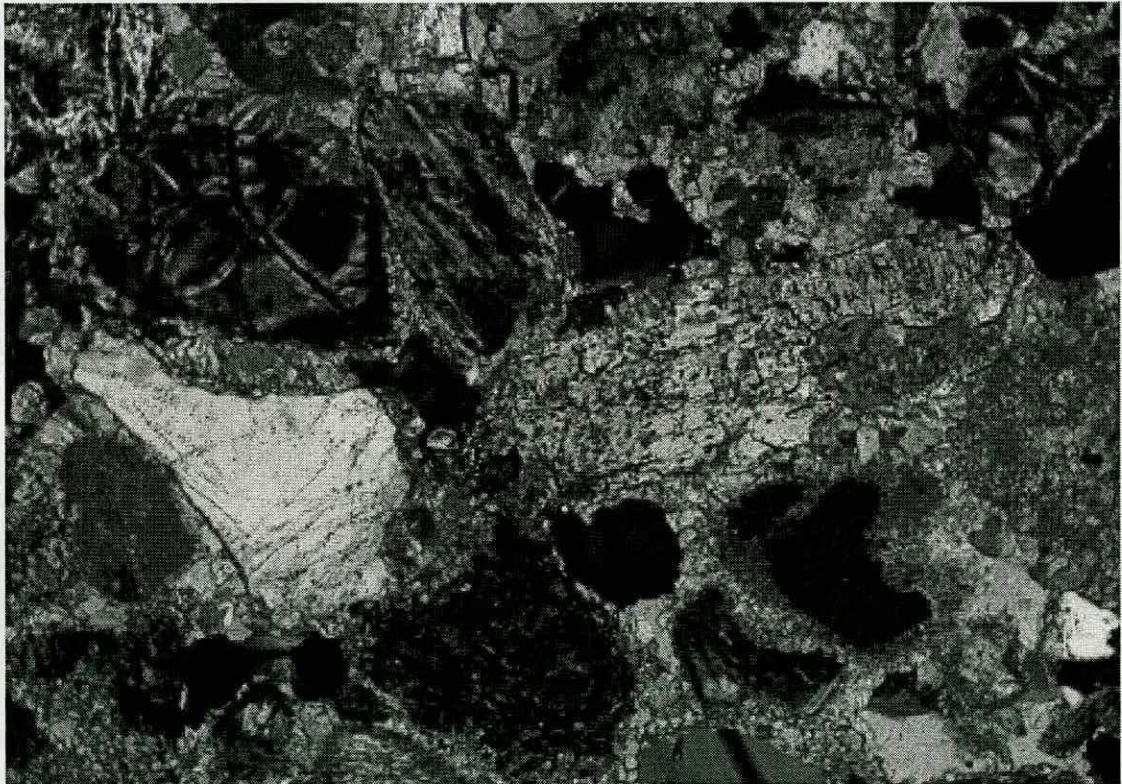


**SB26** – XPL view of fine grained sandstone, note alignment of muscovite grains. Magnification x 10.



**SB27** – PPL litharenite with coarse sparite cement. Note chert clast bottom centre.

Magnification x 10.



**SB29** – XPL of litharenite. Note presence of primary porosity gradually being infilled by sparite and the wide variety of clasts present. Magnification x 10.

## **SB24**

Location 8

Siltstone, grainsize <0.1mm

Grains are sub-angular to sub-rounded, it is poorly sorted and matrix supported with micrite cement >15%.

Very small fragments of siliciclastic material

- Monocrystalline and polycrystalline quartz
- Altered volcanic glass
- Muscovite
- Biotite
- Serpentine
- Chlorite
- Plagioclase
- Micrite
- Opaques

Present also; bioclastic material, planktic forams and bryozoa.

Greywacke

## **SB26**

Location 8

Laminar structure to limestone, very fine grained.

Micrite matrix >50%

Contains a significant amount of siliciclastic material

- Muscovite (long grains show minor alignment)
- Qtz
- Bioclasts
- Opaques
- Pyroxene
- Serpentine
- Hypersthene?
- Micritic/peloidal limestone
- Bioclastic limestone

**SB27**

Medium grained, with grading across the thin section. Medium grained, sub-angular to sub-rounded. Moderate sorting, carbonate cement and matrix supported.

## Clasts

- Siltstone/mudstone
- Serpentine
- Micrite (pos peloids)
- Bioclasts
- Chert
- Bioclastic limestone

## Grains

- Monocrystalline quartz (vacuoles)
- Polycrystalline quartz)
- Muscovite
- Biotite (very abundant pos from mica schists)
- Feldspar (some is quite fresh, others are altered to sericite)
- Pyroxene

Quartz and fine grained sediments dominate clast composition, there are occasional reworked benthic forams.

## Lithicarenite

Quartz ~50%

Feld ~1%

Lithics ~49%

**SB29**

## Location 7

Medium grained ~1mm, grains mostly rounded, clast supported, quite well sorted.

Carbonate cement, very little matrix.

## Clasts

- Serpentinite
- Chert (ordinary red chert, jasper, radiolarian chert)
- Micritic limestone
- Reworked bioclastic material (forams; generally contains quite a lot of well rounded lithoclasts, matrix is removed from clasts, millioids planktics)
- Mudstone/siltstone
- Iron rich sediments
- Biomicrite
- Microbial limestone

#### Grains

- Monocrystalline quartz
- Polycrystalline quartz
- Feldspars (mostly relatively unaltered)
- Hornblende
- Olivine
- Pyroxenes
- Muscovite
- Calcite crystals
- Bivalve fragments

Sources are sedimentary (limestone) and from the ophiolite (all levels are represented)

Litharenite

Qtz ~10%

Feldspars 1%

Lithics ~89%

#### **SB37**

Location 62

Medium grained ~1mm, clasts sub-angular to sub-rounded, matrix supported, moderately sorted. There is an insignificant amount of matrix but there has been extensive carbonate cementation, up to ~50% of the rock in places in filling primary porosity.

## Clasts

- Serpentine
- Siltstone/mudstone
- Chert
- Iron rich sed
- Micrite and biomicrite
- Carbonate
- Bioclasts (planktic forams)
- Peloids
- Basalt

## Grains

- Feldspars (plagioclase and k-feld)
- monocrystalline quartz (mostly clear but some grains contain vacuoles)
- Polycrystalline contacts
- Hypersthene?
- Epidote

Compositionally quite mature, more quartz than seen in some samples and less serpentine.

Litharenite

Qtz ~20%

Feld ~5%

Lithics ~75%

**SB69**

Location 107

Grainsize up to 3mm; moderate-poor sorting; sub-angular to sub-rounded grains. Carbonate matrix and cement present (<15%), clasts have micrite envelopes. Matrix supported.

## Clasts

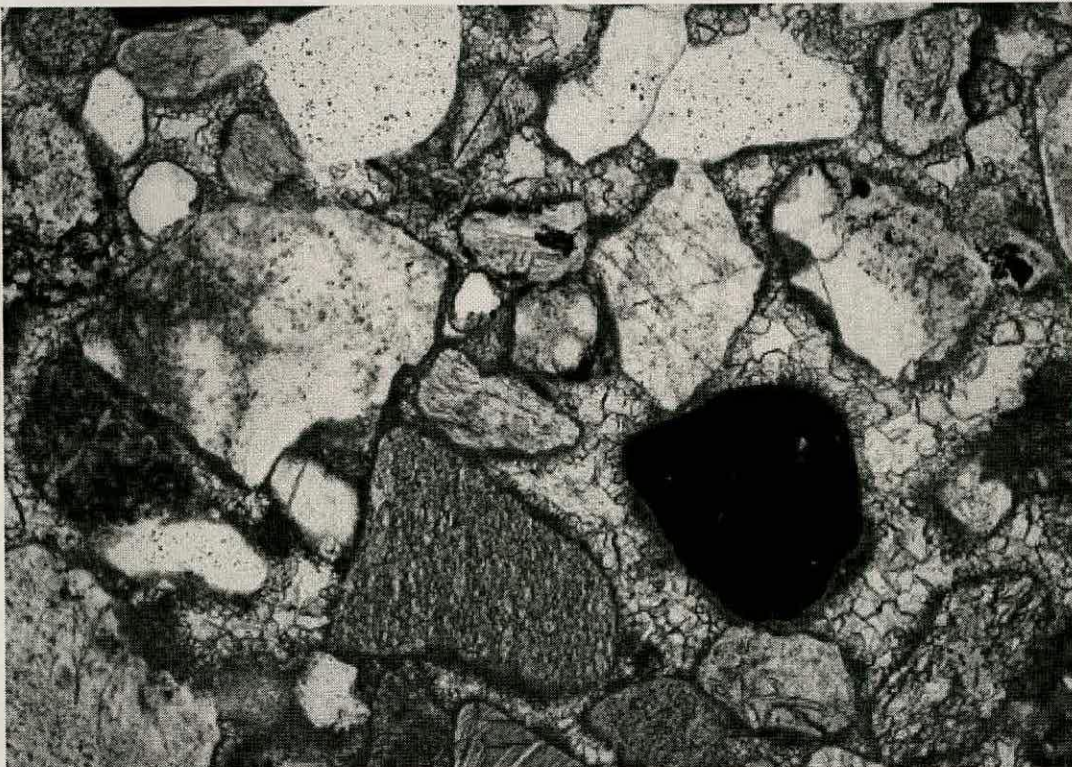
- Red chert
- Micritic limestone
- Serpentine
- Bioclasts (forams)



- Siltstone (qtz and muscovite)
- Clasts of sparite
- Feldspar laths in a very fine opaque matrix (basalt?)
- Bioclastic limestone

#### Grains

- Monocrystalline quartz (some contain lines of fluid inclusions and vacuoles)
- Polycrystalline quartz (sutured contacts)
- Calcite
- Rare feldspars



**SB69** – PPL view showing clearly the micrite envelopes around the grains and the two phases of cement growth, firstly forming small acicular crystals and then infilling completely the pore spaces. Note clasts of chert, opaques and fine grained carbonate.

Lots of fine grained siliciclastic material. The largest clasts are of micrite, one also contains siliciclastic material.

Litharenite

Qtz ~10%

Feldspars <1%

Lithics ~90%

**SB85**

Location 147

Grainsize 1-2mm, poorly sorted, angular to sub-rounded grains, clast supported. Some clasts have a micrite envelope and a fine sparite in fills the original porosity.

Clasts

- Muscovite
- Radiolarian and ferruginous chert
- Serpentinite
- Basalt
- Silt
- Biomicrite and intramicrite
- Sparite
- Altered volcanic glass

Grains

- Olivine
- Monocrystalline quartz
- Clinopyroxene
- opaques
  
- Planktic forams

No isopachous cements

Qtz ~1%

Feldspars ~1%

Lithics ~98%

Lithic greywacke.

**SB86**

Location 147

Grainsize ~1mm, grains are sub-angular to rounded. The sample is moderately poorly sorted and matrix supported.

Clasts

- Serpentine
- Bioclastic limestone
- Micritic limestone
- Silt
- Radiolarian chert
- Other cherts (i.e. ferruginous chert)

Grains

- Monocrystalline and polycrystalline quartz
- Plagioclase
- Clinopyroxene
- Epidote
- Muscovite
- Chlorite
- Olivine
- Opaques

Bioclasts

- Benthic forams (inc. *milliolid* sp.)
- Planktic forams

Lithic greywacke

**SB87**

Location 148 - Sandstone

Cream with opaque minerals

Medium – coarse grained

The sandstone has a clast-supported fabric with calcite cement, grains are angular to sub-rounded and it is generally poorly sorted. Contains >15% matrix.

Lithic Clast composition

- Serpentine
- Chert
- Micritic limestone

Individual grains

- Quartz
- Glauconite?

Bioclastic material

- Foraminifera (benthic sp. dominate also pelagic)
- Bivalve fragments
- Echinoid spines
- Algal material

The sandstone composition is dominated by the serpentinite clasts.

Quartz -1%; feldspar – 0%; lithics – 99%

Lithicwacke

**SB3.3**

Location 405

Pale coloured sandstone, medium grained (<1mm), poorly sorted, angular to subrounded.

Calcite (sparite) cement, <15% micrite matrix. Litharenite.

Clasts – single grains

- Quartz (some with inclusions)
- Feldspar (non-twinned but sericite alteration and Carlsbad-albite)
- Epidote
- Mica
- Hematite

Lithic fragments

- Polycrystalline quartz
- Chert
- Serpentinite
- Basalt
- Limestone (biomicrite)
- Sandstone (arenite)

- Peloids

#### Planktonic forams

Calcite crystals have optically continuous cement overgrowths. Carbonate grains have small calcite crystals growing on edges, but siliciclasts do not have these halos.

Some quartz is metamorphic.

### **SB4.3**

Location 406

Sandstone (litharenite)

Grainsize <0.5mm, moderately well sorted. Clasts well rounded to subangular. Sparite cement, clast supported but once quite porous.

2 stages of cement growth,

- 1) formation of small crystals on edges of clasts (good nucleation sites)
- 2) infilling of pore space by large sparite crystals.

#### Clasts

- Polycrystalline quartz
- Monocrystalline quartz
- Sparite crystals
- Ophiolite
- Calcarenite
- Feldspar (variable, most not twinned but altered)
- Mixed sparite and micrite clasts
- Chert
- Arenite
- Pyroxene
- Basalt

Some single calcite crystals have optically continuous calcite crystals.

No relict porosity.

**SB34.3**

Location 452

Pale coloured medium-grained, poorly sorted sandstone.

>15% matrix ~10% clasts. Siliciclasts are matrix supported, micrite, and are sub-angular to sub-rounded.

Clasts-

- Metamorphic quartz and unstrained quartz
- Epidote
- Clinopyroxene
- Plagioclase
- Opaques
- Alkali feldspar
- Peloids.

Lithic Fragments-

- Quartz and plagioclase
- Serpentine
- Chert
- Basalt
- Glass with needles in.

Much of the quartz and plagioclase are angular clasts compared to the ophiolite derived clasts that are rounded.

Lithic greywacke.

**SB57.3**

Location 8

Medium-grained sandstone, clasts sub-rounded to sub-angular and poorly sorted. Sparite cement but with micritic envelopes surrounding the clasts.

Clasts-

- Monocrystalline and polycrystalline quartz
- Plagioclase

- Limestone (micrite clasts, sparite, iomicrite)
- Single calcite grains
- Pink pelagic chert – radiolarian chert
- Quartz – plagioclase
- Quartz arenite
- Very fine calcareous lithicarenite clasts (silt)
- Basalt
- Quartz – plagioclase clast that has graphic texture (granphyre)
- Quartz with laths of alkali feldspar

Very heterogenous source for this rock.

Calcareous litharenite.

## **Belen Area**

### **Upper Cretaceous**

#### **SB92A**

Location 274

Fine grained <0.5mm, grains sub-angular to sub-rounded, poorly sorted. >15% cement mostly fine-grained spar there is minor matrix.

#### Clasts

- Serpentinite
- Limestone
- Chert
- Basalt
- micrite

#### Grains

- Polycrystalline quartz
- Monocrystalline quartz
- K-feldspar

#### Bioclasts

- Reworked forams both Benthic and planktic.

Qtz ~5%

Feld ~1%

Lithics ~94%

Litharenite

## **Eocene**

#### **SB129A**

Location 352

Mudstone



Dense micrite matrix with sparite infilling biological porosity (inside of shells). Micrite has a patchy fabric (peloidal) with some parts denser than others. Contains lots of bivalve fragments, ostracods, clasts of sparite and micrite clasts with circles of sparite.

### **SB130A**

Location 352

Large calcite vein runs through the centre of the slide.

Limestone is dense micrite, could be compacted peloidal matter or algal.

## **Kepez Formation**

### **SB68A**

Location 225 - Limestone.

These samples contain a lot of bioclastic material;

- Coralline algae
- Forams (Benthic and planktic)
- Echinoid fragments (optically continuous overgrowths)

Much of this material appears to be reworked. Micrite matrix. Sparite in fills minor porosity and is also present as veins.

- After Folk - Biosparite
- After Dunham – Wackestone

### **SB158A**

Location 380

Bioclastic material

- Echinoid fragments
- Coralline algae
- Forams
- Bivalves
- Gastropod

Small sub-angular serpentinite clasts.

Matrix is a mixture of micrite and sparite. One echinoid fragments had a calcite isopachous fringe.

Packstone.

## **Kici**

### **SB73A**

Location 229

Red sandstone, fine grained <0.5mm, poorly sorted, grains sub-angular. No micrite and little sparite cement <<15%.

Clasts

- Serpentinite (~50%)
- Basalt

Grains

- Microcrystalline quartz possibly chert (~50%)
- Monocrystalline quartz
- Microcline
- Peloids
- Iron oxides

Composition is quite different from sandstones from Antakya region.

Litharenite

### **SB77A**

Location 229

Grainsize up to 5mm, very poorly sorted with sub-angular to sub-rounded grains. >15% micrite matrix.

Clasts

- Foraminiferal limestone

- Microcrystalline quartz (chert?)
- Serpentinite
- Peloids

#### Grains

- Calcite crystals
- Opaques

#### Bioclasts

- Oyster fragments
- Forams (some replaced by pyrite)
- Echinoid fragments
- Coralline algae (possibly reworked)

Coarser material appears to be concentrated in layers.

Lithicwacke.

### **SB154A**

Location 380

Beach Rubble – microbial limestone

Composed mainly of reworked algal material – rip up clasts.

Other material has been incorporated into the algae;

- Planktic forams
- Benthic forams (*milliolid* sp. etc.)
- Encrusting foraminifera
- Coral
- Bivalve fragments
- Pisolith
- Serpentinite (sub-rounded)
- Quartz
- Plagioclase
- Opaques

Porosity has been in-filled by sparite, and there is plenty micrite between the large algal clasts.

Boundstone

Shallow marine material reworked either slightly down slope or within a beach environment.

**SB155A**

Location 380 - Beach Rubble

This sample is basically the same as the sample above with slightly more bioclastic material in.

**SB39.3**

Kandildere log (abandoned village). Fine-grained sandstone containing large bioclasts and siliciclastic material. Greater than 15% matrix also a lot of micrite cement

- Gastropods
- Coralline algae
- Bivalve fragments
- Foraminifera.
  
- Serpentinite
- Chert
- Epidote
- Clay minerals – smectite?
  
- Quartz
- Carbonate grains
- peloids

**Gokdere**

**SB71A**

Location 228

Grainsize <0.5mm, moderate sorting and clasts are sub-angular to sub-rounded. Cemented by sparite (>15%).

Clasts

- Basalt
- Ferruginous chert
- Serpentine
- Micrite (peloids)
- Quartz and chlorite
- Polycrystalline quartz plus accessory minerals

Grains

- Polycrystalline quartz
- Monocrystalline quartz
- Plagioclase altering to sericite
- Calcite crystals
  
- Rare foraminifera

Quartz ~50%

Feldspar ~15%

Lithics ~35%

Feldspathic litharenite

**SB94A**

Location 281

Grainsize <0.5mm contains also a large mudclast, poorly sorted.

Angular to sub-angular grains, clast supported. Very little micrite some sparite <15%.

Clasts

- Sparite
- Peloids
- Cherts
- Serpentine
- Chlorite present in some clasts

Grains

- Polycrystalline quartz
- Monocrystalline quartz
- Plagioclase and k-feldspar (very altered)
- Biotite
- Muscovite
- Planktic forams

Litharenite

**SB96A**

Location 281

Grainsize 0.5-1mm. Sub-angular grains, moderate sorting, clast supported with a sparite cement <15%

Clasts

- Serpentine
- Biotite + chlorite
- Limestone
- Quartz + muscovite

Grains

- Muscovite
- Biotite
- Polycrystalline quartz
- Monocrystalline quartz
- Plagioclase

Litharenite

**SB103A**

Location 310

Grainsize ~1mm, poorly sorted with angular to sub-rounded clasts, clast supported. <15% matrix and some sparite.

Clasts

- Serpentine
- Radiolarian chert
- Micrite
- Polycrystalline quartz and plagioclase

Grains

- Polycrystalline quartz
- Monocrystalline quartz with fluid inclusions
- Plagioclase (some have micro-fractures prior to deposition)
- Muscovite

Qtz ~65%

Feld ~5%

Lithic ~30%

**SB121A**

Location 346

Fine grained <0.5mm, moderately sorted, angular to sub-angular grains, matrix supported.  
>15 matrix and some cement.

Clasts

- Micrite
- Serpentine
- Ferruginous chert
- Chert
- Basalt

Grains

- Polycrystalline quartz
- Monocrystalline quartz
- Muscovite (some has chlorite)
- Plagioclase
- Biotite

- Opaques

Clasts have iron oxide crusts.

Qtz ~45%

Feldspar ~15%

Lithics ~40%

### **SB142A**

Location 364

Grainsize ~1mm. Moderately well sorted, grains sub-rounded to rounded, clast supported.

Sparite cement <15%.

#### Clasts

- Plagioclase
- Micrite (peloid)
- Quartz + mica
- Serpentine
- Bioclastic limestone + coralline algae
- Ferruginous chert

#### Grains

- Polycrystalline quartz
- Monocrystalline quartz (fluid inclusions in some grains)
- Calcite
- Biotite
- Muscovite

#### Bioclasts

- Reworked material
- Bivalve fragments
- Planktic forams



Sparite has formed a poikiliptic texture around clasts but additionally clasts have a thin envelope of calcite around the edge. Some calcite grains have optically continuous overgrowths of sparite.

Quartz ~30%

Feldspars ~10%

Lithics ~60%

Litharenite

### **SB27.3**

Gökdere Log

Very fine-grained mudstone. Laminated micrite, layers of ostracods follow the laminations. These bivalves are articulated and disarticulated. There is no preferred way-up and there has possibly been some compaction. The articulated clasts are infilled with sparite. Appear to be two forms of shelly material (thick and thin shelled). Also there are small gastropods and angular quartz grains. Restricted environment? Lagoonal/lacustrine

## ***Serinyol***

### **Eocene conglomerate**

#### **SB36.3**

Location 259

Sample taken from a clast of limestone from a conglomerate horizon. The limestone is pale in colour, very fine-grained packstone/biomicrite.

Very rich in bioclastic material and very tightly packed. Porosity is 100% infilled by later sparite and most of the original calcite of the shells has been replaced by sparite.

- Bivalve fragments
- Benthic and planktic foraminifera
- Echinoid and crinoid fragments
- Bryozoan
- Coralline alage

**SB61.3**

Serinyol log

Fine-grained calcareous sandstone, moderately well-sorted with angular to sub-angular clasts. Sparite cement, but it is clast supported.

Clasts

- Serpentine
- Chert
- Limestone (micrite, biomicrite, coralline algae)
- Plagioclase (altering to sericite)
- Bivalve fragments
- Quartz (mono and polycrystalline)
- Muscovite

***Potential Source Rocks*****Palaeozoic Pink Arkose Sample 182A**

Grainsize 1.2mm, >99% Quartz (quartz arenite). The quartz grains are anhedral and have undergone substantial compaction and have partially sutured grain boundaries. The quartz is a mixture of monocrystalline (very pure quartz although straight trails of tiny fluid inclusions are very common) and polycrystalline (undulose extinction, and subgrain rotation observed). Clay minerals are present in the interstitial spaces and the whole rock has a faint pink colour due to the presence of haematite.

Some quartz crystals have secondary quartz rims and overgrowths in optical continuity.

Quartz cementation has not been recognised in any of the younger sediments.

One clast of a very fine siliciclastic rock was observed.

**Greywacke Sample 183A**

Very fine grained, fine groundmass of clay mineral >15%.

Grains

- Quartz, monocrystalline (with small fluid inclusions, and larger inclusions) and polycrystalline.
- Fine grained siliciclastic material

- Plagioclase (quite altered but twinning is still visible in many grains)
- Muscovite (rare)
- Chert?

### **Olivine Basalt Sample 185A**

Fine-grained

- 60% Plagioclase (twinned and zoned, some are phenocrysts, very fresh)
- 30% Olivine (some are phenocrysts)
- 10 % Pyroxenes

Lots of vesicles.

## **Appendix 4**

### *Point counting data*

Table showing the point-counting results for the fine-grained sandstones in percentage.

Sampl e No	Feld - spar	Silici- clastic	Carbon- ate	Bio- mica	Bio- clast	Ophiolite	Qtz(p)	Qtz(m)	Micrite	S .Calcite	opaque	other
SB94A	4	8	12.5	2	2	13.5	10	10.5	6.5	28.5	2.5	0
SB84	5.5	5	7.5	0.5	0.5	7	9	10.5	7	41.5	4	2
SB73A	0	14.5	5.5	0	0	51.5	1.5	1	2	20	4	0
SB37	5	5	19	0	0	13	15.5	9	0	33.5	0	0
SB79	4	11	16.5	1	0	7	8.5	6	0	36.5	2.5	7
SB23	4	5	17	0	0	11	12	11	1	39	0	0
SB29A	4.5	9	21	2	0	6	3	9	5.5	37	3	0
SB27	1	8	15.5	0	0	8.5	9	9.5	1.5	43.5	1	2.5
SB71A	1	17	19	0.5	0	7	6.5	7.5	1.5	31	4	5
SB142 A	0.5	6	30	0	0	11.5	11.5	5.5	7	19.5	2	6.5

Table showing the point-counting results for the coarse-grained sandstones.

Sample No.	Silici-clastic	Carbon-ate	mica	Bio-clast	Ophiolite	Acidic vol?	Feld-spar	Qtz(p)	Qtz(m)	Micrite	S. Calcite	opaque	other
SB8	4.5	16	0.5	4	50	0	0	0.5	0.5	4	13	1	6
SB86	3.5	14	0	0.5	32.5	0	0	0	2	9	28.5	1	9
SB85	16	13	0	0.5	42	0	0	0	1	11.5	14.5	0.5	1
SB69	2	14.5	0	0	16.5	5	0	11	8	16	24	0	3
SB29	6.5	15.5	0	1.5	29.5	0	2	3	2.5	2	31	0.5	6
SB160A	0	26	0	9.5	15.5	0	0	0	0	4.5	37.5	0	7
SB77A	0.5	1.5	0	1	48.5	0	0	0	0	10.5	37.5	0	0.5
SB90A	1	42	0	20	1	0	0	0	0	10	23	1	2
SB177A	5.5	2	0	0	68.5	0	0	2.5	0	0	19.5	2	0
SB14.3	0	19	0	0	48.5	0	0	0	0.5	21	8	0	3
SB46.3	0	1	0	0	67	0	0	0	0	16	15	1	0
SB43.3	9	20	0	0	41.5	0	0	1.5	2	0	19	0	7
SB57.3	10	15	0	0	19	0	6.5	8.5	22.5	3.5	12	0.5	2.5



## Appendix 5


*Table of Historical Earthquakes recorded in Antioch*

<i>Date of earthquake</i>	<i>Description</i>
21/02/148 B.C.E	Destruction of buildings in Antioch
c.65 B.C.E	Destruction of buildings in Antioch, possibly 170,000 dead in Syria.
23/03/37 C.E	No record of effects
c. 47	Violent earthquake, cracks in walls and collapse of some buildings.
13/12/115	Antioch badly damaged, many buildings destroyed, possibly generated a landslide on Mt Casius. Many dead.
341	Ground shaking; after shocks continued for a year.
13/09/458	Destruction of buildings, many deaths and injuries. Possibly cracks opened in the ground.
29/05/526	250,000 people dead in Antioch, devastation to the city and surrounding areas, destruction of buildings followed by fire. The port of Seleucia Pieria also destroyed. After shocks for a year afterwards.
532	Many small earthquakes but no damage occurred.
580/581	Daphne totally destroyed, some buildings damaged in Antioch.
October 587/588	Destruction of buildings, ~60,000 dead.
28/02 - 10/03/713	Destruction of buildings over a wide area (including Antioch and Aleppo), many dead.
05/01 – 25/12/835	Earthquakes for forty days, destruction of Antioch.
972	Collapse of the city walls and towers.



## **Appendix 6**

### *Conglomerate Clast Count*

	Eocene	E. Miocene 						
	loc 259	loc 282(1)	loc 282(2)	loc 282(3)	Gokdere 1	Gokdere 2	Gokdere 3	Gokdere 4
Limestone	0	74	42	35	5	20	5	0
Num lmst	0	0	0	0	0	0	4	1
Serp	0	0	27	10	95	80	33	40
Pink Pel	0	0	0	0	0	0	0	0
lmst breccia	0	0	0	0	0	0	0	0
Chert	14	9	12	2	0	0	3	2
Conglomerate	0	0	0	0	0	0	0	0
Algal lmst	73	0	0	0	0	0	0	0
sst	0	0	0	0	0	0	0	0
Palaeosol	0	0	0	0	0	0	0	0
Mica schist	0	0	0	0	0	0	0	0
Chert + lmst	13	20	26	21	0	0	0	0
Bioclastic lms	0	5	12	13	0	0	0	0
Pink calcar	0	0	0	0	0	0	0	0
Chalk	0	0	0	0	0	0	0	0
Red mud	0	0	0	0	0	0	0	0
Basalt	0	0	0	0	0	0	0	0
other	0	0	0	0	0	0	0	0
<b>Total</b>	<b>100</b>	<b>108</b>	<b>119</b>	<b>81</b>	<b>100</b>	<b>100</b>	<b>45</b>	<b>43</b>





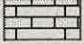




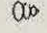


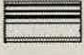

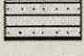







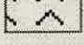

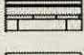

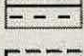

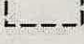




	E. Miocene →								
	loc 163	Enek 1	Enek 2	loc 440	loc 456	Rubbish 1	loc 470	loc 471	loc 472
Limestone	20	0	0	23	5	1	30	0	61
Num Imst	50	0	0	0	0	0	0	0	13
Serp	7	96	43	15	88	94	53	27	0
Pink Pel	5	2	0	8	0	0	0	0	0
Imst	0	0	0	0	0				
breccia						0	0	0	0
Chert	11	2	1	22	3	1	2	18	11
Conglome									
rate	5	0	0	0	7	0	0	0	0
Algal Imst	4	0	0	0	0	0	0	0	0
sst	1	0	0	0	0	0	2	0	0
Palaeosol	0	0	1	0	0	0	0	0	0
Mica									
schist	0	0	0	0	2	0	0	0	0
Chert +									
Imst	0	0	0	0	0	0	0	0	7
Bioclastic									
Imst	0	0	0	0	0	0	0	0	0
Pink									
calcar	0	0	0	0	0	0	18	0	11
Chalk	0	0	0	0	0	0	10	7	0
Red mud	0	0	0	0	0	0	5	0	0
Basalt	0	0	0	0	0	0	0	0	2
other	3	0	0	0	0	0	0	0	0
Total	106	100	45	68	105	96	120	52	105

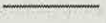

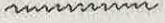
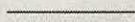
	E. Miocene					U. Miocene		
	Mid		Miocene					
	loc 410	loc 448	loc 474	Koz Kalesi	Asi river	loc 492a	loc 492b	loc 493
Limestone	63	3	0	25	58	30	30	63
Num lmst	30	0	0	20	0	0	10	3
Serp	4	47	36	21	70	3	10	5
Pink Pel	0	0	0	2	0	0	0	0
lmst breccia	0	0	0	2	0	0	0	1
Chert	0	0	0	0	4	0	5	3
Conglomerate	0	0	2	0	0	0	0	0
Algal lmst	0	0	0	0	0	0	0	5
sst	0	0	1	0	0	2	2	0
Palaeosol	0	0	0	0	0	0	0	0
Mica schist	0	0	0	0	0	0	0	0
Chert + lmst	0	0	0	0	0	0	0	4
Bioclastic lms	5	0	6	0	0	13	0	0
Pink calcar	0	0	0	0	0	0	0	3
Chalk	0	0	0	0	0	0	0	0
Red mud	0	0	0	0	2	7	0	0
Basalt	0	0	0	0	0	1	0	0
other	0	0	0	0	3	1	0	0
<b>Total</b>	<b>102</b>	<b>50</b>	<b>45</b>	<b>70</b>	<b>137</b>	<b>57</b>	<b>57</b>	<b>87</b>

# Appendix 7

## Key to Sedimentary logs

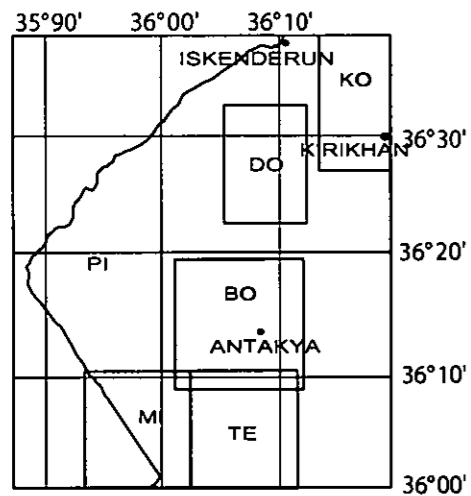
### KEY

	Biorudite		Oncolite
	Biosparite, beds >20cm		Bivalve
	Biosparite, beds <20cm		Dewatering structure
	Biosparite and marl		Whole echinoid
	Calcareenite		Gastropod
	Arenite		Parallel lamination
	Interbedded arenite and marl, bed thickness 0.01-0.3m		Rip-up clasts
	Mudstone with thin sandstone interbeds <15cm		Slump
	Silt		Horizontal burrows
	Marl		Vertical burrows
	Conglomerate		Carbonate nodules
	Ophiolite(serpentinite)		Chert nodules
	Interbedded biomicrite and marl, bed thickness 0.1-0.6m		Siliciclastic pebbles
	Thin bedded marl, bed thickness <0.07m		Plant material
	Individual beds not shown, largest grainsize represented		Coral
			Foraminifera
			Ripples
			Oyster

	Measured beds
	Inferred beds
	Bioturbation
	Amalgamated beds

## **Appendix 8**

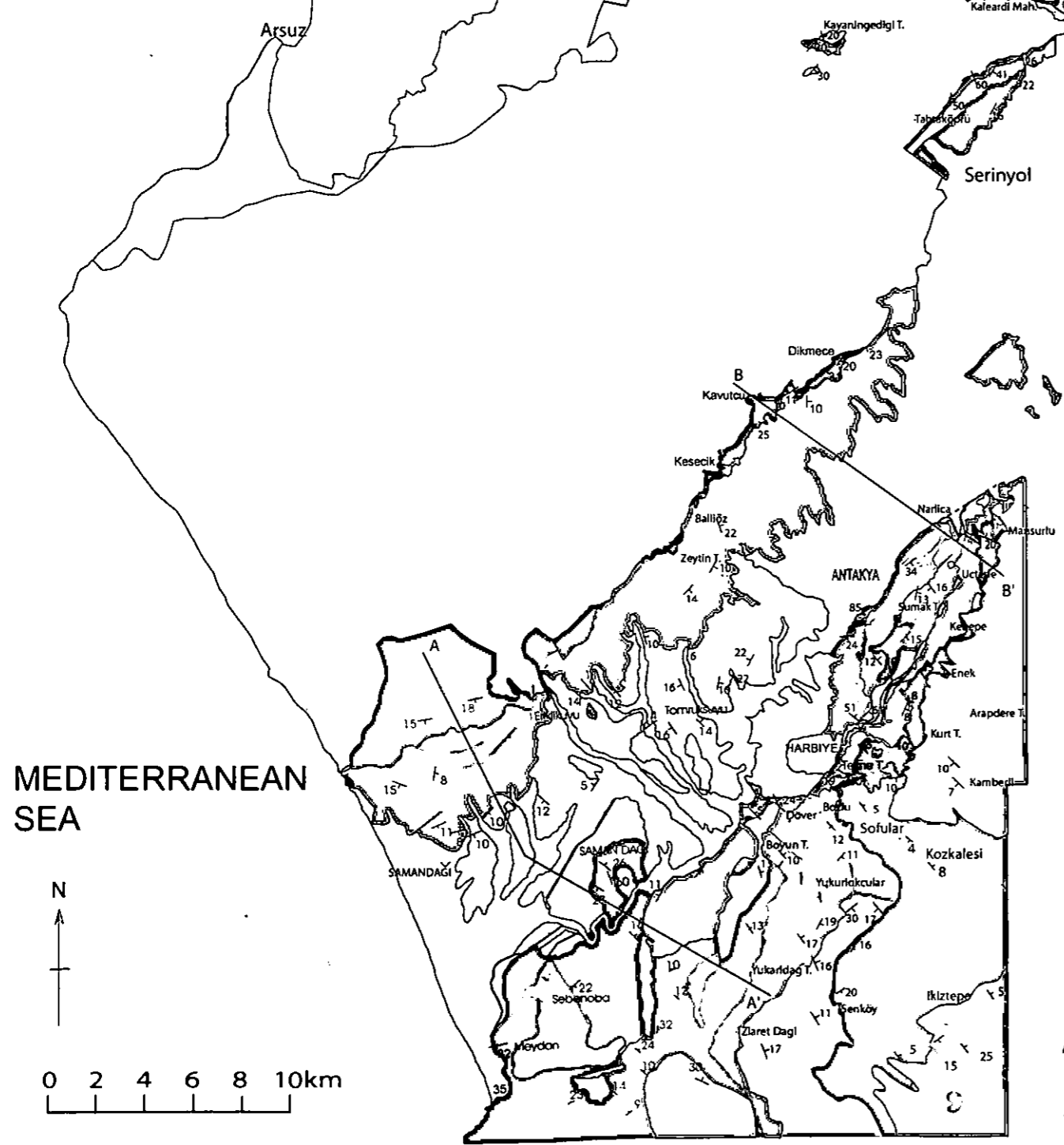
*Geological map and cross-sections of the study area*



BO: Boulton, this study;  
 DO: Dokumacı, 1997;  
 KO: Kop, 1996; MI: Mistik, 2002; TE: Temizkan, 2003; PI: Pişkin, 1985.

Geological Map of the Hatay Region, Southern Turkey.

Compiled by S. J. Boulton 2006.  
 School of GeoSciences, University of Edinburgh



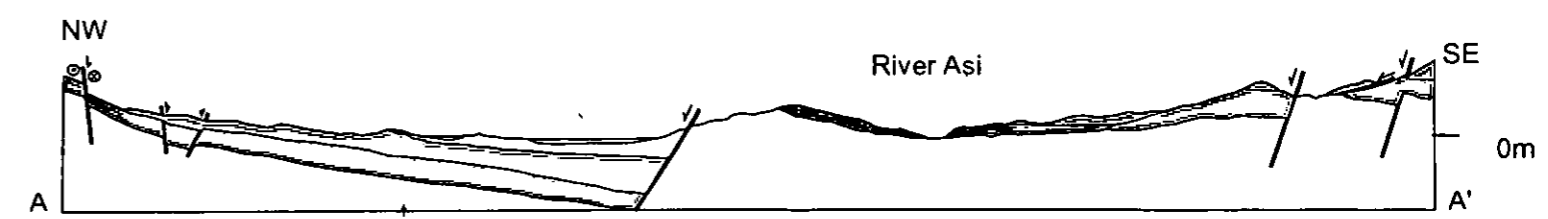
Key to the Stratigraphy of the KIRIKHAN area

C E N O Z O I C	Quaternary	Quaternary	Alluvium
		Quaternary	Karasu Basalt
	Pliocene	Pliocene	Gökdere Fm. (sandstone & marl)
		Pliocene	Kepez Fm. (limestone)
		Pliocene	Kıcı Fm. (sandstone & conglomerate)
	Oligocene	Oligocene	Hacıdağ Fm. (limestone)
		Oligocene	Cona Fm. (marl)
		Oligocene	Eşmişek Fm. (limestone)
	Miocene	Miocene	Terbüzek Fm.
		Miocene	Koçali Complex (ophiolite)
Miocene		Delibekirli Fm.	
Eocene	Eocene	Kalecik Fm.	
	Eocene	Arilik Fm.	
	Eocene	Seydişehir Fm.	
Paleocene	Paleocene	Sosink Fm.	
	Paleocene	Koruk Fm.	
	Paleocene	Zabuk Fm.	
Cretaceous	Cretaceous	Sadan Fm.	
	Cretaceous		

Key to the Stratigraphy of the ANTAKYA area

C E N O Z O I C	Quaternary	Quaternary	Alluvium
		Quaternary	Samandağ Fm. (sandstone, muds and marls)
	Pliocene	Pliocene	Tepehan Fm. (limestone & marls)
		Pliocene	Sofular Fm. (limestone)
		Pliocene	Balyatağı Fm. (conglomerates)
	Oligocene	Oligocene	Kıslak Fm. (limestone)
		Oligocene	Okçular Fm. (limestone)
		Oligocene	Kaleboğazi Fm. (limestone)
	Cretaceous	Cretaceous	Hatay Ophiolite
		Cretaceous	

- 35 Dip and strike of bedding
- Normal faults
- Strike-slip fault
- Thrust fault
- Syncline axis
- Anticline axis



## UNIVERSITY OF EDINBURGH THESIS

Author (surname, initials): *BOULTON, SARAH J.*

Degree: *Ph.D.*

Year: *2006*

This thesis is an unpublished typescript and the copyright is held by the author. *All persons consulting this thesis, or having copies made, must sign the Copyright Declaration below.*

Copying regulations: (1) This thesis may be copied in whole or in part for the use of individuals and for libraries wishing to add this thesis to their stock. *Copying must be done by Edinburgh University Library.*

Copyright Declaration: I undertake fully to observe the author's copyright in this thesis, not to publish the whole or any part of it without the author's written permission, and not to allow any other person to use any copy made for me.

Date	Name and Address (BLOCK CAPITALS)	Signature	Pages copied (if any)



BOULTON, SARAH J.

Ph.D. 2006